THE UNIVERSITY OF HULL

PARTICLE-STABILISED FOAMS AND FOAM FILMS

being a Thesis submitted for the Degree of Doctor of Philosophy

in the University of Hull

by

Dulce Alexandra Braz

BSc (Hertfordshire University)

February 2009

ACKNOWLEDGEMENTS

First and foremost I acknowledge with sincere gratitude my academic supervisor Prof. Bernard P. Binks for offering the opportunity to carry out this PhD work. I also thank him for his continuous and excellent guidance throughout this research and for reviewing this thesis with constructive comments.

Special thanks to my second academic supervisor Dr. John H. Clint for his encouragement during this research. My appreciation also goes to Dr. Tommy S. Horozov for giving me technical assistance in the laboratory and for his fruitful contribution to various parts of this work.

I am grateful to Unilever (Colworth, U.K.) for financial support in sponsoring this research project and to Dr. Andrew Cox for useful discussions as my industrial supervisor. I also thank Mr. M. Kirkland, from Unilever Colworth for carrying out the freeze fracture SEM measurements.

Special appreciation is also given to Prof. Paul D.I. Fletcher and Dr. Vesselin N. Paunov for valuable discussions and to all members of the Surfactant & Colloid Group, for their assistance, friendship and support.

Special thanks to all my family for their unconditional love, understanding and endless support from miles and miles away.

Last but certainly not least, I would like to thank both my husband Richard and my son Iuri for their patience and constant support and encouragement during the time I spent in researching and writing this thesis.

ABSTRACT

This thesis aimed to investigate and understand the properties of foams and foam liquid films stabilised by colloidal solid particles, in the absence of any surface active substances, *e.g.* surfactants. Foams occur as end products or during the processing of products in many industries, including detergents, food and the cosmetic industries. A controlled level of foam formation is desirable in many consumer products. Therefore understanding the mechanisms for their control was also important in this research. Colloidal particles act in many ways like traditional surfactant molecules but offer distinct advantages. The main advantage is that particle-stabilised foams offer longer stability in comparison to surfactant-stabilised foams. Most of the studies, however, were focused on mixtures of surfactant systems and solid particles. Physical mechanisms for foam formation in the presence of colloidal particles alone are less known. However, in response to an increasing interest for this subject, a number of research papers on foams stabilised by solid particles alone have been published recently and during the past 5 years.

The first study was concerned with understanding the properties of foams, such as foaming ability and stability of aqueous dispersions of nanosized silica particle (*i.e.* 100 nm) systems alone, where their hydrophobicity was changed *in situ*. The key parameters investigated were solid particle concentration, particle size, effect of electrolytes and the effect of pH. The results show that foamability and foam stability were directly proportional to particle concentration and particle size of the aqueous silica dispersions. By changing the pH of the aqueous dispersions a maximum in foaming ability was found at an intermediate pH around 4.5. Furthermore, by increasing the concentration of NaCl in the aqueous silica dispersions, it was observed that the foaming ability also increased and a maximum in foam stability was found. These results suggest that by increasing the salt concentration, the silica particles become more hydrophobic and therefore they are able to adsorb at the air-water interface and stabilise the foams. However, at very high concentrations of salt, flocculation of particles is increased and as a result particles may lose their mobility and not be able to promptly adsorb on the air bubble surface. This will hinder foam formation, as shown with this study. Characterisation of the aqueous particle dispersions and foams produced was studied by optical microscopy, light scattering and rheology. The wettability of solid

particles was also investigated by measuring the contact angle of water drops on solid surfaces.

The properties of foams stabilised solely by monodispersed spherical silica particles of diameter 0.6 µ,m that exhibit different extents of hydrophobicity, was also investigated in the absence surface-active agents. The hydrophobicity of the silica particles was modified *ex-situ* to different extents by reacting the hydrophilic silica with different concentrations of dichlorodimethylsilane (DCDMS) in the presence of dry toluene. The foaming ability and foam stability of these aqueous dispersions of nanosized silanised silica particles were investigated by using the glass cylinder shaking test and by homogenisation using an Ultra - Turrax homogeniser. The key parameters investigated were particle hydrophobicity, particle concentration and NaCl concentration. The results show that the foamability of the aqueous dispersions reached a maximum at intermediate particle hydrophobicity ($\theta = 95°$). However, foam stability was enhanced when particles of greater hydrophobicity were used ($\theta = 105°$). Foamability was also enhanced by creating the foams using rotor – stator mixing. By increasing the particle concentration and by adding salt to the aqueous silica dispersions, more particles were transferred to the air - water interface, resulting in better foamability and foam stability observed with these systems. Freeze – fracture SEM studies revealed hexagonally close – packed monolayers and multilayers of silica particles at the air - water surface of the most stable foams obtained.

Vertical foam films with dilute and close–packed modified silica particle monolayers at their surfaces has been investigated by direct microscope observations using a Scheludko type cell. Monodispersed silica particles (3 µm in diameter) hydrophobised to different extents have been used. By keeping the contact angle constant, the density of particles at the water surface was changed by spreading more particles. Several challenges were identified and discussed in this study. It is well known that particles need to accumulate at the thinnest region of the film in order for it to become stable. If they move away from the thinnest part of the film, the film eventually breaks (instability). It is found that their structure and stability depend strongly on the particle hydrophobicity, on the mechanism of opening and closing the films (fast or slow), and also on the monolayer density. With dilute particle monolayers at their surfaces, hydrophilic particles are expelled from the film centre towards its periphery, giving a dimple surrounded by a ring of particles bridging the film surfaces. In contrast, hydrophobic particles tend to move inside the film centre, making the film more unstable and causing it to rupture.

The three phase contact angle of small solid particles adsorbed at the air-water interface is directly related to the particle hydrophobicity and this knowledge is of great importance. Therefore, isolated thin liquid foam films were investigated with a view to developing a novel method for determining the contact angle of small solid particles with interfaces. As a result a simple and reliable film-calliper method for measuring the particle contact angle at the air - water interface in real time has been developed. Its applicability to micrometer latex and silica particles is demonstrated.

The foaming ability and stability of aqueous dispersions of clay Laponite RD particles was also investigated. The effect of different electrolytes was investigated in order to determine the influence of salt valence on the wettability of the clay particles. Laponite RD dispersions were prepared at either constant concentration of Laponite RD with increasing concentration of salt, or at constant salt concentration for a range of clay concentrations by using two different protocols. Foams of salt, water and Laponite RD clay particles were only formed under conditions where the particles are flocculated (via salt) but not gelled. However, all foams formed were very unstable (burst within minutes) and after one day sedimentation of particles occurs, in which a grey, turbid phase separates from a clear, supernatant liquid.

Finally, an investigation into the behaviour of foams stabilised by a mixture of silica nanoparticles and pure cationic surfactant is reported. A systematic study was carried out on the foaming ability and foam stability of aqueous dispersions of CTAB or silica nanoparticles alone by using the glass cylinder shaking method. The key parameters investigated were CTAB or particle concentration and the effect of pH. In mixtures, the synergism between the surfactant and silica particles leads to enhanced foam stability at an intermediate CTAB concentration, where particles were found to be most flocculated. Complementary experiments, including the particle diameter, contact angle and zeta potential measurements have been undertaken in order to offer an explanation for the latter synergy.

PUBLICATIONS AND PRESENTATIONS

This thesis has contributed to the following publication:

1.   T.S. Horozov, D.A. Braz, P.D.I. Fletcher, B.P. Binks and J.H. Clint, 'Novel Film-Calliper Method of Measuring the Contact Angle of Colloidal Particles at Liquid Interfaces', *Langmuir*, **24**, 1678 (2008).

This work has also been presented by the author at the following events:

1.   Oral presentation entitled: 'Particle-stabilised foams', Surfactant & Colloid Young Researcher Workshop, 6th June 2005, University of Hull, U.K.

2.   Oral presentation entitled: 'Particle-stabilised foams', European Student Colloid Conference, 12-15 July 2005, The Netherlands.

3.   Oral presentation entitled: 'Particle-stabilised foams', New Developments in Emulsions and Foams, 12-14 December 2005, The University of Manchester, U.K.

4.   Oral presentation entitled: 'Thin Foam Films', Surfactants and Colloids Group Seminar, 19th May 2006, University of Hull, U.K.

5.   Oral presentation entitled: 'Foams and foam films stabilised by small solid particles', Departmental Research Colloquium, 19th June 2006, University of Hull, U.K.

6.   Poster Presentation: 'Foams and foam films stabilised by small solid articles', Eufoam 2006 Conference: 6th European Conference on Foams, Emulsions and Applications, 02-06 July 2006, Potsdam, Germany.

7.   Oral presentation entitled: 'Particle-stabilised foams and foam films', 1st March 2007, Unilever R&D, Colworth, U.K.

8.   Poster Presentation: 'Particle-stabilised foams', Poster Competition and Networking Event, 9th May 2007, Leeds Metropolitan University.

CONTENTS

CHAPTER 4   STABILISATION OF FOAMS WITH EX-SITU MODIFIED COLLOIDAL SILICA PARTICLES

CHAPTER 5   THIN FOAM FILMS WITH SILICA PARTICLES AT THEIR SURFACES

CHAPTER 8   PARTICLE-SURFACTANT INTERACTIONS IN FOAMS

CHAPTER 9   SUMARY OF THE MAIN CONCLUSIONS AND FUTURE WORK

APPENDIX: TABLES OF EXPERIMENTAL RESULTS

CHAPTER 1

CHAPTER 1

INTRODUCTION

1.1   Industrial relevance of current research

This project was sponsored by Unilever, an international manufacturer of leading brands in foods, home care and personal care. Solid-stabilised foams offer the advantage of longer stability in comparison to surfactant or protein-stabilised ones, and therefore the company wanted to apply this new technology to their products. One example is ice cream, which is a complex food colloid consisting of air bubbles and ice crystals. The air bubbles in the ice cream are mainly stabilised with fat globules of average diameter of a few micrometres, which is a colloidal particle. During the various steps in the manufacturing process of ice cream, such as cooling, the air bubbles in the ice cream coalesce causing a loss of creaminess of the product. This loss of creaminess is often compensated for by introducing a higher fat content and the long term stability of the ice cream is achieved due to the product being frozen, *i.e.* solid-like structure. The challenge for Unilever R&D in Colworth, U.K. was to develop a new technology that retains the small air bubbles and the fine microstructure of freshly produced ice cream whilst lowering the fat content. This research project mainly focused on the preparation and characterisation of foams stabilised solely by solid particles in order to gain a better understanding of their adsorption at the air-water interface, thus enabling the important factors involved in the formation and stability of particle-stabilised foams to be understood.

1.2   Introduction to surfactants and colloids

Foam stabilisation generally relies on the presence of surfactants. Therefore, although this work is mainly based on solid particle-stabilised foams, a brief introduction to surfactants is given here, as they are the most commonly used foaming agents. This is followed by an introduction to the basic concepts and principles of colloids.

A surfactant is a surface-active molecule that is amphiphilic, meaning it contains both hydrophobic groups ("tails") due to the presence of straight or branched hydrocarbons and hydrophilic groups ("heads") that can be either cationic (positively charged), anionic (negatively charged), zwitterionic (positive and negative charges) or nonionic. Therefore, surfactants are soluble in both organic solvents and water depending on the nature of the hydrophilic and hydrophobic groups. Figure 1.1 shows the schematic representation of a straight chain surfactant molecule and shows the two distinct parts of its nature.

Figure 1.1 Schematic representation of a single tailed surfactant molecule. The hydrophobic tail-group favours air (or oil) and the hydrophilic head-group favours water.
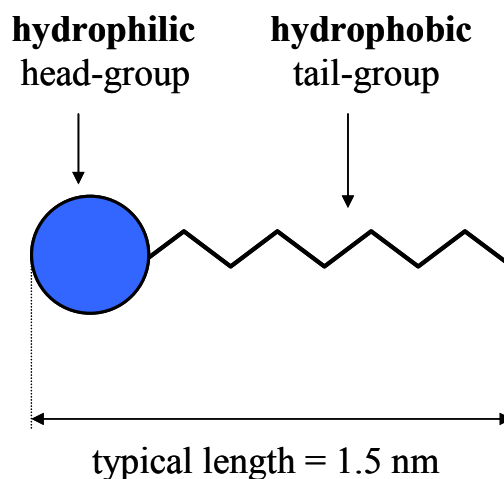
Surfactant molecules can adsorb at interfaces due to the amphiphilic nature of their molecular structure. The hydrophilic head-group is always situated in the aqueous phase, whereas the hydrophobic tail-group is situated in the air or oil phase. Therefore, in two-phase air or oil and water systems a surfactant may partition itself between the air or oil and water phases. If the hydrophilicity of the head-group exceeds the hydrophobicity of the tail-group the surfactant may be expected to partition in favour of the aqueous phase. When the hydrophobicity of the tail-group exceeds the hydrophilicity of the head-group, the surfactant may be expected to partition to a greater extent into the air or oil phase.

In aqueous solution, the hydrophobic tail-groups of a surfactant prefer to minimise their contact with water while the hydrophilic head-groups prefer to maximise their contact with water. The result is generally a spherical aggregate of surfactant monomers with a core of hydrophobic tails and a surface layer of head-groups known as a micelle (Figure 1.2).[1,2] Individual surfactant molecules that are in the system but are not part of a micelle are called monomers.

Figure 1.2   Schematic arrangement of a cross-section of a spherical micelle.
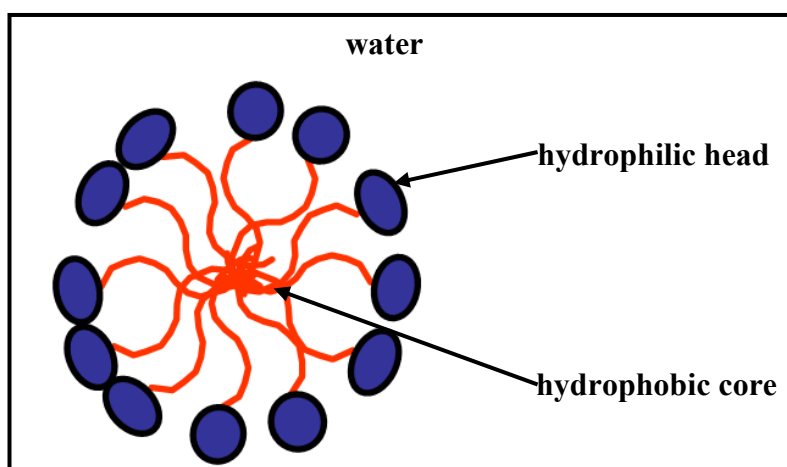
If the surfactant is present in oil, reversed micelles will form, which have a hydrophilic core and a hydrophobic outer layer. Micelles exist in rapid dynamic equilibrium with their monomers.[3] The concentration for the onset of micellisation is known as the critical micelle concentration (cmc) and is marked by a distinct change in the colligative properties of the solution. Below the cmc the surfactant exists in its monomeric form. When the concentration of surfactant is increased above the cmc, the concentration of monomers remains constant and the number of aggregates (micelles) increases.[4]

Surfactants have a tendency to adsorb at air-water and oil-water interfaces, leading to a reduction in the surface or interfacial tension, respectively. When a surfactant is dissolved in water, the presence of the hydrophobic moiety causes unfavourable distortion of the liquid structure, which increases the overall free energy of the system. Water molecules surrounding the hydrophobic tail-groups become ordered which decreases the total entropy of the system.[2]

The entropy is increased when a surfactant molecule is transported to an interface. As less work is required to bring a surfactant molecule to an interface compared to solvent molecules the surfactant will preferentially adsorb at the interface in order to lower the free energy of the system. The hydrophilic moiety retains its affinity for the solvent molecules which causes the surfactant to orient itself at the interface with the hydrophilic group in aqueous solution and the hydrophilic group protruding into the vapour or oil phase. The work required to increase the interfacial area decreases which causes a decrease in the surface or interfacial tension.[5] The amount of surfactant adsorbed at the interface can be calculated by measuring the surface tension and applying the Gibbs' adsorption equation.[6] The surface tension decreases with increasing surfactant concentration as the amount of adsorbed surfactant increases and reaches a saturation value at a critical concentration (Figure 1.3). The surface tension continues to decrease and then reaches a plateau value at the cmc of the surfactant.[5]

Surfactant molecules can also adsorb at the solid-liquid interface. Adsorption onto solid surfaces is an important process in many applications of surfactants including detergency and waterproofing. Adsorption mechanisms are controlled by interactions between the adsorbing surfactant and the substrate, as well as interactions between adsorbed surfactant molecules. The nature of these interactions is determined by the properties of the solid surface, the nature and concentration of the surfactant and environmental factors such as temperature, pH and the type of the solvent.[7] Generally, adsorption mechanisms are evaluated from an adsorption isotherm, which can be obtained using solution depletion methods or techniques such as ellipsometry.[8] A variety of isotherm shapes has been determined experimentally to describe different mechanisms for the adsorption of surfactants onto solid surfaces from aqueous solution.[2]

Figure 1.3   The effect of adsorption of surfactant at the air-water or oil-water interface on the surface tension.
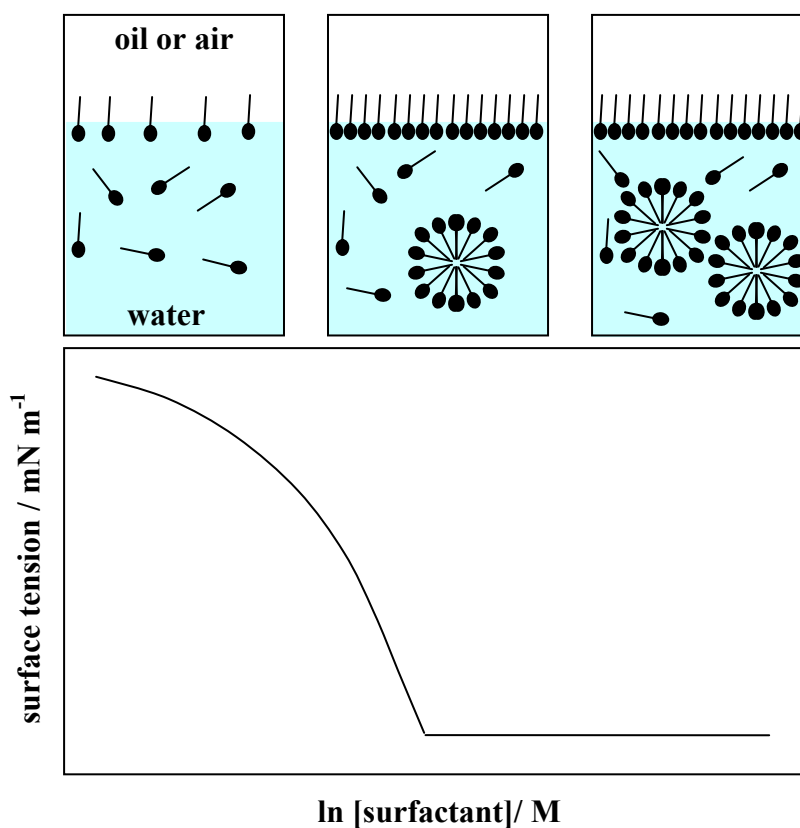
1.2.2   Colloids

Colloids are heterogeneous systems in which finely divided matter (particles) is dispersed in a liquid or gas. Their size usually ranges from 1 nm to several tens of micrometers. These particles are too small to be seen with a microscope but are large enough to scatter light. Colloids can be classified according to the phases of the substances involved as described below:[9,10]

i.   Aerosols are dispersions of fine liquid droplets or solid particles in a gas (*e.g.* fogs, smokes).

ii.   Emulsions are colloidal systems in which the dispersed and continuous phases are both liquids, *e.g.* oil-in-water (mayonnaise) or water-in-oil. Such systems require an emulsifying agent to stabilise the dispersed particles.

iii. Sols are dispersions of fine solid particles in a liquid medium (*e.g.* paints, muds, slurries).

iv. Gels are colloids in which both dispersed and continuous phases have a three-dimensional network throughout the material, so that it forms a jelly-like mass (*e.g.* gelatin).

v. Foams are dispersions of gases in liquids or solids (*e.g.* shaving foam, aluminium foams).

vi. Association colloids are systems in which the dispersed phase consists of clusters of molecules that have hydrophilic and hydrophobic parts (*e.g.* surfactants) and are associated together to form small aggregates (micelles) in water.

Colloidal dispersions are thermodynamically unstable owing to their high surface free energy and the particles tend to combine to form larger aggregates to reduce the interfacial energy. An initially formed aggregate is called a floc and the process of its formation is termed flocculation. The floc may or may not separate out. If the aggregate changes to a much denser form, it is said to undergo coagulation. An aggregate usually separates out either by sedimentation (if it is more dense than the medium) or by creaming (if it is less dense than the medium). The terms flocculation and coagulation have often been used interchangeably. Usually coagulation is irreversible whereas flocculation can be reversed by the process of deflocculation. Figure 1.4 represents some of these processes.[10]

Colloidal particles exhibit Brownian motion, which is the random movement of these particles driven by their thermal energy in a liquid medium.[11] This causes the collision of particles inducing the formation of aggregates. However, this process can be prevented by modifying the forces acting between the colloidal particles. Derjaguin-Landau-Verwey-Overbeek (DLVO) theory is the classical explanation of the stability of colloids in suspension. It looks at the balance between two opposing forces - van der Waals attraction and electrostatic repulsion - to explain why some colloidal systems agglomerate while others do not.[9, 10]

Figure 1.4 Schematic diagram showing various mechanisms of colloidal instability.
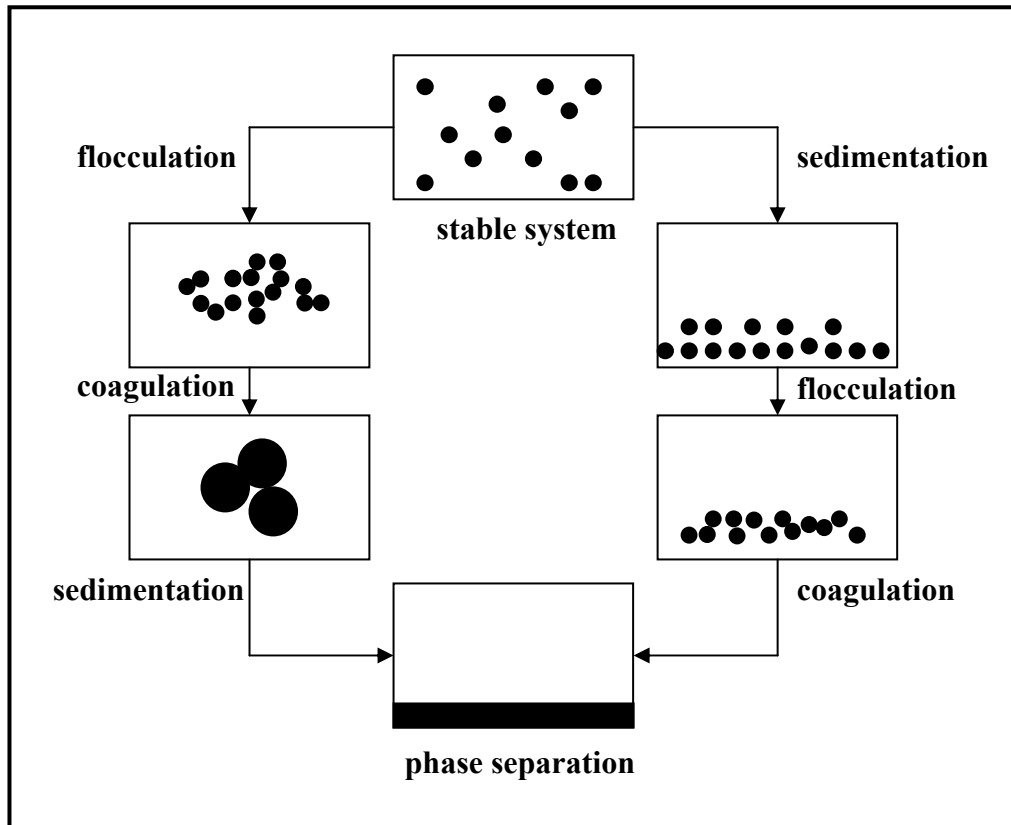
van der Waals forces result from attractions between the electric dipoles of molecules. It was introduced by van der Waals in 1873 to explain the properties of non-ideal gases and liquids, forces between dipole moments and the polarising action of one molecule in another molecule. Attractive van der Waals forces between colloidal particles arise from dispersion interactions between the molecules on each uncharged particle by inducing dipoles in other particles. These instantaneous dipoles create a long-range attractive force between particles. For two spherical particles of radius r, where the interparticle separation (h) is very small (h << r), the attractive energy between two curved surfaces is given by[12]

$$V_A = -\frac{Ar}{12h} \tag{1.1}$$

where A is the Hamaker constant, which determines the effective strength of the van der Waals interaction between colloidal particles. The Hamaker constant is a material property with dimensions of energy; for many materials its order of magnitude is around 10^{-20} J.

Most colloidal dispersions in aqueous media carry an electric charge. There are many origins of this surface charge depending upon the nature of the particle and its surrounding medium. For particles dispersed in liquids, two of the most important causes are the ionisation of chemical groups at the surface and the differential adsorption of ions of different charges from solution.

The development of a net charge at the particle surface affects the distribution of ions in the surrounding interfacial region, resulting in an increased concentration of counter ions, ions of opposite charge to that of the particle, close to the surface. Thus an electrical double layer exists around each particle. The liquid layer surrounding the particle exists as two parts; an inner region (Stern layer) where the ions are strongly bound and an outer (diffuse) region where they are less firmLy associated. Charged particles will attract ions of opposite charge in the dispersant. Ions close to the surface are strongly bound; those further away form a more diffuse region. Within this region is a notional boundary known as the slip plane within which the particle and ions act as a single entity. The potential at the slip plane is known as the zeta potential (Figure 1.5).[13]

Figure 1.5   Schematic representation of zeta potential (taken from ref. 13).
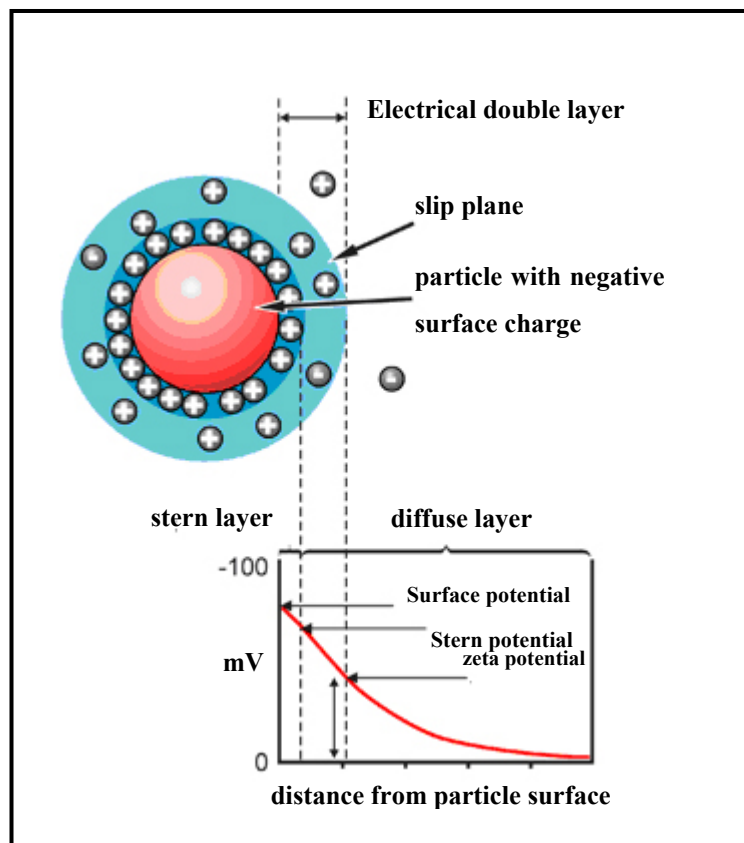
The magnitude of the zeta potential gives an indication of the stability of the colloidal system. The most important factor that affects zeta potential is pH. A zeta potential value on its own without a quoted pH is a virtually meaningless number. If a particle in suspension has a negative zeta potential and more alkali is added to this suspension, then the particles tend to acquire more negative charge. If acid is added to this suspension then a point will be reached where the charge will be neutralised. Further addition of acid will cause a build up of positive charge. Therefore a zeta potential versus pH curve will be positive at low pH and lower or negative at high pH. There may be a point where the plot passes through zero. This point is called the isoelectric point and is very important from a practical consideration. It is normally the point where the colloidal system is least stable.

Electrostatic repulsion becomes significant when two colloids approach each other and their double layers begin to interfere. The electrostatic interactions are screened by dissolved ions; it is found that the screened Coulomb interaction exponentially decays with distance.[14] The repulsive energy due to electrical double layer interactions between two spherical particles of identical radius r, is given by[12]

$$V_R = \frac{\varepsilon r \psi_o^2}{2} \ln\left(1 + \exp(-\kappa h)\right) \tag{1.2}$$

where ε is the permittivity of free space, ψ_o is the surface potential, κ is the reciprocal length and h is the inter-particle separation. Equation 1.2 may be used only if the double layer thickness is small in comparison to the particle radius ($\kappa r \gg 1$). The Debye length ($1/\kappa$) is the thickness of the electrical double layer. The reciprocal length is given by[1]

$$\kappa = \left(\frac{e^2 \sum_i c_i z_i^2}{\varepsilon k T} \right)^{1/2} nm^{-1} \tag{1.3}$$

where c_i is the molar concentration of each ionic species of valence z_i, e is the electronic charge, k is the Boltzmann constant and T is the temperature. In most systems $1/\kappa$ varies from about 1 to 100 nm.

The basic idea of the DLVO theory is that the stability of a colloidal dispersion is determined by the sum of the van der Waals attractive and electrical double layer repulsive forces that exist between particles as they approach each other due to the Brownian motion they are undergoing. Therefore, the total interaction energy between colloidal particles is expressed as the sum:

$$V = V_A + V_R \qquad\qquad (1.4)$$

where V_A is the attractive energy and V_R is the repulsive energy between two spherical particles. These interactions are represented by equations 1.1 and 1.2 for van der Waals attractive forces and electrical double layer repulsive forces respectively. This theory proposes that an energy barrier resulting from the repulsive force prevents two particles approaching one another and adhering together (Figure 1.6). But if the particles collide with sufficient energy to overcome that barrier, the attractive force will pull them into contact where they adhere strongly and irreversibly together. This is known as the primary minimum (Figure 1.7). Therefore if the particles have a sufficiently high repulsion, the dispersion will resist flocculation and the colloidal system will be stable. However if a repulsion mechanism does not exist then flocculation or coagulation will eventually take place.

Figure 1.6 Schematic diagram of the variation of free energy with particle separation according to DLVO theory. The net energy is given by the sum of the double layer repulsion and the van der Waals attractive forces that the particles experience as they approach one another.
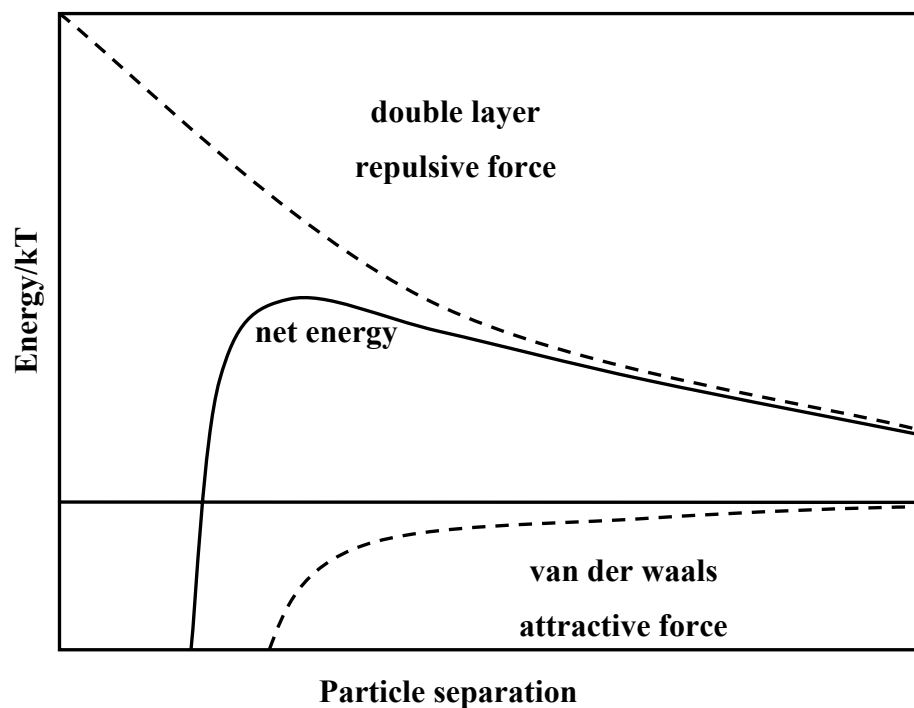
Figure 1.7 Schematic diagram of the variation of free energy with particle separation at high salt concentration showing the possibility of a secondary minimum.

Particle separation
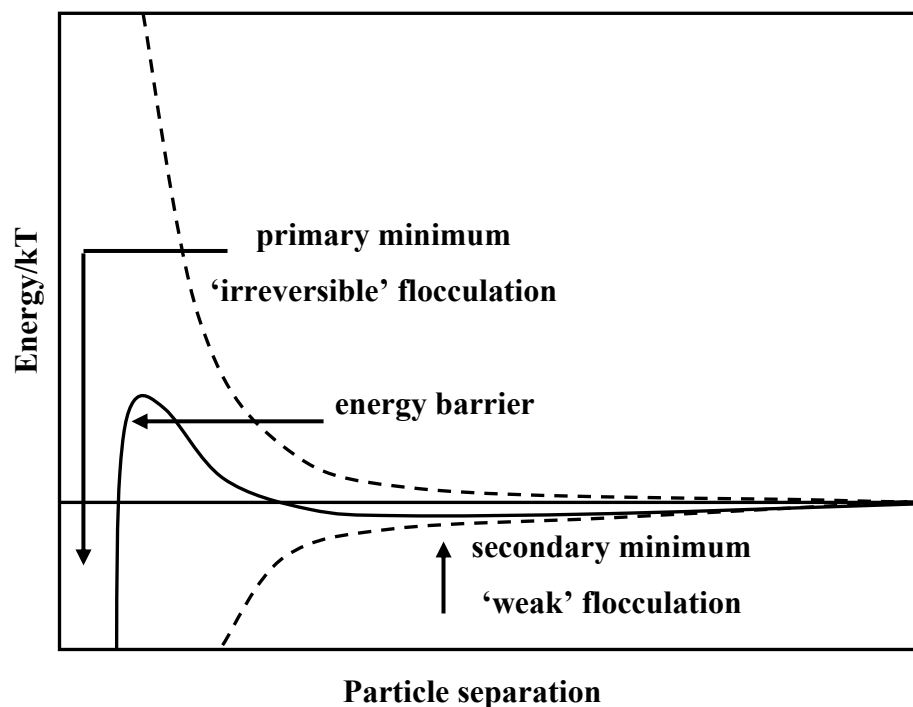
In certain situations (*e.g.* at high salt concentration), there is a possibility of a secondary minimum where a much weaker and potentially reversible adhesion between particles exists together (Figure 1.7). These weak flocs are sufficiently stable not to be broken up by Brownian motion, but may dissociate under an externally applied force such as vigorous agitation. Therefore to maintain the stability of the colloidal system, the repulsive forces must be dominant. In many cases we can alter the environment to either increase or decrease the energy barrier, depending upon our goals. Various methods can be used to achieve this, such as changing the ionic environment, pH or adding surface-active materials to directly affect the charge of the colloid. In each case, zeta potential measurements can indicate the impact of the alteration on overall stability.

The stabilisation of colloidal particles against aggregation can be typically achieved via two main mechanisms.[1] Firstly, by varying the charge at the particle surface, which is known as electrostatic or charge stabilisation. Secondly, by modifying the particle surface by attaching polymer chains increasing the repulsion between particles, known as steric stabilisation (Figure 1.8). In addition, there is a third mechanism, known as electrosteric stabilisation. It is based on the combination of both charge and steric repulsion; this is achieved by attaching polymer groups with ionisable functional groups on the particle surface.

Figure 1.8 Steric and electrostatic stabilisation mechanisms of colloidal dispersions.

steric stabilisation   electrostatic stabilisation
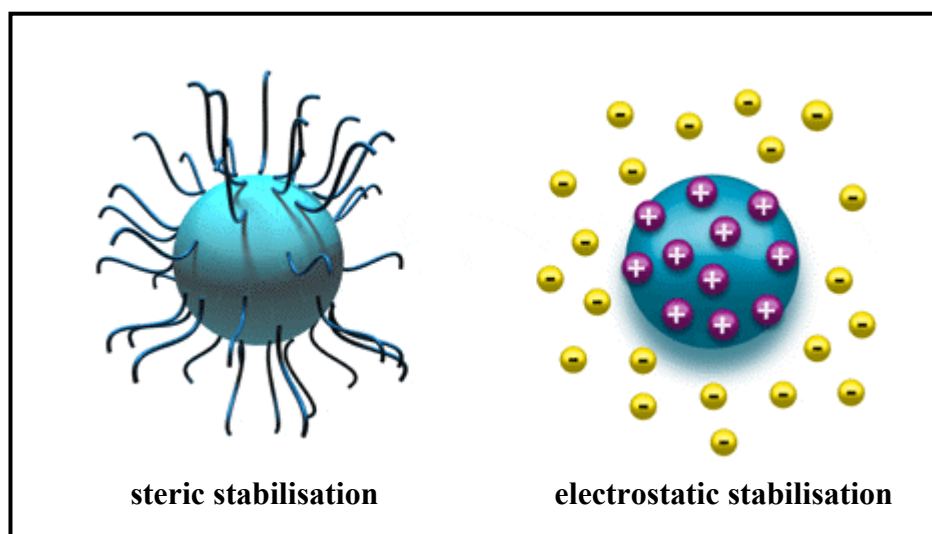
1.3   Adsorption of colloidal particles at air-water surfaces

Colloidal particles, similar to surfactant molecules, can spontaneously accumulate at the interface between two immiscible fluids (liquid-gas or liquid-liquid); they are therefore surface-active.[15] This fact was realised in the beginning of the last century by Ramsden[16] and Pickering.[17] However, unlike surfactant molecules, most colloidal particles, although surface active , are not amphiphilic. The exceptions are the so–called Janus particles, in which two separated regions of different wettability exist on the surface of a given particle. Such particles are both surface-active and amphiphilic.[18] The particles used in this work are not amphiphilic, they are homogeneous. In contrast to surfactant molecules, adsorption of solid particles to fluid/liquid interfaces does not change the interfacial tension.[19] A key parameter that affects adsorption appears to be the contact angle, θ, (measured through water), that particles exhibit at the interface. The angle θ increases with the hydrophobicity of the particle. If θ is large enough, particles prefer to stay in air rather than in water (Figure 1.9). However, if adsorbed, they are strongly held at the fluid interface. This can be explained by the energy of attachment of a solid particle at the air-water interface.

12

Figure 1.9   Position of a small spherical solid particle at a planar air-water interface for a contact angle (measured through the aqueous phase) less than 90° (left) and greater than 90 ° (right).
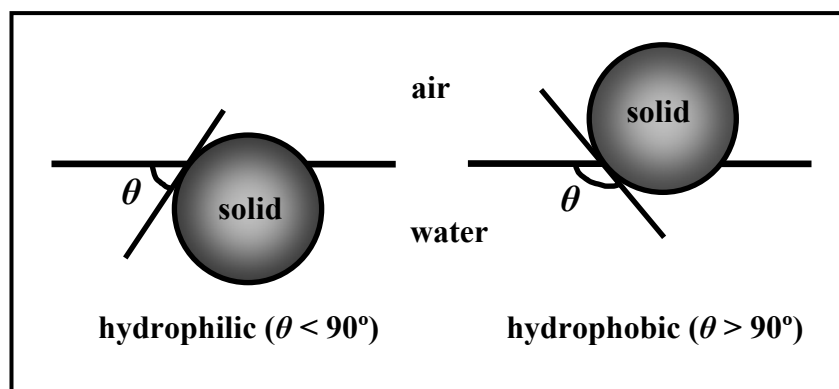
The energy of attachment of a solid particle at the air-water interface is related not only to the contact angle, but also to the tension of the interface γ_{aw} and the particle radius, r (see ref. 20 and references therein). The energy E required to remove the particle from the interface can be simplified to:

$$E = \pi r^2 \gamma \left(1 \pm \cos\theta\right)^2 \qquad (1.5)$$

The sign within the bracket in the latter equation becomes negative for the removal of the particle from the interface into the water phase and positive for removal into the air phase. The influence of contact angle of an adsorbed particle on the energy of attachment at the air-water interface is shown in Figure 1.10. According to equation 1.5 for given r = 10 nm and γ_{aw} = 36 mN m^{-1}, particles are most strongly adsorbed at the interface when θ = 90° with E being ~ 2750 kT as shown in Figure 1.10. The energy of attachment falls rapidly on either side of 90° such that for θ between 0 and 20° or between 160 and 180°, the energy is relatively small (< 10 kT). Therefore, particles with very low or high contact angles are easily removed from the interface resulting in rapid destabilisation of foams. One consequence of the very high energy of attachment of particles to interfaces is that particles once at interfaces are practically irreversibly adsorbed. This is in contrast to surfactant molecules that adsorb and desorb reversibly. Since E depends on the square of the particle radius, the energy of attachment is reduced markedly for smaller and smaller particles (< 1 nm radius) of the size comparable to most surfactant molecules and thus they may not be too effective as foam stabilisers.[18]

Figure 1.10 Variation of energy of attachment, E, of a spherical silica particle of radius r = 10 nm at the planar air - water interface of interfacial tension γ_{aw} = 36 mN m^{-1} with the contact angle θ the particle makes with the interface at 298 K.
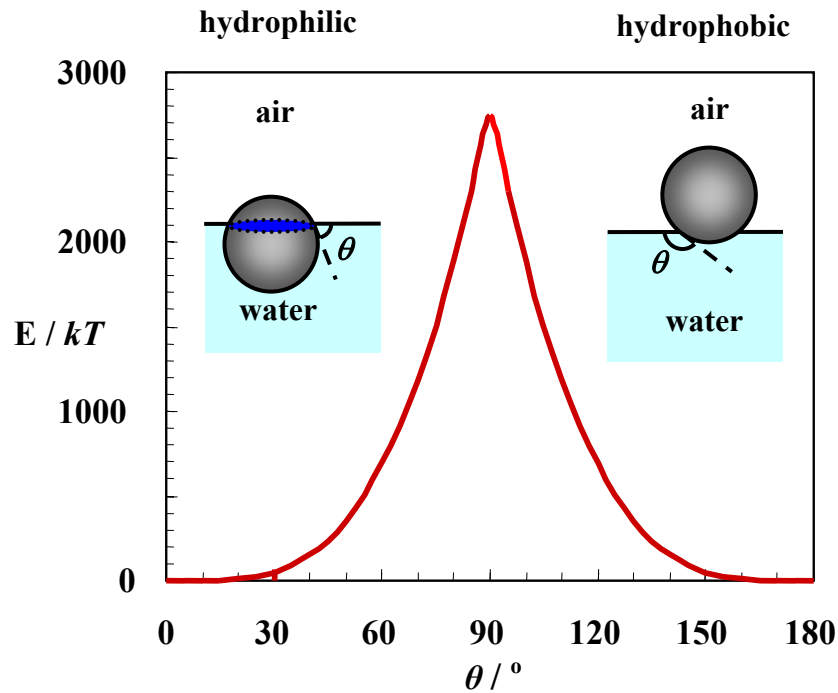
1.4 An introduction to foams

Technologies which are impacted by foams and foaming are widespread. Some well known liquid foams are bubble baths, detergents, shaving foam and the foam head on a glass of beer, as shown in Figure 1.11. Gas bubbles can also give a desirable texture to a diverse range of food products such as ice cream, whipped toppings, bread and cakes. However, due to their complex nature, the material properties of many food foams remain insufficiently understood. Also industrial processes which bring gases and liquids together often form foams. These foams, however, may be unwanted as they can block flow or damage pumps. The petroleum and chemical processing industries are therefore interested in destroying foams. Certain chemical additives can accomplish this. Subsequent sections will provide some general information on the formation, structure and stability of foams in industry and every day life.

Figure 1.11 Examples of foams found in everyday life.

Bath foam

Beer head foam

Ice – cream

Shaving foam

1.4.1   Foam formation and structure

Foams are colloidal dispersions in which the dispersed phase is gas bubbles in a liquid (or solid) continuous phase. This system is thermodynamically unstable, but could be kinetically stable in the presence of surfactants, proteins or particles. The most important physical characteristic of the liquid phase in the foam is surface tension. The surface tension of pure water is 72 mN m^{-1} at 25°C, a value too high for foaming to occur, which explains why pure liquids do not foam. The surface tension needs to be reduced for foaming to occur (*e.g.* by adding surfactants to the water). The most common expansion gas used in aqueous foam systems is compressed air, an insoluble gas. Soluble expansion gas systems are also possible (*e.g.* carbon dioxide).

Liquid foams can be made by: [21]

- mixing or agitation; examples are draught beer, whipped cream and sea foam,
- evolution of dissolved gas; for example canned beer, soft drinks, shaving foam and hair mousse, and
- bubbling gas through liquid.

Depending on the process used when generating the foam, the geometrical shape of the gas bubbles will change as observed in Figure 1.12. The simplest way to form a nearly monodisperse foam is to introduce gas slowly into the liquid through a capillary tube. In that way individual bubbles of (almost) equal size will break off from the capillary tip under the action of surface tension. A much more rapid but less controllable procedure is to bubble gas into the system through a porous plug. In this process a polydisperse foam will result since many small bubbles will coalesce. Even less consistent results will be obtained in foams produced by agitation.

Figure 1.12 Two-dimensional foams produced by various processes (taken from ref. 21).

| Blowing gas | Blowing gas (turbulent flow) | Sparging |
| Blending | Shaking | Nucleation of gas |
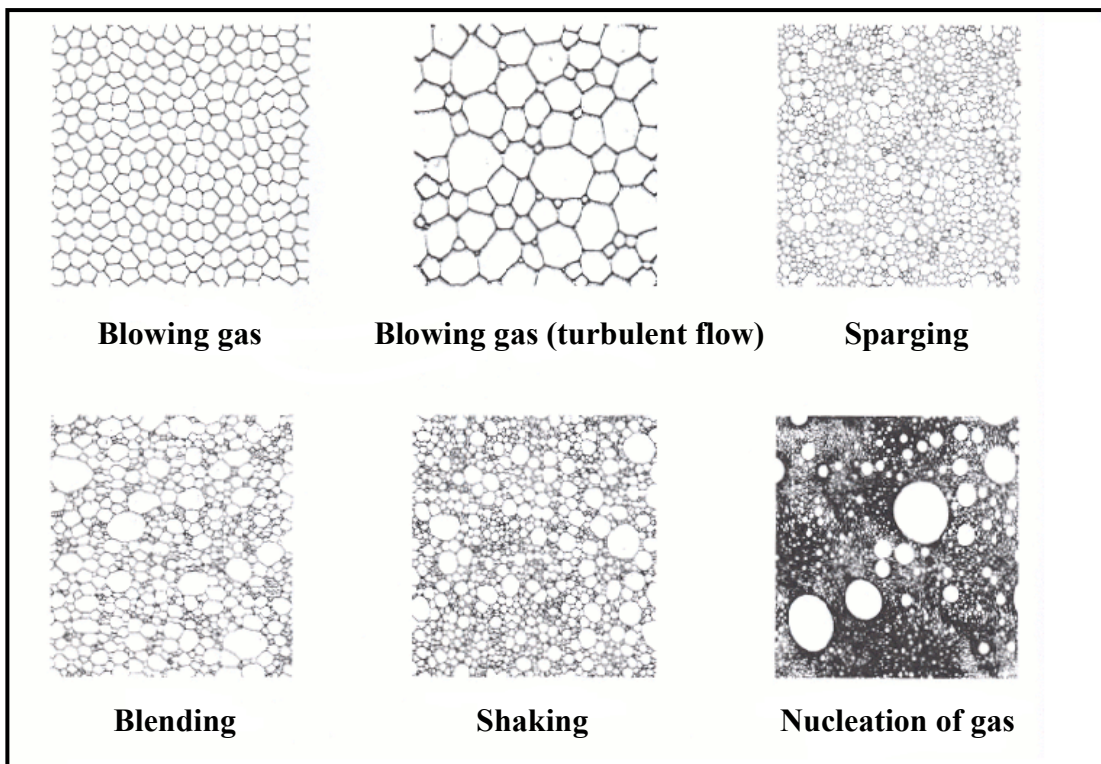
In aqueous surfactant foams, towards the lower part or near the solution of the foam, bubbles are spherical of small size and are called *kugelschaum.* At the upper part of the foam, bubbles are deformed into polyhedral shapes separated by continuous thin liquid films with larger size because of the liquid drainage and are called *polyederschaum*. The polyhedral foams have a larger gas volume fraction, and therefore lower density (Figure 1.13).

Figure 1.13   Typical foam structure formed with surfactant systems.
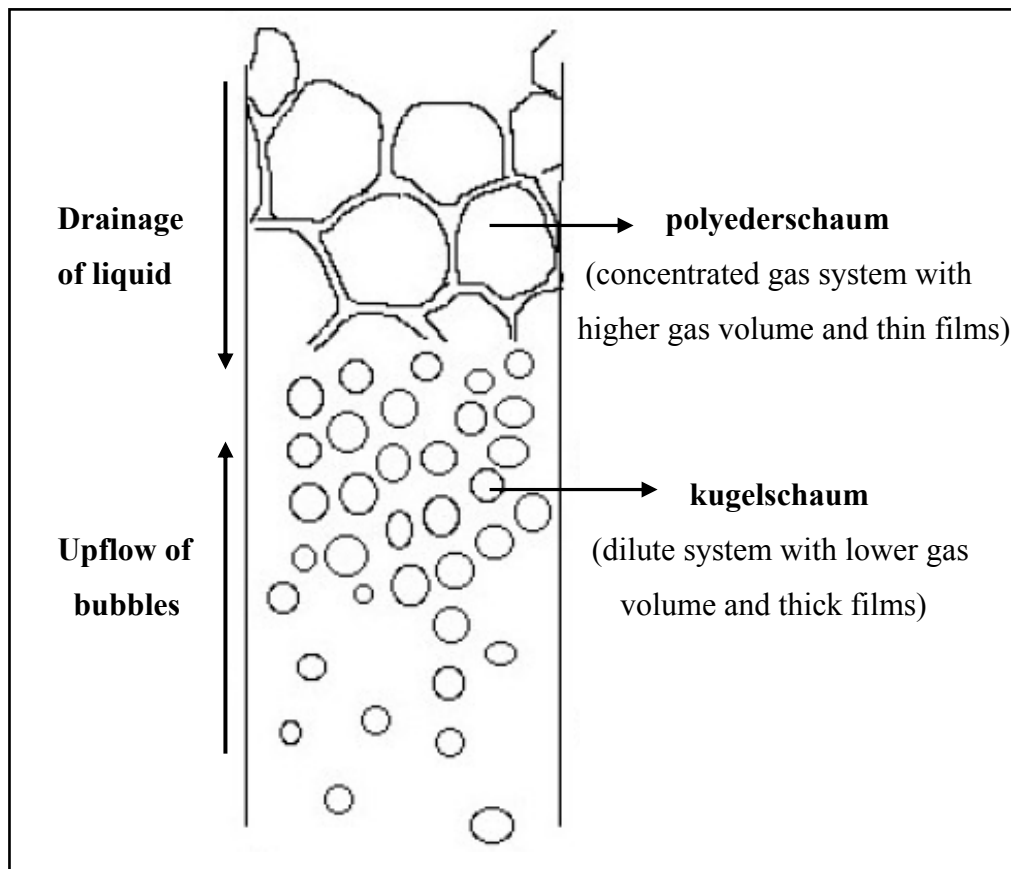
When bubbles are formed or created in a surfactant solution, adsorption of the surfactant starts at their surface. Surfactant adsorption at bubble surfaces occurs because the hydrophobic part of the surfactant molecule is oriented away from the liquid, while the hydrophilic part remains in the liquid (as shown in Figure 1.14). As a result of this the surface tension of the liquid is reduced which eases foam generation (surfaces are more easily stretched). Adsorbed surfactants dissociate causing repulsion necessary to overcome van der Waals attraction and hence stabilise the foam.

17

Figure 1.14   The representation of adsorption of surfactants at bubble surfaces.
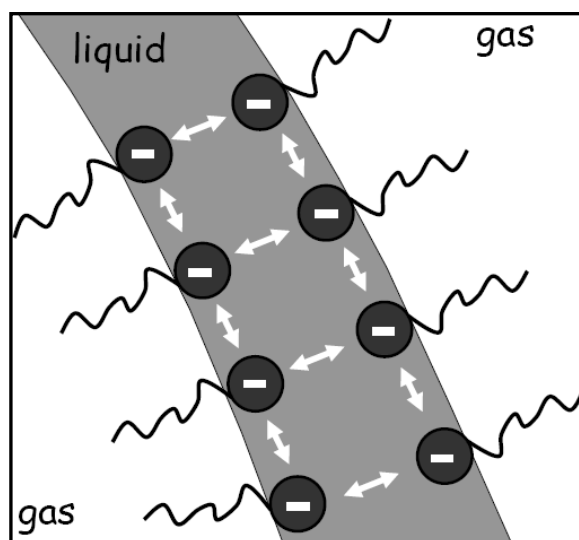
Foam structures can be very complicated. Another example is ice cream, which is essentially a foam consisting of air bubbles dispersed in a mixture of fat, water and ice crystals.[22] The air fraction is typically around 50% by volume, and this is crucial for the product to have the consistency and texture desired by customers. The air bubbles have to be smaller than 0.1 mm otherwise the ice-cream loses the 'creamy' texture. Between the bubbles is a watery phase, with small ice crystals. Also, in order to have a stable ice cream, sufficient fat globules have to be present to form a network enclosing the air cells. These milk fat globules are in turn stabilised by the protein called casein. Most ice creams also have an edible surfactant or emulsifier added. Finally there can be an open matrix formed by polymers like gelatine. This helps to thicken the aqueous phase and therefore improve the foam stability in the ice cream. Various steps in the manufacturing process, including pasteurisation, homogenisation, ageing, freezing, and hardening contribute to the development of this structure. An example of ice cream structure is shown in Figures 1.15 and 1.16.

The foaming ability of a solution is a property characterising each particular foaming system. This property can be expressed quantitatively by the volume of foam (or the foam column height), obtained under certain conditions, such as pH, foaming method, temperature, etc. from a definite volume of the foaming solution.

Figure 1.15 The structure representation and typical composition of an ice cream.
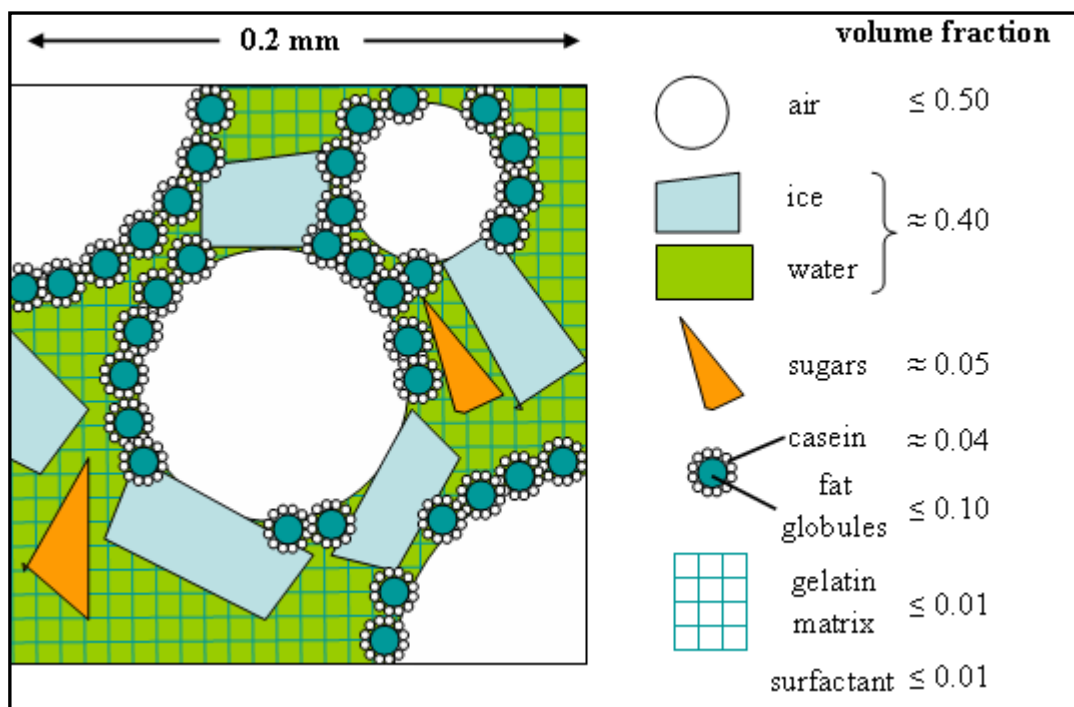
Figure 1.16 (a) Cryo-scanning electron micrograph of the structure of ice cream and (b) the close-up structure of air bubbles in ice cream provided by Unilever, Colworth Science Park.

(a)
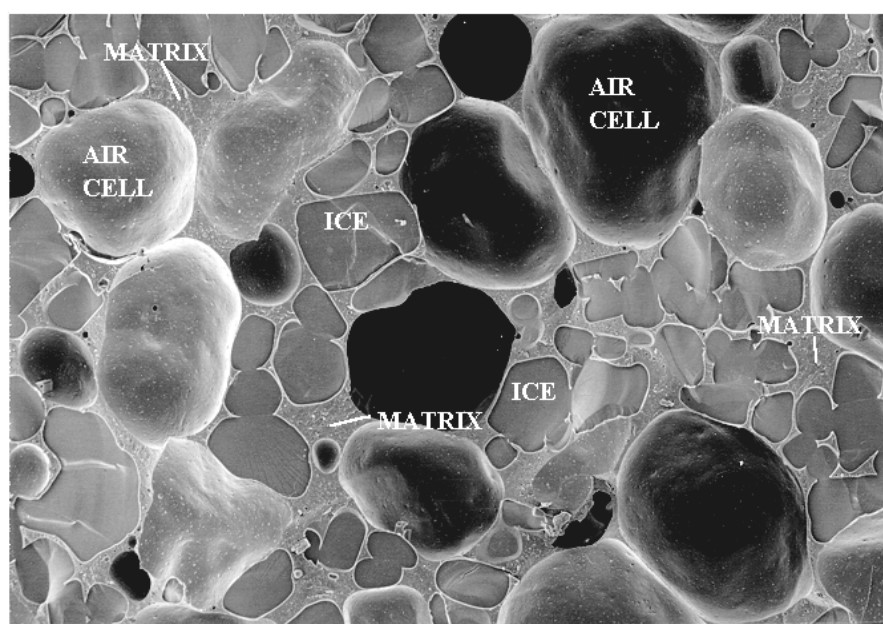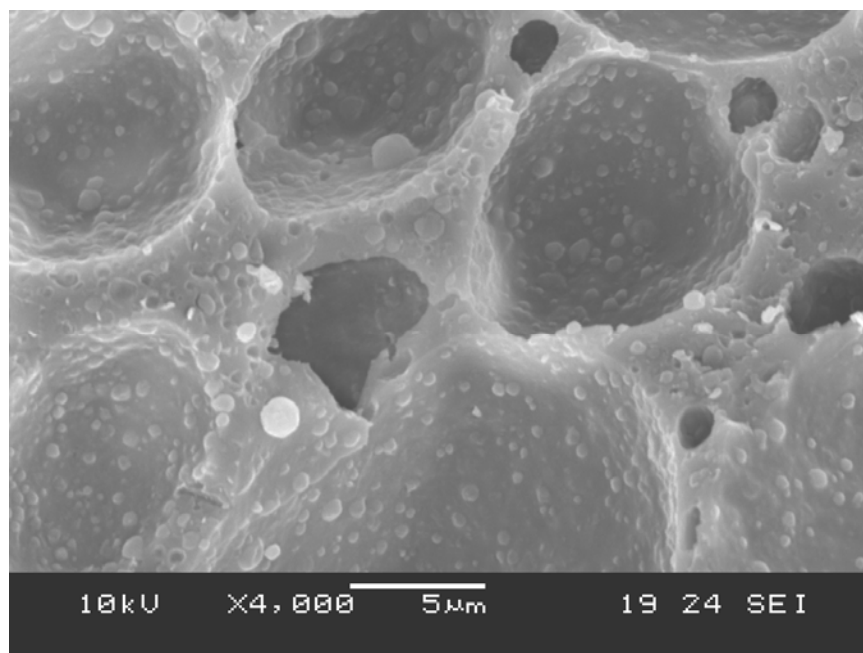
1.4.2   Foam stability

Immediately after foam formation, a close approach between the gas bubbles occurs. Foam stability is directly related to the properties of foam films separating the gas bubbles. The stability of foams depends on many factors including the surface tension of the liquid, the type of foaming agents, the viscosity of the film separating the bubbles, the physical properties of the film, the addition of electrolytes (the double-layer effect), the size of the bubbles, the gas used in the foam and the temperature. Some distinction can be made between *unstable* and *metastable* foam structures. *Unstable* or *transient* foams (e.g. champagne bubbles) are classified by those formed from aqueous solutions of short-chain fatty acids and alcohols, whose lifetime is measured in seconds (or minutes). *Metastable* foams (e.g. meringue) are classified by those formed from solutions of soaps, synthetic detergents, proteins, particles, etc. whose lifetime is measured in days. In the absence of disturbance influences (such as vibration, draughts, evaporation, diffusion of gas from small bubbles to large bubbles, heat, temperature gradients, dust and other impurities) these foams would persist almost indefinitely.[23]

The stability of aqueous foams is governed by various processes, the most important being: (i) rearrangement of the films between bubbles (film thinning), (ii)

liquid drainage due to gravity, (iii) disproportionation - gas diffusion from smaller bubbles through the liquid films to bigger bubbles (the net result of this process is that the average bubble size grows with time), (iv) rupture of films, the latter causing coalescence of neighbouring bubbles.[24]

When three or more gas bubbles meet, the liquid films are curved, forming what has become known as a Plateau border, which is shown within the magnified region of Figure 1.17. As drainage progresses, films at the top of the foam will be thinner than those lower down in the foam. The arrangements of films coming together at equal angles of 120° results from the equalization of the surface tension vectors, or contracting forces, along the liquid films.[25] Drainage continues until a metastable equilibrium is reached or until the film ruptures spontaneously at a critical film thickness. Disproportionation will occur if the dispersed gas is soluble in the continuous phase (*i.e.* soft drinks where the solubility of CO_2 is 50 times greater than N_2). Throughout the foam, neighbouring bubbles will be of different size and disproportionation is driven by the higher Laplace pressure present in smaller bubbles.

Figure 1.17   Illustration of a generalised foam system showing aspects of a liquid foam film (taken from reference 25).
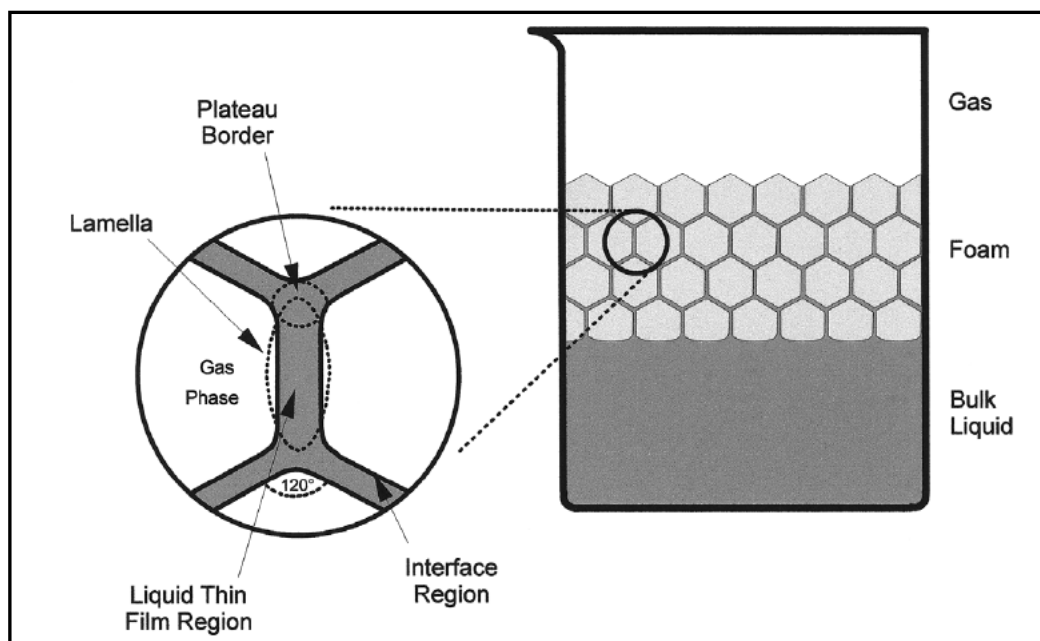
For example, the air phase in an ice cream is unstable due to temperature fluctuations. Disproportionation of bubbles occurs, and the structure of ice cream ends up with fewer and larger bubbles[26] (Figure 1.18).

21

Figure 1.18 Cryo-scanning electron micrograph of the structure of air bubbles in a freshly made ice cream (a) and after temperature fluctuations (b); provided by Unilever, Colworth Science Park.

(a)
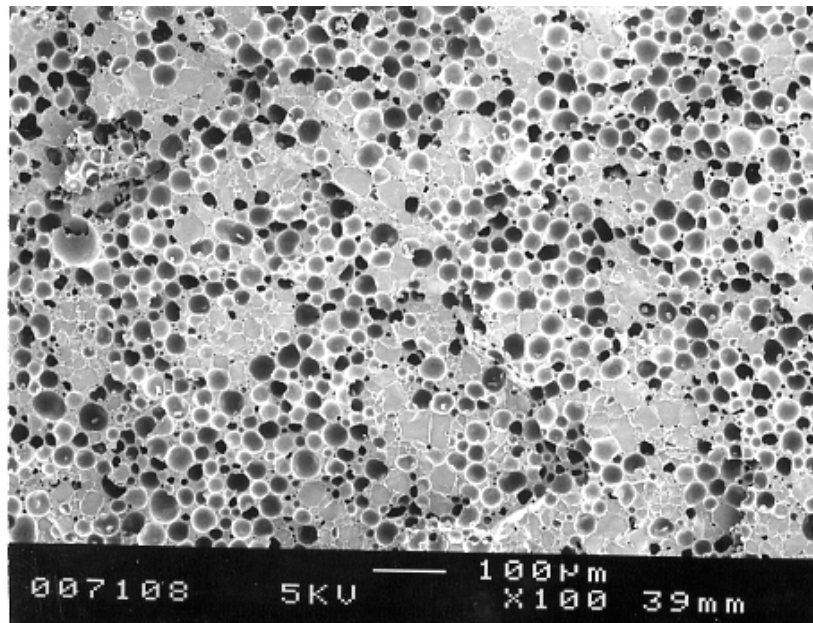
(b)
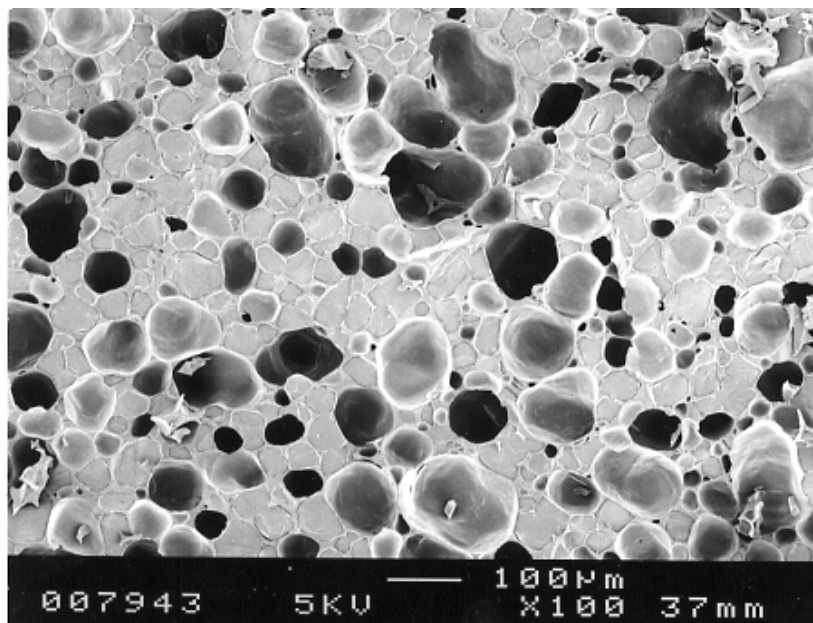
Laplace's law of capillary pressure states that at a gas-liquid interface, the pressure difference between two phases is:

$$p_1 - p_2 = \gamma \left(\frac{1}{R_1} \right) + \left(\frac{1}{R_2} \right) \qquad (1.6)$$

where γ is the surface tension of the liquid and R_1 and R_2 are the radii of curvature of the interface. Due to Laplace's law, the pressure in the Plateau border is lower than the pressure in the flat films, which causes a flow of liquid out of the film, hence thinning it.[23,24]

For a foam to be stable the pressure within the thin liquid films that separates the gas bubbles must be equal to the pressure at the Plateau border (also known as capillary pressure) so that there is no film drainage. This is achieved via a repulsive force within the liquid film known as disjoining pressure (Π). The relationship between Π and $\mathit{\Delta P}$ ($p_1 - p_2$) can be expressed as:

$$p_1 - p_2 = \left(\frac{\sigma}{r_p} \right) - \Pi \qquad (1.7)$$

where r_p is the radius of curvature of the Plateau border. When the disjoining pressure is positive (repulsive), it opposes film thinning. On the other hand, when it is negative (attractive), it increases the driving force (ΔP) and accelerates film thinning.[23,24]

The thickness of foam films and their rate of thinning are of great importance for foam stability and the lifetime of foams. Therefore, any factor that prevents film rupture or slows down the rate of liquid drainage will increase the stability of the foam. Thus stability can be enhanced by controlling certain parameters, such as film elasticity, surface shear viscosity and electrostatic repulsive forces between films. The common understanding of foam stability usually refers to the ability of a foam to maintain its main parameters constant with time, *i.e.* bubble size, liquid content (expansion ratio) and total foam volume. Foam lifetime is therefore the most often used and the simplest measure of foam stability.

Small solid particles can also adsorb at the air – water interface (see Figure 1.19) and therefore they may behave in a similar way to surfactants. Particle adsorption reduces the total surface energy at the air-water surface, therefore contributing to the

stability of the foam. One of the advantages of using solid particles rather than conventional surfactants in the formation of foams is due to the improved bubble stability towards coalescence, disproportionation and liquid drainage and as a result more robust reproducible formulations can be produced.

Figure 1.19   Representation of solid particle adsorption at a bubble surface.

solid particles, *e.g.* silica, latex
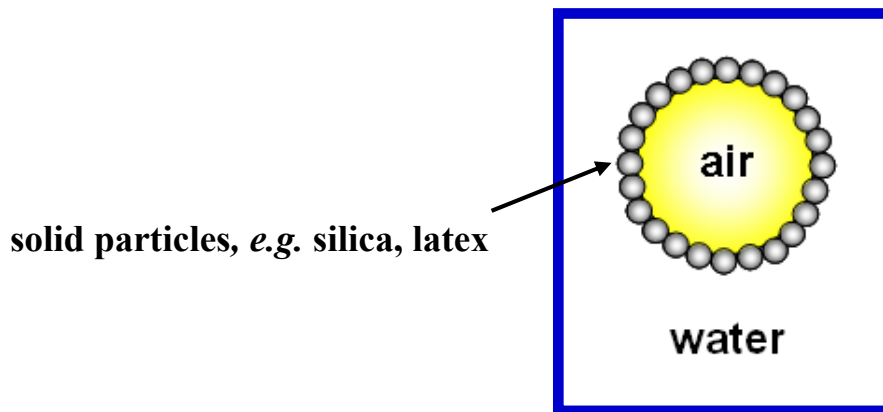
Foam stabilisation by solid particles will depend on several parameters, including the nature of the particles, their size, shape, concentration, hydrophobicity, surface charge, state of aggregation, surface area, density, etc. Several mechanisms are involved in this stabilisation, such as cohesive interactions, disjoining pressure, drainage of thin films and structural inter-particle interactions. Figure 1.20 shows the mechanism of foam film stabilisation by solid particles. The foam films are relatively thick and therefore foams can be very stable against disproportionation. A more detailed explanation on foams and foam films stabilised by solid particles is given in the next section.

Figure 1.20   Representation of a foam film stabilised by solid particles (taken from reference 27).

1.5 Foams and foam films stabilised by solid particles

Stable foams seem to rely on the presence of surfactants, which are able to separate the neighbouring liquid-gas interfaces with a relatively stable liquid film in between. The earlier studies therefore have focused on the foaming and foam stability mechanism of simple aqueous surfactant solutions.[21,23,24] Solid particles have been incorporated into surfactant-stabilised aqueous foams for many years, and their influence on the formation and stability of the foam is very dependent on the surfactant type, particle size and concentration.[28,29] On the other hand, oil and particles were added into the foam systems with the development of antifoams.[30-32] If particles are hydrophilic, foam stability is enhanced since particles collect in the Plateau borders slowing down film drainage. However, hydrophobic particles can enter the air-water surfaces of the foam and cause destabilisation via the bridging – dewetting or bridging – stretching mechanism. This is thought to be the mode of action of particles (frequently in the presence of oil drops) contained within traditional antifoam formulations. It is worth pointing out that some of the principles involved in the use of particles in antifoams and in the process of froth flotation are similar. A study by Ip *et al.*[33] describes the effect of particle concentration, size and hydrophobicity on the stability of both aqueous and molten aluminium foams, both in the presence of surfactant. For the aqueous system utilising silica particles (> 45 μm), they found that only particles of the correct wettability (varied by adsorption of cationic surfactant) could stabilise the foam, and foam stability increased with decreasing particle size and increased concentration. Partially wetted particles were shown to accumulate at bubble surfaces, providing a barrier preventing rupture and coalescence. Therefore, the ability of the particles to stabilise bubbles and emulsion droplets was recognised a long time ago, but the potential and ability of particles to act as foam stabilisers in the absence of any other surface – active material has only been a subject of considerable attention recently.[15,18,34,35] Remarkable progress in this field was achieved within the last three years and important aspects of solid-stabilised foams have been reported very recently. A review of the literature concerned with bulk foams, bubbles and aqueous films stabilised by solid particles is given here.

Colloidal particles act in many ways like surfactant molecules, particularly if adsorbed to a fluid-fluid interface. As the water or oil-liking tendency of a surfactant is quantified in terms of the hydrophile-liphophile balance (HLB) number, a spherical particle can be described in terms of its wettability via contact angle. However,

important differences exist between the two materials, due in part to the fact that particles are strongly held at interfaces.[15]

Work by Wilson[36] was aimed at determining the important factors involved in the formation of particle-stabilised aqueous foams. The thesis described the conditions necessary to achieve foam stabilisation using relatively large charged latex particles of diameter 3.88 μm. Addition of salt, lowering of pH or addition of cationic surfactant to aqueous dispersions all lead to an increase in foam stability and an increase in contact angle (θ). Their results indicated that θ approaches 90° for systems that display high foamability and stability. Foaming was also linked to particle coagulation in bulk. The combination of particles of low charge and of relatively high hydrophobicity seems an essential requirement for making it energetically favourable for them to be situated at the air-water surface compared with bulk.

It is well known that solid particles can stabilise aqueous foams under dynamic conditions of continuous bubble generation and their role in froth flotation of minerals[37,38] or boiling suspensions[39-43] has been extensively investigated. However, the dynamic foams are very unstable and rapidly collapse once the bubbling is terminated. Some of these works are worth considering in more detail.

Bindal et al.[39] studied short living foams stabilised by sludge particles alone in the absence of surface-active agents. They found that foaminess has a maximum with increasing particle concentration and this maximum was a net result of two counter-effects: structure stabilisation and depletion destabilization, which arose due to particle-particle interactions in the foam lamellae. The stability of curved foam films containing small monodisperse particles alone in the absence of surfactant has been investigated.[40] Spherical, hydrophilic silica particles of diameter between 8 and 39 nm dispersed in pure water are shown to stabilise thin films by a layering mechanism within the film since none of the particles adsorb to the film surfaces. The number of stepwise transitions increases with the volume fraction of particles within the film. Eventually a black spot appears indicative of a part of the film containing no particles. The rate of film thinning was found to be high when the particle concentration was low and when both the particle size and film diameter were large. The foamability of a system (foaminess) by aerating a suspension of nanosized hydrophilic silica particles in the absence of surfactant has also been studied by Bindal et al.[41] in which the effects of particle size, particle concentration and bidispersity on foaming were examined. The studies discovered that the foaminess is directly proportional to particle concentration and inversely proportional to particle size. More importantly bidispersity in particle size

drastically reduced foaminess. However, the foam generated with this study had negligible stability. As soon as the aeration was stopped, the foam collapsed.

Mileva and Nikolov[44] studied the collective efficiency of particles by bubbles. They found that there is a range of particle and bubble dimensions for which entrapment is optimal. Mata and Joseph[45] studied the foam control by particles and found that hydrophobic particles suppress foam and break foam better than hydrophilic particles. And most recently, particles alone have been shown to be effective in stabilising metal foams, *i.e.* air bubbles in molten metal.[46]

Paunov *et al.*[47] pointed out that an energy barrier exists between charged particles in bulk water and the charged air-water surface which must be surmounted if particles are to adsorb. The height of this barrier can be reduced by addition of salt or by changing the pH, such that when the kinetic energy of the particles exceeds the barrier height, they adsorb to the surface and become trapped. This has also been demonstrated clearly by Wan and Tokunaga[48] for sub-micron-sized clay particles (by tuning pH) and by Hu *et al.*[49] for silver nanoparticles (by adding KCl).

In addition to coalescence, the other major mechanism by which foams collapse is disproportionation, in which gas diffuses from smaller to larger bubbles due to the higher Laplace pressure within the former. Although theory suggests that films around bubbles with high mechanical rigidity should be able to prevent this and bubble shrinkage, experimental measurements reveal that even the most viscoelastic protein films cannot halt disproportionation. However, one of the most striking findings in the ultrastable particle-stabilised foams is that bubbles do not change their size for a very long time. This does not happen in foams stabilised by surfactants or proteins, in which coarsening of the bubbles occurs with time as gas diffuses from smaller to larger bubbles.[34] As a result larger bubbles grow at the expense of smaller ones which shrink and eventually disappear. Based on this, stabilisation of bubbles against shrinking by solid particles has been investigated both theoretically and experimentally.

Kam and Rossen[50] analysed a two-dimensional theoretical model for solids-coated or armoured bubbles by showing how the armour can support a liquid-vapor interface of reduced or reversed curvature between the particles, giving the bubble zero or even negative capillary pressure. The inward capillary force pulling the particles into the center of the bubble is balanced by large contact forces between the particles in the armour. Thus the bubble is stabilised against dissolution of gas into the surrounding liquid, which otherwise would rapidly collapse the bubble. The stresses between particles in such cases are large and could drive sintering of the particles into a rigid

framework. Earlier work on solids-coated bubbles assumed that solids can freely enter or leave the bubble surface as the bubble shrinks or expands. In such a case, armoured bubbles would not be stable to gas dissolution. This analysis[50] however, suggests that particle ejection from the stressed armour is energetically unfavourable and argued that particles may sinter into a rigid shell, thus making the bubble shrinking impossible. These predictions are supported by the results from recent experiments with single bubbles under a planar air-water surface.[51-53] Du *et al.*[51] showed that solid particles associated with high adsorption energies could generate a sufficiently rigid shell to prevent bubble shrinkage using fumed silica nanoparticles which were partially hydrophobic (40% residual SiOH). Various methods were employed to generate air bubbles in an aqueous particle dispersion beneath a planar air-water surface, including direct injection of bubbles and a sudden reduction of pressure within the cell containing the dispersion causing bubble nucleation. Although some large bubbles (radius 250 μm) were unstable to disproportionation, smaller bubbles (radius 50-100 μm) were completely stable to shrinking over a period of several days. Bubbles of intermediate size shrank to a certain extent and then remained stable subsequently. This is in contrast to bubbles stabilised by either gelatin or ß – lactoglobulin proteins which shrank rapidly and disappeared completely in 1-2 hours. They found that particles form a dense layer around the bubbles, contributing to their stability. Dickinson *et al.*[52] also demonstrated that stable bubbles could be formed from an aqueous dispersion of fumed silica nanoparticles of lower hydrophobicity (67% and 80% SiOH), by adding salt (*i.e.* NaCl) to the water. The bubble stability was found to increase with increasing particle concentration and increasing salt concentration. In addition, formation of a weak gel with a finite yield stress was observed in some suspensions at high salt concentration.[52,53] Therefore, both the dense particle layer around the bubbles and gel formation in bulk are believed to contribute to the bubbles stability against shrinking. A recent quantitative study[54] of the coarsening of foams stabilised by partially hydrophobic silica nanoparticles has been able to correlate the interfacial properties and the macroscopic evolution of the foam. This study has shed some light on the origin of the remarkable stability of aqueous foams stabilised by nanoparticles. Such particle-stabilised foams appear to be the only known foam system where coarsening is inhibited by surface elasticity. A threshold in particle concentration could also be observed, both in the microscopic and macrosopic behaviour. Below full bubble coverage, coarsening was not avoided and the particle-containing foam was unstable behaving as surfactant foam.

Only very recently has it been demonstrated that solid particles alone[55-58] or with appropriate surfactant[59,60] are able to stabilise aqueous foams to an extent that they survive for weeks or more. These recent studies are described here in more detail. A review of the mechanisms of foam film stabilisation by solid particles and their role in the film stability is also given here.

Alargova et al.[55] have demonstrated that particles with non-spherical shape can act as an effective foam stabiliser in the absence of any additives. They used polymeric microrod particles with an average length of 23.5 μm and an average diameter of 0.6 μm and produced 'superfoams' that could be stable almost indefinitely. The likely reason for the super-stabilisation is that the epoxy microrod particles were partially hydrophobic and readily adsorb on the interface of the foam bubbles. Their contact angle at the air-water surface measured through the water was $\theta \sim 80°$. It was found that fairly dilute microrod suspensions (0.2-2.2 wt.%) in pure water readily produce foams upon shaking. The foams were stable for more than 3 weeks even under drying in an open vessel or under harsher conditions such as fast drying and expansion in a vacuum. Microscopic examination revealed that the bubbles were covered with dense hairy shells of entangled microrods. The bubbles were fairly spherical in shape and small (10-100 μm). The films were rather thick (~1-2 μm) and very stable which was attributed to the mechanical rigidity of the continuous net of overlapping and entangled microrods at film surfaces. They also found that these stable foams can be destroyed by addition of SDS (sodium dodecyl sulphate) solution, with SDS thus acting as a defoamer and suppressing the stabilising effect of the particles. The authors concluded that the likely cause of this destabilising action is due to adsorption of surfactant monomer on the particle surfaces rendering them more hydrophilic and thus causing them to lose their affinity to air-water surfaces.

Very stable aqueous foams have also been obtained by means of spherical nanoparticles. Binks and Horozov[56] used near spherical fumed silica nanoparticles of primary diameter approximately 30 nm hydrophobised to different extents to investigate the effect of particle hydrophobicity on foam stability in the absence of any surfactant. Foams were prepared either by shaking by hand the system of powdered particles resting on water (3 w/v%) or by aerating an aqueous dispersion of particles (0.86 w/v%) using an Ultra - Turrax homogeniser. Stable foams were obtained by both methods (either with or without 8.5 mM NaCl in the water) when particles with intermediate hydrophobicity were used. Therefore, they showed a maximum in the foaming ability with respect to the hydrophobicity of particles. The foams were wet (containing about

60 % water even after several days) and very stable to collapse. Similar to the foams stabilised by microrod particles[55], a slow decrease in their volume was detected during the first 24 hours as a result of water drainage and bubble compaction, but not of gas loss. Optical microscope images revealed that the foam contained micron-sized non-spherical bubbles (5-50 μm) surrounded by branched particle aggregates.

Preparation of stable foams from latex suspensions in the absence of any additives has been reported recently by Fujii *et al.*[57,58] In contrast to previous studies[34] they used sterically-stabilised latex particles, therefore additional additives (electrolyte or surfactant) were not needed to induce foaming. A series of sterically and charge-stabilised polystyrene latexes of diameters in the range 0.2-1.6 μm were synthesised by dispersion or emulsion polymerisation. Foams were prepared from purified aqueous suspensions (1-10 wt.%) either by shaking by hand or by bubbling nitrogen through the suspensions. The most stable foams were those obtained at the largest concentration of particles with biggest size. They were stable to drying with little or no change in volume. They also identified highly ordered particulate bilayers in the dry foam by means of SEM and optical microscopy, thus supporting the previous finding[34] that the films between the bubbles in the wet foam are composed of a bilayer of particles separated by water.

The above findings demonstrate that aqueous suspensions of certain solid particles with inherent hydrophobicity are able to make extremely stable foams in the absence of any surfactant. Particle size, shape, concentration and hydrophobicity have been identified as the main factors for foam stabilisation.

An *in-situ* hydrophobisation of initially hydrophilic particles can be accomplished through the adsorption of appropriate amphiphiles on the particle surface. This approach is widely used in froth flotation[37,38] but its potential and versatility for the preparation of stable aqueous foams stabilised by inorganic particles was demonstrated only recently. Gonzenbach *et al.*[59,60] applied short-chain amphiphiles (carboxylic acids, alkyl gallates and alkyl amines) to concentrated suspensions (15-45 vol.%) of different inorganic particles such as silica, alumina, calcium phosphate, etc. and produced high-volume foams by mechanical frothing of the suspensions. The foams containing air contents between 45% and 90% and average bubble sizes between 20 and 80 μm were completely stable against drainage, coalescence and disproportionation. This remarkable foam stability was attributed to the strong attachment of particles at the air-water interface and the formation of an attractive particle network at the interface and throughout the foam lamella. They also demonstrated that the microstructure of these

foams can be tailored in a wide range by adjusting the composition of the initial colloidal suspension[60] and can also be useful for various applications including the fabrication of macroporous ceramics.[61]

It has been shown from previous studies mentioned above, that the behaviour of solid particles in foaming systems is very dependent on the particle hydrophobicity. Partially hydrophobic particles with contact angle, θ, close to 90° can act as a foam stabiliser, whereas hydrophobic particles ($\theta > 90°$) act in the opposite way and are used as antifoams, usually in combination with oily additives. However, very hydrophobic particles were found to stabilise water droplets in air[62] which makes them very resistant against coalescence. Therefore, a free-flowing powder material containing up to 95% water could be prepared.[63] Binks and Murakami[64] have also shown recently that the inversion of particle-stabilised aqueous foams into water-in-air powder (dry water), and vice versa, can be achieved in a single system comprised of air, water, and fumed silica nanoparticles of diameter approx. 20-30 nm hydrophobised to different extents. The inversion of the air-water-particle system was achieved either by a progressive change in silica particle hydrophobicity at constant air-water ratio or by changing the air-water ratio at fixed particle wettability. The phase inversion resembles that observed with particle-stabilised emulsions[15] and therefore, demonstrates the similarity in the particle behaviour in emulsion and foam systems.

Further progress in understanding the stabilisation of bubbles by solid particles has been made recently due to work of Stone's group in Harvard.[65-70] A microfluidic method that allows direct visualisation and understanding of the dynamics and delivery of colloidal particles to curved interfaces (surface of bubbles or drops) has been reported.[65] The particles were periodically ejected to form stable jammed shells, which they refer to as colloidal armour, without the aid of any additives (electrolyte or surfactant). Armoured bubbles covered with 4 μm polystyrene latex particles have been used to investigate their stability to shrinking.[68] It is shown that isolated bubbles covered with jammed particle shells take on non-spherical shapes as they become stable against gas dissolution. The non-spherical bubble remains stable, keeping its volume and shape for at least 2 days. It is also shown with this work that when surfactant is added to the water the non-spherical bubbles become unstable and progressively shrink by ejecting particles into the water. However, the key finding here is that the particle shell around the stable bubble is stressed. Very recent numerical simulations confirm that these bubbles evolve to form faceted polyhedral or crumpled shapes that are stable to dissolution in air-saturated water.[70] This is accompanied by a simultaneous decrease of

the surface energy and Laplace pressure until a local energy minimum is reached. The repulsive interactions between particles cause a reduction of the curvature of the gas-liquid interface, which is the mechanism that arrests dissolution and stabilises the bubbles. The same stabilising mechanism could operate in the ultrastable particle-stabilised foams reported recently.

Since many cosmetics (emulsions) or food related foams contain a mixture of both surfactant and particles, it is of interest to study foams stabilised by such mixtures. Despite some activity in this area, systematic studies of the behaviour and properties of foams in mixtures of surfactant and solid particles are lacking. Therefore, a detailed investigation into the behaviour of air-in-water foams stabilised by a mixture of hydrophilic silica particles and CTAB cationic surfactant at different pH values has been made during this research and the results are shown in Chapter 8. Another similar and very recent study[71] investigated the behaviour of a mixture of Ludox HS-30 silica nanoparticles and a di-chain cationic surfactant, *i.e.* di-decyldimethylammonium bromide (di-C_{10}DMAB) at high pH. Both these studies found that in mixtures the synergism between the foaming agents leads to enhanced foam stability at intermediate surfactant concentration. It was also shown that surfactant addition initially transforms particles from anionic to uncharged and hydrophobic and subsequently to cationic as a result of adsorption. The most hydrophobic particles, possessing an adsorbed monolayer of surfactant, yield foams which are completely stable to disproportionation and coalescence. This is in agreement with the results obtained recently by another study,[72] where aqueous foams were prepared with CTAB surfactant and disk-like Laponite particle dispersions. It was shown from this study that clay/CTAB dispersions have a synergistic effect on foam stability at intermediate CTAB concentrations. The most stable foams were obtained by particles with maximum hydrophobicity ($\theta < 90°$).

The link between the stability of aqueous foams and that of isolated foam films stabilised by surfactant or protein has been extensively investigated.[23,73] Much less is known about foam films stabilised solely by solid particles in the absence of surface–active molecules. Two distinct cases regarding the mechanism of film stabilisation by solid particles are considered: (i) the particles are present only inside the film but not at its surfaces and (ii) some of the particles are firmLy attached to the air-water interfaces (see ref. 35 and references therein). In the first case, solid particles at high concentrations can form a layered structure inside the thinning film, thus stabilising it by the so called oscillatory structural force. This mechanism of film stabilisation has been extensively studied and covered in recent reviews.[15,34] The second case of foam

films with particles at their surfaces in the absence of surfactant is considered only in a few recent experimental studies dealing with microrod particles[55] and complex particulate systems stimulating radioactive waste slurries.[42,43]

Recently, Horozov et al.[74] reported a systematic study on vertical emulsion films with 3 μm silica particle monolayers at their surfaces in the absence of any surfactant. This experimental work clearly demonstrates the behaviour of solid particles in liquid films and the mechanisms of stabilisation by a bridging monolayer or a bilayer of particles attached to the film surfaces. The stabilising mechanisms identified in aqueous emulsion films could be relevant to aqueous foam films. Ordered monolayers of bridging particles in foam films in the absence of surfactant were also observed previously.[75] Similar film stabilisation by a bridging monolayer or a bilayer of close-packed particles was also observed in the work presented here in Chapter 5. This suggests that the behaviour of solid particles in aqueous emulsions and foam films could be rather similar. Recent studies[76-78] explains the liquid film stability by solid particles theoretically, assuming either a bridging monolayer or a bilayer of hexagonally close-packed particles. Detailed equations explaining how particles can stabilise liquid films have been reported in those studies, assuming that interfacial forces are primarily responsible for the stability of such liquid films. They predicted through those equations that the optimum value of the contact angle that a particle exhibits at an air-water surface, being able to stabilise liquid foams, has a unique value, but is in the interval between 50 and 90°.[77] Another mechanism of foam film stabilisation by a network of particle aggregates (gel) inside the film has also been discussed[78]. It occurs when the excess particles in the bulk aqueous phase are flocculated and form a three-dimensional network (gel). This seems to be the most effective mechanism of stabilisation due to the particle network keeping the bubbles well separated, thus preventing coalescence of bubbles and drainage. This explains the high stability of particle-stabilised foams and bubbles recently reported in refs: 52, 56, 57, 59 and 60.

1.6   Aims of the present study and structure of the thesis

The overall aim of this project was concerned with understanding the properties of foams and foam films stabilised by solid particles alone with mechanisms for their control. The preparation and characterisation of foams stabilised solely by solid particles were investigated in order to be used as a replacement for surfactant/protein-stabilised foams in many industrial formulations.

Chapter 2 details all of the experimental techniques used during this study. The results of the present work are grouped into 6 main sections. The initial approach of this research was to make foams with initially hydrophilic silica particles of diameter 100 nm by engineering conditions and changing *in situ* their hydrophobicity. This is described in Chapter 3. In contrast to the 100 nm hydrophilic silica particle systems, the hydrophobicity of silica particles of larger diameter, *i.e.* 600 nm, has been modified *ex-situ* by silanisation with DCDMS (dichlorodimethylsilane) and further studies on the foaming ability and stability of these modified silica particles are reported in Chapter 4.

Vertical foam films with silica particle monolayers at their surfaces have been studied by direct microscope observations and by using a Scheludko type cell. This work was carried out in order to gain a better understanding of the mechanisms of foam stabilisation by solid particles. Therefore, the effects of particle wettability and surface coverage on the structure and stability of foam films in water have been investigated and are described in Chapter 5. In Chapter 6 isolated thin liquid foam films were investigated and a novel method for determining the contact angle of small solid particles with interfaces was developed. The search for new particles of different size and shape, chemistry and hydrophobicity is very important in this project. This is the main reason for studying the foamability and foam stability of dispersions of Laponite RD particles as these are of different shape and chemistry to those of silica particles and are of interest for comparison. This study is described in Chapter 7.

Chapter 8 looks at the effect that silica particles have on the foaming properties of cationic surfactant when they are used in combination. Finally, a summary of conclusions and suggestions for future work are presented in Chapter 9. An appendix with experimental data is also given at the end of the thesis

References

1. I.D. Morrison and S. Ross, Colloidal Dispersions: Suspensions, Emulsions and Foams, Wiley-Interscience, New York (2002).

2. D. Myers, Surfaces, Interfaces and Colloids: Principles and Applications, 2nd Ed., Wiley-VCH, New York (1999).

3. Y. Moroi, Micelles: Theoretical and Applied Aspects, Plenum Press, New York (1992).

4. J.H. Clint, Surfactant Aggregation, Blackie, London (1992).

5. M.J. Rosen, Surfactants and Interfacial Phenomena, 2nd Ed., Wiley- Interscience, New York (1989).

6. K. Tsujii, Surface Activity: Principles, Phenomena and Applications, Academic Press, London (1998).

7. R. Atkin, V.S.J. Craig, E.J. Wanless and S. Biggs, *Adv. Colloid Interface Sci.*, **103**, 219 (2003).

8. H.G. Tompkins, A Users Guide to Ellipsometry, Academic Press, London (1993).

9. D.J. Shaw, Introduction to Colloid and Surface Chemistry, 4th Ed., Butterworth Heinemann Ltd, Oxford, Chapter 10 (1992).

10. R.J. Hunter, Introduction to Modern Colloid Science, Oxford Science Publications, New York, Chapter 3 (1993).

11. D.H. Evertett, Basic Principles of Colloid Science, Royal Society of Chemistry, London, Chapter 6 (1988).

12. J.Th.G. Overbeek in *Colloid Science,* H.R. Kruyt (Ed.), Vol. 1, Elsevier, Amsterdam, p. 245 (1952).

13. Malvern Instruments Theory, PCS Training Manual, Part 1: The measurement of zeta potential using electrophoresis (1998).

14. R.A.L. Jones, Soft Condensed Matter, Oxford University Press, New York (2002).

15. B.P. Binks, *Curr. Opin. Colloid Interface Sci.*, **7**, 21 (2002).

16. W. Ramsden, *Proc. Roy. Soc.*, **72**, 156 (1903).

17. S.U. Pickering, *J. Chem. Soc*., **91**, 2001 (1907).

18. B.P. Binks and T.S. Horozov, Colloidal Particles at Liquid Interfaces, Cambridge University Press, Cambridge, Chapter 1 (2006).

19. E.Vignati, R. Piazza and T.P. Lockhart, *Langmuir*, 19, 6650 (2003).

20. R. Aveyard, B.P. Binks and J.H. Clint, *Adv. Colloid Interface Sci.*, **100**, 503 (2003).

21. D. Weaire and S. Hutzler, The Physics of Foams, Oxford University Press, Oxford (1999).

22. E. Dickinson, An Introduction to Food Colloids, Oxford University Press, Oxford, Chapter 5 (1992).

23. D. Exerowa and P.M. Kruglyakov, Foams and Foam Films: Theory, Experiment, Application, Elsevier, Amsterdam (1998).

24. R.K. Prud'homme and S.A. Khan., Foams: theory, measurements and applications, Marcel Dekker, New York (1996).

25. L.L. Schramm, Emulsions, Foams and Suspensions: Fundamental and Applications, Wiley VCH, Verlag GmbH, Chapter 1, p.7 (2005).

26. H.D. Goff, *Curr. Opin. Colloid Interface Sci.*, **7**, 423 (2002).

27. N. Denkov, Online Presentation entitled Foam Films: Properties and Stability, http://www.maths.tcd.ie/~foams/PRESENTATIONS/Thursday12/Thursday12_Lecture2_Nikolai.pdf.

28. F. Tang., Z. Xiao, J. Tang and L. Jiang, *J. Colloid Interface Sci*., **133**, 498 (1988).

29. J.B.N. Hudales and H.N. Stein, *J. Colloid Interface Sci*., **140**, 307 (1990).

30. R.J. Pugh, *Adv. Colloid Interface Sci.*, **64**, 67, (1996).

31. N.D. Denkov, *Langmuir*, **20**, 9463, (2004).

32. N.D. Denkov and K.G. Marinova in *Colloidal Particles at Liquid Interfaces*, B.P. Binks and T.S. Horozov (eds), 1st Ed., Cambridge University Press, Cambrige, p. 383 (2006).

33. S.W. Ip, Y. Wang and M. Toguri, *Can. Metall. Quart.* **38**, 81 (1999).

34. B.S. Murray and R. Ettelaie, *Curr. Opin. Colloid Interface Sci.*, **9**, 314 (2004).

35. T.S. Horozov, *Current Opinion in Colloid & Interface Sci.,* **13**, 134, (2008).

36. J.C. Wilson, A study of particulate foams, Ph.D. thesis, *University of Bristol* (1980).

37. A.V. Nguyen and H-J. Schulze, Colloidal Science of Flotation, Surfactant Science Series, Vol.118, Marcel Dekker, New York (2004).

38. R.J. Pugh, *Adv. Colloid Interface Sci.*, **114**, 239 (2005).

39. S.K. Bindal, A.D. Nikolov, D.T. Wasan, D.P. Lambert and D.C. Koopman, *Env. Sci. Technol.*, **35**, 3941 (2001).

40. G.N. Sethumadhavan, A.D. Nikolov, and D.T. Wasan, *J. Colloid Interface Sci.*, **240,** 105 (2001).

41. S.K. Bindal, G. Sethumadhavan, A.D. Nikolov and D.T. Wasan , *AIChE J*, **48**, 2307 (2002).

42. D.T. Wasan, A.D. Nikolov and A. Shah, *Ind. Eng. Chem. Res.*, **43**, 3812 (2004).

43. K. Vijayaraghavan and A.D. Nikolov, *Adv. Colloid Interface Sci.*, **123**, 49 (2006).

44. E.N. Mileva and L. Nikolov, *J. Colloid Interface Sci.*, **265**, 310 (2003).

45. C. Mata and D.D. Joseph, *Int. J. Multiphase flow*, **25**, 63 (1999).

46. Th. Wübben and S. Odenbach, *Colloids Surf. A*, **266**, 207 (2005).

47. V.N. Paunov, B.P. Binks and N.P. Ashby, *Langmuir*, **18**, 6946 (2002).

48. J. Wan and T.K. Tokunaga, *J. Colloid Interface Sci.*, **247**, 54 (2002).

49. J-.W. Hu, G.-B. Han, B. Ren, S.-G. Sun and Z.-Q. Tian, *Langmuir*, **20**, 8831 (2004).

50. S.I . Kam and W.R. Rossen, *J. Colloid Interface Sci.*, **213**, 329, (1999).

51. Z. Du., M.P. Bilbao-Montoya, B.P. Binks, E. Dickinson, R. Ettelaie and B.S. Murray, *Langmuir* , **19**, 3106 (2003).

52. E. Dickinson, R. Ettelaie, T. Kostakis and B.S. Murray, *Langmuir*, **20**, 8517 (2004).

53. T. Kostakis, R. Ettelaie and B.S. Murray, *Langmuir*, **22**, 1273 (2006).

54. A.C. Martinez, E. Rio, G. Delon, A. Saint-Jalmes, D. Langevin and B.P. Binks, *Soft Matter*, **4**, 1531 (2008).

55. R.G. Alargova, D.S. Warhadpande, V.N. Paunov and O.D. Velev, *Langmuir*, **20**, 10371 (2004).

56. B.P. Binks and T.S. Horozov, *Angew. Chem. Int. Ed.*, **44**, 3722 (2005).

57. S. Fujii, A.J. Ryan and S.P. Armes, *J. Am. Chem. Soc.*, **128**, 7882 (2006).

58. S. Fujii, P.D. Iddon, A.J. Ryan and S.P. Armes, *Langmuir*, **22,** 7512, (2006).

59. U.T. Gonzenbach, A.R. Stuart, E. Tervoort and L.J. Gauckler, *Ange.w Chem. Int.*, **45**, 3526 (2006).

60. U.T. Gonzenbach, A.R. Stuart, E. Tervoort and L.J. Gauckler, *Langmuir*, **23**, 1025 (2007).

61. U.T. Gonzenbach, A.R. Stuart, E. Tervoort and L.J. Gauckler, *J. Am. Ceram. Soc.*, **89**, 1771 (2006).

62. P. Aussillous and D. Quéré, *Nature*, **411**, 924 (2001).

63. S. Hasenzahl, A. Gray, E. Walzer and A. Braunagel, *SOFW-J*, **131**, 4 (2005).

64. B.P. Binks and R. Murakami, *Nat. Mater.*, **5**, 865 (2006).

65. A.B. Subramaniam, M. Abkarian and H.A Stone, *Nat. Mater.*, **4**, 553 (2005).

66. A.B. Subramaniam, M. Abkarian, L. Mahadevan and H.A Stone, *Nature*, **438,** 930 (2005).

67. R.S. Subramaniam, R.J. Larsen and H.A Stone, *Langmuir*, **21**, 4526 (2005).

68. A.B. Subramaniam, C. Mejan, M. Abkarian and H.A Stone, *Langmuir*, **22**, 5986 (2006).

69. A.B. Subramaniam, M. Abkarian, L. Mahadevan, H.A Stone, *Langmuir*, **22**, 10204 (2006).

70. M. Abkarian, A.B. Subramaniam, S. Kim, R.J. Larsen, S. Yang, H.A Stone, *Phys. Rev. Lett.*, **99**, 188301 (2007).

71. B. P. Binks, M. Kirkland and J. A. Rodrigues, *Soft Matter*, **4**, 2373 (2008)

72. Z. Shuiyan, L. Qiang, L. Qian, X. Jian and S. Dejan, *Colloids Surf. A,* **317**, 406 (2008).

73. D. Platikanov and G. Yampolskaya, *Adv. Colloid Interface Sci.*, **128**, 159 (2006).

74. T.S. Horozov, R. Aveyard, J.H. Clint and B. Neumann, *Langmuir*, **21**, 2330 (2005).

75. K.P Velikov, F. Durst and O.D. Velev, *Langmuir*, **14**, 1148 (1998).

76. P.M. Kruglyakov and A.V. Nushtaeva, *Colloid J.*, **65**, 341 (2003).

77. G. Kaptay, *Colloids Surf. A*, **230**, 67 (2004).

78. G. Kaptay, *Colloids Surf. A*, **282**, 387 (2006).

CHAPTER 2

CHAPTER 2

EXPERIMENTAL

This chapter contains a detailed description of the materials used along with a comprehensive review of all experimental methods.

2.1   Materials

2.1.1   Water

Water was purified by passing through an Elgastat Prima reverse osmosis unit followed by a Millipore Milli-Q reagent water system. The surface tension of this water was periodically checked and found to be 71.9 ± 0.2 mN m^{-1} at 25 °C, which is in excellent agreement with the literature value[1], thus indicating that the water was free from surface active impurities. The resistivity of the water used was always around 18 mΩ cm.

2.1.2   Silica particles

2.1.2.1 Precipitated hydrophilic silica in water

Eleven dispersions of precipitated hydrophilic silica in water at alkaline pH were obtained from Eka Chemicals (Sweden) with average particle diameters ranging from 3.5 nm to 110 nm. These sub-microscopic particles consist of pure amorphous silicon dioxide and are negatively charged. There are several different methods to produce an aqueous colloidal silica.[2] At present, the ion-exchange method is the most common and used technique for manufacturing silica sols. The silica sol manufacturing method using ion-exchange is shown in Figure 2.1.

Figure 2.1 The production process using the ion-exchange method for manufacturing silica sols. This diagram has been re-drawn from ref. 2.

40
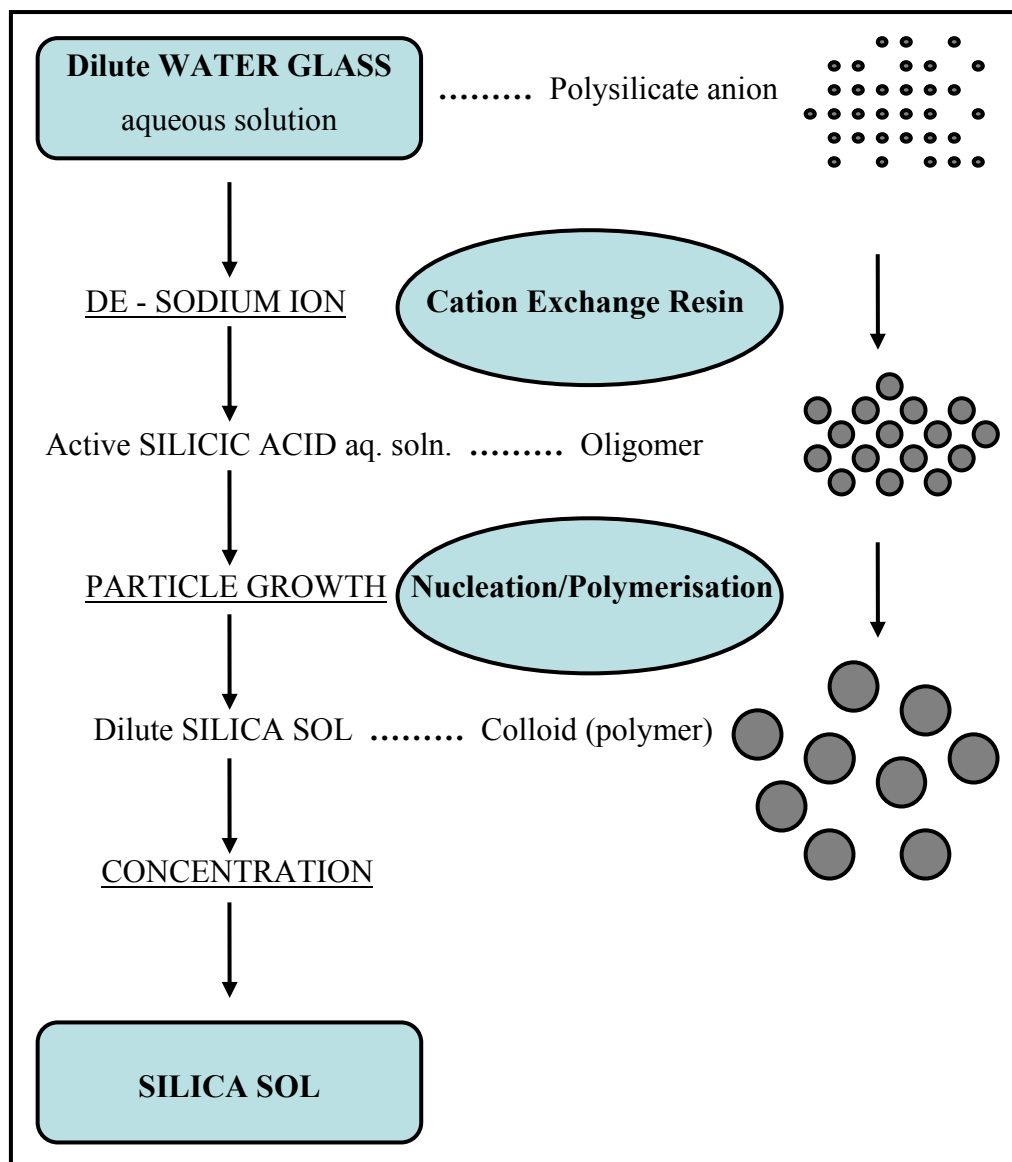
The production of silica sol initiates with a dilute aqueous water-glass solution, where the silica takes the form of polysilicate anion. This solution is passed through a bed of cation-exchange resin in a column for which hydrogen ions have been regenerated in advance to allow the sodium ions to be adsorbed onto the resin bed and leave an aqueous solution of active silicic acid. This liquid is a microscopic colloidal solution with a pH of 2-4 containing 2-6 % SiO_2 comprising particles with a diameter of 2 nm or less. The colloidal solution is also in an unstable state and easily gels upon standing. Nucleation, polymerisation and particle growth are performed on this active silicic acid in the presence of alkali at a temperature of at least 60 °C, a pH of 8-10.5, and a molar ratio of SiO_2:Na_2O of about 20-500, and thus a dilute silica sol is formed. The formed dilute silica sol generally consists of spherical particles having a diameter of 4-100 nm, a pH of 8-10.5 and a SiO_2 content of 2-6 %. This silica sol is a colloidal liquid in a stable state, and therefore it causes no gelling. As illustrated in Figure 2.2, the dilute aqueous water-glass solution is in an ionic state (polysilicate anion). In contrast to this, the active silicic acid is in the form of an oligomer, that is, a colloid of microscopic particles, and finally the dilute silica sol is a polymer in the colloidal state. Next, this dilute silica sol is concentrated so that the SiO_2 content is increased to 15-60 %. Finished products are obtained after the concentration, pH and conductivity of the concentrated sol are adjusted to maintain their stability.[2]

In Table 2.1, the nominal and measured (by evaporation) concentrations of the silica particles in the dispersion, density and pH of the dispersions used are listed together with a code for each silica grade quoted by Eka Chemicals. The primary sizes of some of these hydrophilic silica particles were also measured by transmission electron microscopy TEM (some results were taken from ref. 3) and light scattering (determined in this work). These properties are given in Table 2.2, together with the nominal primary particles diameter quoted by Eka Chemicals. Figure 2.2 is a TEM image of a carbon-coated Cu-Pd grid with hydrophilic silica particles deposited by evaporation from a solution containing dispersed silica particles of grade NYACOL 9950. It can be seen from the figure that the primary particles are fairly monodisperse with a diameter around 100 nm but a few smaller particles are present (~ 20 nm in diameter). This is in agreement with the diameter quoted by the manufacturer.

Table 2.1   Properties of the silica dispersions obtained from Eka Chemicals.

Grade	Solids / wt. %	Solids [a] / wt. %	pH	dispersion density / g cm^{-3}
Eka NP 090	10	11.7 ± 0.1	-	1.07
BINDZIL 15/500	15	-	10	1.1
BINDZIL 30/360	30	-	10	1.2
BINDZIL 40/220	40	42.6 ± 0.1	9.7	1.3
BINDZIL 30/220	30	32.0 ± 0.5	9.7	1.2
BINDZIL 40/130	40	43.0 ± 0.1	9.0	1.3
BINDZIL 50/80	50	53.0 ± 1.0	9.3	1.4
NYACOL 9950	50	54.0 ± 1.0	9.0	1.4
Exptl Lot: 1	50.6	50.4 ± 0.1	9.0	-
Exptl Lot: 2	20.7	31.5 ± 0.5	9.3	-
Exptl Lot: 3	9.3	11.1 ± 0.1	9.9	-

[a] Determined in this work.

Table 2.2   Sizes of hydrophilic silica particles from TEM, light scattering and nominal primary diameter.

Grade	TEM primary diameter / nm	Light scattering mean diameter / nm	Nominal primary diameter / nm
Eka NP 090	-	-	3.5
BINDZIL 15/500	~ 5	-	6
BINDZIL 30/360	~ 6	-	9
BINDZIL 40/220	15 ± 3	-	15
BINDZIL 30/220	15 ± 2	-	15
BINDZIL 40/130	25 ± 5	-	25
BINDZIL 50/80	25 ± 10	-	40
NYACOL 9950	20 - 90	87	100
Exptl Lot: 1	106 - 112	109	170
Exptl Lot: 2	63 - 68	68	35
Exptl Lot: 3	68 - 75	75	43

Figure 2.2   Transmission electron micrograph of hydrophilic silica particles of diameter approximately 100 nm.

100 nm
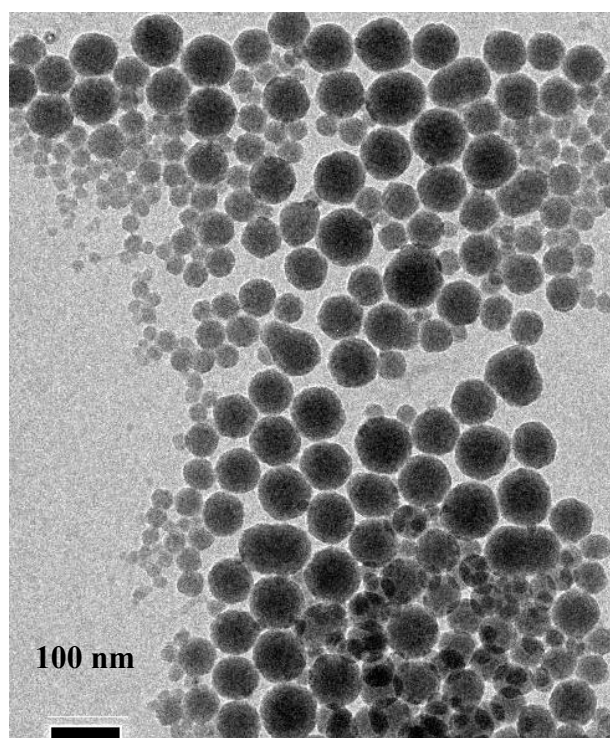
2.1.2.2 Synthetic amorphous silica particles

Eight samples of synthetic amorphous monodisperse silica particles with diameters ranging from 50 nm to 2000 nm and a density of $\sim$ 2.2 g/cm^3 were purchased from the Blue Helix Company (UK). These particles are hydrophilic in nature because of the presence of silanol groups on their surface.[4] Monodisperse spherical silica nanoparticles that range in size from 5 – 2000 nm can be prepared by the Stöber synthesis.[5] Many studies have been published on understanding the mechanisms of formation and growth that yield such stable and monodisperse particles.[6,7] The Stöber route consists of a simple procedure from tetraalkoxysilanes (*e.g.* tetraethoxysilane, TEOS) in alcoholic solutions. In general, the hydrolysis reaction,

$$Si(OC_2H_5)_4 + H_2O \xrightarrow{\ OH^-\ } (OC_2H_5)_3 \, Si(OH) + C_2H_5OH \qquad (2.1)$$

produces the single-hydrolysed TEOS monomer [$(OC_2H_5)_3 \, Si(OH)$]. Subsequently, this intermediate reaction product condenses to eventually form silica,

$$(C_2H_5O_3)Si(OH) + H_2O \xrightarrow{\hspace{3cm}} SiO_2 \downarrow + \ 3 \ C_2H_5OH \qquad (2.2)$$
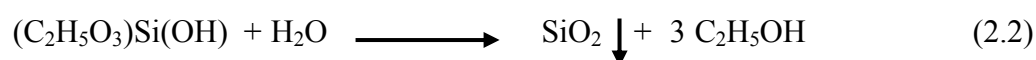
This reaction scheme is a simplification of the condensation process that leads to the formation of silica particles.

The particle size distribution was determined using scanning electron microscopy, SEM and dynamic light scattering using the Malvern Zetasizer 3000 HS. These properties are given in Table 2.3, together with the nominal primary particle diameter quoted by the producer. Figure 2.3 shows the SEM images of the various silica particles. The size distribution obtained from the SEM images and light scattering are in very good agreement with each other.

Table 2.3 Sizes of hydrophilic silica particles (Blue Helix) obtained from SEM and dynamic light scattering with their nominal primary diameter.

Grade	SEM primary diameter / nm	Light scattering mean diameter / nm	Nominal primary diameter / nm
SIO2P005-01	170 ± 10^a 70 ± 20^b	167 ± 6	50
SIO2P010-01	162 ± 10^a	160 ± 3	100
SIO2P020-01	258 ± 5	259 ± 3	200
SIO2P040-01	434 ± 20	433 ± 10	400
SIO2P060-01	547 ± 20	560 ± 5	600
SIO2P080-01	900 ± 50^b 750 ± 20^c	950 ± 10	800
SIO2P100-01	1150 ± 55^b 940 ± 10^c	1205 ± 9	1000
SIO2P200-01	2110 ± 45^b 1860 ± 20^c	2100 ± 34	2000

[a] Majority of small aggregates were observed (~160-170 nm)

[b] When joined particles were observed

[c] When discrete (non-joined) particles were observed

Figure 2.3 SEM images of silica particles of diameter: (a) 50 nm, (b) 100 nm, (c) 200 nm, (d) 400 nm, (e) 600 nm, (f) 800 nm, (g)1000 nm and (h) 2000 nm.

(a)

(b)

(c)

(d)

(e)

47

(f)

(g)

(h)
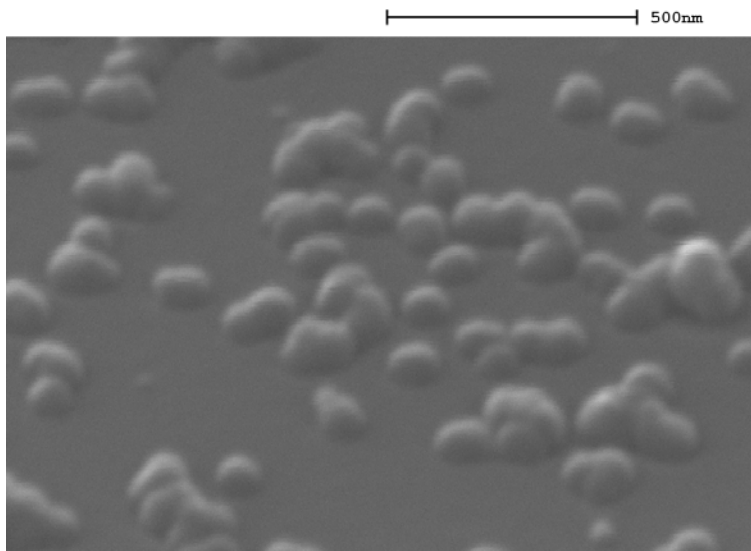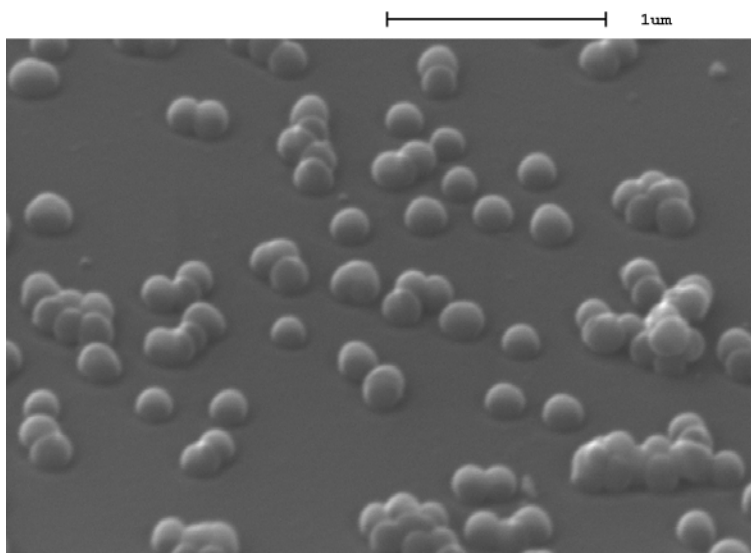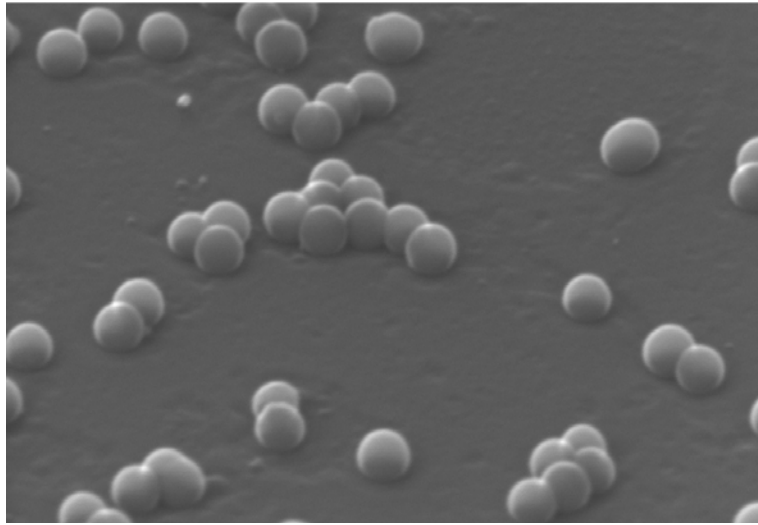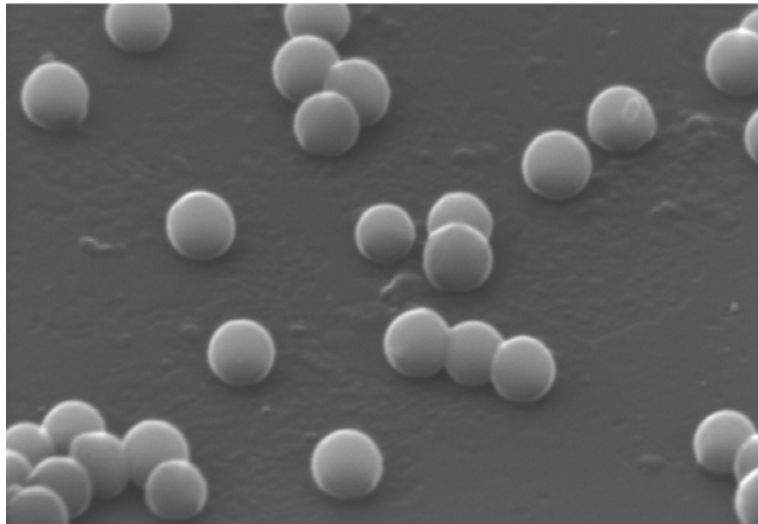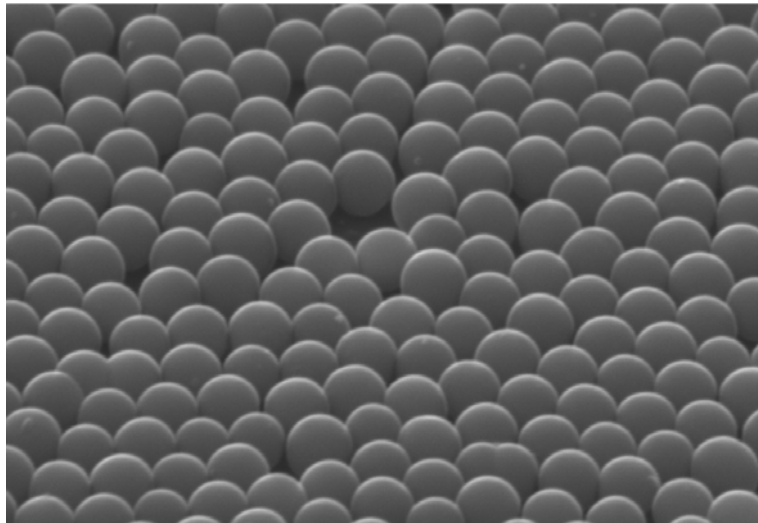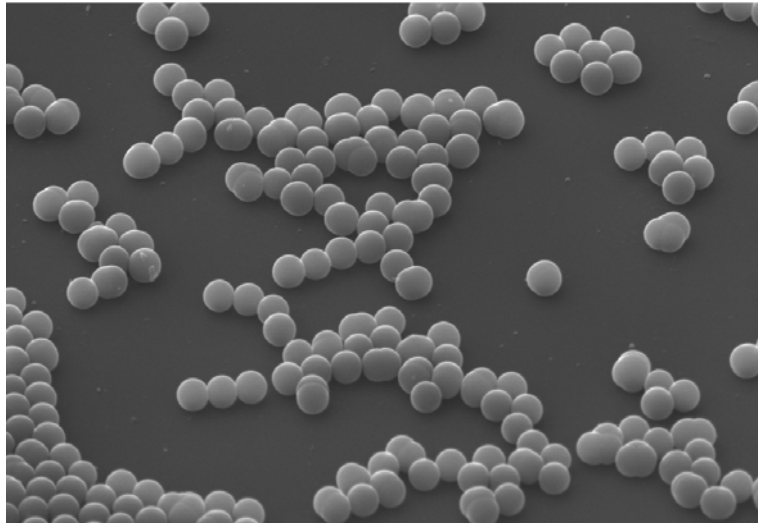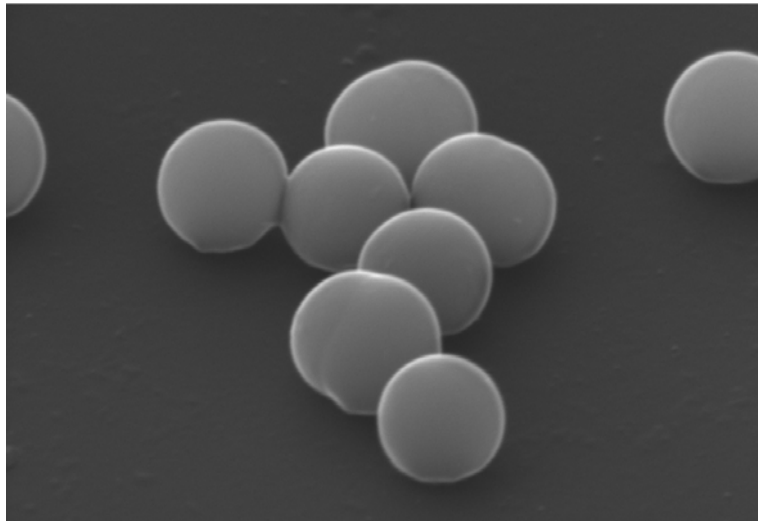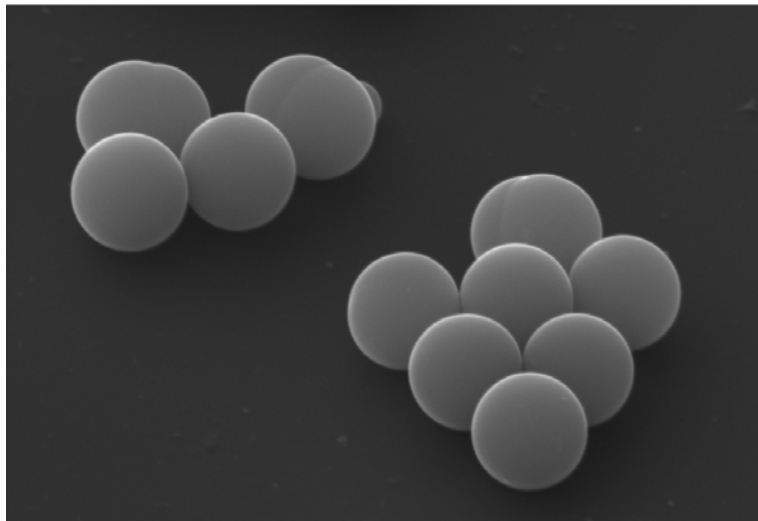
Synthetic amorphous silica particles with a diameter of 3.00 ± 0.05 μm and a density of 2.0 ± 0.2 g/cm^3 were obtained from Tokuyama Corp., Japan. The particle wettability was adjusted by silanisation of their surfaces by Dr. T. Horozov. The procedure is fully described in ref. 8. The silanising agents used were hexamethyldisilazane (HMDS, 99%, Lancaster) or dichlorodimethylsilane (DCDMS, > 99.5 %, Fluka AG) both dissolved in dry cyclohexane (99.7 %, Prolabo) at concentrations within the range 1×10^{-4} to 1×10^{-1} M. The contact angles of water drops under air on glass slides hydrophobised simultaneously with the particles was in the range 50 - 105° as seen in Table 2.4.

Table 2.4   Properties of coated monodisperse silica particles of diameter 3 μm.

[Silanising agent] / M	Silanising agent	Contact angle / deg.
1×10^{-1}	HMDS	50
1×10^{-2}	HMDS	65
1×10^{-3}	HMDS	75
1×10^{-4}	DCDMS	105

2.1.3   Laponite RD particles

The clay sample, Laponite RD, was provided as a white free - flowing powder by Laporte Industries Ltd. (Widnes). Laponite is an entirely synthetic product that resembles the natural smectite mineral hectorite in both structure and composition. The batch used had the chemical composition (wt. %): SiO_2, 59.5; MgO, 27.5; Na_2O, 2.8; Li_2O, 0.8.[9] The synthesis process involves combining salts of sodium, magnesium and lithium with sodium silicate at carefully controlled rates and temperatures.[9,10] This produces an amorphous precipitate which is then partially crystallised by a high temperature treatment. The resulting product is filtered, washed, dried and milled to give a fine white powder. As a result of its high chemical purity and small particle size, Laponite forms colourless and transparent suspensions which are particularly suited for light scattering studies. Laponite RD has a layer structure which, in dispersion in water, is in the form of disc-shaped particles. Their thickness is 1 nm and the disc diameter is around 30 nm as shown below in Figure 2.4. The particle surface has a negative charge on faces and the edges have small localised positive charges, generated from the

dissolving of surface attached ions (Na, Ca, Mg) into the surrounding liquid. The surface charge distribution is fixed due to the crystalline structure of the particle.

Figure 2.4 Schematic picture of the disc-like shape of the primary Laponite RD particle.

30 nm

1 nm
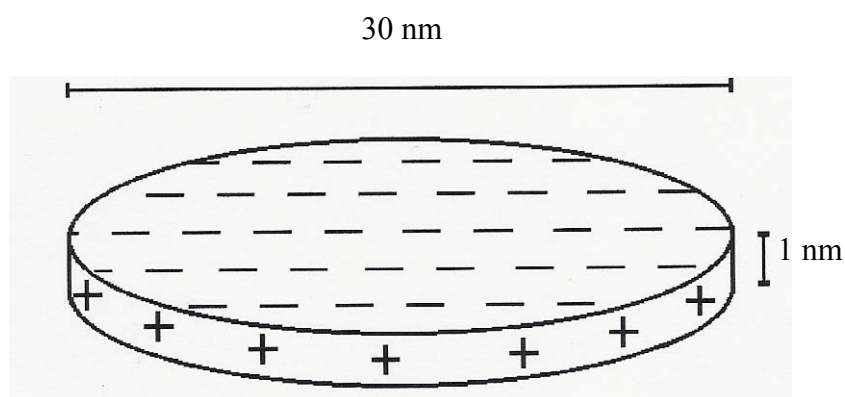
2.1.4 Sulphate latex particles

Sulphate polystyrene latex particles were obtained from Interfacial Dynamics Corporation (IDC, Portland) and used as received. These microspheres are stabilised by sulphate charges as shown in Figure 2.5.

Figure 2.5 Schematic representation of polystyrene latex particle with sulphate functional group at the surface.

$OSO_3^- Na^+$

OH
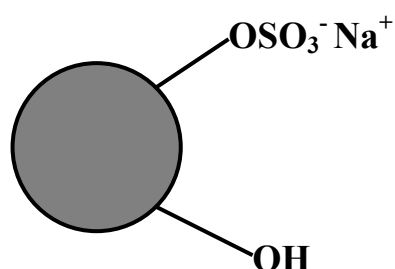
The pKa of the sulphate group is less than 2 and consequently the particles are stable in acidic media. According to the manufacturer's information, the mean diameter of these particles is 9.6 μm and the stock solution has 8.3 % solids.

Polystyrene latex particles are produced by surfactant-free emulsion polymerisation.[11] The polymerisation is initiated by adding an aqueous solution of potassium persulphate to the mixture of water and styrene at 70 ºC. The reaction normally lasts 24 hours. The polystyrene particles are then removed from the unreacted styrene by decantation through glass wool. These latex particles are cleaned by dialysis against deionised water for 24 hours in order to remove sodium chloride, unreacted monomer, unreacted initiator and sulphuric acid formed during the reaction. The dialysate is changed every day until its conductance is close to that of deionised water. The cleaning of latex particles is crucial. An extensive review has shown that the presence of impurities such as unreacted monomer, carbon dioxide, bacteria and fungi in the particle dispersion affect notably the size, morphology, surface group and surface charge density of these particles.[12]

2.1.5   Surfactant

Cetyltrimethylammonium bromide (CTAB) is a cationic surfactant purchased from BDH with a stated purity of > 99 %. It was used as received without further purification. The literature value for the critical micelle concentration (c.m.c.) of CTAB at 25 °C in water is reported as 0.97 mM.[13] Its structure is shown in Figure 2.5.

Figure 2.5 Schematic representation of cetyltrimethylammonium bromide (CTAB).
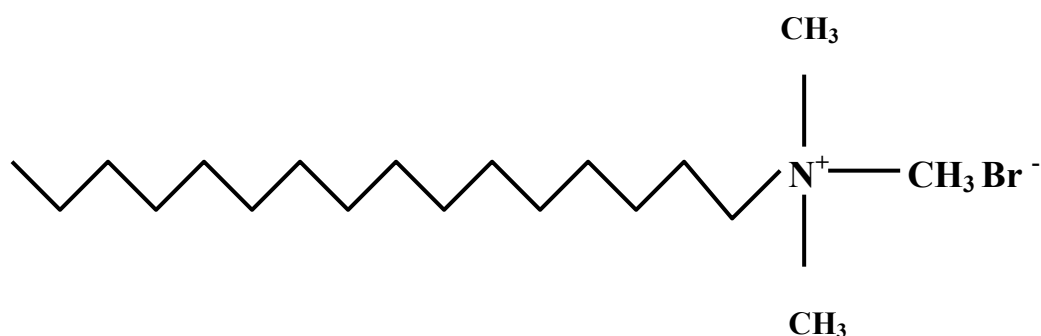
2.1.6   Other chemicals

Table 2.5 lists the other chemicals used in this project with their suppliers and purities. All oils were purified by columning through alumina (activated basic) in order to remove polar surface - active impurities and dried with molecular sieve 5A (Lancaster) for at least 24 hours. The other chemicals were used as received.

Table 2.5   Supplier and purity of chemicals.

Chemicals	Supplier	Purity / %
sodium chloride (NaCl)	BDH	> 99.5
phosphorous pentoxide	Fisher Chemicals	> 98
sodium hydroxide (NaOH)	Prolabo	98
potassium hydroxide (KOH)	BDH	AnalaR grade
ethanol (EtOH)	Fisher Scientific	> 99.9
isopropyl alcohol	Fisher Scientific	> 99.5
hydrochloric acid (HCl)	Fisons	97.5
toluene	Fisher Chemicals	> 99.9
cyclohexane	Prolabo	> 99.7
chloroform	Fisher Chemicals	> 99.9
dichlorodimethylsilane (DCDMS)	Fluka AG	> 99.5

2.1.6   Glassware

Great care was taken to ensure glassware was not contaminated by surfactant or any impurities. All glassware used was first cleaned with alcoholic KOH, then rinsed with copious amounts of Milli-Q water and finally dried in an oven overnight at 50 °C.

2.2   Methods

2.2.1   Ex - situ modification of hydrophilic silica particles and glass slides

2.2.1.1 Washing procedure of silica particles and glass slides

The silica particles were washed with ethanol first and then several times with fresh Milli-Q water prior to silanisation to remove any impurities or surface - active agents. Dispersions of hydrophilic silica particles were prepared using the ultrasonic vibracell processor (Sonics and Materials). A known amount of particles was dispersed in ethanol by operating the processor with a probe tip of 3 mm diameter at 20 kHz and

up to 10 W for 2 minutes. During sonication, the vessel containing the dispersion was immersed into an ice bath in order to keep the mixture cool. The dispersions obtained were settled by centrifugation (10 minutes at 3000 rpm) using a Baird and Tatlock auto bench centrifuge (Analytical Supplies Ltd, UK). The supernatant liquid was replaced with pure water, and particles were re-dispersed. The centrifugation-redispersion cycle was repeated several times by replacing the supernatant liquid with pure water. Surface tension measurements of all supernatants obtained were determined with a Krüss tensiometer K12, using the du Noüy ring method. Microscopic glass slides were cut to 12x15 mm and washed with ethanol (sonicated for 30 minutes in a water bath) and then rinsed with copious amounts of Milli-Q water. These glass slides were then dried in an oven at 60 °C prior to silanisation alongside the silica particles.

2.2.1.2 Silanisation of silica particles and glass slides

The silanising agent used was dicholorodimethylsilane (DCDMS). Silanisation was carried out in a dry nitrogen atmosphere (relative humidity about 10 – 15 %) using phosphorous pentoxide, *i.e.* P_2O_5, as drying agent and a glove bag (Aldrich). It is crucial to maintain minimum water conditions, because the chlorine atoms in the silane reagent can hydrolyse readily with water and form silicone polymer, such as polysiloxanes. Silica particles (approximately 5 - 5.5 g) were dried on a hot plate at ~ 100 °C after being washed with ethanol and water. After cooling, silica particles were mixed with 130 mL of DCDMS solution in dry toluene. The microscope glass slides were immersed in the dispersion after being carefully washed and dried. After 1 hour of continuous agitation using a magnetic stirrer, silanisation was halted. The glass slides were removed and placed in a beaker with chloroform to remove any unreacted silane reagent. The suspension obtained was transferred to six different vessels (~ 25 mL solution in each) and particles were settled by centrifugation (3 minutes at 2000 rpm). The supernatant liquid was replaced with pure chloroform and particles were re-dispersed using an ultrasonic vibracell processor at 10 W for 1 minute. The centrifugation - re-dispersion cycle was repeated several times replacing the supernatant liquid with pure chloroform. The last cycle was done with absolute ethanol. Silanised particles were isolated by removing the ethanol and finally dried on a hot plate at 100 °C for 10 minutes and then in an oven at 50 °C overnight. Different extents of silanisation (hydrophobicity) were achieved by varying the concentration of the silanising agent in the range ~ 8×10^{-4} to 0.2 M. This reaction results in the formation of

covalent siloxane bonds between the silica atoms of the organosilane molecules and the silica atoms of the solid surface. However, it is possible for the remaining chlorine molecule to react with an adjacent silanol group or another dimethyldichlorosilane group to form doubly bound bidentate siloxane bridges and polymerised coatings respectively[14] as shown in Figure 2.6.

Figure 2.6 Schematic representation of hydrophobic silica formation.
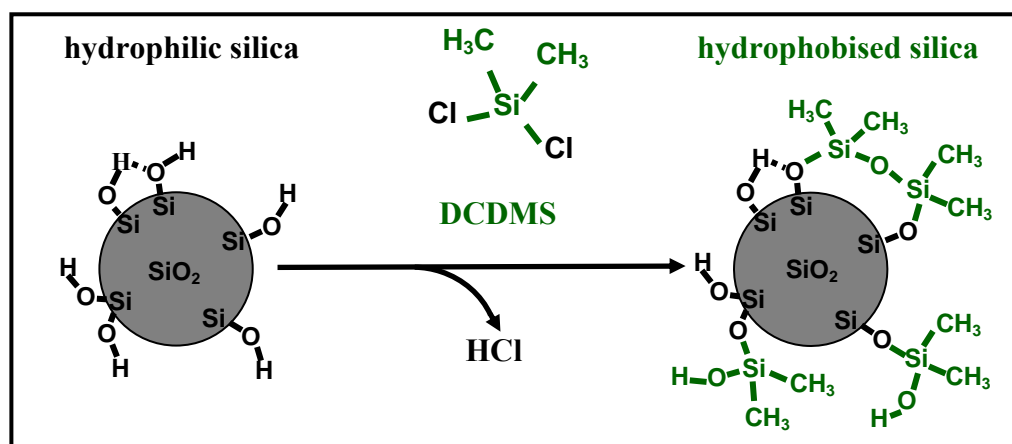
2.2.2 Preparation of colloidal dispersions

2.2.2.1 Precipitated hydrophilic silica in water

Known masses of the stock dispersions of hydrophilic silica were mixed with solutions of hydrochloric acid at concentrations such that the final volume of the dispersion was at the required pH. Sodium chloride was then added to the dispersions after dilution and pH adjustment. This method was denominated as protocol 1. In protocol 2, known masses of the stock aqueous dispersions of silica particles were diluted in aqueous solutions of sodium chloride first by using a magnetic stirrer and then hydrochloric acid was added to the dispersion.

2.2.2.2 Powdered particles

Dispersions of the unmodified and silanised silica particles (0.6 and 2 μm in diameter) were prepared in the following way. A known amount of particles (0.75 or 1.5 g) was dispersed in 25 mL of water by using a magnetic stirrer for at least 1 hour

(stock). Then 5 mL of the aqueous stock dispersions of silanised silica particles were placed in 5 different glass vessels and mixed with 5 mL solutions of aqueous salt (previously prepared) at concentrations such that the final volume of the dispersion was at the required [NaCl]. Finally all systems were sonicated for 1 minute at 10 W. During sonication, the vessel containing the dispersion was immersed in an ice bath in order to keep the mixture cool. Foams were prepared immediately after sonication of all systems, at room temperature (~ 22 °C).

The spreading suspension of silica particles (3 μm in diameter) used in the thin foam film experiments was prepared by diluting a small amount of silica particles in water and isopropanol, giving a total concentration of approximately $(2.6 - 5) \times 10^{-2}$ g cm^{-3}. To improve the attachment of particles to the air - water surface and enable formation of close – packed particles the spreading suspension of silica particles was prepared in a different way. This was achieved by diluting a small amount of silica particles, $e.g.$ 0.0157 g, in water (~10x weight of particles = 0.1680 g) and isopropanol (3 x weight of particles = 0.0489 g), giving a total concentration of particles of 0.068 g cm^{-3}.

Dispersions of Laponite RD in pure water were prepared by dispersing a known amount of powder into 10 mL or 20 mL of water using a high intensity ultrasonic vibracell processor (Sonics and Materials, tip diameter 3 mm) operating at 20 kHz and up to 10 W for 2 minutes or by simply using a magnetic stirrer for about 30 minutes. Subsequently, different known masses of NaCl were added such that the dispersion was at the required concentration of salt. This method was denominated as protocol 1. In protocol 2, known masses of Laponite RD powder were directly dispersed into the aqueous salt solution (previously prepared) by using a magnetic stirrer for approximately 30 minutes or by sonication for 2 minutes at 10 W.

2.2.2.3 Surfactant - particle mixtures

Hydrophilic silica particle dispersions in water were prepared by using an ultrasonic vibracell processor (Sonics and Materials, tip diameter 3 mm) operating at 20 kHz and up to 10 W for 2 minutes. Different concentrations of CTAB solution (5 mL) were added to 5 mL of silica dispersion previously prepared at different pH values. The final particle concentration in the dispersion was 3 wt. %. These dispersions were stirred gently for 30 minutes to allow equilibrium at room temperature.

55

The pH measurements of all dispersions were determined with a Fisherbrand Hydrus 400 pH meter, using a glass electrode. The pH meter was calibrated with buffer solutions at pH 4, 7 and 10. The pH of all aqueous colloids was varied by the addition of hydrochloric acid or sodium hydroxide.

2.2.3   Method for dispersing hydrophobic particles

The most hydrophobic silica particles (hydrophobised to a higher extent, *e.g.* [DCDMS] = 4×10^{-3} M) were dispersed in the following way. A minimum amount of ethanol was added to the particles, in order to sufficiently wet the particles and allow them to enter the aqueous phase. Then water was added and particles were dispersed by gentle agitation of the glass vessel (to avoid particles getting trapped at the air-water surface). The ethanol was removed by washing with Milli-Q water and centrifugation cycles. Each wash / centrifugation cycle comprised of 10 minutes centrifugation at 3500 rpm after which the clear supernatant was removed from above the sedimented silica particles. Some of the silica particles rose to the air/water surface (probably due to some trapped air). After each centrifugation the supernatant was removed and fresh water was added and then dispersed gently. After the final centrifugation, fresh water was added so that the sample was at the required weight. After this number of washes the amount of ethanol remaining in the system was very small (0.0005 wt. %) and considered negligible.

2.2.4   Preparation of foams

2.2.4.1 Hand-shake method

Foams were prepared either in 100 mL stoppered graduated measuring cylinders or in sample tubes (inner diameter 2 cm, height 7.5 cm) by vigorously shaking an aqueous dispersion of particles (10 mL or 20 mL) by hand for approximately 20 seconds. Foams were then monitored over time. All foam measurements were made at room temperature.

2.2.4.2 Homogenisation

Foams were also prepared by aerating an aqueous dispersion of particles using an Ultra Turrax homogeniser (Janke & Kunkel) with a 10 mm diameter head operating at 13000 or 17000 rpm for 2 minutes (2 x 1 min. with 30 s rest period). Photographs of the vessels were taken with an Olympus C – 765 Ultra Zoom digital camera.

2.2.5   Measuring foamability and foam stability

The foam shake test enabled a quick and quantitative assessment of the effect of the presence of particles and concentration of the electrolyte (NaCl) on both the initial volume of foam produced immediately after solution agitation (foamability) and the rate at which this initial volume decays over a period of time (foam stability). In this work the foam stability was expressed in different ways. For example, the foam stability was measured as the time taken for the foam to collapse to half its initial volume ($t_{1/2}$). Another way was by calculating the overrun, the variation of the volume fraction of air and liquid in the foam with time. Overrun is a term used to describe the amount of air that the total dispersion contains. It refers to the increase in the volume of the dispersion (after being foamed) over the initial volume of dispersion used. The value of overrun can be used to determine the quality of the foams formed. The % overrun can be calculated as follows:

$$\% \text{ overrun} = (V_T - V_0)/V_0 \text{ x } 100 \%$$ (2.3)

where V_T is the total volume of dispersion and V_0 is the initial volume of dispersion. $V_T - V_0$ corresponds to the volume of gas incorporated. The volume fraction of air (ϕ_{air}) in the foam is given by:

$$\phi_{air} = V_g / (V_g + V_l)$$ (2.4)

where V_g and V_l are the volume of gas and liquid in the foam respectively ($V_g + V_l = V_{foam}$). The liquid fraction in the foam is then given by:

$$\phi_l = 1 - \phi_{air}$$ (2.5)

2.2.6 Contact angle measurements

All contact angles measurements carried out in this work were measured using a Krüss DSA10 drop shape analyzer as shown in Figure 2.7. The apparatus comprises three parts:[15] the drop-making chamber with thermostat jacket and syringe holder, the CCD camera and the drop profile analysis program.

The instrument measures the three-phase contact angle from a digital image of a drop placed on a solid surface (sessile drop) as shown in Figure 2.8. The shape that this drop exhibits on the solid surface is the result of the free energy of the system controlled by the interfacial tensions between the three phases acting at the interface. This is explained theoretically by Young's equation:

$$\gamma_{sl} - \gamma_{sg} + \gamma_{lg} \cos \theta = 0 \qquad (2.6)$$

where γ_{sl}, γ_{sg} and γ_{lg} are the interfacial tensions of the solid-liquid, solid-gas and liquid-gas interfaces respectively. This equation is valid for a system where the three phases are in thermodynamic equilibrium.[16]

Figure 2.7   Krüss DSA 10 apparatus.
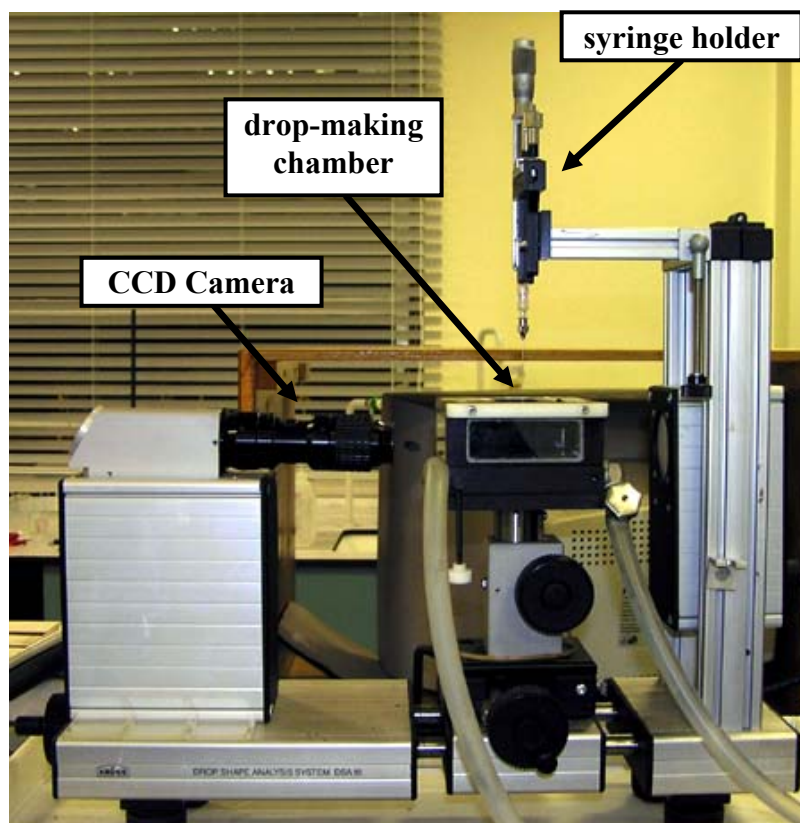
Figure 2.8 Schematic diagram of a sessile drop on a solid substrate in air and respective interfacial tensions acting at the contact line between the three phases.
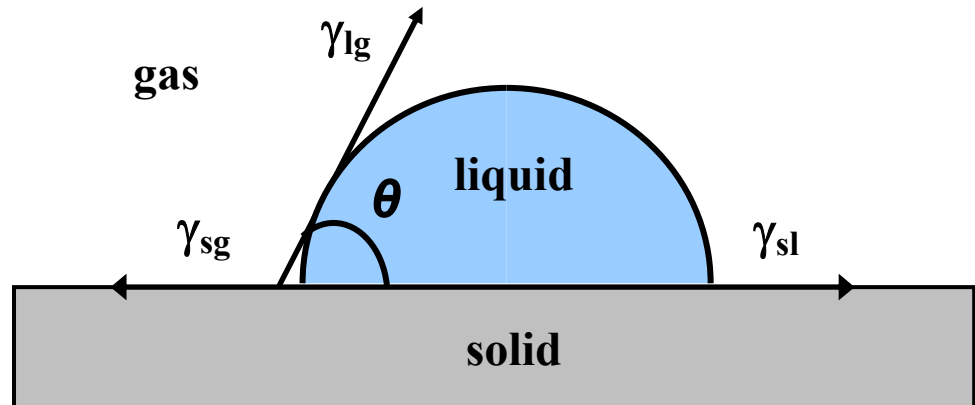
In order to obtain a clear image of the drop on the solid surface in the drop image window as shown in Figure 2.9 the focus of the CCD camera and the light intensity were adjusted. The baseline was matched exactly with the contact angle of the liquid and the solid substrate.

Figure 2.9 Drop profile analysis programme showing the typical shape of a sessile drop during the analysis.
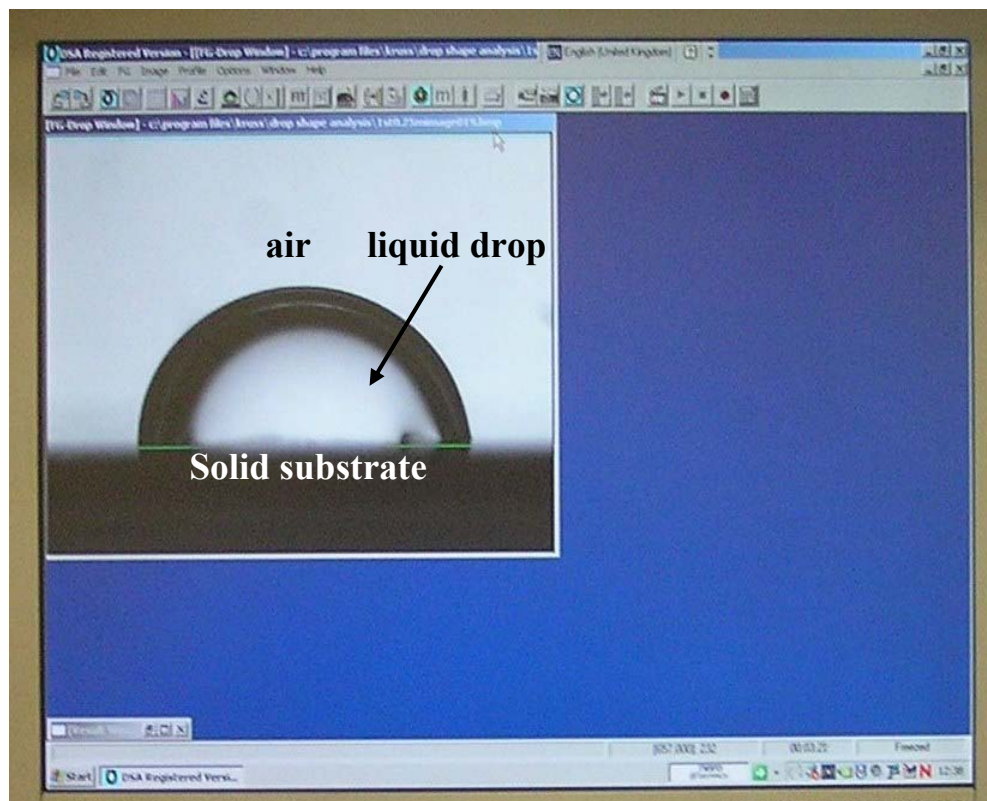
Different methods for the evaluation of sessile drops and the determination of the contact angles can be obtained from the DSA program.[15] The evaluation method used in this work was the tangent method, where the software fits a polynomial equation to the drop profile obtained digitally using a video camera and the angle is then obtained as the slope of that equation exactly at the three-phase contact point at the baseline. This angle is measured for both sides of the drop (left and right) and the software determines an average.

All contact angle measurements were carried out at 25 °C using a Grant LTD-6 thermostat on either completely hydrophilic or hydrophobised glass slides (Chance Propper) and also on silicon wafers (Compart Technology Ltd., UK). All angles quoted are those measured through the liquid phase.

Advancing contact angles of water and aqueous NaCl drops under air on hydrophilic glass slides and on silicon wafers were measured. Microscope glass slides were previously immersed in a hot mixture (50 °C) of water (70 %) and sodium hydroxide (30 %) for two hours and then rinsed thoroughly with Milli-Q water and dried in an oven (45 °C) for about 20 hours. Silicon wafers were also treated with nitric acid prior to measurements to render them hydrophilic. The hydrophilic glass slide or silicon wafer was then put in the measuring chamber with temperature control and a drop (~ 5 μL) of pure water or aqueous solution of NaCl was released from a 25 μL syringe.

Both advancing and receding three-phase contact angle measurements of water drops were made on silanised glass slides under air measured through water. Glass slides were silanised simultaneously with silica particles and at different [DCDMS]. At each value of [DCDMS], three measurements of the advancing and receding contact angle were made on 6 different glass slides. The silanised glass slide was put in the measuring chamber (the chamber was closed to avoid evaporation of water) with temperature control and a drop (~ 5 - 10 μL) of pure water was released from a 25 μL syringe. The contact angle was measured using the tangent method from the images. The receding contact angle was determined by removing a volume of water from the drop until the three - phase contact line began to recede. Once movement of the contact angle line had begun, the receding contact angle was measured. The difference between advancing and receding contact angles of water drops on glass slides under air was less than 6°; therefore their average was used.

Advancing contact angles of aqueous CTAB drops (~ 5 - 10 μL) at pH 9 on a silicon wafer have been measured and recorded within 5-10 minutes to allow the system to reach equilibrium. Silicon wafers were treated with concentrated nitric acid and rinsed with Milli-Q water before use rendering them hydrophilic. A mean contact angle of at least 2 drops was taken for each surfactant concentration.

2.2.7 Particle size and zeta potential measurements

The particle size and zeta potential of aqueous dispersions was measured using a Malvern ZetaSizer 3000 HS instrument. A brief outline of the principles of operation of the Malvern Zetasizer for particle size and zeta potential measurements is described below.

Photon Correlation Spectroscopy (PCS), also known as Dynamic Light Scattering (DLS), is the method used for measuring the particle size using the Malvern Zetasizer.[17] This technique is one of the most popular methods used to determine the size of particles. Shining a monochromatic light beam, such as laser, into a solution with spherical particles in Brownian motion causes a Doppler Shift when the light hits the moving particle, changing the wavelength of the incoming light. Due to their higher average velocity, smaller particles cause a greater shift in the light frequency than larger particles. It is this difference in the frequency of the scattered light among particles of different sizes that is used to determine the size distribution of the particles present. Analysis of the time dependence of the intensity fluctuation can therefore yield the translational diffusion coefficient of the particles (D_T) from which, via the Stokes Einstein equation (2.7) knowing the viscosity of the medium (η), the hydrodynamic diameter (d_H) of the particles can be calculated.

$$d_H = \frac{k_b T}{3\pi \eta D_T}$$

(2.7)

where k_b is the Boltzmann constant and T is the absolute temperature. This diameter is referred to as a hydrodynamic diameter because it is a value that refers to how a particle diffuses within a fluid.

Although simple in principle, light scattering measurements present a number of experimental difficulties, the most notable being the necessity to free the sample from impurities such as dust, the relatively large particles of which would scatter light

strongly and introduce serious errors. The method chosen depends on the size of the particles in relation to the wavelength of light. It is convenient to divide the scattering of light by independent particles into three classes: [18]

(i)   Rayleigh scattering – where the scattering particles are small enough to act as point sources of scattered light.

(ii)   Debye scattering – where the particles are relatively large, but the difference between their refractive index and that of the dispersion medium is small.

(iii)   Mie scattering – where the particles are relatively large and have a refractive index significantly different from that of the dispersion medium.

Micro-electrophoresis is the method employed by the Malvern ZetaSizer used to measure zeta potentials. The sample under investigation is contained within an electrophoresis cell. A known electric field is applied and the sample illuminated by the crossed focused laser beams. Particles moving through the measurement volume scatter light. The intensity of the light fluctuates with a frequency proportional to the velocity of particles. The velocity is calculated from the measured frequency then expressed as mobility by dividing by the applied field. This is then converted to zeta potential using established theories.[19]

The velocity of a particle in a unit electric field is referred to as its electrophoretic mobility (μm s^{-1} V^{-1} cm) and is best considered as the velocity of flow (μm s^{-1}) per unit electric field (V^{-1} cm). Zeta potential is related to the electrophoretic mobility by the Henry equation:

$$U_E = \frac{2\varepsilon\zeta f(\kappa a)}{3\eta}$$

(2.8)

where U_E is the electrophoretic mobility, ζ is the zeta potential of particles in solution, ε is the dielectric constant of the solvent, η is the viscosity of the medium and $f(\kappa a)$ is the Henry's function. The units of κ, termed the Debye length, are reciprocal length and κ^{-1} is often taken as a measure of the 'thickness' of the electrical double layer. The parameter 'a' refers to the radius of the particle and therefore κa measures the ratio of the particle radius to the electrical double layer thickness. Electrophoretic determination of zeta potential is most commonly made in aqueous media and moderate electrolyte concentration. For small κa the Henry's function approaches 1, for large κa it

approaches 1.5. These correspond to limiting cases where the particle is much smaller than the double layer thickness or much larger. These are also known as the Hückel and Smoluchowski limits respectively (see Figure 2.10). The Hückel limit applies for very small particles in low dielectric constant media. The Smoluchowski applies for particles larger than about 0.1 μm dispersed in aqueous solutions with an ionic strength $>10^{-3}$ M (this ionic concentration is high enough to significantly compress the double layer).

Figure 2.10 Schematic illustrating Hückel and Smoluchowski approximations used for the conversion of electrophoretic mobility to zeta potential.
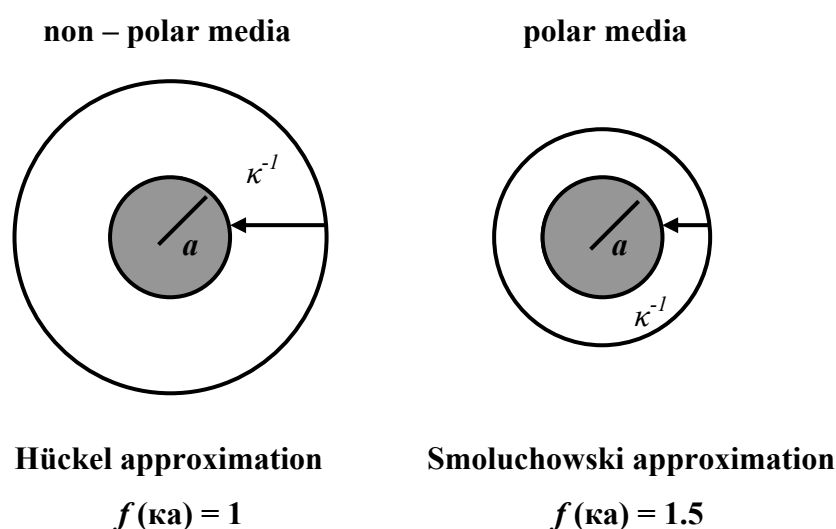
A zeta potential measurement system comprises of six main components as shown in Figure 2.11. First of all a laser (1) is needed to provide a light source to illuminate the particles within the sample. This light source is split to provide an incident and reference beam. The laser beam passes through the centre of the sample cell (2), and the scattering at an angle of 17° is detected. When an electric field is applied to the cell, any particles moving through the measurement will cause the intensity of light detected to fluctuate with a frequency proportional to the particle speed. A detector (3) called photomultiplier sends this information to a digital signal processor (4). This information is then passed to a computer (5) where the software produces a frequency spectrum, from which the electrophoretic mobility and hence the zeta potential are calculated.

The intensity of the scattered light within the cell must be within a specific range for the detector to successfully measure it. If too much light is detected then the detector will become overloaded. To overcome this, an attenuator (6) is used to reduce the

intensity of the laser and hence reduce the intensity of the scattering. To correct for any differences in the cell wall thickness and dispersant refraction, compensation optics (7) are installed within the scattering beam path to maintain alignment of the scattering beams.[20]

Figure 2.11 Schematic representation of a zeta potential measurement system (taken from ref. 21).
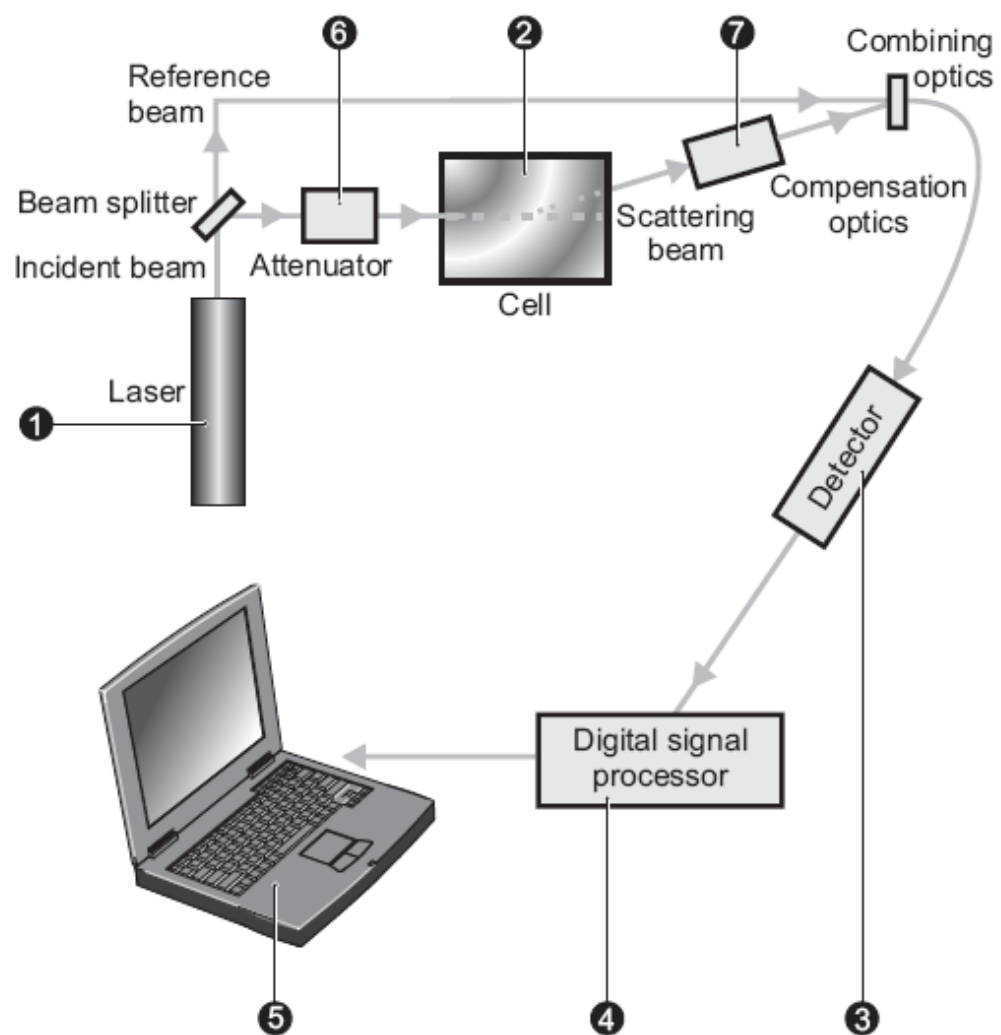
2.2.8   Viscosity measurements

The viscosity of aqueous dispersions of precipitated silica particles was measured with a Bohlin CVO 120 High Resolution rheometer in the controlled rate mode. The instrument applies a controlled shear stress to the sample and detects the sample deformation as shear strain, which is converted into shear rate. The rheometer contains a constant torque motor that works by a drag cup system.[22] The angular position sensor detects the movement of the measuring system. The software automatically converts the applied torque into shear stress and the resultant displacement in the dispersion is measured using the position sensor. By monitoring the change of shear strain as a function of time, the instrument calculates the shear rate. The viscosity η is then calculated by the software using the equation:

$$\eta = \frac{\sigma}{\dot{\gamma}}$$
(2.9)

where σ is the shear stress in pascal and $\dot{\gamma}$ is the shear rate in s^{-1}.

A (truncated) cone (4° cone angle, 40 mm cone diameter) and plate geometry (150 μm gap width) roughened by sand blasting (Bohlin) was used. The geometries were cleaned by rinsing in propan-2-ol. A solvent trap was used to avoid evaporation of the solutions during measurements. Prior to sampling for measurements, the solutions were gently shaken with a magnetic stirrer to reverse any sedimentation effects.

2.2.9   Optical, Transmission and Scanning Electron Microscopy

Optical microscopy was used to observe the shape and size of the bubbles in the foams and also to determine the particle size in order to make comparisons with the particle size distribution obtained by the light diffraction method. Different methods for viewing the bubbles were used as described below:

(i)   A small amount of bubbles within the foam were placed on a haemocytometer cell (Web Scientific) and the structure of the thin films was observed from the top of the slide with an optical microscope using reflected light.

(ii)   Bubbles were observed within the glass cylinder with an optical microscope positioned horizontally facing the sides of the cylinder.

(iii)   Foam was transferred to an open glass dish and thin films between the bubbles were observed from the top with an optical microscope using reflected light.

The method to view the particles involved diluting a small amount of particles in water and spreading the dispersion in a haemocytometer cell (Web Scientific) and covering with a cover slip. All samples were viewed at 4X, 10X and 40X magnification with a Nikon Labophot microscope fitted with a DIC-U camera (World Precision Instruments). All images were processed using Adobe Photoshop 5.0 software. A graticule (National Physical Laboratory) was used to calibrate the microscope at different magnifications in order to calculate the number of pixels per micron of the images on the screen.

Transmission Electron Microscopy (TEM) images of hydrophilic silica particles were obtained using a JEOL 100C 80 kV electron microscope. Prior to analysis by TEM, the original aqueous precipitated silica obtained was diluted with water and a single drop of the diluted dispersion was placed on a carbon-coated copper grid (300 mesh). The dispersion was then allowed to evaporate.

Scanning Electron Microscopy (SEM) images of the monodispersed silica particles used obtained by coating the samples with a layer of carbon, since the specimens examined by SEM must be able to withstand the strong electric currents produced by the electron beam. Therefore, before imaging, all samples were coated with ~ 10 nm carbon (spectrally pure graphite) using an Edwards High Vacuum evaporator fitted with a planetary-motion sample rotation device. The SEM images were taken after observation of the whole sample in order to obtain a representative image. The observation angle was also varied from 0° (view from the top) to ~ 90° (side view).

2.2.10 Freeze-fracture Scanning Electron Microscopy

Scanning Electron Microscopy freeze fracture (Cryo-SEM) images of particle-stabilised foams were obtained at Unilever Colworth (UK). Aqueous foams were first frozen by immersing the vessels into liquid nitrogen. The aqueous foam was fronzen as rapidly as possible so that ice crystal damage is minimal, and to as low a temperature as practical to avoid the possibility of sublimation. The frozen samples were then kept inside a box containing dry carbon dioxide (ice) and kept in a freezer. The principal operational steps are shown in Figure 2.12 and described below:

Figure 2.12 Schematic representation of the cryo-SEM technique step by step (taken from ref. 23).
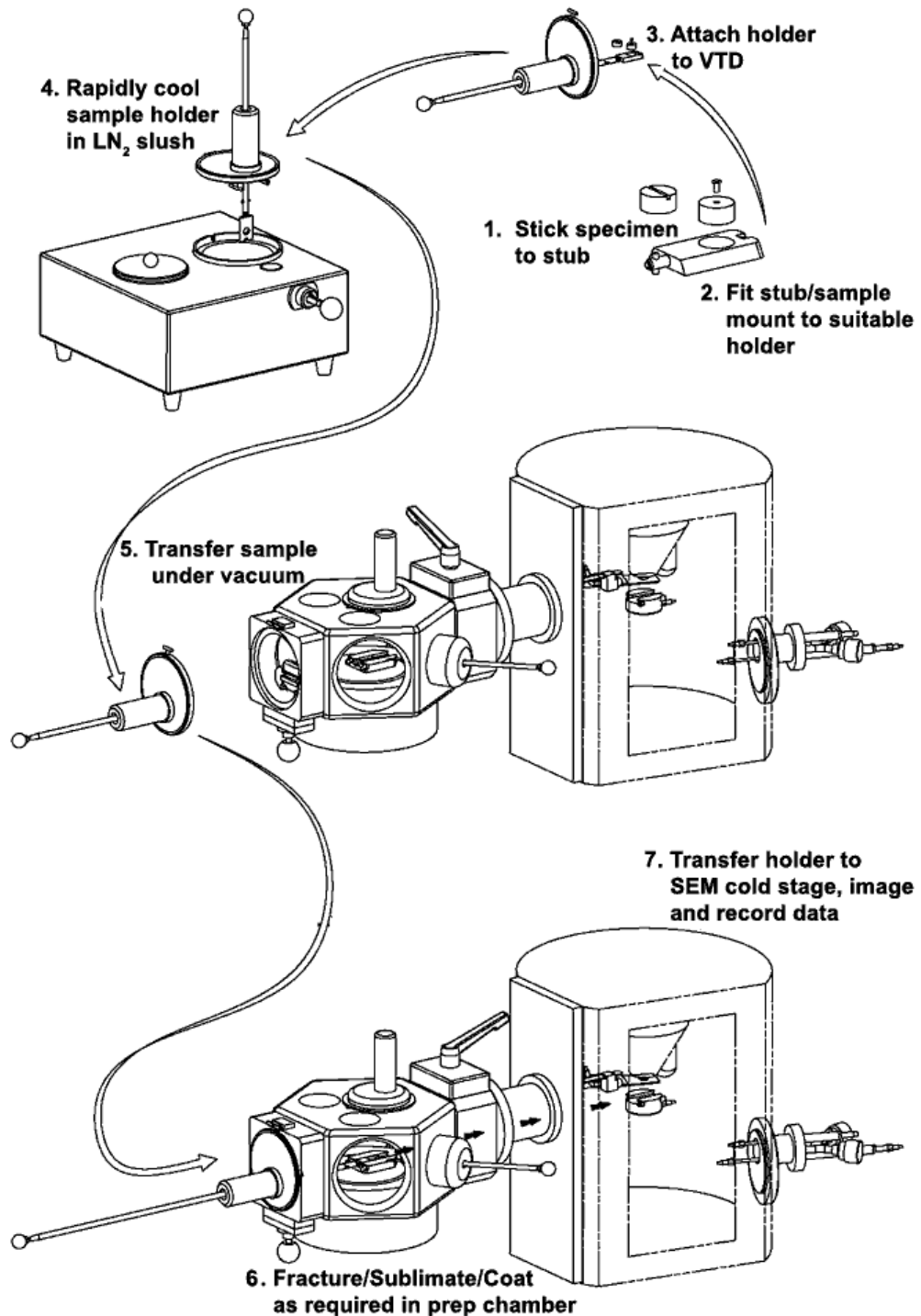
Step one   A small sample of the frozen foam was fractured on the surface of an aluminium plate (previously cooled with dry carbon dioxide). The holder and tweezers to handle the foam were pre-cooled in slushy nitrogen (sub-cooled liquid nitrogen). The small fraction of the foam was 'glued' on to the SEM stub using O.C.T. compound. O.C.T. compound is an optimum cutting temperature formulation of water-soluble glycols and resins. It is a special low-temperature embedding medium for cryo-sectioning techniques. This material is not toxic, is water soluble and will leave no traces.

Step two   The stub containing the frozen foam is then inserted into a suitable holder.

Step three   The holder is then attached to a vacuum transfer device (VTD).

Step four   The sample holder is then cooled quickly by plunging into liquid nitrogen slush.

Step five   The stub containing the frozen foam was then transferred under vacuum to a preparation chamber.

Step six   In the preparation chamber, temperature and pressure levels were carefully controlled. The foam was fractured at different positions: close to the surface of liquid (bottom of foam) or at the top of the foam, using an aluminium cold plate and then etched to remove any frozen ice from the surface of the foam (this was achieved by controlled raising of the temperature until sublimation occured) in order to reveal the inner structure of the foam. The exposed foam surface was sputter coated with 2 nm of platinum – palladium coating. The amount of coating was controlled with time (*e.g.* platinum - 2 Å per minute). The sputter coater is used to coat non-metallic samples. This makes them conductive and ready to be viewed by the SEM.

Step seven   Finally, the gate valve between the preparation chamber and the SEM was raised and the sample of foam transferred onto the cooled stage of the SEM by using the VTD. Images were captured and data recorded by the software.

2.2.11 Tursbican measurements on stability of aqueous dispersions

The stability of aqueous silica dispersions was studied using a Turbiscan Lab Expert instrument, at Unilever Colworth, (UK). The Turbiscan Lab. Expert (Formulaction) as shown in Figure 2.13 uses multiple light scattering, which allows monitoring of concentrated dispersions without any dilution.

Figure 2.13 Turbiscan Lab Expert (Formulaction) apparatus.

Multiple light scattering allows the measurement of the photon mean free path (λ) and transport mean free path (λ^*), absolute parameters which describe the real state of dispersions, without mathematical approximations. The multiple light scattering theory is briefly described below.[24]

In diffusive optics, λ^*, the photon transport mean free path, corresponds to the distance of penetration of the photon in the dispersion. The central part of the backscattered light spot has a radius of 4 λ^*. The Tursbican mainly analyses this central part. Therefore, the measured backscattered flux BS can be linked to λ^*. As a first approximation, BS is inversely proportional to the square root of λ^*

$$BS \sim 1/(\lambda^*)^{1/2} \tag{2.10}$$

From Mie theory, λ^* is inversely proportional to the volume fraction of the particles ϕ and proportional to their mean diameter d

$$\lambda^*(d, \phi) = 2\,d\,/\,[3\phi\,(1\text{-}g)\,Qs] \tag{2.11}$$

where g and Qs are optical parameters given by Mie theory. Therefore, the backscattering measurement by the Turbiscan is directly dependent on particle mean diameter d and on volume fraction ϕ.

In diffusive optics, λ, the photon mean free path, represents the mean distance travelled by photons before undergoing a diffusion phenomenon. This measurement is performed by the Turbiscan by sending a light beam through the cell and detecting the photons that cross the dispersion, without being diffused. Therefore, the more photons that cross the cell, the more important the λ value.

The Lambert-Beer law gives an analytical expression of the transmitted flux T measured by the Turbiscan as a function of the photon mean free path λ:

$$T(\lambda, ri) = T_0 \times e^{\,2ri\,/\,\lambda}, \text{ with } \lambda(d, \phi) = 2\,d\,/\,3\phi\,Qs \tag{2.12}$$

where ri is the measurement cell internal radius and T_0 the transmittance of the continuous phase. Therefore, as for backscattering, the transmission is directly dependent on the particle mean diameter d and the volume fraction ϕ.

The measurement principle of the Turbiscan is shown in Figure 2.14. The dispersion analysed is contained in a cylindrical glass cell. The light source is an electro luminescent diode in the near infrared (λ_{air} = 880 nm). Two synchronous optical sensors receive respectively light transmitted through the sample (180° from the incident light, transmission sensor), and light backscattered by the sample (45° from the incident radiation, backscattering detector).

Figure 2.14 Measurement principle of the Turbiscan Lab Expert instrument.
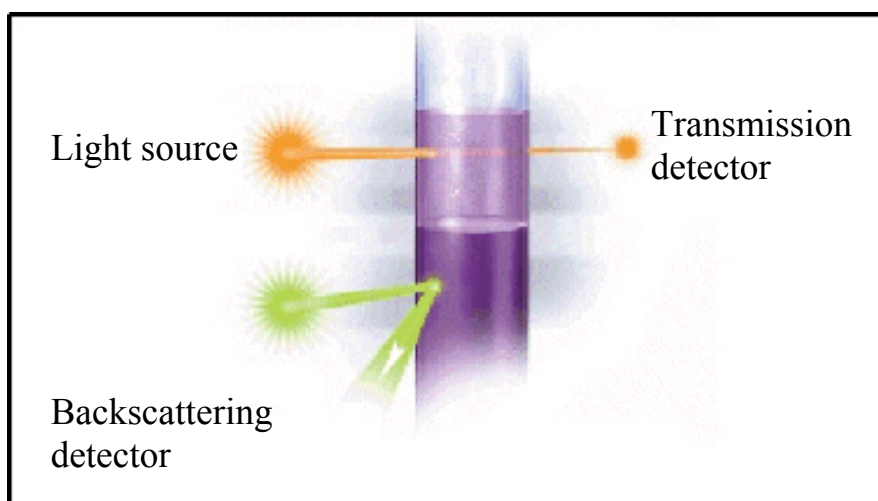
The Turbiscan reading head acquires transmission and backscattering data or at a chosen position on the sample cell (fixed position mode), or every 40 μm while moving along the 55 mm cell height (scan mode). The scan mode was used in this study, as this is the most complete analysis mode enabling the detection of the migration phenomena. The results are then represented on the software screen by a curve showing the percentage of backscattered or transmitted light relative to standards as a function of the sample tube length in mm. The acquisition scan is then repeated over and over with a programmable frequency and results are superimposed on a time scan graph as shown in Figure 2.15. The stability or instability of the sample can then be determined by analyzing the time graph. Transmission is used to analyse clear to turbid dispersions and backscattering is used to analyse opaque dispersions.

Sedimentation is one of the parameters that can be very easily detected using the Turbiscan as it induces a variation of the concentration of the dispersed phase between the top and the bottom of the sample. Backscattering increases at the bottom of the sample due to an increase of the concentration of the dispersed phase (sediment) and decreases at the top of the sample due to a decrease of the concentration (clarification).

Figure 2.15 Turbiscan profile analysis programme showing the typical curves of transmitted (top) and backscattered (bottom) light flux in % (y axis) as a function of the sample height in mm (x axis) of an aqueous dispersion. The times of acquisition are shown in different colours on the right-hand side of the screen.

From the backscattering and transmitted light flux (%) data obtained from the aqueous silica dispersions, the following parameters can be calculated in order to determine the sedimentation kinetics:

(i)   The variation of backscattering (ΔBS) between the top and the bottom of the cell.

(ii) The phase thickness (ΔH) of the sediment layer and/or the clear phase, in order to be able to follow its formation (calculation in reference mode).

(iii) The migration velocity of the clarification front (slope of the clarified phase thickness), in order to follow the kinetics of sedimentation (calculation in no-reference mode).

2.2.12 Surface tension measurements

Surface tension (γ) measurements for some systems studied in this work were determined using a Krüss K12 Digital Tensiometer (thermostatted) applying the du Noüy ring method and appropriate correction.

The du Noüy ring method was the first method for measuring the surface tension to be developed and is named after the French physicist who developed it in the late 1800s. The ring used is this work is made from an alloy of platinum and iridium (with high energy surface) and welded on a frame of the same alloy that is used to suspend the ring on a balance and brought into contact with the liquid surface tested. The forces experienced by the balance as the ring interacts with the surface of the liquid can be used to calculate the surface tension. The ring hanging from the balance hook is first immersed into the liquid and then carefully pulled up, by lowering the sample cup, through the surface of the liquid. The microbalance is recording on-line the force applied on the ring while pulling through the surface. The surface tension is the maximum force needed to detach the ring from the liquid surface. At the maximum the force vector is exactly parallel to the direction of motion; at this moment the contact angle, θ (as shown in Figure 2.16) is 0°.

Figure 2.16 Schematic diagram of the ring method.
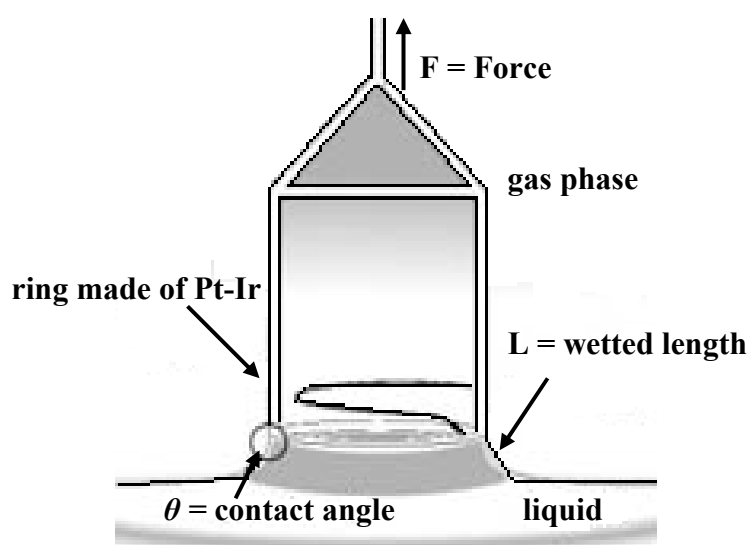
The following illustration (Figure 2.17) shows the change in force as the distance of the ring from the surface increases.

Figure 2.17 Change of force with ring distance.
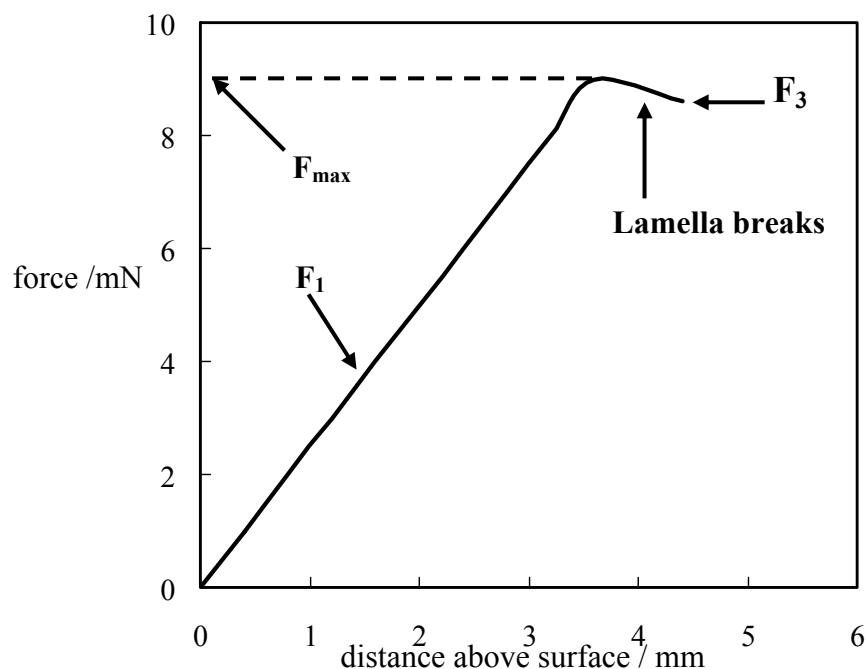
In practice, however, the distance is first increased until the area of maximum force has been passed through. The sample vessel containing the liquid is then moved back so that the maximum point is passed through a second time. The maximum force F_{max} is only determined exactly on this return movement and used to calculate the tension. When the maximum pulling force is operative on the ring:

$$F_{max} = mg = 4\pi R\gamma \tag{2.13}$$

where m is the mass of the solution raised by the ring, g is the acceleration due to gravity, R is the average radius of the ring (obtained by adding the value of the inner radius of the ring and the radius of the wire making up the ring) and γ is the surface tension. The term $4\pi R$ corresponds to the wetted length of the ring (L). However, a solution must be found for a particular problem: the curve of the film is greater on the inside of the ring compared with the outside. This means that the maximum force (at which the contact angle $\theta = 0°$) is reached at different ring distances for the inside and

outside of the ring. As a result the measured maximum force does not agree exactly with the actual value. Hakins and Jordan[25] pointed out that a factor relating to the shape of the meniscus should be taken into account and a modified equation was given,

$$\gamma = mgF / 4\pi R = \Delta\rho VgF / 4\pi R \qquad (2.14)$$

where F is the correction factor which is a function of R^3/V and R/r, where V is the volume of liquid pulled from the surface by the maximum pull of the ring and r is the radius of the wire from which the ring is made. The correction factors are applied by measuring the radii of the ring, the wire and the density difference between the fluids $\Delta\rho$. A value of R^3/V is calculated for each determination and the correction factor is obtained from tables according to the value of R/r. The accuracy of these tables has been shown to be within $\pm$ 0.25 % of those obtained from theoretical variations in meniscus shapes by Freud and Freud.[26] This method was extended by Zuidema and Waters[27] to include the measurement of interfacial tension below 25 (mN) m^{-1}.

The ring used for measuring the surface tension in this work was cleaned before each use by rinsing in alcoholic KOH and then in Milli-Q water. Finally the ring was dried by briefly heating it in a blue Bunsen burner flame until it glowed red. The glass vessel was also cleaned in alcoholic KOH and then rinsed in Milli-Q water. The vessel containing the sample was then placed in the thermostatted dish and allowed at least 10 minutes to reach equilibrium. The torsion balance was first zeroed with the ring suspended in air close to the liquid. The ring was then immersed in the liquid and the servo-motor in the tensiometer lowered the vessel until the maximum force was measured.

2.2.13 Thin foam film experiments

2.2.13.1 Apparatus

The films are formed in a Scheludko cell and air – water systems are used because of their applications to foams. The scheme of the experimental setup[28] is shown in Figure 2.18. First a rectangular glass cuvette with inner dimensions 20 × 50 mm and 40 mm height is partially filled with water and then a fresh suspension of silica particles is spread (see later) on the water surface. The vertical foam films are formed by crossing the particle monolayer (formed in advance at the air-water interface) with a

circular frame with an inner diameter of 6.2 mm and a thickness of 2 mm. The frame consists of a glass ring fitted inside a PTFE holder. A U-shaped steel needle is connected into the holder and the glass ring through a small hole at the bottom of the frame. The other end of the needle is connected to a glass syringe (Hamilton, 1 mL) by means of flexible PTFE tubing. The frame is mounted on a holder attached directly to the microscope stage and fitted with micrometer screws allowing vertical movement and adjustment of the frame. The syringe is mounted on a separate stage near the microscope. The observations are carried out using a microscope (Optiphot 2, Nikon) with infinity-corrected optics. It was modified by inserting a first surface mirror in the optical path between the objective and the tube lens. In this way, observations in a horizontal direction (*i.e.* parallel to the microscope stage) can be made.

Figure 2.18 Sketch of (a) the experimental setup and close-up of the frame for water films, (b) side view cross - section and (c) front view (re-drawn from ref. 28).
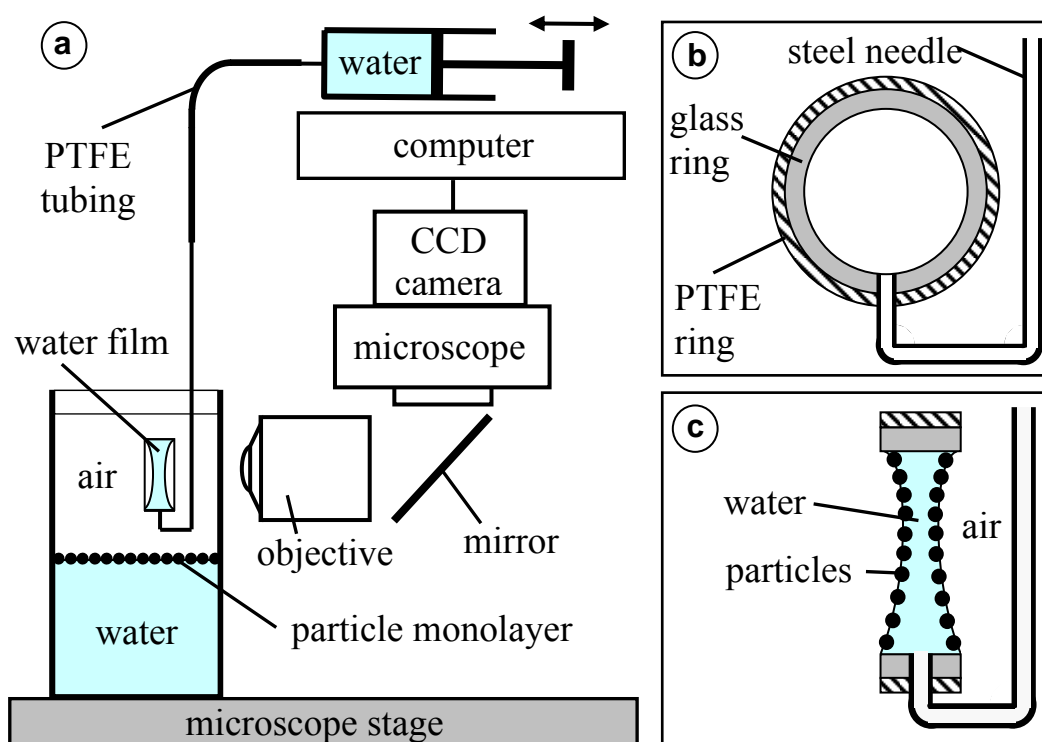
The images of the film taken in transmitted or reflected light are captured by the CCD camera (TK-C1381, JVC), recorded by VCR and processed with Image Pro Plus image analysis software (Nikon).

2.2.13.2 Experimental procedure

All parts of the experimental setup which were in contact with the liquids used were cleaned thoroughly before the experiments. The PTFE tubing was flushed several times first with ethanol and then water. The frame was immersed in ethanol and sonicated for at least 15 minutes by using an ultrasonic bath. The sonication was repeated replacing the ethanol with deionised water. Then, the tubing and frame were rinsed with copious amounts of deionized water and dried before use. The cuvette and the syringes were cleaned with sulfochromic acid and rinsed with large amounts of deionized water. The experiments were performed in the following way. The syringe and tubing were filled entirely with water. Then the rectangular glass cuvette was partially filled with water and the freshly prepared suspension of silica particles was spread at the water surface to form a monolayer of particles at the air-water interface. The density of the monolayer was varied from very dilute to very dense by changing the spread volume in the range 2 - 160 μL. The ring frame was immersed in water (with particles at the surface) and very thick vertical films (air-water-air) were formed after lifting the glass frame from water into the air phase. The film thickness was decreased by sucking out (or increased by pumping in) liquid from the film meniscus using the syringe.

2.2.14 Measurement of contact angles by side imaging technique with an optical microscope

The method used for measuring the contact angle of sulfate latex particles at the air-water interface was based on side imaging of the particles and on simple relations between the contact angle and the geometrical parameters of the adsorbed spherical particle. The particle diameter chosen was 9.6 μm, which is large enough and suitable for measuring the particle contact angle by side imaging technique. The experimental setup was modified in comparison to those described in the literature[29,30]. The sketch of the experimental setup used is shown in Figure 2.19. Particles are spread at the air-water interface by means of isopropyl alcohol to form a dilute monolayer. Then a PTFE tube with an inner diameter of 6.2 mm is immersed into the water, therefore some of the particles are captured at the surface of the air bubble formed at the tip of the bubble. The air-water surface at the tip of the tube is made almost flat by sucking/pumping air using a syringe. The particles attached to the fluid interface are observed with a horizontal

microscope Optiphot 2 (Nikon) supplied with a digital camera (QICAM Fast 1394) in transmitted light and their side images are captured and processed by the computer using Image Pro Plus software. Further details on these measurements will be explained later in Chapter 6.

Figure 2.19 A sketch of the experimental setup for measuring the contact angle of particles at the air-water interface by side imaging with optical microscopy.
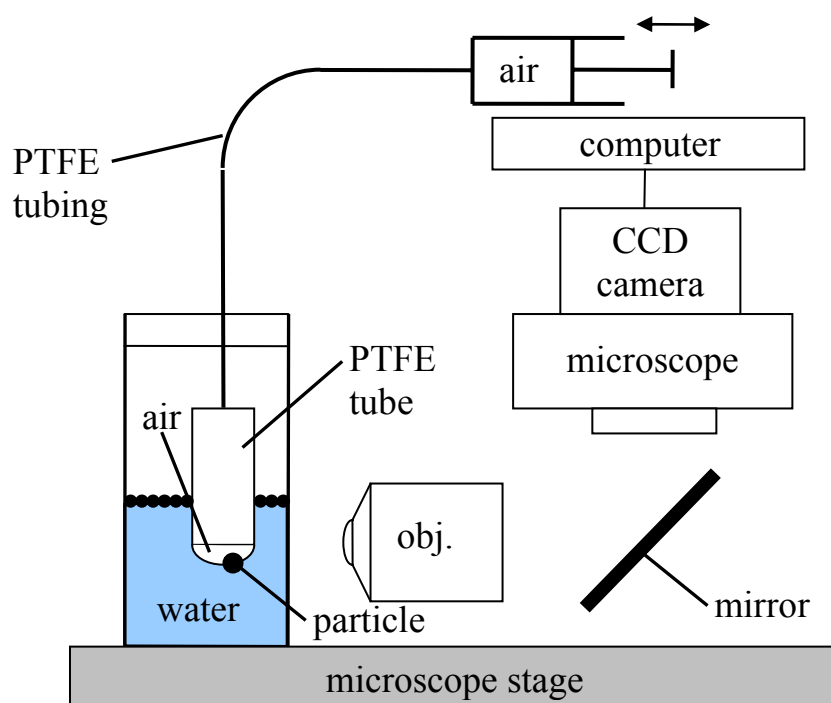
References

1.   CRC Handbook of Chemistry and Physics, 72nd Ed., CRC Press, Boca Raton, (1991).

2.   H.E. Bergna, The Colloid Chemistry of Silica, Advances in Chemistry Series 234, American Chemical Society, Washington (1994).

3.   B.P. Binks and C.P. Whitby, *Colloids Surf. A*, **253**, 105 (2005).

4.   R.K. Iler, The Chemistry of Silica, John Wiley & Sons, New York (1979).

5.   W. Stöber, A. Fink and E. Bohn, *J. Colloid Interface Sci,*, **26**, 62 (1968).

6.   A. Van. Blaaderen, J. V. Geest and A.Vrij, *J. Colloid Interface Sci*., **154,** 2 (1992).

7.   D.L. Green, J.S. Lin, Y-F Lam, M.Z.C. Hu, D.W. Shaefer and M.T. Harris, *J. Colloid Interface Sci.,* **266,** 346 (2003).

8.   T.S. Horozov, R. Aveyard, J.H. Clint and B.P. Binks, *Langmuir*, **19**, 2822 (2003).

9.   Laponite - The Technical Directory, Laporte Industries Ltd., Widnes, (1999).

10.   Laponite Performance - Focused attributes in rheology and speciality film forming applications, CommuniClay, Rockwood Specialities Inc., Vol. 1, (2001).

11.   IDC Ultraclean Uniform Latex Particle Microspheres, Interfacial Dynamics Corporation, Oregon (2000).

12.   M.C. Wilkinson, J. Hearn and P.A. Steward, *Adv. Colloid Interface Sci.*, **81**, 77 (1999).

13.   M.J. Rosen, Surfactants and Interfacial Phenomena, 3rd Ed., John Wiley and Sons, New Jersey (2004).

14.   M.L. Hair, *J. Colloid Interface Sci.*, **60**, 154 (1977).

15.   Krüss DSA10 Drop Shape Analysis, User Manual, V010905, Hamburg (2001).

16.   A.W. Adamson, Physical Chemistry of Surfaces, 5th Ed., John Wiley and Sons, New York, (1990).

17.   Size measurements, Malvern Instruments Ltd., Manual Number MAN0149, Issue 1.1 (1997).

18.   R.J. Hunter, Introduction to Modern Colloid Science, Oxford Science Publications, New York, Chapter 3 (1993).

19.   PCS Training Manual, Malvern Instruments Ltd., Part 2: Zeta Potential – theory of operation (1998).

20. Zeta Potential measurements, Malvern Instruments Ltd., Manual Number MAN0150, Issue 1.1 (1997).

21. Zetasizer Nano Series User Manual, Manual Number MAN0317, Issue 1.1, http://www.indiana.edu/~physbio/images/Zetasizer%20Nano%20user%20manual%20---%20Man0317-1.1.pdf (2004).

22. User Manual for Bohlin Rheometers, Brochure 800014, Bohlin Instruments, (2001).

23. Cryo Transfer Scanning Electron Microscope (Cryo-SEM) Made Easy, Marilyn Carey, Gatan, UK, http://www.gatan.com/knowhow14/cryo.htm (2006).

24. Tursbican Lab guide, Formulaction, UK (2006).

25. W.D. Harkins and H.F. Jordan, *J. Am. Chem. Soc.*, **52**, 1751 (1930).

26. B.B. Freud and H.Z. Freud, *J. Am. Chem. Soc.*, **52**, 1772 (1930).

27. H.H. Zuidema and G.W. Waters, *Ind. Eng. Chem.*, **13**, 312 (1941).

28. T.S. Horozov, R. Aveyard, J.H. Clint, *Langmuir*, **21**, 2330 (2005).

29. Z. Horvolgyi, S. Nemeth, J.H. Fendler, *Colloids Surf. A*, **71**, 327 (1993).

30. R. Aveyard, J.H. Clint, D. Nees, V.N Paunov, *Langmuir*, **16**, 1969 (2000).

CHAPTER 3

CHAPTER 3

FOAMING ABILITY AND STABILITY OF AQUEOUS HYDROPHILIC SILICA PARTICLES

3.1   Introduction

Aqueous foams are both thermodynamically and kinetically unstable systems that collapse as a result of liquid drainage, rupture of films and bubble disproportionation due to gas diffusion. It is known that it is not possible to obtain stable (long-living) foams from pure liquid. To stabilise foams, surfactants or proteins are generally used, whose molecules cover the air-liquid interfaces. This is possible because surfactant molecules have an amphiphilic structure where part of the molecule prefers to be in air and the other part prefers to be in water. Solid particles do not have an amphiphilic structure, but exhibit some similarities with such molecules by adsorbing at interfaces.[1] In the literature, it has been mentioned that solid particles can enhance foaming if they have suitable wetting properties that allow them to go to the air-liquid interface (as described in more detail in Chapter 1). In most of the foams studied previously, the solid particles have been used in combination with surfactants, in which they were found to either stabilise or destabilise bubbles in foams. It is only recently, however, that their precise role is being elucidated in surfactant-free systems. Foam stabilisation solely by particles may be valuable for applications in which surfactants are to be avoided. Foam stability can also be drastically improved by using particles instead of surfactants, since particles tend to adsorb irreversibly at the air-water interface.[1] The adsorption of particles reduces the highly energetic interfacial area and lowers, therefore, the free energy of the system. Such a reduction in free energy makes the interfacial adsorption of particles an irreversible process, as opposed to the continuous adsorption and desorption of conventional surfactant molecules at the air-water interface. However, physical mechanisms for foam formation in the presence of colloidal particles alone are poorly understood.

This study is aimed at enhancing the basic understanding of the mechanisms that produce foaming in a three-phase system, containing solid, liquid and gas, and identifying key parameters that enhance the foaming ability and stability in the absence of surface–active agents. Therefore, a first attempt was made to establish that silica particles, which are hydrophilic in nature, could cause foaminess in the absence of

surface-active agents by engineering conditions and changing *in situ* their hydrophobicity. In order to prove this hypothesis, a systematic study was carried out on the foaming ability (initial foam volume) and foam stability (time that foam decays) of aqueous dispersions of nanosized hydrophilic silica particles by using the glass cylinder shaking test. The key parameters investigated, and described in this chapter, were particle size, particle concentration, effect of NaCl and effect of pH. In this study no surfactant was used either to modify surface characteristics or to create foam, therefore foam stability can confidently be assigned to the solid alone. Stock dispersions of hydrophilic silica particles of different diameters were dispersed in pure water and as expected such particles do not cause foaming. Two different protocols were used to disperse the stock silica dispersions in aqueous NaCl at different pH values (as described in Chapter 2). When protocol 1 was used, it was observed that when NaCl was added to the aqueous silica dispersions of smaller diameter (3.5 and 5.5 nm), the dispersion starts to become viscous which then gels very quickly at any pH. However, when NaCl was added to the aqueous dispersions with larger particles (*e.g.* ~ 100 nm) at pH ~ 9, the dispersion remained stable for longer and only started to become viscous and particle sedimentation observed at a later stage (after days). No gel formation or precipitation of particles was observed for all pH and [NaCl] when protocol 1 was used. When protocol 2 was used, it was found that after adding aqueous NaCl solution (*e.g.* 3 M NaCl) directly to the concentrated stock aqueous silica dispersion (pH ~ 9) without dilution, the silica particles start to form a white precipitate and the dispersion gelled. It seems that adding the stock of silica directly into the salt solution instead of first dispersing it in salt-free water and subsequently raising the ionic strength causes the silica to precipitate and gel before it can fully disperse. After adding HCl to this solution, particles do not re-disperse (particles are strongly coagulated and remain at the bottom of the vessel). Therefore, protocol 1 was the method chosen and used in this study as dispersions seemed initially more stable and easier to control. The first parameter studied was the effect of particle size and is discussed below.

3.2   Effect of particle size

One of the most important features of colloidal particles is their physical dimension. The effectiveness of a colloid can be predicted on the basis of the particle surface area. Particle size is one of the two main factors that determine the particle surface area of a colloid. Another important parameter in determining the total particle surface area is the particle concentration, which is described below in section 3.3. Particle surface area is inversely proportional to particle size, which means that for a constant concentration of particles, the surface area increases as the particle size decreases.[2]

Researchers have found conflicting results concerning the effect of the size of solid particles on the foaming ability and stability of aqueous systems. These studies are briefly reviewed here. Most of these studies, as mentioned before, were carried out in the presence of surfactants. For example, Ralston[3] reported that the presence of small solid particles enhances foam stability. Tang *et al.*[4] found that the most important factor governing foam stability was particle size; the smaller the particle, the more stable the foam. However, the role of solid particles on foam stabilisation was not explained. The particle size investigated was below 0.7 μm. Hudales and Stein[5] by contrast found that larger particles of hydrophilic glass in a cetyltrimethylammonium bromide (CTAB) solution increased foam stability by decreasing the drainage of free vertical films, while smaller particles had no influence on foam drainage. The particle size used in their study was in the range of 1-10 μm. Recently, there has been increased interest from researchers and an increase in literature regarding foams stabilised solely by solid particles. However, most of these studies, reported foaming systems of one particular size of particles. Therefore, the effect that particle size has on the foaming ability and stability of aqueous systems is still not fully understood. Wilson[6] explored the foaming behaviour of relatively large, charged polystyrene (PS) latex particles with diameters ranging from 1.02 to 3.89 μm. The results showed that the foam quality decreased as the particle diameter was reduced, with the minimum particle diameter required to obtain stable foams being approximately 1.50 μm (stable foams could not be prepared using 1.02 μm PS latex). Bindal *et al.*[7] used silica particles of diameters ranging from 8 nm to 100 nm to investigate the effect of particle size on foaminess in water-containing systems. The results revealed that foaminess was inversely proportional to the size of the particles in their system, since a larger size implies a lower effective volume fraction

(and smaller particle layering) for a constant volume fraction. However, it is worth commenting that the foam generated by their study using different particle sizes had negligible foam stability. As soon as the aeration was stopped, the foam collapsed. Therefore, the stability and structure of the foams generated could not been studied in any detail. Another study by Ip et al.[8] investigated the effect of different sized SiO_2 particles ranging from 45 to 150 μm on the stability of aluminium foams. Their results showed that foam stability increased with decreasing particle size. This was attributed to the fact that for smaller particles at constant volume fraction, the number of particles in the slurry increased and consequently a higher surface coverage of the bubbles was obtained. Aluminium foams are thought to be primarily stabilised by ceramic particles such as SiC, but the underlying physics is not understood, and surface-active impurities are commonly present.[9] Recently, Fujii et al.[10] evaluated a wide range of latexes as possible foam stabilisers. This study used different latexes ranging in diameter from 170 nm to 1.62 μm. The results showed that the minimum latex diameter (260 nm) required to form stable foams is significantly lower compared to that reported by Wilson[6] who required latexes of at least 1.50 μm diameter. It can be concluded by the contradictory results reported by the various authors that more studies are needed concerning the effect of particle size on both foaming ability and foam stability of aqueous systems.

To investigate the effect of particle size on foaming ability and foam stability, 3.5, 25, 34 and 100 nm aqueous dispersions of hydrophilic silica particles at a fixed concentration of 5 wt. %, [NaCl] = 3 M and at pH 4.2 were used. The reason for choosing this particular concentration of NaCl and pH is due to the fact that at this stage in the investigation these were the conditions found to give the more stable foams. The results reveal that foamability increases gradually with particle size (see Figure 3.1). However, for 3.5, 25 and 34 nm particles, the ratio of the initial foam volume to the foam bursting time was very similar (~ 1), therefore they were all equally unstable (foams collapsed completely after a few seconds). The largest silica particles of diameter ~ 100 nm were found to give the most stable foam. After 48 hours, 5 mL of foam was still remaining at the top of the aqueous dispersion.

Figure 3.1 Initial foam volume formed from 20 mL aqueous dispersion of silica particles at [particle] = 5 wt. %, pH = 4.2, [NaCl] = 3 M.
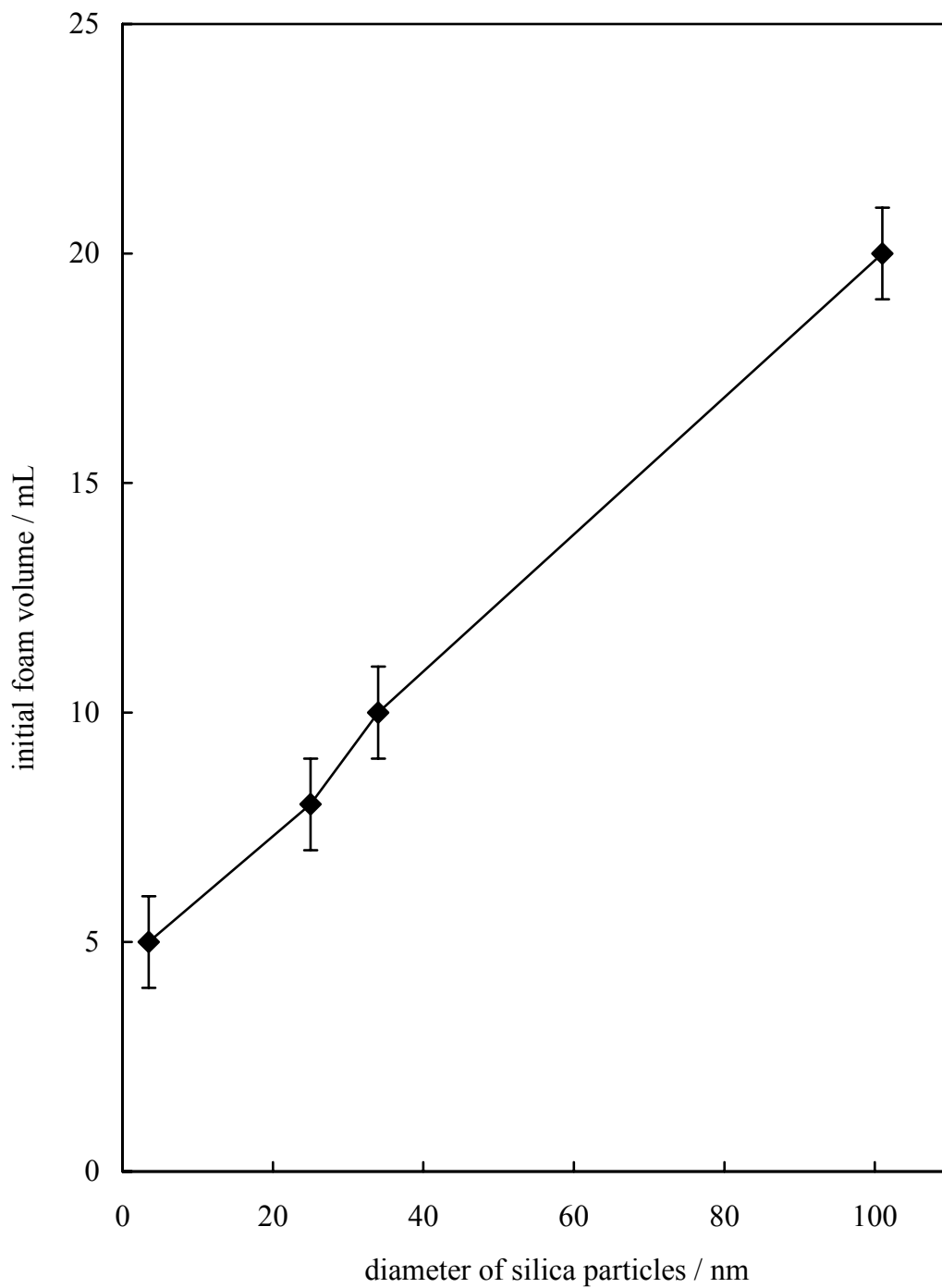
As mentioned before, aqueous dispersions containing smaller silica particles were more unstable and gelled quicker than the larger silica particles of diameter 100 nm at a fixed particle concentration. The rate of gelling appears to be proportional to the total area of silica surface present in a given volume of dispersion. Since the specific surface area of silica varies inversely with the particle diameter, dispersions having the same ratio of concentration to particle diameter gel at about the same rate.[11] Thus, at a fixed particle concentration of 5 wt. %, a dispersion of 5 nm particles is expected to gel much quicker than the 100 nm particles. In order to enhance foamability, particles should be able to promptly adsorb on the air bubble surface, thus if the aqueous phase is gelled quickly, particles will lose their mobility and this will hinder foam formation. This could explain why the smaller size particles used here were unable to produce a reasonable amount of foam and they were very unstable. Since the energy of attachment of a particle to an interface, E, depends on the square of the particle radius, it decreases markedly for very small particles and detachment is easy and therefore they may not be too effective as foam stabilisers compared to the larger particles. Therefore, it can be concluded that the size of particles has implications with respect to the rate at which particles can diffuse and arrive at the surface of newly formed bubbles, to prevent disproportionation.

All further experiments were performed with silica particles of diameter 100 nm, as it was discovered at this stage that only these particles could give reasonable foam volumes and stable foams, depending on particle concentration, pH and NaCl concentration.

3.3   Effect of particle concentration

Particle concentration is an important parameter in particle-stabilised foams, which can influence both foamability and stability. To understand how the concentration of silica particles in the dispersions would affect the nature and amount of foaminess, a systematic study was carried out for four concentrations of silica particles of 101 nm at a fixed concentration of NaCl (*e.g.* 3 M) and pH ~ 4-5. When the particle concentration was increased from 1-10 wt. %, the initial foam volume increased from 12 to about 25 mL (Figure 3.2) and the foam stability increased as well (Figure 3.3). The bubbles were polydisperse in size with an approximate size of 0.5-3 mm, with

smaller size bubbles at the bottom and the bigger bubbles at the top of the solution which burst quicker. The smaller size bubbles remained for longer time at the bottom.

The foam volumes (foamability) obtained here was not very high compared to that formed by surfactant, like for example, sodium dodecyl sulphate (SDS). Nevertheless, the stability of these foams was greater than SDS foam (see Figure 3.4). As a thermodynamically unstable system, the breakdown of the foam is inevitable. The SDS foam was completely broken after 24 hours. The instability of the foams (air + water) formed in this study seems to be mainly due to drainage of water; it was observed after some time that the volume fraction of liquid in the foam was lower at the top of the foam and higher at the bottom. For the foams formed with silica particles it can be seen that not all the particles are in the foam sice a cloudy dispersion was observed in the liquid below. An increase in particle concentration seems to cause a closer packing of particles, resulting in an increase in surface viscosity, a decrease in drainage rate, and therefore, an increase in foam stability. The foams seemed stable against disproportionation and coalescence of bubbles. This is in agreement with the results reported by other researchers. The same concentration effect on foaminess is reported by Tang *et al.*,[4] but for silica particles which were surface treated and in the presence of surfactants. They found that the presence of silica particles decreased the surface tension, which implies that hydrophobic particles were concentrated at the interface and the drainage process governed the foam collapse.

A number of non-DLVO surface forces have been discovered experimentally. The oscillatory structural force is one of them and appears during the thinning of thin liquid films containing colloidal particles.[1] This force affects the stability of foam films. At high particle concentrations this force stabilises the films, whereas at low concentrations it degenerates into the depletion force which is found to destabilise films.

Figure 3.2 Initial foam volume versus particle concentration for 20 mL aqueous dispersions of silica particles of diameter 100 nm at pH = 4.5 and [NaCl] = 3 M.
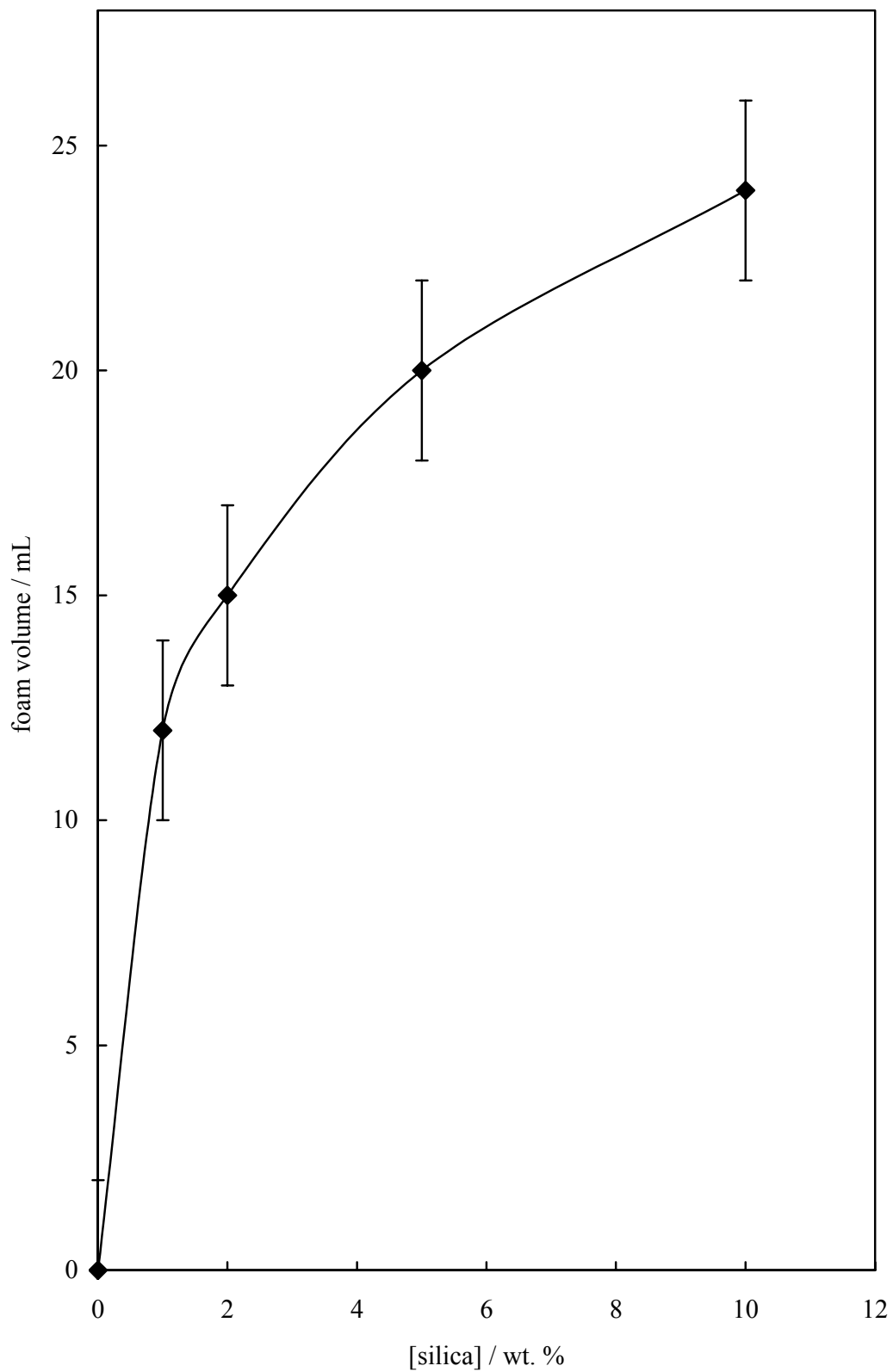
Figure 3.3 Foam volume versus time for 20 mL aqueous dispersions of silica particles of diameter 100 nm, [NaCl] = 3M and pH ~ 4.25 at different concentrations.
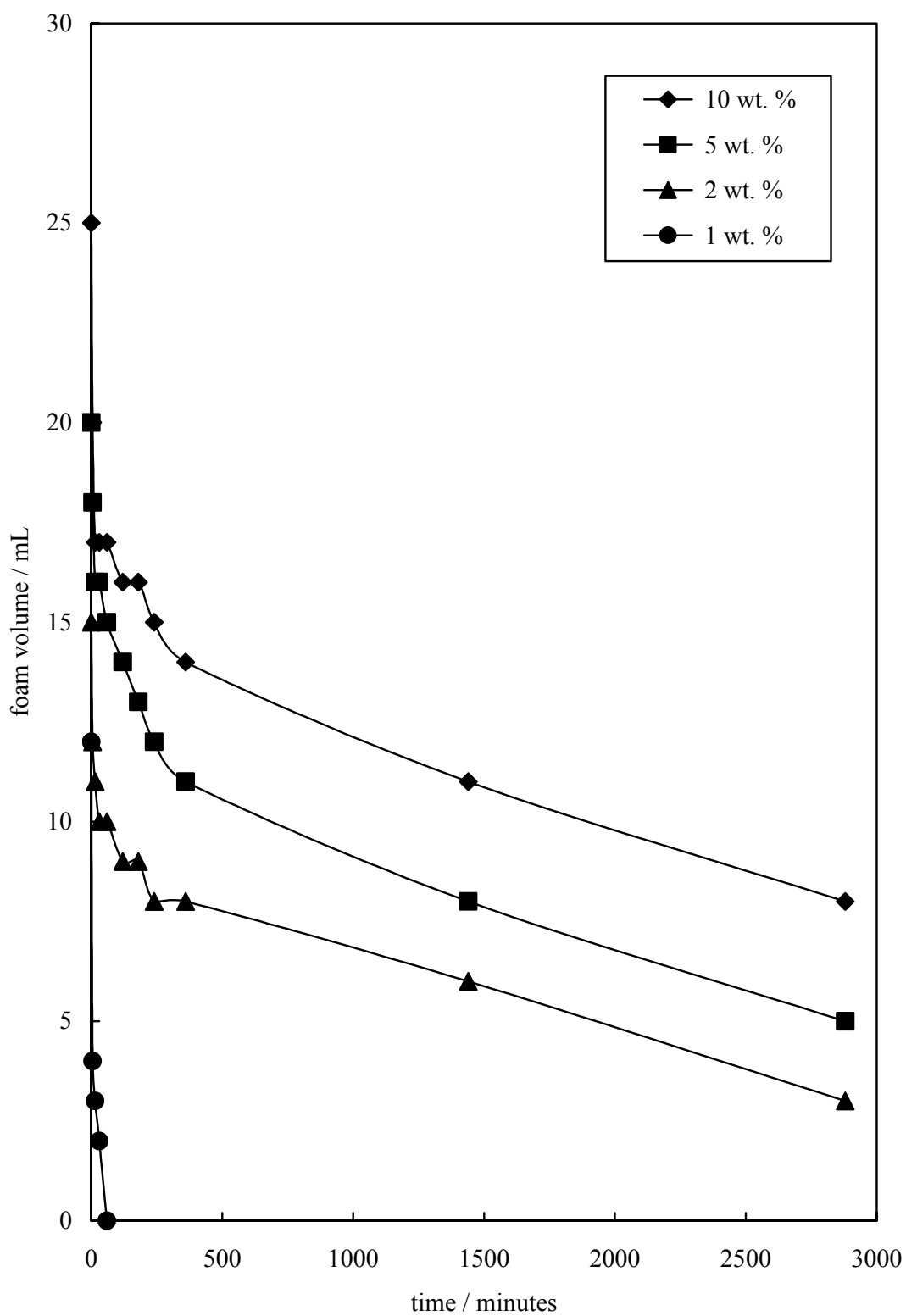
Figure 3.4 Appearance of vessels after 30 minutes (a), 24 hours (b) and 48 hours (c). The left vessel is an aqueous SDS foam at the c.m.c. (8×10^{-3} M). The right vessel corresponds to the foam formed with 5 wt. % aqueous silica particles of diameter 100 nm at pH ~ 4.50 and [NaCl] = 3 M.

(a)
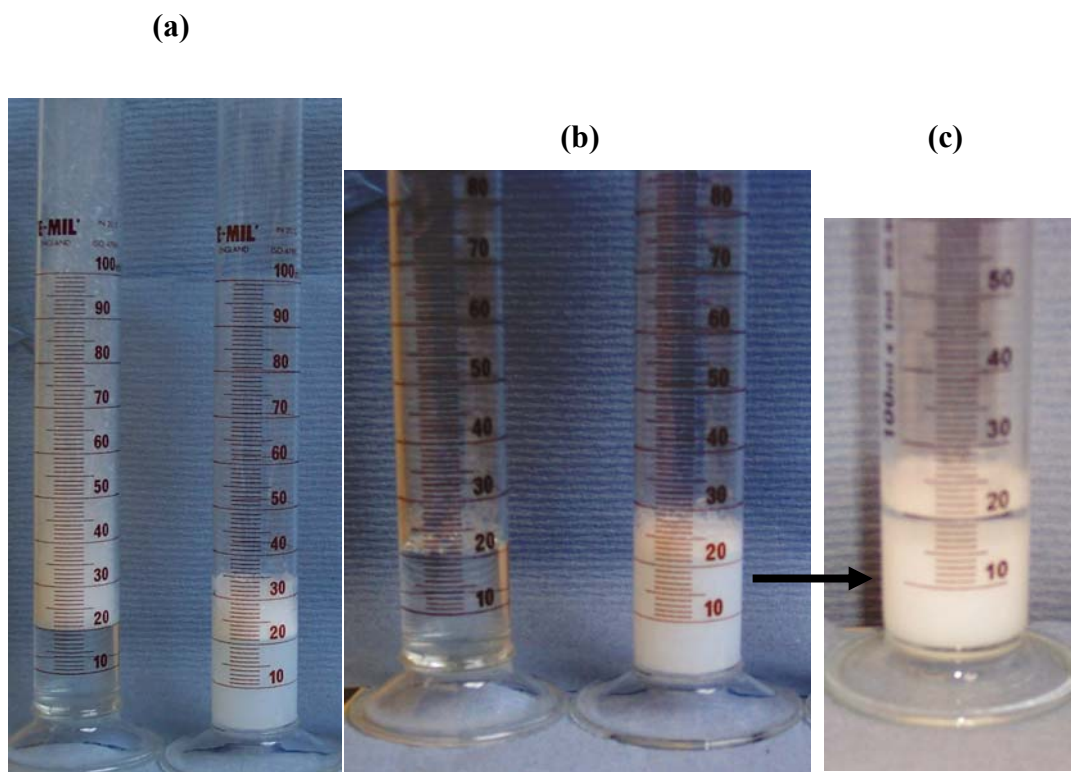
The study of Bindal *et* al.[7] also showed that particle concentration is directly proportional to foaminess. They proposed that in the absence of surface-active agents, foaminess is caused by the colloidal particle self-layering phenomenon inside the confined boundaries of the foam lamellae, *i.e.* bare interfaces. This kind of particle self-layering provides a structural barrier against the coalescence of bubbles. A higher concentration of solid particles leads to a better particle-layered structure inside the film, which is in turn reflected in the higher foam lamella stability and foaminess observed in their systems. However, the foams generated in their system collapsed a few seconds after the aeration was stopped, so their results are important in terms of foaming ability (foaminess) but not in terms of foam stability. Monte Carlo simulations showed that at high particle concentrations the energy needed to withdraw a particle from the film is high, due to the improved in-layer structure, thus inhibiting particle diffusion and enhancing film stability.[1] It is still unclear, however, how hydrophilic silica particles accumulate at the interface and provide any kind of stabilisation, without

using any other surface-active agent. This stabilization effect can be attributed to the addition of sodium chloride to the silica dispersions at a particular pH value.

3.4   Effect of pH

The pH of silica dispersions is one of their most important characteristics. Silica dispersions may vary greatly with only minor change in pH as observed in this study. The effect of pH is also very important on the foaming properties. To study the effect of pH, a fixed concentration of silica particles (5 wt. %) and fixed concentration of NaCl (e.g. 3 M) was used. Varying the pH of the dispersions, from alkaline to acidic conditions, a maximum in foamability and foam stability was found at approximately pH 4-4.5. Figure 3.5 shows the foamability data and Figures 3.6 and 3.7 display the foam stability in two different ways. Figure 3.6 show the foam volume decay with time at different pH whereas Figure 3.7 show the foam half-life (time taken for the foam to decay to half its initial volume) versus pH.

Destabilisation of the particle dispersion at pH around 4-4.5 was noticed due to the flocculation of particles, followed by their sedimentation with time, which was observed visually. The aggregation of particles occurred at this pH since particles were uncharged and did not repel each other. At acidic pH (lower than 4) and at alkaline conditions dispersions were more stable. Thus interparticle interactions in the particle dispersion had an influence on the foamability and foam stability of the aqueous dispersions, as discrete particles were not able to stabilise foams, in contrast to aggregated particles which gave the more stable foams. This will be discussed in detail in section 3.7.

Figure 3.5 Initial foam volume versus pH for 20 mL aqueous dispersions of silica particles of diameter 100 nm, [particle] = 5 wt.% and [NaCl] = 3 M.
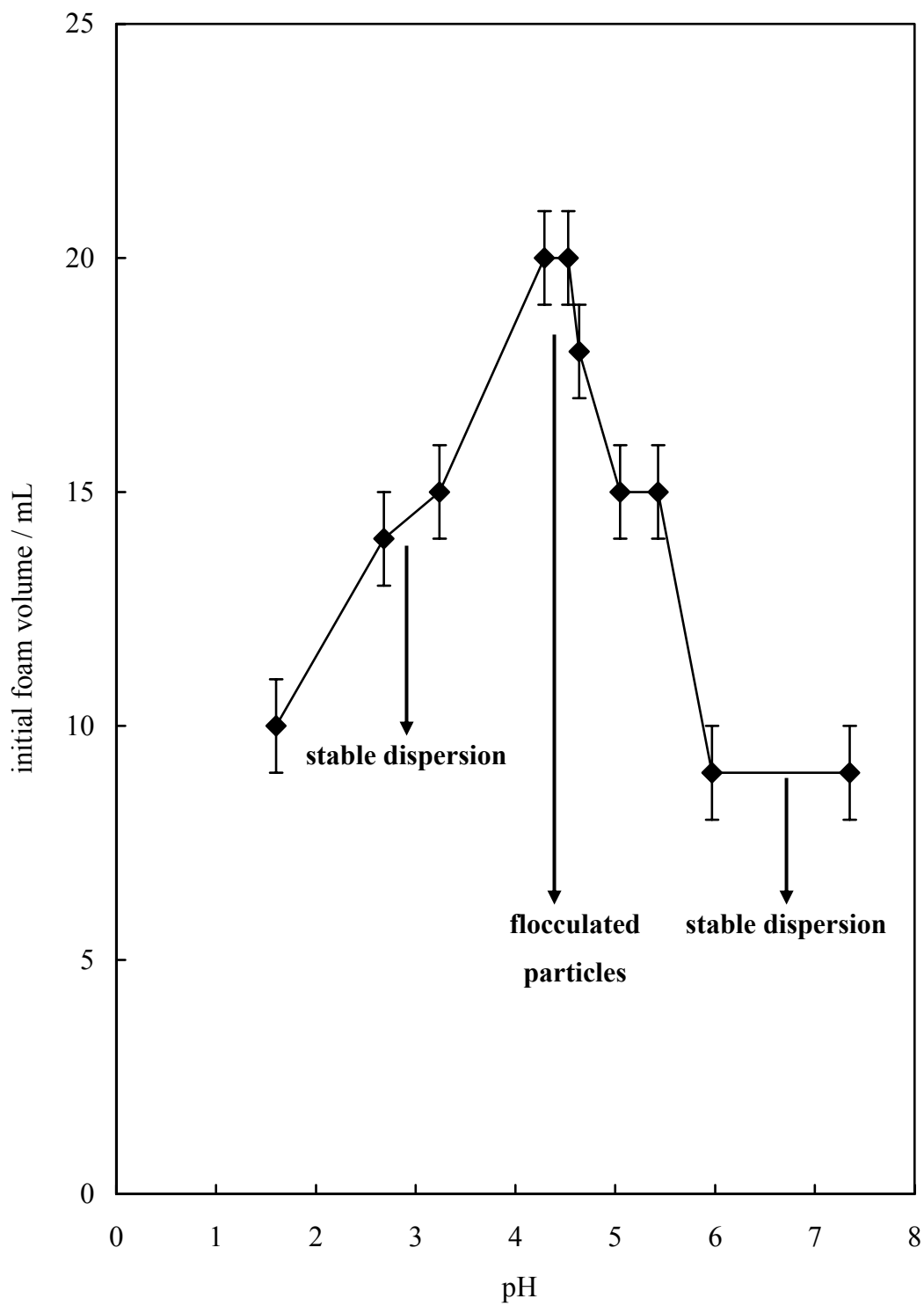
Figure 3.6 Foam volume versus time for 20 mL aqueous dispersions of silica particles of diameter 100 nm, [particle] = 5 wt. %, [NaCl] = 3M at different pH. The points at pH = 7.35, 2.68 and 1.60 can not been seen in the graph because they were very unstable and burst in a few seconds.
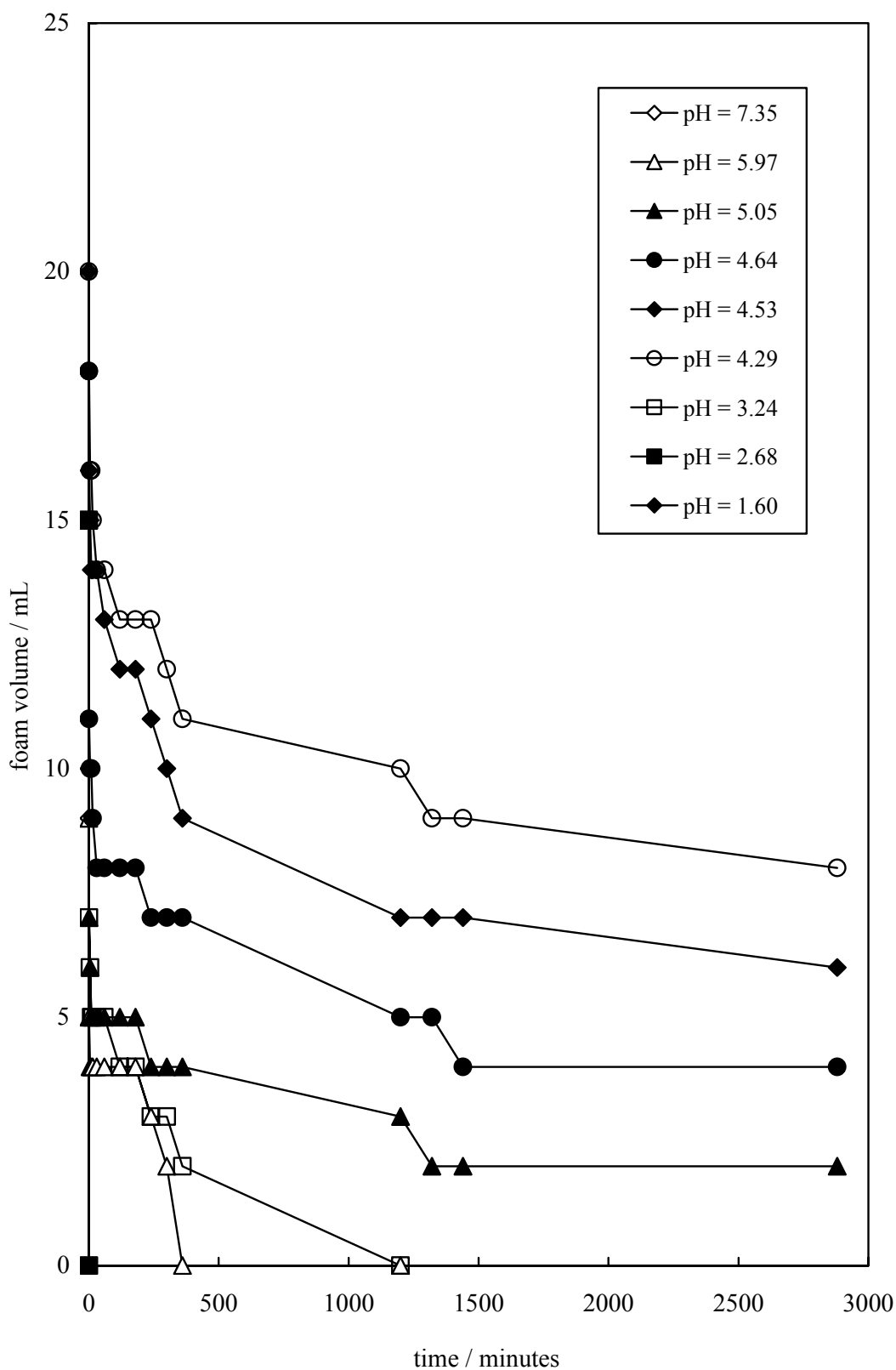
Figure 3.7   Foam half-life versus pH for 20 mL aqueous dispersions of silica particles of diameter 100 nm, [particle] = 5 wt. %, [NaCl] = 3M.
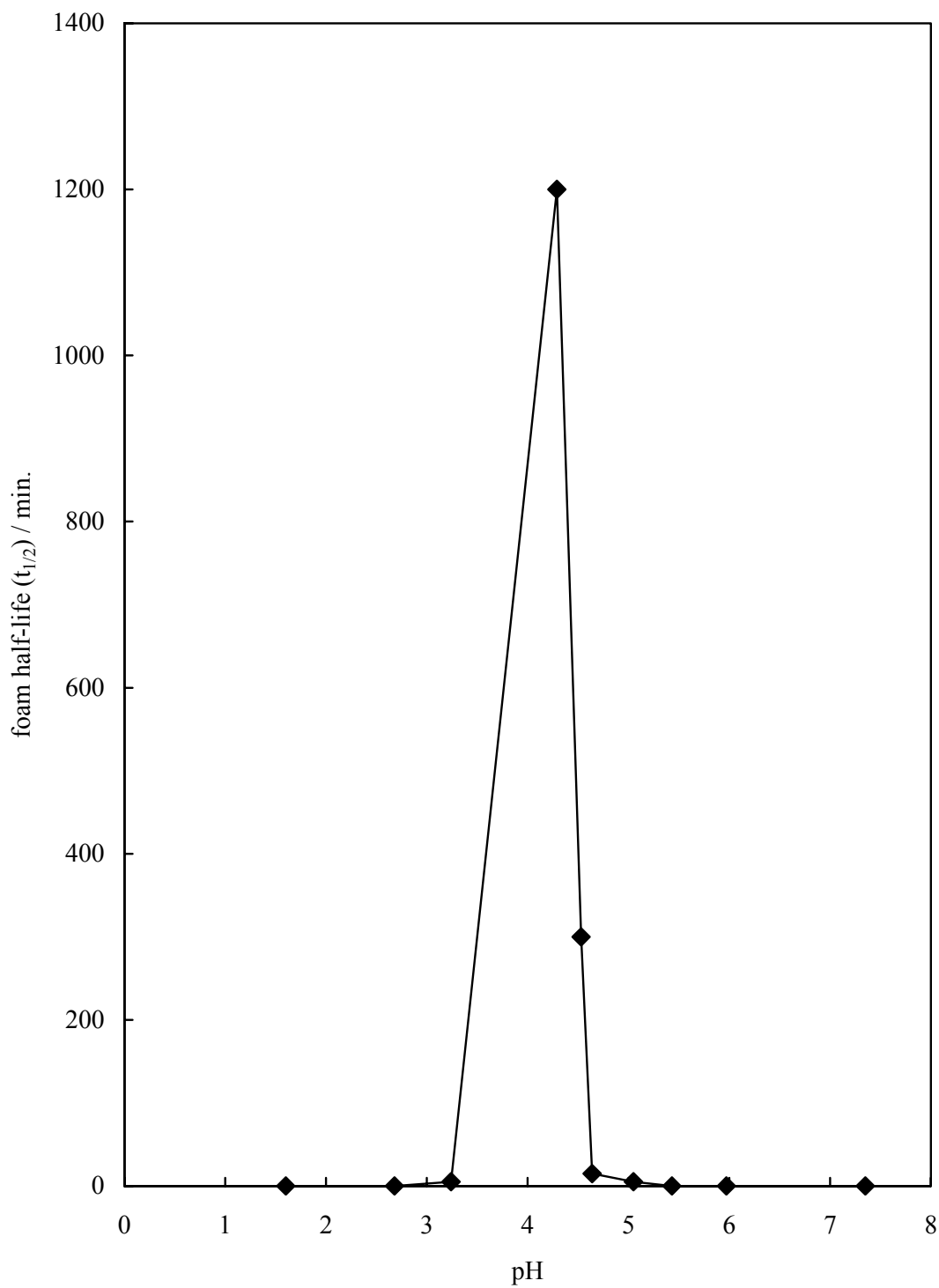
After observing that at pH 4-5, the foams volumes were higher and foam stability increased dramatically, more experiments were carried out with dispersions in this narrow pH range. Again, a maximum in foaming occurs at pH 4.4, see Figure 3.8. However, the foam stability taken by calculating the foam half-life ($t_{1/2}$), shown in Figure 3.9, shows a sharp decrease from pH 4.0 to pH 5.2. This means that at pH 4.0 the top of the foam takes longer to decay initially, therefore they are more stable compared to the foams obtained with other pH values, where a rapid foam decay occurs. Although these foams initially decay quite quickly, once they reach a certain volume they all behave similar and remain stable for a longer period of time (see Figure 3.10).

By increasing the concentration of silica in the aqueous dispersion from 5 to 10 wt. % and fixed [NaCl] = 3 M, at 3 different pH around 4-5 it was found again that the foamability and stability decrease from pH 4 to 5 (see Figures 3.11 and 3.12). To check the reproducibility of the experiments performed, two experiments at the same conditions were repeated: particle concentration = 5 wt. %, pH around 4.20, [NaCl] = 3 M (see Figure 3.13). The results show that foamability is approximately the same (error of ± 2 mL) and therefore foam volumes start to decrease at a similar rate. The foam half-life was found to be about 18-20 hours for both systems studied.

Figure 3.8 Initial foam volume versus pH for 20 mL aqueous dispersions of silica particles of diameter 100 nm, [particle] = 5 wt. %, [NaCl] = 3 M.

Figure 3.9   Foam half-life versus pH for 20 mL aqueous dispersions of silica particles of diameter 100 nm, [particle] = 5 wt. %, [NaCl] = 3M.

Figure 3.10 Foam volume versus time for 20 mL aqueous dispersions of silica particles of diameter 100 nm, [particle] = 5 wt. %, [NaCl] = 3M at different pH.
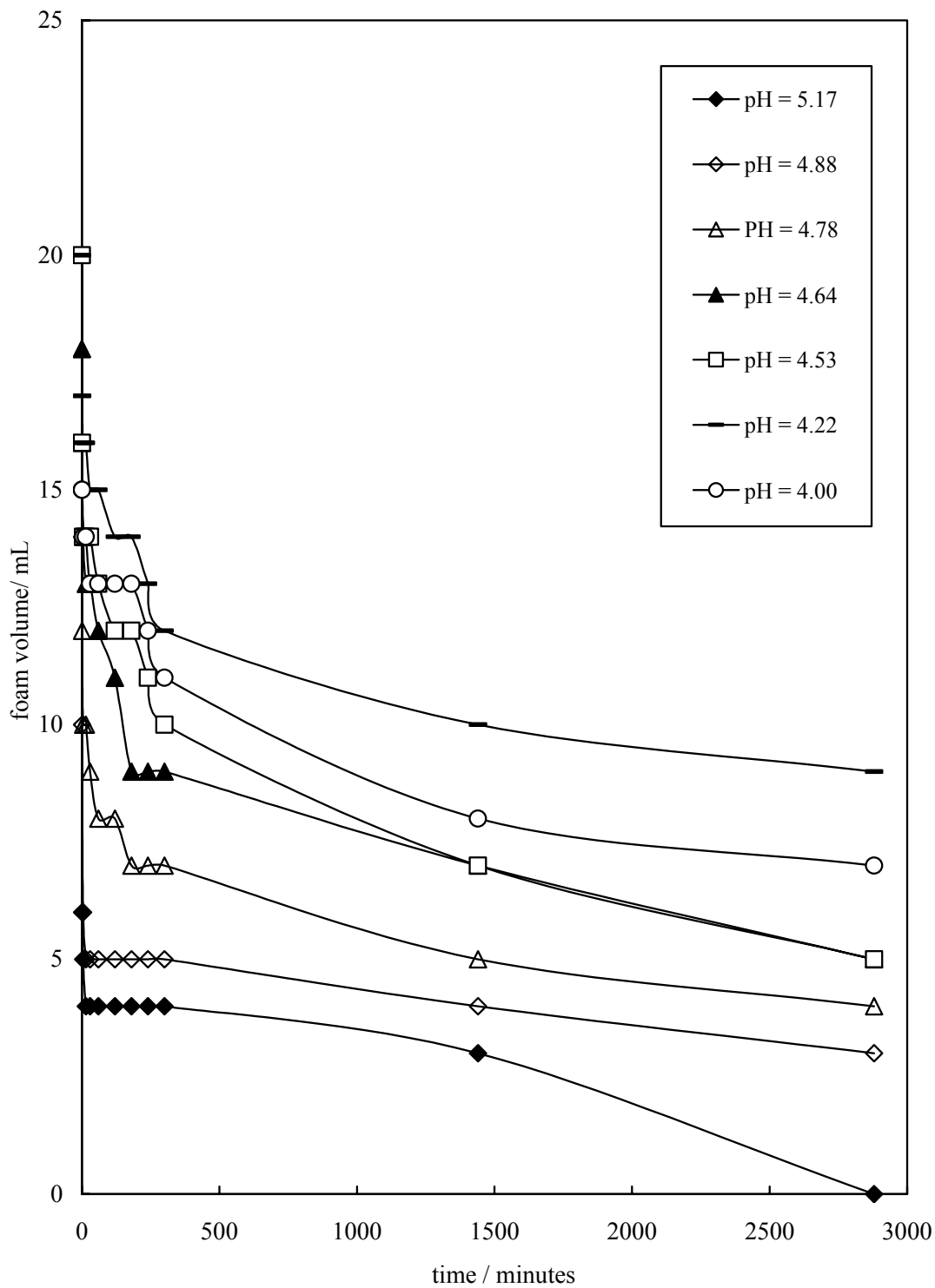
Figure 3.11 Initial foam volume versus pH for 20 mL aqueous dispersions of silica particles of diameter 100 nm, [particle] = 10 wt. %, [NaCl] = 3 M.
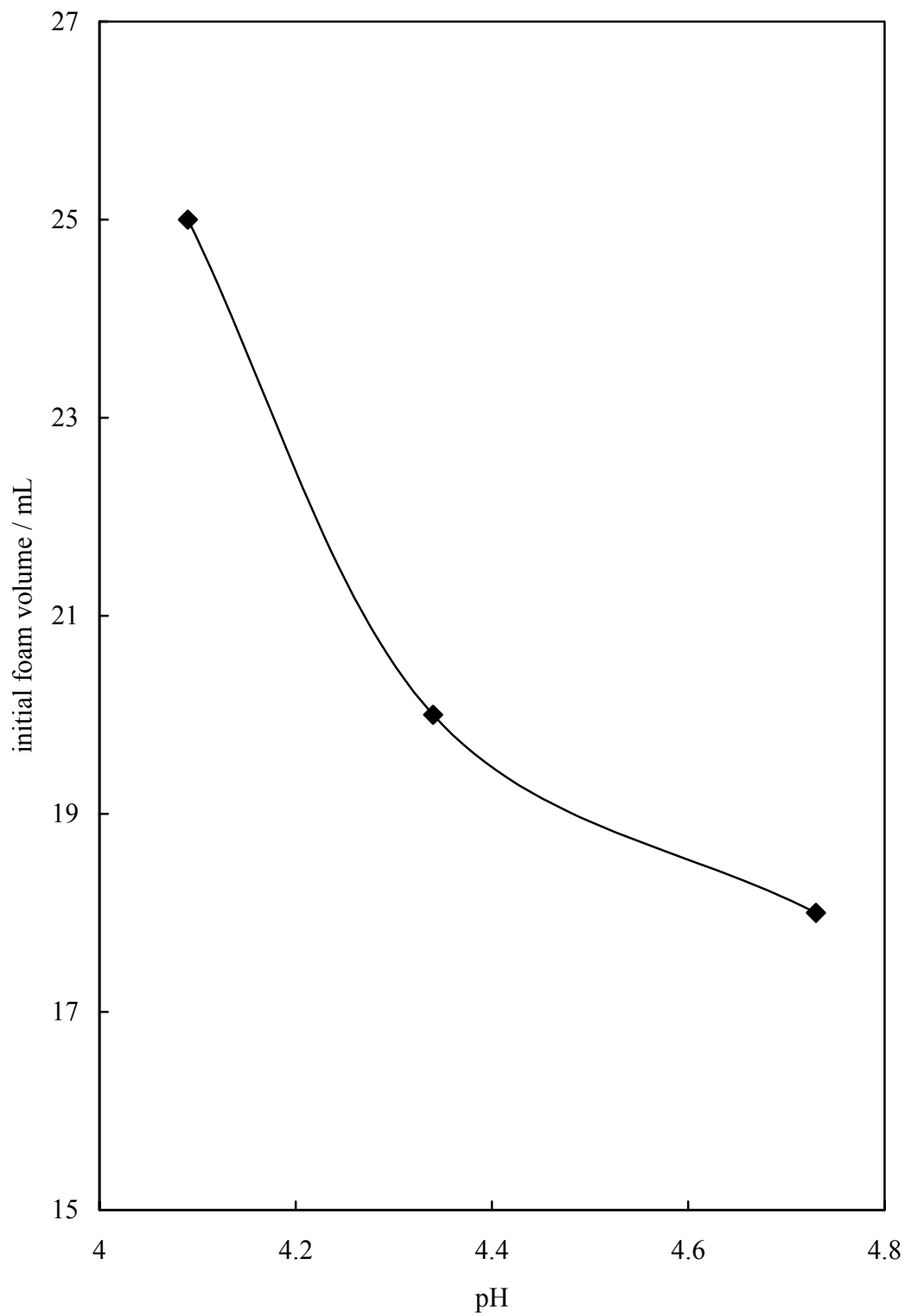
Figure 3.12 Foam volume versus time for 20 mL aqueous dispersions of silica particles of diameter 100 nm, [particle] = 10 wt. %, [NaCl] = 3 M at different pH.
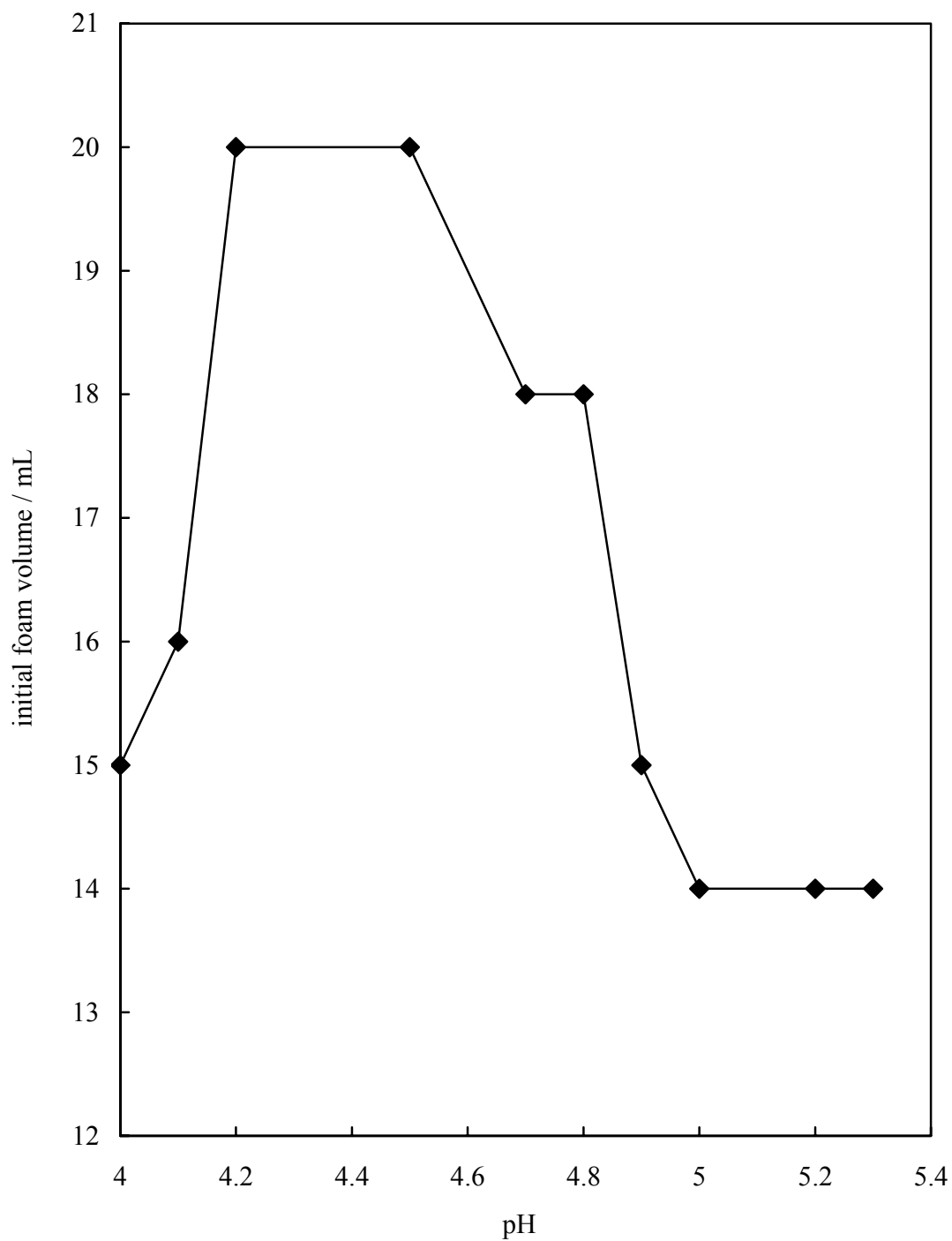
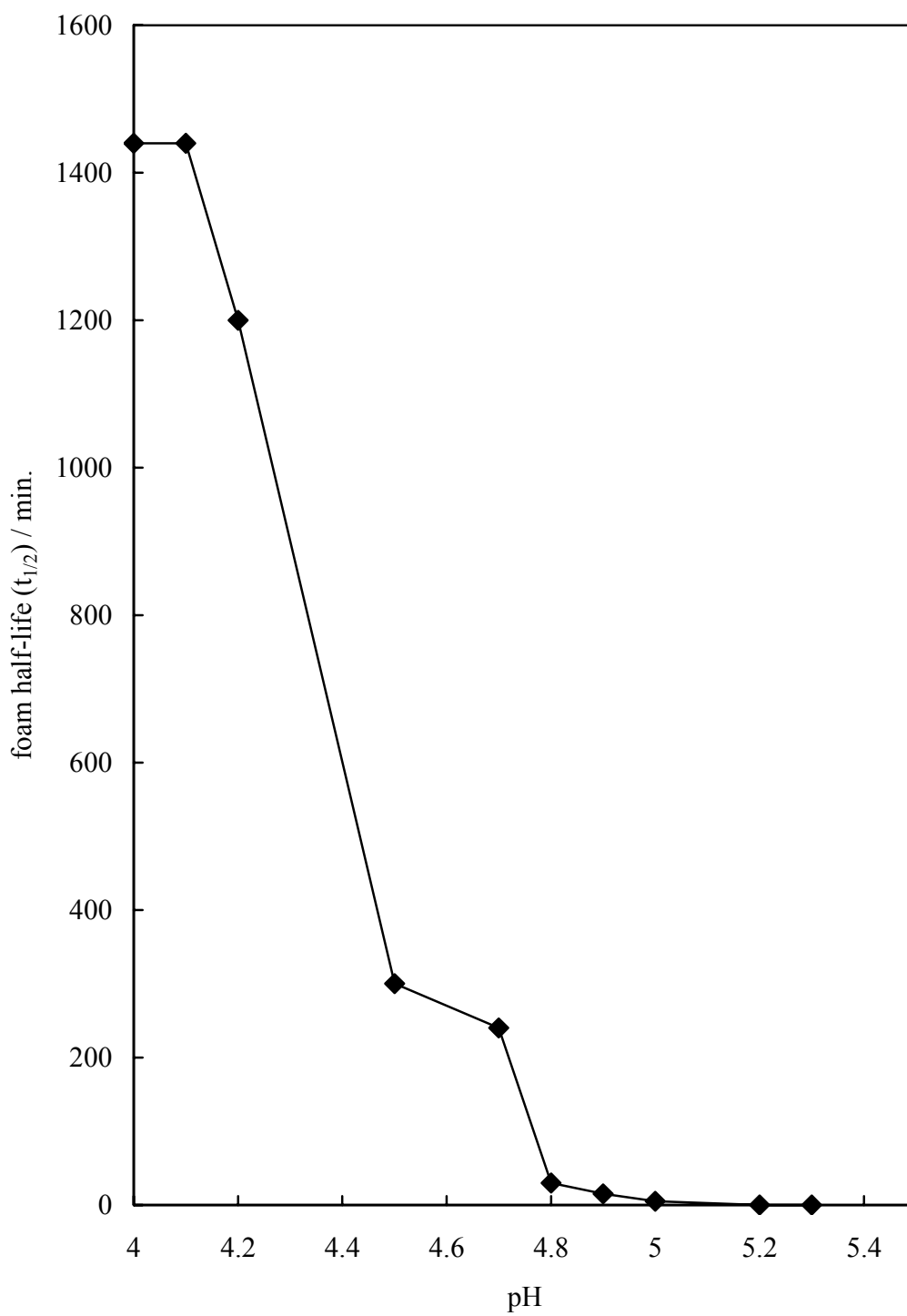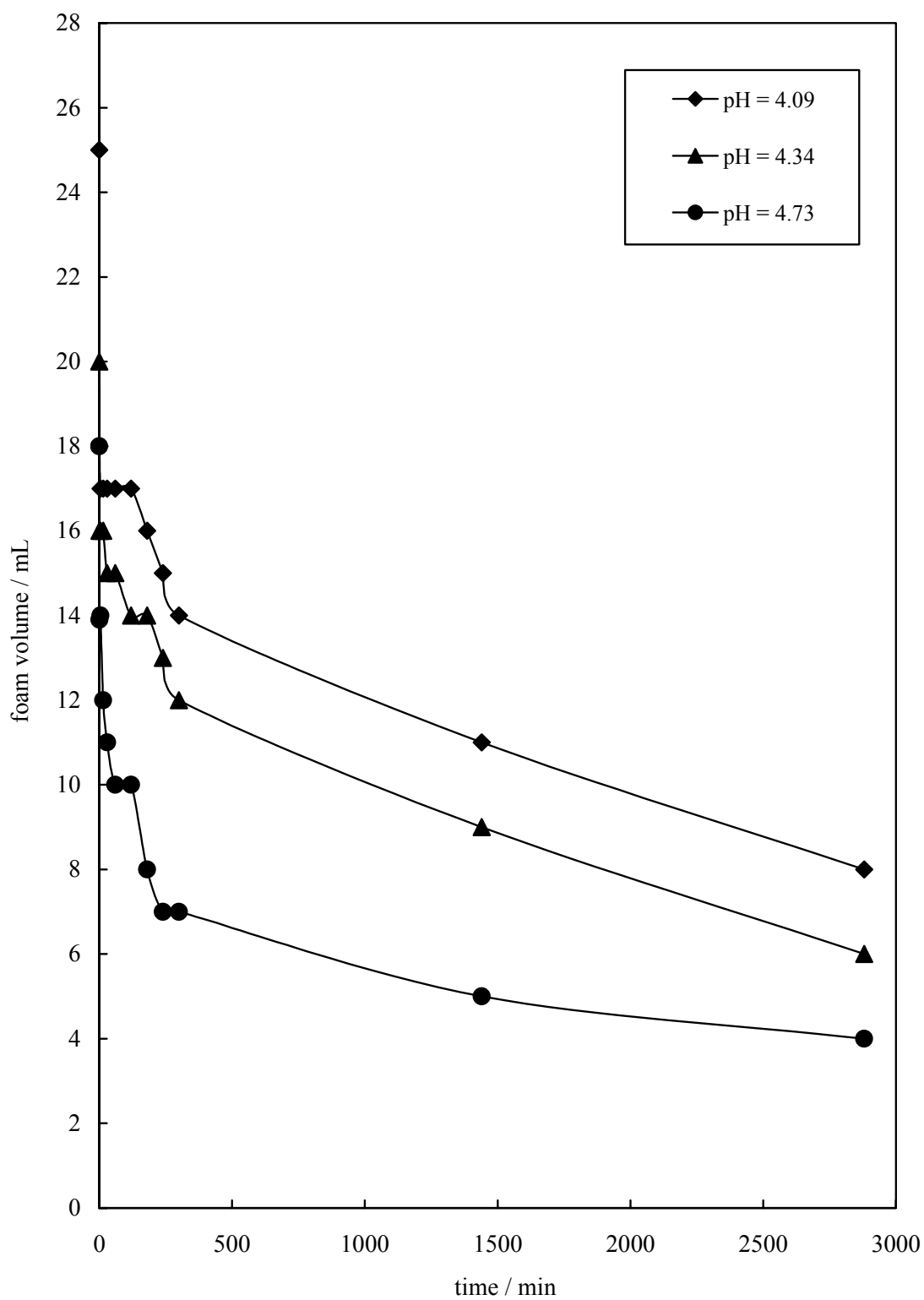**Figure 3.13** Foam volume versus time for 20 mL aqueous dispersions of silica particles of diameter 100 nm, [particle] = 5 wt. %, [NaCl] = 3 M and pH around 4.20 for two separate dispersions.
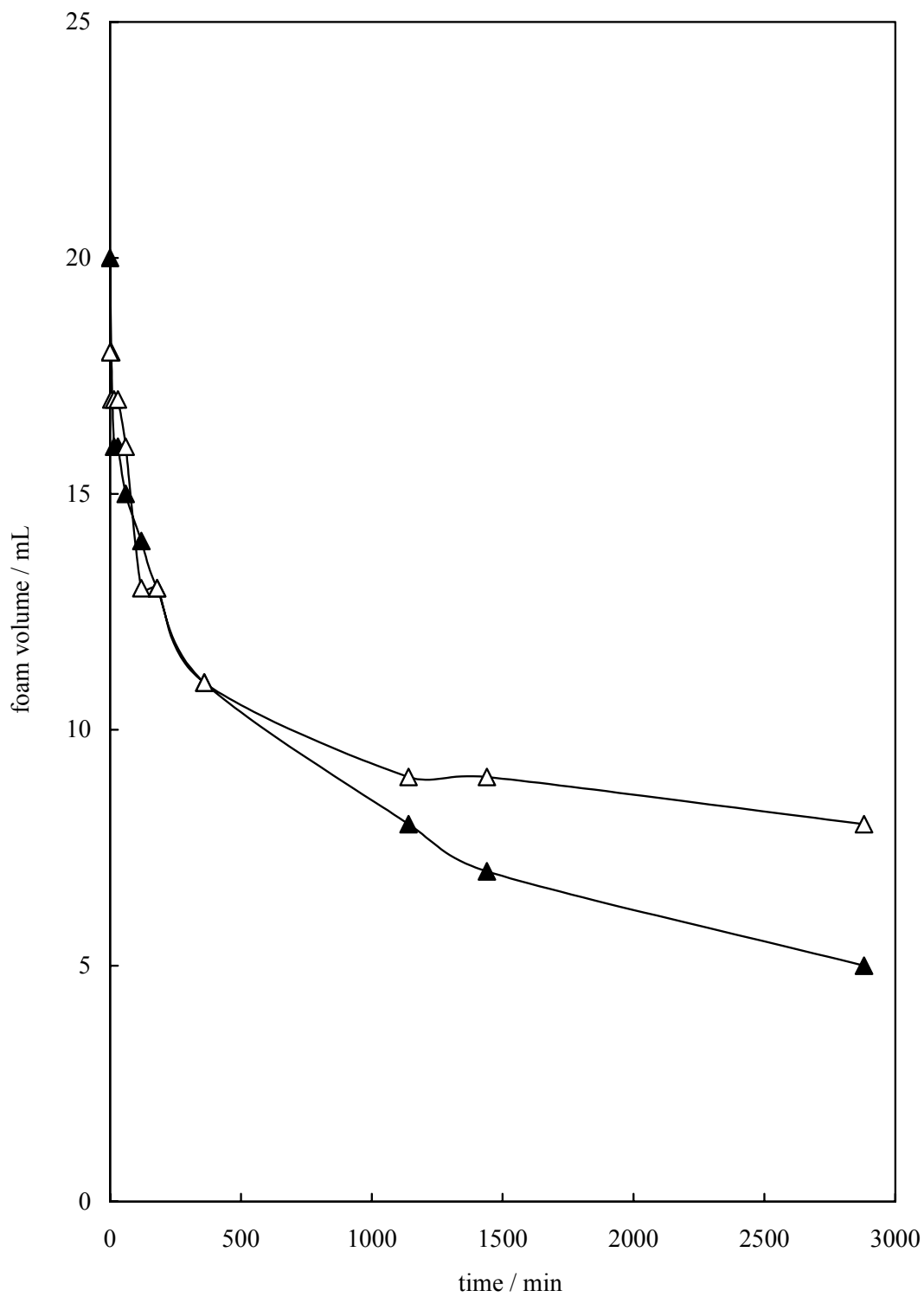
3.5   Effect of NaCl

As silica particles in water and bare air-water surfaces are negatively charged, it is anticipated that addition of salt to water should enhance the transfer of particles to the surface by reducing the energy barrier to adsorption.[12] It may also increase their contact angle as hydrophobicity increases, with both of these factors leading to improved stabilisation of the foam. Therefore, the effect of salt on foamability and foam stability of aqueous silica dispersions was investigated. The state of aggregation of particles in aqueous dispersions before foaming is an important factor to consider and this depends on the interparticle forces, both attractive and repulsive. It was observed that by increasing the NaCl concentration, dispersions become more unstable. However, at pH = 9 or pH = 3, dispersions remained stable for longer, compared with the silica dispersions at an intermediate pH = 4.5-5 where particles flocculated, followed by their sedimentation which was observed visually in the aqueous phase before foaming. As discussed in the previous section, at this intermediate pH the particles were uncharged or weakly charged having a low surface charge density and thus they are more hydrophobic. Figure 3.14 shows the different vessels containing aqueous dispersions of silica particles at a fixed pH value of 4.5 and fixed concentration of 5 wt. % at different salt concentration, after a few days. It can be seen that the dispersions containing more salt (e.g. 4 and 5 M NaCl) are the most unstable and more viscous, with the higher volume of sediment observed.

Figure 3.14 Appearance of vessels after a few days for aqueous dispersions of silica particles of diameter 100 nm at pH = 4.5, [particle] = 5 wt. % and different concentrations of NaCl (1 - 5 M left to right).

Addition of sodium chloride to the aqueous silica dispersions at a fixed concentration and pH around 4.5 causes a progressive increase in foamability with NaCl. In order to obtain foam stability, the breakdown of foam generated by the shake test was monitored over time; see Figure 3.15. Foams produced up to 2 M NaCl are very unstable and burst very quickly. From 3 to 5 M NaCl, the top of the foams (bigger bubbles) start to coalescence and collapse quickly, until they reach a plateau (~ 5 mL foam) after 48 hours, where foams remain stable for days. Another way of measuring foam stability is shown in Figure 3.16, where the foam half-life ($t_{1/2}$) is plotted. The graph shows a maximum in foam stability at 3 M NaCl. This does not necessary mean that foams produced with 3 M NaCl were most stable overall, because as observed in Figure 3.14, after 2 days all foams reach a plateau in stability. This maximum at [NaCl] = 3 M, shows that the foams produced with such concentration of salt decay at a much slower rate initially ($t_{1/2}$ = 18 hours), compared with the foams obtained with the higher salt concentration (*e.g.* 4 and 5 M), which collapse to half their initial volume in a few hours. It seems that, at 3 M NaCl, silica particles flocculate in bulk and these flocs adsorb on the surface of the bubbles, preventing coalescence of the bubbles. However, at a higher salt concentration, particles may aggregate to a higher extent and these flocs may be too big compared to the size of the bubbles formed and therefore they can be easily detached from the bubble surfaces, and cause instability between bubbles. This was confirmed as the vessels containing foams produced with such high salt were very sensitive to mechanical vibration and silica particles detached from the bubbles and sediment when those vessels were tapped. The particles may also aggregate to different extents and introduce a certain level of polydispersity. It was revealed by Sethumadhavan *et al.*[13] that polydispersity in particle size can disrupt the in-film packing significantly such that films thin much more rapidly and indeed coalesce quite rapidly. More recently, other studies[14-17] revealed that if particles extensively coagulate in the aqueous phase, this will hinder foam formation. In this study the extensive particle flocculation observed at high NaCl concentration, *e.g.* 5 M, did not seem to hinder foam formation, as a similar amount of foam (~ 25 mL) was obtained compared to the foam formed with 3 M NaCl (~ 22 mL). However, the bubbles within the foams produced with 5 M NaCl collapse quicker initially compared to the other foams. The reason for all foams reaching a plateau in stability may be related to the viscosity of the bulk dispersions underneath the foams.

Figure 3.15 Initial foam volume and foam volume after different times versus concentration of NaCl for 20 mL aqueous dispersions of silica particles of diameter 100 nm, [particle] = 5 wt. % at pH around 4.5.
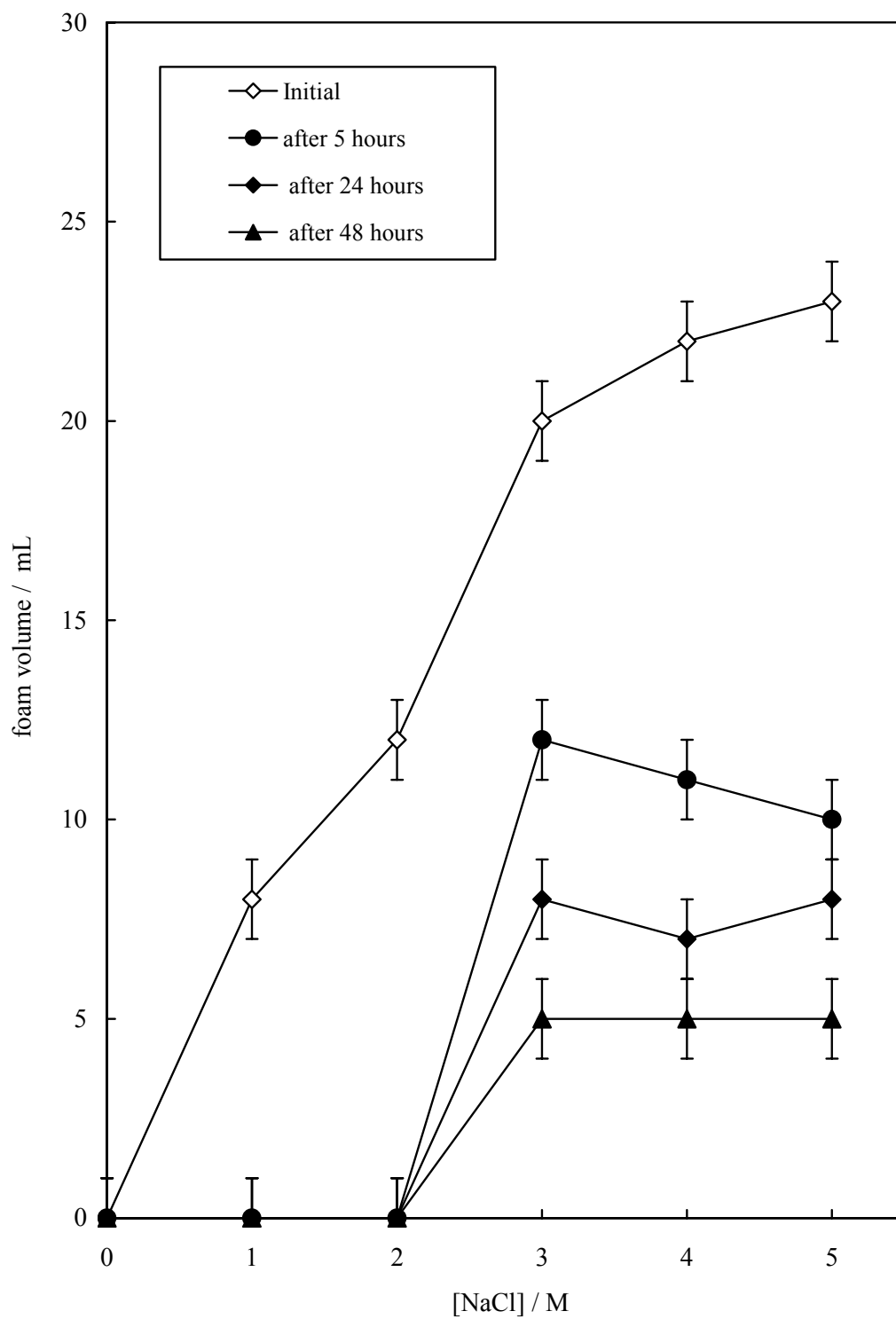
Figure 3.16 Initial foam volumes (circles) and foam half-life (diamonds) versus [NaCl] for 20 mL aqueous dispersions of silica particles of diameter 100 nm, [particle] = 5 wt. % at pH around 4.5. The sketches in the graph show that particles are becoming more flocculated with salt and the flocs attach to the air bubbles.
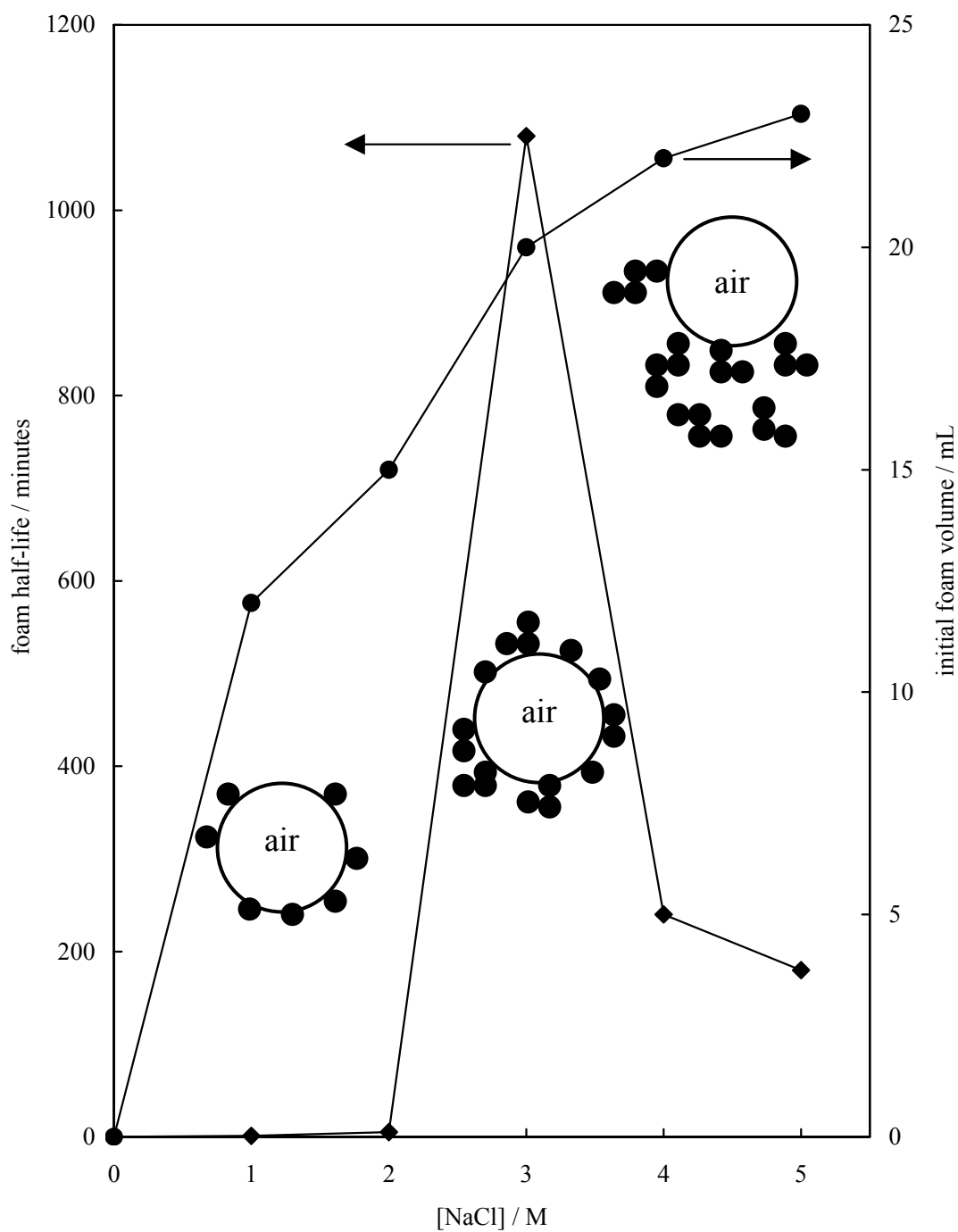
This is also in agreement with other studies. Wilson[6] also noticed that stable bubbles were only formed under circumstances when the latex was close to conditions for its coagulation in bulk. Some authors (see ref. 18 and references therein) claim that particles stabilize liquid foams by increasing the effective viscosity of the liquid. They found that there is a correlation between the viscosity of the film and foam stability. It was also shown that adding additives to foams can increase the viscosity and improve the stability of foams. Du *et al.*[19] have demonstrated that partially hydrophobic silica nanoparticles can indeed give highly stable air bubbles in an aqueous phase. They used particles of primary size 20 nm, but aggregates considerably larger than this were present at the interface. Stable bubbles were only formed when the hydrophobicity of the particles was such that there was always a strong tendency for the particles to aggregate in bulk as well. Dickinson *et al.*[20] also analysed the shrinkage kinetics of a single bubble as the same time it gathered more particles in its surface. They showed an existence of a critical bubble size, above which the bubble surface was covered rapidly enough with particles for dissolution of the bubble to be relatively insignificant. However, below this critical size, they concluded that bubbles shrank too fast to be stabilised by the particles. The critical bubble size depended on the size of the particles or aggregates of particles in the dispersion, amongst other factors. However, according to Kaptay[21] increased viscosity cannot explain the primary stabilisation of the foam, although it can play a secondary role in decreasing the drainage rate of the foam. This point of view is also supported by the observed foaming during the in situ production of solid particles at the bubble-liquid interface, while there were no particles in the bulk liquid, and thus bulk viscosity was not affected by the particles at all.[22]

3.6   Contact angles of aqueous drops in air

In order to explain the effect of NaCl on the foamability and foam stability of the systems studied, a knowledge of the contact angle that these particles make with the interface is essential in interpreting some of the phenomena. Different methods for determining the contact angle when the particle are large enough (> 2 μm) to be seen microscopically are available (see ref. 1). However, those methods are unsuitable for sub-micron particles whose size is below the limit of resolution of an optical microscope. Therefore the interfacial phenomena associated with colloidal systems such as emulsion and foams are often studied by means of experiments on artificially prepared flat surfaces rather than on the colloidal systems themselves. Such methods

provide a most useful indirect approach to the various problems. In this work hydrophilic glass slides and silicon wafer substrates previously treated with nitric acid were used to resemble the hydrophilic particles studied. Figure 3.17 shows the foamability of aqueous silica dispersions and the average results obtained for the advancing contact angles versus [NaCl]. An increase in contact angle with increasing NaCl concentration was observed. This increase in contact angle, suggests that the particle hydrophobicity is increasing with NaCl concentration, which explains the increase in foamability of the aqueous dispersions observed. However, when the contact angles of aqueous drops were measured on a silicon wafer, an increase in contact angle was observed up to 3 M NaCl and then decreased at higher NaCl concentration (see Figures 3.18 and 3.19). Silicon wafer may be chemically different to borosilicate glass and therefore the trend of contact angle with [NaCl] is different, however the magnitude of the contact angles is very similar. These results show that particle hydrophobicity may increase with NaCl up to a certain value and then at very high salt concentration, *e.g.* 5 M NaCl, may decrease. Fokkink and Ralston[23] measured contact angles on charged substrates and they have shown that the presence of an electrical double layer at the solid-liquid phase boundary accounts for the maximum hydrophobicity of solids at their point of zero charge. This could explain why bubbles collapsed quicker with the foams obtained at high salt concentrations, after a few hours, compared with the foams produced with 3 M NaCl which were more stable to collapse in the same period of time. These results also suggest that increasing concentrations of NaCl may modify the solvent structure within the interfacial region and may provide insight into particle-particle interactions at high ionic strengths where the DLVO theory typically diverges from experimental observations.[24]

Figure 3.17 Initial foam volumes (diamond) for 20 mL aqueous silica dispersions of diameter 100 nm, at a fixed [particle] = 5 wt. % at pH = 4.5 and advancing contact angles (circle) of aqueous NaCl drops under air on hydrophilic glass slides versus [NaCl].
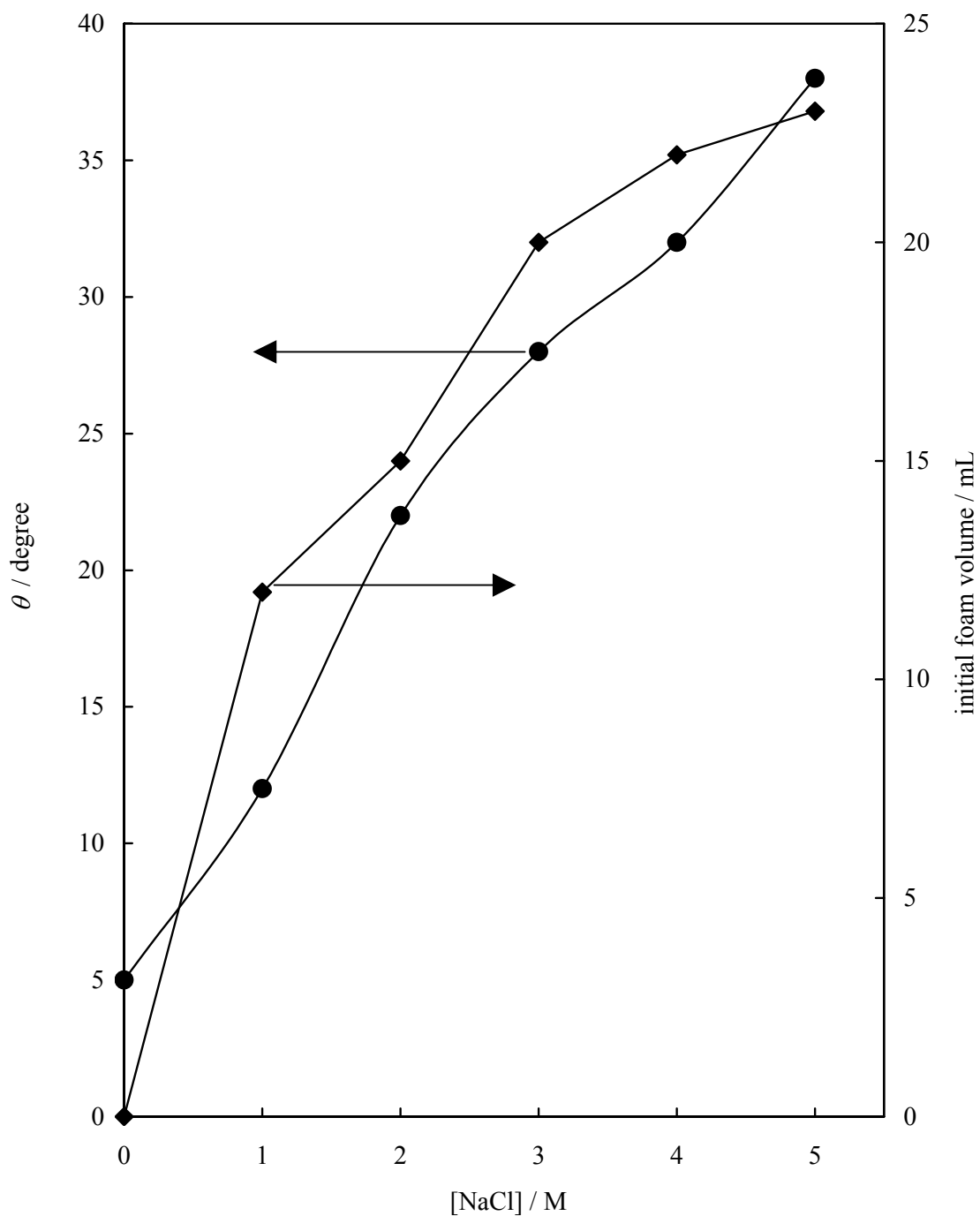
Figure 3.18 Contact angles of NaCl drops at pH around 4.2 under air on a silicon wafer chemically treated with nitric acid; (a) 0 M NaCl, 14.3°, (b) 1 M NaCl, 29.2°, (c) 2 M NaCl, 35.8 °, (d) 3 M NaCl, 46.8°, (e) 4 M NaCl, 48.5°, (f) 5 M NaCl, 36.9°. These images are side views of the drops taken with the Krüss DSA 10.

.

(a)
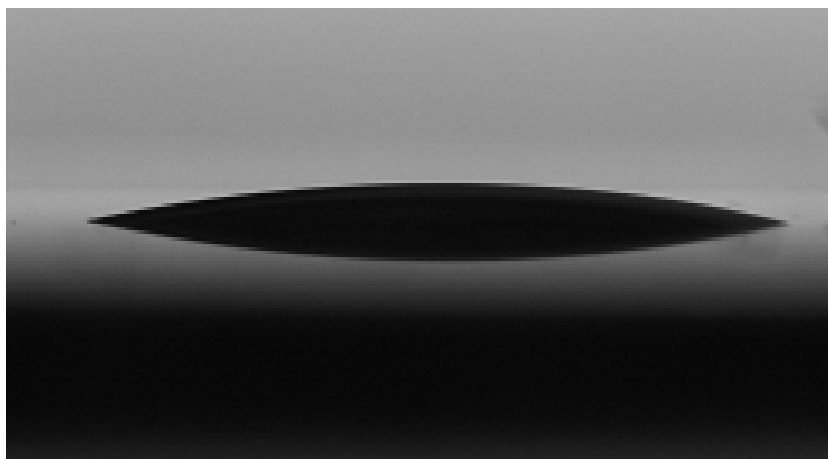
(b)
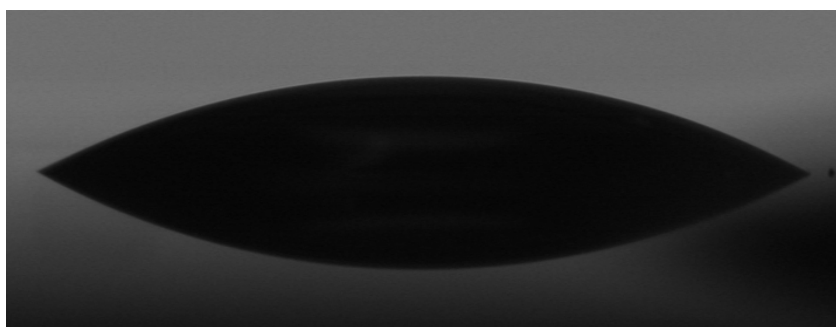
(c)
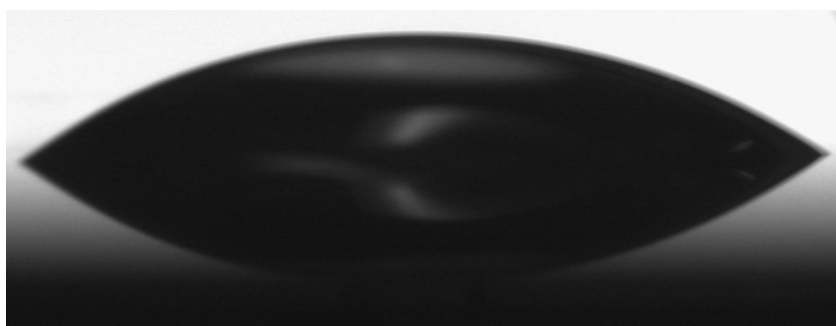
(d)
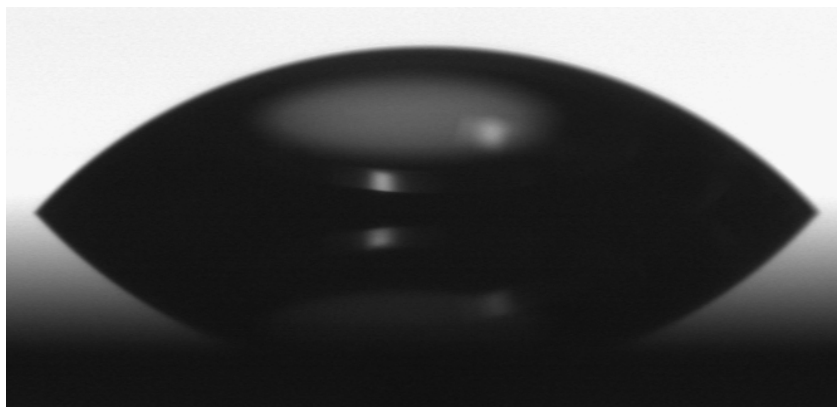
(e)
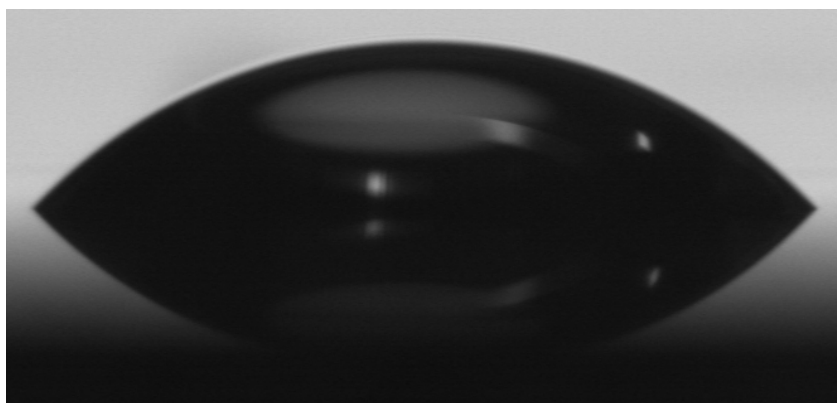
(f)
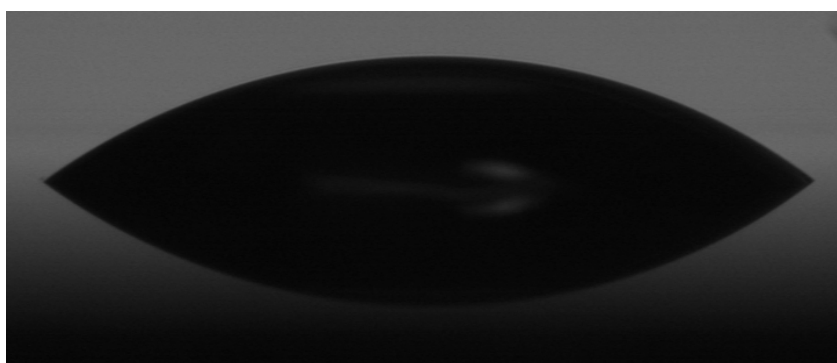
Figure 3.19 Foam half-life (circles) for 20 mL aqueous silica dispersions of diameter 100 nm, [particle] = 5 wt. % at pH = 4.5 and contact angles (diamonds) of aqueous NaCl drops under air on silicon wafer at pH = 4.5 versus [NaCl].
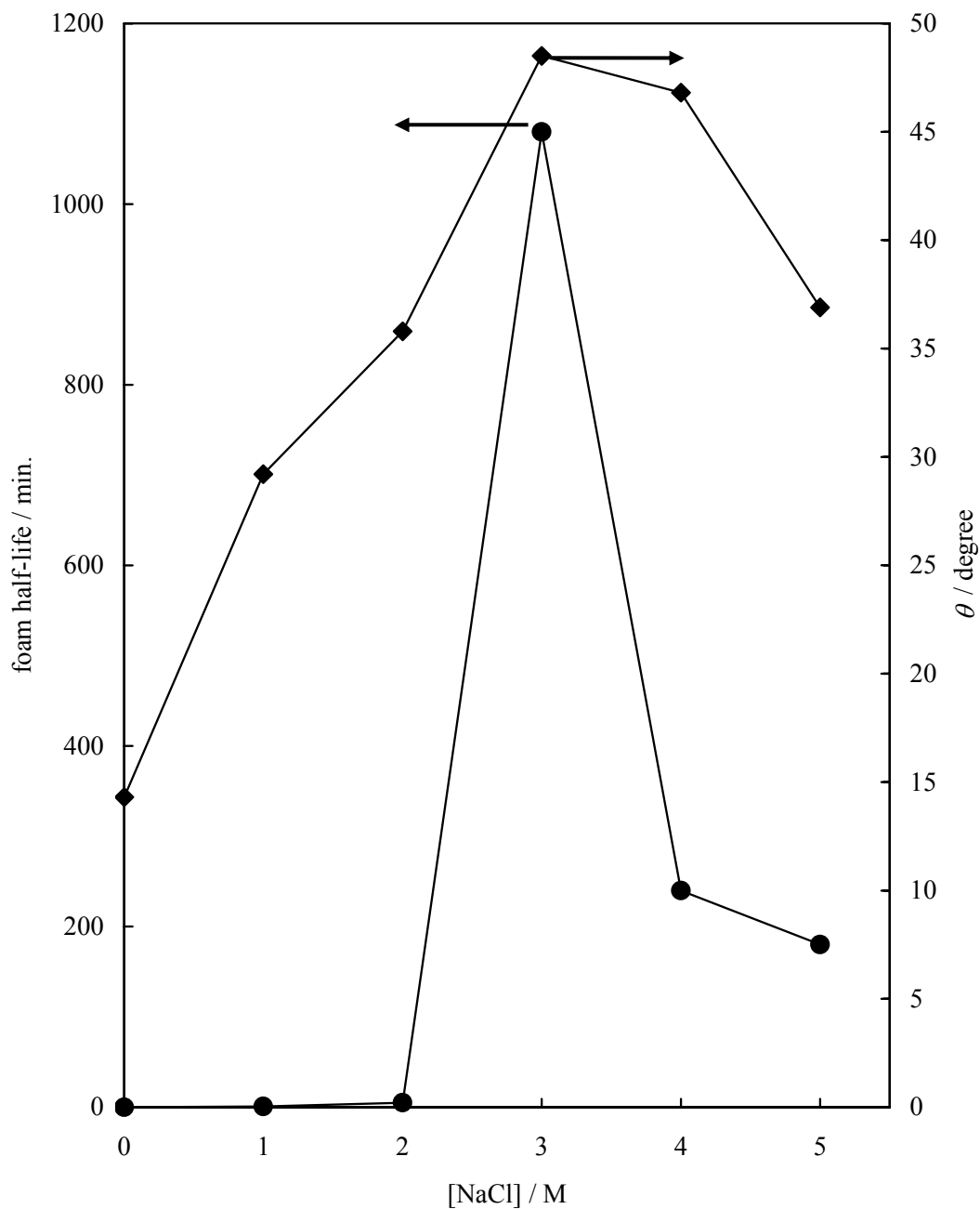
A study on the impact of aqueous electrolytes on interfacial energy has been reported[24] where they aimed to determine the change in contact angle as a function of salt concentration. They measured contact angles formed by salts solutions up to 1 M on a hydrophilic clay surface (sodium montmorillonite) and reported that the presence of electrolytes ions near the solid-water interface resulted in an increase in solid-water interfacial energy. The change in these properties as a function of ionic strength may be affected by the hydrophobicity of the substrate due to orientation between the water and the solid surface.

Contact angles for a set of probe liquids on solid surfaces have been used to determine the components of the solid surface energies.[25] The Young-Dupré equation for a non-spreading liquid (L) on a solid surface (S), is

$$\gamma_S = \gamma_{SL} + \gamma_L \cos\theta \qquad (3.1)$$

where θ is the contact angle and γ_S, γ_L and γ_{SL} are the equilibrium solid , liquid and solid-liquid interfacial tensions, respectively. Expressing the three tensions in equation (3.1) in the form of the total interfacial tension between the solid and liquid phases gives

$$(1 + \cos\theta)\gamma_L = 2\left(\sqrt{\gamma_S^{LW}\gamma_L^{LW}} + \sqrt{\gamma_S^{+}\gamma_L^{-}} + \sqrt{\gamma_S^{-}\gamma_L^{+}} \right) \qquad (3.2)$$

Equation (3.2) contains three unknowns related to the solid surface, γ_S^{LW}, γ_S^{+} and γ_S^{-}. As a result, contact angle data for at least three different liquids (of which two must be polar) enable all three parameters to be calaculated from the various simulataneous equations of type (3.2).

Data taken from reference 24 was used to predict the contact angles of aqueous NaCl on hydrophilic glass using glass surface energy components from reference 25. It was found from the calculations that a water drop on hydrophilic glass has a contact angle of approximately 9.9° and 0.5 M NaCl gave a contact angle of 20.4°. These results are shown in table 3.1[26] and the findings are in good agreement with the results found in this work. Unfortunately, no datum was obtained for higher salt concentrations, in order to compare with the results obtained here.

Table 3.1.   Predicted contact angles of aqueous NaCl (taken from ref. 26).

I / M	γ^{LW} / mJ m^{-2}	γ^{+} / mJ m^{-2}	γ^{-} / mJ m^{-2}	Predicted θ / deg.
0	21.60	25.5	25.5	9.9
0.001	20.30	-	-	-
0.01	19.16	24	29	16.6
0.1	18.30	22	31.5	17.6
0.5	17.73	22.5	32.2	20.4
1	16.91	-	-	-

A study by Paunov et al.[12] derived analytical expressions for particle adsorption at the air-water surface. They predicted that the higher the salt concentration the larger the depletion of the bulk concentration of particles as more particles become adsorbed onto the interface. According to their study one of the effects explaining why salt enhances particle adsorption to the surface is that the true contact angle, θ, increases as the salt concentration increases, making the particles more hydrophobic. The predictions of this model are in accord with relevant experimental data and the results are directly relevant for understanding the behaviour of solid particles as emulsifier agents and foam stabilizers. A more recent study by Hu et al.[27] investigated the origin of assembling silver particle films by adsorbing nonoparticles from bulk colloids to the air-water interface. It was revealed that it is thermodynamically favourable for a colloidal particle in bulk to adsorb to the air-water interface. However, a finite sorption barrier between it and the nearby particles usually restrains the adsorption process. They found that when an electrolyte such as KCl was added to the silver colloids, it largely reduced the sorption barrier. Thus, silver nanoparticles could break through the sorption barrier, pop up, and become trapped at the air-water interface. The trapped silver particles are more inclined to aggregate at the interface than those in bulk due to the increase in van der Waals forces and the reduction of electrostatic forces. Partially immersed silver particles have one part exposed to air, resulting in the increase of the Hamaker constant A_{eff}. Therefore, attractive van der Waals interactions between two trapped particles enhanced. On the other hand, electrostatic forces fall due to the decreasing surface potential of trapped particles. With the increase of the ionic strength, the 'screening

effect' shields partly the repulsive electrostatic forces. As a result, attractive van der Waals interactions prevail over repulsive electrostatic interactions at any distance of the two separated, partially immersed silver particles, leading to an irreversible bonding.

It has also been shown that solid particles can stabilize liquid foams only if the contact angle is above a certain value, ensuring the stability of bubble-particle agglomerates. The energy of attachment of a particle to a fluid-fluid interface is related not only to the contact angle but also to the tension of the interface γ_{aw}.[1] Assuming the particle is small enough (typically less than a few microns in diameter) so that the effect of gravity is small, the energy E required to remove the particle from the interface is given by

$$E = \pi \, r^2 \, \gamma_{aw} \, (1 \pm \cos \theta)^2 \qquad\qquad (3.3)$$

in which the sign inside the bracket is negative for removal into the water phase, and positive for removal into the air or phase. The extreme variation of E observed with wettability has a major influence on the ability of particles of different hydrophobicity to stabilise foams or emulsions.[1] However, the literature concerning the wettability of particles in stabilising aqueous foams is still very sparse, compared to the studies performed with emulsions. The first systematic study of the influence of particle wettability on emulsion type and stability using a range of silica particles of increasing hydrophobicity was reported by Binks and Lunsdon.[28] Emulsions containing either very hydrophilic or very hydrophobic particles contain large drops and are unstable to coalescence. Those with particles of intermediate hydrophobicity are sub-micron and completely stable to coalescence. The findings are discussed in relation to the effect of particle wettability on the energy of attachment of particles to interfaces. Other work described by Binks et al.[29] was aimed at preparing and stabilising multiple emulsions using particles alone as emulsifier. Hydrophilic silica particles are used to stabilise o/w drops/globules and hydrophobic silica particles are used to stabilise w/o drops/globules in multiple emulsions of either o/w/o or w/o/w. It was found that emulsions are very stable to coalescence as a result of adsorbed particles. According to Binks,[1] the optimum contact angle for foam stabilization is about 90°, as at this value the energy to remove the particle from the interface is at maximum. The optimum contact angle of about 85° was experimentally established for aqueous foams stabilised by polysterene latex particles at conditions of coagulation (clustering) in bulk.[6] Another study reported

that the optimum contact angle interval ensuring highest foam stability was found between 40 and 70°[o30] and 75-85°.[8] However, some of the systems used in those studies had surfactants.

3.7   Zeta potentials of aqueous dispersions

3.7.1 Effect of silica surface charge

Hydrophilic solids exhibit an affinity for water. Their surface chemistry allows these materials to be wetted forming a water film or coating on their surface. The surface functional groups have the ability to form hydrogen bonds with water. The solid-liquid interface is considered to develop a surface charge as a result of surface equilibrium involving potential-determining ions which give rise to positive, negative and for some systems, neutral surface sites. The charge on the mineral colloids depends on the nature of the colloid, pH, ionic strength and other solution conditions.[31]

The hydrophilic silica surface chemistry must be considered when trying to explain the foaming behaviour and foam stability observed in the system studied. The effect of silica surface chemistry on the behaviour of colloidal suspensions of silica in water has been extensively studied,[32] yet many aspects of the surface are still poorly understood. The silica surface represents a dynamic system that undergoes slight to notable changes depending on the conditions of the environment. Therefore, the surface charge of silica particles is of great importance and interest. Like other mineral oxide surfaces, the principal mechanism by which silica surfaces acquire a charge in contact with water and potential determining ions (H^+ and OH^-) is shown by the following equations:[11]

$$SiOH + H^+ \rightleftharpoons SiOH_2^+ \tag{3.4}$$

$$SiOH + OH^- \rightleftharpoons SiO^- + H_2O \tag{3.5}$$

The isoelectric point (point of zero charge) for silica occurs at approximately pH = 2, in the absence of electrolyte and will depend on the type of silica (amorphous or quartz). Above this pH the particles are negatively charged but below pH 1 the particles bear a positive charge. In one study the isoelectric point of silica was reported to be about pH

5.[33] The origin of this unusual behaviour is not yet clear. In this current study the surface charge properties of aqueous silica dispersions of diameter 101 nm were determined in terms of the zeta potential using electrophoresis. Figure 3.20 shows the zeta potential versus pH data obtained in the absence of NaCl. From this graph it can be seen that there is an intimate relation between zeta potential and pH. If the data is extrapolated from Figure 3.20, the isoelectric point (IEP) of the silica is found to be about 2-3, which is within the limits of other studies reported.[11] The surface charge of silica comes from the dissociation of the silanol groups, so in this case the pH controls the zeta potential of silica particles through the following process:

$$\text{SiOH}_2^+ \underset{+H^+}{\overset{-H^+}{\rightleftharpoons}} \text{SiOH} \underset{+H^+}{\overset{-H^+}{\rightleftharpoons}} \text{SiO}^- \qquad (3.6)$$

3.7.2 Effect of electrolyte on zeta potential

In this study, the particle surface chemistry and the nature of the aqueous phase seems to affect both foamability and foam stability. However, it is unclear how the charging behaviour of particles at the air-water interface will be affected by the addition of high concentrations of NaCl to the water phase. It is possible though to speculate about the effect of the addition of electrolytes to the solid-aqueous phase interface and thus particle interactions in the dispersions. In general, the zeta potential is an important factor controlling the dispersion stability of silica suspensions, which results in the existence of an energy barrier preventing the approach of particles. According to the DLVO theory, the energy barrier arises as a result of the electrostatic energy of repulsion and the attractive van der Waals energy between charged particles as they approach each other. The magnitude of the zeta potential determines the height of the energy barrier. The control of silica sol coagulation by pH and by addition of simple electrolytes is said to be 'anomalous' in that it is not simply predicted by conventional DLVO theory.

Figure 3.20 Zeta potential versus pH for aqueous dispersions of silica particles of diameter 100 nm, [particle] = 0.1 wt. % in pure Milli-Q water.
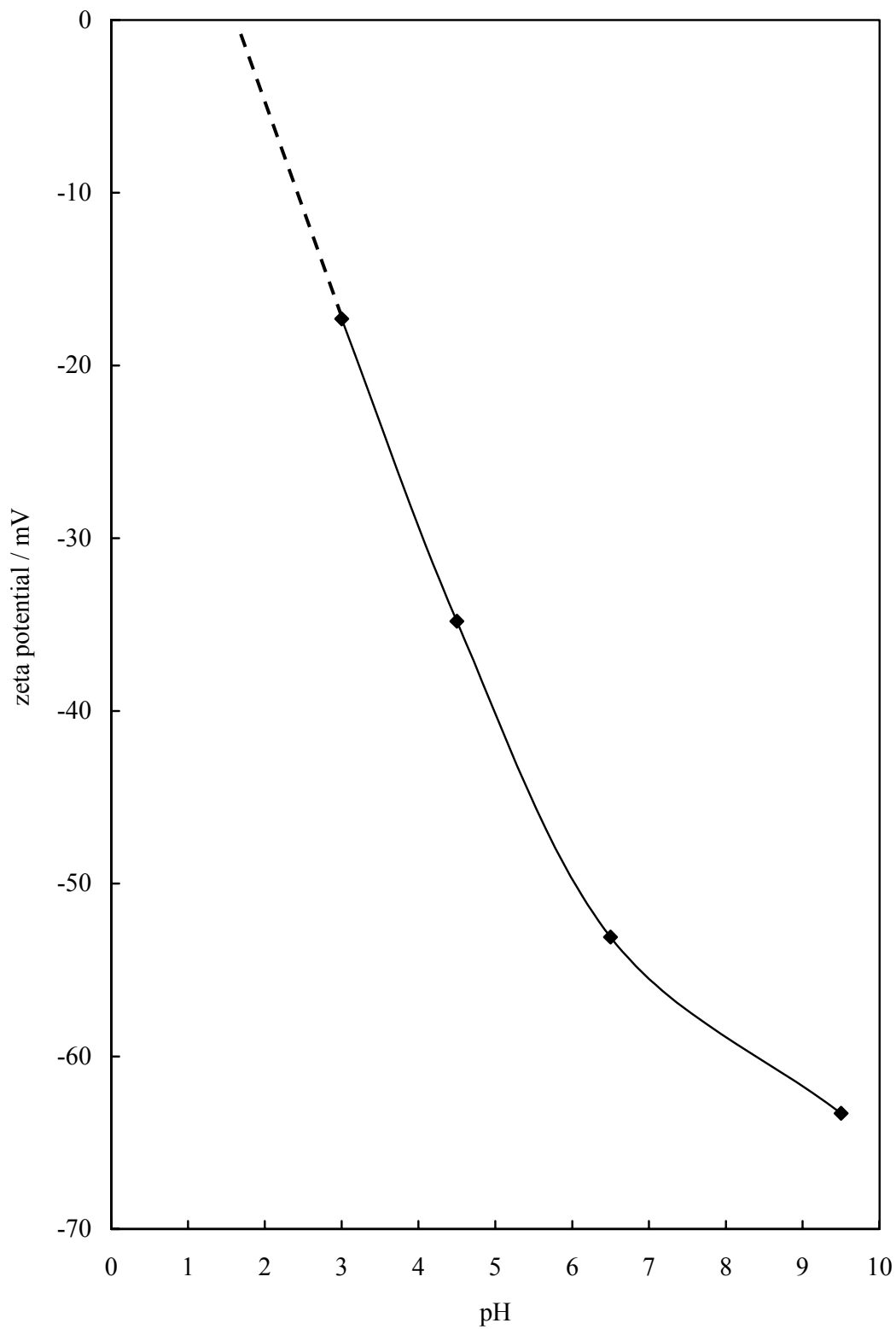
Iler[11] noted that at pH 2, where the charge of silica particles is zero (IEP), silica sols were remarkably stable to electrolyte. The short-range repulsion as well as the low Hamaker constant of silica in water (1.2×10^{-20} J) are the likely cause of the unusual stability of silica at its IEP.[34] Due to the low Hamaker constant, the dispersions forces are very low and it appears that one monolayer of water is quite enough to screen dispersion forces between particles preventing coagulation. A number of reasons for the enhanced stability of silica at low pH have been postulated. For example, Allen and Matijevic[35] proposed that the stability of silica in acidic conditions is caused by particle hydration, with the silanol groups being capable of hydrogen bonding with water, such that silica behaves more like a lyophilic than a lyophobic colloid. Substitution of silanol protons by cations (*e.g.* Na^+) of the electrolyte as the pH increases leads to destabilisation of the sol by eliminating sites for hydrogen bonding (dehydration):

$$(3.7)$$
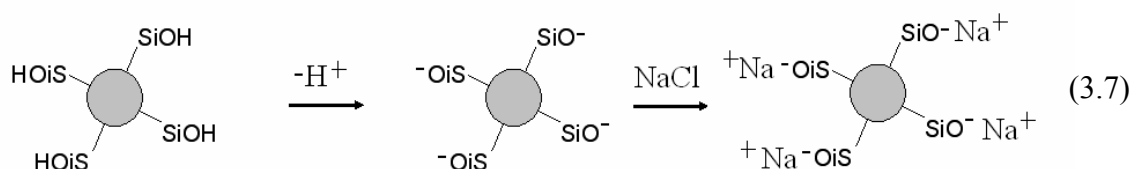
The applicability of the DLVO theory to various inorganic sols has been discussed.[24] If an electrolyte is added to a charged colloidal dispersion, this will cause marked compression of the electrical double layer around the silica particles and the reduction of surface charge. Unfortunately, there is no information in the literature concerning the addition of high concentrations of NaCl to aqueous silica dispersions. Only small concentrations of electrolytes have been added to silica dispersions in previous work.[11] Therefore, reliable electrophoretic data for silica at higher ionic strengths are not available.

In this study, the effect of NaCl concentration on the zeta potential (ζ) of aqueous SiO_2 dispersions of diameter 101 nm at different pH was investigated. The results are shown in Figure 3.21. An increase in the NaCl concentration from 0 to 0.5 M causes a sharp increase in the absolute value of the zeta potential from a negative value to zero charge at pH around 4.5; further increase in NaCl concentration caused a surface charge reversal. This charge reversal was also observed at pH around 3 and pH = 9.5.

Figure 3.21 Zeta potential versus NaCl concentration for aqueous dispersions of silica particles of diameter 100 nm, [particle] = 0.1 wt. % at different pH.
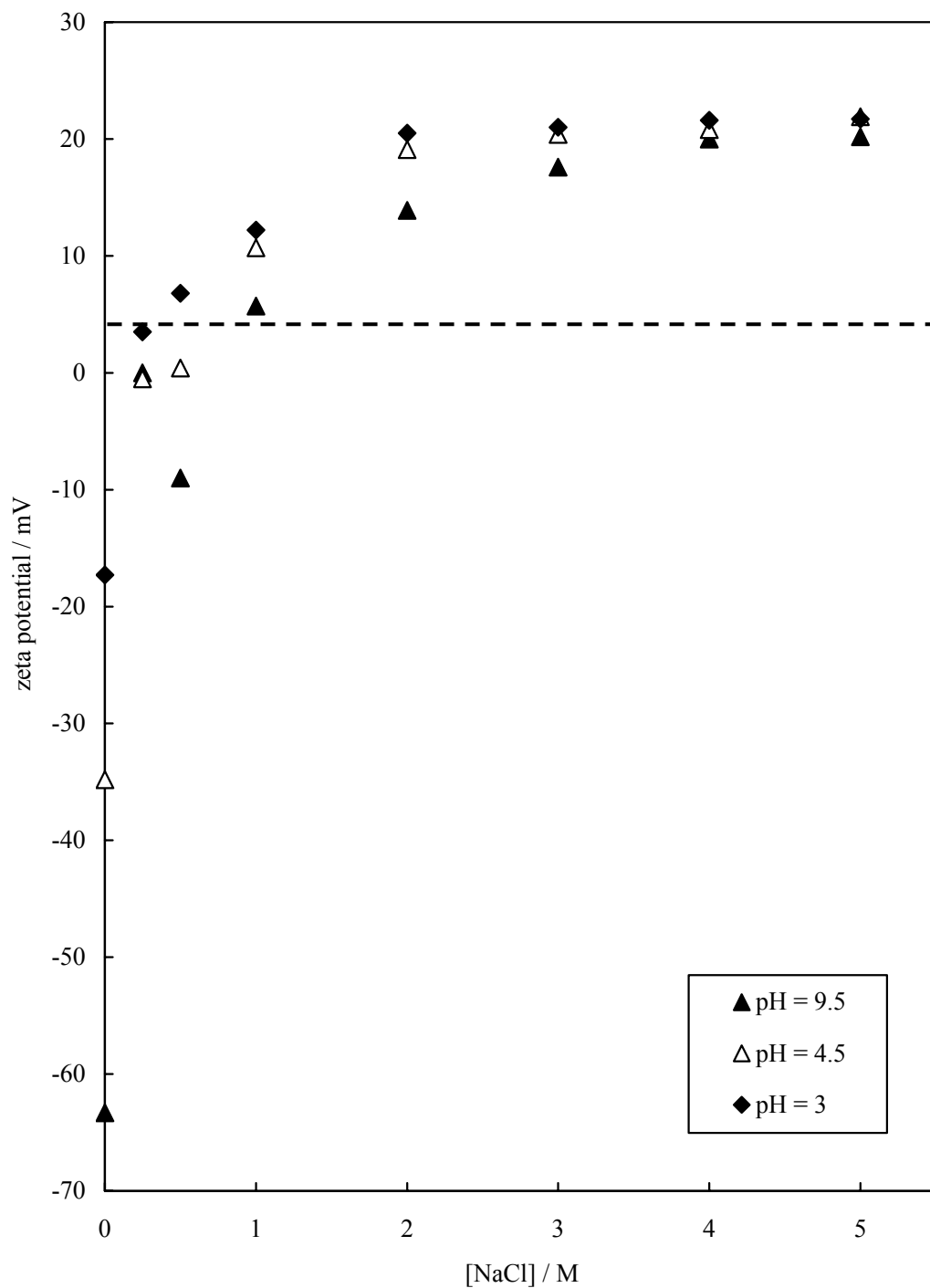
Figure 3.22 shows the zeta potentials at different pH values for systems containing different concentrations of NaCl. At high NaCl concentration, the reversal of zeta potential from negative to positive indicates that the adsorption of Na^+ takes place on the negatively charged silica particle surfaces, as mentioned in other studies.[36-38] The zeta potential results indicate that by increasing the concentration of salt from 0 to 0.5 M, the IEP of the silica particles shifted from pH 2 to pH around 4.5. At high concentrations of NaCl (from 1 M to 5 M) the surface of the silica remains positive for all pH values. This may not correspond to the actual zeta potential of the aqueous dispersions used to produce the foams as the concentration of silica particles used was 5 wt. %, while the zeta potential measurements were performed with only 0.1 wt. % of particles at the same high salt concentrations used in the aqueous foams. However, recent studies shows very similar results to the ones obtained here. A study by George[36] describes the effect of concentrated monovolent electrolytes on the zeta potentials of silica suspensions. According to this work an explanation for some of the anomalous behaviour of silica is likely to be related to the shifting IEP and the additional attraction found at high salt concentrations not predicted by the DLVO theory. The zeta potentials of silica suspensions were measured over a wide range of monovalent electrolyte concentrations. The counterions investigated were Li^+, Na^+, K^+ and Cs^+, while the co-ion was always Cl^-.

Figure 3.23 shows his results at 0.4 M NaCl. These results are very similar to the results obtained in this study, for 0.5 M NaCl, where a shift of IEP from pH 2 to pH around 4.5 is clearly observed. Another study[37] concerns the surface charge properties and dispersion stability of aqueous silica suspensions. The same effect of electrolyte (especially multivalent metal ions) on zeta potential was observed. This investigation also concluded that in some cases the electrolyte can cause a surface charge reversal, which depends on the properties and concentration of electrolyte. Again this investigation focused on the effect of counterions (co-ions do not have an obvious effect on zeta potential). As mentioned before, electrophoretic data for silica at very high salt concentrations is sparse. However, other studies on surface properties with other types of particles at high electrolyte concentration have been reported.[39-45] There is one study worthy of comment which aimed to determine the ζ-potential of precipitated aluminium hydroxide particles in NaCl solutions at concentrations up to 3 M.[39]

Figure 3.22 Zeta potential versus pH for aqueous dispersions of silica particles of diameter 100 nm, [particle] = 0.1 wt. % at different [NaCl].
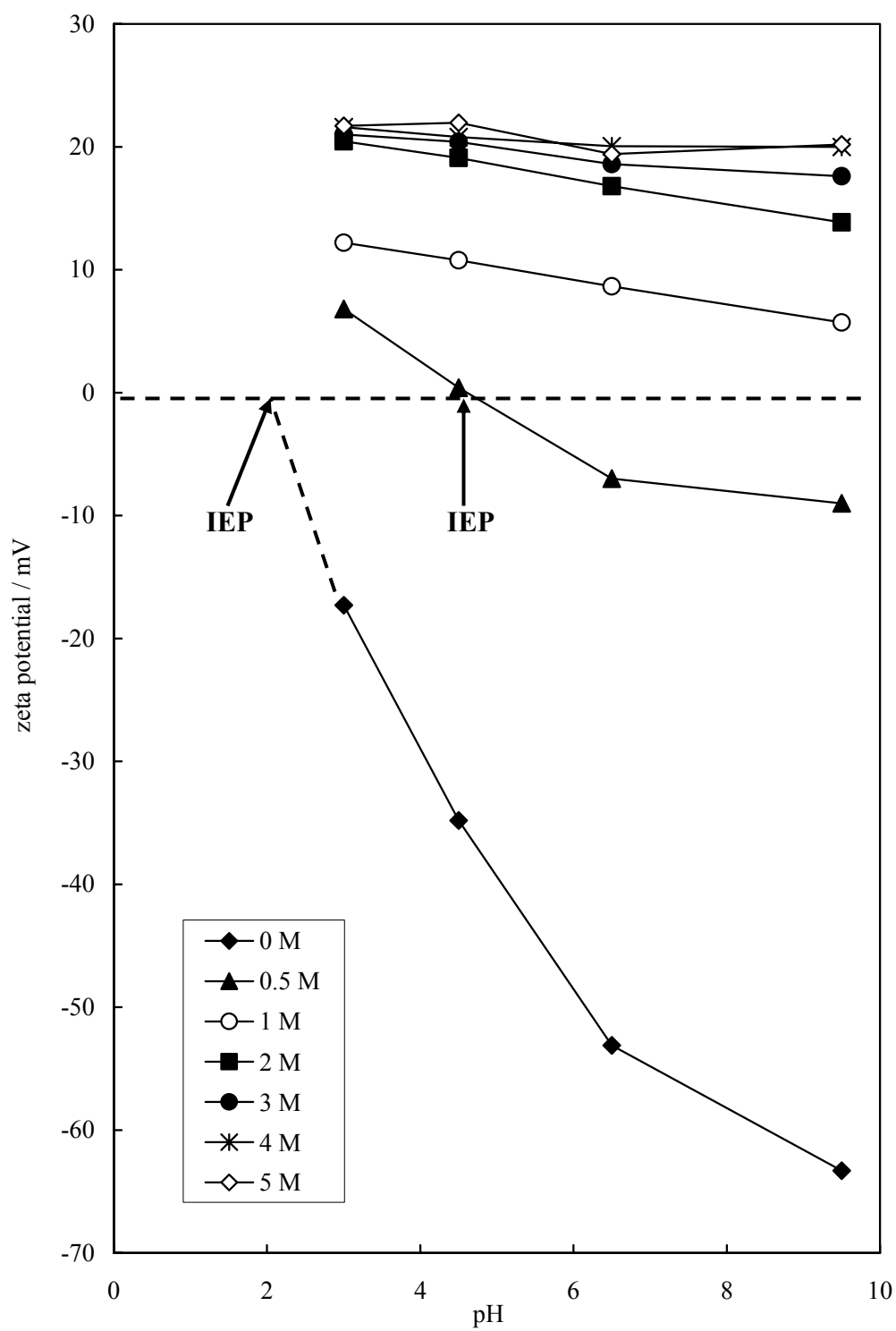
**Figure 3.23** Zeta potential versus pH for aqueous dispersions of silica particles of diameter 100 nm, [particle] = 0.1 wt. % with no salt (in this work) and with [NaCl] = 0.4 M (data obtained by George[36]).
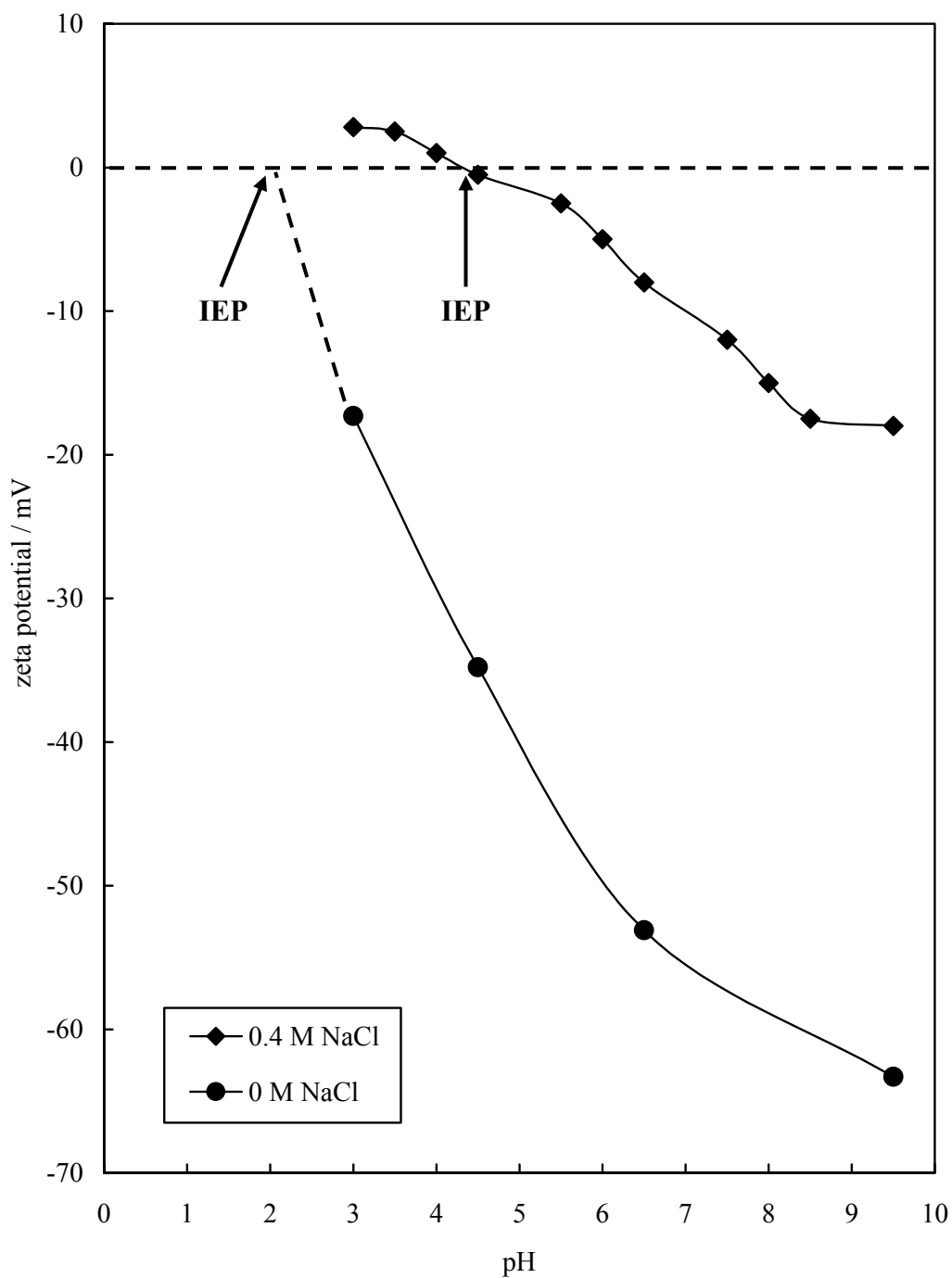
The result of the study was that at 0.5 M NaCl, the IEP shifted up by about two pH units, and that at 3 M NaCl there was no IEP. It appears that the sodium ions are preferentially adsorbed on the hydroxide surface at high concentrations, and at the highest concentration studied the surface remains positive for all pH values. The results described in this study suggest that, in alkaline solution, this highly hydrated alumina tends to adsorb sodium ions close up to the particle surface so that the net charge at the surface where liquid flow begins to develop is positive. There may be many negative charges residing in the solid but they are overwhelmed in number by the adsorbed cations.

It may be inferred that charged particles at low pH (positively charged) and high pH (negatively charged) were unable to adsorb at the air-water interface, however at an intermediate pH their adsorption as uncharged particles was significant. It is therefore concluded that particle adsorption is promoted at pH around 4 as the particle is uncharged or more hydrophobic and the aqueous dispersions were more viscous as a result of flocculation of particles. It is believed that flocs are adsorbing around bubbles preventing water drainage, coalescence and disproportionation of bubbles in the foams, which explains the maximum in foamability and foam stability observed at this pH. At the low or high pH particle desorption is promoted as the particles are charged and therefore more hydrophilic. This is schematically shown in Figure 3.24.

Figure 3.24 Schematic representation of the influence of pH on the particle adsorption at the air-water interface. The charge on bare air-water surface is always negative.
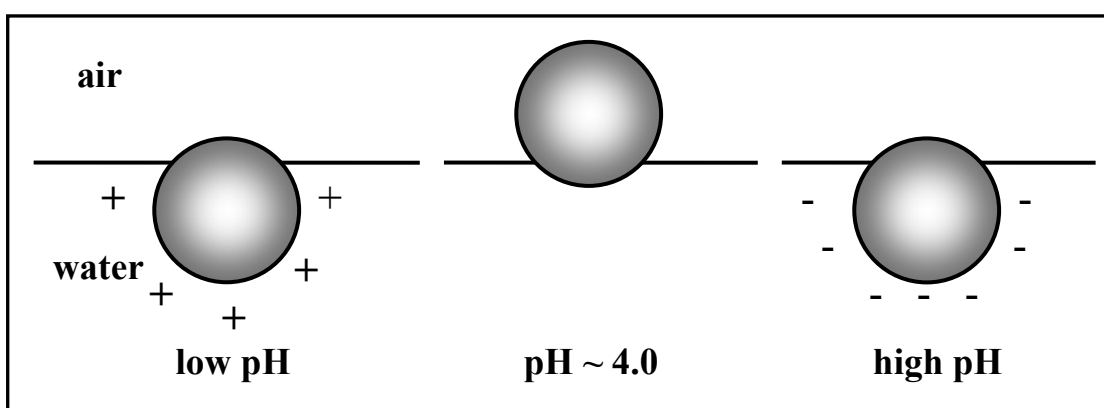
3.8   Viscosity of aqueous dispersions

The properties of a foaming system fall into two categories; those which affect the foaming ability of the system and those which stabilise the foam. One criterion for foaming is that the foaming agent must be able to adsorb at the air-liquid interface to give a mechanically strong film. The common understanding of foam stability usually refers to the ability of the foam to maintain its parameters constant with time, i.e. bubble size, liquid content and total foam volume. The stability of foams has been found to be dependent on the strength and rheological properties of the thin liquid films. Rheology is the study of the deformation and flow of materials under the influence of an applied stress. The response of a material to shear depends on the type of material, there are two limiting behaviours: an elastic solid or a viscous liquid.[46] Under an applied stress, a solid resists flow whereas a liquid flows in response. These materials can be described as a Hookean solid and Newtonian liquid respectively. For a Newtonian liquid, the shear rate ($\dot{\gamma}$) is constant under an applied shear stress (σ). The flow of a viscous fluid is described earlier on equation (2.9), where η is the viscosity. The shear rate is proportional to the shear stress, and the viscosity is the constant of proportionality. The viscosity is a measure of the resistance to flow when a fluid is subjected to a shear stress. However, for a Hookean solid, the application of a shear stress ($\dot{\gamma}$) to the material results in a shear strain (γ) in response. The flow of an elastic solid is described by

$$\sigma = G\gamma$$

(3.8)

where G is the shear modulus. The shear strain is proportional to the applied stress, with the constant of proportionality being the shear modulus G. Elastic materials have a critical value to flow which is known as the yield stress. This is defined as a narrow range of stresses where the material shows a dramatic transformation in flow.[47] An elastic material stretches and returns to its original shape when the shear stress is below the yield point, however it will stretch, flow and be permanently deformed for a stress higher than the yield point. Most materials have both viscous and elastic characteristics and exhibit some form of intermediate behaviour known as viscoelasticity. The flow behaviour of many dispersions cannot be simply described by equations 2.9 and 3.8, because there is a complex interplay between the motion of the liquid itself and the

interactions and rearrangement of suspended particles to flow.[48] In addition, a fluid can respond to an applied stress in different ways, in contrast to a Newtonian fluid. There are two typical types of non-Newtonian behaviour. Firstly, a shear-thinning fluid, in which the viscosity gradually decreases with the shear stress, i.e. the fluid flows as the sample is sheared more. Secondly, a shear-thickening fluid, in which the viscosity gradually increases with the shear stress, i.e. the fluid flows at low shear stress but becomes more resistant to flow when sheared at higher stresses.

Many rheological properties have been studied in detail for emulsions which are very similar to foams.[49] Research has also been carried out on the rheological properties of aqueous foams. However, they have been hidden in many past foam viscosity experiments due to the confounding effects of wall slip, variation in foam structure with foam age and mode of foam generation.[50] Until recently, foam rheology has been described by undefined physical parameters. For example, the rate at which a vertical glass tube passes through the foam to the vessel bottom[51] or the time needed for a glass rod placed initially in a vertical position to reach the vessel walls have been suggested for characterising foam 'strength'. However, many general characteristics of foam rheology are known. Foams display shear-thinning behaviour, and often a yield stress is reported.[52, 53] Several authors have found that high surface viscosity of the liquid film correlates with high foam stability. High surface viscosity can retard the drainage of the thin liquid film.[54] However, other researchers have found that high viscosity is desirable but not essential for high foam stability.

It is difficult to study the rheological properties of a foam since at deformation its properties change. This applies to the liquid outflow from the foam, the phase separation into liquid and gas and the local foam destruction under mechanical stress, especially in 'dry' foams. That is why rheology data for silica dispersions will be obtained here, instead of the foams, since solid particles are rigid and non-deformable during the measurement.

The viscosity of the aqueous silica dispersions were observed over time and an attempt to study their rheology was made in order to better understand the effect that NaCl concentration has on the foamability and foam stability of the systems studied. It was observed with the aqueous dispersions of silica particles of diameter 101 nm that at high enough concentration of NaCl (*e.g.* 3 M) the higher the foamability and foam stability. It can be seen that with time the dispersion with higher concentration of NaCl starts to become more viscous (like gel) and sedimentation of the liquid underneath the

foam starts to take place (see Figure 3.25). It seems that at high salt and with time these dispersions form strong gels, where the attractive interactions between particles are large enough to form connecting paths along the gel network (see Figure 3.26).

Figure 3.25 Image of a foam formed with 30 mL aqueous dispersions of silica particles of diameter 100 nm, [particle] = 5 wt. % at [NaCl] = 3 M and pH ~ 48 days after foam formation.

Figure 3.26 Image showing the space filling network formed with silica particles.
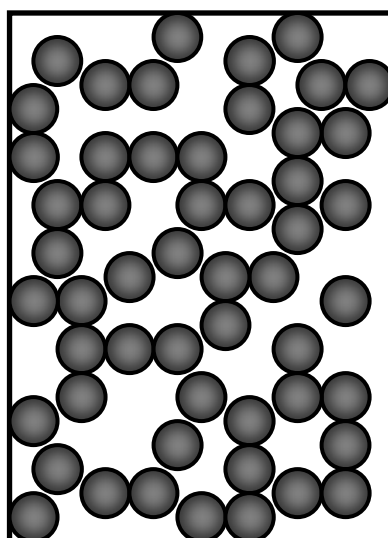
Viscosity measurements of aqueous dispersions of silica particles of diameter 100 nm, [particle] = 5 wt. % at pH ~ 4-5 (20 mL) and different NaCl concentration were taken at different times and the results are shown in Figures 3.27 - 3.30. Aqueous

dispersions of silica particles without salt showed Newtonian flow behaviour (Figure 3.27). However, dispersions with NaCl showed shear thinning behaviour in which the viscosity gradually decreases with the shear stress, i.e. the fluid flows as the sample is sheared more (Figure 3.28). Figures 3.29 and 3.30 showed that the viscosity of these aqueous dispersions increased with time and with concentration of NaCl. Although at high salt the foams formed are relatively stable, most of the particles are still in the bulk liquid, which means that only some of the silica flocs adsorb at the air-water interface enabling the stabilisation of air bubbles. However, due to the high viscosity of these dispersions, foaming ability can be hindered due to the build-up of massive particle clusters in the aqueous phase and therefore they are not able to promptly adsorb on the air bubble surface. The dispersions with lower NaCl concentration (< 3 M) were less viscous and gave rise to unstable foams. Based on these results, it seems that foam formation is favoured by the adsorption of small flocs at the air-water interface and foam stability can be attributed to the irreversible adsorption of these flocs at the interface. These results also confirm that the enhanced stability of the foams with high salt cannot be explained solely by an increase in the liquid viscosity in the foam lamella as the most stable foams were observed with 3 M NaCl and the viscosity of the aqueous silica dispersions increased with concentration of NaCl and no maximum was observed.

Most materials have both viscous and elastic characteristics and exhibit some form of intermediate behaviour known as viscoelasticity. Therefore, further measurements should be taken in order to obtain more accurate results and determine whether these dispersions exhibit viscoelastic properties or not.

127

Figure 3.27 Viscosity (square) and shear stress (circle) versus shear rate for aqueous silica dispersion of diameter 100 nm, 5 wt. %, pH = 4.30, no salt.
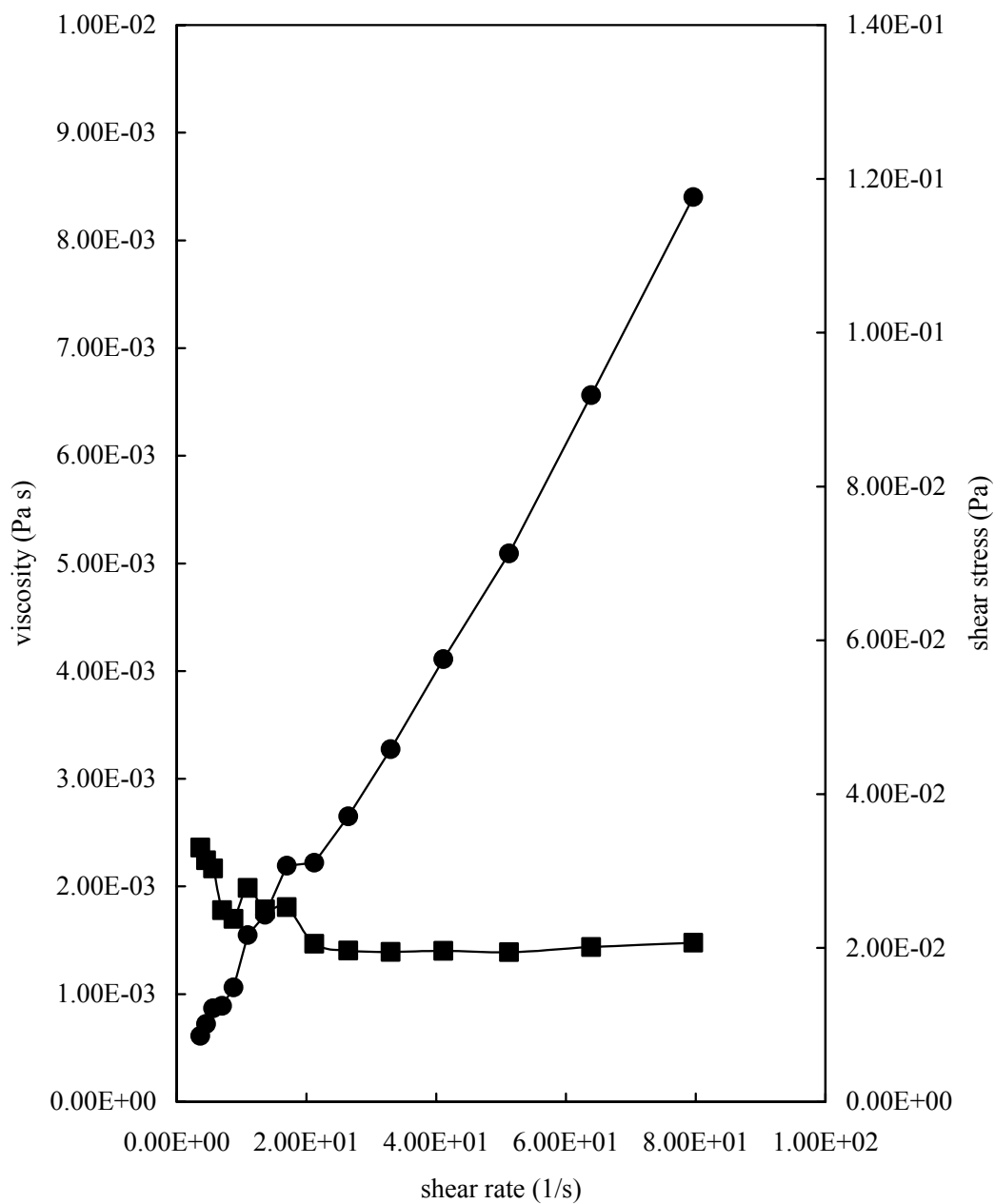
Figure 3.28 Viscosity (square) and shear stress (circle) versus shear rate for aqueous silica dispersion of diameter 100 nm, 5 wt. %, pH = 4.30, [NaCl] = 5 M.
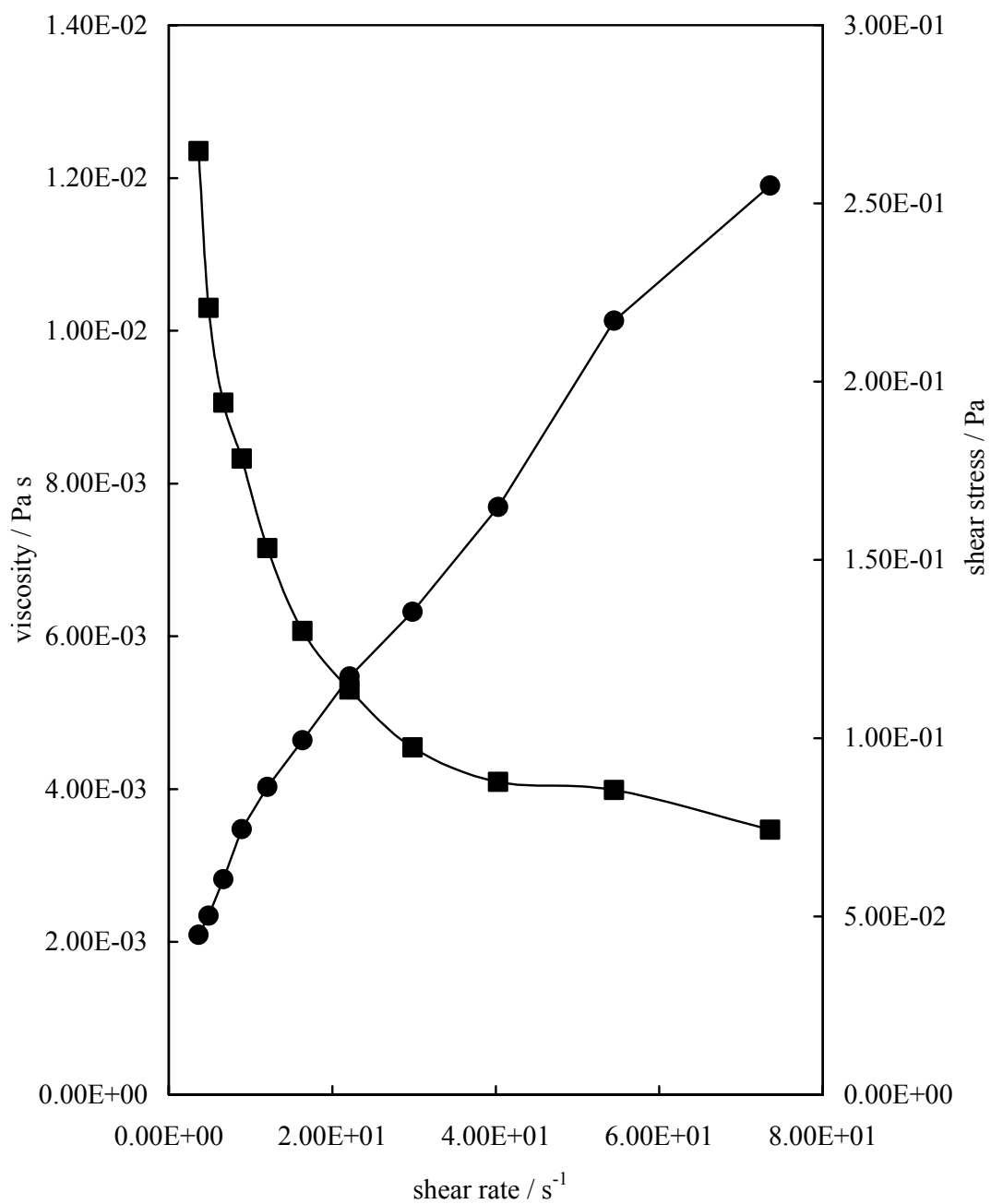
Figure 3.29 Viscosity at a shear rate 22 s^{-1} versus time for aqueous silica dispersions of diameter 100 nm, 5 wt.%, pH = 4.30 at different NaCl concentration.
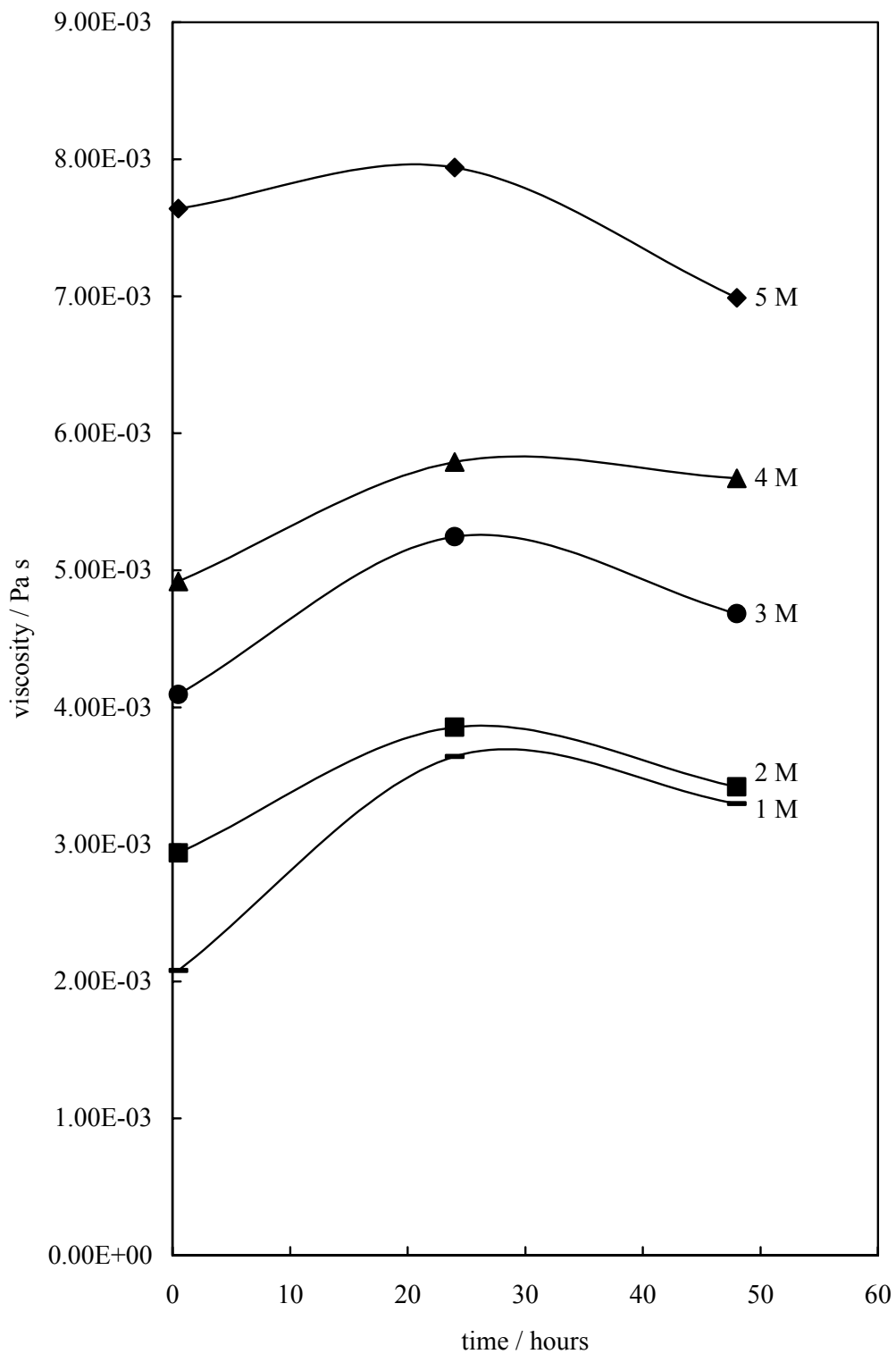
Figure 3.30 Viscosity at shear rate 22 s^{-1} versus [NaCl] for aqueous dispersions of silica particles of diameter 100 nm, 5 wt.%, pH = 4.30 at different times.
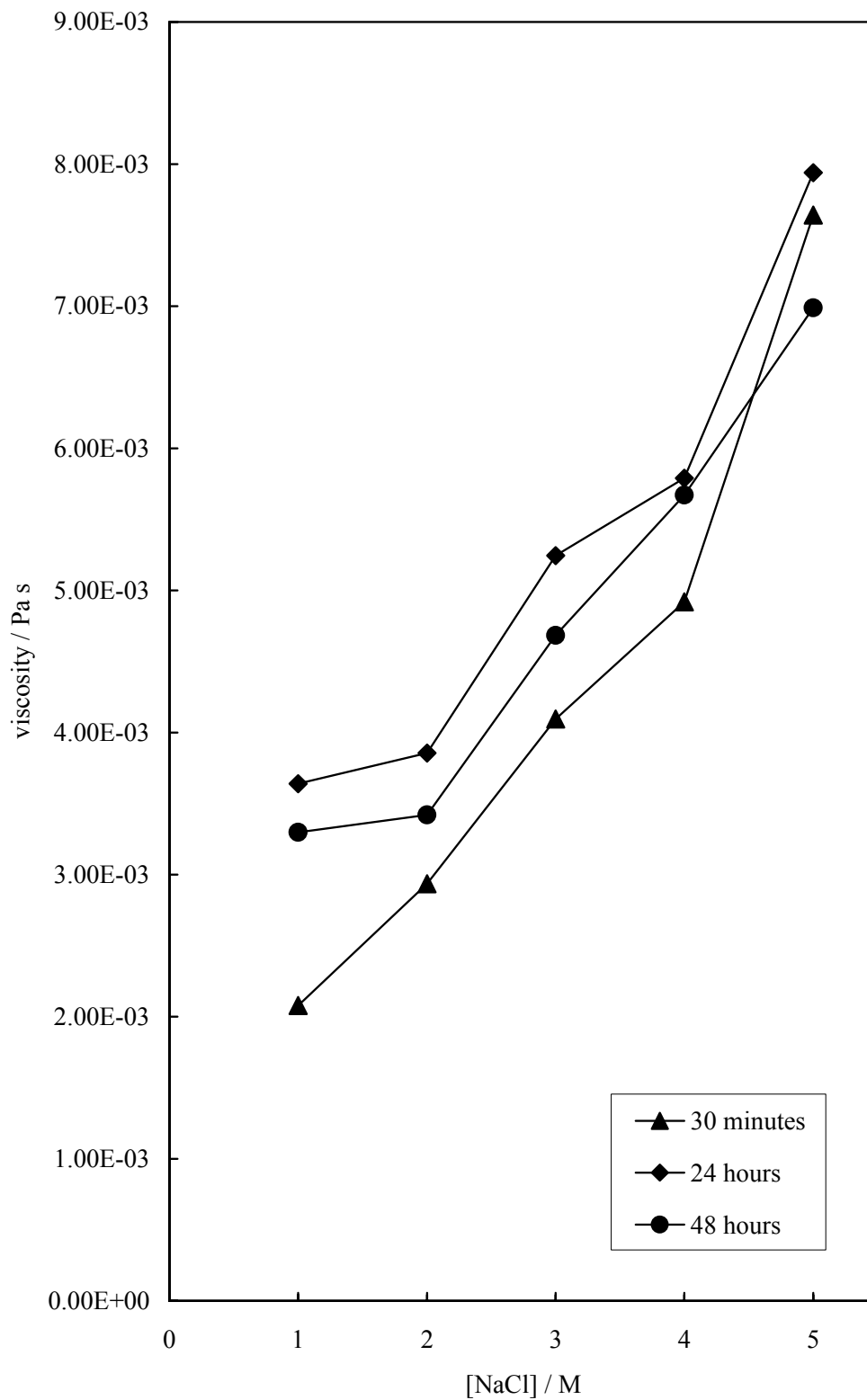
3.9   Structure of the bubbles in foams

The foam produced by shaking aqueous dispersions of silica particles under the appropriate foaming conditions as described in this chapter is particle stabilised. Here the bubbles are very stable compared with surfactant foams. The bubbles appear to be mainly spherical although liquid bridges joining two or more bubbles are also seen. The bubbles observed varied in size from micro-bubbles (bottom of foam, 10-20 µm) to bubbles having a diameter of the order of 0.4 cm (top of foam). Some of these long-living spherical foams are formed by high viscosity liquids as showed in the previous section, which impede the movement, contact and coalescence of individual gas bubbles. These are the case of the silica particles of diameter 100 nm, at pH ~ 4-5 and 3 to 5 M NaCl concentration. Figure 3.31 shows images of thin films of the bubbles at the air-water interface of one of the systems studied. Since bubbles always try to minimize surface area, two bubbles will merge to share a common wall, Figure 3.31 (a). Regardless of their relative sizes, the bubbles will meet the common wall at an angle of 120 degrees. This can be clearly seen in Figure 3.31 (b), where all three bubbles meet at the centre at an angle of 120 degrees.

If the liquid is not so viscous, bubbles tend to move more freely and are more unstable. This was observed with the same silica particles of diameter 100 nm but at pH ~ 2.5 and [NaCl] = 3 M, which gave unstable foams (Figure 3.32). This could be explained by the effect of pH on the foaming properties as discussed in section 3.4. The silica particles used to produce these foams are too small to be seen with an optical microscope however; interference was observed on the bubbles as the film drains, which could indicate the regularity of the packing of the silica particles on the bubble surfaces (Figure 3.33).

Figure 3.31 Images of thin films of bubbles at air-water interface formed with aqueous silica dispersions of diameter 100 nm, 5 wt. %, 5 M NaCl and pH = 4, observed on a microscope slide of single cavity with an optical microscope (viewing from the top at reflected light). (a) - (c) shows the liquid film between two, three and six bubbles.

(a)

(b)
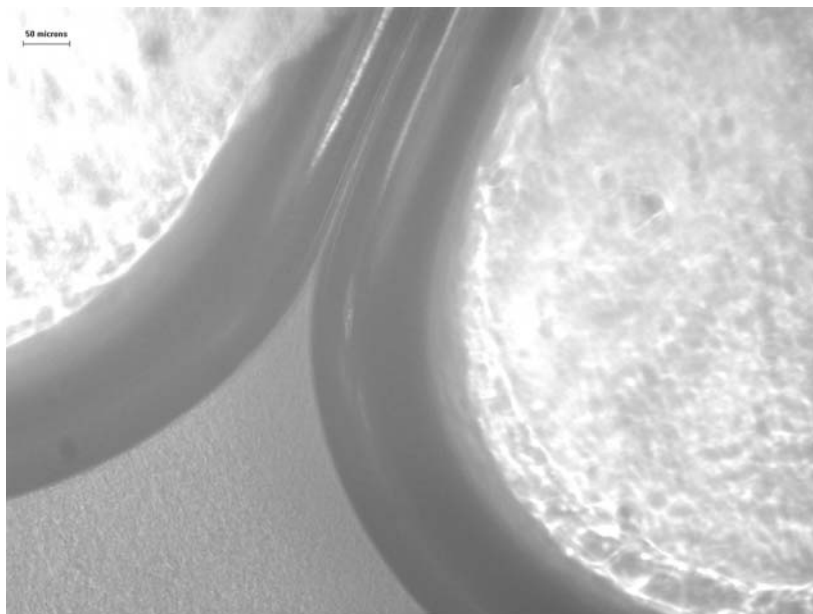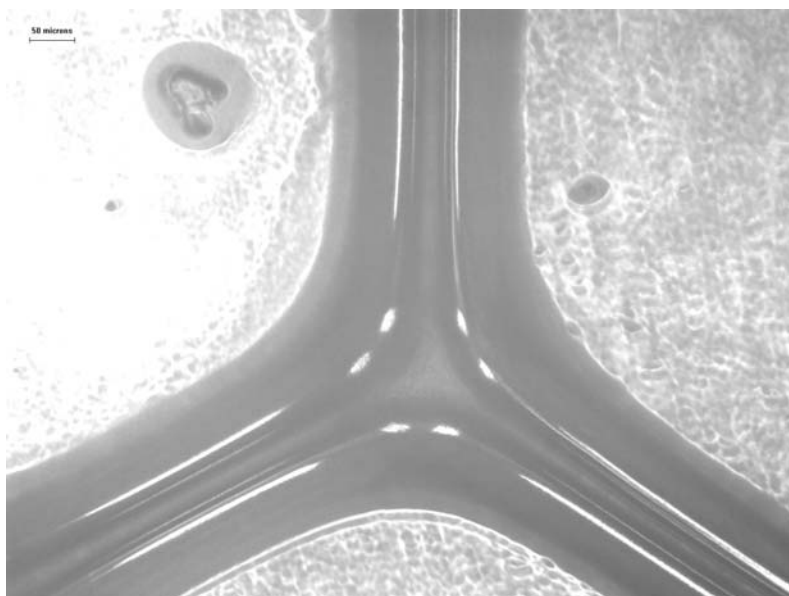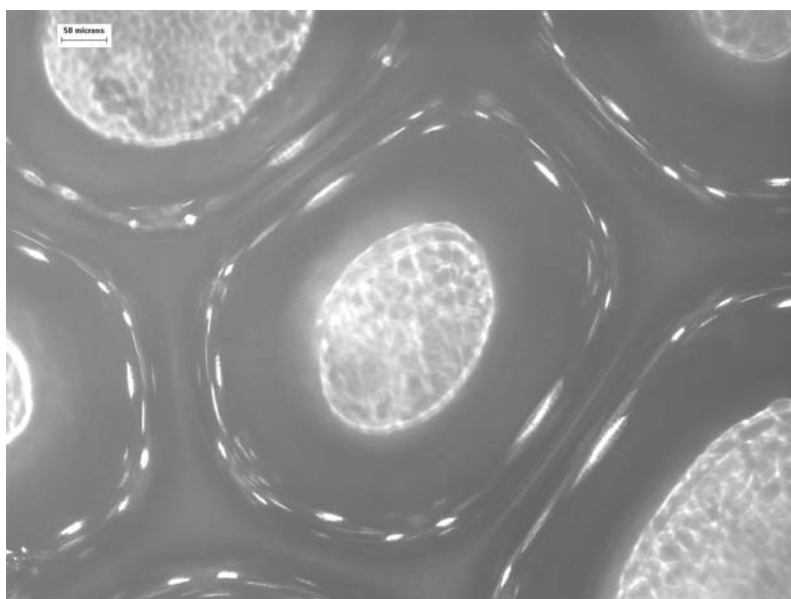
Figure 3.32 Image of unstable bubbles at air- water interface formed with aqueous silica dispersions of diameter 100 nm, 10 wt. %, 3 M NaCl at pH = 2.5 taken from the sides of a glass cylinder by viewing it with a horizontal optical microscope.
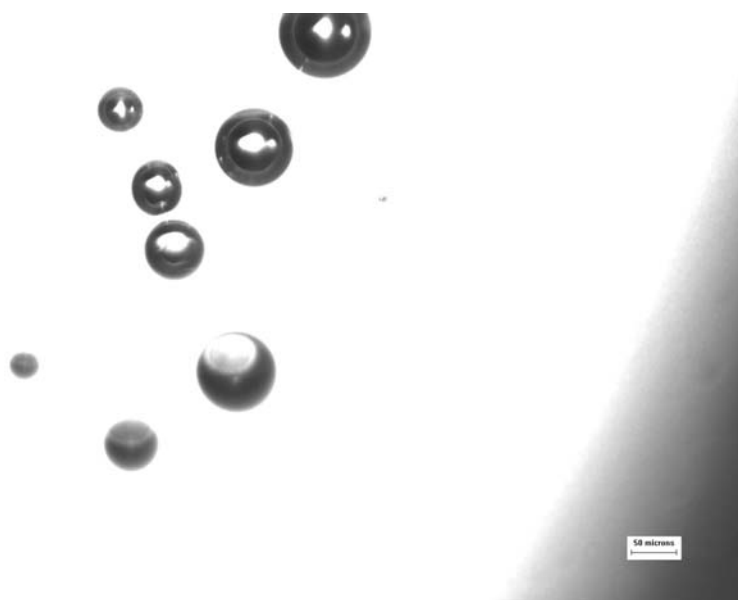
Figure 3.33 Appearance of foam formed with aqueous silica particles of diameter 100 nm, 5 wt. %, 5 M NaCl at pH ~ 4.5 (a) and image of bubbles taken from the same system by viewing from the top with an optical microscope in reflected light (b).

(a)

(b)

50 microns
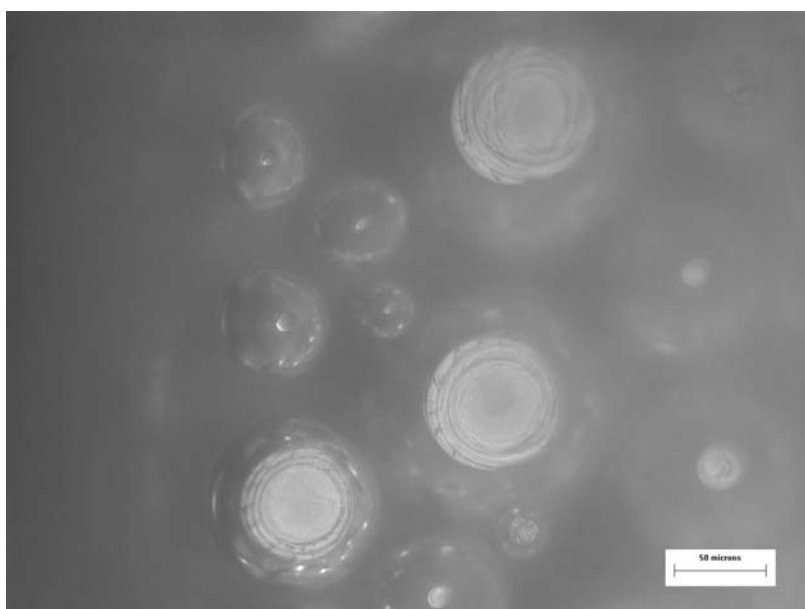
The main stages of foam formation can be described through observing the behaviour of a certain number of rising bubbles. When bubbles are formed with the aqueous silica dispersions studied an adsorption of the silica particles starts at their interface. When the number of bubbles starts to increase at the surface they begin to

draw closer. Furthermore, the capillary attraction between bubbles helps the process of bubble contact and deformation, resulting in thin liquid film formation between neighbouring bubbles. Thus, a monolayer of gas bubbles is formed at the surface, followed by a second layer and so on until a three dimensional foam is obtained (see Figure 3.34). At the very moment of its formation the foam begins to decay due to various processes occurring in it, the most important being film thinning, liquid drainage due to gravity, gas diffusion from smaller bubbles through the liquid films to bigger bubbles and rupture of films, the latter causing coalescence of neighbouring bubbles. The change in bubble size and their disappearance leads to structural reorganisation of the foam. Moreover, evaporation of liquid as well as destruction of the foam column occurs when the foam is open to the atmosphere.

Figure 3.34 Appearance of bubbles viewed at the sides of the glass cylinder formed with aqueous dispersions of silica particles of diameter 100 nm, 5 wt. %, 3 M NaCl at pH ~ 4.5 (a) bubbles at the top of foam attached to one side of the surface of glass cylinder and (b) bulk foam.

(a)

(b)
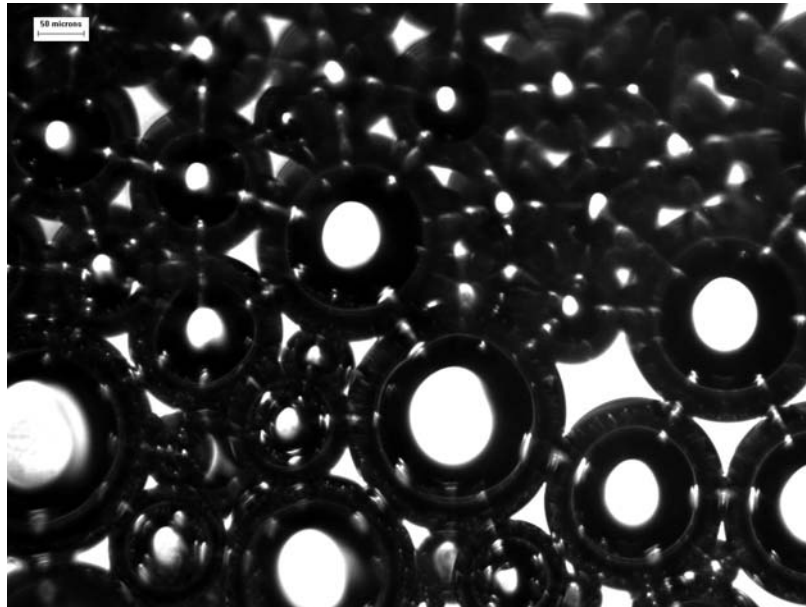
The geometrical shape of gas bubbles in the foam depends on the ratio of gas and liquid volumes, on the degree of polydispersity and on bubble packing. It is well known that the most stable shape for a bubble is a sphere. However, foams tend to be polydisperse, thus resulting in a pressure difference between bubbles of different sizes. The pressure inside a bubble is related to its curvature and is equal to $2\gamma/R$ where R is the bubble radius. Therefore, a small bubble is at higher pressure than a large bubble. Gas diffuses from the high to the low pressure region thus causing a small bubble to grow smaller and a large bubble to grow larger. This is called Ostwald ripening in the case of emulsions. Bubbles observed at the top of all foams formed are polydispersed in size (Figure 3.35 (a)) compared to the bottom of the foam where bubbles are much smaller and monodisperse (Figure 3.35 (b)). Therefore, bubbles at the bottom of the foam are much more stable than the bubbles at the top where the smaller bubble (which always has a higher internal pressure) will bulge into the larger bubble causing rupture of films.

The shaking procedures also influence the amount of foam produced (foamability) and foam stability. Figure 3.36 shows that after applying several hand shake tests to the foam system, the bubbles at the bottom increase in diameter and the foam becomes more unstable. This may be due to increased drainage of the liquid between the bubbles.

Figure 3.35 Appearance of bubbles formed with aqueous dispersions of silica particles of diameter 100 nm, 5 wt. %, 3 M NaCl at pH ~ 4.5. (a) bubbles at the top of foam of diameter 50 - 300 μm, (b) bubbles of diameter 10-20 μm rising up from the bottom of solution to the bottom of foam.

(a)   **(b)**
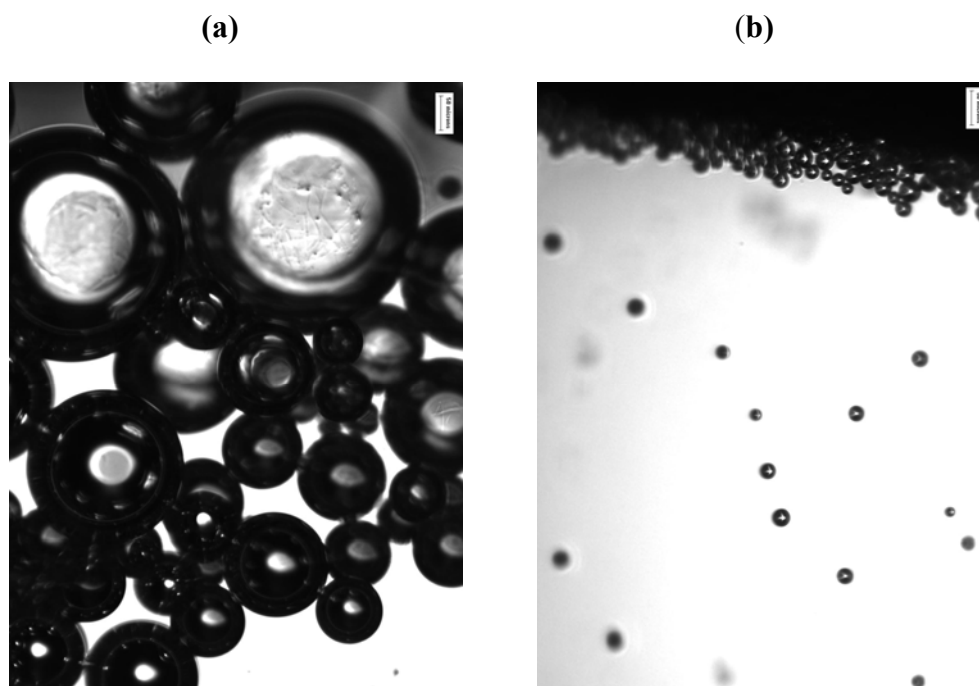
Figure 3.36 Appearance of bubbles formed with aqueous dispersions of silica particles of diameter 101 nm, 5 wt. %, 3 M NaCl at pH ~ 4.5 after applying several hand shakes (bubbles of diameter ~ 40-50 μm).
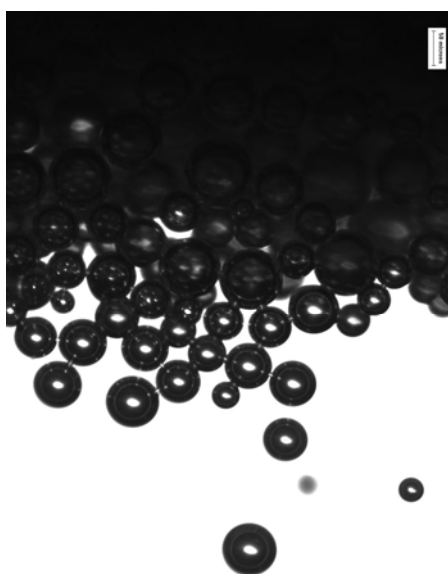
3.10   Conclusions

The purpose of this study was to investigate the foamability and foam stability of aqueous silica dispersions using the simplest method of foam production, the shake test. It was proposed that in the absence of surface–active agents, *e.g.* surfactants, hydrophilic particles can be modified in situ in order to make them more hydrophobic and therefore adsorb at the air-water interface. The key parameters investigated were particle size, particle concentration, pH and NaCl concentration. It was discovered that foamability and foam stability is very dependent on the particle size as only the larger particles (*i.e.* 100 nm) studied gave relatively good stable foams. It was also found that a higher concentration of solid particles and [NaCl] leads to a more viscous dispersion, which is in turn reflected in the higher foam volume and foam stability observed in these systems. It can be concluded that by changing the pH of the aqueous dispersions to about 4 - 4.5 and by adding high concentrations of salt, particles become more hydrophobic and therefore believed to go to the air-water interface.

Zeta potential results show that at high salt concentrations and low pH the charge of silica particles becomes positive and therefore particles behave as hydrophilic. At high pH, silica particles are negatively charged, therefore hydrophilic in nature. At an intermediate pH of 4, particles are uncharged and more hydrophobic. The fact that similar behaviour was observed in other zeta potential studies may suggest that the negative charge on silica can be reversed by adsorbing an excess of positively charged ions on the surface and therefore the IEP of the silica particles can be shifted to higher pH. This can explain why very good foams could be prepared at pH around 4, and not at pH 2 as would be expected. The contact angles of aqueous NaCl on hydrophilic glass were also measured and it was observed that they increase with increasing concentration of NaCl drops. This implies that the particle hydrophobicity is increasing with salt concentration and so particles adsorb at the air-water interface enhancing foamability and foam stability. However, the contact angles of aqueous NaCl on a silicon substrate (previously treated to render them hydrophilic), increased to up to 3 M NaCl and then slightly decreased at higher salt concentrations. This may suggest that at very high salt concentrations particles are positively charged and therefore hydrophilic in nature.

References

1. B.P. Binks, *Current Opin. Colloid Interface Sci.*, **7**, 21 (2002).

2. P.C. Hiemenz and R. Rajagopalan, Principles of Colloid and Surface Chemistry, 3rd Ed., Marcel Dekker, New York (1997).

3. J. Ralston, *Adv. Colloid Interface Sci.*, **23**, 1 (1983).

4. F. Tang., Z. Xiao, J. Tang and L. Jiang, *J. Colloid Interface Sci.*, **133**, 498 (1988).

5. J.B.N. Hudales and H.N. Stein, *J. Colloid Interface Sci.*, **140**, 307 (1990).

6. J.C. Wilson, A study of particulate foams, Ph.D. thesis, University of Bristol (1980).

7. S.K. Bindal, G. Sethumadhavan, A.D. Nikolov and D.T. Wasan, *AIChE J.*, **48**, 2307 (2002).

8. S.W. Ip, Y. Wang and M. Toguri, *Can. Meta. Quart.*, **38**, 81 (1999).

9. J. Banhart, N.A. Fleck and A. Mortesen, Cellular Metals: Manufacture, Properties, Applications, MIT-Verlag, Berlin (2003).

10. S. Fujii, P.D. Iddon, A.J. Ryan and S.P. Armes, *Langmuir*, **22**, 18 (2006).

11. R.K. Iler, The Chemistry of Silica, John Wiley & Sons, New York (1979).

12. V.N. Paunov, B.P. Binks and N.P. Ashby, *Langmuir*, **18**, 6946 (2002).

13. G. Sethumadhavan, S.K. Bindal, A.D. Nikolov and D.T. Wasan, *Colloids Surf. A,* **204**, 51 (2002).

14. E. Dickinson, R. Ettelaie, T. Kostakis and B.S. Murray, *Langmuir*, **20**, 8517 (2004).

15. R.G. Alargova, D.S. Warhadpande, V.N. Paunov and O.D. Velev, Langmuir, 20, 10371 (2004).

16. U.T. Gonzenbach, A.R. Studart, E. Tervoort and L. Gauckler, *Angew. Chem. Int. Ed.,* **45**, 3526 (2006).

17. U.T. Gonzenbach, A.R. Studart, E. Tervoort and L. Gauckler, *Langmuir*, **22**, 10983 (2006).

18. R.K. Prud'homme and S.A. Khan, Foams: Theory, Measurements and Applications, Marcel Dekker, New York (1996).

19. Z. Du, M.P. Bilbao-Montoya, B.P. Binks, E. Dickinson, R. Ettelaie and B.S. Murray, *Langmuir*, **19**, 3106 (2003).

20. E. Dickinson, R. Ettelaie, T. Kostakis and B.S .Murray, *Langmuir*, **20**, 8517 (2004).

21. G. Kaptay, *Colloids Surf. A.*, **230**, 67 (2004).

22. B. Wu and R.G. Reddy, *Mettal. Mater. Transf. B.,* **33**, 543 (2002).

23. G.J. Fokkink and J. Ralston, *Colloids and Surf.*, **36**, 69 (1989).

24. M.A. Butkus and D. Grasso, *J. Colloid Interface Sci.,* **200**, 172 (1998).

25. J.H. Clint and A.C. Wicks, *International Journal of Adhesion and Adhesives*, **21**, 267 (2001).

26. J.H. Clint and T.Dunstan, University of Hull, unpublished results.

27. J-W. Hu, G-B. Han, B. Ren, S-G. Sun and Z-Q Tian, *Langmuir*, **20**, 8831 (2004).

28. B.P. Binks and S.O. Lumsdon, *Langmuir*, **16**, 8622 (2000).

29. B.P. Binks, A.K.F. Dyab, P.D.I. Fletcher and H. Barthel, European patent assigned to Wacker-Chemie GmbH (2002).

30. G. Johansson and R. Pugh, *Int. J. Min. Proc.*, **3**, 1 (1992).

31. S. Paria and K.C. Khilir, *Adv. Colloid Interface Sci.*, **110**, 75 (2004).

32. H.E. Bergna, in *Advances in Chemistry Series*, Vol. 234, American Chemical Society, Washington, (1994).

33. R. Denoyel, F. Rouquerol and J. Rouquerol, in *Fundamentals of Adsorption*, A.I Liapis (ed.), Engineering Foundation*,* p. 199, New York (1987).

34. F. Dumont, in *Advances in Chemistry Series*, Vol. 234, H.E. Bergna (ed.), Washington, p. 143 (1994).

35. L.H. Allen and E. Matijevic, *J. Colloid Interface Sci.,* **31**, 287 (1969).

36. V.F. George, *J. Colloid Interface Sci.*, **249**, 44 (2002).

37. G. Xu, J. Zhang and G. Song, *Powder Technology,* **134**, 218 (2003).

38. C.E. McNamee, M. Matsumoto, P.G. Hartley and M. Nakahara, *Colloids Surf. A,* **193**, 175 (2001).

39. W.N. Rowlands, R.W. O' Brien, R.J. Hunter, and V. Patrick., *J. Colloid Interface Sci.,* **188**, 325 (1997).

40. J. Senne, B. Robillard and M. Vignes-Adler, *Colloids Surf. B,* **21**, 59 (2001).

41. M. Kosmulski and J.B. Rosenholm, *J. Colloid Interface Sci.,* **248**, 30 (2002).

42. M. Kosmulski, J. Gustafsson and J.B. Rosenholm, *J. Colloid Interface Sci.,* **209**, 200 (1999).

43. M. Kosmulski and J.B. Rosenholm, *J. Phys. Chem.*, **100**, 11681(1996).

44. M. Kosmulski, S. Durand-Vidal, J. Gustafsson and J.B. Rosenholm, *Colloids Surf. A,* **157**, 245 (1999).

45. J-P Hsu and Y-T Chang, *Colloids Surf. A*, **161**, 423 (2000).

46. J.W. Goodwin and R.W. Hughes, Rheology for Chemists: An Introduction, Royal Society of Chemistry, Cambridge (2000).

47. H.A. Barnes, *J. Non-Newtonian Fluid Mech.*, **81**, 133 (1999).

48. I.D. Morrison and S. Ross, Colloidal Dispersions: Suspensions, Emulsions and Foams, Wiley-Interscience, New York, (2002).

49. P. Sherman, Emulsion Science, Academic Press, London, (1968).

50. J.P. Heller and M.S. Kuntamukkula, *Ind. Eng. Chem. Res.*, **26**, 318 (1987).

51. J.J. Bikerman, Foams, Springer-Verlag, Heidelberg, Berlin, New York (1973).

52. S.A. Khan, C.A. Schnepper, and R.C. Armstrong, *J. Rheol.*, **32**, 69 (1988).

53. B.S. Gardener, B.Z. Dlugogorski, G.J. Jameson and R.P. Chhabra, *J. Rheol.*, **42**, 1437 (1998).

54. D. Exerowa and P.M. Kruglyakov, Foams and Foam Films: Theory, Experiment, Application, Elsevier, New York (1998).

CHAPTER 4

CHAPTER 4

STABILISATION OF FOAMS WITH EX-SITU MODIFIED
COLLOIDAL SILICA PARTICLES

4.1   Introduction

Small solid particles of colloidal dimensions (nm – μm) adsorb to liquid surfaces in many products and processes, for example, fat crystals around air bubbles in certain foods and the selective attachment of mineral particles to bubbles in froth flotation. Manipulation of the behavior of particles adsorbed at fluid interfaces enables the development of a novel range of foams for use in the food industry, detergent, and cosmetic formulations. The properties of these systems are due in part to the irreversible nature of particle adsorption and such particles behave in may ways like surfactant molecules.[1] Particle–stabilised foams offer the advantage of longer stability in comparison to surfactant–stabilised foams. Small spherical or quasi-spherical solid particles with an appropriate hydrophobicity can stabilise foams.[2-6] The attachment of particles at the gas-liquid interface requires an optimum balance between the solid-liquid, solid-gas, and liquid-gas interfacial energies and is therefore dependent on the wetting behaviour at the particle surface. Therefore this study aimed to determine if it is possible to adjust the hydrophobicity of silica particles by silanisation and investigate if these modified particles can stabilise foams.

This study is concerned with understanding the properties of foams stabilised solely by monodisperse spherical silica particles that exhibit different extents of hydrophobicity. In contrast to the previous chapter where the hydrophobicity of hydrophilic silica particles is changed *in situ*; in this chapter the hydrophobicity of silica particles of different diameters were modified *ex-situ* by silanisation with dichlorodimethylsilane (DCDMS) in the presence of dry toluene. The reaction of dichlorodimethylsilane results in the formation of dimethylsiloxy groups on the particle surface. Figure 4.1 shows a representation of both a hydrophilic and a hydrophobic silica particle.

Figure 4.1 Schematic representation of a hydrophilic (left) and a hydrophobic silica particle (right).
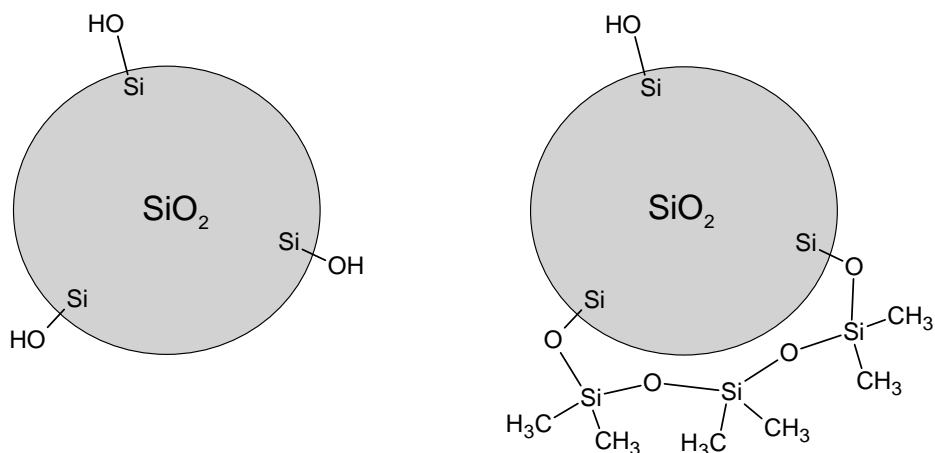
The foaming ability and foam stability of aqueous dispersions of sub-micron silanised silica particles were investigated by using the glass cylinder shaking test and by homogenisation using Ultra-Turrax homogeniser. The key parameters investigated were particle hydrophobicity, particle concentration, salt concentration and particle size.

4.2 Surface tension measurements

Silica particles of different diameters were washed with Milli-Q water and ethanol before silanisation. Surface tensions of all supernatants obtained from the washing procedures were determined using the du Noüy ring method. Tables 4.1 and 4.2 show the results collected for the 0.1, 0.6 and 2 μm silica particles, respectively.

Table 4.1 Surface tension of Milli-Q water and the supernatants obtained from centrifuging a dispersion containing 10 wt. % of 0.1 μm silica particles (measured at 25 °C).

Liquid	γ / (mN) m^{-1}
Milli - Q water	72.38
1st supernatant	71.81
2nd supernatant	72.00

Table 4.2   Surface tension of Milli-Q water and pure ethanol and the supernatants obtained from centrifuging a dispersion containing 5 wt. % of 0.6 μm silica particles (measured at 25 °C).

Liquid	γ / (mN) m^{-1}
Milli - Q water	73.02
Pure ethanol	22.30
1st supernatant	71.89
2nd supernatant	72.30
3rd supernatant (ethanol)	22.70

It was observed that when the smallest silica particles (*e.g.* 0.1 and 0.6 μm) were dispersed in water, they did not foam and the surface tension of the resultant supernatants are very close to the surface tension of pure water or pure ethanol. It can be concluded that these particles did not contain surface-active impurities. However, higher concentrations of the larger silica particles, *e.g.* 2 μm, when dispersed in water cause foaming after only shaking the contents in the glass vessel. Tables 4.3 and 4.4 shows the results of surface tension measurements of all supernatants obtained from the washing procedures in the case of two different concentrations of the 2 μm silica particles.

Table 4.3   Surface tension of Milli-Q water and the supernatants obtained from centrifuging a dispersion containing 30 wt. % of 2 μm silica particles (measured at 25 °C).

Liquid	γ / (mN) m^{-1}
Milli - Q - water	71.58
1st supernatant - water	61.94
2nd supernatant - water	67.72
3rd supernatant - water	71.50

Table 4.4   Surface tension of Milli-Q water and the supernatants obtained from centrifuging a dispersion containing 10 wt. % of 2 μm silica particles (measured at 25 °C).

Liquid	γ / (mN) m^{-1}
Milli - Q water	71.58
1st supernatant - water	67.93
2nd supernatant - water	71.53

From the results, it can be seen that by reducing the concentration of silica particles, less washing cycles are necessary in order to achieve the surface tension close to pure water. The foam shake test was applied to all the supernatants to see if they foamed and only a few bubbles were observed at the top of the glass vessel, which burst very quickly. Therefore, it seems that although the surface tension results show that these particles contain some surface impurities, these are not the principal cause for the formation of foam itself. After washing these particles at least twice with pure water no foam was observed and the surface tension of the second supernatant was very close to the surface tension of pure water.

4.3   Particle contact angles

A key parameter when dealing with solid particles at fluid interfaces is the three-phase contact angle, θ that particles exhibit at the interface. The contact angle is directly related to the particle hydrophobicity (wettability) and its knowledge is of great practical importance. The wettability of the silica particles in this study was modified *ex-situ* to different extents by reacting the hydrophilic silica with different concentrations of dichlorodimethylsilane (DCDMS) in the presence of dry toluene for a fixed period of time. As a monolayer of dimethylsiloxy groups on the particle surface forms, particles become increasingly hydrophobic (alkyl chains exposed to solution). The actual microscopic contact angle of the individual particles was unknown. So, in order to know whether the modified silica particles are increasing in hydrophobicity by simply increasing the silanising agent concentration, an assumption was made (as may other researchers usually do) that the microscopic contact angle of these particles is a same as the macroscopic contact angle on a flat smooth substrate of the similar material

146

chemically modified at the same conditions as the solid particles. Therefore, an attempt to measure their contact angle was made through the water on glass slides hydrophobised simultaneously with the particles. The results obtained are shown in Table 4.5, which shows that the air- water contact angles of 0.6 μm size silica particles gradually increase with an increase in DCDMS concentration. This means that the hydrophobicity of these particles is increasing as the [DCDMS] is increased. However, the contact angle measured on the modified glass slides are not the actual contact angle of the modified particles, because the contact angle of individual particles could be different from the macroscopic one on the flat solid with the same surface composition, due to their chemical and roughness differences. However, this indirect method gives an estimation of the contact angle of the particles at the air-water interface and also shows that there is a relationship between the concentration of DCDMS used and the hydrophobicity of the particles.

Table 4.5   Average of advancing and receding three - phase contact angles of water drops on glass slides silanised simultaneously with silica particles of diameter 0.6 μm at different [DCDMS] in dry toluene in the range 3×10^{-4} to 0.2 M. The contact angle on the unmodified bare glass slide (without DCDMS) is also shown.

[DCDMS] / M	air-water average contact angle / deg.
0	5
3×10^{-4}	46
8×10^{-4}	58
3×10^{-3}	77
4×10^{-3}	95
8×10^{-2}	105
0.2	110

4.4 Stability of aqueous silica dispersions before foaming

The stability of aqueous silica dispersions was investigated using a Turbiscan Lab Expert instrument in the scanning mode, which follows the evolution of the dispersion with time through the height of the sample (bottom to top) so particle migration can be easily detected (see Chapter 2 for details). The sample analysis can be done in two modes:

(a)   Reference mode: This means that a given profile (the profile at t = 0 is used by default) is subtracted from all other profiles. By subtracting the reference profile, variations are emphasised. In this mode it is possible to compute the kinetics (mean value for particle size variations and peak thickness for particle migrations)

(b)   No reference mode: The profiles are shown as acquired. In this mode it is possible to compute data on one sample (*e.g.* BS (t), I*(t), d (t), etc.). However, the variations can be difficult to observe.

Therefore, in order to see the variations of the profiles more easily it is recommended to put the profiles in reference. The main instabilities observed with colloidal systems are of two types:

(a)   Particle migration, *i.e.* local variations of the concentration of particles in the sample, hence local variations of the transmissions or backscattering level measured.

(b)   Particle size increase, *i.e.* global variations of the particle size in the sample due to flocculation, hence global variations of the transmission or backscattering level measured.

Graphs obtained when analysing the turbiscan profiles can be interpreted in three parts: bottom, middle and top. Variations in the bottom and top of the sample are linked to migration phenomena. Variations in the middle are due to particle size variations. The effect of particle hydrophobicity and salt concentration on the stability of aqueous silica dispersions studied was investigated and the results obtained are described below.

4.4.1   Effect of particle hydrophobicity

The effect of particle hydrophobicity on the stability of aqueous dispersions containing a fixed particle concentration of 3 wt. % and no salt was first investigated. Figure 4.2 shows the raw data obtained for transmission (top) and backscattering (bottom) light flux in percentage versus height in the vessel in mm for an aqueous dispersion of hydrophilic (unmodified) silica particles. Low height corresponds to the bottom of the sample. The time of acquisition of the profiles is shown in different colours on the right – hand side of the graphs.

Figure 4.2   Turbiscan profile analysis programme showing the curves of transmitted (top) and backscattered (bottom) light flux in % as a function of the sample height in mm for an aqueous dispersion of 3 wt. % hydrophilic silica particles of diameter 0.6 μm at pH ~ 6 and no salt. These profiles are displayed in the 'reference mode' (t = 0). The times (in day, hr, min and s) are given on the right.
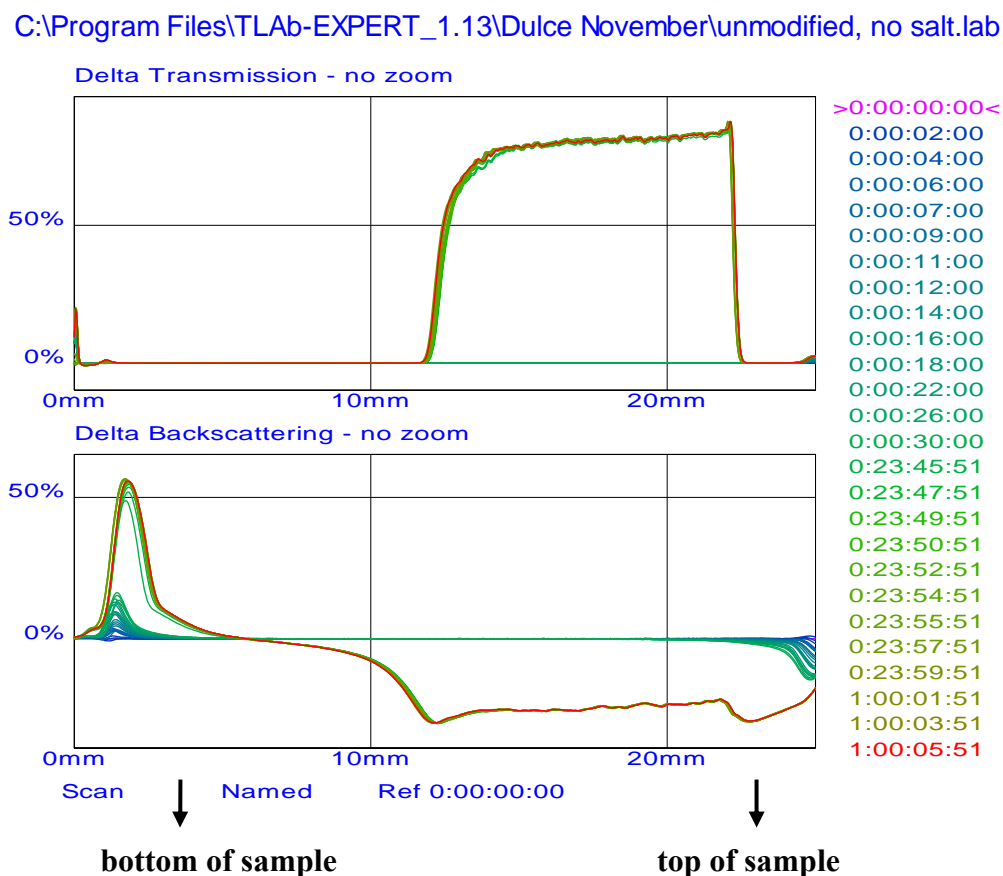
Sedimentation is a common phenomenon of instability for suspensions, encountered when the density of the dispersed phase is greater than the density of the continuous phase. This phenomenon is very easily detected using the Tursbiscan as it induces a variation of the concentration of the dispersed phase between the top and the bottom of the sample. As can been seen in Figure 4.2 the backscattering increases at the bottom of the sample with time due to an increase in the concentration of the dispersed phase (sediment) and decreases at the top of the sample due to a decrease of the concentration (clarification). Although, sedimentation occurs with these unmodified silica particles, the sedimentation is rather slow and it is observed over a long period of time. This can be confirmed by the transmission profile, which shows that there is no transmission signal in the first few hours after preparation of the dispersion as the whole vessel appeared turbid. Only after around one day is a clear phase separation observed and a transmission signal is then seen at the top of the vessel (from approx. 12 to 22 mm). Once the destabilisation phenomenon in this case sedimentation, has been identified the following parameters can be computed by the software:[7]

(a)   The variation of backscattering (ΔBS) between the top and the bottom of the cell to compare quickly various dispersions.

(b)   The phase thickness (ΔH) of the sediment layer and/or the clear phase, in order to be able to follow its formation.

(c)   The migration velocity of the clarification front (slope of the clarified phase thickness), in order to follow the kinetics of the sedimentation phenomenon.

The mean value kinetics (ΔBS or ΔT) at the top and the bottom of the vessel can be obtained by computing a mean value for each Delta backscattering or Delta transmission profile in between two defined limits (height of vessel) as a function of time. Figures 4.3 and 4.4 shows the variation of ΔBS at the bottom and top of vessels with time. The vessels contained dispersions of silica particles of different hydrophobicity, at a fixed particle concentration of 3 wt. % and no salt.

Figure 4.3 ΔBS at the bottom of the vessel (0 - 6 mm) versus time for 3 wt. % aqueous dispersions of silica particles of diameter 0.6 μm at different hydrophobicity and no salt.
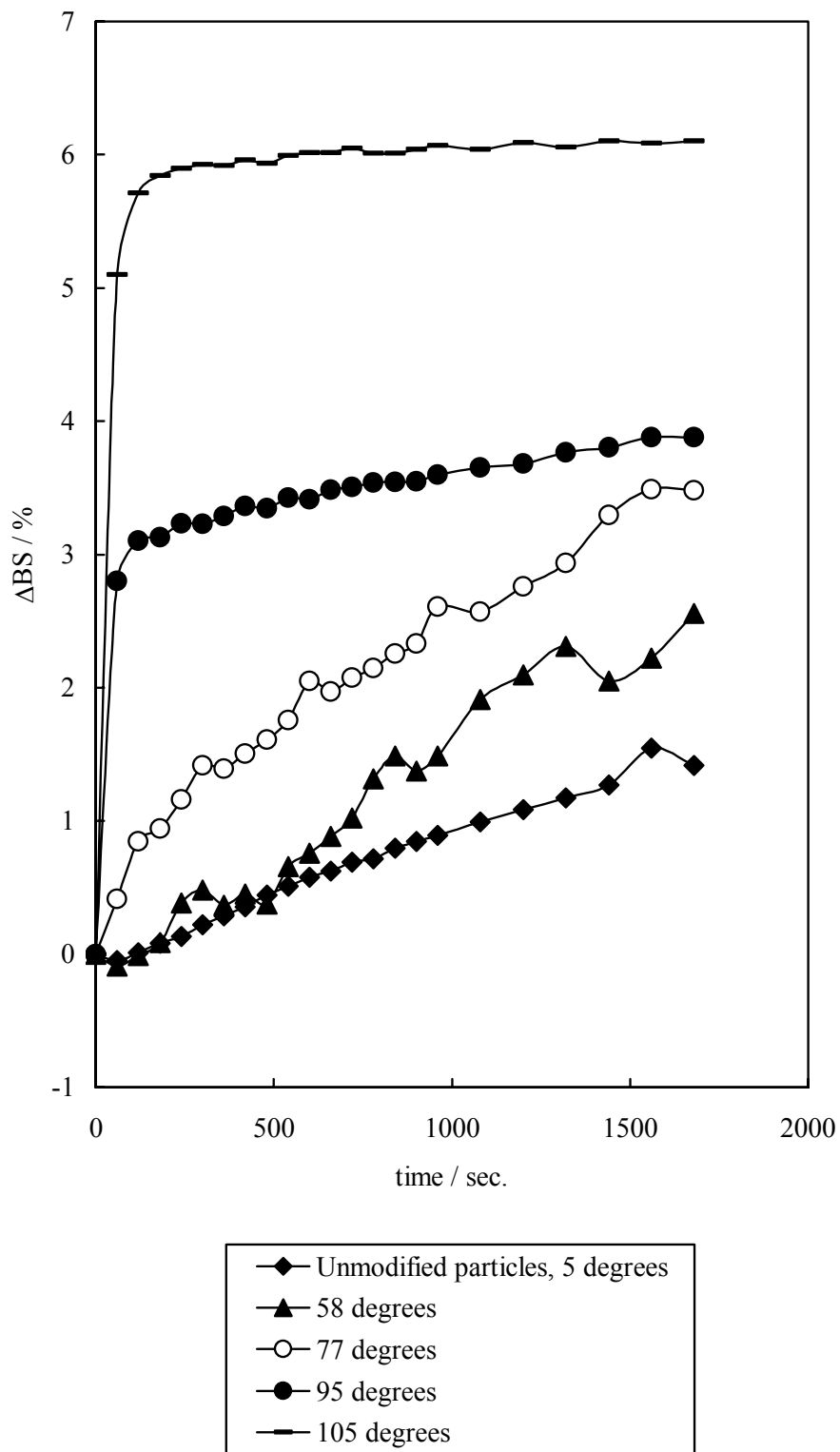
Figure 4.4 ΔBS at the top of the vessel (12 - 22 mm) versus time for 3 wt. % aqueous dispersions of silica particles of diameter 0.6 μm at different hydrophobicity and no salt.
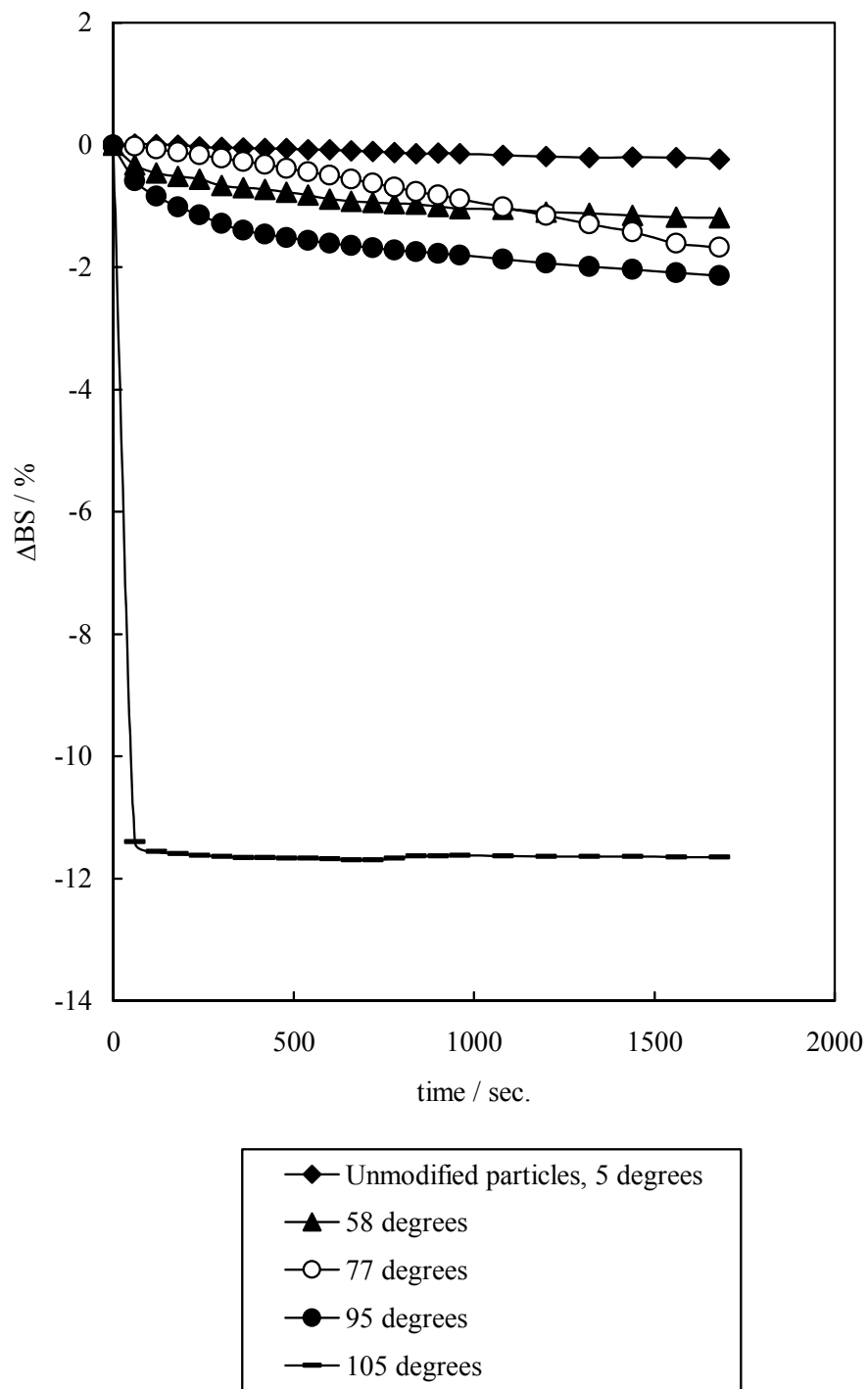
It can be clearly seen that ΔBS increases at the bottom of all samples due to an increase of the sediment layer and decreases at the top of the samples due to a decrease of the concentration (clarification). However, ΔBS for dispersions containing the most hydrophobic particles (*e.g.* 95 and 105°) increases very quickly initially (steep curve) at the bottom of the vessel and then reaches a plateau. This means that the most hydrophobic particles sediment at a much faster rate until reaching a certain height of sediment. This sediment remains constant for a long period of time and then slowly with time starts to become more compacted in the bottom of the vessels. ΔBS for the dispersions containing the less hydrophobic particles (*e.g.* 5 to 77°) increases gradually with time.

When backscattering and transmission profiles are displayed in a reference mode a peak appears (as shown in Figure 4.2). This peak enlarges over the course of time and its thickness at a ΔBS or ΔT threshold can be computed as a function of time. Figure 4.5 shows the phase thickness (ΔH) of the sediment layer (left peak) computed from the backscattering data at the bottom of the vessels (0 to 8 mm) versus time for 3 wt. % aqueous dispersion of silica particles at different particle hydrophobicity. The sediment layer measured here corresponds to the same as would be measured by eye with a ruler. It was found that the dispersions containing the most hydrophobic silica particles (*e.g.* 105°) sediment very quickly immediately after the preparation of the dispersion and then reach a plateau in the thickness of the sediment. The higher the hydrophobicity of the particles the higher is the sediment layer, showing their instability compared with the unmodified or less hydrophobic particles (*e.g.* 58°) which sediment gradually with time at a much slower rate. However, after one day, all vessels showed a sediment layer at the bottom of the vessels (see Figures 4.6 and 4.7).

Figure 4.5 ΔH (phase thickness of the sediment layer) from backscattering data obtained between height limits (0 to 8 mm) versus time for 3 wt. % aqueous dispersion of silica particles of diameter 0.6 μm at different particle hydrophobicity and with no salt.
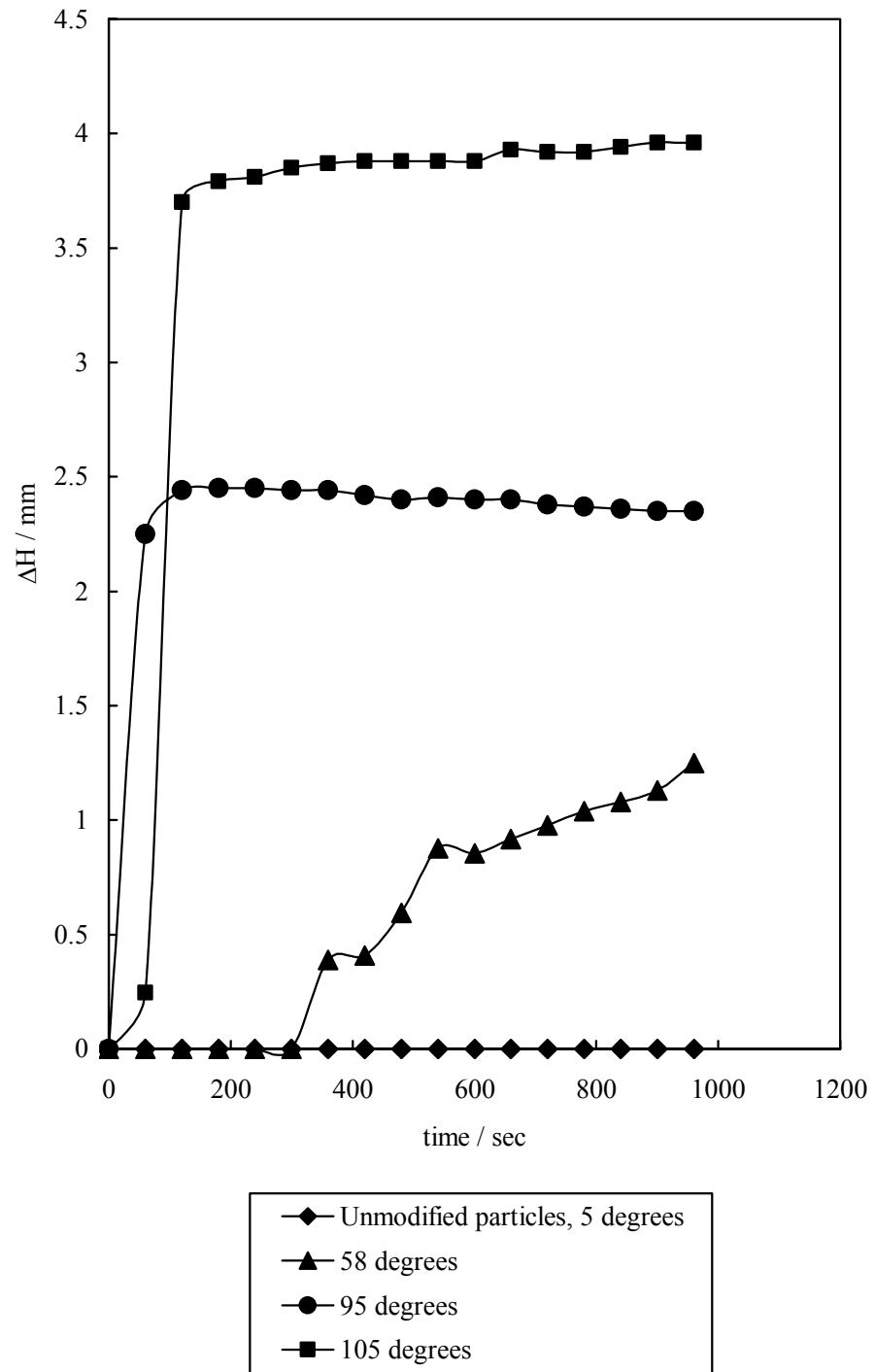
Figure 4.6 ΔH (phase thickness of the sediment layer) from backscattering data obtained between height limits (0 to 8 mm) at long time for 3 wt. % aqueous dispersion of silica particles of diameter 0.6 μm at different particle hydrophobicity and no salt.
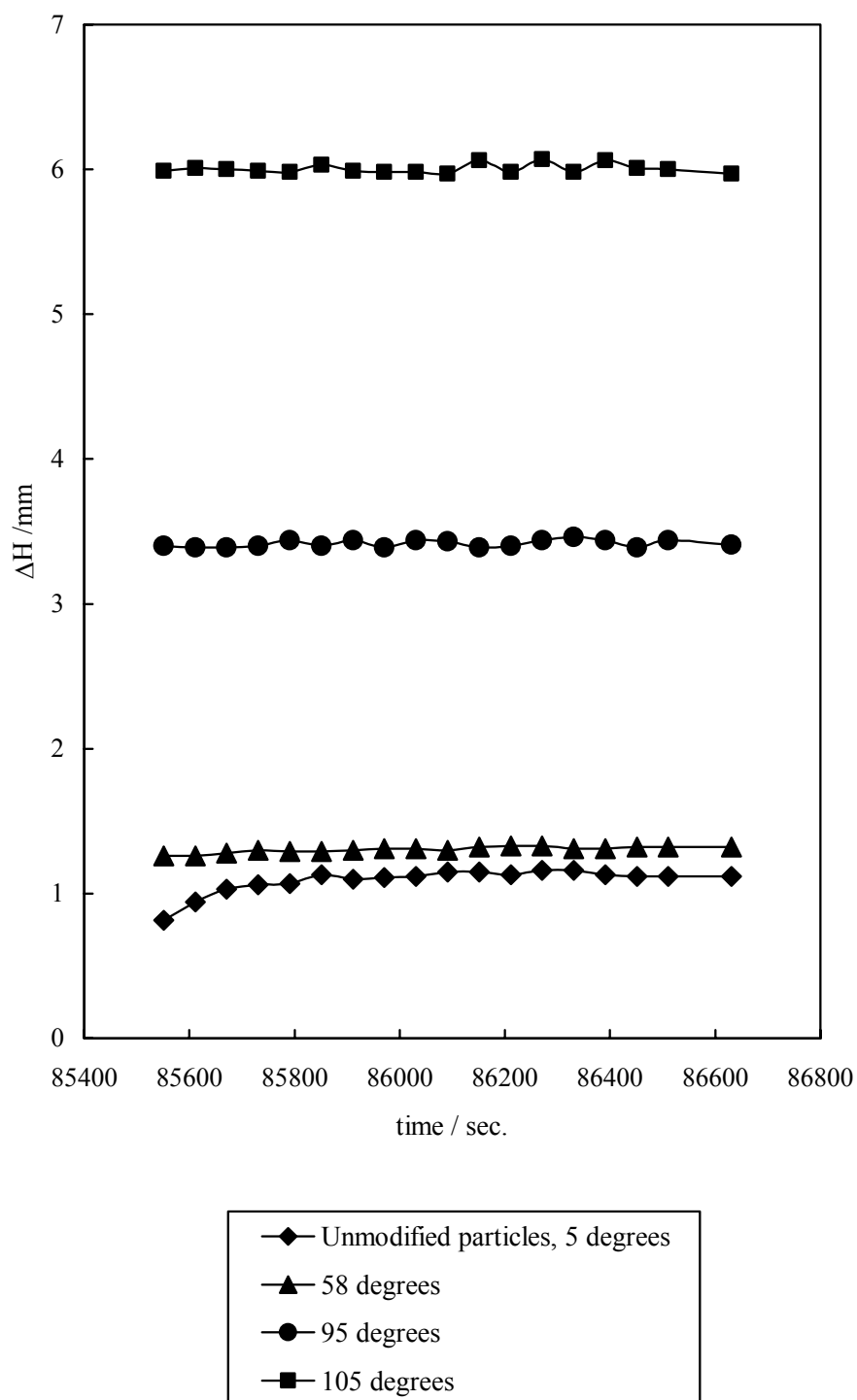
Figure 4.7   Appearance of vessels after one day for aqueous silica dispersions of diameter 0.6 μm at a fixed [particle] = 3 wt. %, pH around 6 and at different particle hydrophobicity: (a) hydrophilic (unmodified) particles, 5°, (b) 58°, (c) 95°, (d) 105°.
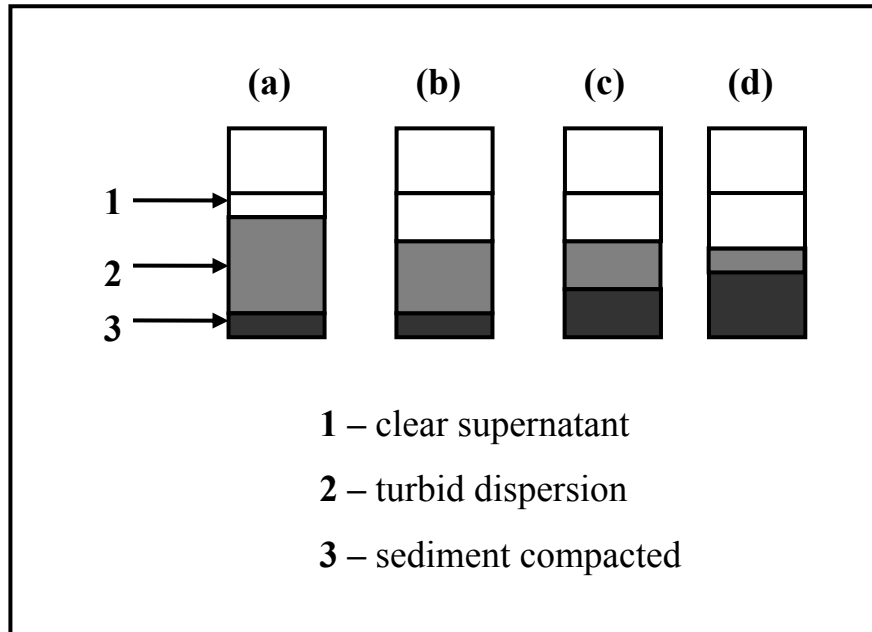
In the case of a destabilisation like sedimentation, when the backscattering and transmission profiles are displayed in 'no reference mode', a front that is moving over time is observed. A function, V (t), is available in the Graph menu of both transmission or backscattering profile graphs and computes the velocity of this front as a function of time. From the V (t) graph the migration rate mean velocity (V) can be computed. In order to compute V two limits are chosen. As V is a mean value of the velocity data, it is important that the V (t) is stable within the calculated zone. The software uses the general law of sedimentation to compute V and other hydrodynamic parameters. The Stokes Law extended to concentrated dispersions is:[8]

$$V(\phi,d) = \frac{|\rho_P - \rho_C| \times g \times d^2}{18 \times v \times \rho_C} \cdot \frac{[1-\phi]}{\left[1 + \dfrac{4,6\phi}{(1-\phi)^3}\right]} \qquad (4.1)$$

where V is the particle migration velocity (ms^{-1}), ρ_c is the continuous phase density (kgm^{-3}), ρ_p is the particle density (kgm^{-3}), g is the gravity constant (9.81 ms^{-2}), d is the particle diameter (μm), v is the continuous phase dynamic viscosity (cP) and ϕ is the volume fraction of the dispersed phase (%). One of the following parameters can be computed (by knowing the other ones): the continuous phase dynamic viscosity, the volume fraction, the continuous phase density, the dispersed phase density and the hydrodynamic diameter.

In order to confirm if the silanised particles sediment quicker than the unmodified particles due to an increase of the primary particle size (aggregation of the particles) further parameters were investigated and computed. The particle size variation induced by flocculation is easily detected by the Turbiscan, as it leads to a decrease of the backscattering over the whole height of the sample. Figure 4.8 shows an example of the graphs obtained from the Turbiscan profile analysis for backscattering light flux when displayed in 'no reference mode' and V (t) computed from backscattering as a function of time for an aqueous dispersion of hydrophilic silica particles (unmodified). From the graph of V (t) versus time, the migration velocity V and the hydrodynamic particle diameter d can be obtained (as clearly seen in Figure 4.8). The hydrodynamic particle diameter is obtained from the value of V calculated between two limits defined on the curve V (t) and by knowing other parameters like, for example, the volume fraction of the particles used (*e.g.* 3 wt.%) and the density of the particles (~ 2 g/cm^3). The mean velocity and the mean particle diameter for different aqueous dispersions of silica particles of different hydrophobicity was obtained as described above over a fixed period of time (*e.g.* from ~ 0 to 20 min). Figure 4.9 shows the hydrodynamic silica particle diameter and the mean velocity of the same particles as a function of particle hydrophobicity. It can be seen that the particle diameter increases from ~ 0.6 μm (unmodified silica) to up to 3 μm (silanised silica particles of θ = 105°), showing that the aggregation of particles is increasing with the hydrophobicity of the particles. As a result of this, their mean velocity is also higher and particles sediment quickly to the bottom of the vessel. The appearance of the aqueous silica dispersions at different particle hydrophobicity is shown in Figure 4.10.

Figure 4.8 Turbiscan profile analysis programme showing the graphs of backscattering light flux in % as a function of the sample height in mm (top) and particle migration velocity, V (t) computed from the backscattering graph as a function of time (bottom) for an aqueous dispersion of 3 wt. % hydrophilic silica particles of diameter 0.6 μm at pH ~ 6 and no salt. These profiles are displayed in the 'no reference mode'.

C:\Program Files\TLAb-EXPERT_1.13\Dulce\unmodified silica - no salt.lab
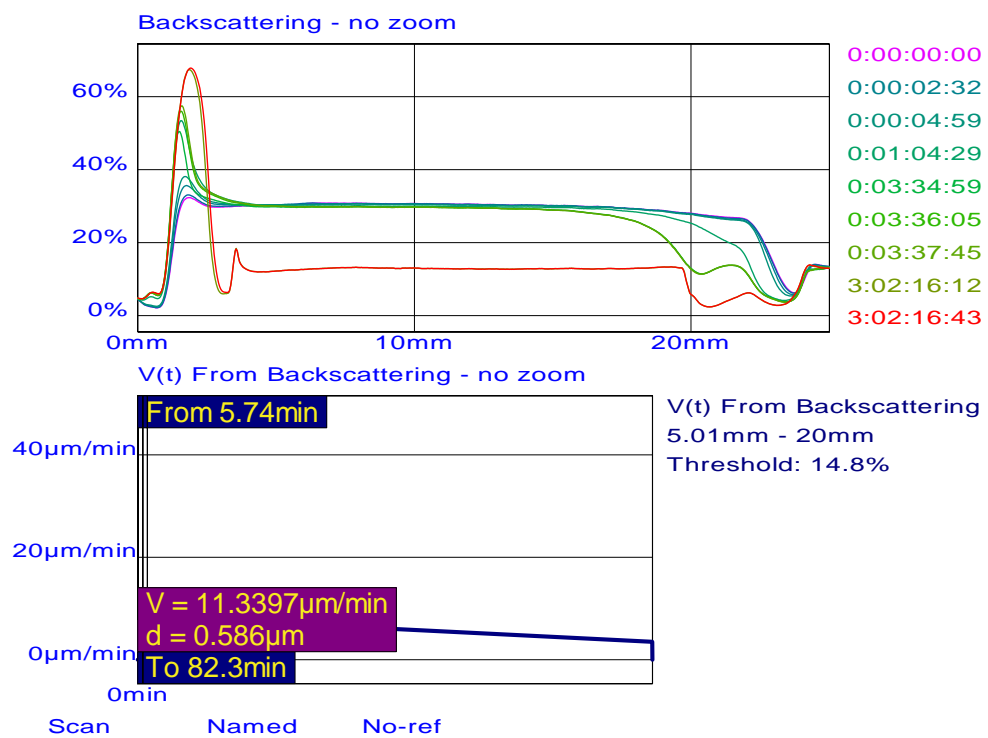
Figure 4.9 Hydrodynamic particle diameter and mean particle velocity versus particle hydrophobicity for 3 wt. % aqueous dispersions of silica particles of diameter 0.6 μm and no salt (data obtained in the first 20 minutes after sample preparation).
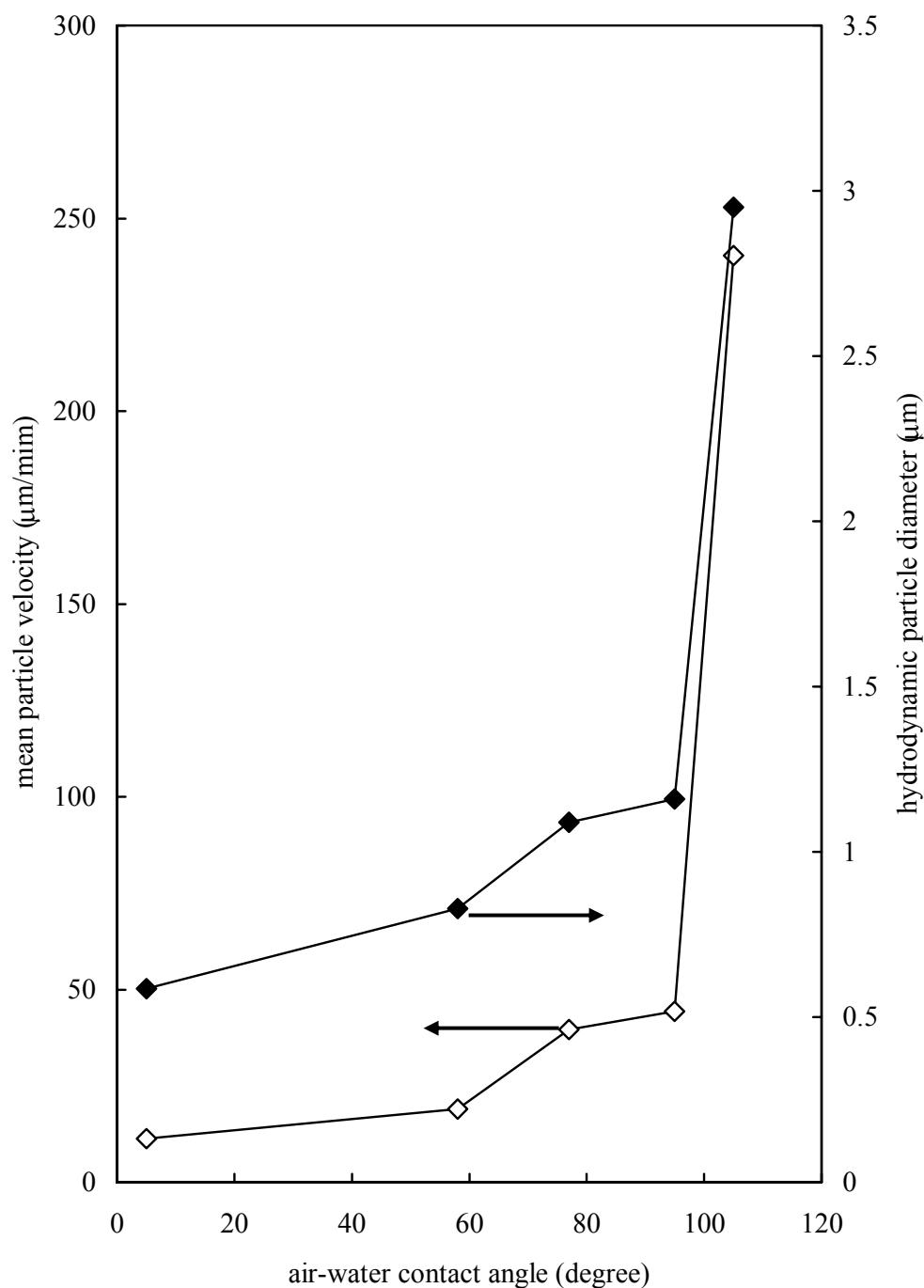
Figure 4.10 Appearance of vessels immediately after preparation containing aqueous silica dispersions of diameter 0.6 μm at a fixed [particle] = 3 wt. %, no salt, pH around 6 and for different particle hydrophobicity.

$\theta \sim 5°$ $\theta \sim 58°$ $\theta \sim 77°$ $\theta \sim 95°$ $\theta \sim 105°$ $\theta \sim 110°$
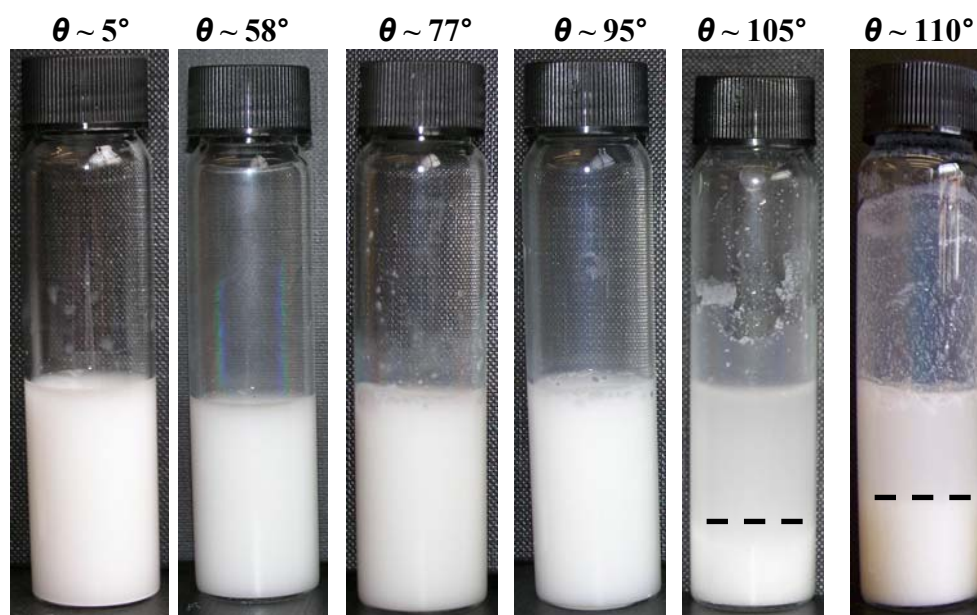
4.4.2   Effect of NaCl concentration

The effect of salt concentration on the stability of the aqueous unmodified and silanised dispersions before foaming was also investigated. At a fixed particle concentration of 3 wt. %, addition of NaCl leads to a dramatic change in the stability of the dispersions. This happens when salt is added to the unmodified silica particles and to all of the different silanised silica particles studied. A few examples are given in Figure 4.11. It can be seen that the initial stable dispersion, at no salt, begins to sediment very quickly by increasing the NaCl concentration to up to 1 M. It is also clear that the degree of flocculation obtained with NaCl depends on the initial hydrophobicity of the silica particles. Figure 4.12 shows that for unmodified silica particles, the hydrodynamic silica particle diameter increases from ~ 0.6 μm (no salt) to up to 4.25 μm (1 M NaCl), showing that extensive flocculation has occurred at high salt concentrations leading to sedimentation of particles. The critical coagulation concentration (c.c.c.) of salt just required to flocculate the dispersion decreases progressively with increasing in particle hydrophobicity as the repulsion between charged particles decreases.

Figure 4.11 Appearance of aqueous silica dispersions of diameter 0.6 μm previously silanised with (A) [DCDMS] = 8 × 10^{-4} M (θ_{aw} average = 58°), (B) [DCDMS] = 4 × 10^{-3} M (θ_{aw} average = 95°) and (C) [DCDMS] = 8 × 10^{-2} M (θ_{aw} average = 105°), at a fixed particle concentration of 3 wt. %, pH = 6 and different [NaCl]: (i) no salt, (ii) 0.05 M, (iii) 0.1 M, (iv) 0.5 M and (v) 1 M NaCl after a few minutes.
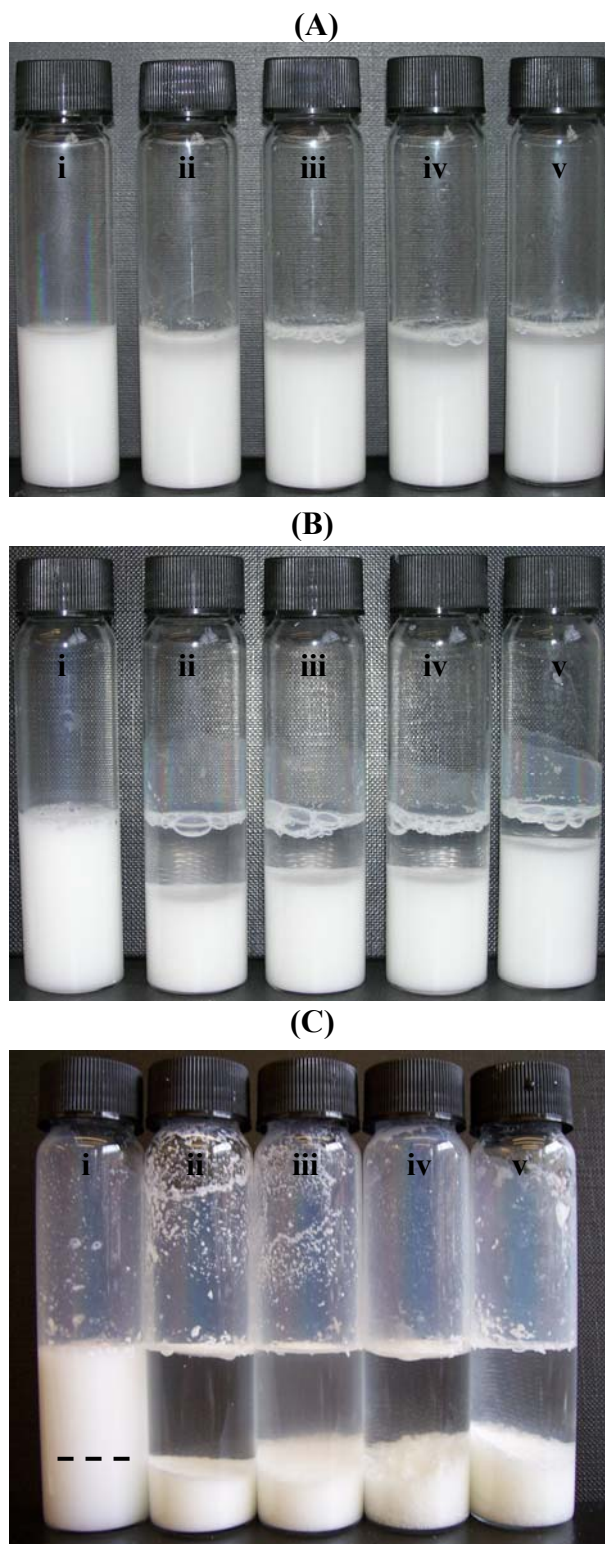
(A)

(B)

(C)

Figure 4.12 Hydrodynamic particle diameter and particle velocity (clarified phase) versus NaCl concentration for 3 wt. % aqueous dispersions of unmodified silica particles of diameter 0.6 μm at different [NaCl] (data obtained in the first 20 minutes after sample preparation).
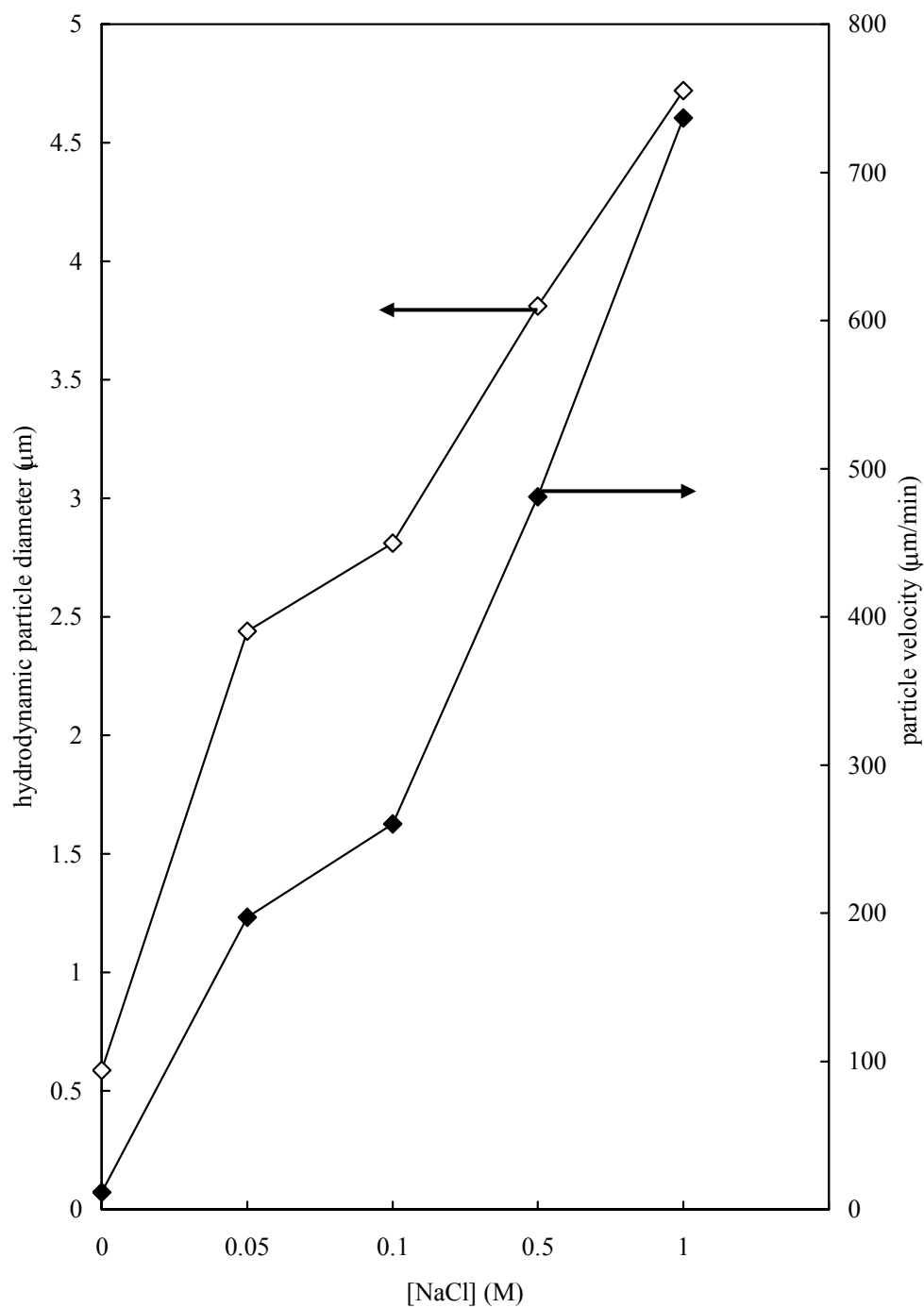
4.5   Foaming ability and foam stability of aqueous silica dispersions

To understand the effect of the inherent hydrophobicity of the silica particles on their ability to stabilise aqueous foams, a systematic study was initiated with monodisperse silica particles of different diameters. However, this study was mainly focused with silica particles of diameter 0.6 μm. The effects of different methods of foam production, particle hydrophobicity, particle concentration and addition of salt on foamability and foam stability were investigated. First the foamability and foam stability of the aqueous unmodified silica particles was investigated in order to compare with the foaming systems prepared with the hydrophobised silica particles.

4.5.1   Hydrophilic (unmodified) silica particles

The foamability and foam stability of the aqueous unmodified hydrophilic silica particles of diameter 0.6 μm (θ_{aw} estimated = 5 - 10°), at a fixed concentration (*e.g.* 3 wt. %) at different [NaCl] and pH around 6 (no salt) – 4.5 (1 M NaCl) was investigated. Without salt, such particles do not cause foaming by either hand shaking or homogenisation using the Ultra - Turrax. However, addition of salt (*e.g.* 0.5 and 1 M NaCl) enhances the foamability of these aqueous hydrophilic silica dispersions (see Figure 4.13). It was found that silica particles in aqueous salt sediment quicker than in those without salt.

As silica particles in water and bare air-water surfaces are negatively charged, addition of salt to water may enhance the transfer of particles to the surface by reducing the energy barrier to adsorption.[9] This may lead to improved foamability and stability of the foam as shown in Chapter 3. A higher volume of foams was obtained with the Ultra - Turrax homogeniser compared with the foams generated by hand shaking. Foams formed with the Ultra - Turrax homogeniser are also different from those formed by hand shaking. The bubbles formed by hand shaking are spherical and much smaller than the bubbles formed by the Ultra - Turrax, where bubbles are bigger in size and polyhedral in shape (dry foams). One reason for this may be the fact that when the Ultra – Turrax is used, vessels are open and more air is incorporated from the top of the dispersions. The bubbles at the top of the foam are bigger and more unstable than the bubbles at the bottom of the foam. After 24 hours, the bubbles in the dry foams formed by either homogenisation or hand shaking are bigger in size and distorted (disproportionation and coalescence of bubbles). However, foam remains stable to total

collapse. It seems that particles adsorb at air bubbles and stabilise the films between the bubbles. It was also observed, after 24 hours, that the supernatant in all vessels increased and became much clearer. The sediment was also more compacted at the bottom of the vessel.

Figure 4.13 Appearance of foams from aqueous hydrophilic silica dispersions of diameter 0.6 μm (θ_{aw} estimated to ~ 5°) at a concentration of 3 wt. %, pH ~ 6 at different [NaCl]: (a) no salt, (c) 0.5 M, (c) 1 M NaCl. The times refer to times after foam generation by (A) hand shaking or (B) homogenisation at 13, 000 rpm.

(A)

(B)
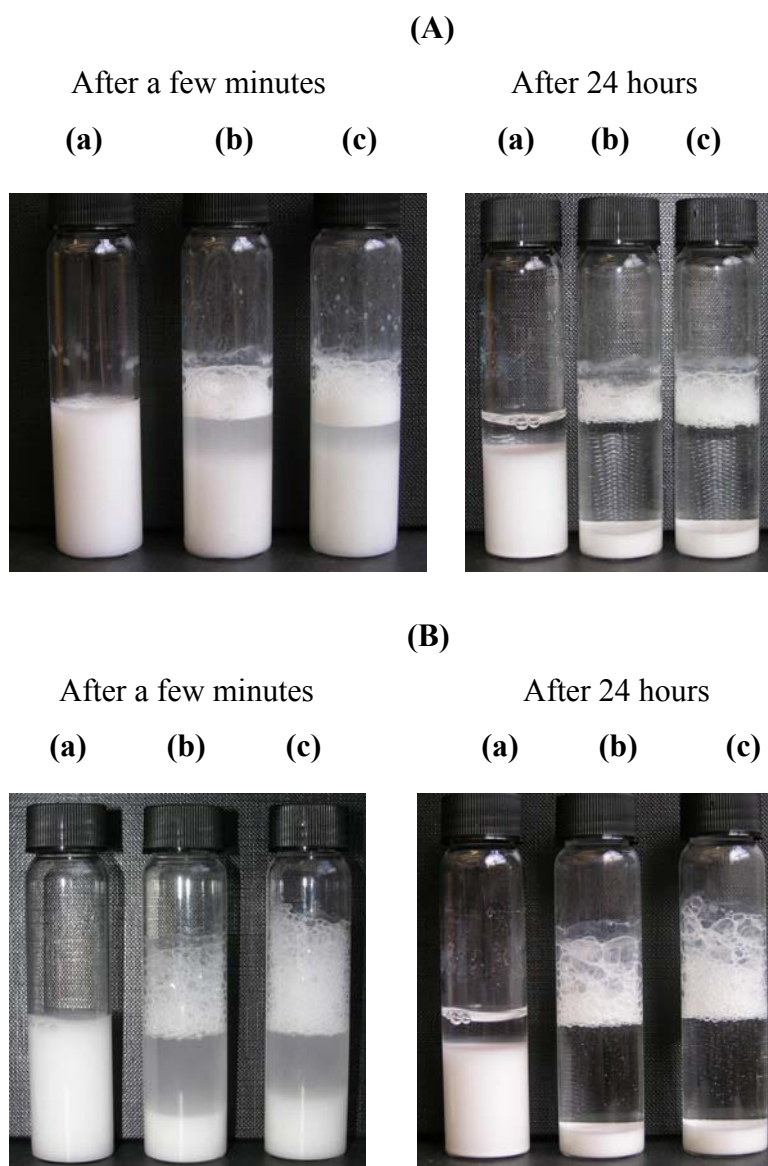
Silanised silica particles with contact angles of 46° and 58° were easily dispersed in water like the unmodified silica particles. However, when silica particles with contact angles ranging from 77° to 110° were dispersed in water, these particles exhibited hydrophobic behaviour. The silica particles remained at the air–water surface rather than entering the bulk and during shaking, rapid film growth on the glass vessel surfaces was observed. An example is given in Figure 4.14. Therefore, an alternative method to disperse the most hydrophobic particles was used as was described in detail in Chapter 2.

Figure 4.14 Appearance of vessel containing silica particles of diameter 0.6 μm previously silanised at [DCDMS] $= 3 \times 10^{-3}$ M (θ_{aw} average $= 77°$) at a concentration of 3 wt. % and no salt, immediately after hand-shaking (particles were not dispersed in the bulk).

particle film
climbs up
the vessel wall
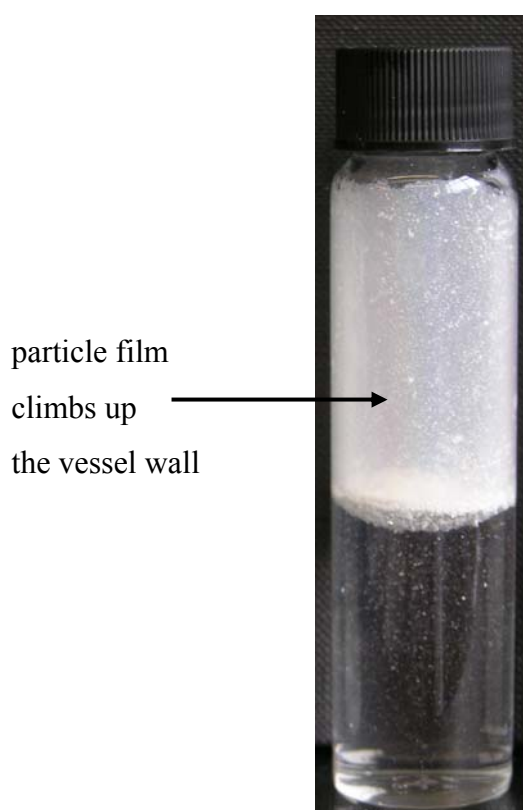
Since these findings, a paper by Binks *et al.*[10] was published which describes the particle film growth driven by foam bubble coaslescence. Shaking the initial two phase mixture forms foam bubbles. The foam bubbles are unstable with respect to coalescence with the flat air-water interface, possibly because the adsorption of silica particles at the curved and flat air-water surfaces is too low to prevent coalescence. Coalescence of the foam bubbles with the flat air-water surface transfers particles to the interface between the bulk phases and the additional surface pressure of the adsorbed particles causes the film to climb up the hydrophilic walls.[10]

4.5.2.1 Effect of particle hydrophobicity

The effect of particle hydrophobicity was investigated with 1.5 or 3 wt. % aqueous dispersions of silica particles of different diameters, containing no salt or salt by using different methods for foam production. Only some of these systems will be shown here. In the absence of salt no foam is formed for very hydrophilic particles of $\theta \sim 5°$. As described in the previous section, by increasing the particle hydrophobicity particles become more aggregated and the foaming ability of the aqueous dispersions of silica particles of diameter 0.6 μm is enhanced until intermediate contact angle ($\theta \sim 95°$), after which it decreases (see Figure 4.15). In the case of extreme aggregation, observed with the most hydrophobic particles ($\theta = 110°$), the foamability (the capacity to produce the foam in the first place) was reduced compared with particles of intermediate hydrophobicity (bigger aggregates diffuse slower, thus hindering the attachment of particles at the air-water interface). Big flocs were observed at the foam-water interface at high hydrophobicity ($\theta \sim 105°$ and 110°). They are very sensitive to mechanical vibration and detach very easily from the bubble-water surface. If the glass vessels are left undisturbed the big flocs remain below the foam for a longer period of time (they eventually sediment with time but at a very slow rate). Nevertheless the most stable foams are those formed with the most hydrophobic particles, where the adsorbed particles form a coagulated solid network preventing coalescence and disproportionation of bubbles. Figure 4.16 shows more clearly the effect of particle hydrophobicity on the foaming ability and foam stability of the same aqueous silica dispersions shown in Figure 4.15 (the most hydrophobic particles, *e.g.* 77 to 110° were first dispersed in water and ethanol mixtures before foaming). Another possible reason for the fact that the most hydrophobic particles achieved here (*e.g.* 105 and 110°) foamed less than the particles of intermediate hydrophobicity, may be due to their

antifoaming behaviour. It is known from the literature that particles exhibiting contact angle higher than 90° can behave as antifoaming agents for surfactant – stabilised foams.[11-13]

Figure 4.15 Appearance of foams from 10 mL aqueous silica dispersions of diameter 0.6 μm previously silanised at different [DCDMS] at a concentration of 3 wt. %, pH = 6 and no salt after a few minutes of foam generation by homogenisation at 17, 000 rpm.

$\theta \sim 5°$ $\theta \sim 46°$ $\theta \sim 58°$ $\theta \sim 77°$ $\theta \sim 95°$ $\theta \sim 105°$ $\theta \sim 110°$

no foam **1 cm** **1.5 cm** **3 cm** **3.5 cm** **2.5 cm** **2.5 cm**
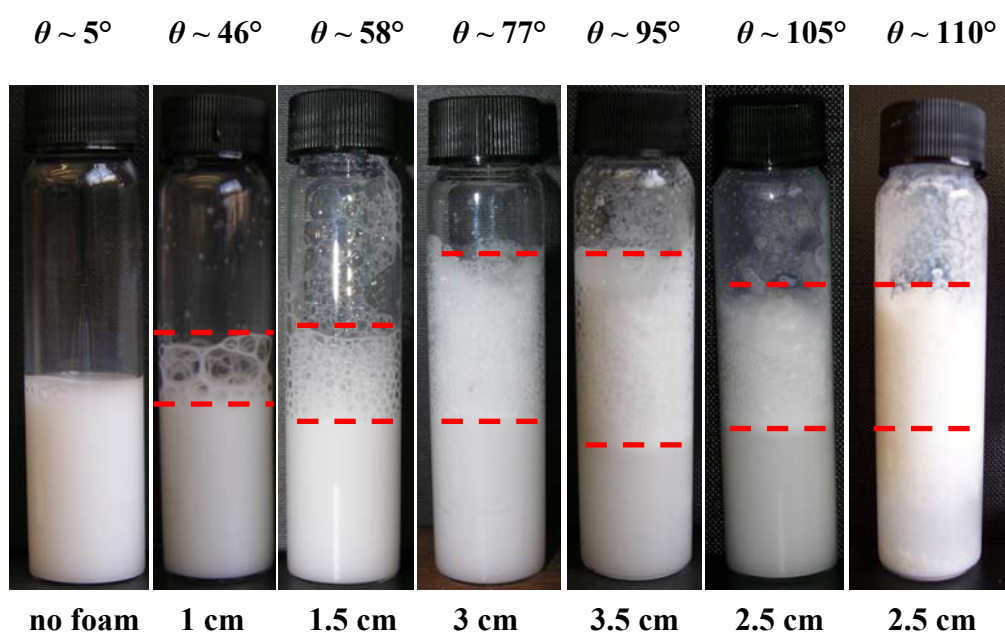
Figure 4.16 Graph of initial foam height and foam height after 48 hours versus estimated particle hydrophobicity for 10 mL aqueous silica dispersions of diameter 0.6 μm previously silanised at different [DCDMS] at a concentration of 3 wt. %, pH = 6 and no salt. Foams were produced by homogenisation at 17, 000 rpm.
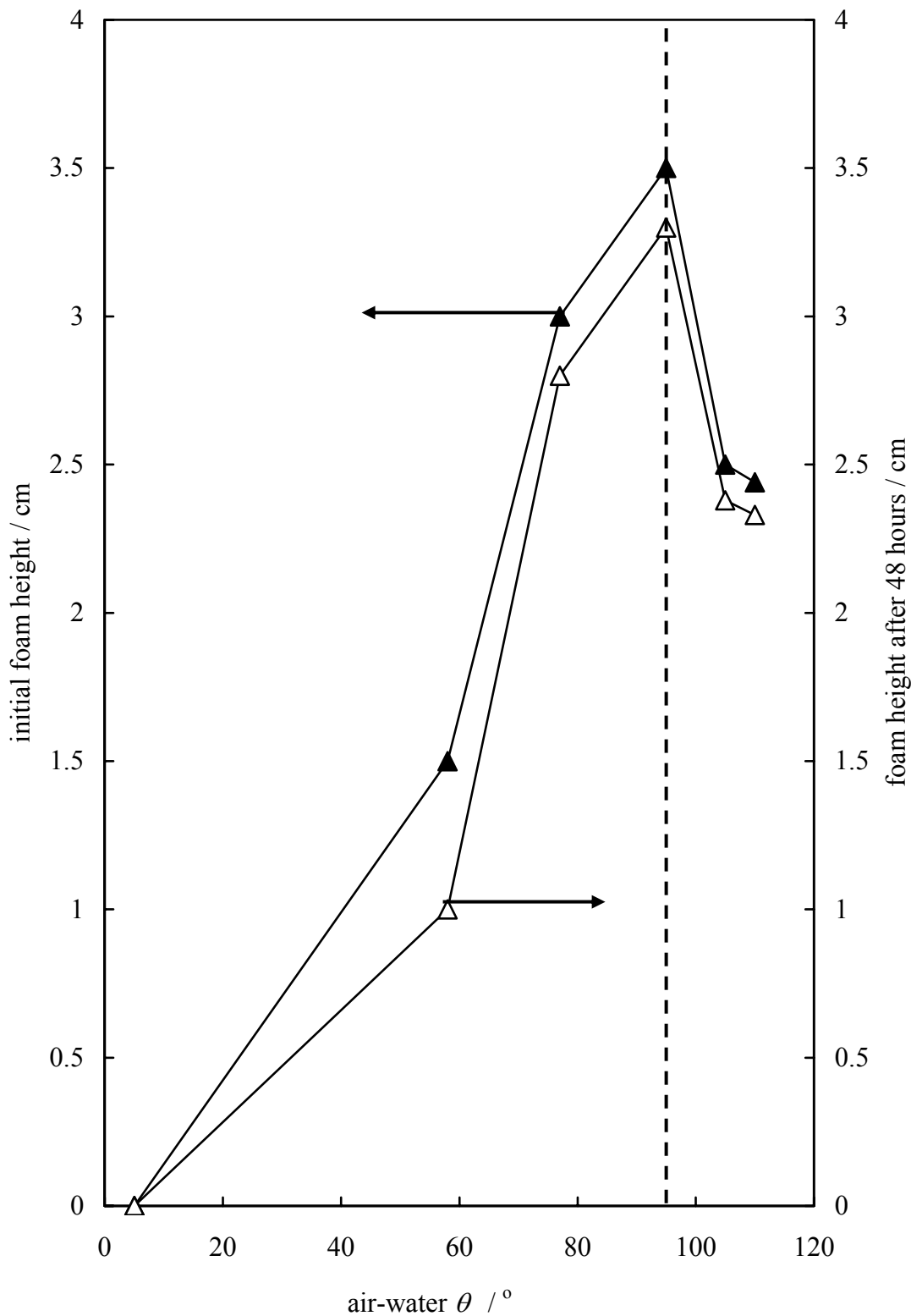
Figure 4.17 shows foams that were produced without dispersing the most hydrophobic particles, *e.g.* 77 to 110°, in the bulk (particles stayed at the air-water surface and homogenisation was applied at 17, 000 rpm).

Figure 4.17 Appearance of foams from 10 mL aqueous silica dispersions of diameter 0.6 μm previously silanised at different [DCDMS]: (a) 77°, (b) 95°, (c) 105° with dry toluene at a concentration of 3 wt. %, pH = 6 and no salt. The times refer to times after foam generation by homogenisation at 17, 000 rpm.

(a)

Before foaming	After a few minutes	After 24 hours

(b)

Before foaming	After a few minutes	After 24 hours
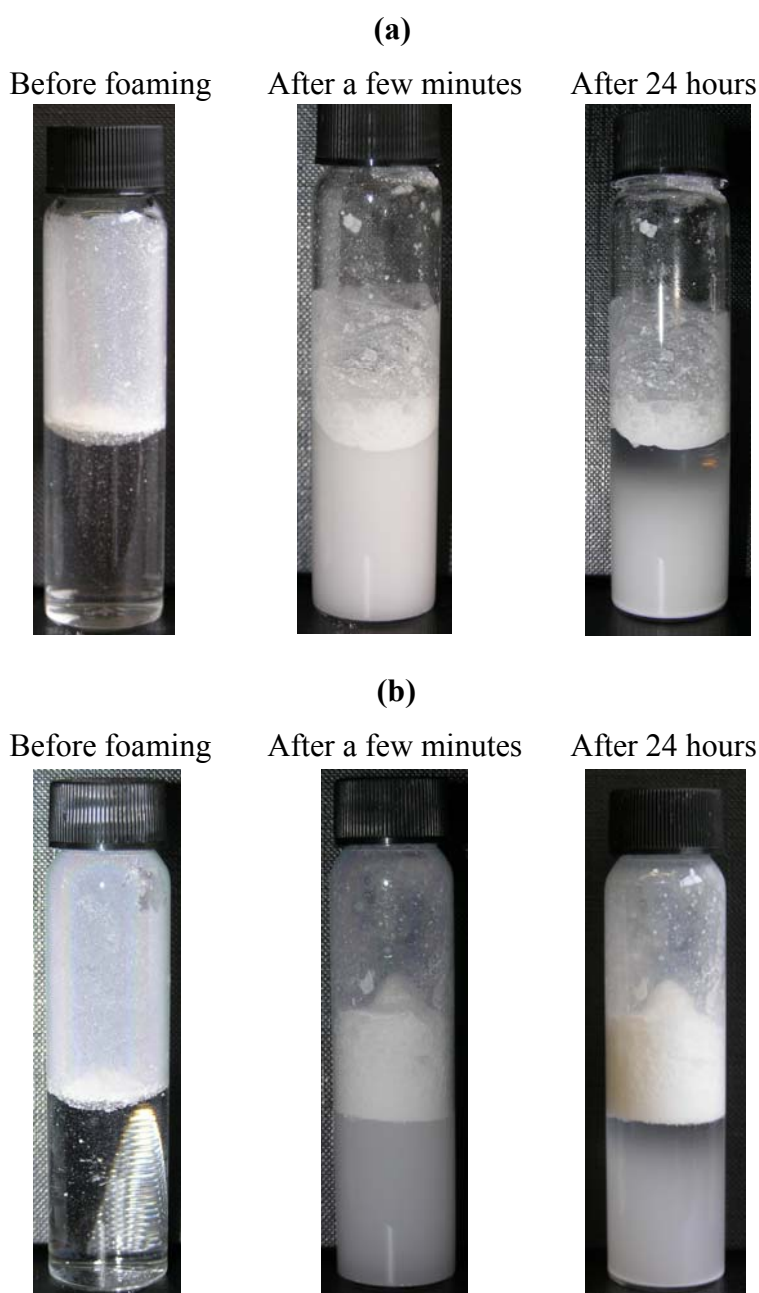
(c)

Before foaming   After a few minutes   After 24 hours
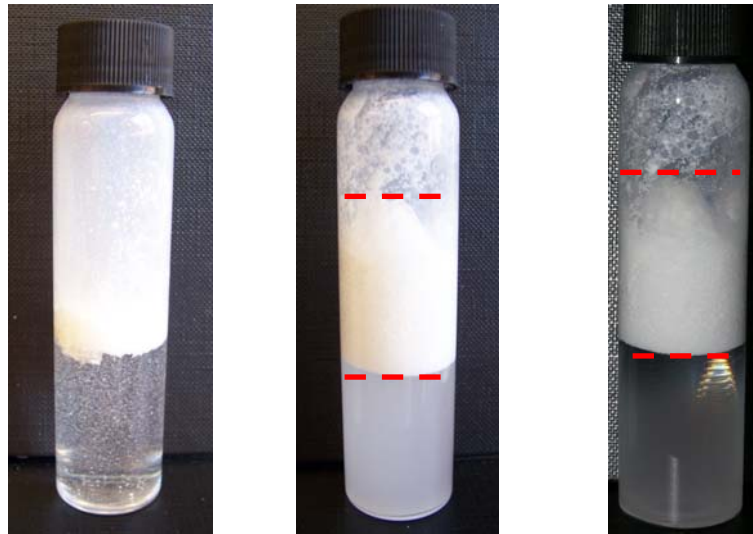
After 5 days

(a)   **(b)**   **(c)**
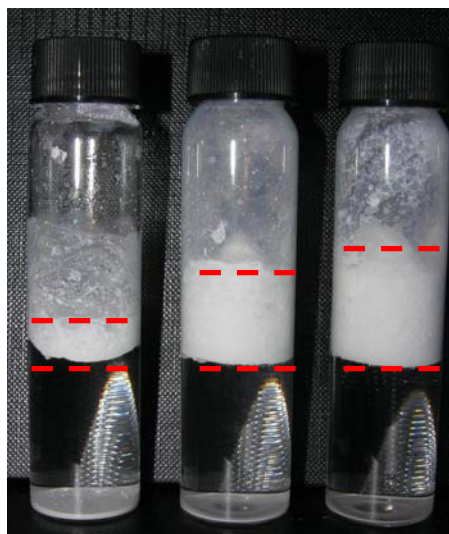
In the case where the most hydrophobic particles are not initially dispersed in bulk before foaming, it is observed that by increasing the particle hydrophobicity the foaming ability is enhanced. This may be due to the fact that the most hydrophobic particles ($\theta = 105°$) have the capacity to readily coagulate at interfaces and form a strong gel network whereas in the case of the particles with $\theta = 77°$ this doesn't happen.

Theoretical studies on liquid films stabilised by solid particles has been reported by Kaptay[14,15], assuming either a bridging monolayer or a bilayer of hexagonally close-packed particles. The stability of the film in both cases is determined by the maximum capillary pressure (p_c^{max}), which is depedent on the particle contact angle, θ, at the air-water interface and also on the arrangement of particles in the liquid film between the bubbles. The following general equation was derived for the maximum capillary pressure:[15]

$$p_c^{max} = 2\, p\gamma\, (cos\,\theta + z)/r \qquad (4.2)$$

where r is the radius of the spherical solid particle, γ the interfacial tension between the liquid and gas, θ is the contact angle of the solid particle at the air-water interface, p and z are functions of the particle arrangement. A higher positive value of p_c^{max} ensures that a thin liquid film between the bubbles of a foam can withstand a higher pressing force. The main finding obtained from these theoretical studies was that particles with contact angles $\geq 90°$ should not be able to stabilise water films by a bridging monolayer mechanism. However, aqueous films could be stabilised by a close-packed bilayer of hydrophobic particles with contact angles smaller than ~ 129°, because p_c^{max} is greater than zero up to θ ~ 129°. This is in agreement with the results shown here, where the foams obtained with the most hydrophobic silica particles of contact angle higher than 90° were very stable against disproportionation or coalescence of bubbles. These results are quite interesting. However, more studies are needed in order to obtain conclusive data for foam films or foams stabilised by hydrophobic solid particles alone ($\geq 90°$).

4.5.2.2 Effect of NaCl and particle concentration

Addition of sodium chloride (in the range 0.05 to 1 M) to the aqueous silica dispersions of diameter 0.6 μm, previously silanised at [DCDMS] = 8×10^{-4} M (θ_{aw} average ~ 58°), at a fixed particle concentration (*e.g.* 1.5 or 3 wt. %) was investigated. It was found that addition of salt causes a slight increase in foamability but foam stability is very similar in all systems (see Figure 4.18). When these silanised silica particles were dispersed in water (without NaCl) such particles do not cause foaming as observed with the unmodified silica particles.

Figure 4.18 Appearance of foams from aqueous silica dispersions of diameter 0.6 μm previously silanised at [DCDMS] = 8×10^{-4} M (θ_{aw} average = 58°) at a concentration of 1.5 wt. % (pH ~ 5) at different [NaCl]: (a) no salt, (b) 0.05 M, (c) 0.1 M, (d) 0.5 M and (e) 1 M NaCl. The times refer to times after foam generation by hand shaking.

Before foaming   After a few minutes

(a)   (b)   (c)   (d)   (e)   (a)   (b)   (c)   (d)   (e)

After 1 hour   After 48 hours

(a)   (b)   (c)   (d)   (e)   (a)   (b)   (c)   (d)   (e)
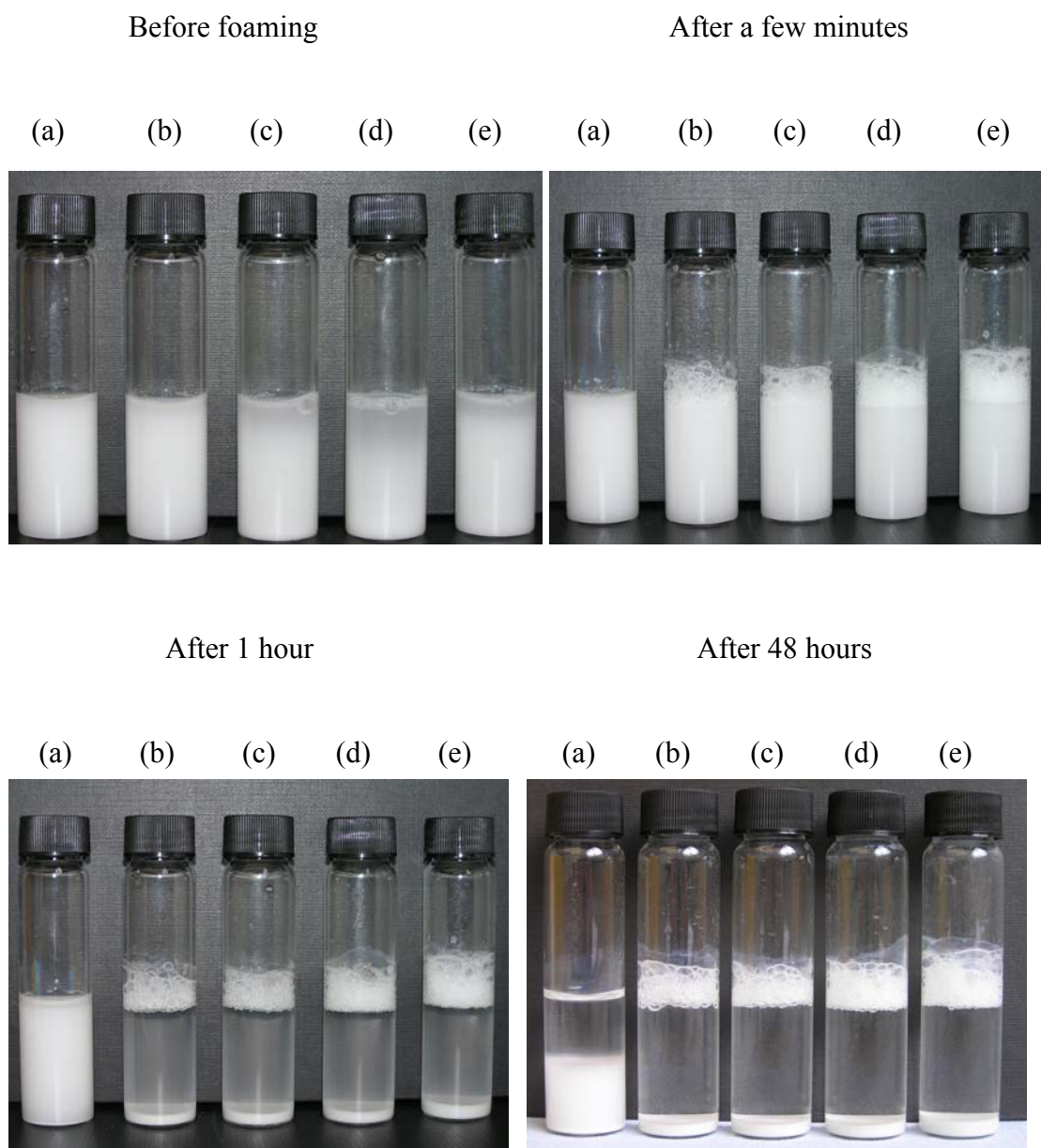
Overrun is a term used to describe the amount of air that the total dispersion contains. It refers to the increase in the volume of the dispersion (after being foamed) compared to the initial volume of dispersion used. The value of Overrun can be used to determine the quality of the foams formed. The % Overrun can be calculated as follows:

$$\% \text{ Overrun} = (V_T - V_0)/V_0 \text{ x } 100 \%\ \quad\quad (4.3)$$

where V_T is the total volume of dispersion after foaming and V_0 is the initial volume of dispersion. $V_T - V_0$ corresponds to the volume of gas incorporated. The volume fraction of air ($\varnothing_{air}$) in the foam is given by:

$$\varnothing_{air} = V_g / (V_g + V_l)\ \quad\quad (4.4)$$

where V_g and V_l are the volume of gas and liquid in the foam respectively ($V_g + V_l = V_{foam}$). The liquid fraction in the foam is then given by:

$$\varnothing_l = 1 - \varnothing_{air}\ \quad\quad (4.5)$$

In the case of 1.5 wt. % aqueous silanised silica dispersions containing 0.05 and 0.1 M NaCl, the % Overrun calculated after a few minutes of foam generation is around 23 % and slightly higher (33 %) with the system containing 1 M NaCl. The breakdown of the foams generated were monitored over time (see Figure 4.19). A slight decrease in foam volume was observed initially due to water drainage, and then a plateau is reached. Foams remain stable to total collapse. However, after 48 hours bubbles are bigger in size, showing disproportionation of bubbles.

By increasing the silica particle concentration from 1.5 wt. % to 3 wt. %, the initial foam volume (foamability) in all systems was increased (an example is given in Figure 4.20). At no salt the 3 wt. % silanised silica particles dispersion gave rise to a small volume of foam, whilst with the 1.5 wt. % (see Figure 4.18) no foam was observed. When a higher concentration of particles was used a better trend in foamability and stability with [NaCl] was observed (Figure 4.21).

Figure 4.19 Foam height *versus* time for 10 mL (~ 3.2 cm) aqueous silica dispersions of diameter 0.6 μm (θ_{aw} average = 58°) at a concentration of 1.5 wt. %, pH = 5.6 to 4.4 at different [NaCl] given (hand shake test).
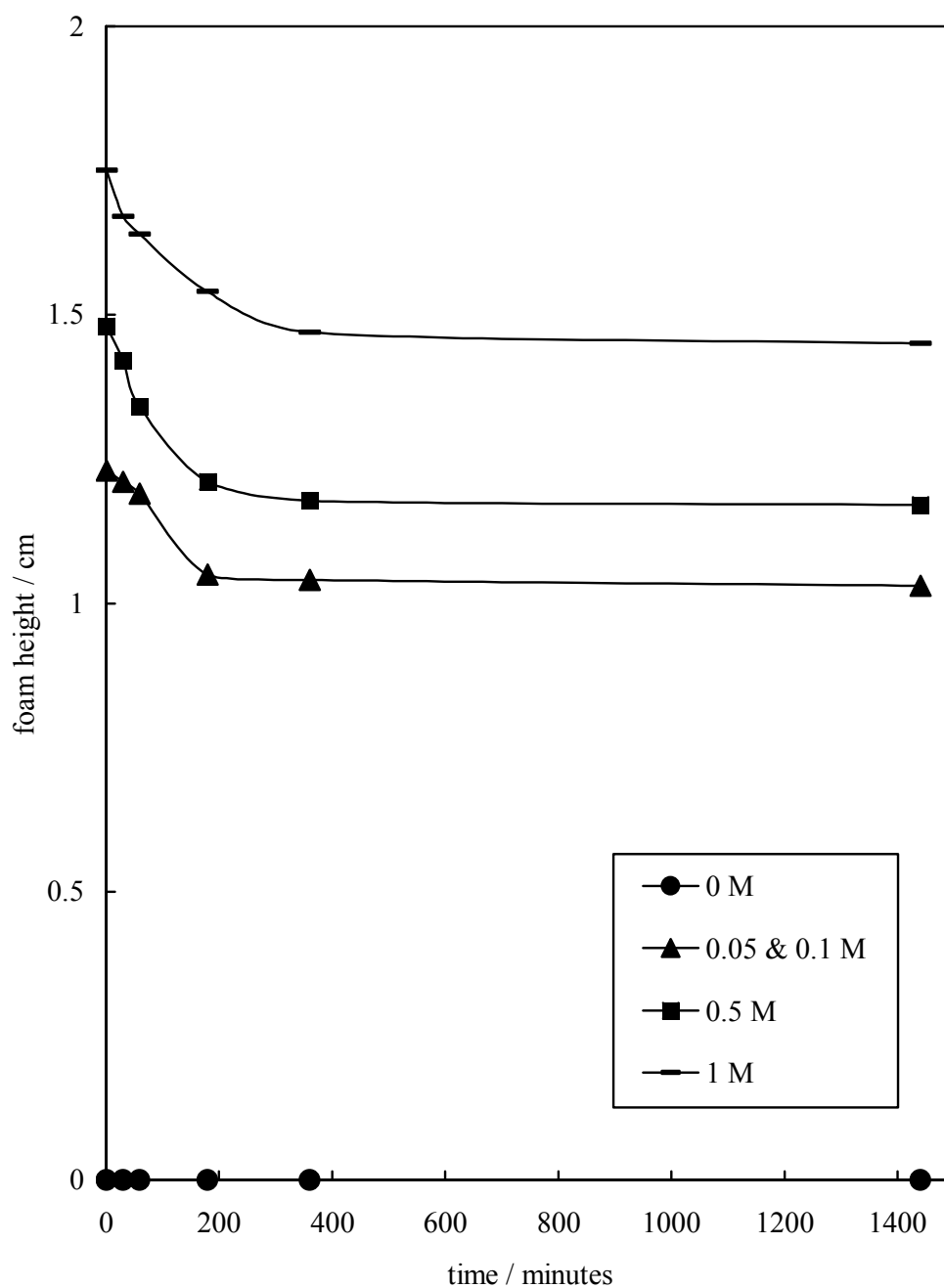
Figure 4.20 Appearance of foams from aqueous silica dispersions of diameter 0.6 μm previously silanised at [DCDMS] = 8×10^{-4} M (θ_{aw} average = 58°) at a concentration of 3 wt. % (pH ~ 5) at different [NaCl]: (a) no salt, (b) 0.05 M, (c) 0.1 M, (d) 0.5 M and (e) 1 M NaCl. The times refer to times after foam generation by hand shaking.
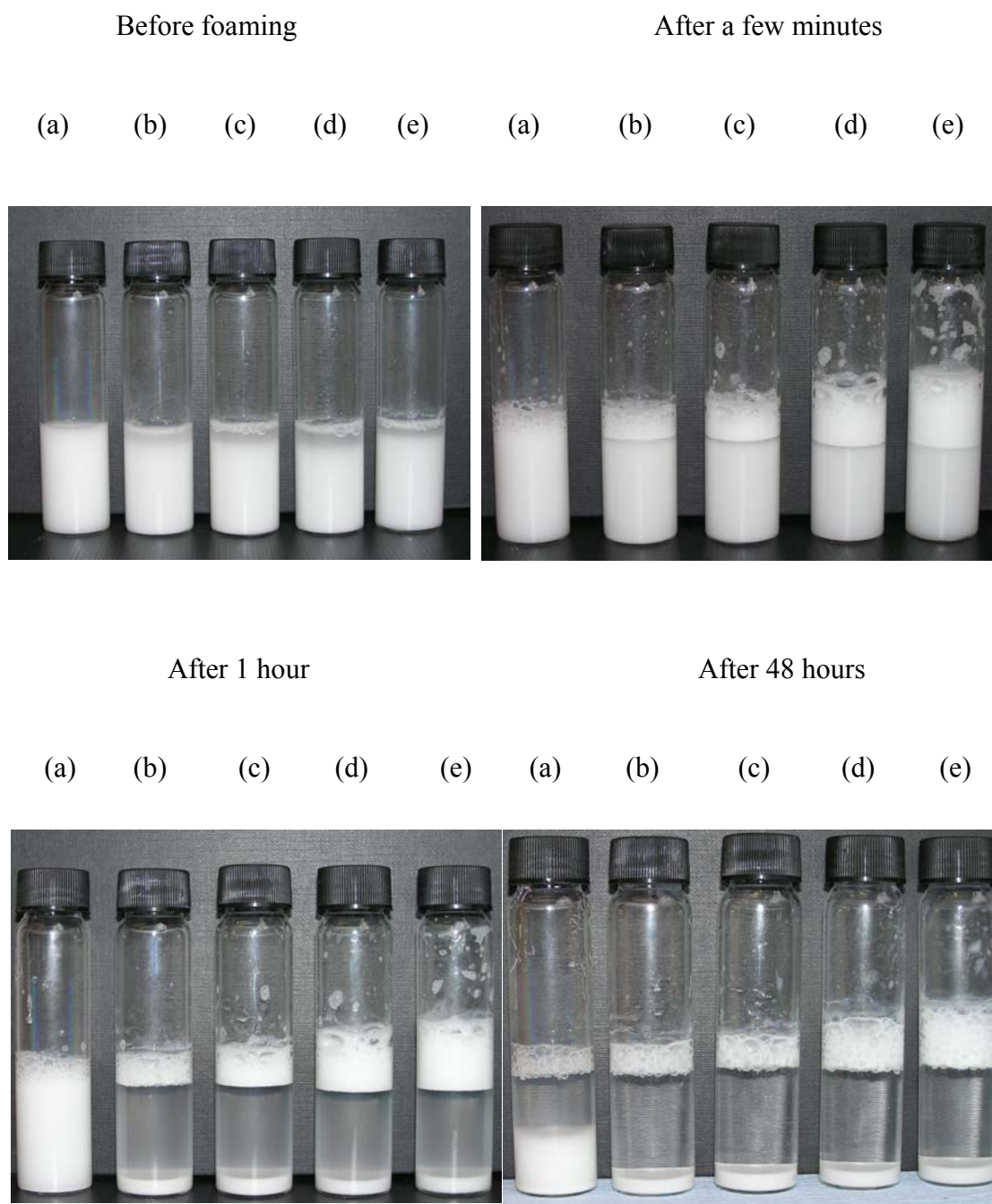
Figure 4.21 Foam height *versus* time for 10 mL (~ 3.2 cm) aqueous silica dispersions of diameter 0.6 μm (θ_{aw} average = 58°) at a concentration of 3 wt. %, at pH around 5 at different [NaCl] given (hand shake method).
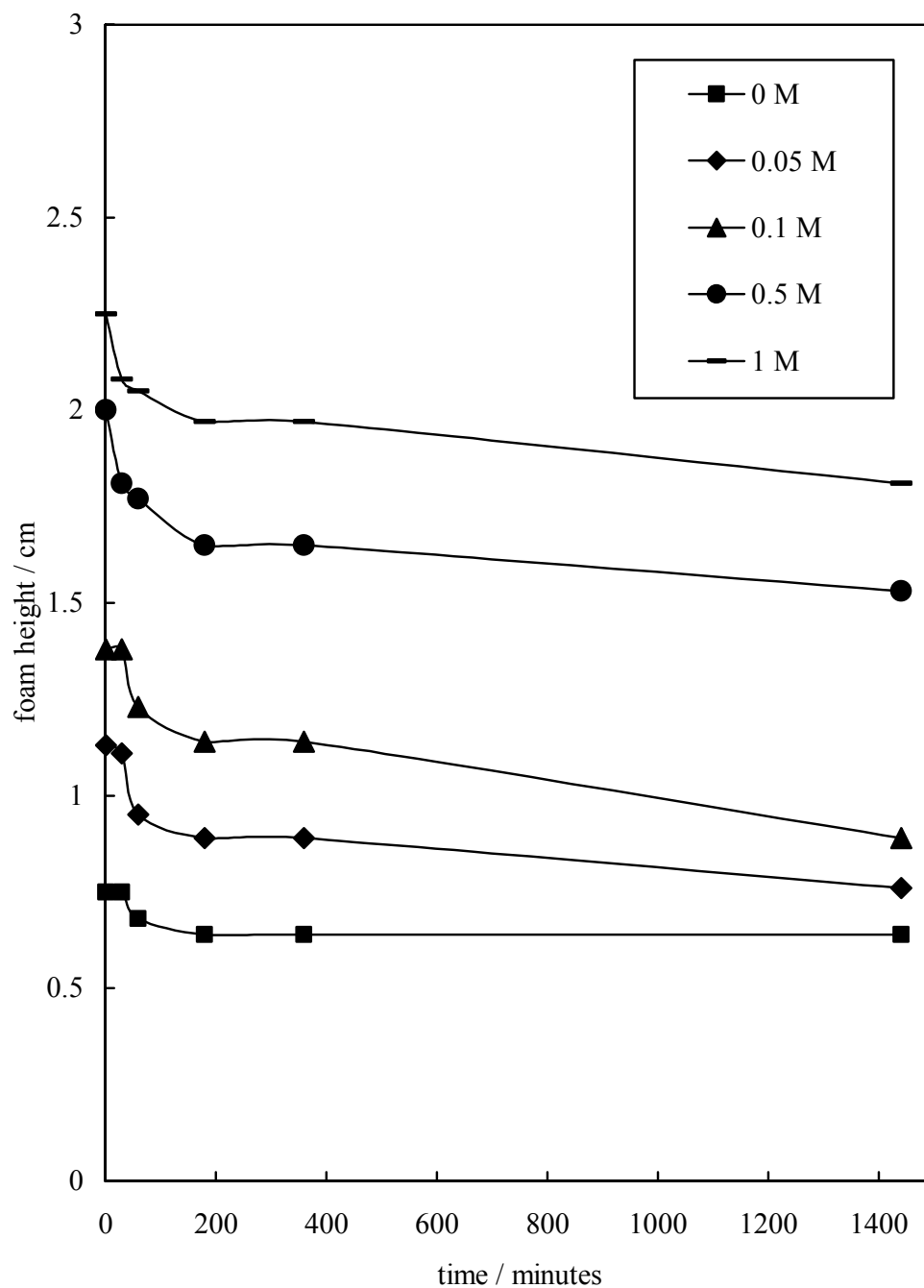
Tables 4.6 and 4.7 show the results of % Overrun, $\varnothing_{air}$ and $\varnothing_l$ in the foams produced with the 3 wt. % silanised silica aqueous systems.

Table 4.6 Summary of the results obtained for the foams formed by hand shaking after a few minutes for the systems shown in Figure 4.20 (3 wt.% particles).

[NaCl] / M	Overrun / %	$\varnothing_{air}$	$\varnothing_l$
0 and 0.05	23	0.72	0.28
0.5	40	0.66	0.34
1	52	0.78	0.22

Table 4.7 Summary of the results obtained for the foams formed by hand shaking after 48 hours for the systems shown in Figure 4.20.

[NaCl] / M	Overrun / %	$\varnothing_{air}$	$\varnothing_l$
0 and 0.05	15	0.77	0.23
0.5	36	0.79	0.21
1	47	0.83	0.17

The bubbles in the foams formed with the higher concentration of particles (*e.g.* 3 wt. %) are much smaller and monodisperse initially, compared to the bubbles formed with the lower particle concentration (*e.g.* 1.5 wt. %). However, the way these foams breakdown (stability) is very similar in both systems. Foams are very stable to collapse, but after 48 hours it was observed that the bubbles in these foams are bigger, possibly due to disproportionation (diffusion of gas from small to large bubbles).

The previous foams were formed by hand shaking all aqueous silanised silica dispersions. In order to assess if different methods of foam production would affect the nature or amount of foaminess, foams were also produced by aerating the same volume of aqueous silica dispersions using an Ultra - Turrax homogeniser (see Figure 4.22). It was observed that the foamability of the aqueous dispersions increased when foams were produced with the Ultra - Turrax homogeniser. These foams rose very quickly to

the top of the glass vessel during homogenisation and have a higher gas fraction (dry foams) compared to foams produced with the hand shaking method. The bubbles formed are polyhedral in shape. After the Ultra - Turrax homogeniser was removed from the vessel, a hole in the foam was observed, which makes it difficult to assess the actual volume of foam initially produced (foamability). Therefore, to access the actual volume of foam, all systems were gently re-shaken after 30 minutes of foam generation. It can be seen from the photographs of foams formed with the partially hydrophobised silica particles (θ_{aw} average = 58°), that both the foaming ability and foam stability are improved, relative to the unmodified hydrophilic particles.

Figure 4.22 Appearance of foams from aqueous silica dispersions of diameter 0.6 μm previously silanised at [DCDMS] = 8 × 10^{-4} M (θ_{aw} average = 58°) at a concentration of 3 wt. % (pH ~ 5) at different [NaCl]: (a) no salt, (b) 0.05 M, (c) 0.1 M, (d) 0.5 M and (e) 1 M NaCl. The times refer to times after foam generation by homogenisation at 13, 000 rpm.

After a few minutes
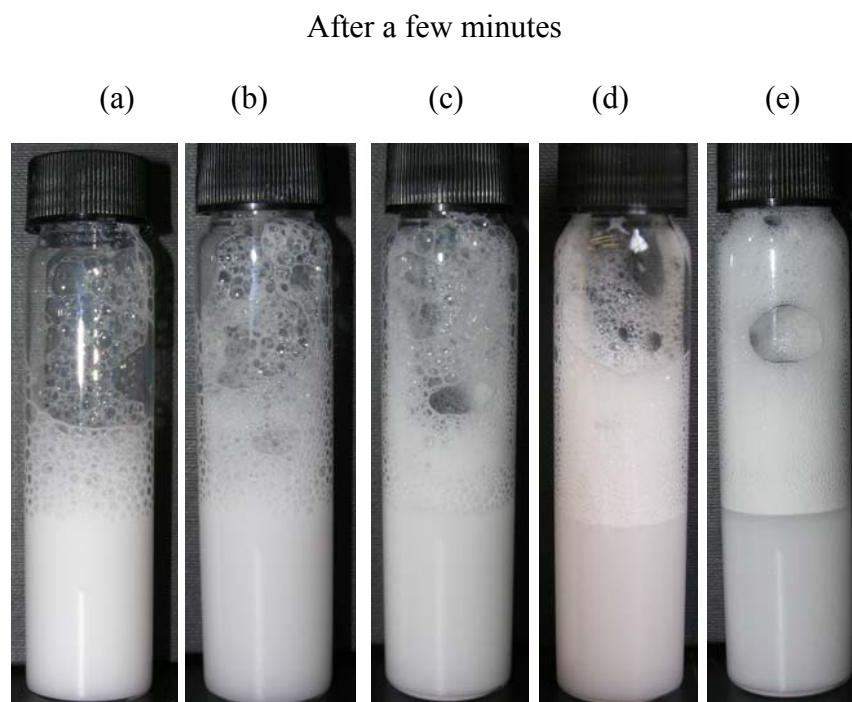
(a)   (b)   (c)   (d)   (e)

After 30 minutes

(a)　(b)　(c)　(d)　(e)

After gentle re-shaking after 30 min.

(a)　(b)　(c)　(d)　(e)

After 6 hours

(a)　(b)　(c)　(d)　(e)

After 48 hours

(a)　(b)　(c)　(d)　(e)

It was also clearly observed that the sizes of the bubbles formed initially decreased progressively with an increase in [NaCl]. The following two tables show the results of % Overrun, Ø_{air} and Ø_l in the foams produced with the 3 wt. % silanised silica aqueous dispersions.

Table 4.8   Summary of the results obtained for the foams formed by homogenisation after a few minutes of the systems shown above in Figure 4.22.

[NaCl] / M	Overrun / %	Ø_{air}	Ø_l
0	43	0.71	0.29
0.05 and 0.1	59	0.77	0.23
0.5	74	0.87	0.13
1	95	0.92	0.8

Table 4.9   Summary of the results obtained for the foams formed by homogenisation after 48 hours of the systems shown above in Figure 4.22.

[NaCl] / M	Overrun / %	Ø_{air}	Ø_l
0	39	0.75	0.25
0.05 and 0.1	58	0.88	0.12
0.5	69	0.92	0.8
1 M	84	0.94	0.6

The results in the above Tables show that these foams are very stable to collapse. The decrease in their volume is a result of water drainage. However after 48 hours, in addition to drainage, coarsening occurs simultaneously due to the diffusion of gas, which results in continual growth of bubble size (as observed in previous foams produced by hand shaking). Therefore, although higher foam volumes are produced by homogenisation, the stability of these foams is very similar to the previous foams produced by hand shaking.

The effect of NaCl and particle concentration on the foaming ability and foam stability of aqueous silica dispersions of diameter 0.6 μm hydrophobised with a higher concentration of DCDMS (3×10^{-3} M, θ_{aw} average ~ 77°) was also investigated. The aqueous dispersions were foamed by hand shaking and using the Ultra-Turrax homogeniser. Figures 4.23 to 4.25 show the appearance of these foams formed under different conditions. By using the hand shaking method, small volumes of foam were observed in all systems compared to those formed by homogenisation. The foamability of these systems also increased with particle concentration, which means that more particles are adsorbing at the air-water surface. Addition of salt causes a slight increase in foamability when using the hand shaking method. However, a more pronounced effect of salt concentration is observed when the Ultra - Turrax homogeniser is used (see Figures 4.24 and 4.25). It can be seen that more particles are residing in the aqueous phase containing low [NaCl] (*e.g.* 0.05 and 0.1 M), whereas at higher [NaCl] (*e.g.* 0.5 and 1 M), they are mainly located within the white, creamy foam initially formed. It was observed that these silanised silica particles (θ_{aw} average ~ 77°) are more flocculated compared to the previous silanised particles studied (θ_{aw} average ~ 58°). Small flocs may adsorb around air bubbles which may increase the surface viscosity, thus resulting in a decrease in drainage rate and therefore an increase in foam stability. However, big flocs remain below all foams. They are very sensitive to mechanical vibration and detach very easily from the bubble – water surface. If the glass vessels are left undisturbed the big flocs remain below the foam for a longer period of time (they eventually sediment with time but at a very slow rate).

Figure 4.23 Appearance of foams from aqueous silica dispersions of diameter 0.6 μm previously silanised at [DCDMS] = 3 × 10^{-3} M (θ_{aw} average = 77°) at a concentration of 1.5 wt. % (A) and 3 wt.% (B) at different [NaCl]: (a) no salt, (b) 0.05 M, (c) 0.1 M, (d) 0.5 M and (e) 1 M NaCl. The times refer to times after foam generation by hand shaking.

(A)
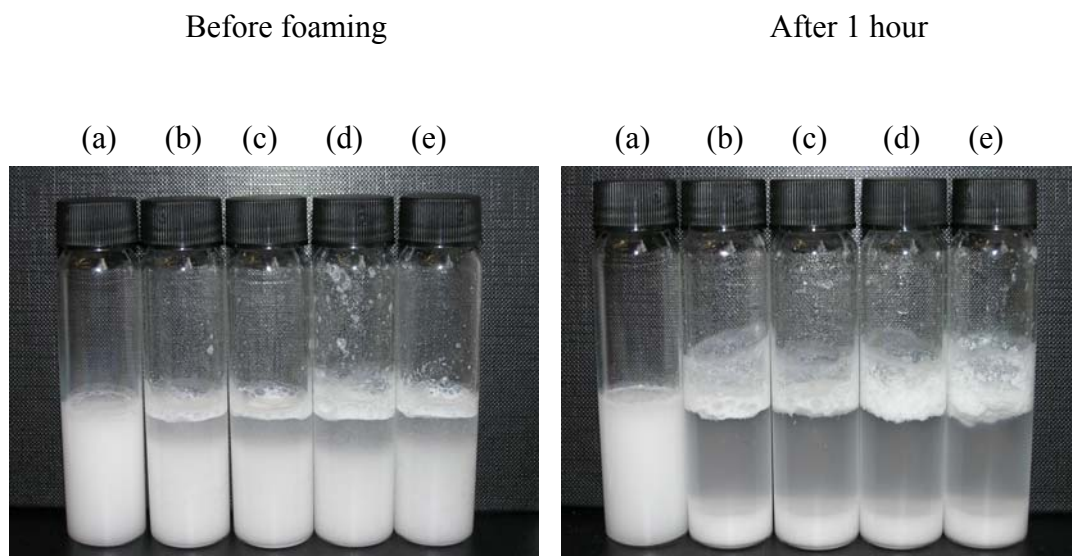
(B)
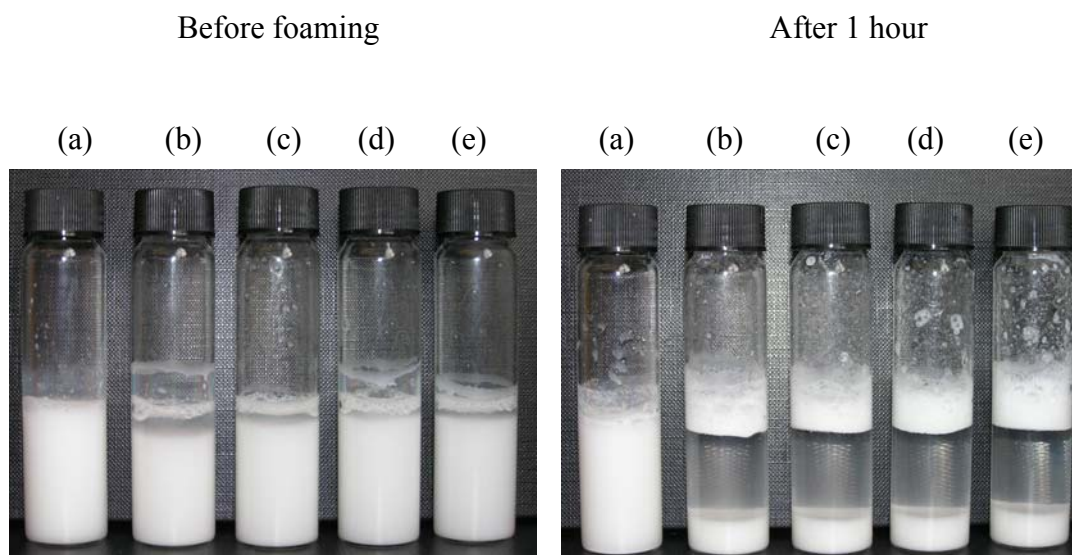
Figure 4.24 Appearance of foams from aqueous silica dispersions of diameter 0.6 μm previously silanised at [DCDMS] = 3 × 10^{-3} M (θ_{aw} average = 77°) at a concentration of 1.5 wt. % (pH ~5) at different [NaCl]: (a) no salt, (b) 0.05 M, (c) 0.1 M, (d) 0.5 M and (e) 1 M NaCl. The times refer to times after foam generation by homogenisation at 13, 000 rpm.

After a few minutes

After 3 hours

After 24 hours

After 48 hours
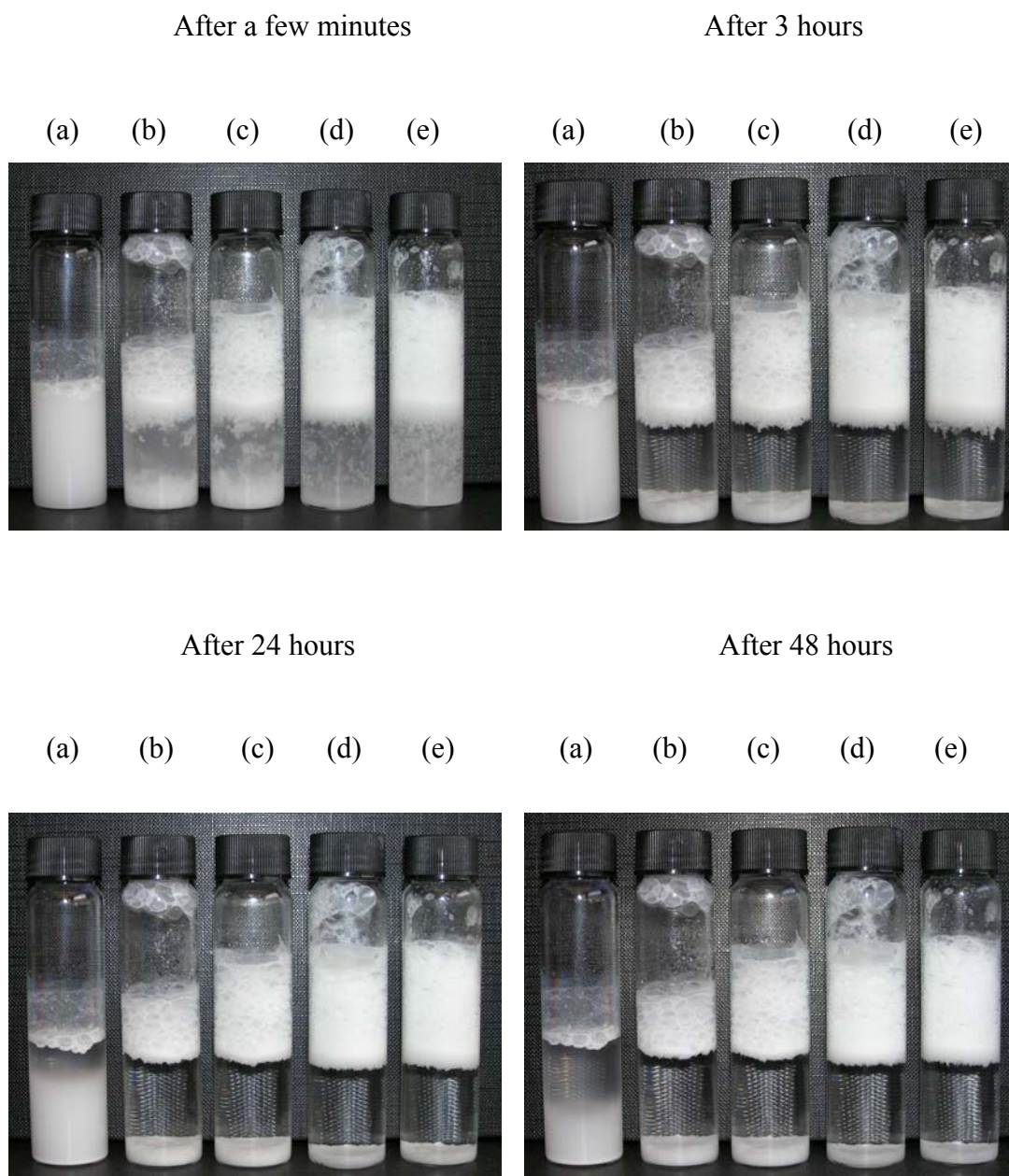
Figure 4.25 Appearance of foams from aqueous silica dispersions of diameter 0.6 μm previously silanised at [DCDMS] = 3 × 10^{-3} M (θ_{aw} average = 77°) at a concentration of 3 wt. % (pH ~ 5) at different [NaCl]: (a) no salt, (b) 0.05 M, (c) 0.1 M, (d) 0.5 M and (e) 1 M NaCl. The times refer to times after foam generation by homogenisation at 13, 000 rpm.

After a few minutes   After 3 hours

(a)   (b)   (c)   (d)   (e)   (a)   (b)   (c)   (d)   (e)

After 72 hours   After 6 days

(a)   (b)   (c)   (d)   (e)   (a)   (b)   (c)   (d)   (e)
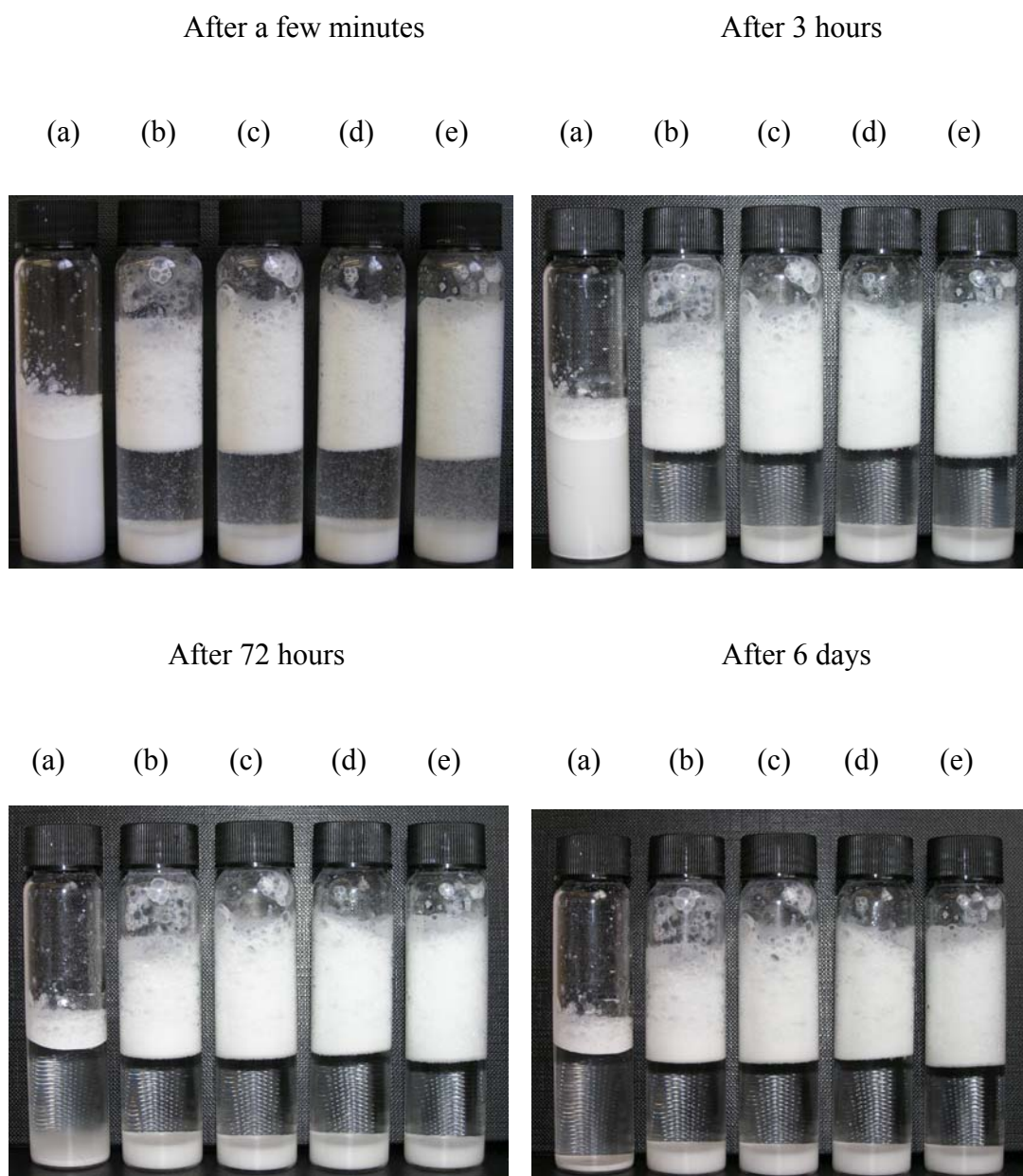
Tables 4.10 and 4.11 give the results of % Overrun, $\emptyset_{air}$ and $\emptyset_l$ in the foams produced with the 1.5 wt. % silanised silica aqueous dispersions.

Table 4.10 % Overrun, $\emptyset_{air}$ and $\emptyset_l$ obtained for the foams formed by homogenisation after a few minutes of the systems shown in Figure 4.23.

[NaCl] / M	Overrun / %	$\emptyset_{air}$	$\emptyset_l$
0.05	40	0.53	0.47
0.1 1	60	0.67	0.33
0.5 and 1	75	0.71	0.29

Table 4.11 % Overrun, $\emptyset_{air}$ and $\emptyset_l$ obtained for the foams formed by homogenisation after 48 hours of the systems shown above in Figure 4.23.

[NaCl] / M	Overrun / %	$\emptyset_{air}$	$\emptyset_l$
0.05	33	0.63	0.37
0.1	57	0.71	0.29
0.5 and 1	71	0.75	0.25

Tables 4.12 and 4.13 show the results of % Overrun, $\emptyset_{air}$ and $\emptyset_l$ in the foams produced with the 3 wt. % silanised silica aqueous dispersions.

Table 4.12 % Overrun, $\emptyset_{air}$ and $\emptyset_l$ obtained for the foams formed by homogenisation after a few minutes of the systems shown in Figure 4.25.

[NaCl] / M	Overrun / %	$\emptyset_{air}$	$\emptyset_l$
0.05	66	0.72	0.28
0.1 and 0.5	79	0.75	0.25
1 M	83	0.74	0.26

Table 4.13 % Overrun, $\emptyset_{air}$ and $\emptyset_l$ obtained for the foams formed by homogenisation after 6 days of the systems shown above in Figure 4.25.

[NaCl] / M	Overrun / %	$\emptyset_{air}$	$\emptyset_l$
0.05	62	0.79	0.21
0.1 and 0.5	71	0.81	0.19
1 M	79	0.80	0.20

As can be seen from the results shown in the above tables, aqueous silica dispersions with higher particle and salt concentration produced the higher % overrum and contained the highest air content in the foam. They were also the most stable foams formed as the rate of liquid drainage was much slower and no disproportionation or coalescence of bubbles occurred. It was also found with this study that the method of foam production is very important in particle-stabilised foams. Therefore, the production of fresh bubbles at very high rates during air incorporation was necessary in the preparation of foams and in this way most of the particles were able to go to the air-water interface. Aqueous silica dispersions of diameter 0.6 μm (θ_{aw} average = 77°) were also aerated by homogenisation at 17, 000 rpm as shown in Figure 4.26, instead of 13, 000 rpm (see Figure 4.25). It was clearly observed that the aqueous silica dispersion containing no salt gave rise to a small volume of foam when the homogeniser was used at 13, 000 rpm, however when 17,000 rpm was used a higher foam volume was observed. It was also noticed that most of the particles are within the foam at higher rpm was used (clear supernatant) while at 13, 000 rpm some particles still remain in the bulk and eventually sediment. Foams produced with homogenisation at 17, 000 rpm were found to be more stable to disproportionation or coalescence of bubbles since bubbles seem to be completely covered with the particles.

Figure 4.26 Appearance of foams from aqueous silica dispersions of diameter 0.6 μm previously silanised at [DCDMS] = 3 × 10^{-3} M (θ_{aw} average = 77°) at a concentration of 3 wt. % (pH ~ 5) at different [NaCl]: (a) no salt, (b) 0.05 M, (c) 0.1 M, (d) 0.5 M and (e) 1 M NaCl. The times refer to times after foam generation by homogenisation at 17, 000 rpm.

After a few hours   After 7 days up to months

(a)   (b)   (c)   (d)   (e)   (a)   (b)   (c)   (d)   (e)
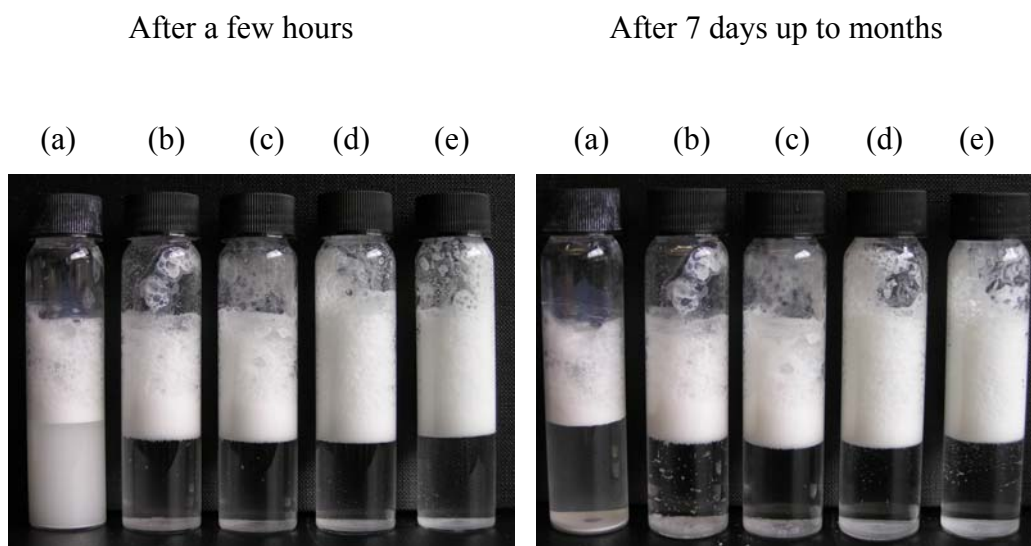
The effect of NaCl concentration on the foaming ability and stability of the most hydrophobic particles ($\theta = 105°$) was also investigated. It was found that the higher the particle hydrophobicity the lower the effect of salt on the foamability of the aqueous dispersions. As can be seen in Figure 4.27 similar foam volumes were formed with all NaCl concentrations used and big flocs were observed underneath the foam. These flocs were bigger than the ones observed with the lower particle hydrophobicity (*e.g.* $\theta = 77°$) and again they were found to be very sensitive to mechanical vibrations as they eventually detach from the foam and sediment. However, these foams were very stable against disproportionation or coalescence of bubbles and their stability was very similar in all systems.

Figure 4.27 Appearance of foams from aqueous silica dispersions of diameter 0.6 μm previously silanised at [DCDMS] = 8×10^{-2} M (θ_{aw} average = 105°) at a concentration of 3 wt. % (pH ~ 5) at different [NaCl]: (a) no salt, (b) 0.05 M, (c) 0.1 M, (d) 0.5 M and (e) 1 M NaCl. The times refer to times after foam generation by homogenisation at 13, 000 rpm.
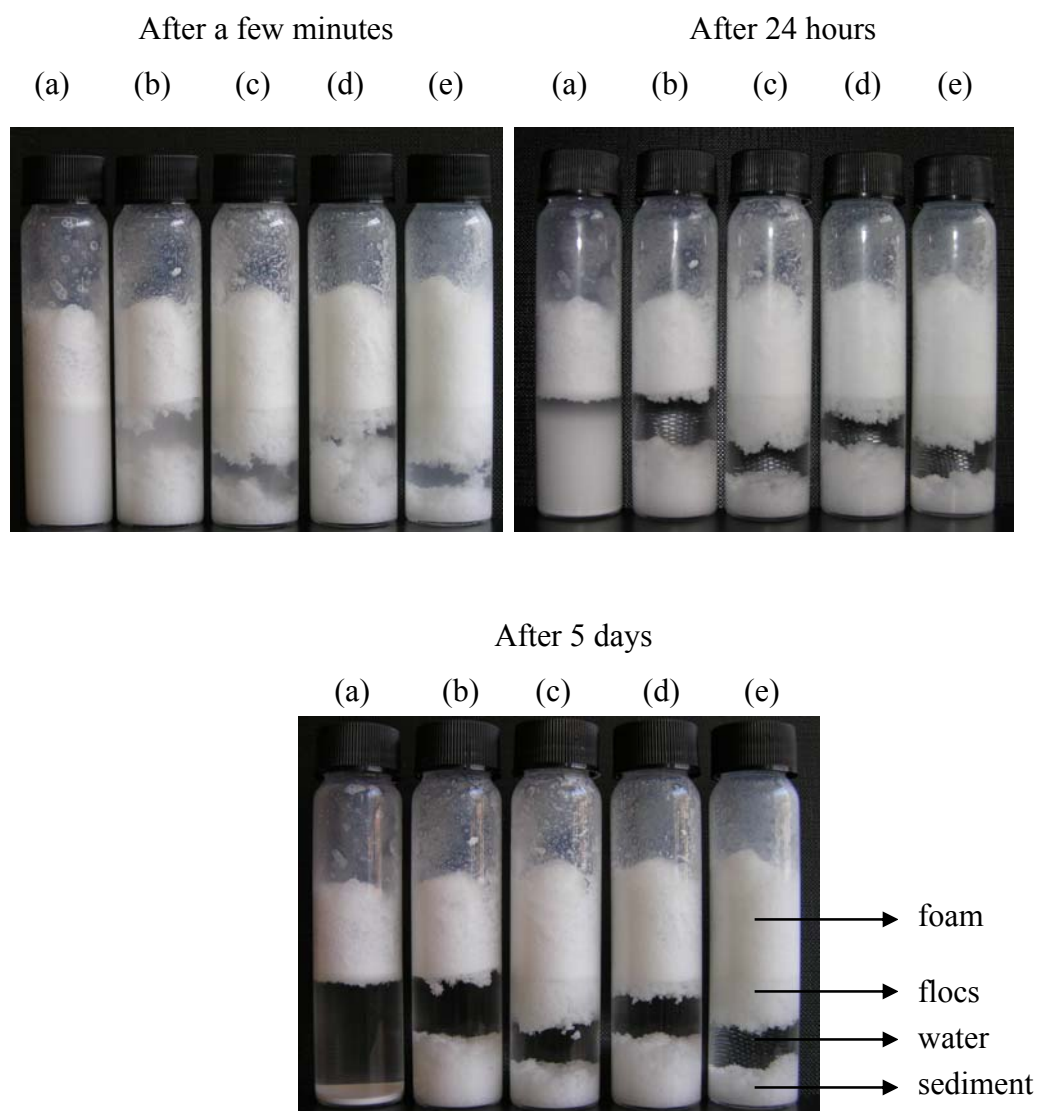

From these results it was found that by increasing the particle concentration in the aqueous dispersions the foaming ability and stability was improved. Therefore, it can be concluded that for foams to be formed there must be sufficient particles to cover the air-liquid interface generated as has been found in many other studies. If the number of silica particles is too small, the bubble surfaces will not be coated with sufficient particles causing 'patches' in the surface which can act as rupture centres. A higher

concentration of solid particles may lead to a better particle-layered structure inside the film (providing a structural barrier against the coalescence of bubbles), which is in turn reflected in the higher foam lamella stability and foaminess observed in these systems.[16] Also, by increasing the salt concentration, the foaming ability and stability was clearly improved, particularly in the systems containing the least hydrophobic particles. This can be explained by the fact that the contact angle of these particles increases with salt concentration, leading to improved stabilisation of the foams as shown in the previous Chapter 3.

The state of the aqueous dispersions before foaming can also be linked to the foaming ability and stability observed. As mentioned before, in section 4.4, flocculation of particles occurs by increasing the particle hydrophobicity and also by adding salt to the dispersions and the degree of flocculation is dependent on the particle hydrophobicity. In Figure 4.28 is seen that in the absence of salt the hydrodynamic particle diameter increases by increasing the particle hydrophobicity and a maximum in the foaming ability of the aqueous dispersions is observed when small flocs are obtained with partially hydrophobic particles (*e.g*. 95°). Figure 4.29 shows that by increasing the salt concentration in the dispersions containing particles of intermediate hydrophobicity (*e.g.* 58°), the hydrodynamic particle diameter gradually increased with salt concentration and also the foaming ability and stability of such dispersions increased. However, in the case of particles with higher hydrophobicity (*e.g.* 105°) the degree of particle flocculation with salt concentration increased dramatically compared with the previous less hydrophobic particles. It is seen in Figure 4.30 that an increase of salt concentration in the aqueous dispersions containing the most hydrophobic particles (*e.g.* 105°) did not had much effect on the foaming ability of such dispersions. Therefore, it is concluded that small flocs can enhance the foaming ability and stability of the aqueous dispersions by adsorbing at the bubble-air interface, while bigger flocs can hinder foam formation and detach themselves from the bubble-air interface.

Figure 4.28 Hydrodynamic particle diameter and initial foam height versus air-water contact angle for 3 wt. % aqueous dispersions of silica particles of diameter 0.6 μm in the absence of salt.
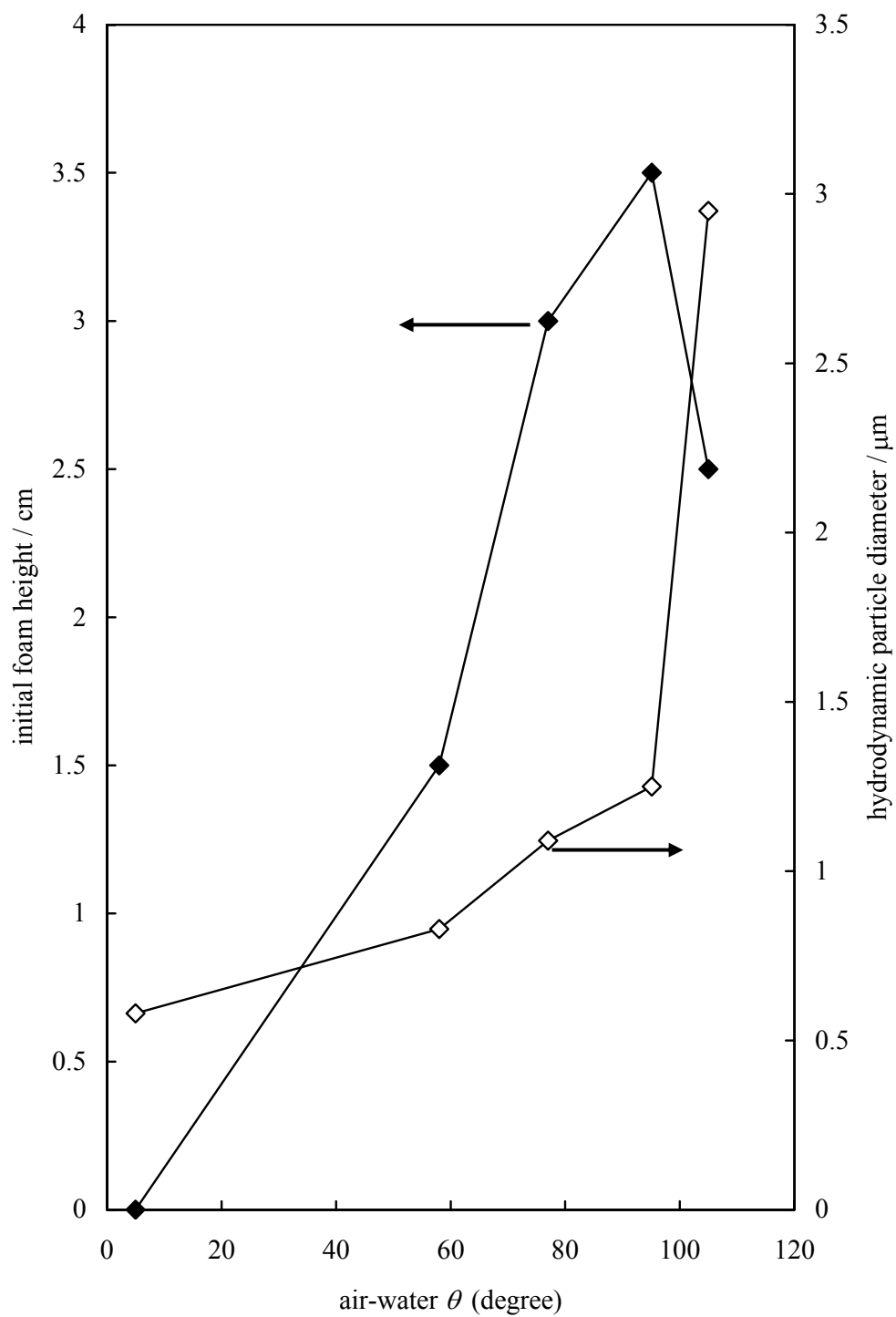
Figure 4.29 Hydrodynamic particle diameter (filled diamonds) and initial foam height (empty diamonds) versus NaCl concentration for 3 wt. % aqueous dispersions of silica particles of diameter 0.6 μm and previously silanised at [DCDMS] = 8 × 10^{-4} M (θ_{aw} average = 58°).
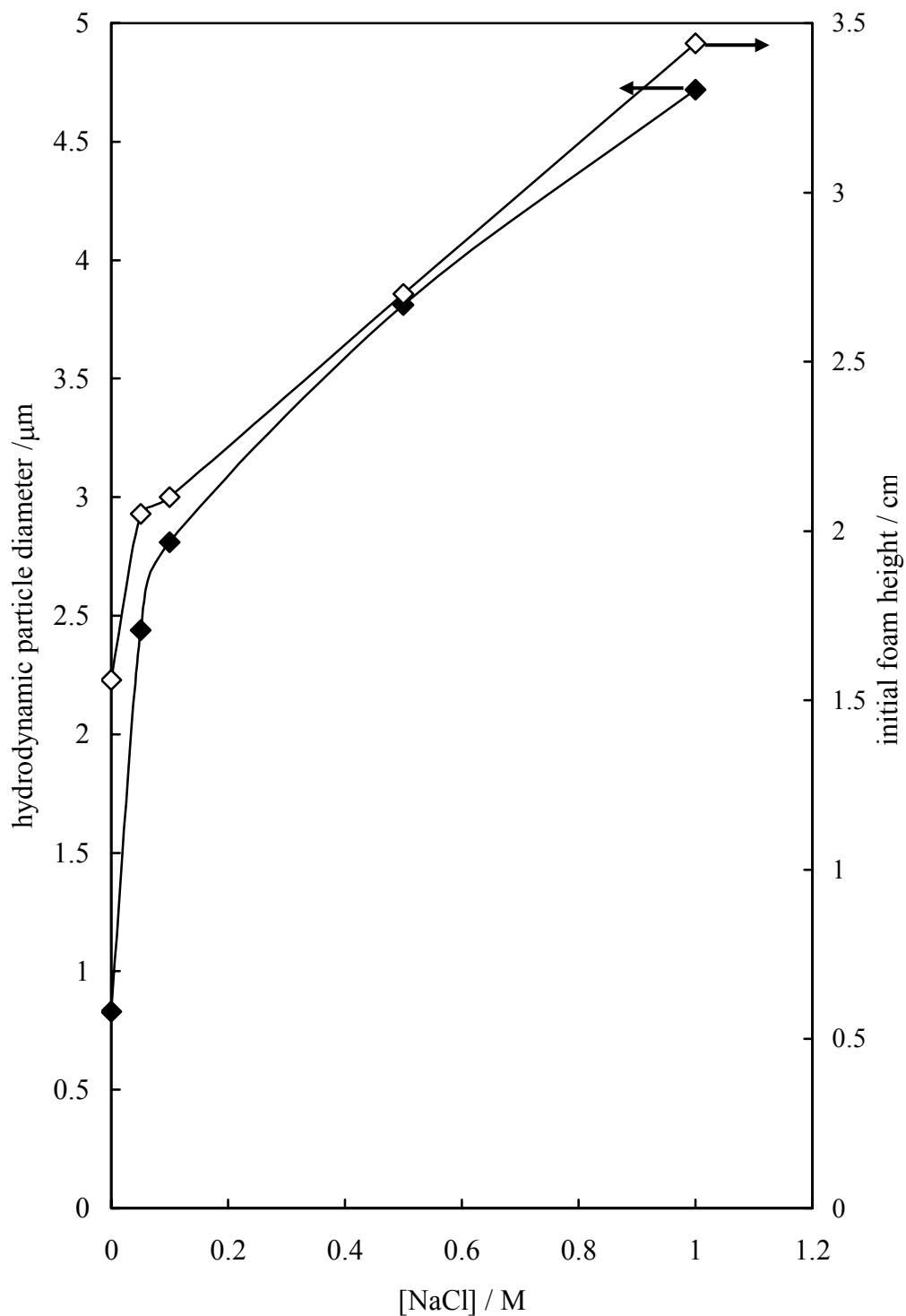
Figure 4.30   Hydrodynamic particle diameter (filled diamonds) and initial foam height (empty diamonds) versus NaCl concentration for 3 wt. % aqueous dispersions of silica particles of diameter 0.6 μm and previously silanised at [DCDMS] = 8 × 10⁻² M (θ_{aw} average = 105°).
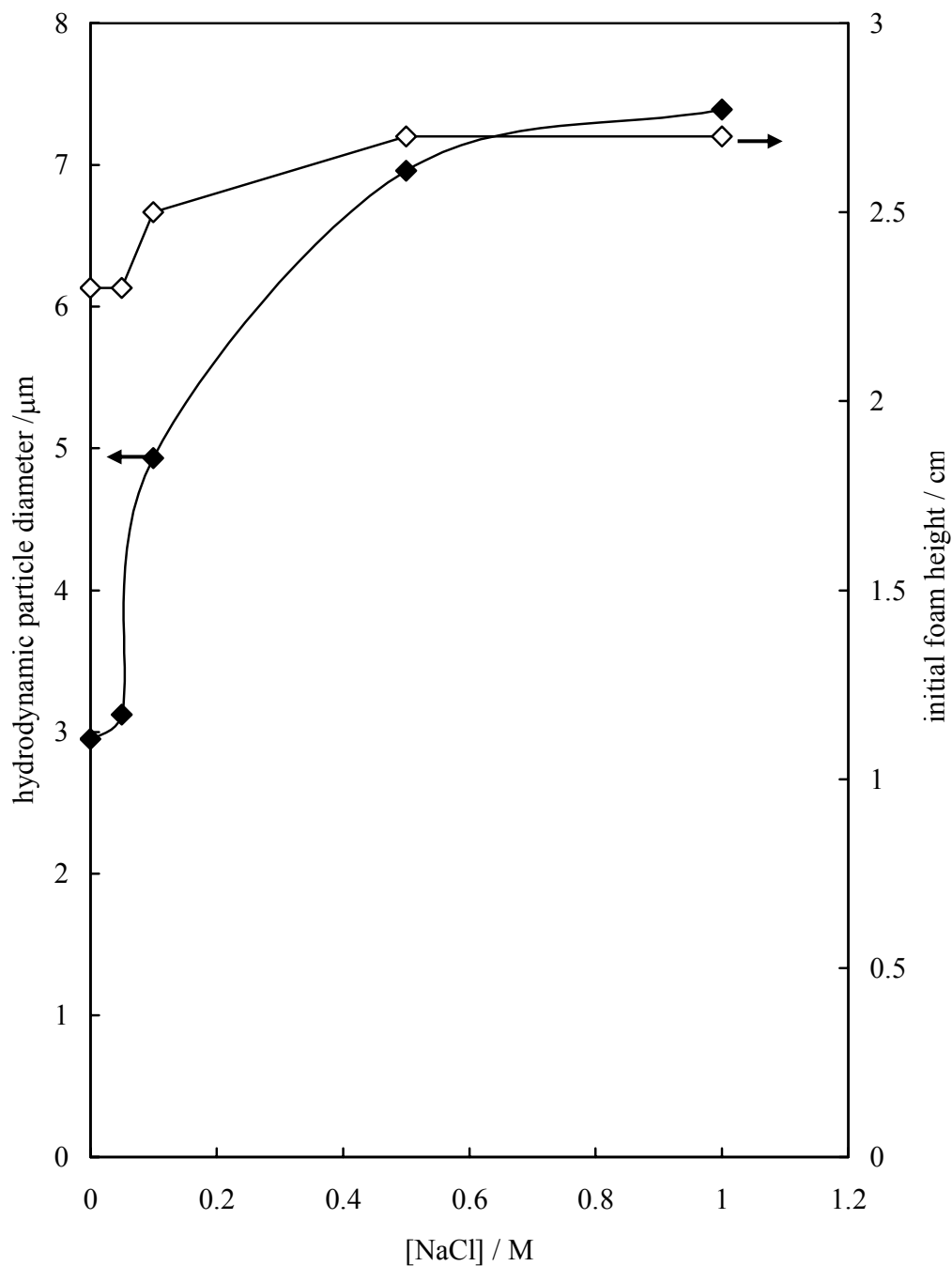
4.5.2.3 Effect of particle size

The effect of particle size on the foaming ability and stability of aqueous dispersions is still not fully understood. To investigate the effect of particle size on foaming ability and foam stability of the aqueous monodisperse silanised silica particles, two other particle sizes were investigated, *e.g.* 0.1 and 2 μm and the results were compared with the previous foams investigated with silica particles of diameter 0.6 μm. Figure 4.31 shows the appearance of foams formed with different particle sizes at a fixed contact angle of 58° and a fixed particle concentration of 3 wt. %. It was clearly observed that the foaming ability of the aqueous silica dispersions increased with the systems containing bigger particles. However, the stability of both systems containing different particle sizes was very similar. After 24 hours, the bubbles in all foams were bigger in size, showing signs of instability.

Figure 4.31 Appearance of foams from aqueous silica dispersions of diameter (A) 0.1 and (B) 0.6 μm previously silanised with [DCDMS] = 8×10^{-4} M (θ_{aw} average = 58°) at a fixed concentration of 3 wt. % and pH ~ 5 at different [NaCl]: (a) no salt, (b) 0.05 M, (c) 0.1 M, (d) 0.5 M and (e) 1 M NaCl. The times refer to times after foam generation by homogenisation at 17,000 rpm.

(A)

After a few minutes   After 24 hours
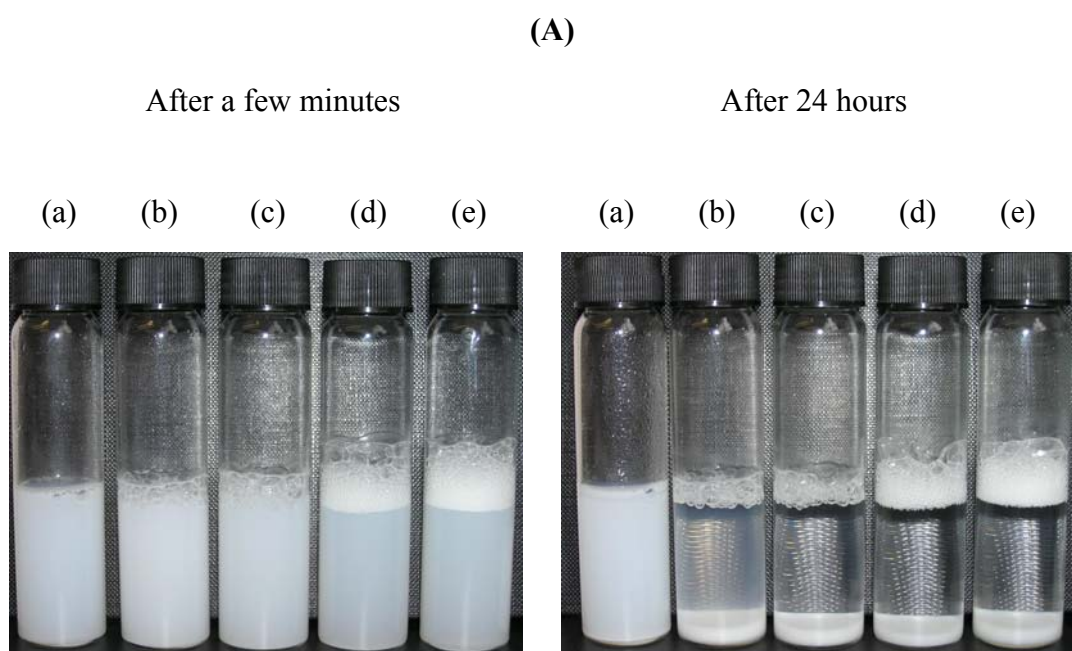
(a)   (b)   (c)   (d)   (e)   (a)   (b)   (c)   (d)   (e)

(B)

After a few minutes   After 24 hours

(a)   (b)   (c)   (d)   (e)   (a)   (b)   (c)   (d)   (e)

The ability of the silica particles to stabilise foam also depends on the number of particles in the system. If there are insufficient particles to sufficiently cover the air cells formed on shaking, the bubbles formed will be unstable and burst quickly. Therefore, in order to compare the foaming ability and stability of aqueous dispersions of silica particles of diameters 0.6 and 2 μm, the same number of particles in all systems was used (*e.g.* 1.33×10^{12}), which means that all systems had the same specific surface area. To achieve this, different concentrations for the different particle sizes were used as shown in Table 4.14.

Table 4.14 Properties of silica particles of different particle sizes.

Specific Surface Area $= 1.5$ m^2	
Number of particles $= 1.33\times10^{12}$ particles	
particle diameter / μm	[particle] / wt.%
0.6	3
2	10

Figure 4.32 shows the appearance of foams from aqueous silica dispersions of diameters 0.6 and 2 μm containing the same number of silica particles and it can be clearly seen that not only the foamability is improved with the larger silica particles but also the foam stability. After 24 hours the bubbles in the foams generated by the smaller particles *e.g.* 0.6 μm were bigger in size possible due to disproportionation and coalescence of bubbles; whereas the bubbles within the foams produced with the larger particles *e.g.* 2 μm are much more stable and remained their structure and physical appearance for several weeks.

Figure 4.32 Appearance of foams from aqueous silica dispersions of diameter (A) 0.6 and (B) 2 μm previously silanised at [DCDMS] = 8×10^{-4} M with dry toluene (θ_{aw} average = 58°) at different concentrations as shown in Table 4.14 and pH ~ 5 at different [NaCl]: (a) no salt, (b) 0.05 M, (c) 1 M NaCl. The times refer to times after foam generation by homogenisation at 17000 rpm.

(A)

After 1 hour   After 24 hours

(a)   (b)   (c)   (a)   (b)   (c)

(B)

After 1 hour   After 24 hours

(a)   (b)   (c)   (a)   (b)   (c)

The effect of particle hydrophobicity on the foaming ability and stability of the larger silica particles of diameter 2 μm was also investigated. As can been seen in Figure 4.33, by increasing the particle hydrophobicity up to a contact angle of 95° the foamability and foam stability was enhanced as observed with the silica particles of diameter 0.6 μm. The effect of particle concentration was also investigated with the larger silica particles at a fixed contact angle of 95°, Figure 4.34. Foaming ability was enhanced by increasing particle concentration and all foams were very stable against disproportionation or coalescence of bubbles. These foams seemed more robust than the ones produced with the smaller particle sizes. Since the energy of attachment of a particle to an interface, ΔG depends on the square of the particle radius, it decreases markedly for very small particles and detachment is easy and therefore they may not be too effective as foam stabilisers compared to the larger particles. Therefore, it can be concluded that the size of particles has implications with respect to the rate at which particles can diffuse and arrive at the surface of newly formed bubbles, to prevent disproportionation.

It can be concluded that particle hydrophobicity is a key factor for foaming ability and stability of these aqueous silica systems and that by increasing particle size both foamability and foam stability are enhanced (see Figure 4.35).

Figure 4.33 Appearance of foams from aqueous silica dispersions of diameter 2 µm previously silanised at different [DCDMS] at a fixed particle concentration of 10 wt. % and pH ~ 5 at different [NaCl]: (a) no salt, (b) 0.05 M, (c) 1 M NaCl. The times refer to times after foam generation by homogenisation at 17, 000 rpm.

Before foaming

$\theta_{aw} = 58°$ $\theta_{aw} = 77°$ $\theta_{aw} = 95°$

(a) (b) (c)   (a) (b) (c)   (a) (b) (c)

After a few minutes

$\theta_{aw} = 58°$ $\theta_{aw} = 77°$ $\theta_{aw} = 95°$

(a) (b) (c)   (a) (b) (c)   (a) (b) (c)

After 96 hours

$\theta_{aw} = 58°$ $\theta_{aw} = 77°$ $\theta_{aw} = 95°$

(a)   (b)   (e)   (a)   (b)   (e)   (a)   (b)   (c)
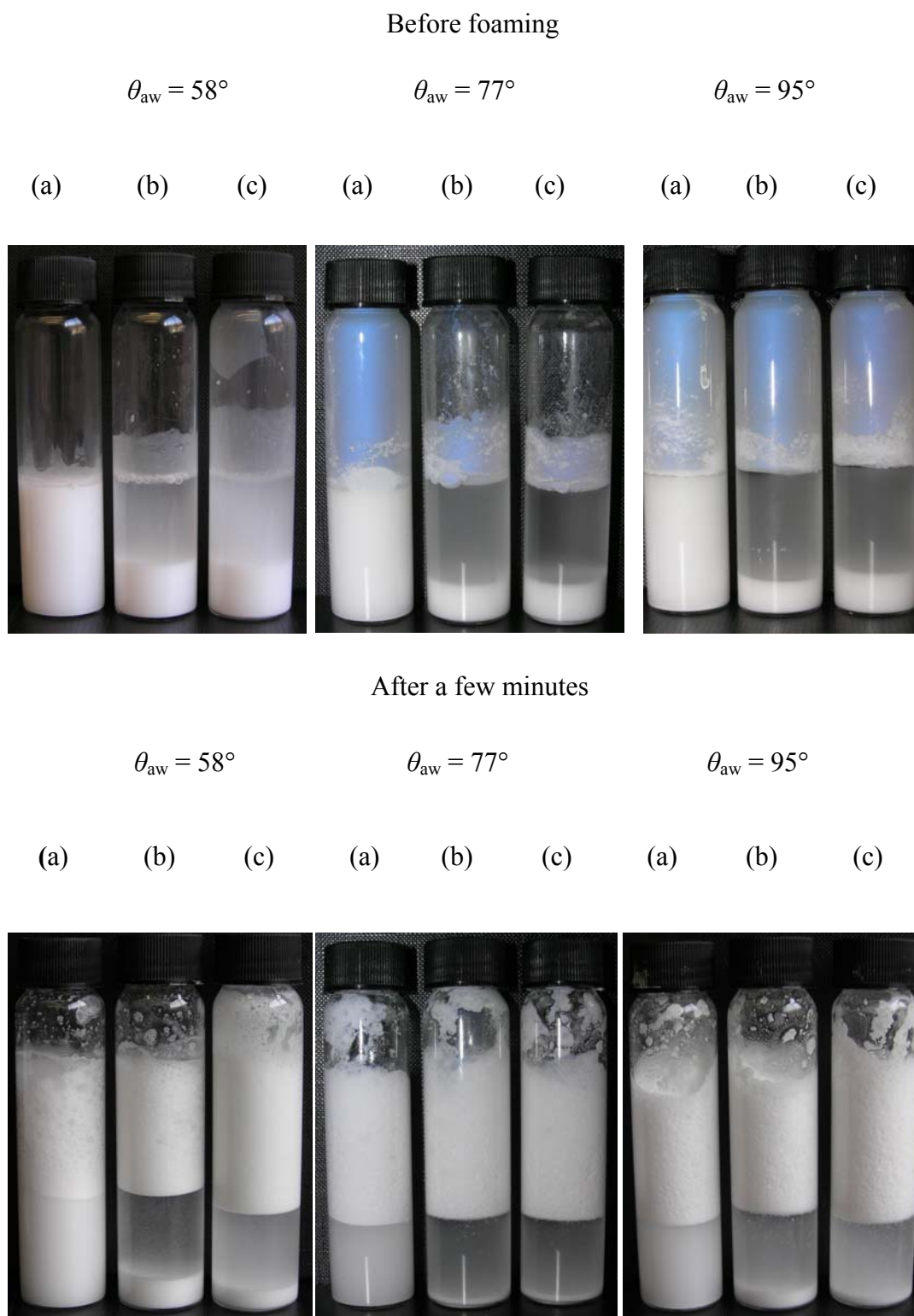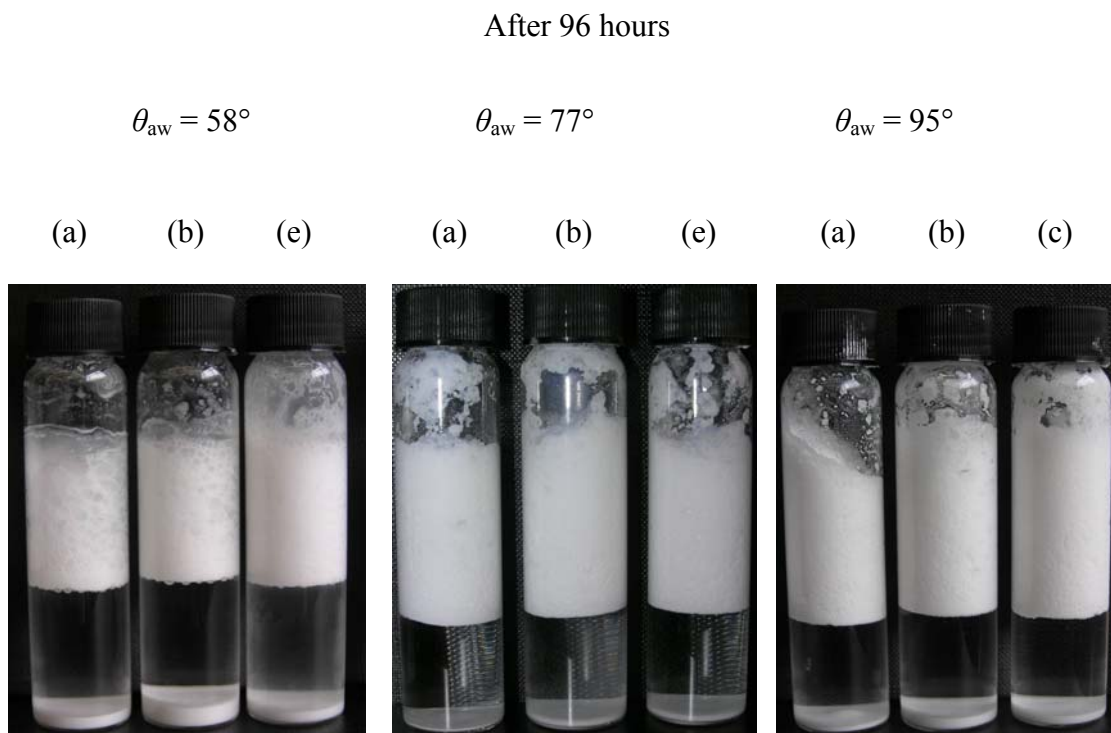
Figure 4.34 Appearance of foams from aqueous silica dispersions of diameter 2 μm previously silanised at [DCDMS] = 4 × 10^{-3} M (θ_{aw} average = 95°) at different concentrations and no salt (pH ~ 5). The times refer to times after foam generation by homogenisation.

After a few minutes   After 5 days up to months

3 wt.%   5 wt.%   10 wt.% | 3 wt.%   5 wt.%   10 wt.%
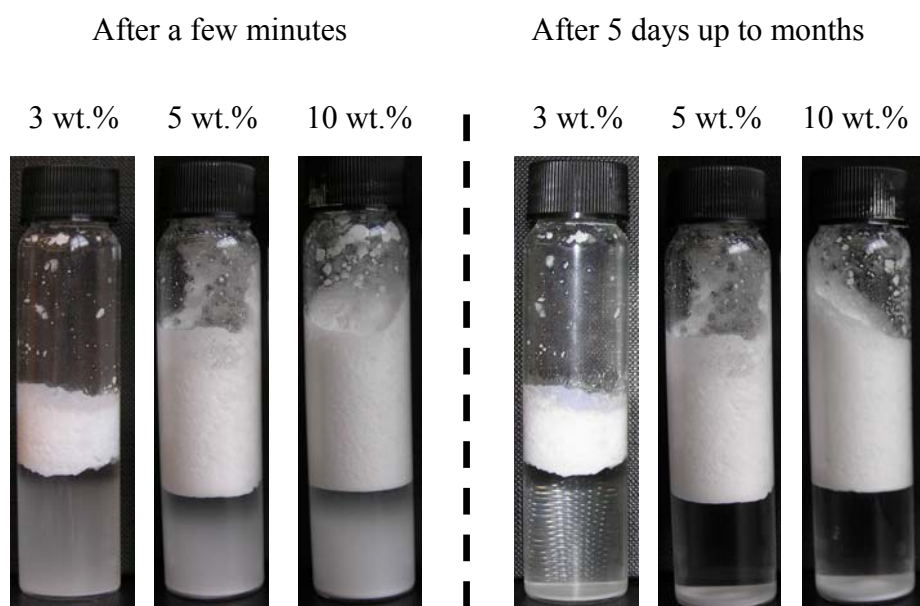
Figure 4.35 Initial foam height (open symbols) and foam height after 48 hours (filled symbols) versus air-water contact angle for aqueous dispersions of silica particles of diameter 0.6 (triangles) and 2 μm (diamonds) at different concentrations as given.
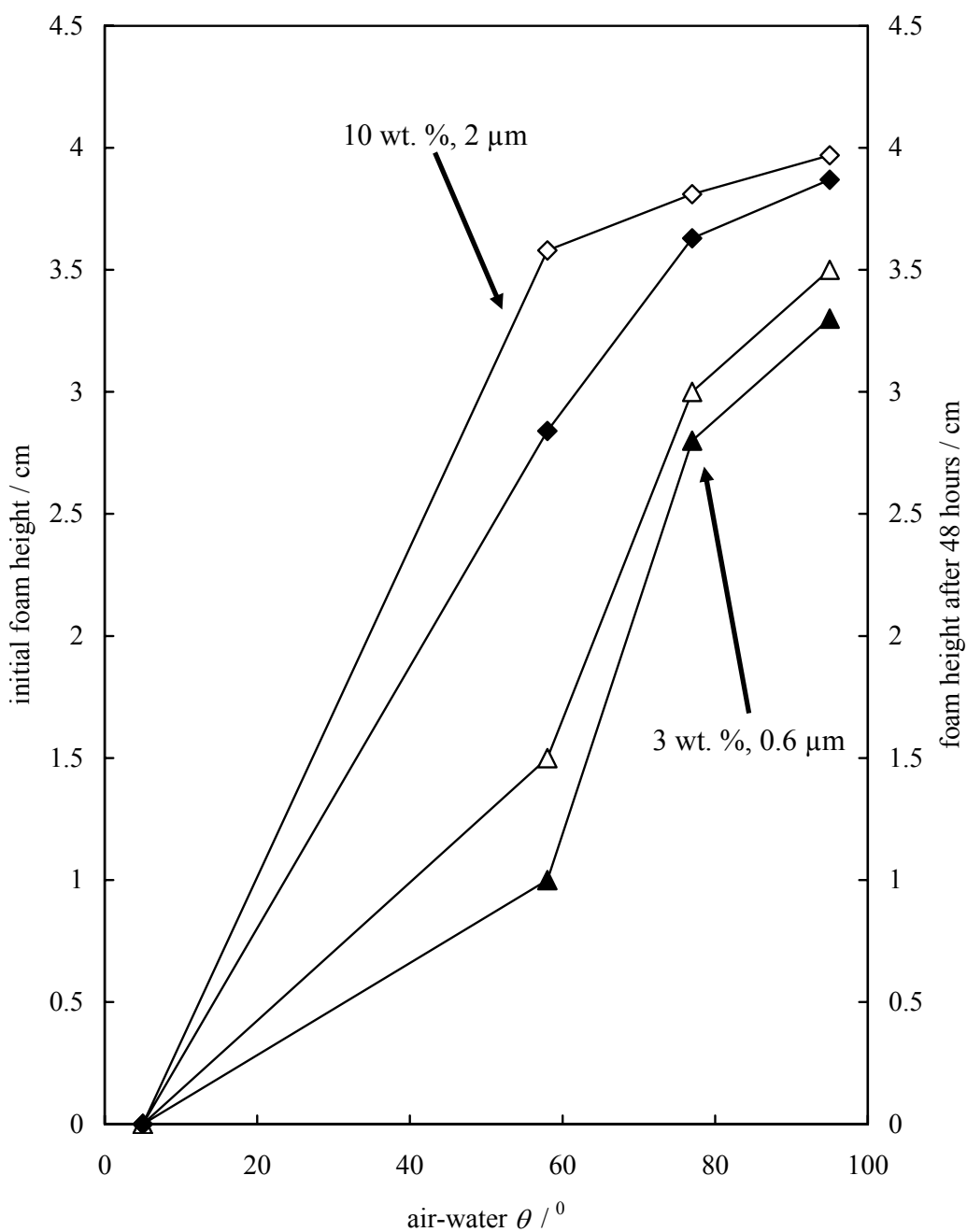
4.6   Foam structure

The foam produced by shaking or homogenising aqueous dispersions of silica particles under the appropriate foaming conditions is particle stabilised. Here the bubbles have a 'solid' appearance and are very stable compared with liquid surfactant foams. The bubbles appeared to be mainly spherical although some bubbles, especially the smaller ones, had distinct non-spherical shape. The bubbles observed varied in size from diameters of the order of 2 cm to microbubbles, depending on the particle hydrophobicity and concentration of salt. Optical microscope and cryo-SEM images of the bubbles within some of the foams produced are shown below.

4.6.1   *Optical microscope*

Optical microscope images of bubbles in foams stabilised by silanised silica particles of diameter 0.6 μm (θ_{aw} average = 58°) in the presence of salt are shown in Figure 4.36. Bubbles are spherical and more rounded when the foam is wet (Figure 4.36 (a)), while bubbles in the dry foam have angular sides (Figure 4.36 (b)). The bubble size in this system was in the range 50 μm - 2 cm. The smaller bubbles were observed in the foams produced from aqueous silica particles of higher hydrophobicity and higher salt concentration. For example, the bubble size in the foam obtained from aqueous dispersions of silica particles of intermediate hydrophobicity, *e.g.* 77° and 1 M NaCl (see Figure 4.37 (c)) was in the range of ~ 20 - 50 μm. Figure 4.38 shows the size and shape of the bubbles within the foam produced with silica particles of higher hydrophobicity, 95°. Distinct non-spherical bubbles, with diameters of 5 - 50 μm, are a feature of these systems. Their surfaces seem to be rough as a result of ripples. This may suggest that the bubbles are covered with dense particle layers. Stable bubbles are possibly formed by coalescence between smaller bubbles that are covered with dilute particle layers during homogenisation.[3] When the bubble area decreases, excess particles cannot be released as they are irreversibly adsorbed and so the surface corrugates to increase in area.

Figure 4.36 Optical microscope images of the bubbles in aqueous foams stabilised by 3 wt. % silica particles of diameter 0.6 μm previously silanised with [DCDMS] = 8 × 10^{-4} M (θ_{aw} average =58°) captured from the top of the foam in a Petri- dish. Conditions and time after homogenization: (a) 0.1 M NaCl, after 1 hour, wet foam, 4 x magnification, (b) 1 M NaCl, after evaporation of water, dry foam, 4 x magnification.

(a)
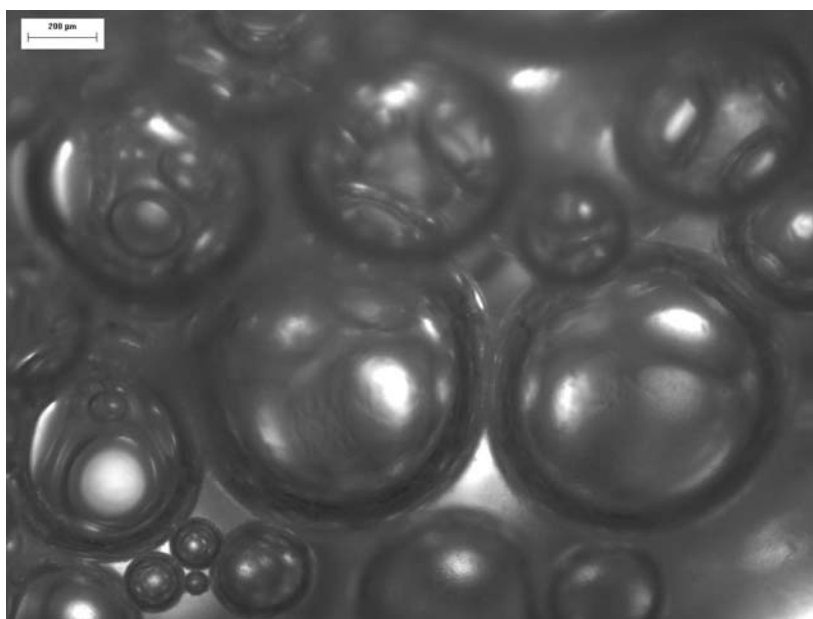
(b)
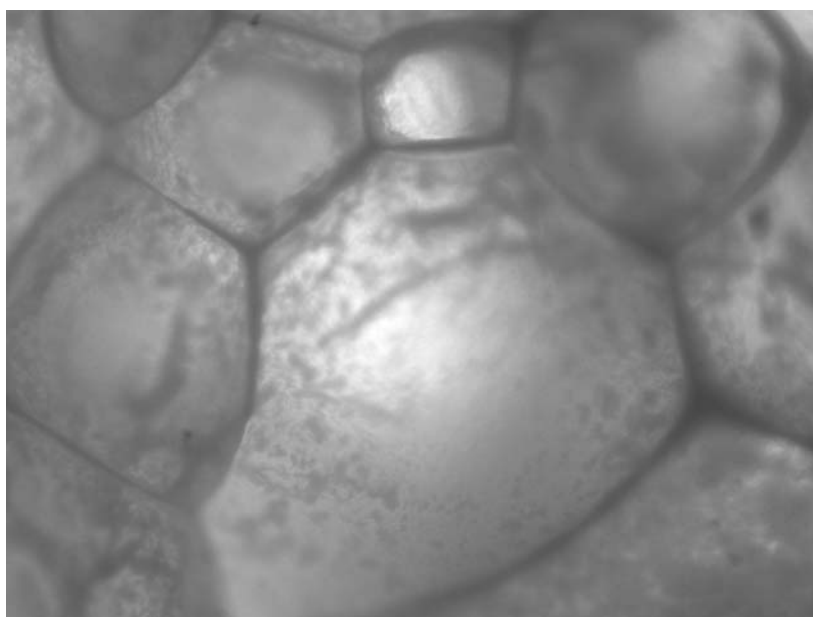
Figure 4.37 Optical microscope images of the bubbles in aqueous foams stabilised by 3 wt. % silica particles of diameter 0.6 μm previously silanised with [DCDMS] = 3 × 10^{-3} M (θ_{aw} average = 77°) captured from the top of the foam in a Petri- dish. Conditions and time after homogenization: (a) 0.05 M NaCl, after 24 hours, wet foam, 10 x magnification, (b) 0.05 M NaCl, dry foam, 10 x magnification, (c) 1 M NaCl, after 24 hours, wet foam, 4 x magnification.

(a)
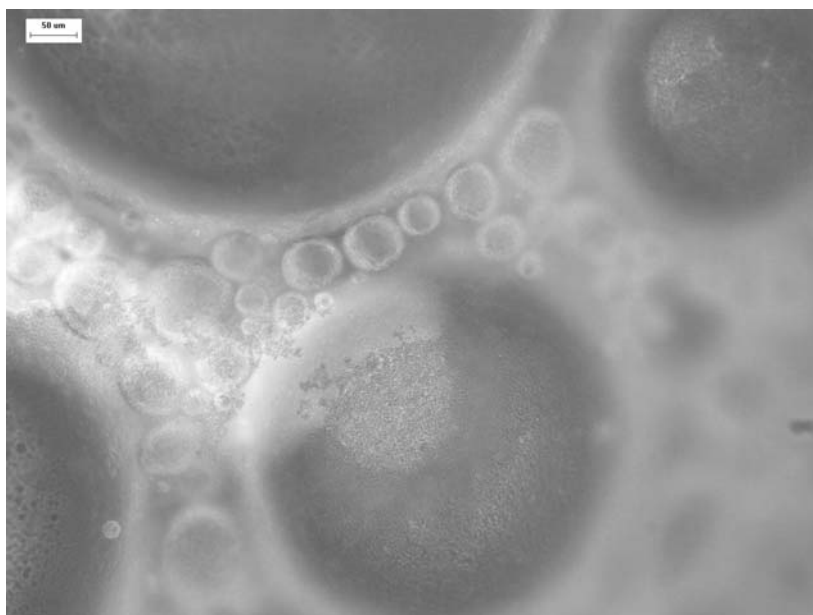
(b)
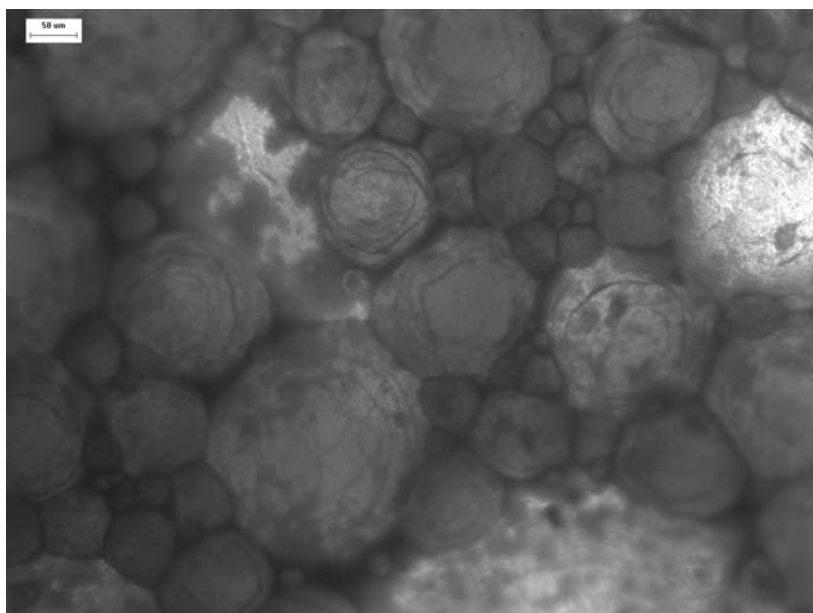
(c)
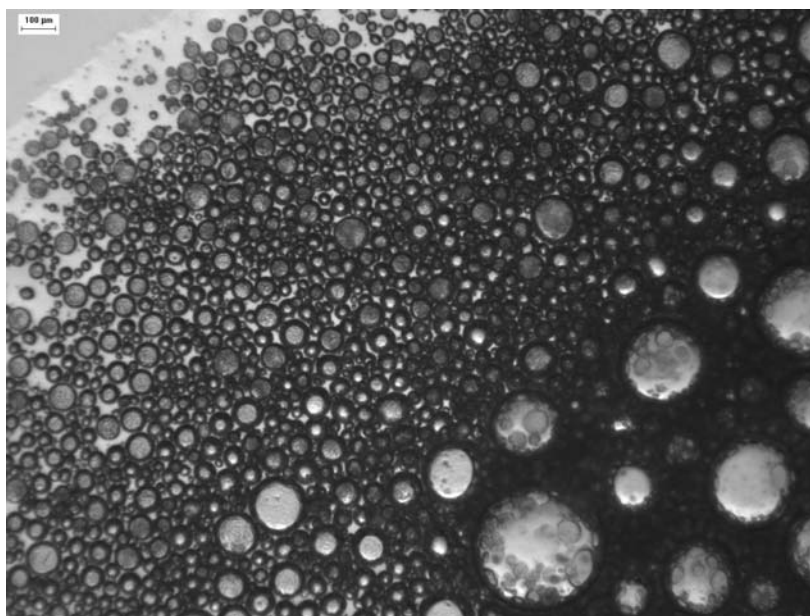
Figure 4.38 Optical microscope images of the bubbles in aqueous foams stabilised by 3 wt. % silica particles of diameter 0.6 μm previously silanised with [DCDMS] $= 4 \times 10^{-3}$ M (θ_{aw} average $= 95°$) captured from the top of the foam in a Petri- dish. Conditions and time after homogenization: (a) 0.05 M NaCl, after 7 days, 10 x magnification, (b) 0.05 M NaCl, after 7 days, 40 x magnification.

(a)
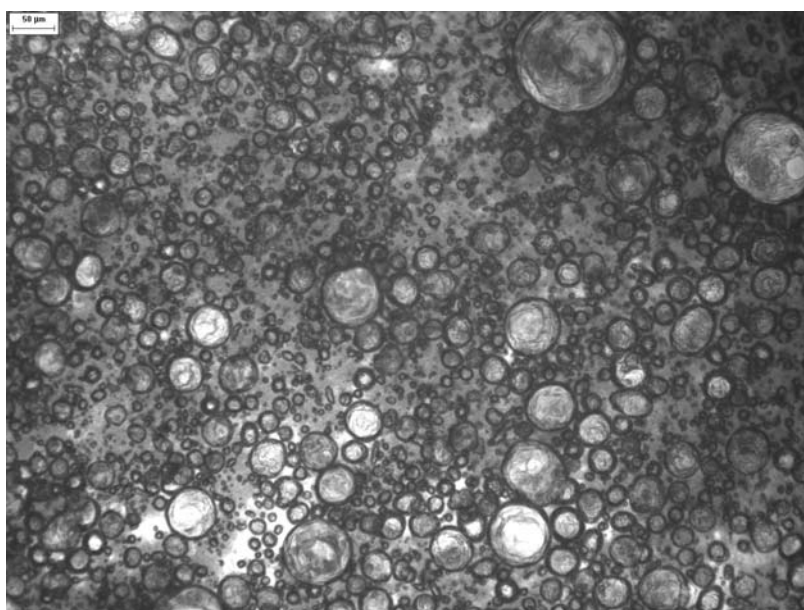
(b)
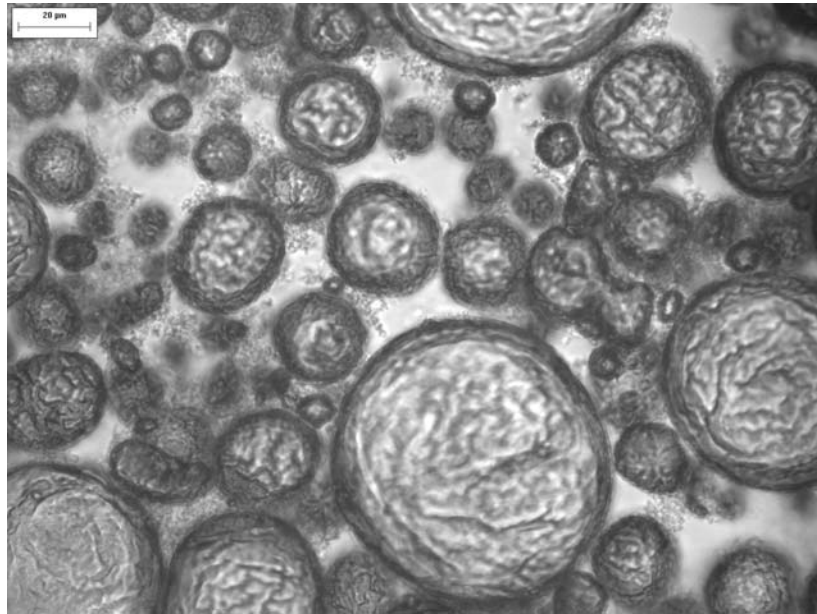
Other researchers[17,18] have also demonstrated that not only are particles useful for making bubbles last longer, they also alter the properties of these bubbles. Instead of behaving like a fluid surface that flows to balance unequal stresses, the 'armor' of particles on the surface of the bubbles actually supports the unequal stresses inherent in non-spherical shapes. Surface tension gives all bubbles their perfectly spherical shape by minimizing the surface area for a given volume. Ordinarily if two bubbles are fused, the product is a larger but still spherical bubble. But when particles are strongly anchored to the bubble surface and the bubbles are fused, a stable sausage shape is produced. The bubble wants to reduce its surface area by going back to a spherical shape, but the strong anchoring of the particles on the surface prevents their expulsion. The particles end up tightly packed, and eventually push against each other strongly, allowing the bubble surface to carry forces to support a non-spherical shape.

4.6.2   Cryo - freeze fracture SEM

Cryo- SEM images of bubbles in foams stabilised by silica particles of different hydrophobicity in the presence and absence of salt are shown in Figures 4.39 and 4.40 respectively.

Figure 4.39 Cryo - freeze fracture SEM micrographs at different magnifications of fragments of aqueous foams stabilised by 3 wt. % silica particles of diameter 0.6 µm at different particle hydrophobicity in the absence of salt.

$\theta = 77°$

$\theta = 95°$
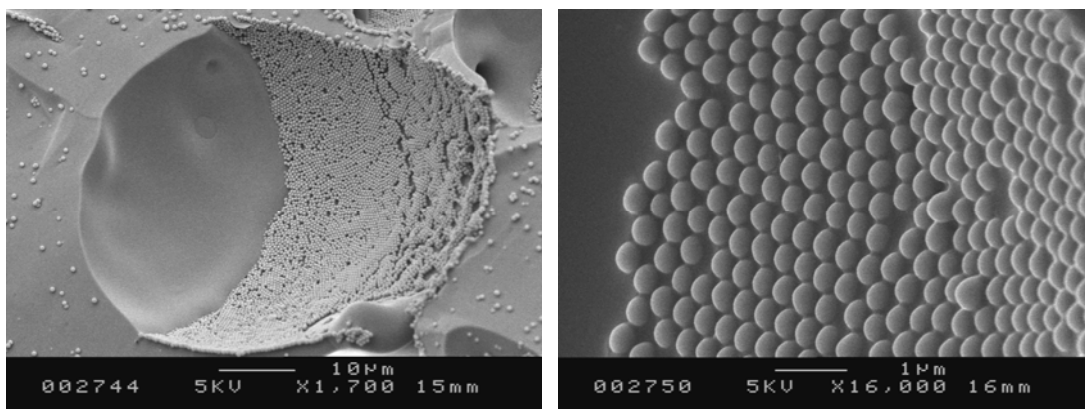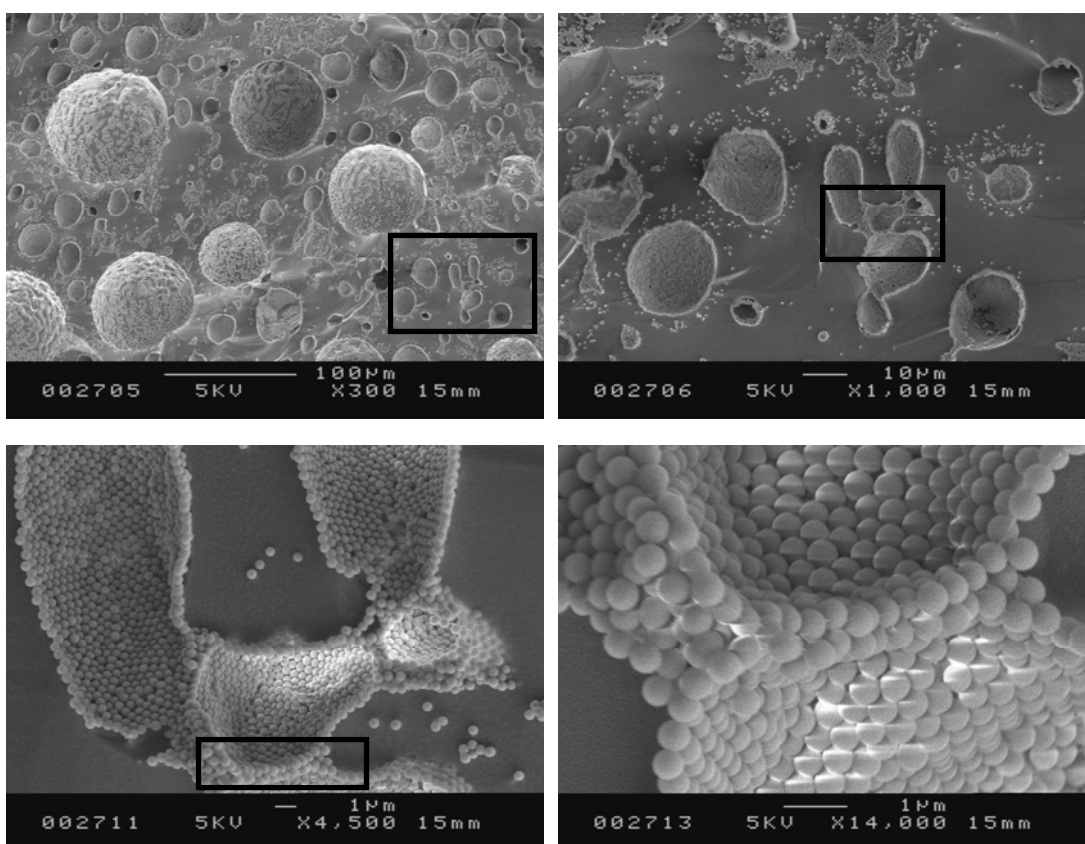
θ = 105°
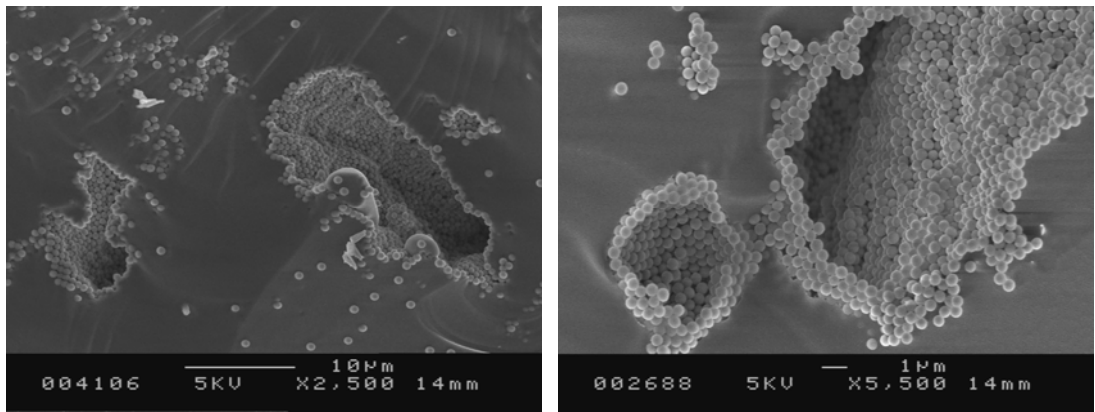
Figure 4.40 Cryo - freeze fracture SEM micrographs at different magnifications of fragments of aqueous foams stabilised by 3 wt. % silica particles of diameter 0.6 µm for different particle hydrophobicity in the presence of 0.05 M NaCl.

θ = 5°

θ = 58°

θ = 77°

θ = 95°
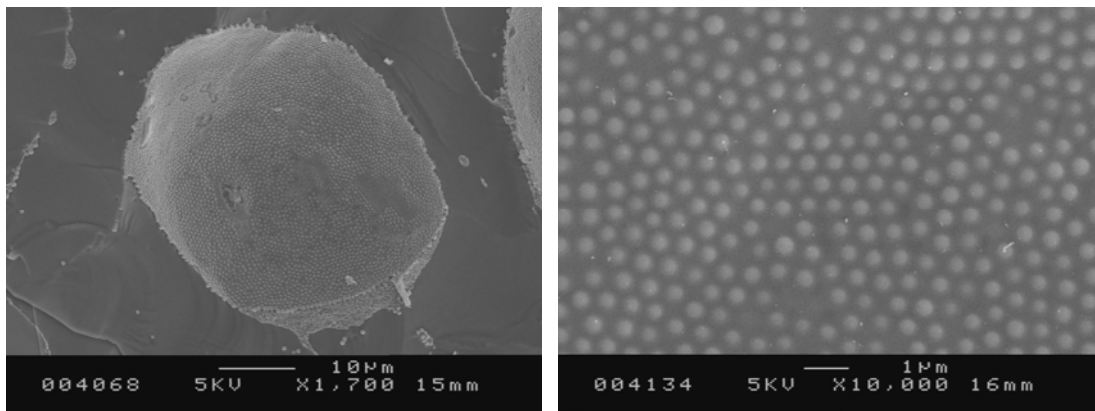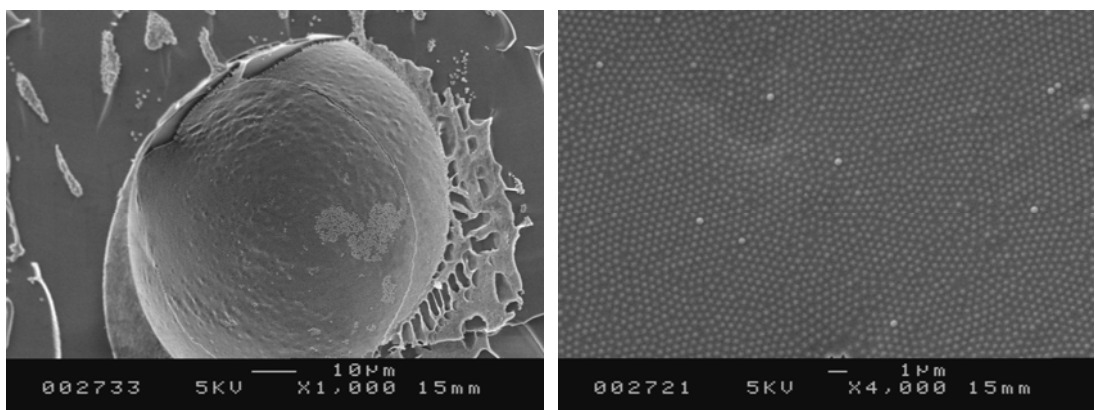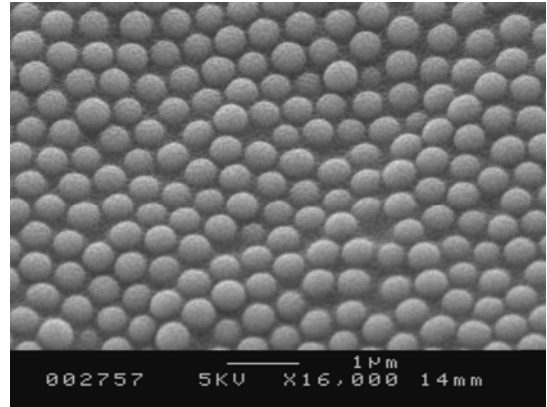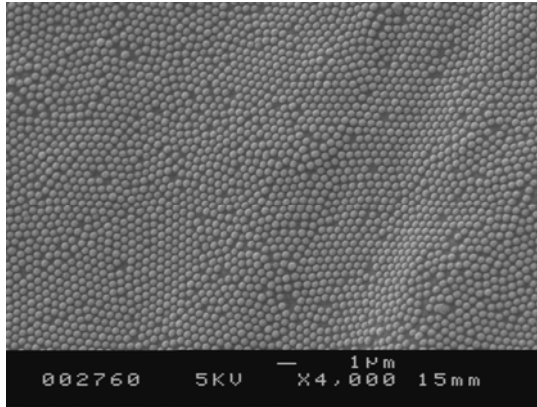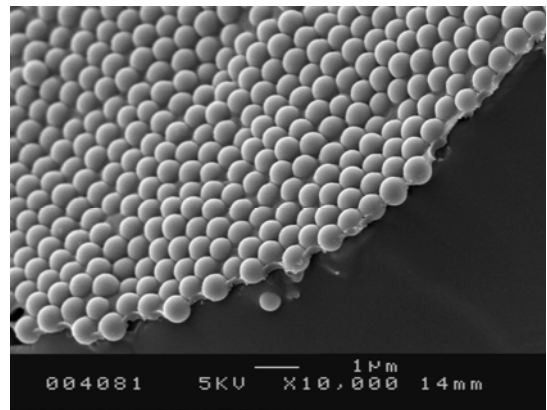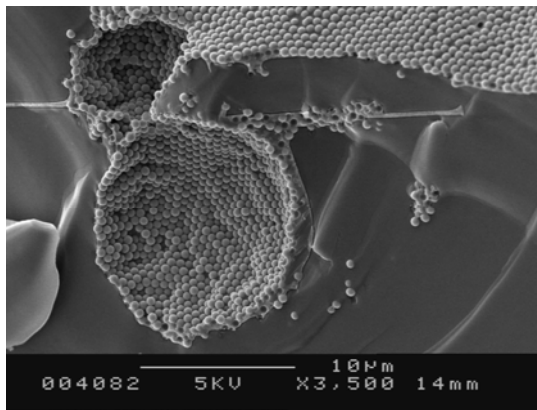
θ = 105°
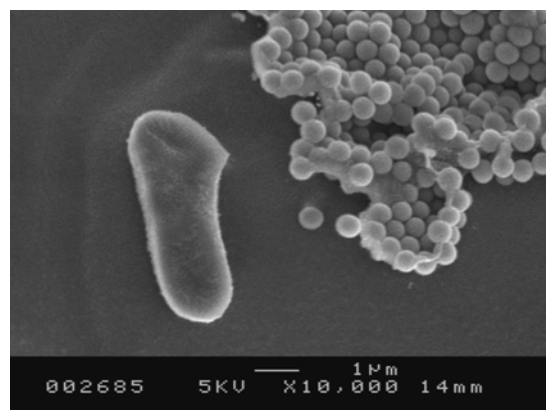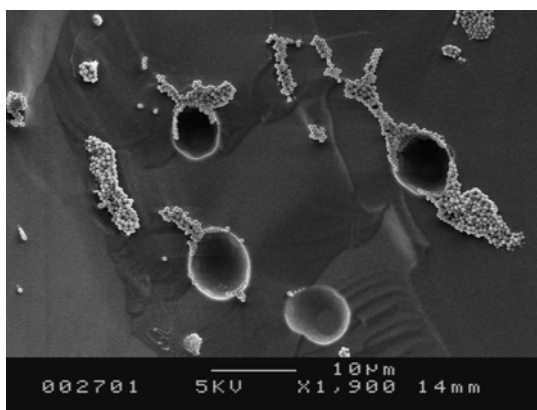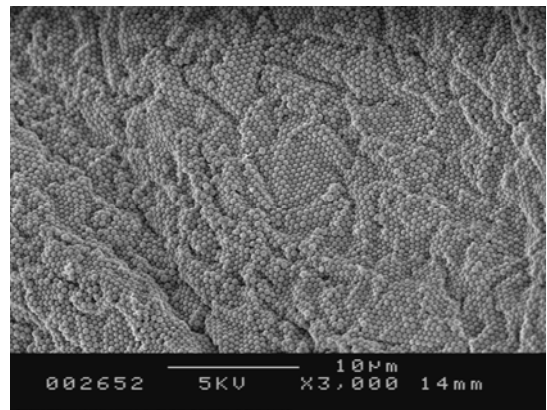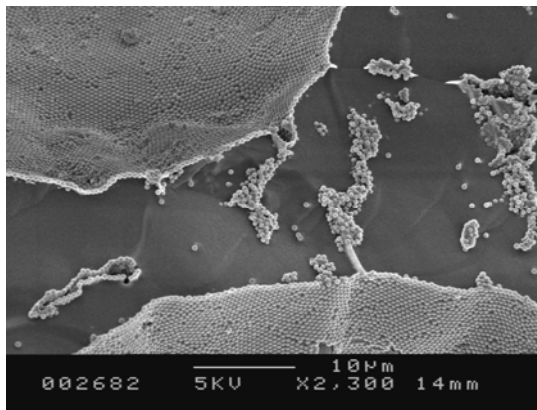
It can be seen from these images that by increasing the contact angle of the silica particles from 77° to 105° in the absence of salt, particles become more closed-packed and aggregates are observed in the systems containing the most hydrophobic particles, 105°. In the case of silica particles with contact angle 77°, particle-free regions at the air-water interface were observed, which can explain why these foams were more unstable compared with the foams produced with particles of higher hydrophobicity. However, even when partial coverage of silica particles at the air-water interface is observed, hexagonal close-packed arrangement of particles is observed in covered areas with some few defects (holes). It is also shown in these images that when two bubbles completely covered by silica particles (*e.g.* 95°) contact each other, the bubbles form a bilayer structure believed to prevent bubble coalescence.

A better coverage of silica particles at the interface is observed with the higher particle contact angle (*e.g.* 95° and 105°) and also with the systems containing salt. The accumulation of particles near the interface of contact between the bubbles was also observed in these systems (which may be also the reason for preventing bubble coalescence). The bubble sizes were found to decrease with increasing contact angle and for the more hydrophobic systems they are in the range 5 – 50 μm (some bubbles have distinct non-spherical shape). It was clearly observed with the systems containing salt (Figure 4.40) that particles of increasing hydrophobicity are more exposed to the air rather than in the aqueous phase. The images also show that the smaller bubbles have a more densely packed particle layer at the interface compared with the bigger bubbles where particle-free regions were observed. The densely packed particles, either in single or multilayer configuration, can provide strong steric hindrance to bubble coalescence. Ripples at the surfaces of bubbles are observed, possibly due to a dense multilayer of silica particles at the air-water interface. It was also observed that the smaller bubbles (~ 5 μm) found at the bottom of the foam (*e.g.* 105°) are not covered with individual silica particles. Instead they have a few flocs around them and because some of these flocs are so big they may be easily detached from the bubbles and go to the aqueous solution and eventually sediment (this was also observed in situ when preparing the foam – flocs were observed underneath the foam and with time they eventually sediment).

4.7   Conclusions

A study of the foamability and foam stability of *ex-situ* modified hydrophilic silica particles of diameter 0.6 μm is presented. The parameters that affect the foamability and foam stability of the aqueous dispersions are particle hydrophobicity, particle concentration, salt concentration and the method used for foam production.

Unmodified hydrophilic silica particles are able to stabilise aqueous foams only in the presence of salt *e.g.* 0.5 and 1 M NaCl. By increasing the particle hydrophobicity, a maximum in foamability was observed at a contact angle equal to 95°. However, the most stable foams are those formed higher particle hydrophobicity ($\theta = 95\text{-}110°$) and in the presence of salt. These foams are very stable against coalescence or disproportionation of bubbles. The decrease in their volume is mainly a result of water drainage and bubble compaction, but not to loss of air. The size of the bubbles decreases progressively with an increase in salt concentration and hydrophobicity of the particles. By increasing particle concentration and size, foamability and foam stability is also enhanced.

Silica particles were found to aggregate in bulk after addition of salt. The extent of aggregation depends on the hydrophobicity of the particle and the concentration of electrolyte. It was found here that the more hydrophobic particles and the higher the salt concentration used, the bigger are the aggregates formed. It seems that when very dense layers of particles and small aggregates adsorb around air bubbles, foam stability is enhanced in comparison to foams formed with discrete primary particles as they are easily detached form the air-water interface. One consequence of particle aggregation is the increased viscosity of the aqueous phase (gelling) which results in slower drainage of foam films and increased stability of the foam. The densely packed particles at the air-water interface, either in monolayer or multilayer configuration provides strong steric hindrance to bubble coalescence.

References

1. B.P. Binks, *Current Opin. Colloid Interface Sci.*, **7**, 21 (2002).

2. R.G. Alargova, D.S. Warhadpande, V.N. Paunov and O.D. Velev, *Langmuir*, **20**, 10371 (2004).

3. B.P. Binks and T.S. Horozov, *Angew. Chem. Int. Ed.*, **44**, 3722 (2005).

4. J.C. Wilson, A study of particulate foams, Ph.D. thesis, University of Bristol (1980).

5. S. Fujii, P.D. Iddon, A.J. Ryan and S.P. Armes, *Langmuir*, **22**, 18 (2006).

6. B.P. Binks and R. Murakami, *Nature Materials*, **5**, 865 (2006).

7. Tursbican Lab guide, Formulaction, U.K. (2006).

8. P. Snabre and P. Mills, *Q. Europhysic Letters 25*, **9**, 651 (1994).

9. V.N. Paunov, B.P. Binks, N.P. Ashby, *Langmuir*, **18**, 6946 (2002).

10. B.P. Binks, J.H Clint, P.D.I. Fletcher, T.J.G. Lees and P. Taylor, *Chem. Commun.*, 3531, (2006).

11. R. Aveyard, B.P. Binks, P.D.I. Fletcher and C.E Rutherford, *J. Dispersion Sci. Technol.,* **15**, 251 (1994).

12. R.J. Pugh, *Adv. Colloid Interface Sci.*, **64**, 67 (1996).

13. N.D. Denkov, *Langmuir*, **20**, 9463 (2004).

14. G. Kaptay, *Colloids Surf. A: Physicochem. Eng. Aspects,* **230**, 67 (2003).

15. G. Kaptay, *Colloids Surf. A: Physicochem. Eng. Aspects,* **282-283**, 387 (2006).

16. S.K. Bindal, G. Sethumadhavan, A.D. Nikolov and D.T. Wasan, *AIChE J.*, **48**, 2307 (2002).

17. A.B. Subramanian, M. Abkarian, L. Mahadevana and H.A. Stone, *Nature*, **438**, 930 (2005).

18. A.B. Subramanian, M. Abkarian, L. Mahadevan and H.A. Stone, *Langmuir*, **22**, 10204 (2006).

CHAPTER 5

CHAPTER 5

THIN FOAM FILMS WITH SILICA PARTICLES AT THEIR SURFACES

5.1 Introduction

The stability of foams or emulsions is a major subject of surface and colloid science. In any foam or emulsion system thin liquid films (TLF) are formed when the bubbles or droplets are pressed against one another under the action of surface forces, Brownian motion or gravity. Many industrial processes and products rely on fundamental interfacial interactions which occur in the thin-film region. In order to stabilise these intervening films, organic or inorganic substances are added to the liquid continuous phase. Understanding the mechanisms behind thinning and stability of the aqueous films separating the foam bubbles is crucial in order to understand coalescence and foam collapse. The link between the stability of aqueous foams and isolated foam films stabilised by surfactants or proteins has been investigated and well documented.[1,2] Much effort has been spent investigating in a controllable and reproducible way the processes of formation, thinning, and rupture of liquid films between bubbles in the presence of surfactant. The first experiments in the field have been performed by the Derjaguin's group[3,4] They designed a few setups that permit manipulation of the gas bubbles in a controllable way and pioneered the investigation of foam films. Sheludko[5,6] refined the construction proposed by Derjaguin and Tatijeskaja[3] and introduced the capillary cell for studying foam films. In this configuration, the film is made by sucking the liquid from a biconcave meniscus. Later, Lykema et al.[7] elaborated the technique of forming macroscopic foam films on glass frame. This method has undergone numerous modifications, but it remains a widely employed tool in studying foams.[8] Another convenient way to study TLF is to press a drop (bubble) to a large interface.[9,10] Currently, TLF are investigated mainly by means of the miniaturised Scheludko cell[11], and Mysels cell.[12,13]

In foams the pressure inside the bubbles (P_1) is higher than the pressure in the bulk liquid (P_2) and as a result a capillary suction occurs.[14,1] The pressure difference:

$$\Delta P = P_1 - P_2 \qquad (5.1)$$

is related to the radius r of the bubbles according to the Laplace equation:

$$\Delta P = P_C = \frac{2\sigma}{r} \qquad (5.2)$$

P_C is the capillary pressure and σ is the interfacial tension of the continuous phase. As the aqueous solution in a TLF (*e.g.* foam) drains, the interfaces approach one another and the phases separated by the solution interact. The drainage of the intermediate thin films induced by P_C is slowed down and eventually prevented when interactions between the film surfaces come into play. These interactions are called the disjoining pressure Π.

One general definition for the mechanical equilibrium disjoining pressure is that $\Pi(h)$, is equal to the difference existing between the component P_3 of the pressure tensor in the TLF and the pressure, P_2, set up in the bulk liquid (equation 5.3).[15]

$$\Pi(h) = P_3 - P_2 = P_1 - P_2 = P_C \qquad (5.3)$$

P_3 is the normal component of the pressure tensor in the film, P_2 is the pressure in the meniscus (bulk of the liquid); P_1 is the pressure in the air (bubble) and P_C is the capillary pressure defined as the pressure difference across the fluid interface. If capillary suction is tending to pull liquid out of the film then, for a plane film in equilibrium with the adjoining plateau border, the disjoining pressure is equal to capillary pressure ($\Pi = Pc$). A schematic representation of a water TLF is shown in Figure 5.1 and a schematic plot of the disjoining pressure isotherm versus *h* is shown in Figure 5.2.

Figure 5.1   Schematic representation of water TLF.
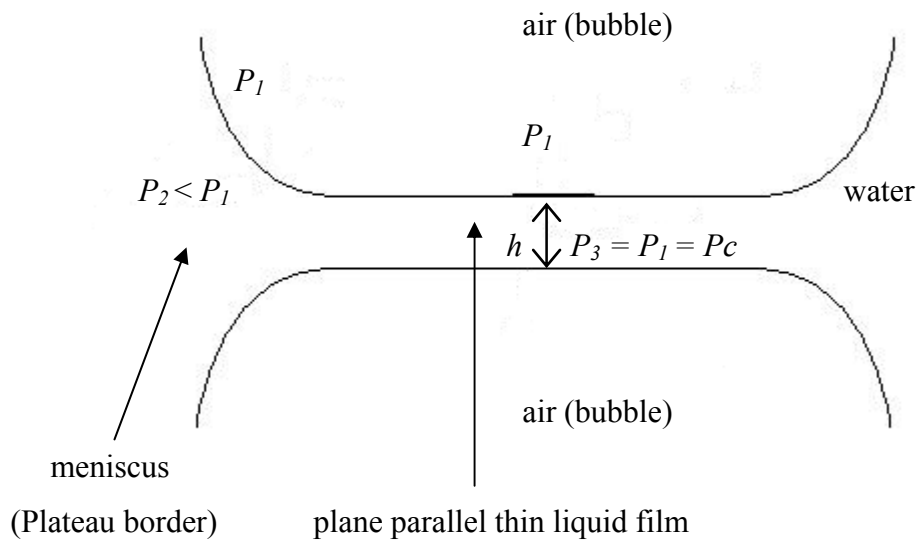
Figure 5.2   Sketch of a disjoining pressure isotherm (Π) versus film thickness (h). Pc is the capillary pressure, h_1 corresponds to a primary film and h_2 to a secondary film (re-drawn from reference 16).
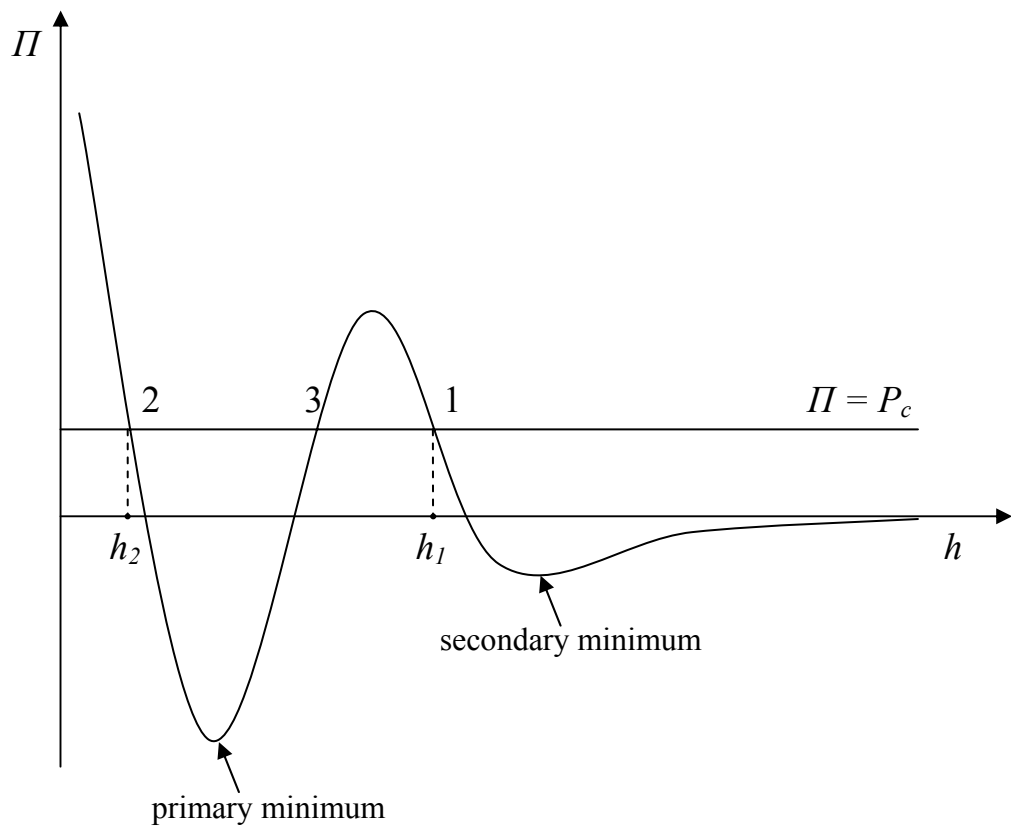
For a system giving rise to such a disjoining pressure isotherm, there will exist a metastable film with thickness h_1, which is stabilised by the double layer repulsion (Figure 5.2, Point 1). If the film can surmount the energy maximum in some way or another, a thinner metastable film with thickness h_2 will form, which is stabilised by the short range repulsion (Figure 5.2, point 2). Films with thickness h_1 and h_2 correspond to the primary film or Common Black Film (CBF) and the secondary film or Newton Black Film (NBF).[16] Transitions from common to Newton black films are often observed with foam films.[17,18] $\Pi > 0$ means that repulsion exist between the film surfaces, whereas $\Pi < 0$ corresponds to attraction. Point 3 in Figure 5.2 corresponds to unstable equilibrium and can not be observed experimentally.

For a planar film in equilibrium with an adjoining meniscus the disjoining pressure in the film is equal to the capillary pressure. Since stability results from the competition between capillary pressure tending to thin the film and disjoining pressure tending to thicken it, it follows that equilibrium is not possible if $d\Pi(h)/dh$ is positive. Although, films are considered to be plane parallel structures, capillary waves are present in the film surface as a result of Brownian motion or mechanical effects. The waves are damped by the action of the surface tension (which is the cause of the Laplace pressure). If there are only attractive forces between the surfaces, this will act to thin even further the thinner parts of the film, increasing the chances of forming a hole which can lead to rupture. The cappilary pressure depends on the amplitude and wavelength of the waves and on the surface tension. However in soap films there are also repulsive surfaces forces in addition to van der Waals forces and this means that in systems were the surfactant concentration is high enough (to keep monolayers close-packed) instead of rupture occurring at the critical thickness (hc), a few tens of nanometres, 'black spots' of thin film can form[19]. This phenomenon probably results from changes occurring in the disjoining pressure isotherms with changes in surfactant concentration. Once formed, the black spots can grow to cover the whole film. In systems exhibiting black spots foam stability tends to be high.

All the film studies mentioned above are relevant to the stability of surfactant foams. However, the present study is related to particle-stabilised foams and a simpler method for studying foam films with particle monolayers at their surfaces was employed. There are a few studies on the properties of emulsion films with particle monolayers at their surfaces which are relevant to particle-stabilised emulsions. However, systematic studies on the foam films stabilised solely by solid particles in the

absence of surface-active molecules is sparse. Therefore, the mechanisms underlying the stability of the surfactant-free particle-stabilised foams are not well understood. Recently, a systematic study of emulsion films with silica particles monolayers at their surfaces was published by Horozov *et al.*[20] where the effect of particle contact angle and surface coverage on the structure and stability of water films in oil (o-w-o) and oil films in water (w-o-w) were investigated. The main findings were found to be very relevant to particle-stabilised emulsions. The experimental setup used in this study (see Chapter 2) was very similar to the one reported by Horozov *et al.*[21], where the films were formed in a Scheludko type cell and observed with a microscope. The main difference is that air-water systems were used in this study because of their applications to foams. We used monodisperse silica particles (3 μm in diameter) hydrophobised to different extents. The density of the particle monolayer at the water surface was changed by spreading different amounts of particles. Vertical foam films with dilute and close-packed modified silica particles monolayers at their surfaces and the effect of both hydrophilic and hydrophobic particles on the stability of foam films has been investigated.

In the literature Denkov *et al.*[21] proposed a theoretical model for the stabilisation of emulsions by solid particles. In this model, they considered theoretically films formed by a particle monolayer pressed between two emulsion interfaces. Their stability was determined by the maximum capillary pressure drop, P_c^{max}, which can be resisted by liquid menisci formed between the adsorbed particles. They also supposed that the particles in the film were not in close contact. From a physical point of view this will be the case when repulsion between the particles in the film takes place. In the case, where there is attraction between the particles and particles are close-packed in the film, another theoretical model has been proposed by Kaptay.[22] In this model, the thin liquid films are stabilised by a double layer of closed packed particles. Therefore, considering these two models[21,22], two different mechanisms have been proposed in this study as possible explanations of stabilisation of foams by hydrophilic solid particles ($\theta < 90°$). Films with dilute particle monolayer (a) and close-packed particles at their surfaces (b) are considered in Figure 5.3. The quantity h shown in Figure 5.3 is denoted film thickness and is the shortest distance between the two film surfaces.

Figure 5.3 Sketch of a foam film with dilute (a) and close-packed (b) monodisperse spherical solid particles at its surfaces.

(a)

(b)

air

water

h

air

film drains

air

water

air

bilayer of close-packed particles

217
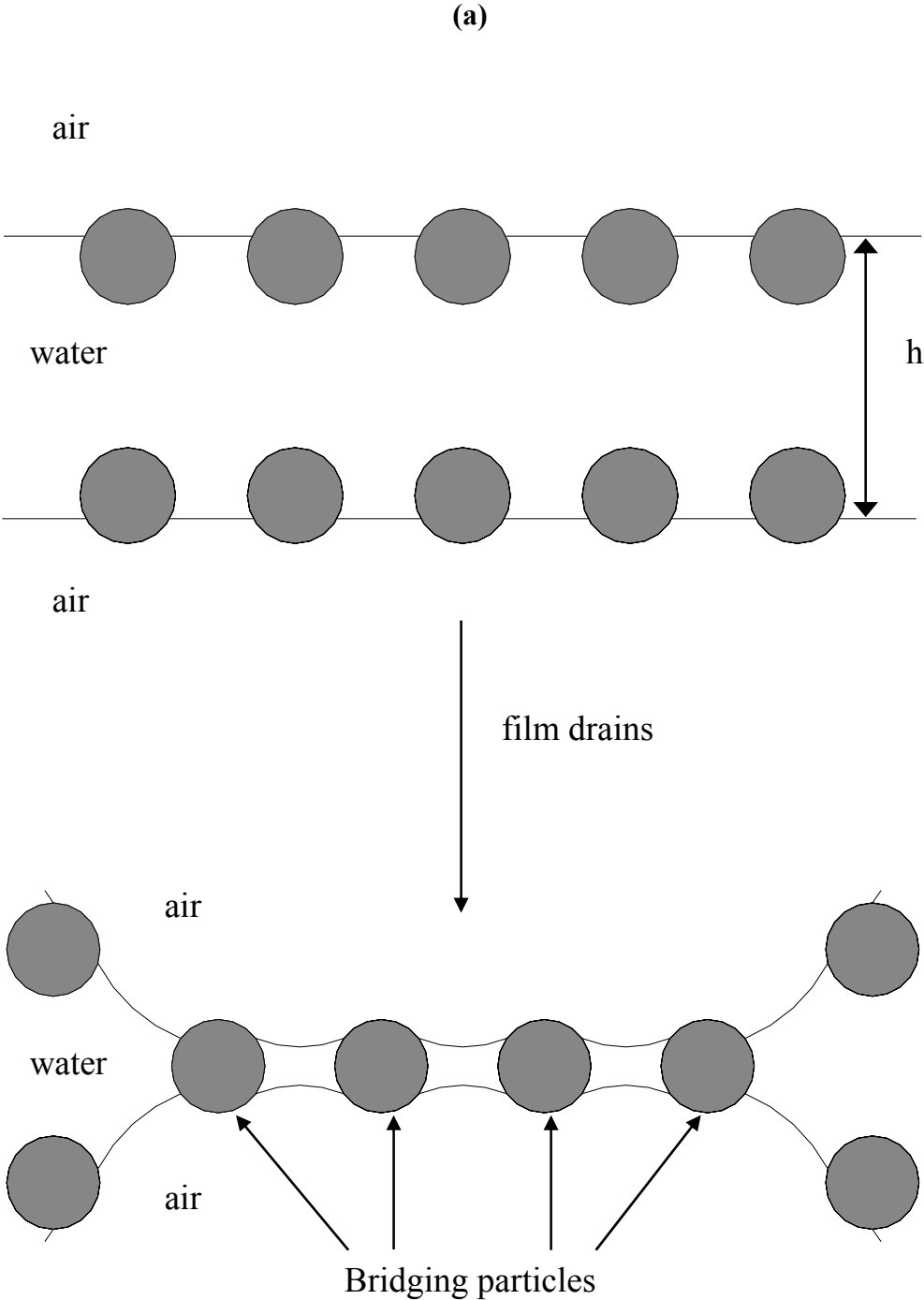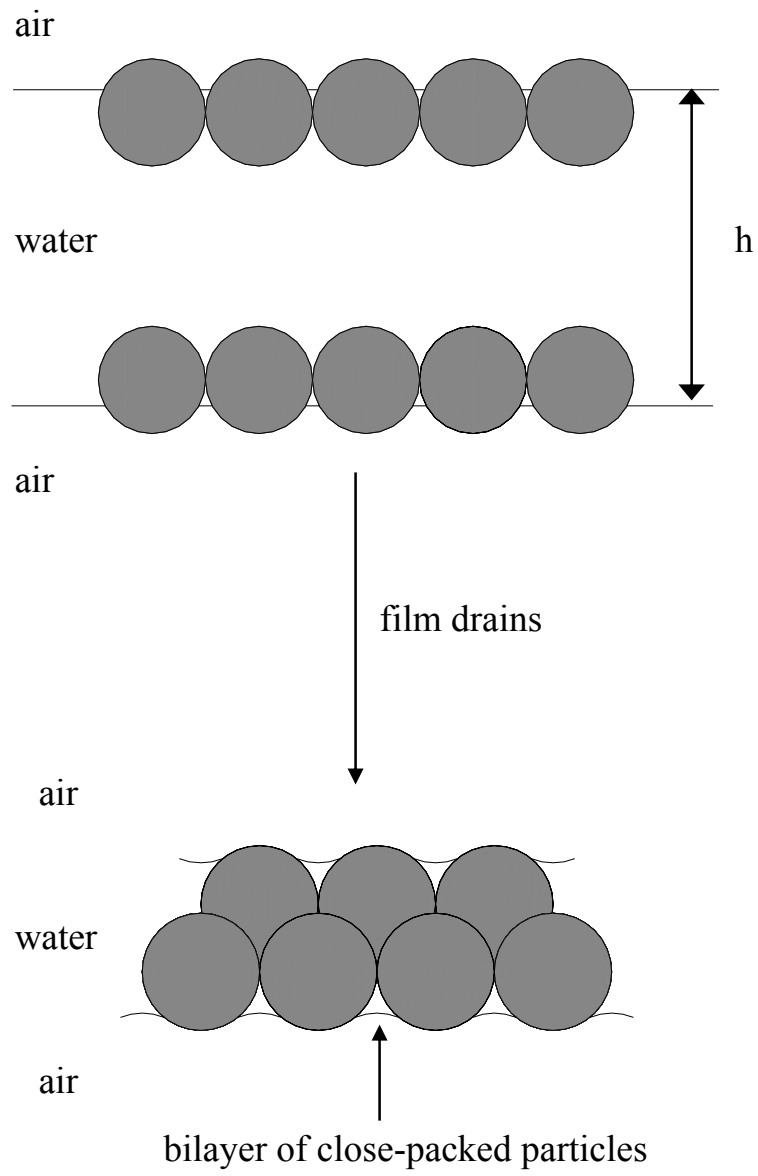
As the film drains curvature of the surfaces is generated which draws liquid towards the particle, thus opposing film thinning. Hence, the particles do not rupture the films. However, two different configurations are possible depending on the arrangement of particles in the film between the bubbles, in the case of films with dilute particle monolayer at their surfaces a stable bridging monolayer configuration is possible, whereas with films covered with close-packed particles a bilayer can be formed. The main purpose of studying thin foam films with hydrophilic silica particles at their surfaces was to investigate if these models could be achieved experimentally and to find out what are the conditions needed for stabilising foam films with particles.

Kaptay[23] also suggested that foam films could be stabilised by a double layer of close-packed hydrophobic particles. This is an interesting hypothesis because it is known that hydrophobic particles are good foam breakers.[24-26] The aim for studying foam films with hydrophobic silica particles was therefore to verify Kaptay's hypothesis.

5.2   Hydrophilic silica particles ($\theta_{aw} < 90°$)

5.2.1   Films with dilute particle monolayers at their surfaces

In this study foam films are formed in a vertical Scheludko cell as shown in detail in Chapter 2. The Scheludko cell was connected to a syringe by mean of flexible PTFE tubing. The syringe and tubing were previously filled with water. Then a rectangular glass cuvette was filled partially with water and the fresh prepared suspension of modified silica particles of diameter 3 μm spread at the water surface to form a monolayer of particles at the air-water interface. The density of the monolayer was then varied from very dilute to very dense by changing the spread volume in the range 2 - 160 μL.

Thick vertical foam films are formed just after crossing the air-water interface with the ring frame. Once formed, these very thick films were forced to thin by sucking water out of the meniscus (so-called "opening of the film"). Vertical films without particles at their surface were studied first. These water foam films were relatively stable and survived for several minutes (see Figure 5.4). They are mainly stabilised by the electrostatic repulsion forces between the film surfaces and such a film is usually referred to as a common black film (CBF).

Figure 5.4 Vertical water films without particles at their surfaces. (a) inhomogenous thickness (formation of a dimple), (b) plane parallel film with a thickness of ~ 100 μm.

(a)

25 microns

(b)

25 microns
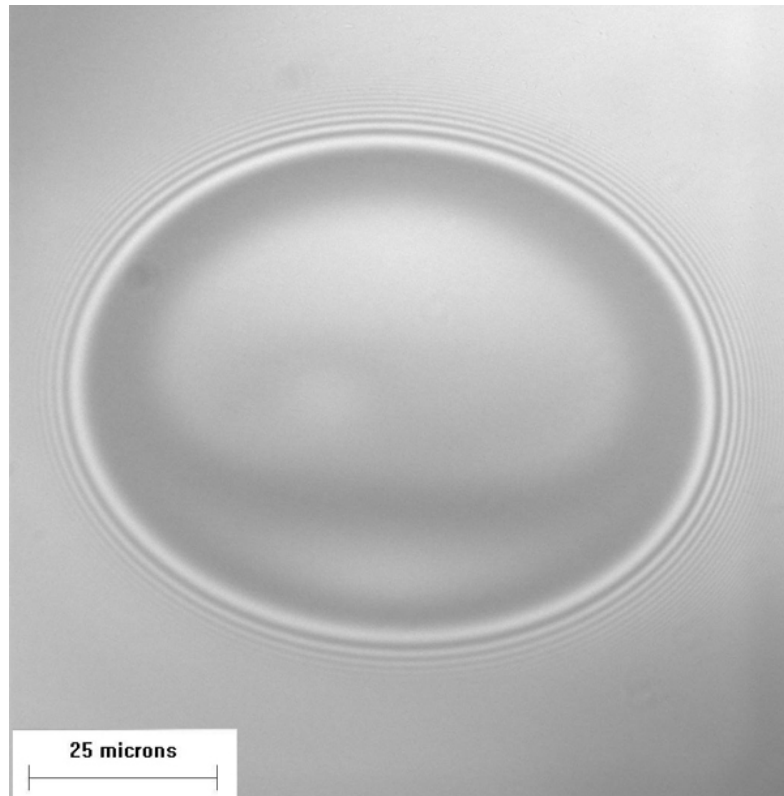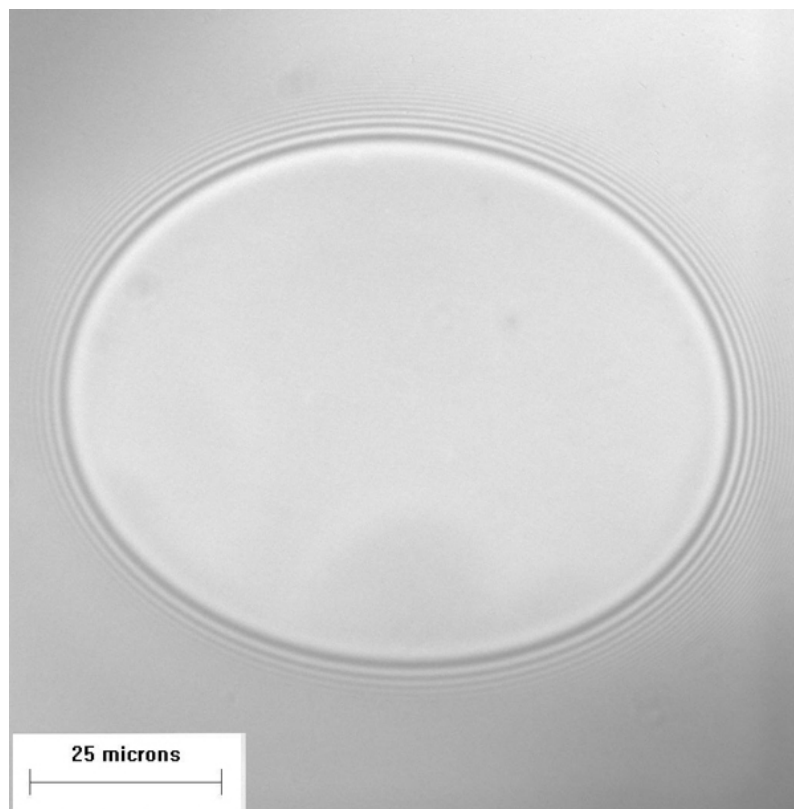
It is known from the literature[27] that in any foam system the driving (capillary) pressure and the film radius are two parameters that crucially affect the rate of thinning of the foam films and, consequently, the stability of the system. The pressure inside and outside the air bubbles are denoted by P_1 and P_2, respectively. The capillary pressure (P_C) of the bubbles is then,

$$P_C = P_1 - P_2 \qquad (5.4)$$

The reason for the existence of such difference between P_1 and P_2 can be either due to the curvature of the bubble surface or gravitational (hydrostatic) sucking pressure as in the case of a foam column. In reality, the water film will break if taking into account the sucking pressure. However, the water films studied here in the absence of any surfactants were relatively stable. Similar observations have been reported by Exerowa et al.[27] were they showed experimentally that foam films could be stable in the absence of surfactant with a measured film thickness $h_w \sim 43$ nm. This stabilisation could be explained by the charge of the air-water interface. It has been suggested that the air-water interface could possess high enough negative charge in the absence of surfactant due to the spontaneous adsorption of hydroxyl (OH^-) ions from water.[28] Therefore, water films without any surfactant could be stable due to repulsive electrostatic interactions between negatively charged surfaces.

The stability and structure of foam films with 3 μm hydrophilic silica particles at their surfaces depended on the mechanism of the speed of opening the films. In the beginning particles were equally distributed at the vertical air-water interface (Figure 5.5 (a)). By opening the film slowly (gentle suction of water out of the meniscus), particles were expelled out of the film with a dimple, as shown in Figure 5.5 (b).

Figure 5.5 Images of a vertical foam film taken in transmitted light in the presence of 3.45×10^5 particles cm^{-2} at the film surfaces. The particle contact angle is 50°. The scale bar is equal to 50 μm.

(a) **(b)**
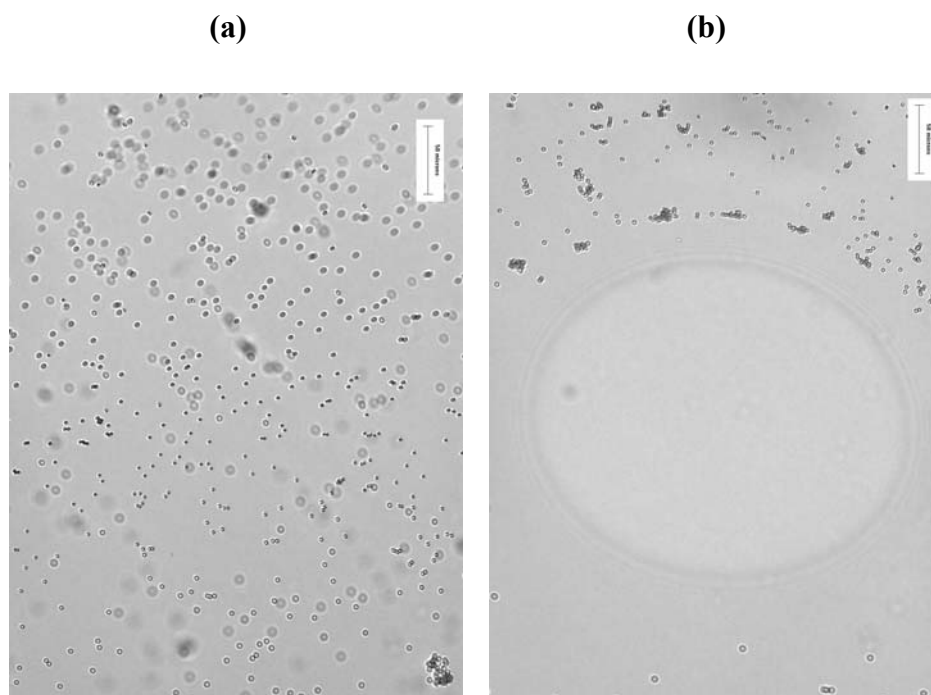
Particles started moving away from the thinnest part of the film, which shows that particles are attached to one of the surfaces therefore particles do not bridge the film surfaces. At rapid film opening, a ring of particles at the film periphery appeared, which shows that the ring consists of particles which bridge the opposite film surfaces. This suggestion is supported by the behaviour of the particles from the ring during the film closing caused by pumping water into the film meniscus (Figure 5.6). During closing, the ring shrunk together with the particle ring. The ring diameter had decreased simultaneously with an increase of its thickness without losing any particles during shrinking (Figure 5.6a-c). This process was fully reversible. The film was opened, thus increasing the ring diameter and decreasing its thickness. Further closing of the film caused shrinking of the particle ring until a crystalline disc of particles was formed spontaneously in the thinnest central part of the water film, which strongly increased its stability against rupture (Figure 5.6d).

Figure 5.6 Consecutive images of a vertical foam film taken in transmitted light during fast film closing by pumping water into the meniscus (in the presence of $\sim 5 \times 10^4$ particles cm^{-2} at their surfaces). The particle contact angle is 65°. The scale bar is equal to 50 µm.

(a) **(b)**

(c) **(d)**
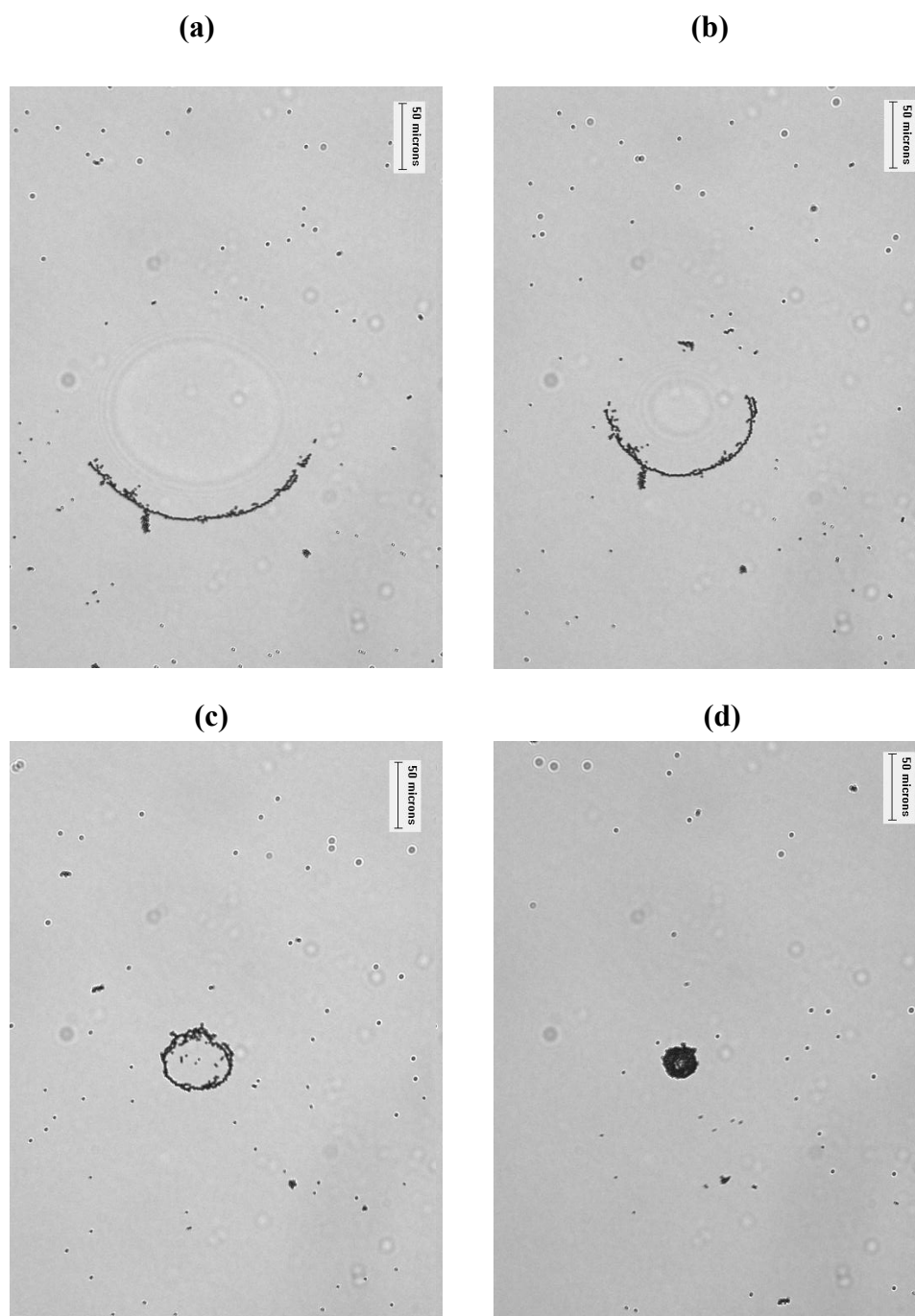
The driving force bridging particles together to give a dense crystalline disk is the capilary attraction between adjacent bridging particles caused by the curved menisci of the fluid interface formed when the particles became attached to both film surfaces.[29-32]

5.2.2 Films with dense particle monolayers at their surfaces

The density of the monolayer was varied from very dilute ($\sim 5\times10^4$ particles cm^{-2}) as shown previously in Figure 5.6, to very dense by changing the spread volume from 2 µL to about 80-150 µL. Foam films with dense particle monolayers containing approximately 20×10^5 particles cm^{-2} at their surfaces were studied shortly after they were formed in order to diminish the effect of particle sedimentation. Figure 5.7 (a) to (f) shows consecutive images taken of the closing up the ring film by putting water inside the film in the case of 20×10^5 particles cm^{-2} at their surfaces and then by opening the film quickly from (e) to (f) a large aggregate is formed outside the film.

Figure 5.7 Consecutive images (a) to (f) of vertical foam films taken during film closing by pumping water inside the meniscus in the case of $\sim 20 \times 10^5$ particles cm^{-2} at their surfaces in transmitted light. The particle contact angle is 65°. The scale bar is equal to 50 µm.

(a)   **(b)**

(c)   **(d)**

223
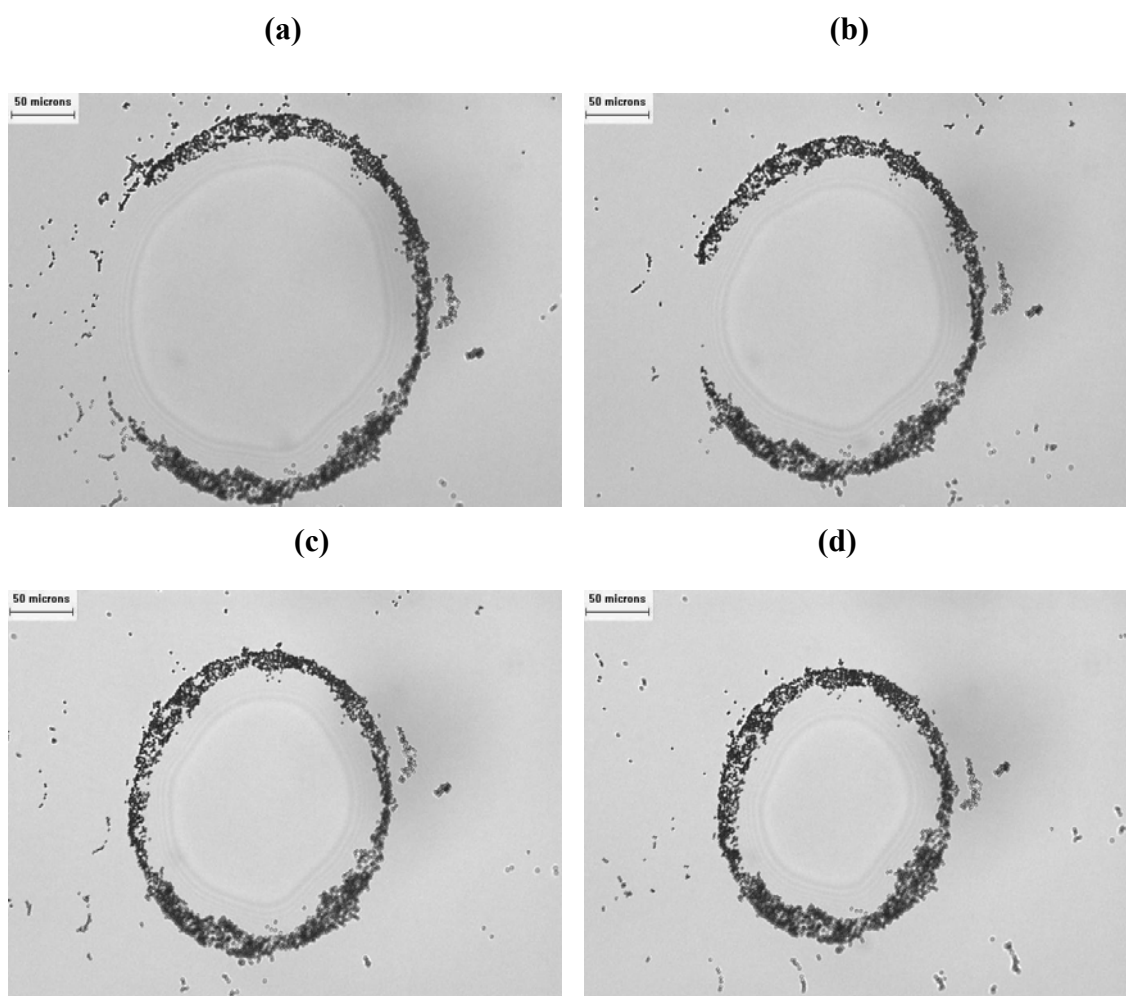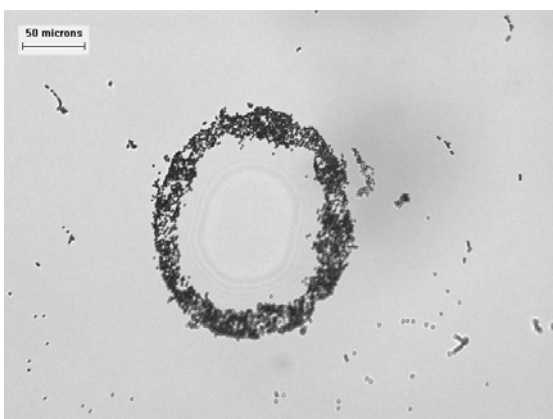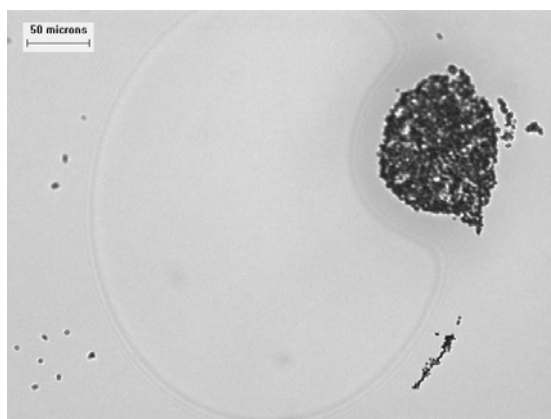
It can be concluded from these results that bridging of particles occurs only at a rapid opening of the foam films. At slow opening, the particles are dragged by the hydrodynamic flow out of the expanding film, due to large lateral mobility of the particles in the dilute monolayers at the foam film surfaces.[33] In the case of faster opening of the film, the particles attached to one of the film surfaces at the periphery of the expanding film move very rapidly in a lateral direction close to the opposite film surface. Such fast particle movement can create deformation of the fluid interface[34] which could be large enough to cause bridging of the film surfaces by some of the peripheral particles. This mechanism of particle bridging at fast opening of foam films as shown in Figure 5.8 is consistent with the results obtained by others.[35]

Figure 5.8 Bridging of water film surfaces by hydrophilic particles with a contact angle smaller than 90° during the film opening (a and b) and increase of the particle ring thickness during the film closing (c). The block arrow points to the deformation of the film surface caused by the fast lateral movement of a particle attached at the opposite film surface (a). This sketch was adapted from ref. 20.
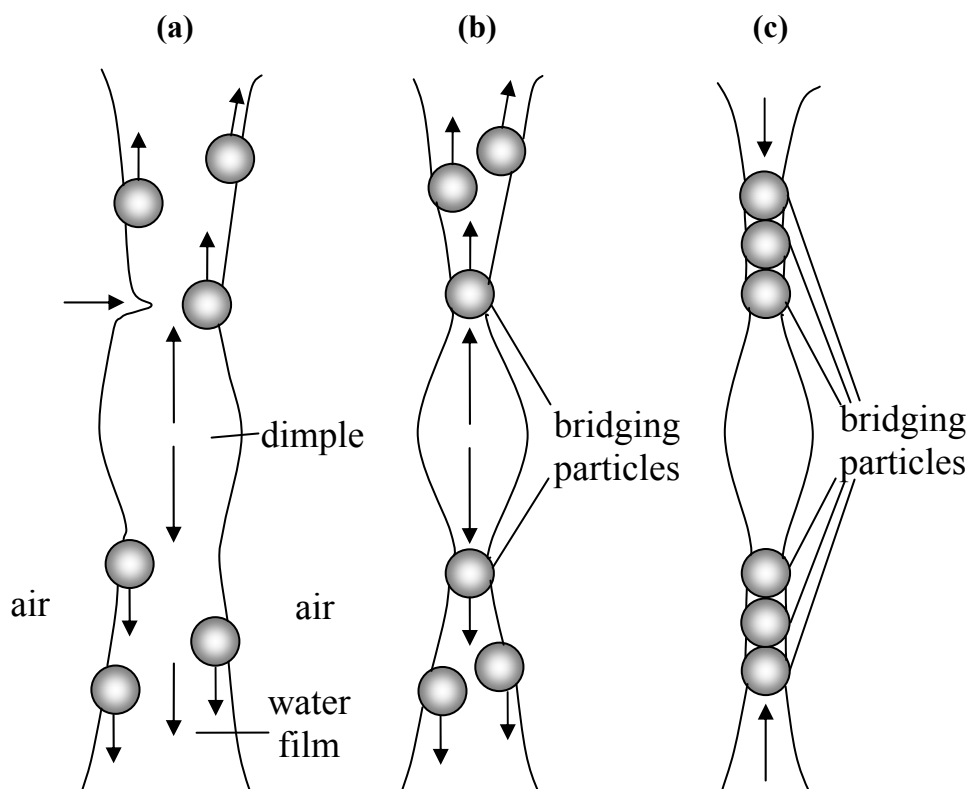
5.2.3   Films with close-packed particle monolayers at their surfaces

Films with close-packed particle monolayers at their surfaces behaved differently from those with dilute or concentrated monolayers. Water films did not contain a dimple. Instead, the films in the case of hydrophilic silica particles (contact angle smaller than 90°) were forced to thin until a spot consisting of a bilayer of sticking particles from the opposite film surfaces was formed (Figure 5.9). These films were very stable and suction of water out of the film meniscus caused a transition from bilayer to monolayer of particles bridging the opposite film surfaces in the centre of the film (Figures 5.10 and 5.11).

Figure 5.9 Formation of a water film with close-packed particles of contact angle ~ 50° measured on glass slides at the air-water interface. A diffraction pattern can be observed due to the bilayer structure of the particles in the film (transmitted light).
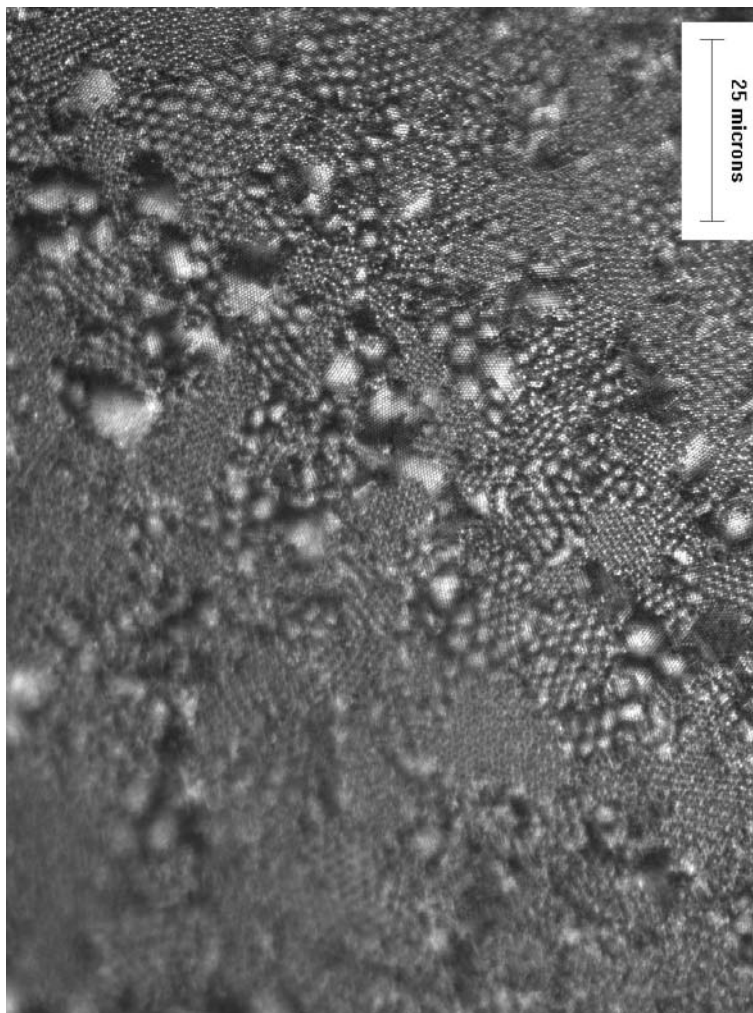
Figure 5.10 Formation of a water film with close-packed particles at their surfaces by sucking water from the film. The particle contact angle is ~ 65° measured through the aqueous phase on glass slides at the air-water interface. A diffraction pattern can be observed showing a bilayer of close-packed particles to monolayer transition (transmitted light). Below the image is the schematic representation of the monolayer and bilayer structure.
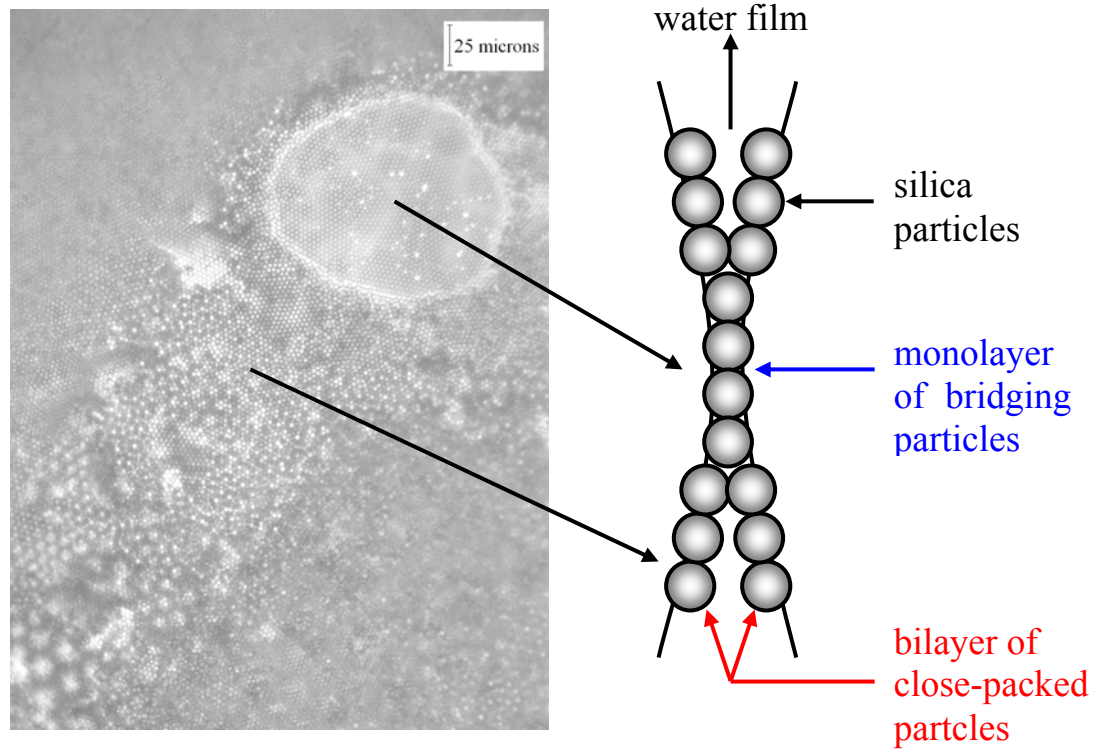
Figure 5.11 Picture showing a monolayer and bilayer at higher magnification. Well ordered hexagonal array of silica particles is observed in the monolayer region.
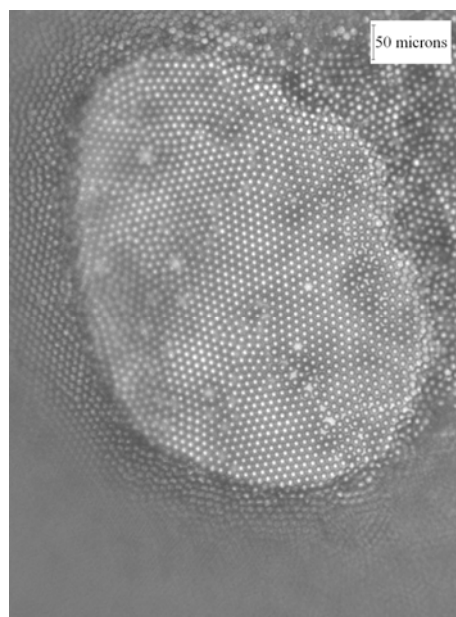
The bilayer structure with hexagonally close-packed silica particles found in these foam films strongly suggests that there is a bilayer of silica particles separated by the water film surrounding each bubble in the foams. This can also be confirmed with the images of Cryo-SEM shown in Chapter 4, where a bilayer of silica particles, which are hexagonally close-packed, was also observed in the foams formed. For foam stability the film covering the bubble must withstand vibrations set up in the system. Obviously the higher the rigidity of the film the more stable the foam will be. However, there still must be a degree of mobility within the film. The presence of a second layer of particles, the two layers being in positions of secondary minimum with each other, will enable there to be a degree of mobility both within the plane of the film and also across it. This also shows that short-range interaction forces are prevailing, which stabilises this very thin film. During film thinning areas of bare air-water interface uncovered by the particles was observed due to the attractive forces between particles as shown in Figure 5.12. These gaps will make the foam films unstable and more vulnerable to break. This is an important finding that can explain the destabilisation of foams with solid particles.

Figure 5.12 Representation of the monolayer and bilayer structure with a bare surface between both structures in the case of hydrophilic silica particles (with contact angle ~ 50° measured on glass slides).
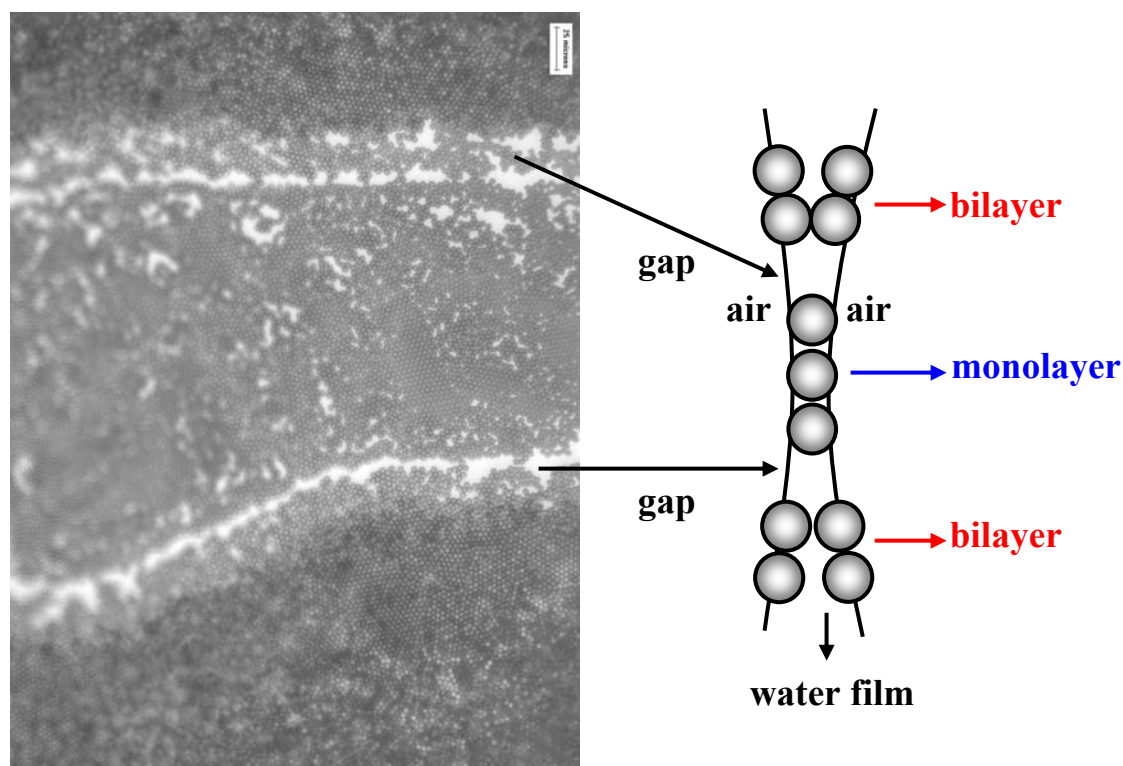
5.3 Hydrophobic silica particles ($\theta_{aw} > 90°$)

5.3.1 Films with dilute particle monolayers at their surfaces

In the case of silica particles with contact angle of 105°, well ordered monolayers at the air-water interface at large interparticle distances were observed (Figure 5.13 (a)). These foam films do not break during slow opening of the film (by sucking liquid out of the meniscus). However, by thinning the film, particles started to move away from the central thinnest region of the water film and no bridging of particles was observed (Figure 5.13 (b) and (c)). Therefore, the unprotected central part of the film becomes vulnerable to rupture. The film breaks almost immediately when the liquid is sucked out of the meniscus quickly. In this case some particles bridge the film surfaces and the film breaks which is in the agreement with the antifoam action of hydrophobic particles.[21,22] Therefore, stable foam films have not been observed when particles with contact angle of 105° were used. The films do not break during slow opening (no bridging of particles) but rupture at fast film opening when some of the particles bridge the film surfaces. In contrast to the hydrophilic particles, the hydrophobic ones give well ordered monolayers at large interparticle distances, which show that very long range repulsion between particles exists. This repulsion is strong and sufficient to oppose the gravity force acting on the particles at vertical fluid interfaces. It is mediated through the air and is mainly due to Coulomb repulsion between charges at the particle non-polar fluid interface. Water (which is a major component of the systems studied) might play a very significant role in charging of the particle surface in contact with the non-polar fluid (air).[20]

Figure 5.13 Foam films with ~ 1.40×10^5 silica particles cm^{-2} at their surfaces with contact angle 105°. (a) Particles well ordered at the centre of film, just before bridging of particles, (b) centre – the thinnest part of the film and (c) particles pushed further away by opening the previous film shown in (b) very slowly. The scale bar in the pictures is 50 µm.

(a)
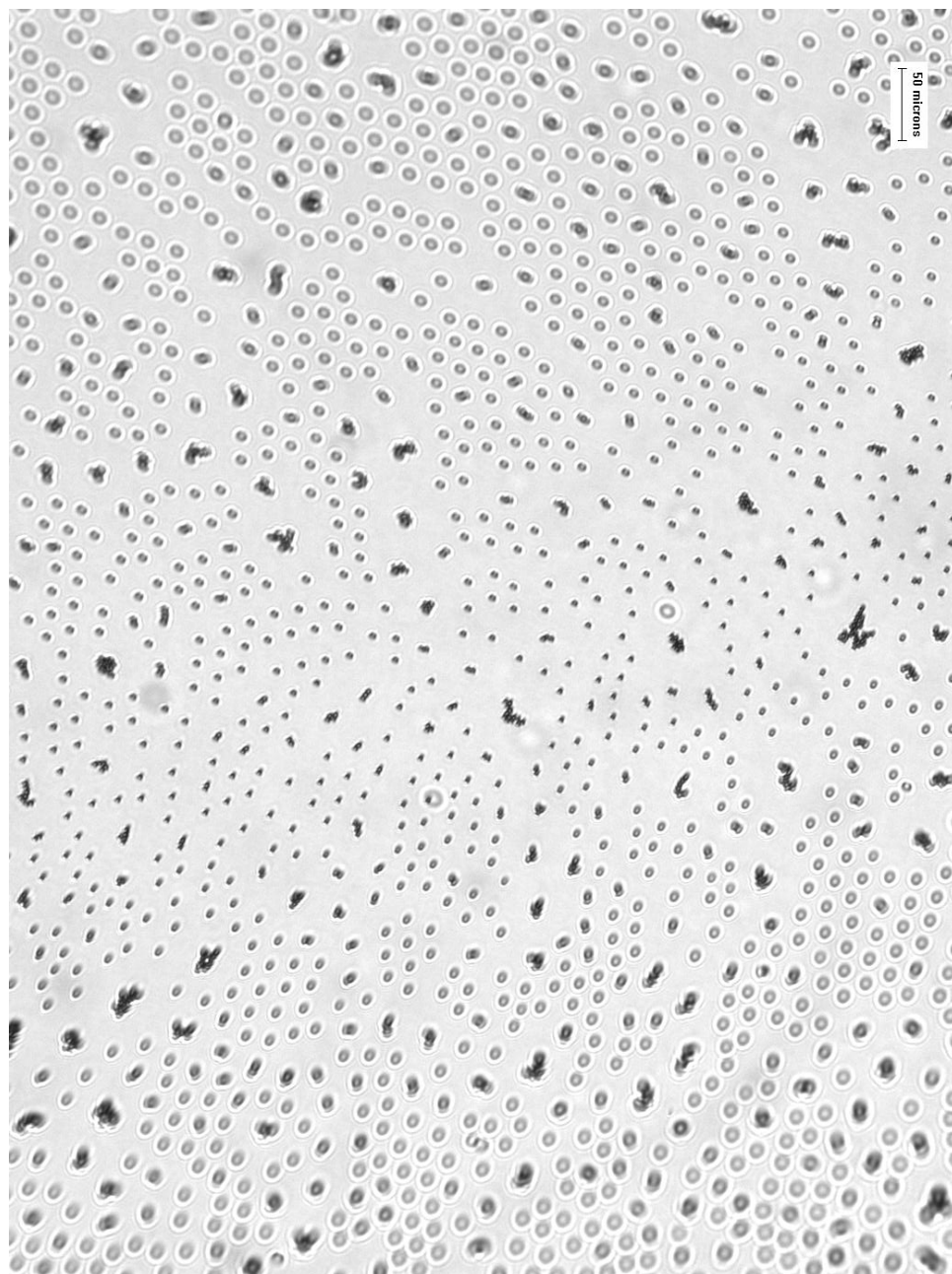
(b)
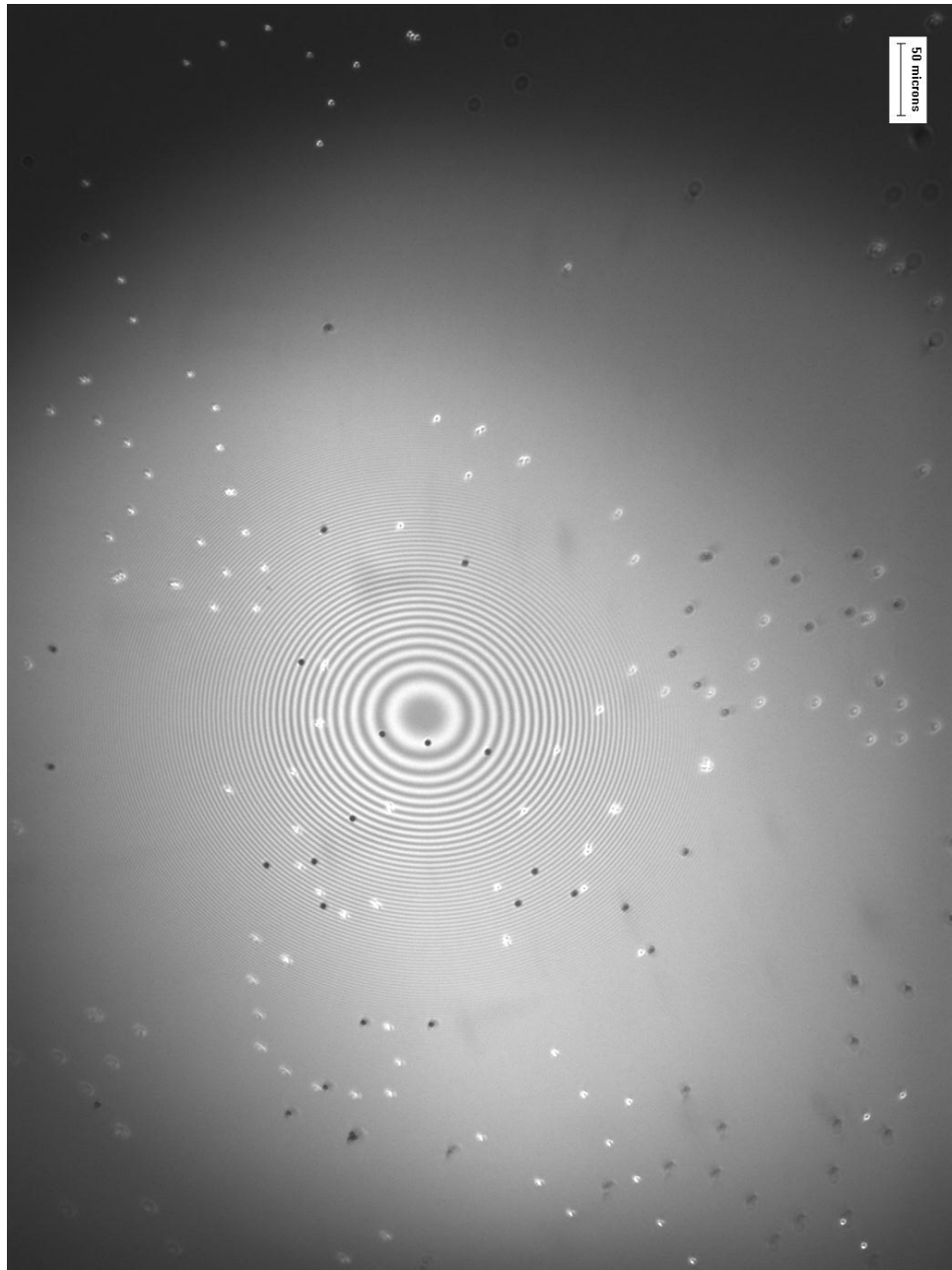
(c)
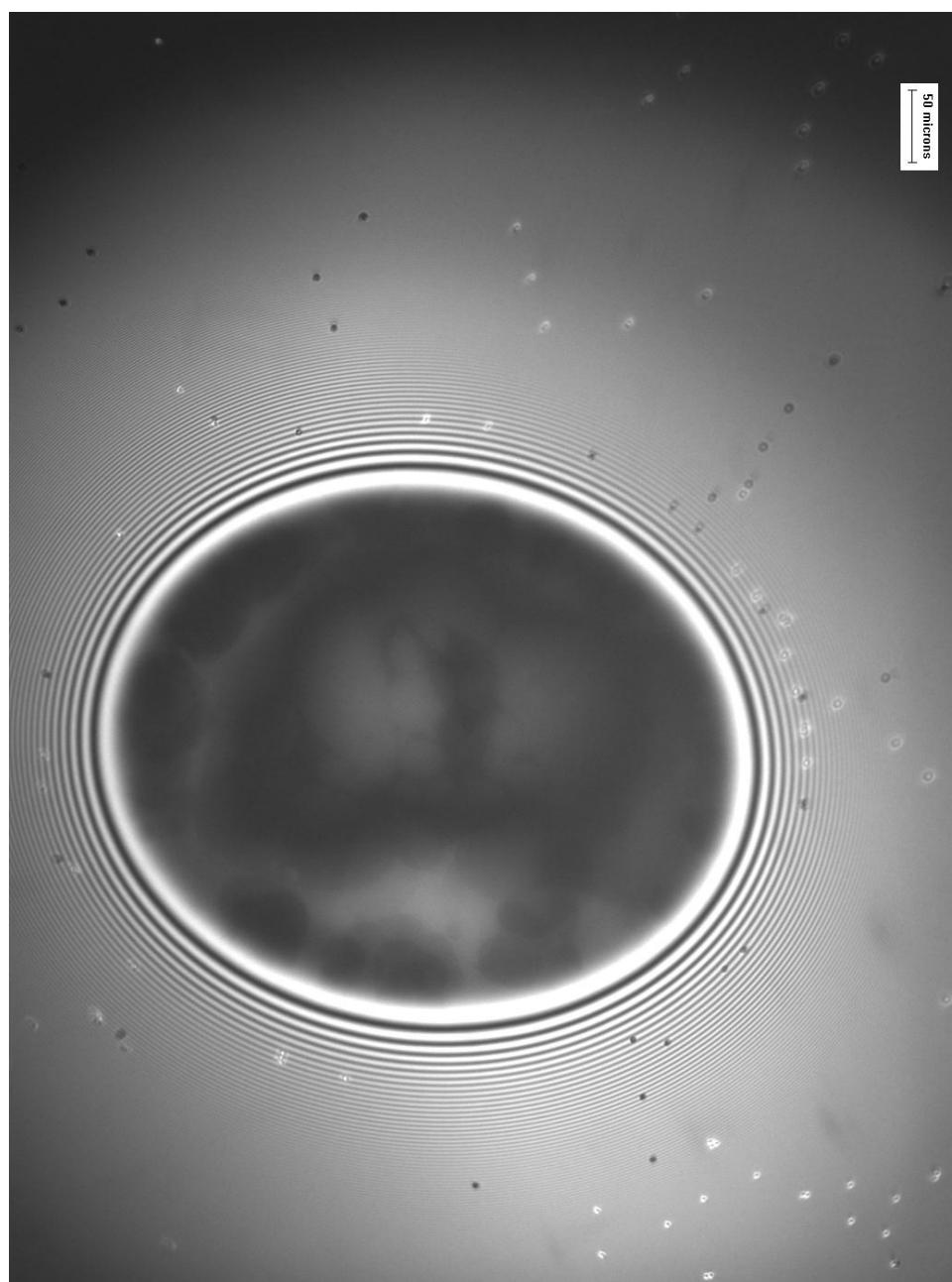
5.3.2 Films with dense particle monolayers at their surfaces

By increasing the volume of spreading suspension of silica particles, particles started to become ordered outside the film. Silica particles at distances larger than three particle diameters are seen (Figure 5.14). Such ordering of silica particles at air-water interface, suggests that there is not a principle difference in particle interactions at the air-water interfaces compared to oil-water interfaces reported before.[36] Obviously, there

is long range repulsion between particles preventing them from aggregation and keeping them apart in well ordered arrays.

Figure 5.14 Foam films with ~ 6 × 10^5 particles cm^{-2} at their surfaces with contact angle 105°. (a) centre of the film – the thinnest part of the film, (b) opening of the film slowly – particles are pushed further away but do not bridge the surfaces, (c) futher opening of the film. The scale bar is 50 μm.

(a)
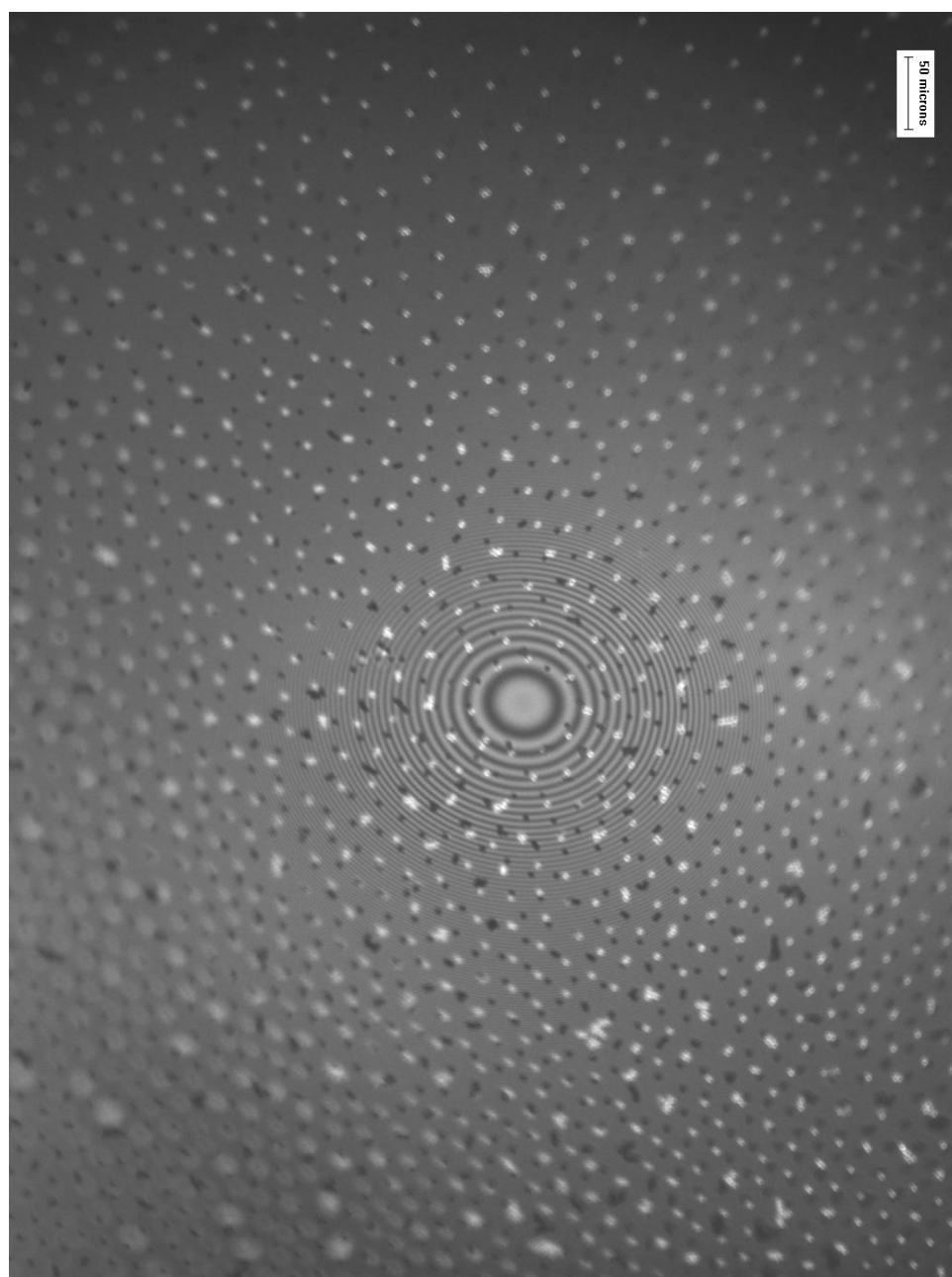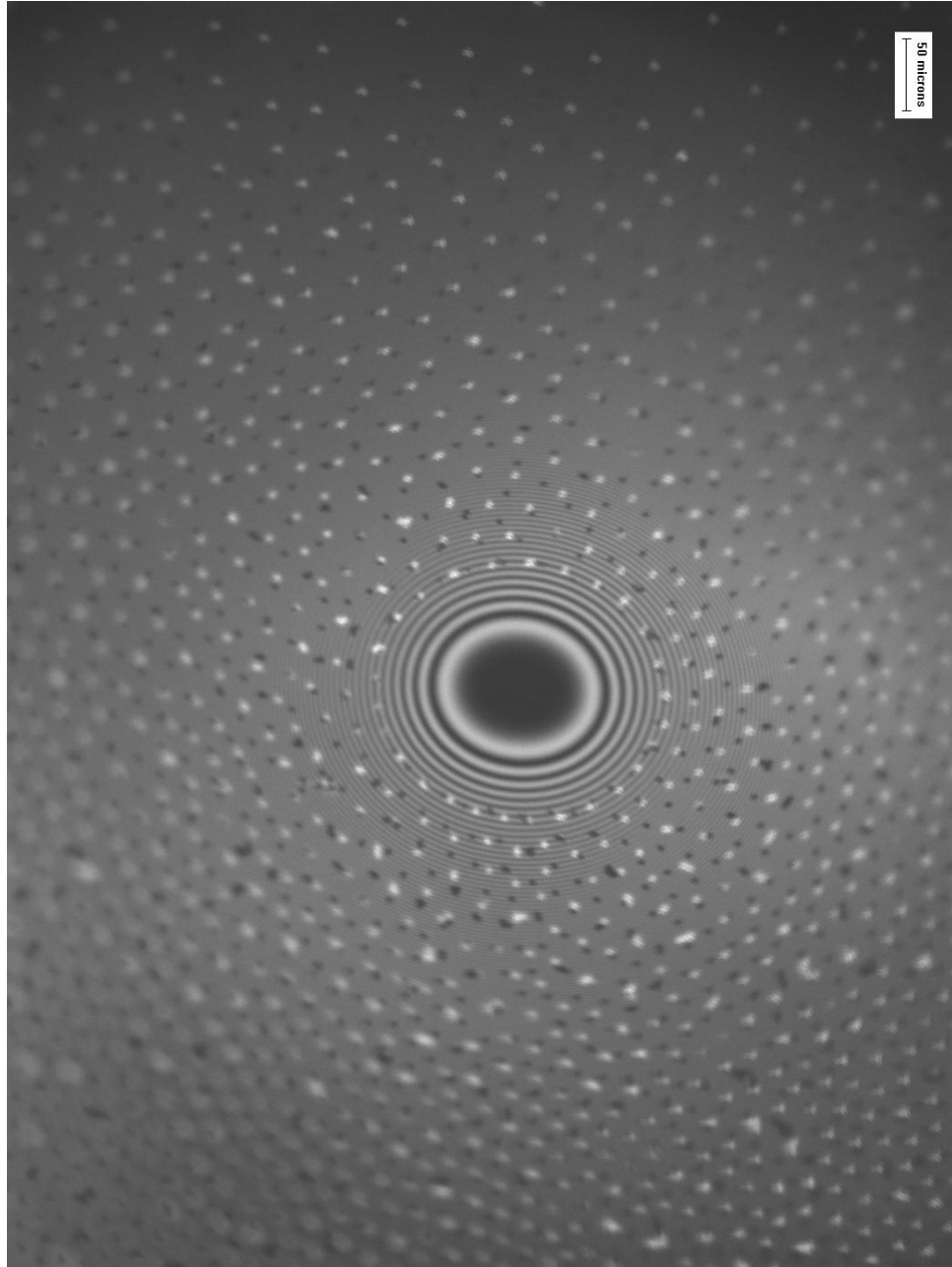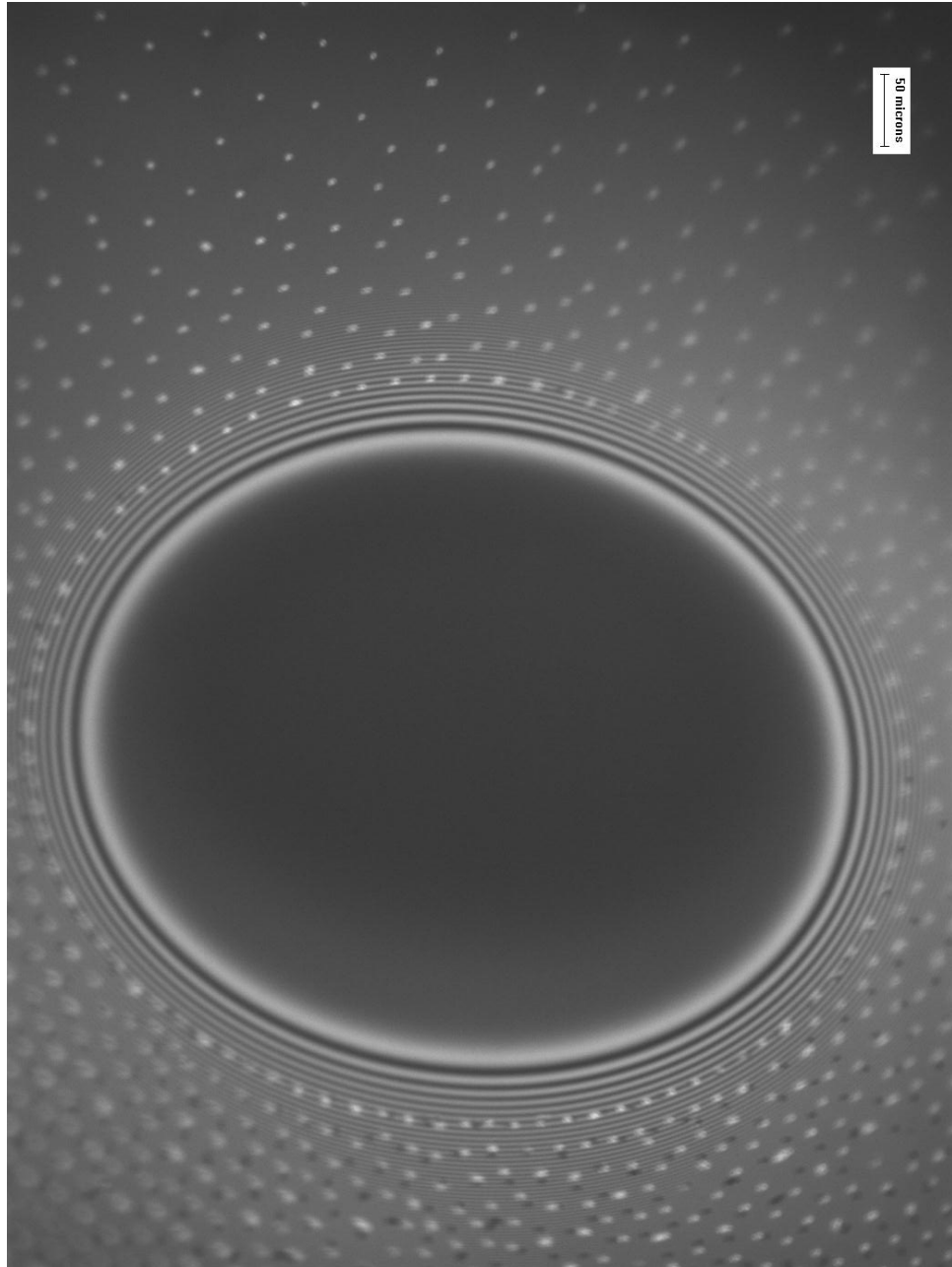
5.3.3   Films with close-packed particle monolayers at their surfaces

In the case of hydrophobic particles (contact angle greater than 90º), the formation of a bilayer structure was not observed which explains the fact that these films were more unstable than the ones formed with close-packed hydrophilic particles. It was observed the coexistence of two types of interactions between the hydrophobic particles in the film: close-packed and well ordered separated particles (see Figure 5.15). This means that there are also repulsive surface forces (well ordered separated particles) in addition to attractive van der Waals forces (close-packed particles). Such strong long-range particle repulsion is absent in the case of hydrophilic particles. By sucking more water from the film shown in Figure 5.15 gaps between the air – water surfaces appear and particles instead of breaking the foam films can bridge themselves. Eventually the film becomes unstable and bursts. Figure 5.16 shows the appearance of the film just before it breaks. These results show that it is not possible to obtain stable foam films with close-packed hydrophobic particles at their surfaces as suggested by Kaptay.[23] However, in real foams it was clearly observed in Chapter 4, that closely packed hydrophobic particles of contact angle around 105° were able to stabilise foams. One possible reason that explains the discrepancy between the results obtained here with the foam films and the real foam systems (in Chapter 4) is that experimentally it was very difficult to achieve a very close-packed particle configuration at the surface of the foam films with the hydrophobic particles. It was a very difficult process as small volume of particles was spread at the water surface each time and then the ring frame was immersed in the water surface and pulled back to the air. This was done several times until the foam films surfaces were densely covered with silica particles but not completely close-packed. In the case of real foam systems the bubbles coalescence and particles accommodate themselves at the surface of the bubbles in a more freely and spontaneous way.

Figure 5.15 Formation of a water film with close-packed and well separated silica particles with contact angle around 105° (measured through the aqueous phase on glass slides) at the air-water interface by sucking water from the film (reflected light).
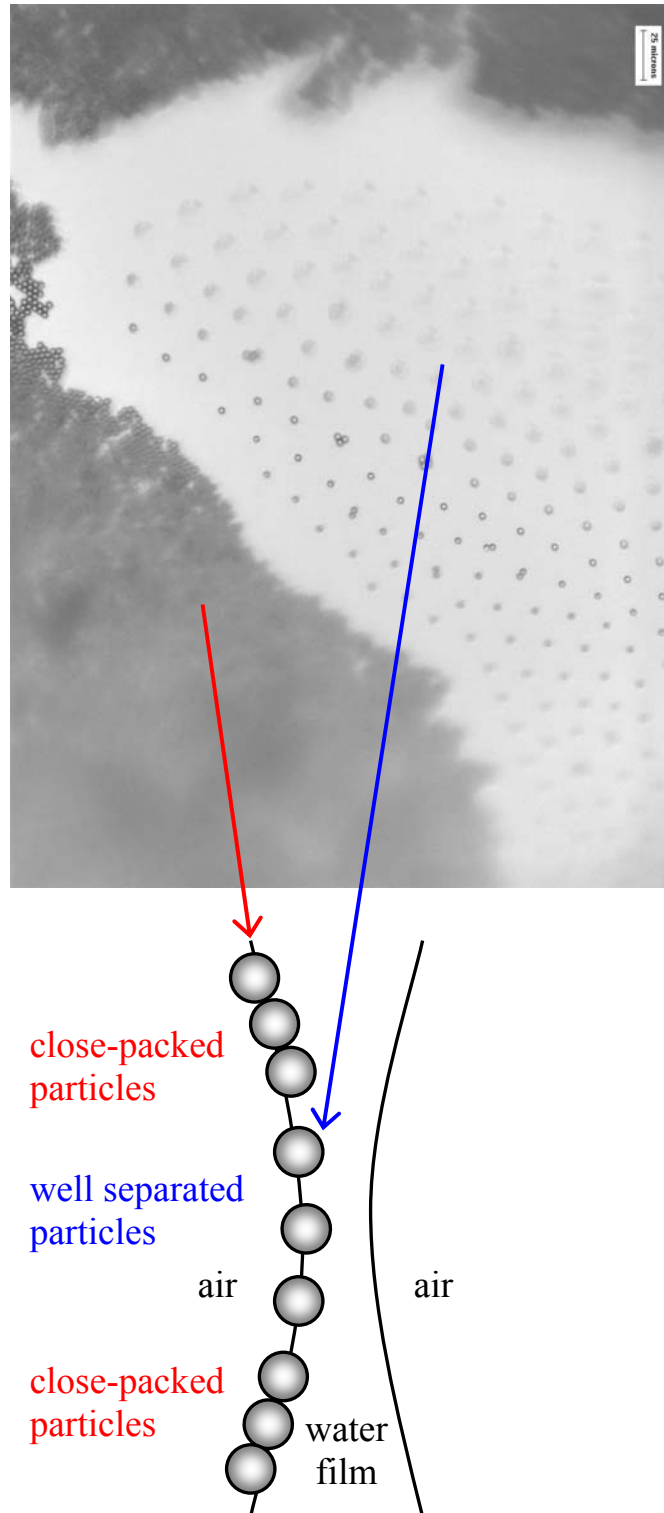
Figure 5.16 Appearance of the water film with close-packed particles with contact angle around 105° (measured through the aqueous phase on glass slides) at the air-water interface just before it breaks.

.
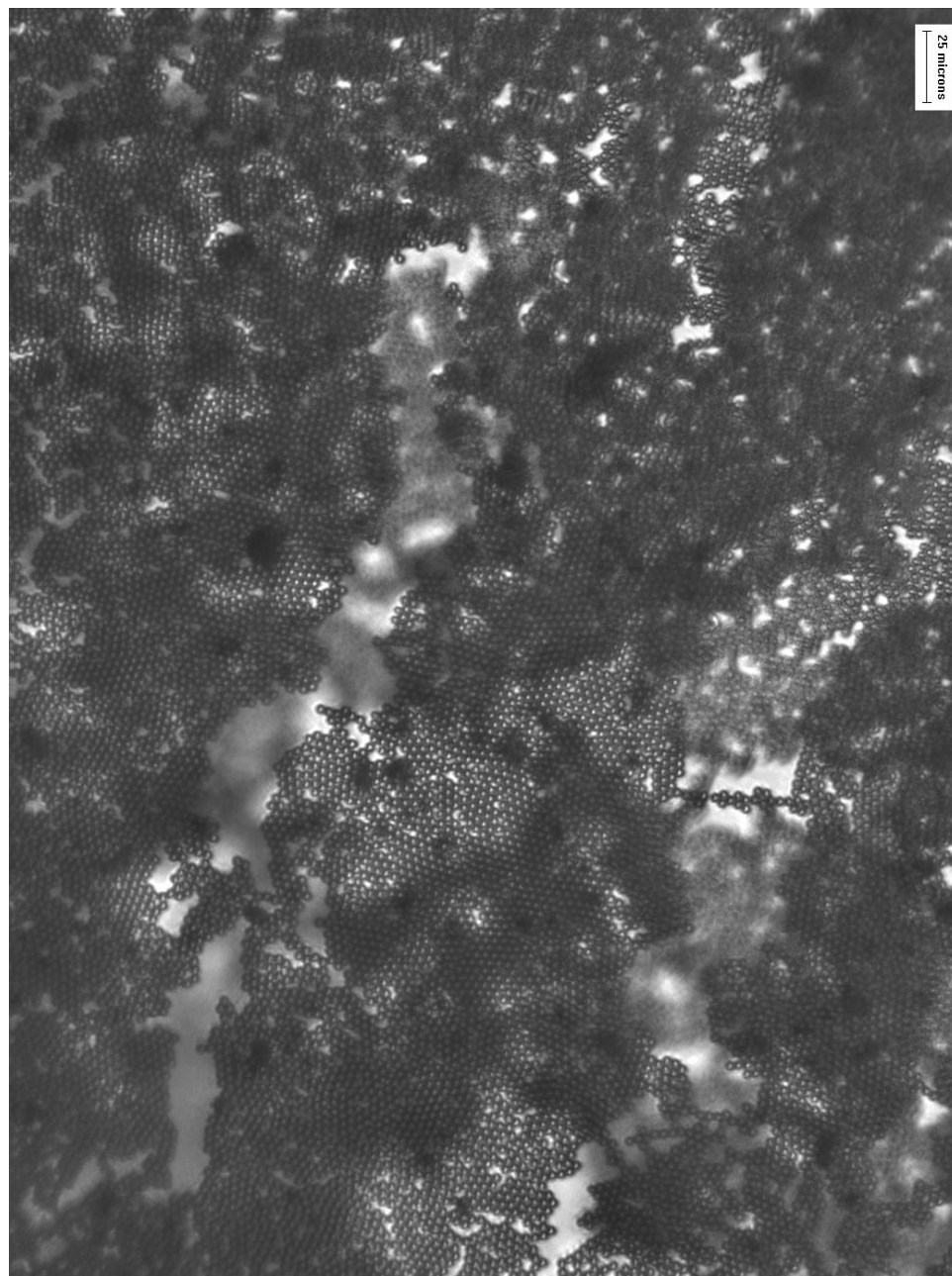
5.4   Conclusions

The behaviour and stability of thinning foam films with particles at their surfaces are of great interest in this research. Vertical foam films with particle monolayers at their surfaces have been studied. Such films are formed between colliding bubbles in particle stabilised foams; therefore the obtained results have an impact on better understanding of the mechanisms of foam stabilisation by solid particles. The structure and stability of foam films strongly depend on particle contact angle, interactions between particles from the same and the opposite monolayer, and monolayer density.

Stable films are observed only in those cases when the particle contact angle, θ, fulfils the condition for a stable particle bridge, that is, $\theta < 90°$ for foam films. These hydrophilic particles seem to possess high lateral mobility during film thinning which is crucial for their rearrangement at the air-water surface and subsequent stabilisation. That is why the hydrophilic particles are expelled out of the thinning foam film, forming eventually a ring of bridging particles at the film periphery. This happens in the case of foam films with dilute particle monolayer at their surfaces. However, in normal conditions, this means that dilute particle monolayer can not protect the bubbles in real foam systems. Only when close-packed particles are achieved, very stable foams films can be obtained. This can be confirmed with real foam systems, where very stable small bubbles are covered with close-packed silica particles as shown in Chapter 4. Closely packed layers of solid particles are known to prevent the coalescence of bubbles in foams.

The main conclusion in the case of foam films with hydrophobic particles at their surfaces is that by opening the film slowly particles start to move away from the thinnest part of film and do not bridge the surfaces. When the film is opened quickly, the film breaks immediately as some particles bridge the film surfaces. The hypothesis for stable foam films with close packed bilayers of hydrophobic particles is not supported with this study; probably because the films studied were not fully covered with close-packed particles. More experiments are needed in order to clarify the hypothesis.

References

1.   D. Exerowa and P.M. Kruglyakov, Foam and Foam Films: Theory, Experiment, Application, Elsevier, Amsterdan (1998).

2.   G. Yampolskaya and D. Platikanov, *Adv. Colloid Interface Sci.*, **128-130**, 159 (2006).

3.   B.V. Derjaguina and E. Obuchov, *Acta Physic. USSR*, **5**, Issue No.1, 1 (1936).

4.   B.V. Derjaguin and A.S. Titijevskaja, *Kolloidn. Zh,* **15**, 416 (1953).

5.   A. Scheludko, *Kolloidn. Zh*, **39**, 155 (1957).

6.   A.Scheludko and D. Exerowa, *Kolloidn. Zh,* **165**, 148 (1959).

7.   J. Lyklema, P.C Scholten and K.J. Mysels, *J. Phys. Chem.*, **69**, 116 (1965).

8.   N.D. Denkov, *Langmuir*, **15**, 3171 (1999).

9.   B.P. Binks, W.G. Cho and P.D.I. Fletcher, *Langmuir*, **13**, 71 (1997).

10.   I.B. Ivanov and D.S. Dimitrov in *Thin Liquid Films*, I.B Ivanov (ed.), Marcel Deckker, New York, chapter 7 (1998).

11.   O.D. Velev, G.N. Constantinides, D.G. Avraam, A.J. Payatakes and R.P. Borwankan, *J. Colloid Interface Sci.*, **175**, 68 (1995)

12.   K. Mysels and A.Jones, *J. Phys. Chem.*, **68**, 3441 (1964).

13.   V.Bergeron, Ph.D. Thesis, University of California, Berkley CA (1993).

14.   C. Stubenrauch and R. Von Klitzing, *J. Phys.: Condens. Matter*, **15**, 1197 (2003).

15.   V.Bergeron, *J. Phys.: Condens. Matter*, **11**, 215 (1999).

16.   K.S. Birdi, Handbook of Surface and Colloidal Chemistry, CRC Press, New York, Chapter 5 (2002).

17.   X.L. Chu, A.D. Nikolov and D.T. Wasan, *J. Chem. Phys.*, **103**, 6653 (1995).

18.   P.A Kralchevsky and A.D. Nikolov, *Chem. Phys. Lett.*, **240**, 385 (1995).

19.   P.R. Garret in *Defoaming: Theory and Industrial Applications*, P.R. Garret (ed.), Marcel Dekker, New York, Chapter 1 (1993).

20.   T.S. Horozov, R. Aveyard, J.H. Clint and B. Neumann, *Langmuir*, **21**, 2330 (2005).

21.   N.D. Denkov, I.B. Ivanov, P.A Kralchevsky and D.T. Wasan, *J. Colloid Interf. Sci.*, **150**, 589 (1992).

22.   G. Kaptay, *Colloids Surf. A: Physicochem. Eng. Aspects*, **230**, 67 (2003).

23.   G. Kaptay, *Colloids Surf. A: Physicochem. Eng. Aspects*, **282**, 387 (2006).

24. R. Aveyard, B.P. Binks, P.D.I. Fletcher and C.E Rutherford, *J. Dispersion Sci. Technol.,* **15**, 251 (1994).

25. R.J. Pugh, *Adv. Colloid Interface Sci.*, **64**, 67 (1996).

26. N.D. Denkov, *Langmuir*, **20**, 9463 (2004).

27. D. Weaire and S. Hutzler, The physics of foams, Oxford, New York (1999).

28. D. Exerowa, N.V. Churaev, T. Kolarov, N.E. Esipova, N. Panchev and Z.M. Zorin, *Adv. Colloid Interf. Sci*., **104**, 1 (2003).

29. K.G. Marinova, R.G. Alargova, N.D. Denkov, O.D. Velev, D.N. Petsev, I.B. Ivanov and R.P. Borwankar, *Langmuir*, **12**, 2045 (1996).

30. P.A Kralchevsky and K. Nagayama, Particles at Fluid Interfaces and Membranes, Elsevier Science, Amsterdam (2001).

31. P.A Kralchevsky and K .Nagayama, *Adv. Colloid Interf. Sci*., **85**, 145 (2000).

32. P.A Kralchevsky and N.D. Denkov, *Curr. Opin. Colloid Interf. Sci.*, **6**, 383 (2001).

33. T.S. Horozov and B.P. Binks, *Colloids Surf. A: Physicochem. Eng. Aspects*, **267**, 64 (2005).

34. K.D. Danov, R. Aust, F. Durst and U. Lange, *Chem. Eng. Sci*, **50**, 263 (1995).

35. K.P. Velikov, F. Durst and O.D. Velev, *Langmuir*, **14**, 1148 (1998).

36. T.S. Horozov, R. Aveyard, J.H. Clint and B.P. Binks, *Langmuir*, **19**, 2822 (2003).

CHAPTER 6

CHAPTER 6

NOVEL METHOD FOR MEASURING CONTACT ANGLES OF SMALL SOLID PARTICLES

6.1   Introduction

The three-phase contact angle of small solid particles adsorbed at the air-water interface is directly related to the particle hydrophobicity (wettability). Its knowledge is of great practical importance for particle-stabilised foams. We have seen in previous Chapters 4 and 5 the importance of particle hydrophobicity for the foaming ability and stability of aqueous foams and foam films. It has been assumed that the particle contact angle is the same as that of a flat smooth glass plate chemically modified at the same conditions as solid particles. However, the contact angle of individual particles could be different from that on the flat macroscopic solid because the surface roughness and composition could never be the same. Therefore, to have a direct method for measuring the contact angle of solid colloidal particles attached to air-water interfaces is important for predicting the foaming or antifoam action of solid particles[1,2] and the type and properties of particle-water-air composite materials.[3]

Several experimental methods for measuring the three-phase contact angle of individual solid particles have been developed.[4-10] However, most of those methods involve sophisticated instruments or complex calculations which makes them difficult to use. The colloidal probe techinique[4] utilises atomic force microscopy (AFM) for measuring the interaction between single micron–sized particles at the air–water interface. The contact angle of single microspheres is determined from the force versus distance profiles. One inconvenience of this method is that the particle must be glued at the cantilever of the atomic force instrument in advance, thus restricting the method to micrometer size particles and making the collection of sufficient data for statistical evaluation of the contact angle very difficult. The "Film trapping technique"[5-7] also allows the contact angle of micrometer sized particles at the air-water interface to be determined. In this technique a micron-sized spherical solid particle is entrapped within a liquid film of equilibrium thickness smaller than the particle diameter. The profile of the deformed film surfaces around the particle is reconstructed from the interface pattern obtained in reflected light by solving the Laplace equation of capillarity. The

contact angle is obtained from the intersection of the extrapolated profile with the particle surface. This involves numerical solutions of the Laplace equation and makes the technique sensitive to errors in the film thickness. The direct measurement of contact angle by taking a side image of the particle attached to the liquid interface is a much simpler technique[8], but due to the restricted spatial resolution of the optical microscope it is not suitable for particles smaller than several micrometres. The "Gel trapping technique" (GTT) has been introduced recently as an extension of the particle side imaging method by means of electron microscopy.[9,10] In this technique particles of interest are spread on the air (oil) – water interface at approximately 50°C. The aqueous phase contains several wt. % of a gelling agent (gelan). After cooling to room temperature the aqueous phase gels and the particles are trapped at the gel-air (oil) interface. Then particles are incorporated in a polymer matrix from the side of the air (oil) by means of a photopolymerisable oil. The adherent gel is then removed and images of the particles incorporated in the polymer matrix are taken by a scanning electron microscope (SEM). The SEM imaging of the particle position on the polymer surface provides information on the particle contact angles at the water-air (oil) interface with much higher resolution than the optical microscope. The great advantage of this technique is that particles of submicron size or non-spherical shape can be studied. However, it is an indirect method of measurement. The effects of the gelling agent itself, gelling procedure, fabrication of the polymer matrix and the significant temperature change on the particle contact angle measured are not clear and could compromise the results.

In summary, the existing methods for measuring the contact angle of individual solid particles at fluid interfaces have limitations. There is not a simple and reliable method for measuring the contact angle of submicron particles in their real environment, which is a challenging problem. Here, a novel experimental method for measuring the particle contact angle at the air-water interface in real time without adding any additional components (*e.g.* gelling agents) to the aqueous phase is described and its applicability to micrometer latex and silica particles is demonstrated.

6.2   Measuring principle

The method is based on the fact that particles can bridge the surfaces of free standing thin liquid films (i.e. to attach simultaneously to both surfaces) and adjust their position with respect to the film thickness in order to minimise the deformation of the fluid interfaces. The experimental set-up (Figure 6.1) is rather simple and similar to that used for studying emulsions (ref.11) and foam films with particles at their surfaces (Chapter 5). Particles are spread at a horizontal water – air interface and the very dilute particle monolayer ($\sim$ 300 particles per mm^2) is crossed with a glass circular frame. The thick vertical foam film with particles attached to its surfaces is forced to thin by sucking liquid out of the meniscus using a syringe. As a result some particles bridge both film surfaces and go in the meniscus where they attain their equilibrium position forming an arc away from the thinnest part of film (Figure 6.2). The film is observed by a horizontal microscope in reflected monochromatic light. Images are captured by a 12-bit digital camera (QUICAM FAAT1394, Qimaging) and are stored and processed by a PC with Image Pro Plus software. The film thickness (h) is determined from the interference fringes by optical interferometry and thus knowing the radius R of a spherical particle, the contact angle can be calculated by a simple formula (see below).

Figure 6.1   Sketch (a) and photographs (b) and (c) of the experimental set-up.

(a)

(b)

cover

cuvette

glass ring

water

attached to a
syringe as shown
in (c)

objective

microscope stage

(c)

syringe

filled with water

245
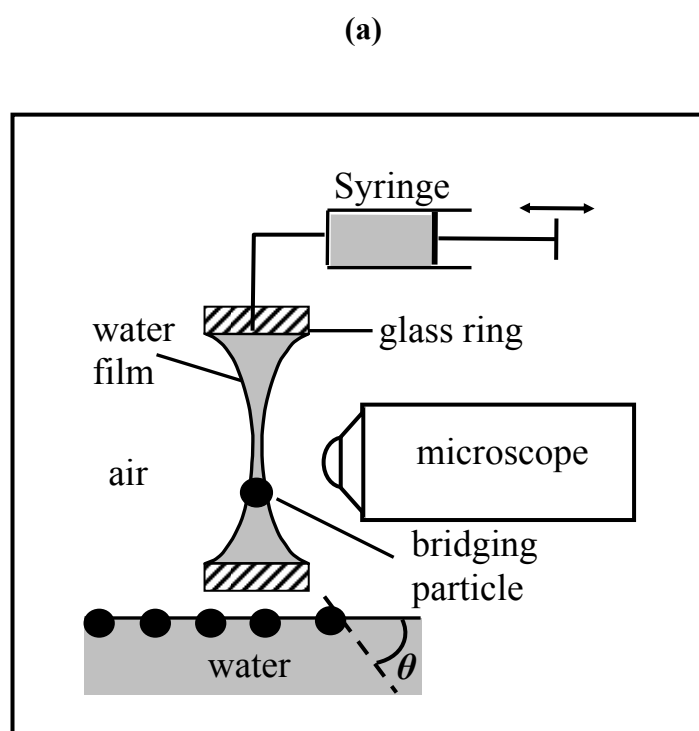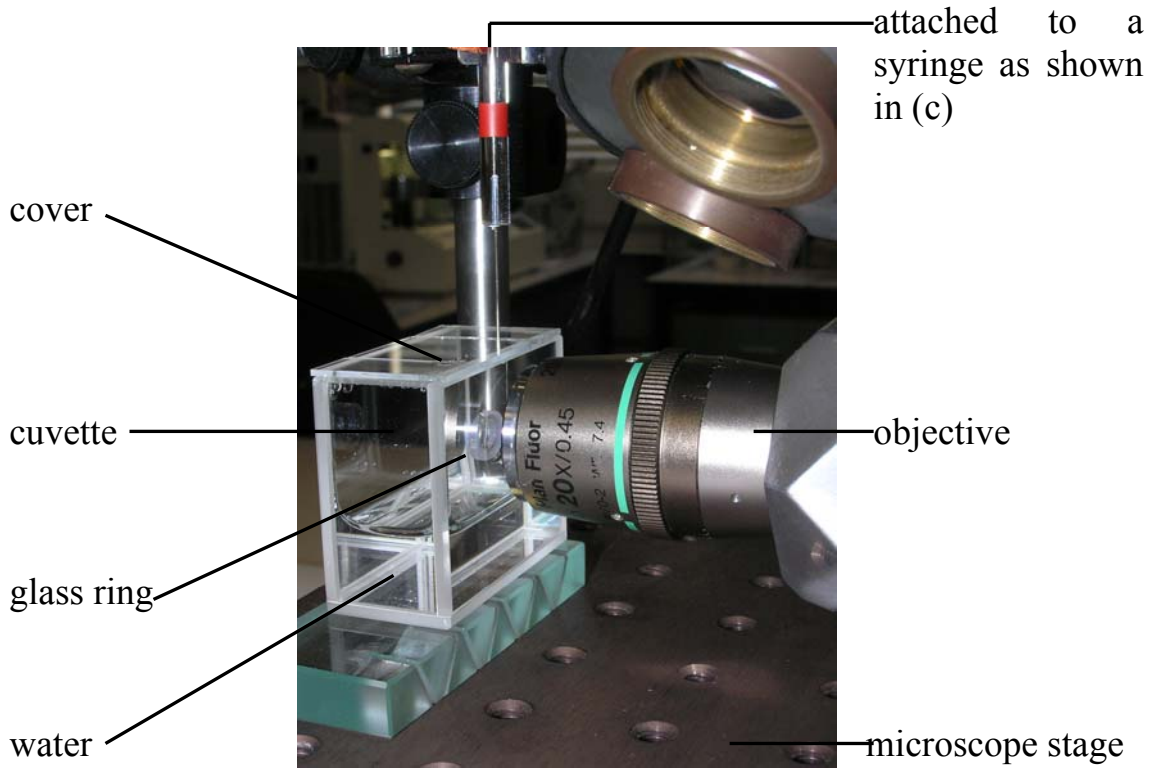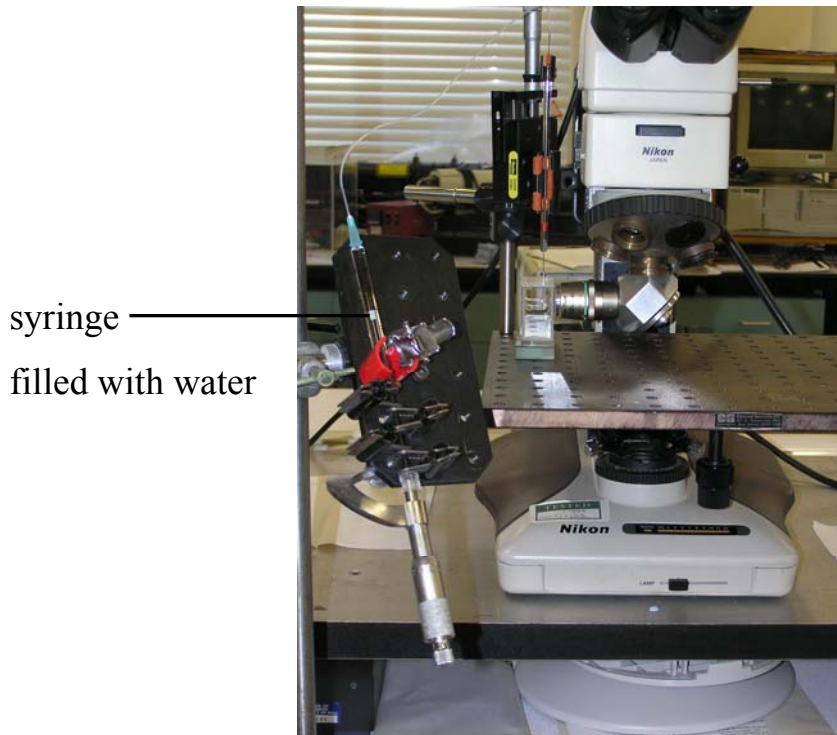
Figure 6.2 (a) Image of a water film in air with bridging silica particles (3 μm) at their surfaces taken in reflected monochromatic light. The line between the film centre O and point M in the meniscus is selected to pass through one of the particles (P₁). The film is not perfectly circular due to the hydrostatic pressure variation with height caused by gravity. (b) Sketch of the film cross section.
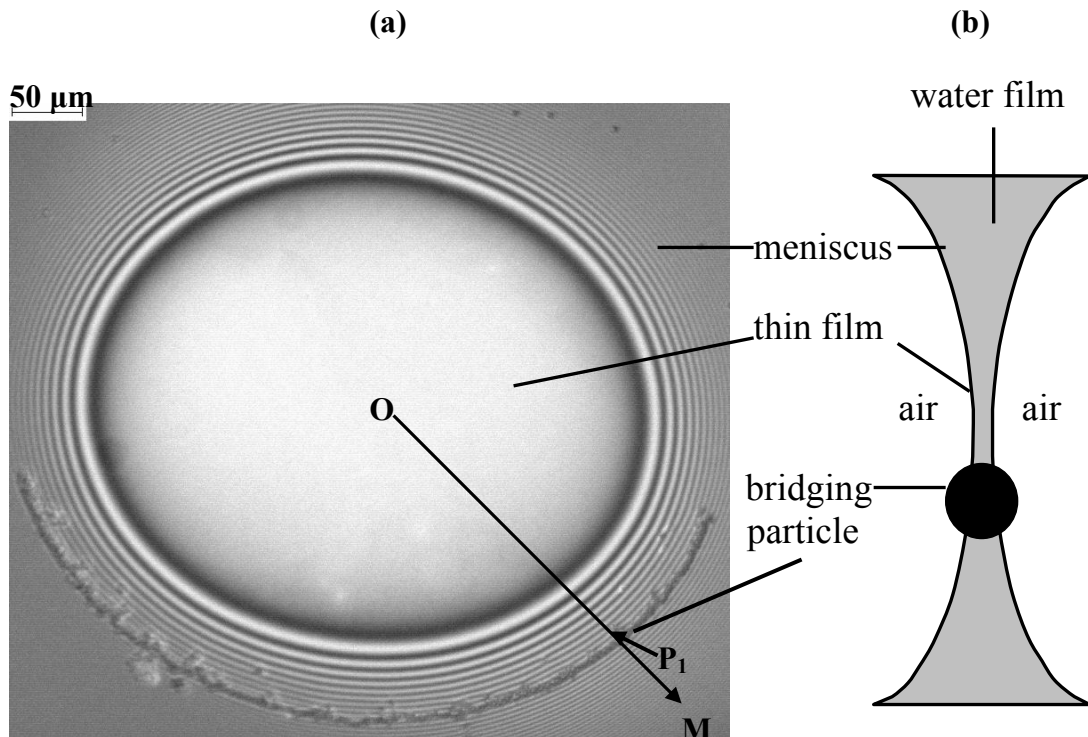
6.2.1   *Determination of the film thickness in the meniscus*

Optical Interferometry is used for measuring the film thickness in the meniscus. Figure 6.3 shows that when a plane parallel water film (thickness h, refractive index n = 1.33) in air (refractive index n = 1) is observed in a mono-chromatic reflected light, the light rays reflected from both film surfaces interfere. The overall intensity of reflected light depends on the phase difference between the reflected rays 1 and 2 as shown in Figure 6.3. The latter depends on the film thickness.

Figure 6.3   Interference in light reflected from a thin film due to a combination of rays reflected from the upper and lower surfaces. h represents the thickness of the film and n the refractive index.
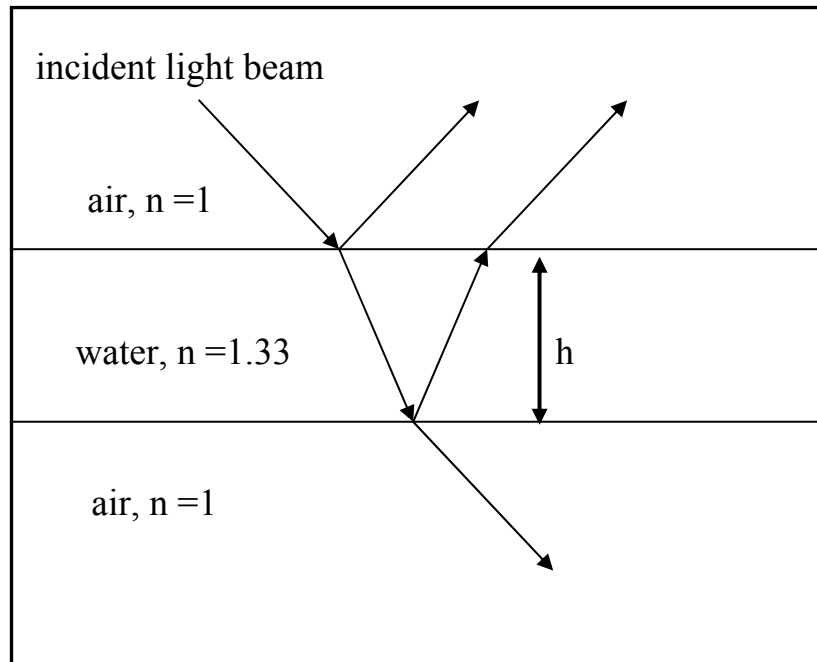
If the light rays in air are nearly normal to the surface then maxima and minima of the light intensity are observed due to constructive and destructive interference, respectively. The film thickness (h) corresponding to the light intensity maxima or minima are given by equations 1 and 2:

$$h = \left(m + \tfrac{1}{2}\right)\lambda / 2n \tag{1}$$

$$h = m\lambda / 2n \tag{2}$$

where m = 0, 1, 2, 3, …is the so-called order of interference. When light reflects from an interface between two media (*e.g.* air-water) there may also be a phase shift. If light travels from a lower index of refraction (*e.g.* air) to a higher index of refraction (*e.g.* water), the reflected light will experience a 180° or λ/2 shift (reflected ray 1). If the light travels from a higher index material (*e.g.* water) to a lower index material (*e.g.* air), however, there is no phase change (reflected ray 2).[12]

When a water film in air is observed in reflected monochromatic light, the characteristic interference pattern of dark and bright fringes in the meniscus can be detected (as shown in Figure 6.2). Bright fringes appear due to constructive interference (in phase light) and dark fringes appear due to destructive interference (counter phase light). The interference pattern shown in Figure 6.2 is then analysed by Image Pro Plus software. The light intensity profiles along the line OM connecting the film centre O (the thinnest part) and point M in the thicker meniscus region is obtained (Figure 6.4). It consists of alternating intensity minima and maxima, which correspond to the dark and bright fringes, respectively. The bridging particle (P_1) was previously marked with a black dot on the image before obtaining the light intensity profile. Therefore its position is well seen in Figure 6.4 and corresponds to the sharp drop in intensity.

Knowing the light wavelength, $\lambda = 546$ nm (Hg-lamp) and the refractive index of the water film, n = 1.33, the film thickness, h, at the maxima and minima light intensity points is calculated by using equations (1) and (2). The first interference minima (dark fringe) has an order of interference m = 1, because when the film was forced to thin by sucking water out of the meniscus, the light intensity at the film centre passed through a maximum (m = 0, h = 102 nm from equation (1)), then the film broke. This can be confirmed by equation (2) which shows that the dark fringe with m = 0 corresponds to a zero film thickness (film rupture). Therefore, the foam film became unstable and broke when its thickness was smaller than $\sim$ 100 nm and this is in agreement with the literature data.[13] By using equations (1) and (2) and starting with m = 1 the film thickness was calculated at the interference minima and maxima, respectively. The film thickness at the interference minima and maxima obtained from the light intensity profile along the line OM (Figure 6.4) are plotted in Figure 6.5 versus the radial distance.

Figure 6.4 Light intensity profile in grey scale units (*g.s.u*) showing the interference maxima (unfilled diamonds) and minima (filled diamonds) obtained from figure 6.2 (a) versus radial distance measured from the film centre (O) to point M passing through one of the bridging particles P_1.
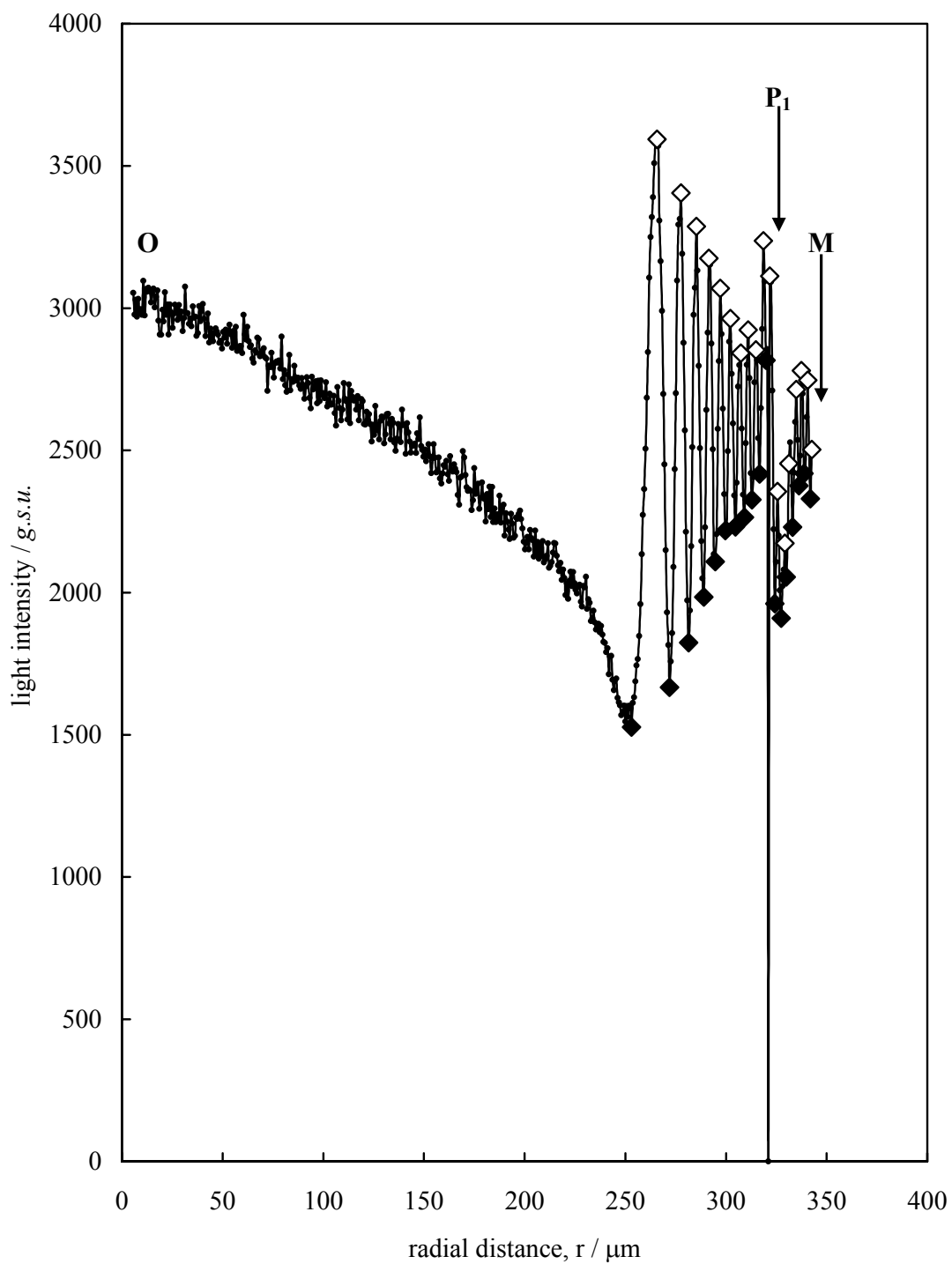
Figure 6.5 Film thickness of the meniscus calculated by equations (1) and (2) for the interference maxima (unfilled diamonds) and minima (filled diamonds) as shown in the light intensity profile along the film centre (O) and point M in Figure 6.4. The red circle corresponds to the film thickness at the location of the particle (P$_1$).
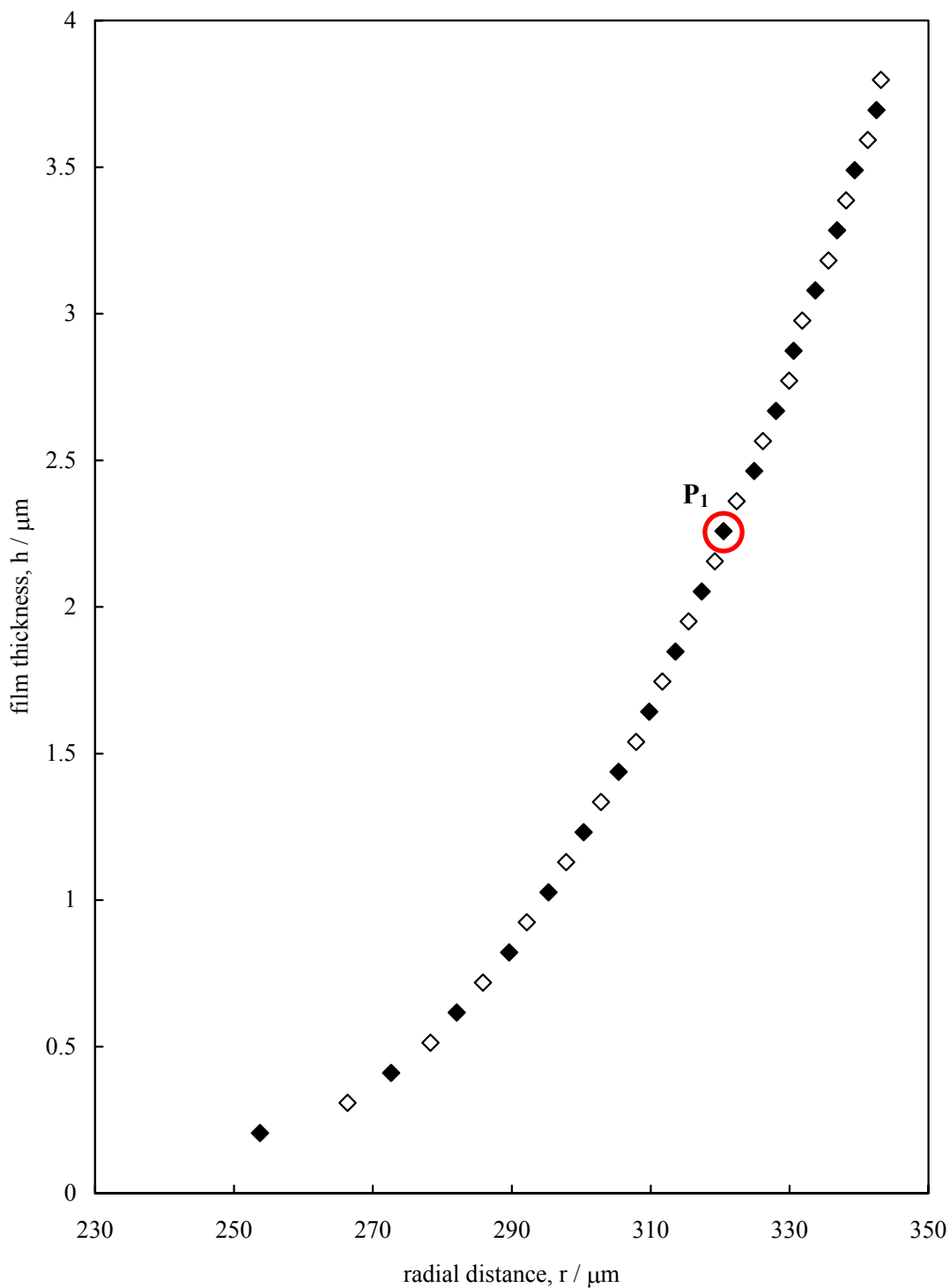
In order to determine the particle contact angle, the thickness profile of the film meniscus is determined firstly, by the interferometric technique as discussed above. The film thickness where the particle is located ($\sim$ 2.3 μm) as shown in Figure 6.5 is smaller than its diameter (3 μm), thus confirming that the particle protrudes the film surfaces. Pumping water into the meniscus causes the film area to shrink and the bridging particles move closer to the film centre (Figure 6.6). Nevertheless, the particles remain at the same film thickness during their movement (see Figures 6.7). This particle behaviour can be understood, if we consider the film profile around a particle bridging the surfaces of a liquid film with variable thickness (see Figure 6.8).

Figure 6.6   Consecutive images taken during the shrinking of a foam thin film with bridging silica particles by pumping water inside the film meniscus. The arrow points towards one of the particles at a distance *r* from the film centre. The silica particles with diameter of 3 μm were partially hydrophobised with 1×10^{-4} M HMDS. Black dots were marked on the images so that the light intensity profile could be obtained for individual particles at a particular position in the foam film.

(a)

251
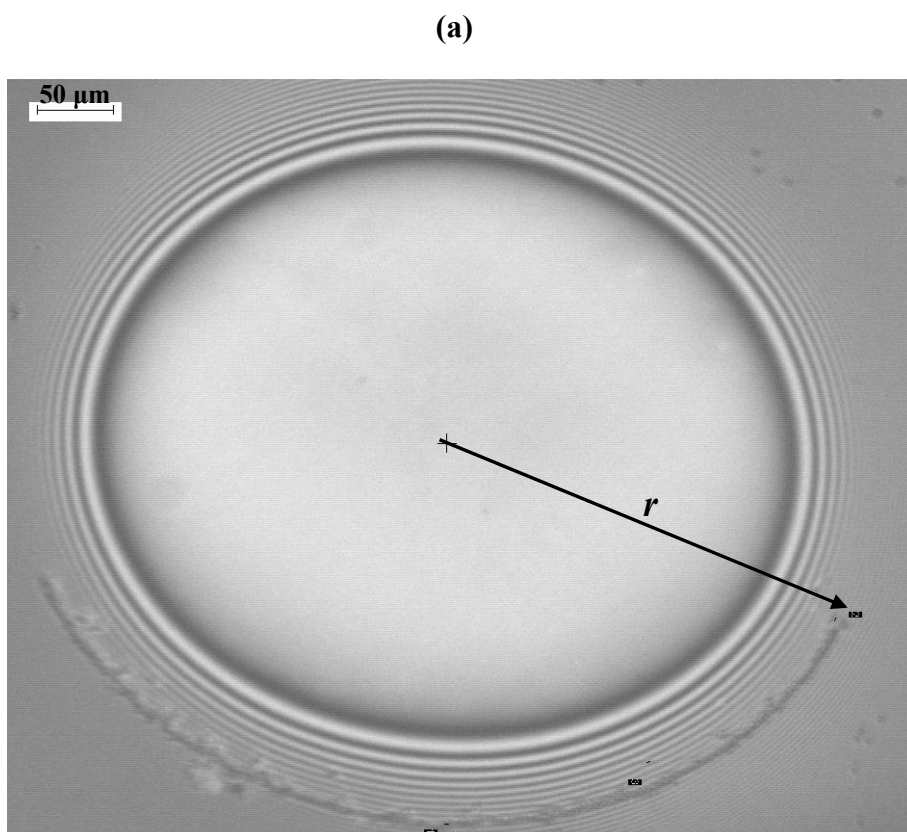
(b)
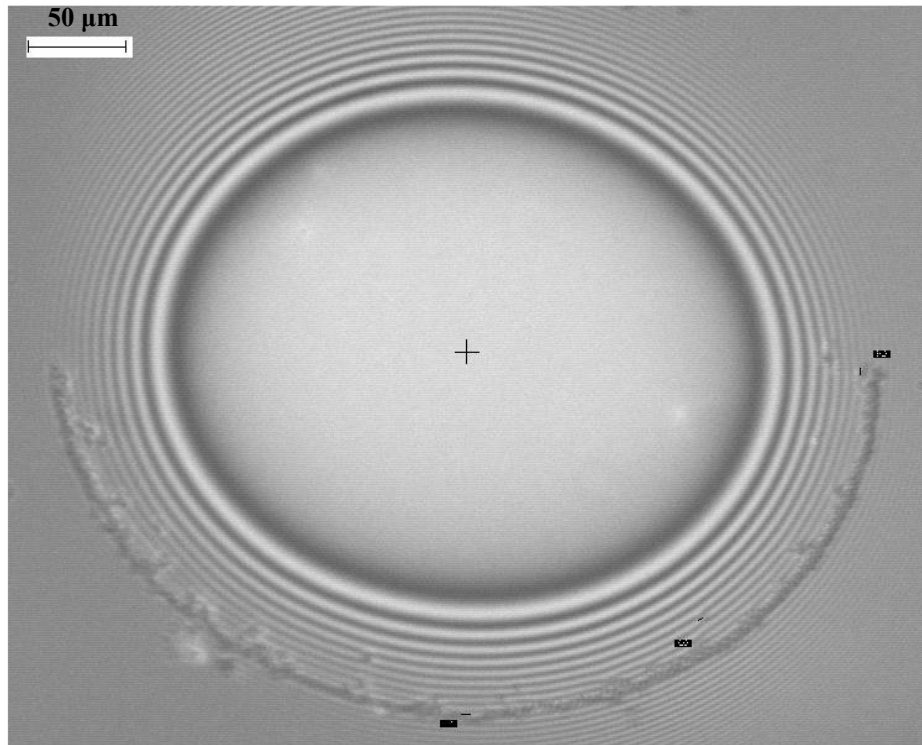
(c)

Figure 6.7 Film thickness, h_e, at the location of one bridging particle of diameter 3 μm taken from Figure 6.6 versus radial distance from the film centre during the shrinking of the film by pumping water into the meniscus. The dashed line shows the average $h_e = 2.28 \pm 0.05$ μm.
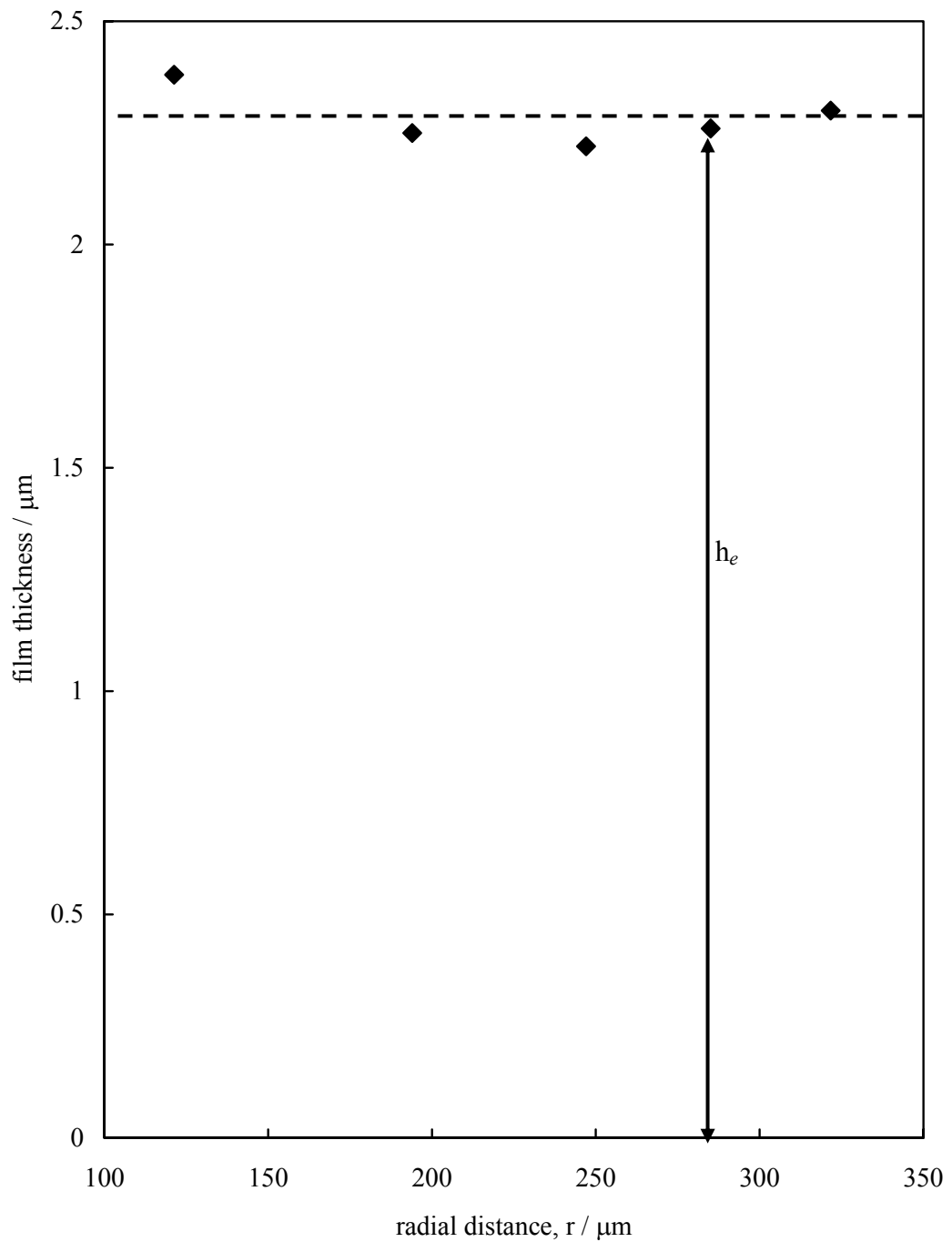
Figure 6.8 Sketch of a bridging particle in a liquid film with variable thickness and the expected increase of the surface free energy, ΔE, due to deformations of the film surfaces if the particle moves in thinner (left) or thicker (right) film regions (taken from ref.14).
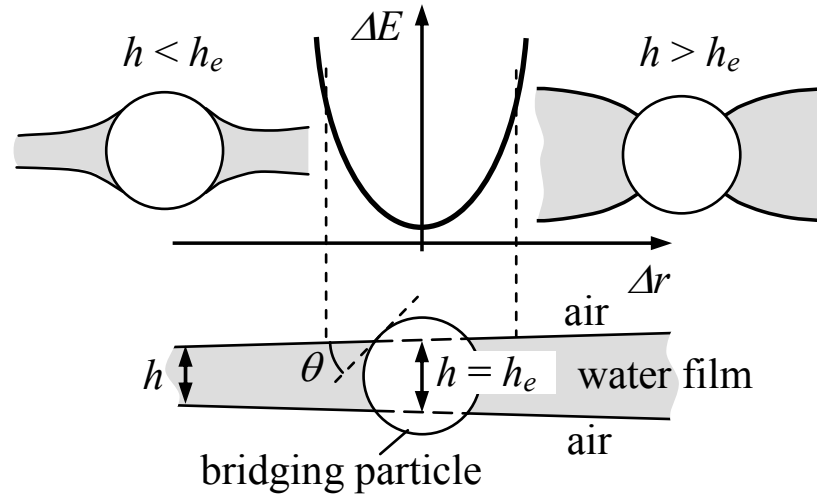
At a given particle diameter, d, and contact angle, θ, there is an unique film thickness, h_e, where the bridging particle will not cause deformation of the film surfaces (Figure 6.8, bottom). Any movement of the particle into thinner (left) or thicker (right) film regions will cause deformation of the film surfaces, the area of the liquid interface will increase, hence the surface free energy, ΔE, will also increase. Therefore the bridging particle will locate at that film thickness $h = h_e$, where the deformation of the film surfaces is practically missing and the surface free energy is minimum. In this case h_e is related to θ by the following simple equation.

$$h_e = d \cos \theta \tag{3}$$

Therefore by measuring h_e and knowing d the contact angle of the bridging particles can be determined by equation (3). Here, we use the liquid film as a calliper to measure the thickness h_e and to obtain the contact angle by equation (3). For this reason we call the new method "Film Calliper Method" (FCM). It relies on the absence of deformation around the bridging particle - a principle difference to the existing film trapping technique.[5] The new FCM is simple and allows determination of the contact angle of many particles bridging simultaneously the film surfaces (see Figure 6.6), thus giving statistically reliable average values

6.3   Results and discussion

6.3.1   Silica particles

Silica particles with diameter of 3 μm (Tokuyama Corp.) were hydrophobised to different extents with hexamethyldisilazane (HMDS) at various concentrations by the procedure described elsewhere.[15] The results for the contact angles of 3 μm silica particles with different wettability obtained with the new Film Calliper Method are shown below for isolated thin films with bridging particles at their surfaces. Table 1 shows the contact angles of 3 μm silica particles hydrophobised with 1×10^{-4} M HMDS obtained for several different isolated foam films as shown in Figure 6.6.

Table 6.1   Film thickness and contact angle of 3 μm silica particles hydrophobised with 1×10^{-4} M HMDS measured at an air-water interface with the new film calliper method. The results shown here are for one particular bridging particle versus radial distance taken from different isolated foam film images.

radial distance, r / μm	film thickness, h_e / μm	particle contact angle / deg.
321.7	2.30	39.92
285.1	2.26	41.03
247.0	2.22	42.25
194.0	2.25	41.41
121.3	2.36	38.12

.

The average film thickness obtained for the bridging silica particles hydrophobised with 1×10^{-4} M HMDS was 2.28 ± 0.05 μm and the average bridging contact angle was 40º ± 2. These values are in very good agreement with the contact angles results obtained with the glass plates previously hydrophobised. Also, it can be confirmed with the results that even at different radial film distances the contact angle of the particle remains constant and therefore it seems that once the particle bridges the film, it remains at the same location whether you open the film (from thin to thick film) or close it (from thick to thin film).

255

Table 2 and Figure 6.2 show the results of film thickness and contact angle obtained for silica particles of 3 μm hydrophobised with 1×10^{-3} M HMDS. The average film thickness obtained was 1.70 ± 0.04 μm and the average bridging contact angle was $56^{\circ} \pm 1$.

Table 6.2   Film thickness and contact angle of 3 μm silica particles hydrophobised with 1×10^{-3} M HMDS measured at an air-water interface with the new film calliper method. The results were obtained at the location of one particular bridging particle versus radial distance from the film centre during the shrinking of the film by pumping water into the meniscus.

radial distance, r / μm	film thickness, h_e / μm	particle contact angle / deg.
422.4	1.75	54.29
426.8	1.70	55.25
378.7	1.69	55.77
367.1	1.68	55.94
345.6	1.67	55.94
315.3	1.69	55.72
278.3	1.73	54.55
244.7	1.68	55.94
200.4	1.70	55.25
147.4	1.64	56.88

Table 6.3 shows the results for film thickness and contact angle obtained for silica particles of 3 μm hydrophobised with 1×10^{-2} M HMDS for 3 different isolated foam films where particles are at different radial distance in the foam film. The average of film thickness obtained from all 3 different isolated foam films was 1.17 μm $\pm$ 0.06 and the average bridging contact angle was 67 ± 2.

The results for the contact angles of silica particles hydrophobised with different concentrations of HMDS are summarised in Table 4. As expected, the contact angle of the silica particles increases with the increase of HMDS concentration used for their hydrophobisation.

Table 6.3   Film thickness and contact angles of 3 μm silica particles hydrophobised with 1×10^{-2} M HMDS measured at an air-water interface with the new film calliper method. Here the results are shown for 3 different particles that are positioned at different radial distances in the foam film.

particle number	radial distance, r / μm	film thickness, h_e / μm	particle contact angle / deg.
1	192.1	1.24	65.7
	224.5	1.25	65.4
	317.4	1.13	67.9
2	171.6	1.08	68.9
	235.4	1.18	66.9
	338.3	1.26	65.2
3	192.9	1.08	69
	247.2	1.19	66.6
	314.1	1.16	65.2

Table 6.4   Average contact angles of 3 μm silica particles hydrophobised with HMDS measured at an air-water interface with the new film calliper method.

[HMDS] / M	particle contact angle / deg.
1×10^{-4}	40 ± 2
1×10^{-3}	56 ± 1
1×10^{-2}	67 ± 2.0

The contact angles of silica particles hydrophobised with 1×10^{-2} M HMDS have also been measured with the FCM in the presence of 10 mM NaCl. The results are shown below in Table 6.5.

Table 6.5   Film thickness and contact angles of 3 μm silica particles hydrophobised with 1×10^{-2} M HMDS measured at an air-water interface in the presence of 10 mM NaCl with the FCM. Here the results are shown for two different particles (P_1 and P_2) at different radial distance in the foam film.

.

	P_1	P_1	P_1	P_2	P_2	P_2
radial distance, r / μm	73.08	106.87	156.46	62.93	114.36	165.22
film thickness, h_e / μm	0.79	1.12	0.78	1.11	1.12	0.70
particle contact angle / deg.	74.79	67.99	74.90	68.33	68.10	76.43

The average of the individual bridging silica particles contact angle (hydrophobised with 1×10^{-2} M HMDS) in the case of water films in the absence of salt was found to be 67° ± 2. However, when salt (*e.g.* 10 mM) was added to the water films containing the same particles, hydrophobised with 1×10^{-2} M HMDS, at their surfaces the average bridging particle contact angle was found to be 72° ± 4 as shown in table 6.5. These results show that salt addition increases the contact angle that these particles make with the air-water interface (~ 10° higher) making them more hydrophobic (Figure 6.9). These findings are in agreement with the results found with the previous studies in this research (Chapters 3 and 4) where addition of salt to the aqueous silica dispersions was found to enhance the transfer of particles to the air-water interface (the contact angle of aqueous NaCl drops on glass slides in air was found to increase with increasing salt concentration).

6.3.2 *Sulfate latex particles*

The contact angle of polystyrene (PS) sulfate latex particles (Interfacial Dynamics Corp.) with diameter 9.6 μm at the air-water interface has also been determined using the novel Film Calliper Method. A typical image of a foam film with bridging latex particles is shown in Figure 6.9.

Figure 6.9   Image of a vertical foam film with bridging 9.6 μm PS latex particles.
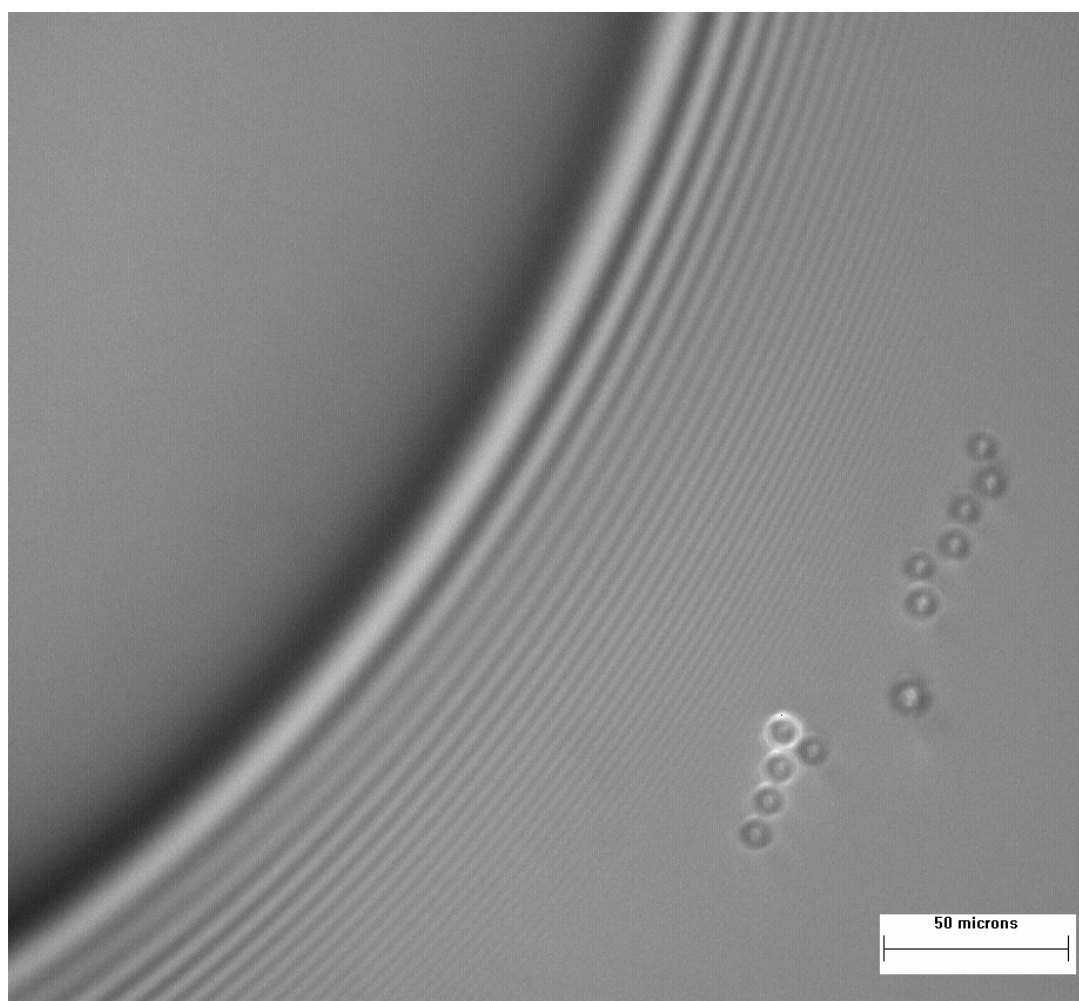
The film thickness, h_e, and the bridging contact angle of several latex particles at the air-water interface determined from a thin foam film (Figure 6.9) are shown in table 6.6. The average contact angle is 40.2° ± 1.5.

Table 6.6   Film thickness and contact angles of 9.6 μm sulphate latex particles measured at an air-water interface with the FCM. Here the results are shown for several different particles versus radial distance in a foam film.

particle number	film thickness, h_e / μm	particle contact angle / deg.
1	7.59	37.69
2	7.29	40.61
3	7.19	41.54
4	7.49	38.68
5	7.49	38.68
6	7.18	41.54
7	7.39	39.66
8	7.18	41.54
9	7.39	39.66
10	7.08	42.46

6.3.3 Comparison with existing methods

In order to compare the results obtained for the contact angle of the silica particles measured by FCM, another indirect method for measuring the contact angle of the same silica particles was used. This method involved the use of microscope glass slides, which were hydrophobised simultaneously with the silica particles and then the contact angles of water drops on the slides in air were measured by the Drop Shape Analysis Instrument (DSA10, Krüss). The average of receding and advancing contact angles are plotted against the HMDS concentration in Figure 6.10. The particle contact angles obtained by the FCM are also plotted for comparison. As shown in Figure 6.10, by increasing the concentration of HMDS, the contact angles of the glass plate hydrophobised simultaneously with the particles and the contact angles of the silica particles at an air-water interface measured by FCM increased, showing the same trend. However, the plate contact angles are slightly higher than those of particles.

Figure 6.10 Contact angles of 3 μm silica particles hydrophobised with HMDS measured at an air-water interface with the FCM (unfilled diamonds) and on glass plates hydrophobised simultaneously with the particles (filled diamonds).
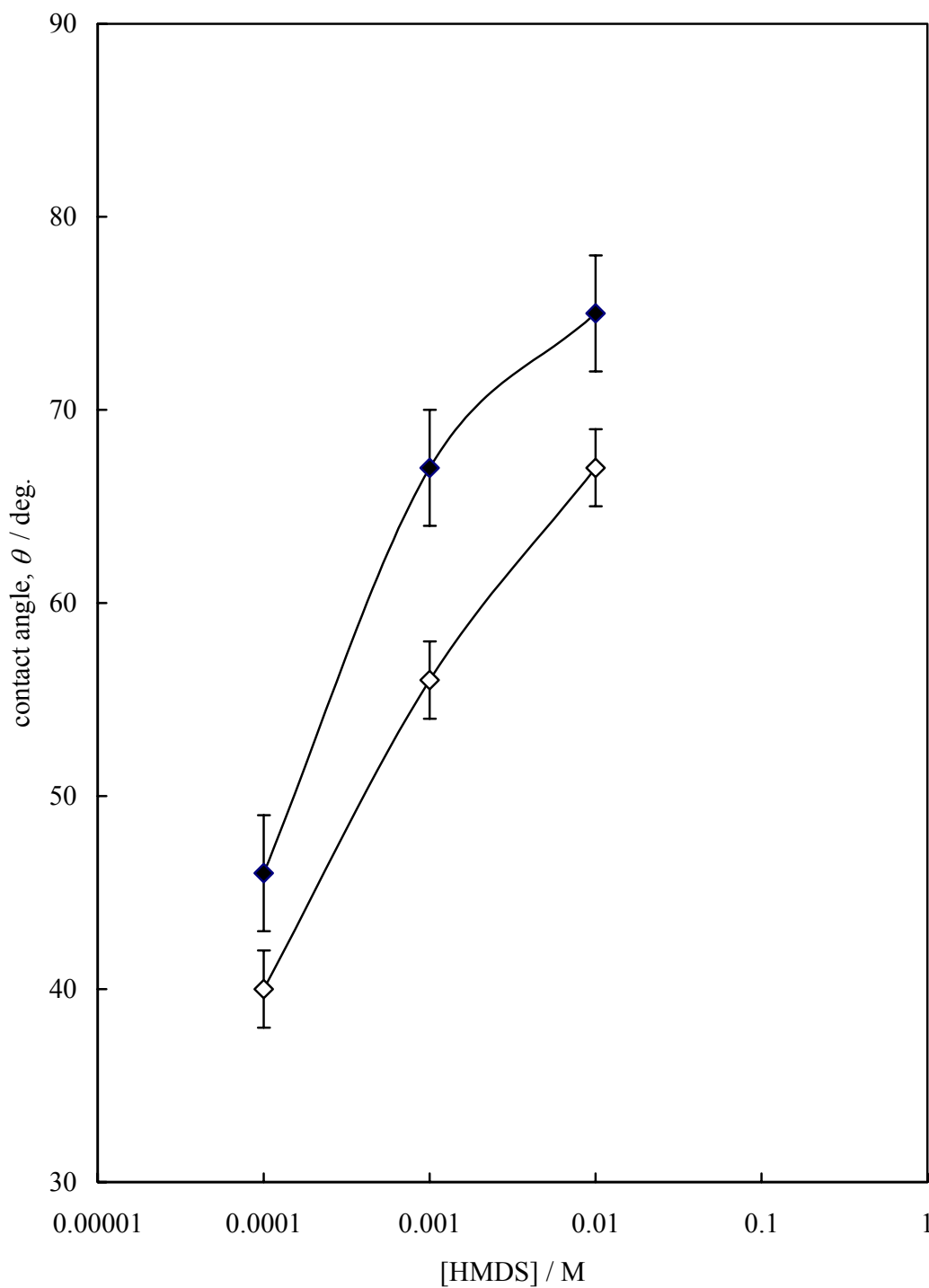
The disadvantage of this indirect method for measuring the particle contact angle is that the surface chemistry and roughness of the macroscopic flat solid cannot be exactly the same as those of the microscopic particles.

The contact angle of 9.6 µm latex particles measured by the FCM were also compared with those determined by side imaging technique.[8] The latter uses the simple relations between the contact angle and the geometrical parameters of the spherical particle attached to the liquid interface. The sketch of the experimental setup and details of the procedure are described in Chapter 2. A typical side image of 9.6 µm latex particles attached to the air-water interface is shown in Figure 6.11.

Figure 6.11 Side image of a polystyrene sulfate latex particle with diameter of 9.6 µm at the air-water interface. The position of the water-air surface (dashed line) coincides with the line of symmetry of the particle and its reflection from the liquid interface.
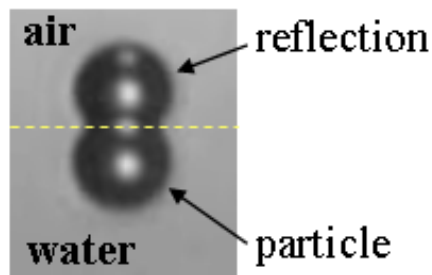
The deformation of the fluid interface around the spherical particle is negligible for particles smaller than ~10 µm.[13] The contact angle through the water can be calculated by using any of the following equations:

$$\sin \theta = \frac{dc}{d} \tag{4}$$

$$\cos \theta = \frac{2hw}{d} - 1 \tag{5}$$

where d and dc are the diameter of the particle and that of the three phase contact line respectively and h_w is the depth of immersion in water (Figure 6.12). Therefore, h_w and dc could be measured directly from the images.

Figure 6.12 Sketch of the side image of a particle with diameter *d* and contact angle θ attached to the air-water interface. The depth of immersion in water, h_w, and the diameter of the three phase contact line, dc, depend on particle hydrophobicity measured by the three phase contact angle θ.
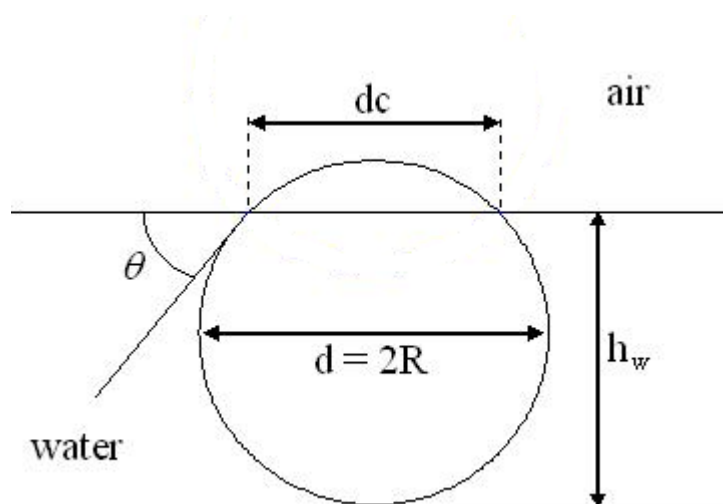
We have measured d, dc and h_w from the images of several latex particles and calculated the contact angle through the water by using the equations (4) and (5). Figure 6.13 shows the results obtained with the side imaging technique and the FCM. The average contact angle determined by side imaging technique is 41 ± 4°. This is in excellent agreement with that obtained by the film calliper method with an average contact angle of 40 ± 1.5°, thus confirming that the new method gives correct and reliable contact angle values. The new FCM, however, is more precise than the latter technique (*cf.* error).

Figure 6.13 Contact angles of PS sulphate latex particles of diameter 9.6 μm at the air – water interface determined by the side imaging technique (filled diamonds: equation 4 and unfiled circles: equation 5) and from the bridging particles in the thin foam films (unfilled triangles: the new film calliper method). The solid line represents the average value of all results obtained from both methods.
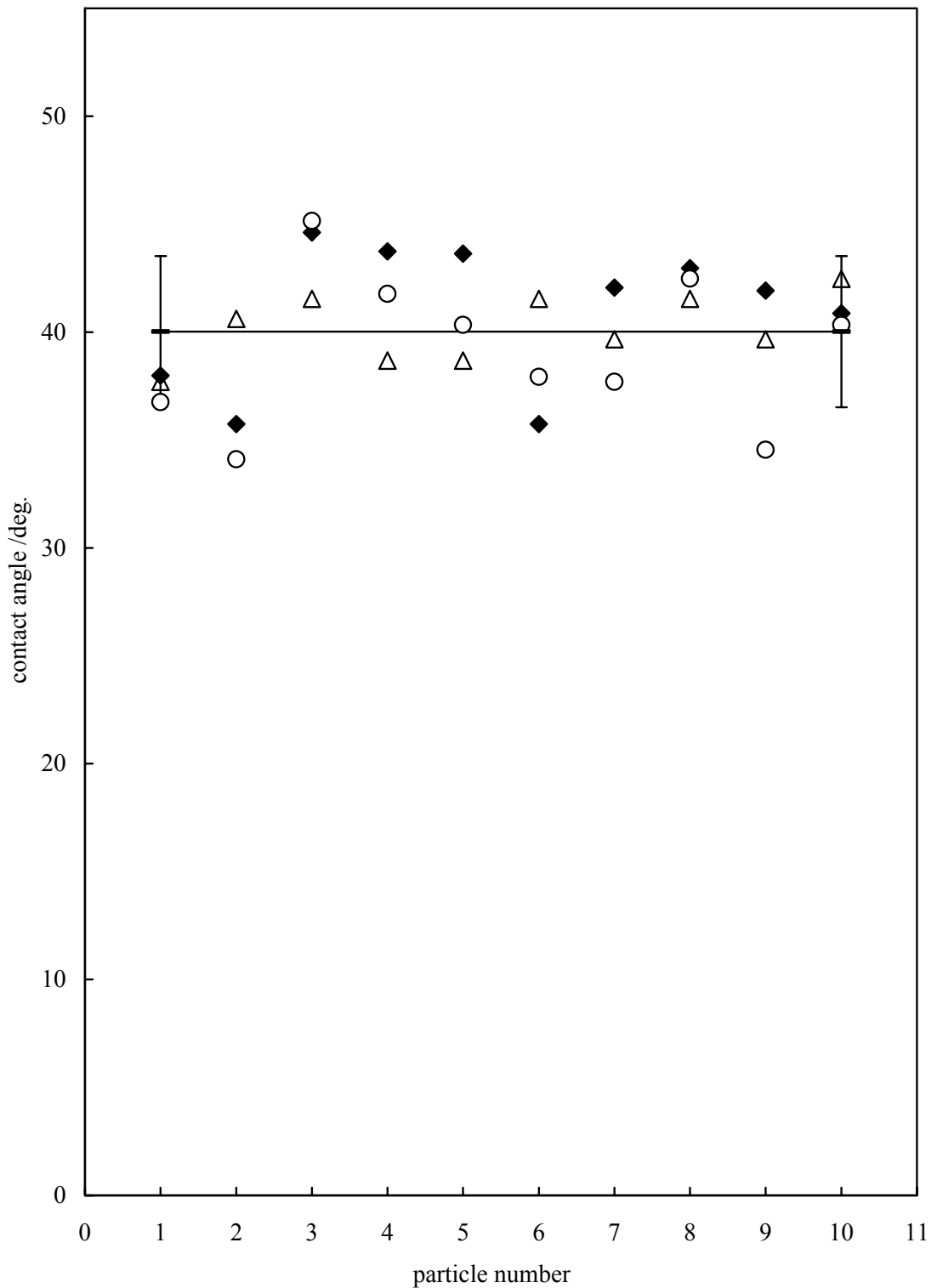
6.4   Conclusions

A new method has been developed for measuring the contact angle of solid particles at liquid interfaces called the Film Calliper Method. The applicability of the new method for measuring contact angles of particles of different chemistry, sizes and wettabilities at the air-water interface is demonstrated.

A prerequisite for the application of the FCM is that the liquid film with bridging particles is sufficiently stable. It has been shown in this study that this requirement is fulfilled in the case of air-water films with hydrophilic and partially hydrophobised silica particles ($\theta < 90°$). It was also shown previously that the latter is fulfilled in the case of water-oil emulsion films with hydrophobised silica particles.[11] Hence the new method could also be applied for measuring the particle contact angles at water – oil interfaces.[14] However, hydrophobic particles ($\theta > 90°$) cannot form stable bridges in water films. Therefore, the FCM can be used for measuring the air-water contact angle of hydrophilic particles ($\theta < 90°$) only. The results obtained here with the new FCM, are in excellent agreement with the contact angle values measured with alternative techniques. Many systems of pratical interest, such as food or pharmaceutical formulations involve hydrophilic particles and the new FCM offers significant advantages over the existing methods. The new method differs from the existing experimental techniques by its simplicity, reliability and applicability for measuring the contact angle of micrometer particles in their natural environment and in real time without using any artificial additives, sophisticated instruments or complex calculations. In contrast to most of the existing techniques, the FCM is easily applicable to sub-micrometer particles as demonstrated in ref. 14 for latex particles with diameters of 810 and 610 nm.

References

1.   B.P. Binks and T.S. Horozov, Colloidal Particles at Liquid Interfaces, Cambridge University Press, Cambridge (2006).

2.   B.P. Binks and T.S. Horozov, *Angew Chem. Int. Ed.*, **44**, 3722 (2005).

3.   B.P. Binks and R. Murakami, *Nature Materials*, **5**, 865 (2006).

4.   G. Gillies, M. Kappl and H-J. Butt, *Adv. Colloid Interface Sci.*, **114-115**, 165 (2005).

5.   A. Hadjiiski, R. Dimova, N.D Denkov, I.B. Ivanov and R. Borwankar, *Langmuir*, **12**, 6665 (1996).

6.   I.B. Ivanov, A. Hadjiiski, N.D. Denkov, T.D. Gurtkov, P.A. Kralchevsky and S. Koyasu, *Biophysical J.*; **75**, 545 (1998).

7.   A. Hadjiiski, S. Tcholakova, I.B Ivanov, T.D Gurtkov and E.F. Leonard, *Langmuir*, **18**, 127 (2002).

8.   Z. Hórvölgyi, S. Németh and J.H. Fendler, *Colloids Surfaces A*, **71**, 327 (1993).

9.   V.N. Paunov, *Langmuir*, **19**, 7970 (2003).

10.   O.J. Cayre and V.N. Paunov, *Langmuir*, **20**, 9594 (2004).

11.   T.S. Horozov, R. Aveyard, J.H. Clint and B. Neumann, *Langmuir*, **21**, 233 (2005).

12.   M. Born and E. Wolf, Principles of Optics, 7th Ed., Cambridge University Press, Cambridge, chapter VII (1999).

13.   D. Exerova, N.V Churaev, T. Kolarov, N.E. Sipova, N. Panchev and Z.M. Zorin, *Adv. Colloid Interface Sci.,* **104**, 1 (2003).

14.   T.S. Horozov, D.A. Braz, P.D I. Fletcher, B.P. Binks and J.H. Clint, *Langmuir*, **24**,1678 (2008)

15.   T.S. Horozov, R. Aveyard, J.H. Clint and B.P. Binks, *Langmuir*, **19**, 2822 (2003).

CHAPTER 7

CHAPTER 7

FOAMING ABILITY AND STABILITY OF AQUEOUS LAPONITE RD DISPERSIONS

7.1   Introduction

The size and shape of colloidal particles are amongst their most important characteristics because they determine many other features of the behaviour of colloidal suspensions[1]. Therefore the search for new particles of different size, shape, chemistry and hydrophobicity is very important in this project. This is the reason for studying Laponite RD particles as these are of different shape and chemistry from that of silica particles and are of interest for comparison in terms of effect of particle shape on the behaviour of foamability and foam stability. Laponite dispersions have been extensively investigated. For example, the type and stability of emulsions stabilised by Laponite RD clay particles are reported[2] and it is concluded that stable o/w emulsions of toluene, water and Laponite RD clay particles were only formed under conditions where the particles are flocculated (via salt) and at intermediate concentrations of clay. Emulsions prepared from either gel or discrete particle dispersions were unstable to coalescence. The ability of electrolyte solutions to control the stability of bubbles and the flotation of hydrophobic particles has been investigated[3]. Therefore, the effect of different electrolytes on foamability and foam stability of aqueous dispersions of Laponite RD particles was also investigated in order to determine the influence of salt valence on the wettability of Laponite RD particles and consequent foam stability.

7.1.1   Suspensions of colloidal clay discs

The colloid chemistry of clays is industrially relevant and academically interesting. For colloid scientists clay mineral dispersions can be considered as suitable model systems based on the fact that the surface structure of these plate-like particles is well known and that minerals with widely differing properties are available. However, clay mineral dispersions never behave as ideal systems. Coagulation and flocculation processes are much more dependent on system parameters than for other dispersions. Several reasons contribute to this behaviour:

(a)   The particles are of irregular shape and of different thickness.

(b)   The charges of the layers are not uniformly distributed.

(c)   The particles also carry charges at the edges which change with the chemical parameters, in particular with pH.

Therefore, stability and coagulation conditions are not so straightforward and are less reliable in clay systems because of these facts. Nevertheless, many practical uses of clay dispersions are just based on the variation of the colloidal stability with the system parameters[4].

The term clay is used in soil science and agriculture to mean any material of particle size less than 2 μm but the term clay mineral refers to a group of silicate minerals. Properties which are considered typical of clays are: plasticity, thixotropy, water retention, swelling, ion-exchange, adsorption of inorganic and organic compounds. These properties are related to the presence of the minerals, and are used on a large scale in industry. Refined natural and synthetic clays find a wide industrial application as shear sensitive anti-settling agents in water based formulations such as paints and inks, personal care products, household products, agricultural detergents and oil drilling fluids.

Most clay minerals are part of a large family of silicate minerals called phyllosilicates[1, 5]. As the Greek name indicates (phyllo means leaf) these materials are built up from leaves, or more precisely from stacks of mineral leaves. A schematic representation of the structure of phyllosilicate minerals is shown in Figure 7.1. Each mineral in a leaf is a monocrystalline structure consisting of two dimensional sheets of silica tetrahedra (SiO_4^{2-}) covalently bonded together. The octahedral sites in between the tetrahedral sheets are occupied by divalent or trivalent ions. The surfaces of each leaf are covered by the oxygen atoms of the silica tetrahedra and are negatively charged. Alkali ions like potassium K^+, sodium Na^+ or calcium Ca^{2+} compensate the charge and form the bonds between the leaves. Synthetic clay-minerals are generally synthesised in a sodium rich environment and the great majority of their interleaf cations are therefore sodium ions[6].

Figure 7.1 (a) Schematic representation of the layered structure of phyllosilicate minerals. Note the stacking of mineral leaves where each leaf consists of a monocrystalline silicate structure. The area in the box is depicted magnified in the lower plot. (b) Idealised tri-octahedral phyllosilicate structure drawn in perspective. The legend on the right displays the elements present in the structure. The presence of sodium atoms can be seen in the basal spacing. Taken from ref. 7.
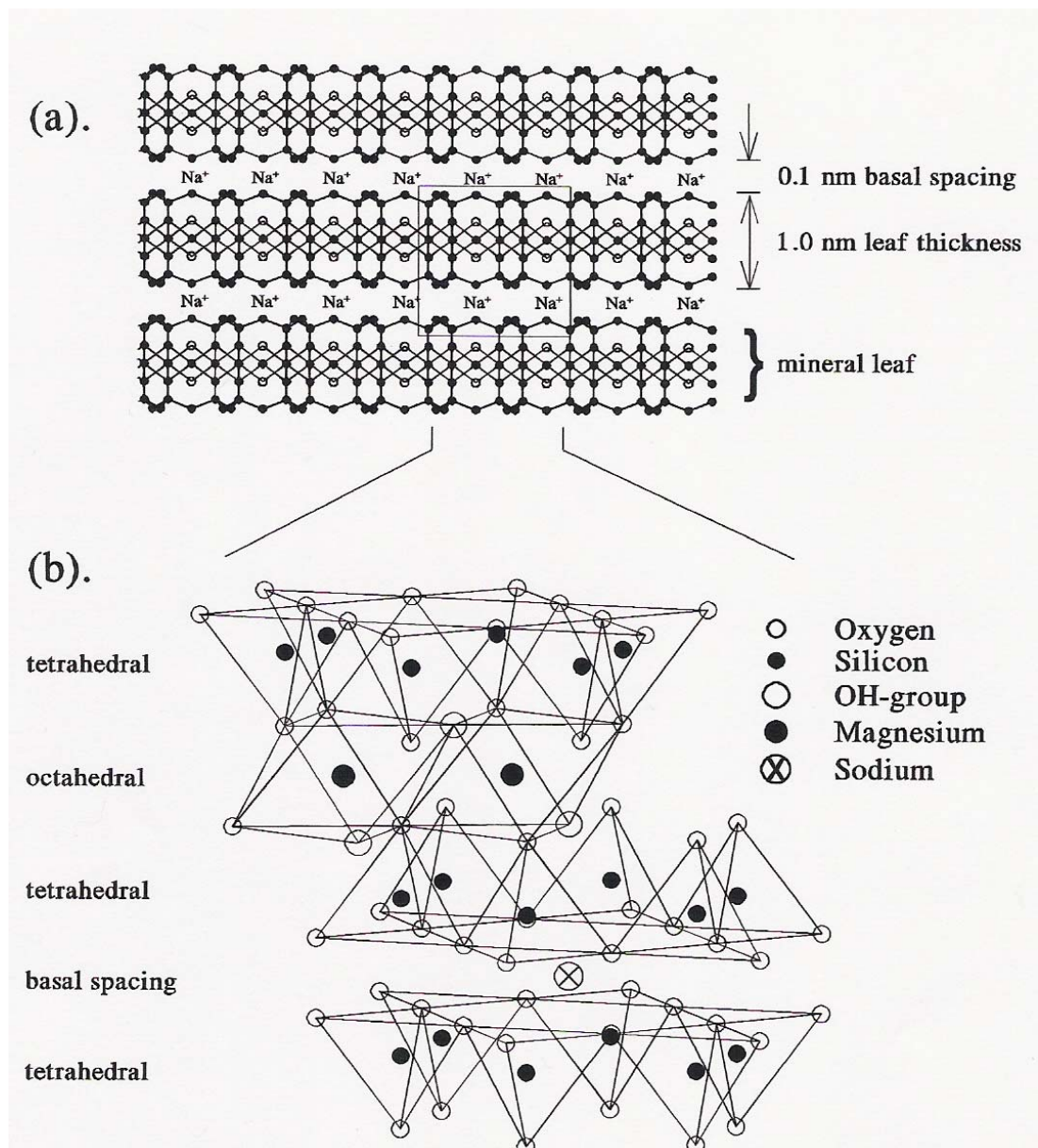
7.1.2 Laponite structure, size and chemistry

In this study we use the grade Laponite RD (rapid dispersion) which is the easiest grade to disperse[8,9]. Laponite is an entirely synthetic product that resembles the natural smectite mineral hectorite in both structure and composition. Its unique properties improve the performance of a wide range of industrial and consumer products. These properties result because the primary platelet size of Laponite is only 25-30 nm across by 1 nm thick, which is significantly smaller than the naturally occurring material. The synthesis process involves combining salts of sodium, magnesium and lithium with sodium silicate at carefully controlled rates and temperatures. This produces an amorphous precipitate which is then partially crystallised by a high temperature treatment. The resulting product is filtered, washed, dried and milled to give a fine white powder. As a result of its high chemical purity and small particle size, Laponite forms colourless and transparent suspensions which are particularly suited for light scattering studies. Laponite has a layer structure which, in dispersion in water, is in the form of disc-shaped crystals and pH ~ 10. The idealised unit cell shows six octahedral magnesium ions sandwiched between two layers of four tetrahedral silicon atoms. These groups are balanced by twenty oxygen atoms and four hydroxyl groups as shown in Figure 7.1(b). The height of the unit cell represents the thickness of the crystal (1 nm). The unit cell is repeated many times in two directions resulting in a disc diameter of around 30 nm as shown below in Figure 7.2. In practise, however, some magnesium ions are substituted by lithium ions to give a composition having the empirical formula: $Na_{0.7}^{+} [(Si_8Mg_{5.5}Li_{0.3})O_{20}(OH)_4]^{0.7-}$.

Figure 7.2 Schematic picture of the disc-like shape of the primary Laponite particle. The surface charge distribution is fixed as a result of the crystalline structure of the particle as shown in Figure 7.1(b).

30 nm

1 nm
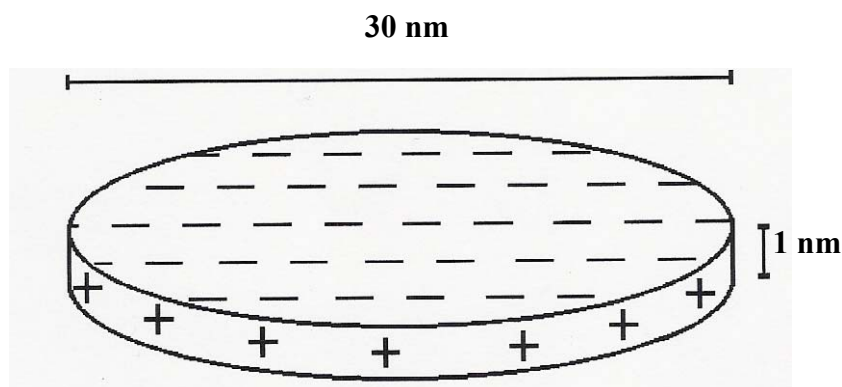
The charge deficiency of 0.7 per unit cell is neutralised during drying as sodium ions are adsorbed onto the surfaces of the crystals. The crystals become arranged into stacks held together electrostatically by sharing of sodium ions in the interlayer region between adjacent crystals. The crystal surface has a negative charge and the edges of the crystal have small localised charges. Electrostatic attractions draw the sodium ions in solution towards the crystal surface and osmotic pressure from the bulk of water pulls them away. An equilibrium becomes established where the sodium ions are held in a diffuse region on both sides of the dispersed Laponite crystal. These are known as electrical double layers. When two particles approach their mutual positive charges repel each other and the dispersion exhibits low viscosity and Newtonian type rheology.

It is necessary to keep the dispersions of Laponite at elevated pH in order to avoid disintegration of the particles.[10] If the pH decreases below 8.5, Laponite may react with hydrogen ions which dissolves the mineral structure and releases Mg^{2+} and other monovalent ions. The rate of this reaction decreases with increasing pH and is negligible for pH > 8.5. The stability, structure and rheology of Laponite dispersions has been the subject of considerable investigation[6-20]. However, there is still debate in the literature over the mechanism of gelation. The formation of a gel above a specific concentration is well known for other types of clay also. However, the addition of salt does not promote the isotropic liquid phase as observed for spherical or rod-like particles, but instead lowers the particle volume fraction at which the gel or glassy phase appears. This finding appears to be contrary to what is expected from predictions of DLVO theory.

Recent small-angle X-ray scattering studies[10] for dispersions at different pH and ionic strength lend support to the proposal of two types of gel structure arising from both opposing mechanisms offered in the literature as mentioned below. According to Saunders *et al.*[11] the charge in ion concentration can change the type of platelet interaction as shown in Figure 7.3. These results are interpreted in terms of an ordered, aligned structure where the particles face and edge electrical double layers are expanded and negative in sign. This is in contrast to a "house-of-cards" structure which results when particle aggregation is promoted by lower pH, higher ionic strength or a lower particle edge charge.

Figure 7.3 Types of platelet interaction.
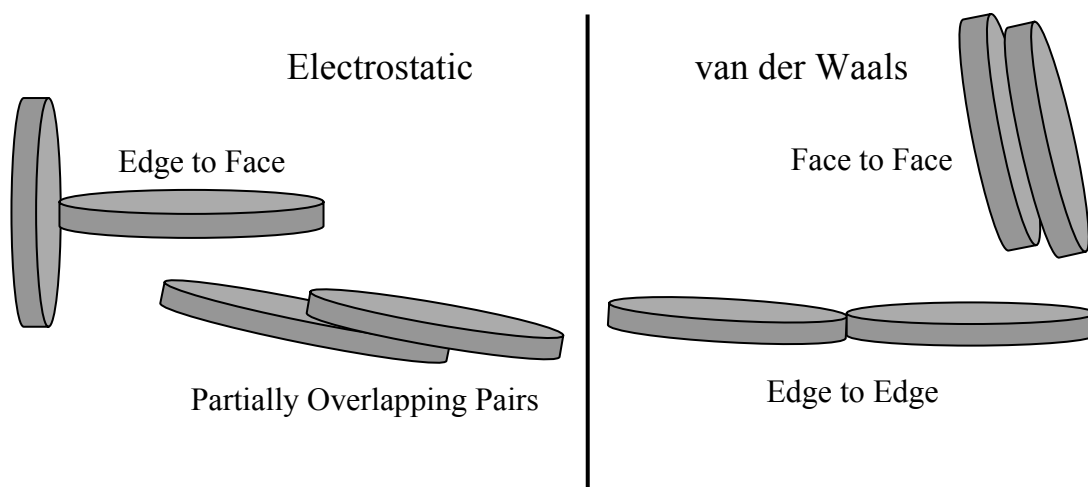
Two opposing origins for the gel formation of Laponite dispersions have been proposed. Norrish[12] originally suggested that gel formation is caused by long range electrical double layer repulsion between the clay platelets. Alternatively, it was suggested by van Olphen[13] and supported by others[14,15] that electrostatic attraction reinforced by van der Waals interactions between the positively charged edges and negatively charged faces of the plate-like particles leads to microflocculation of the Laponite particles and the formation of a "house of cards" structure (see Figure 7.4). However, it was argued that no such aggregation occurs except at high ionic strength ($Cs>10$ mM), but instead that repulsive interaction leads to a glassy state[16-19]. The glassy state is thought to be reached even at Laponite volume fractions below 1% due to strong repulsive electrostatic interaction. The slow development of the gel-like behaviour was interpreted in terms of an aging process of the glass[19].

Recently, it was demonstrated that the presence of positive charges on the rim of the Laponite disks is necessary to induce aggregation and gelation.[20] These charges can be effectively neutralised by added pyrophosphate. Aggregation and gelation is slowed down after addition of pyrophosphate even though the ionic strength is increased. The aggregation is even reversed by adding a large amount of pyrophosphate. The effect of adding pyrophosphate is in contrast with that of adding monovalent salt. In the latter case the aggregation and gelation rate increases dramatically, because electrostatic repulsion between the Laponite disks is screened without neutralising the rim charge.

Figure 7.4 Schematic structure of the Laponite gel formation – ''house of cards''. Laponite gel structure forms under shear forcing systems toremsin homogeneous. Taken from ref. 8.
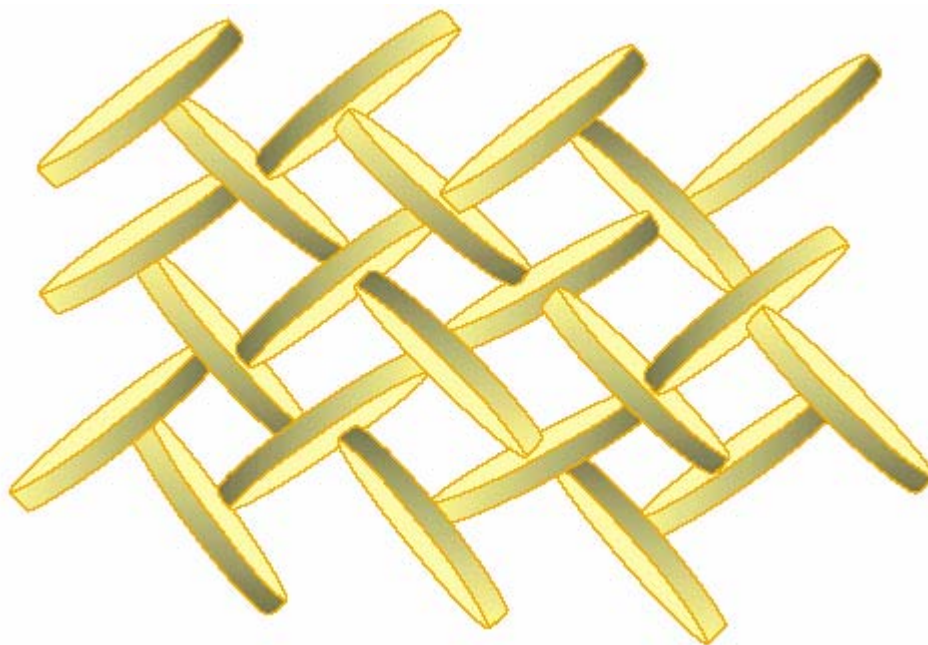
7.2 Dispersions of Laponite RD particles in aqueous NaCl

The particle size distribution (Z_{Ave} diameter) of the Laponite RD particles used in this study was determined by using the Malvern Zetasizer 3000 HS and it was found to be 26 ± 4 nm. This value is very similar to the Laponite RD particle diameter of approximately 30 nm quoted by the manufacture and reported by other studies.

In the absence of added salt, Laponite RD was successfully dispersed in pure water between 0.5 and 5 wt. %. Immediately following dispersion, colourless, fluid colloids were formed for concentrations up to 2 wt. %. They remained clear and non-viscous indefinitely. Above this concentration, the viscosity of the dispersions increased with time such that for 2.5 and 3 wt. % a clear gel which did not flow formed after one day. At high enough Laponite RD concentrations (above 3.5 wt. %) the dispersions do not flow upon tube reversal within 15 minutes and are slightly turbid (Figure 7.5). Dispersions containing between 0.5 and 4 wt. % were also prepared in different concentrations of NaCl in the range 0.01 to 3 M by using two different protocols as already described in Chapter 2.

Figure 7.5   Salt-free Laponite RD dispersions containing different concentrations of Laponite RD at pH ~ 10 after one day.

0.5wt.%   1wt.%   2wt.%   3wt.%   4wt.%   5wt.%
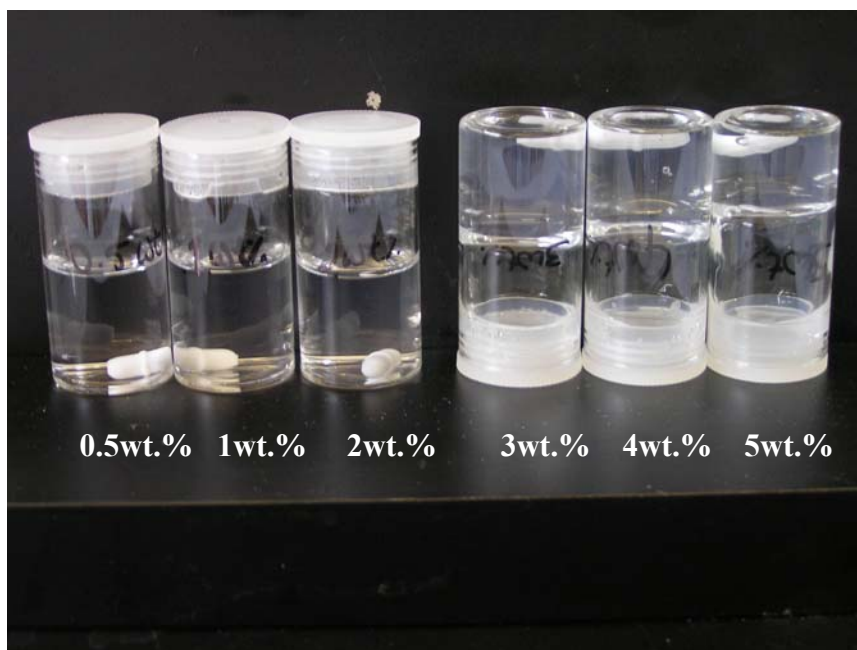
The 'natural' pH values of all the fresh Laponite RD dispersions without salt were around 10, but after few days the pH of these dispersions dropped slightly to about 9.8 (due to CO_2 absorption from the atmosphere). The pH is more or less independent of clay concentration but decreases systematically with an increase in salt concentration. The most noticeable reduction occurs at very high [NaCl] (*e.g.* 2 or 3 M) where the pH decreases to about 8.6. This may be due to the exchange of H^+ ions in the electrical double layer by added cations.[6]

Mourchid *et al.*[17] proposed a sol-gel state diagram of Laponite dispersions as a function of the salt and Laponite concentration. A partial phase diagram similar to that reported by Mourchid *et al.* is also reported by Ashby and Binks[2] where three distinct regions can be identified (see Figure 7.6). At low clay (≤ 2wt. %) and salt concentrations, an isotropic liquid containing discrete disc-like particles exists. At high clay concentrations (≥ 2.5 wt. %) and below 10^{-1} M NaCl, gels are formed which transform from isotropic to nematic with increasing clay content. For high salt concentrations (≥ 0.1 M) flocculation occurs at all clay concentrations in which a grey, turbid phase separates from a clear, supernatant liquid. Mourchid *et al.*[17] also reported flocculation for concentration of salt above 20 mM independent of the concentration of [Laponite].

Figure 7.6 Partial state diagram of aqueous Laponite RD dispersions in the presence of NaCl at 25 °C. Points along the abscissa (10^{-5} M NaCl) refer to dispersions containing no added electrolyte. Vertical arrows signify the clay concentrations for which emulsions were prepared with increasing salt concentration; horizontal arrows refers to the salt concentration at which emulsions were prepared of increasing clay concentration. Taken from ref. 2.
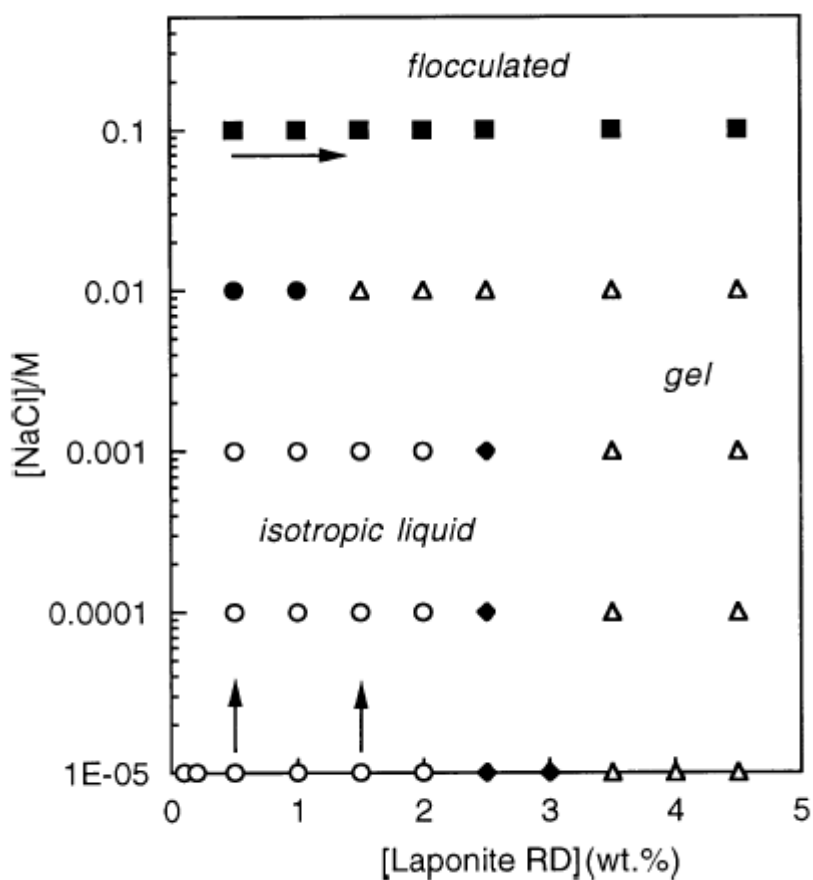
In this study, at a lower concentration of clay, *e.g.* 0.5 wt. % Laponite RD, increasing [NaCl] concentration leads to turbid dispersions of increased viscosity and sedimentation occurs at all salt concentrations ≥ 0.01 M (protocol 1), see Figure 7.7. It was also observed that from 1 to 3 M NaCl, separation of phases occurred quicker but little supernatant was observed at the top, while 0.05 to 0.5 M NaCl produced bigger volume fractions of the supernatant phase at a slower separation rate compared to other dispersions.

Figure 7.7 Photo taken one day after shaking the glass test tubes containing 20 mL dispersions of 0.5 wt. % Laponite RD at different [NaCl] given (protocol 1, using ultrasonic probe).
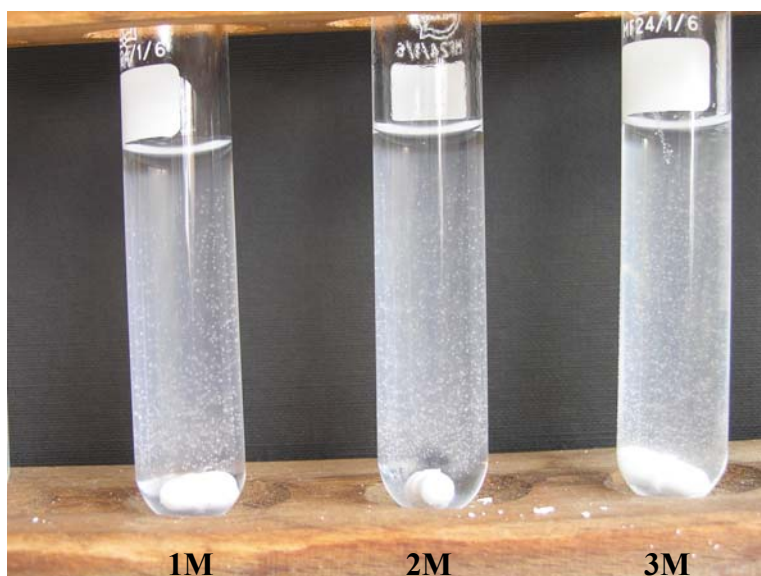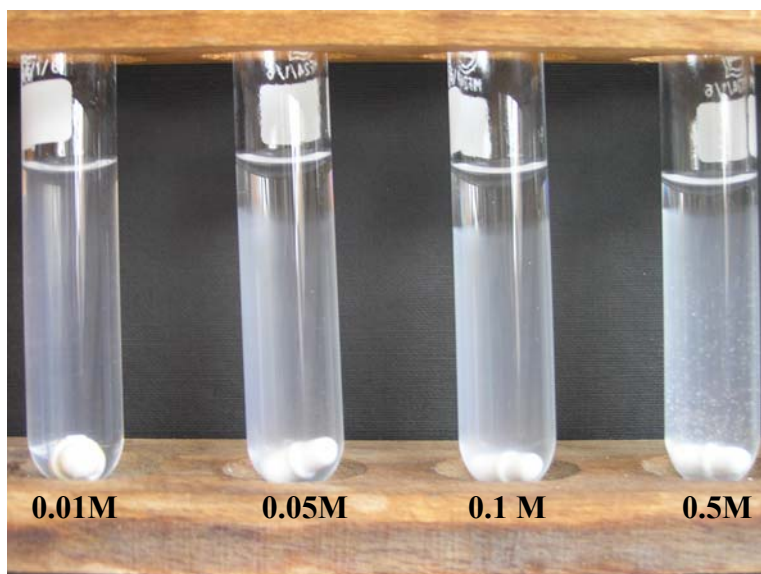
At a higher Laponite RD concentration (*e.g.* 2 wt. %), adding low levels of salt (*e.g.* 0.01 M) leads to a clear non-flowing gel immediately. However, further increasing the salt level up to 3 M leads to more turbid dispersions and flowing gels (Figure 7.8). These are homogeneous dispersions and only after a few days can it be seen that there is a very small supernatant liquid at the top of gels.

Figure 7.8 Photo taken after shaking the glass test tubes containing 20 mL dispersions of 2 wt. % Laponite RD at different [NaCl] given (protocol 1 with magnetic stirrer).
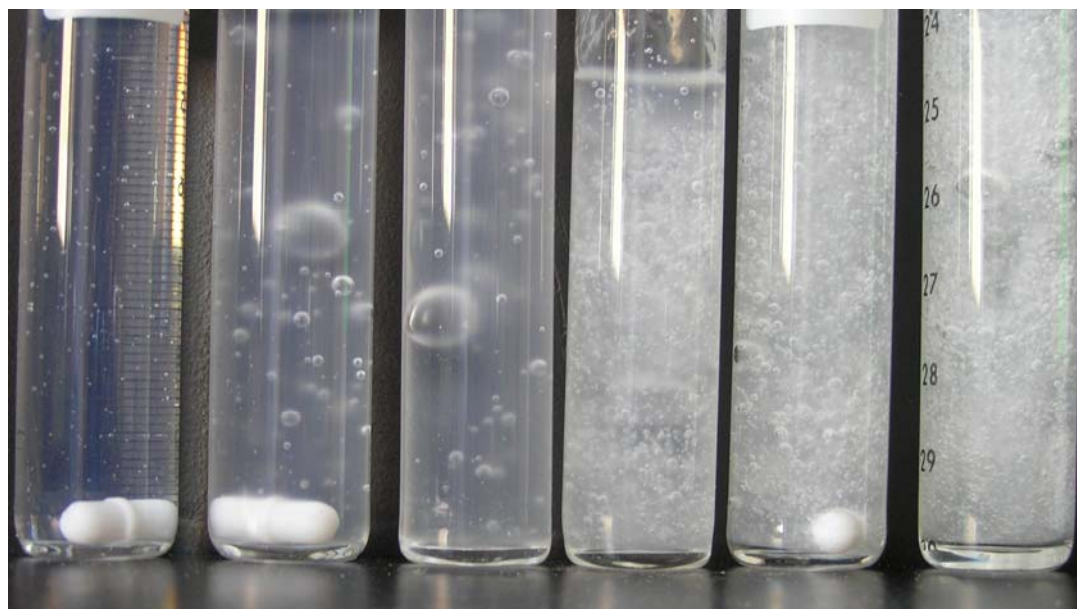
| 01 M | 0.05M | 0.1M | 0.5M | 1M | 2M |
| clear gel | slightly turbid, jelly-like type gel | | | turbid and flowing gels | |

This contradicts the results previously reported by other researchers[2, 17], where they found that flocculation occurred for concentration of salt above 0.02 M independent of the concentration of Laponite RD. However, they dispersed the Laponite powder directly into the salt solution instead of first dispersing it in salt-free water and subsequently raising the ionic strength. As a consequence Laponite aggregates before it can fully disperse[21]. In this study, by dispersing Laponite RD first in salt-free water and subsequently adding the salt (protocol 1), homogenous dispersions at higher salt concentrations were obtained. A partial phase diagram is given in Figure 7.9.

Figure 7.9 Partial phase diagram of 20 mL aqueous Laponite RD dispersions at pH   in the range 8.5 – 10 in the presence of NaCl at room temperature (~ 21 ºC) using protocol 1.   Points along the abscissa (0.001M NaCl) refer to dispersions containing no added electrolyte.
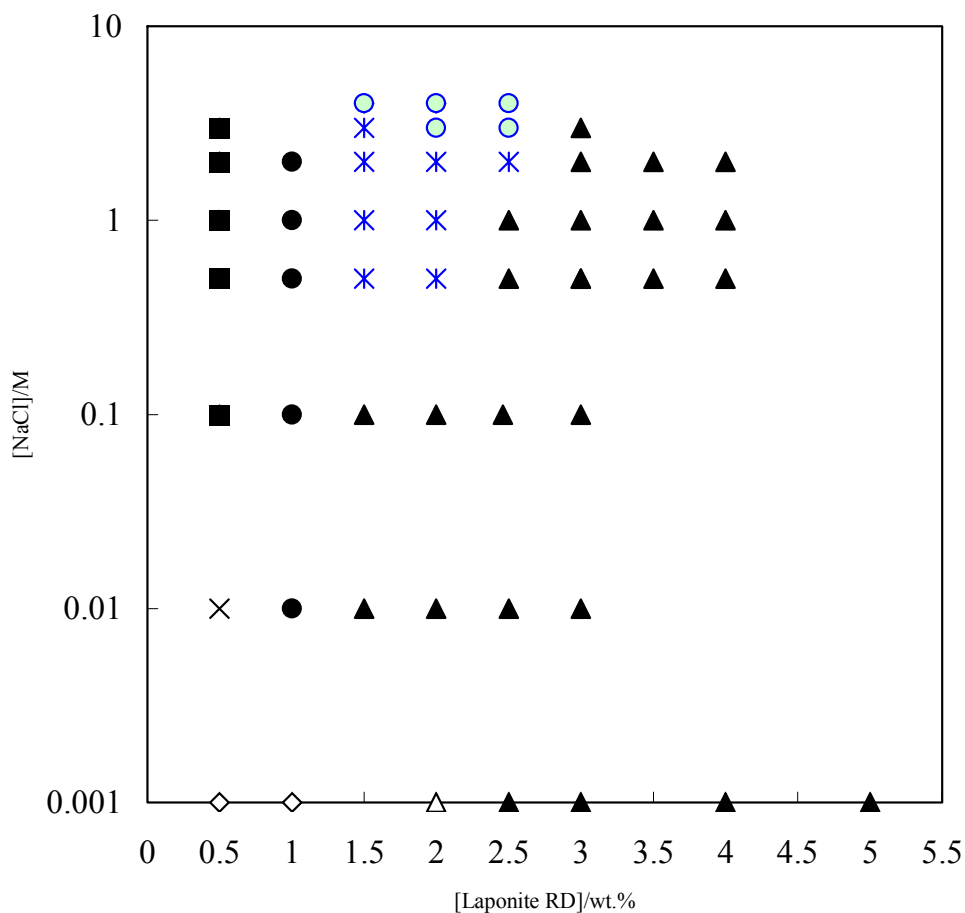
◇ clear fluid

△ clear gel, flows

▲ turbid gel, didn't flow upon reversal of tube but are reversible gels from 0.1 M NaCl

✕ slightly turbid viscous

● slightly turbid gel, flows (turbid from 0.5M NaCl)

■ slightly turbid floc + clear supernatant (from 1M small supernatant at top)

✳ turbid gel (doesn't flow, reversible) + clear supernatant at bottom

○ turbid gel, flows + small clear supernatant at bottom

All state diagrams shown here depend on the waiting time used in the experiment and should not be considered as equilibrium phase diagrams. In Figures 7.10 and 7.11 can be seen the effect of Laponite RD concentration when the salt concentration is fixed. At low salt concentration (Figure 7.11) dispersions are slightly turbid and at low concentration of Laponite RD (0.5 wt. %) the dispersion remained viscous, but after one day a clear supernatant was observed at the top. Increasing the concentration of clay to 2 wt. % the dispersions become more gelled and do not flow upon reversal of the test tube immediately after addition of the salt. However, some gel-like behaviour was not observed immediately but developed slowly with time. This was observed with the dispersion containing 1 wt. % which became gelled and did not flow after one day. At a higher concentration of salt, say 1 M as shown in Figure 7.12, dispersions become gels but remain flowing gels up to 2.5 wt. %; only at a higher concentration (3 wt. %) did the gels not flow.

Figure 7.10 Photo taken after shaking the glass test tubes containing 20 mL aqueous Laponite RD dispersions at different [Laponite RD] and at a fixed [NaCl] = 0.01 M with pH around 10 by using protocol 1 (dispersions a and b were slightly turbid, viscous and only after one day a gel was formed; dispersions from c to e were also slightly turbid but gels formed immediately and didn't flow).
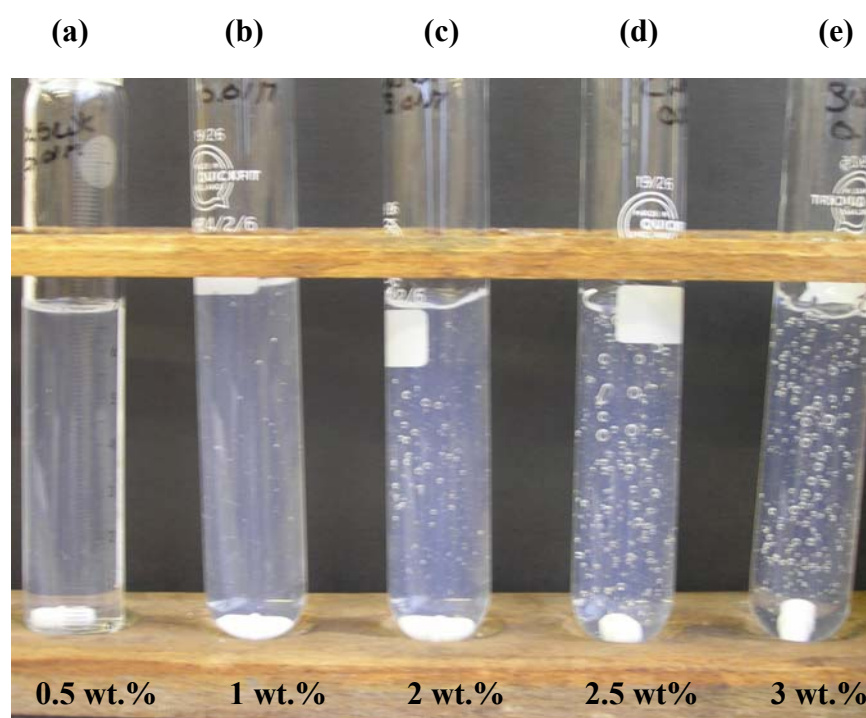
Figure 7.11 Photo taken after shaking the glass test tubes containing 20 mL aqueous Laponite RD dispersions at different [Laponite RD] and at a fixed [NaCl] = 1M with pH around 8.9 by using protocol 1 (dispersion a was slightly turbid and viscous; dispersions from b to d were turbid flowing gels and e was a rigid gel that did not flow).

       (a)   **(b)**   **(c)**   **(d)**   **(e)**

0.5 wt.%   1 wt.%   2 wt/.%   2.5 wt.%   3 wt.%
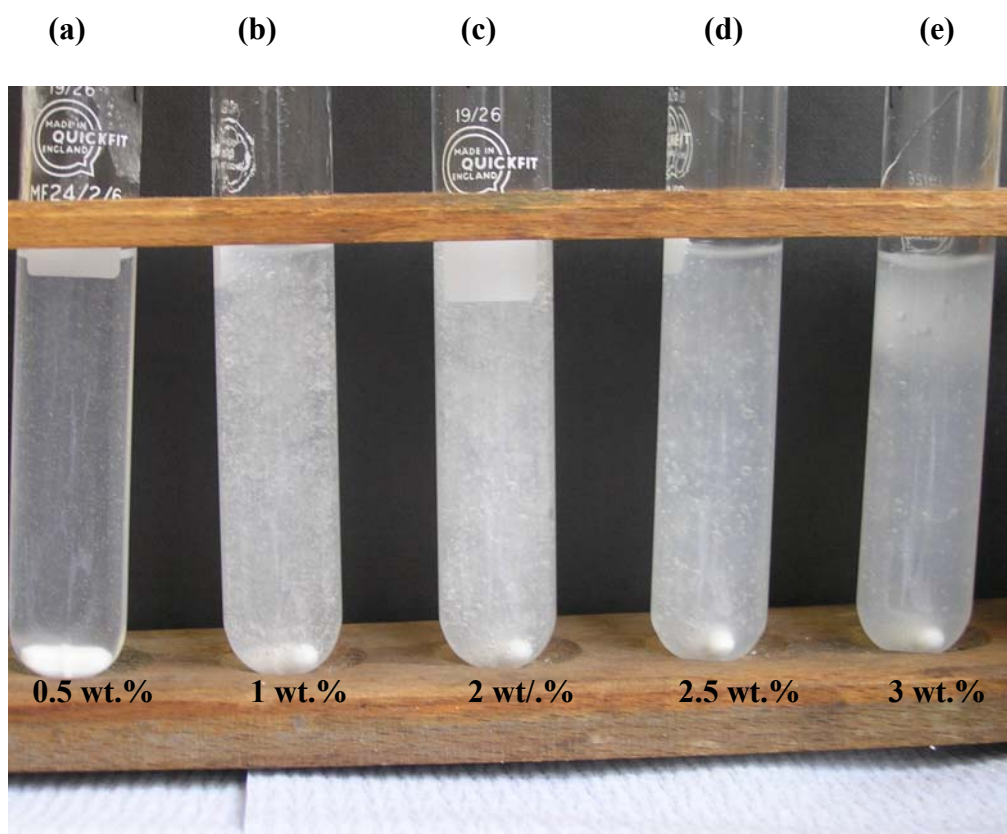
The results obtained in this study are similar to that reported recently by Mongondry et al.[21] where they revised the state diagram of Laponite dispersions. It can be concluded by using protocol 1 that the gelation process increases strongly at high enough Laponite RD concentrations, where they did not flow upon reversal of the tube. However, dispersions of intermediate concentration (1.5 – 2.5 wt. %) which did not flow in the absence of salt or in the presence of low salt (0.01 – 0.1 M), become flowing gels at high salt concentration (≥ 0.5 M) by using protocol 1. It was also observed that the gel state can be reversed by simply re-shaking the test tubes containing ≥ 0.1 M NaCl. However, for concentrations of salt lower than 0.1 M and high Laponite RD concentration the gel state is much stronger and can not be reversed by simply re-shaking the test tubes manually (they need a stronger mechanical stress).

In many of its macroscopic properties, the gel state of the Laponite RD dispersions resembles the gels formed by gelatine[22, 23], commonly encountered in food preparations. The clay gel shows an elastic response to small perturbing forces; it wiggles and behaves like jelly. However, when subjected to shear forces above a certain threshold strength a liquid-like response (thixotropy) is observed. It is well known that Laponite gels are easily broken by mechanical stress, which means that the bonds are weak. This observation simply shows that the bonds are not irreversible. Whether the bonds are caused by charge interactions between a positively charged edge and a negatively charged face or are due to van der Waals interactions, they are reversible to some extent. When left undisturbed (after the mechanical stress stops), the aggregation starts again and the sol returns to a gel state. This process was recently interpreted in terms of rejuvenation of a glass[24]. Unlike gelatine the clay/water system does not form thermotropic gels, *i.e.* clay gels are not reversible under temperature variation. For the clay/water suspensions shear takes the role of temperature.

When using protocol 2, similar results were obtained to that reported by N. P. Ashby and Binks[2]. Some differences may be due to a difference in waiting time. A similar way of sample preparation was used, where the Laponite RD powder was directly dispersed into the salt solution. With this protocol, it was observed that for high salt concentrations (≥ 0.05 M) flocculation occurs at all clay concentrations in which a grey, turbid phase separates from a clear, supernatant liquid (Figure 7.12). The only difference between using a magnetic stirrer and a high energy ultrasonic probe to disperse the clay particles into the salt solution is that the sedimentation of particles slows down when using the ultrasonic probe and more stable dispersions are obtained (0.01 and 0.05 M NaCl) compared to just using the magnetic stirrer where the particles sediment much quicker and bigger volumes of clear supernatant liquid are observed. It can be seen that at the same clay concentration, the volume fraction of flocculated (sedimentation) phase decreases with increasing salt concentration.

Figure 7.12 Photo taken after stirring the glass vessels (a) simply by using a magnetic stirrer for 15 minutes or (b) by using an ultrasonic probe for 2 minutes, containing 20 mL dispersions of 2 wt. % Laponite RD at different [NaCl].

(a)
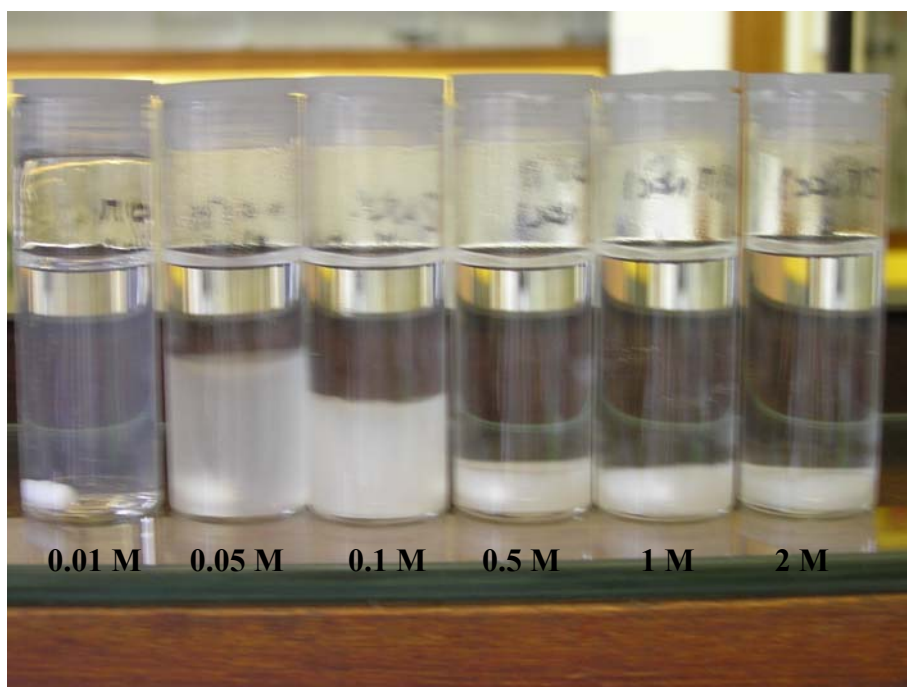
(b)
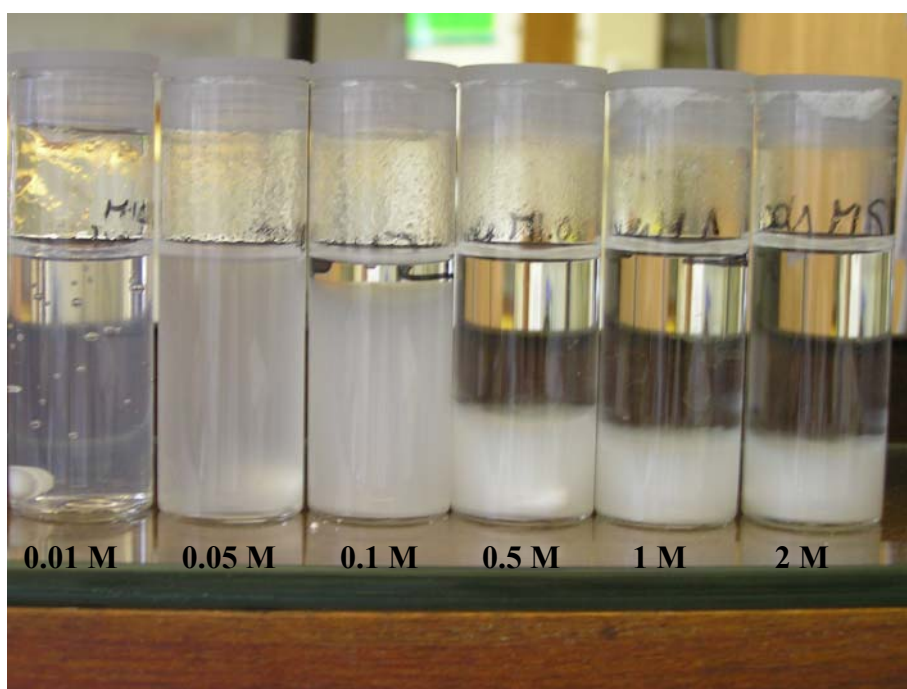
Figure 7.13 shows the appearance of vessels of Laponite RD dispersions at different clay concentration and at a fixed [NaCl] = 1M. It can be seen that the volume fraction of the flocculated phase increases with Laponite concentration as expected. A partial phase diagram is given in Figure 7.14.

Figure 7.13 Photo taken one day after shaking the glass vessels containing 20 mL aqueous dispersions of Laponite RD at different concentrations and [NaCl] = 1M at pH ~ 9 (protocol 2).
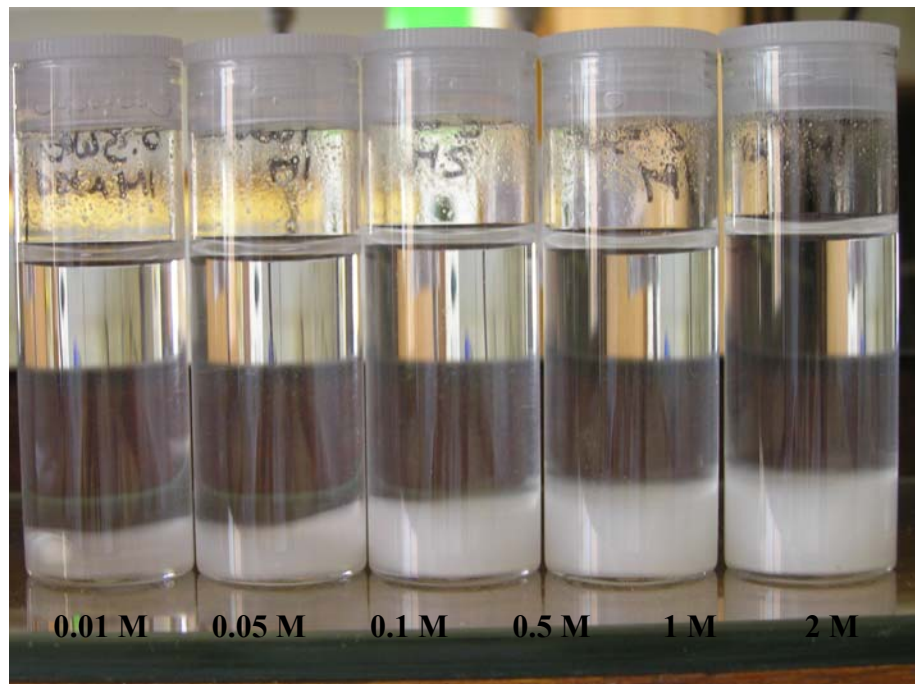
Figure 7.14 Partial phase diagram of 20 mL aqueous Laponite RD dispersions at pH in the range 8.5 – 10 in the presence of NaCl at room temperature (~ 21 ºC) using protocol 2. Points along the abscissa (0.001M NaCl) refer to dispersions containing no added electrolyte.

◇ clear fluid

△ clear gel, flow

■ turbid floc + clear liquid supernatant

▲ sligtly turbid gel (didn't flow upon reversal of tube)

● slightly turbid viscous
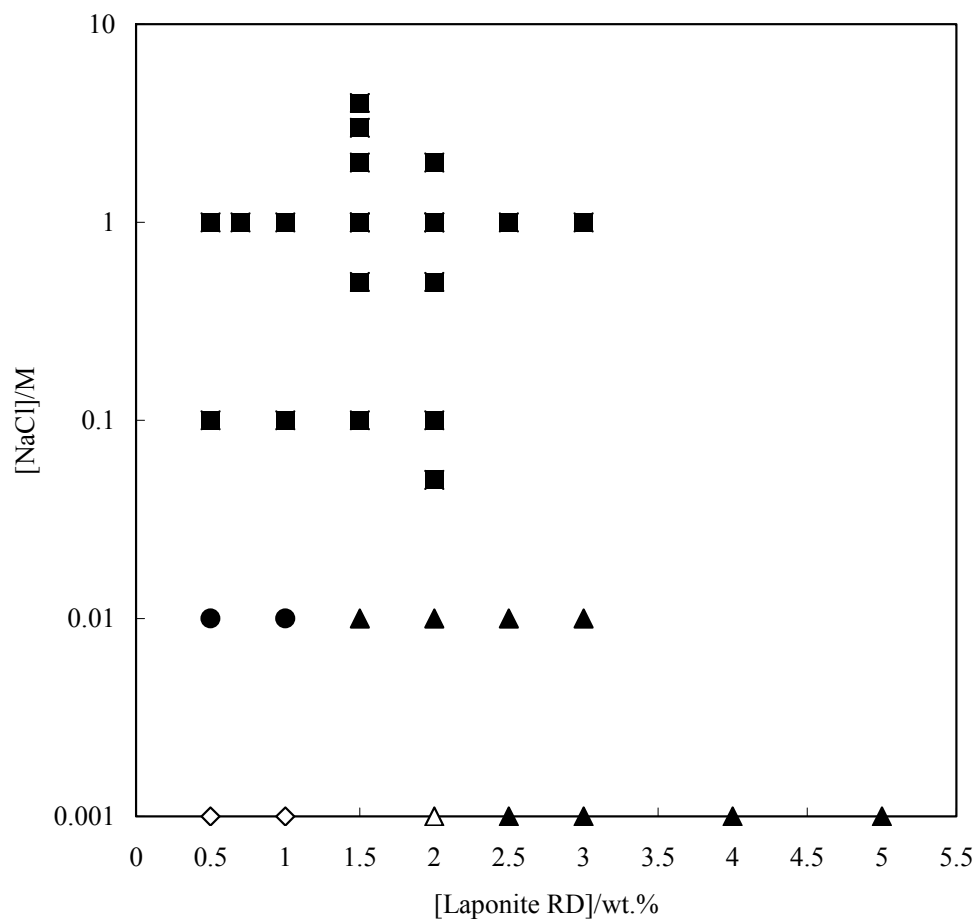
7.3   Foamability of Laponite RD dispersions in aqueous NaCl – protocol 1

In this study, by dispersing Laponite RD first in salt-free water and subsequently adding the salt (protocol 1), homogenous dispersions at higher salt concentrations were obtained. To understand how the [NaCl] in the dispersions would affect the nature and amount of foaminess, a systematic study was carried out for concentrations of NaCl in the range 0.01 to 4 M at a fixed concentration of Laponite RD and pH ~ 8.5 - 10. The shake test was the method used to determine the foamability. When Laponite RD powder was dispersed in water (without NaCl) such particles do not cause foaming. At low clay concentration (0.5 wt. %) and at low salt concentrations, no foams were observed. Only when the salt concentration was ≥ 0.5 M, were small volumes of foam observed (foamability) which increased slightly with [NaCl] (see Figures 7.15 and 7.16). However the foam stability was negligible as all foams burst very quickly, within seconds.

Figure 7.15 Photo taken after a few seconds of shaking the glass test tubes containing 20 mL dispersions of 0.5 wt. % Laponite RD at different [NaCl] (a) 0.5 M, (b) 1 M, (c) 2 M, (c) 3 M; pH ~ 8.5 - 9 (protocol 1).
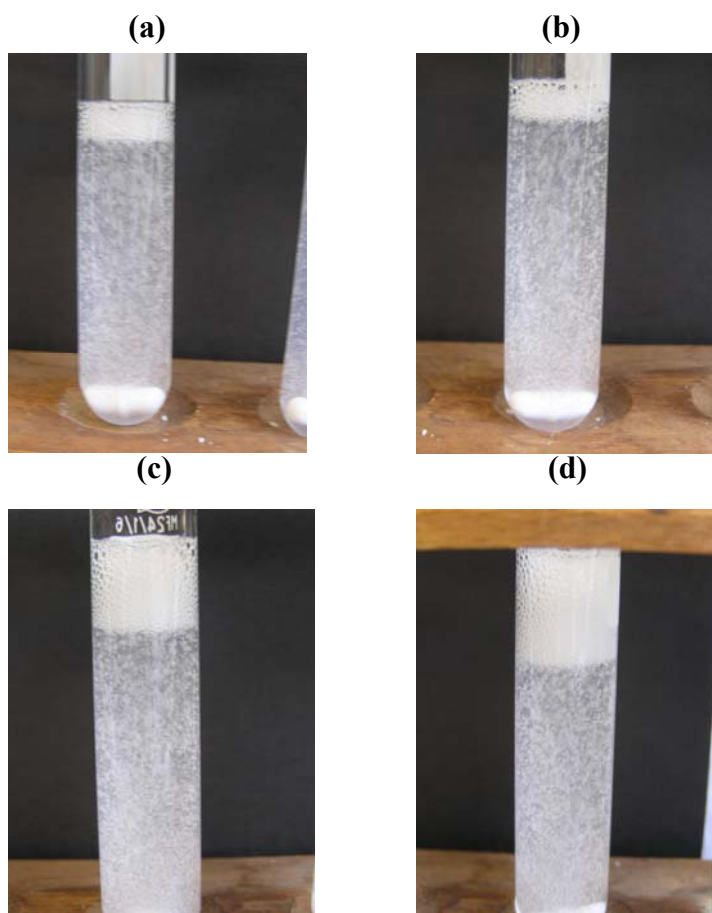
Figure 7.16 Initial foam height versus NaCl concentration for 0.5 wt. % aqueous dispersions of Laponite RD particles (protocol 1).
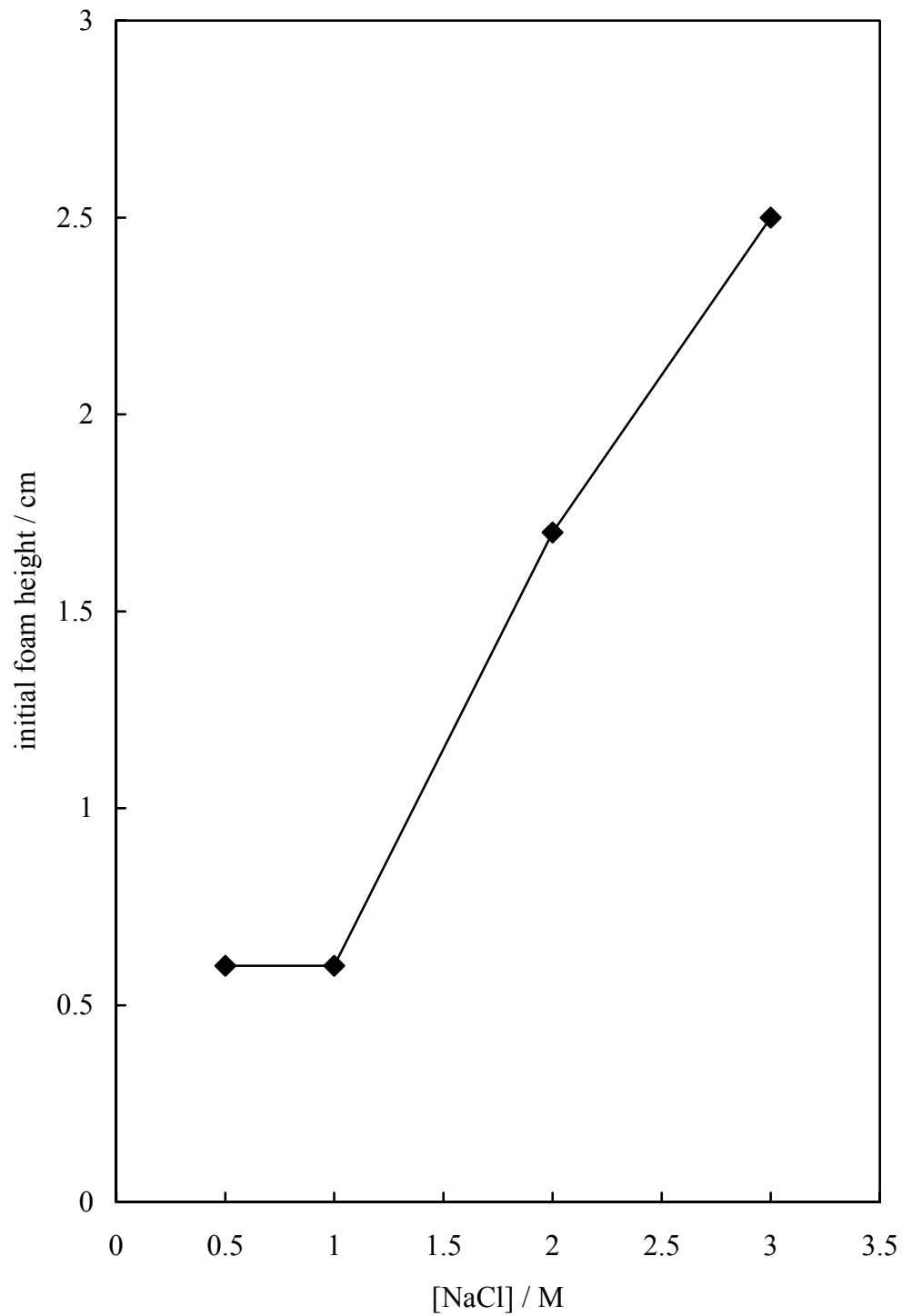
The bubbles were polydisperse in size with an approximate diameter of 0.5-3 mm, with smaller size bubbles at the bottom and the bigger bubbles arising at the top. However, when high salt concentrations (≥ 0.5 M) are added to an intermediate narrow range of clay concentration (1.5 – 2 wt. %), the dispersions become less gelled and give rise to more bubbles. Only a few bubbles reach the surface of the dispersion but they burst very quickly (in seconds) and the majority of bubbles get trapped in the gel. Some clear examples are given in Figure 7.17.

Figure 7.17 Photo taken a few minutes after shaking the glass test tubes containing 20 mL dispersions of 1.5 wt. % Laponite RD at different [NaCl] (a) 0.01 M, (b) 2 M, (c) 3 M and (d) 4 M at pH ~ 8.5 - 9.5 (protocol 1).

(a)　　　　**(b)**　　　　**(c)**　　　　**(d)**
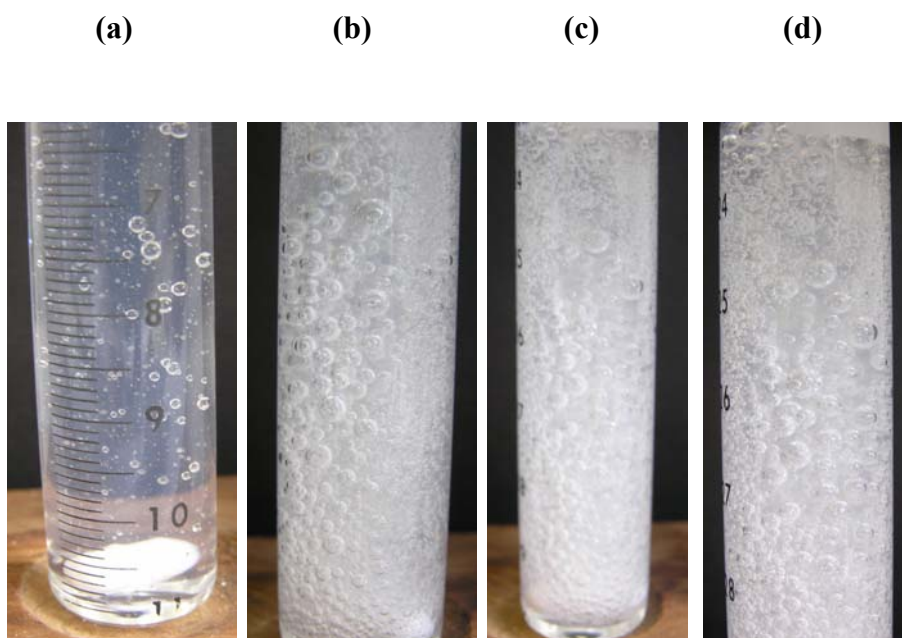
Because of the higher volume content of bubbles in these dispersions, they become lighter and after one day these gelled dispersions rise to the top and the bubble - free liquid can be observed at the bottom. Some of these dispersions contained a clear liquid simultaneously at the top and bottom leaving the Laponite RD gel in the middle (Figure 7.18). However, these are only observed with clay dispersions of intermediate concentration (1.5 – 2 wt. %) and at high salt concentration (≥ 0.5 M).

Figure 7.18 Photo taken after shaking the glass test tubes and leaving to stand at room temperature for one day containing 20 mL dispersions of 1.5 wt. % Laponite RD at different [NaCl]: (a) 0.5 M, (b) 1 M, (c) 2 M and (d) 3 M at pH ~ 8.5 - 9.5 (protocol 1).
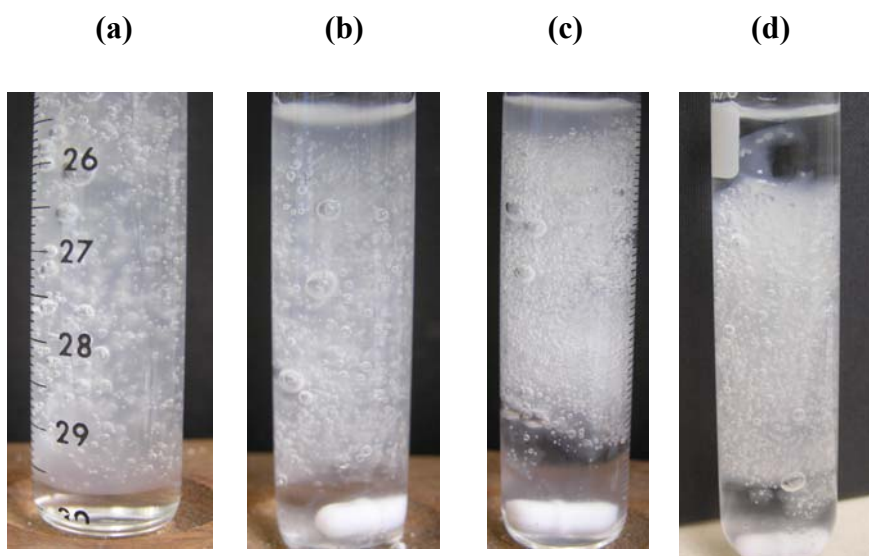
It is known and shown in Chapters 3 and 4 that the addition of salt may increase the particle hydrophobicity and therefore, foaming ability and stability may be enhanced. However, the foams produced here were very unstable. This may be due to the fact that these clay particles are too small. Since the energy of attachment of a particle to an interface, E, depends on the square of the particle radius, it decreases markedly for very small particles and detachment is easy and therefore they may not be too effective as foam stabilisers compared to larger particles. Therefore, it can be concluded that the size of particles has important implications with respect to the rate at which particles can diffuse and arrive at the surface of newly formed bubbles, to prevent disproportionation. Also, in order to enhance foamability, particles should be able to promptly adsorb on the air bubble surface, thus if the aqueous phase is gelled quickly, particles will lose their mobility and this will hinder foam formation. This could explain why no foams were produced when high concentrations of Laponite RD particles were used as they gelled very quickly. These results are in agreement with the results obtained with the smaller hydrophilic silica particles studied (< 100 nm) in Chapter 3.

7.4   Foamability of Laponite RD dispersions in aqueous NaCl – protocol 2

This section describes some examples of the effect of NaCl and particle concentration on the foamability of Laponite RD dispersions prepared by using protocol 2. It was observed that only at high salt concentrations (> 0.5 M) reasonable foam volumes could be obtained but they are very unstable as with protocol 1. However, the higher the salt concentration, the faster is the sedimentation of particles at the bottom of dispersions at all clay concentrations. Figure 7.19 shows the appearance of foams formed after hand shaking under the conditions described and Figure 20 shows the respective foam data plotted.

Figure 7.19 Photo taken immediately after shaking tubes containing 10 mL aqueous Laponite RD dispersions with [Laponite RD] = 1.5 wt. % at different [NaCl] in M (a) 1, (b) 2, (c) 3, (d), (e) and (f) 4 at pH around 8 - 10 (protocol 2).
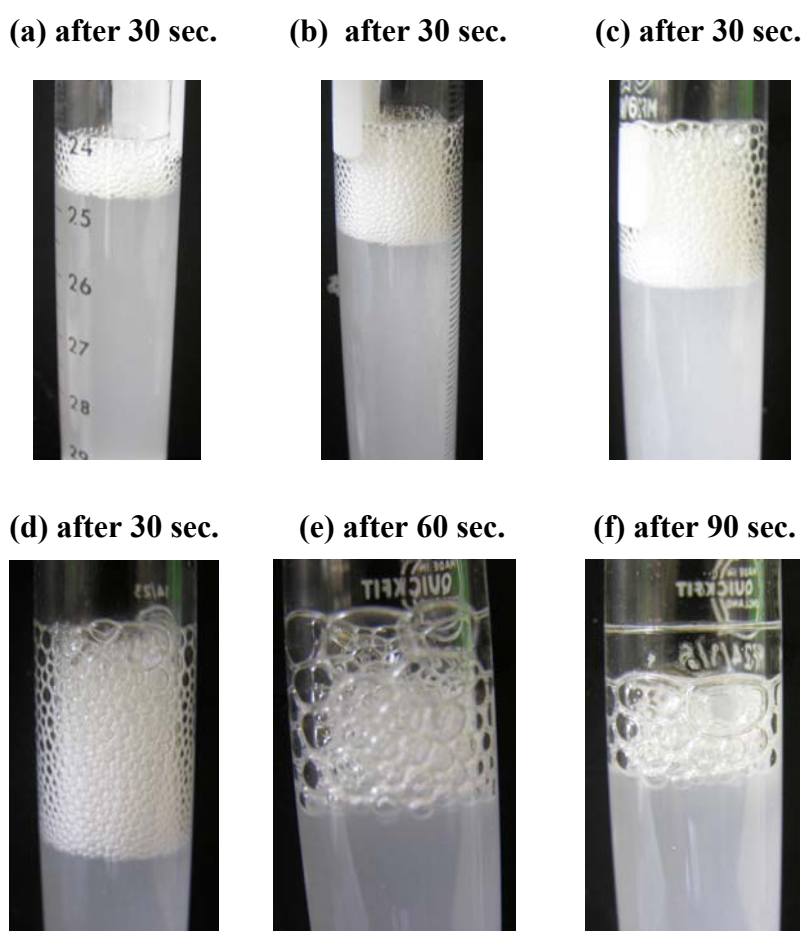
(a) after 30 sec.   **(b) after 30 sec.**   **(c) after 30 sec.**

(d) after 30 sec.   **(e) after 60 sec.**   **(f) after 90 sec.**

Figure 7.20 Initial foam height versus NaCl concentration for 1.5 wt. % aqueous dispersions of Laponite RD particles (protocol 2).
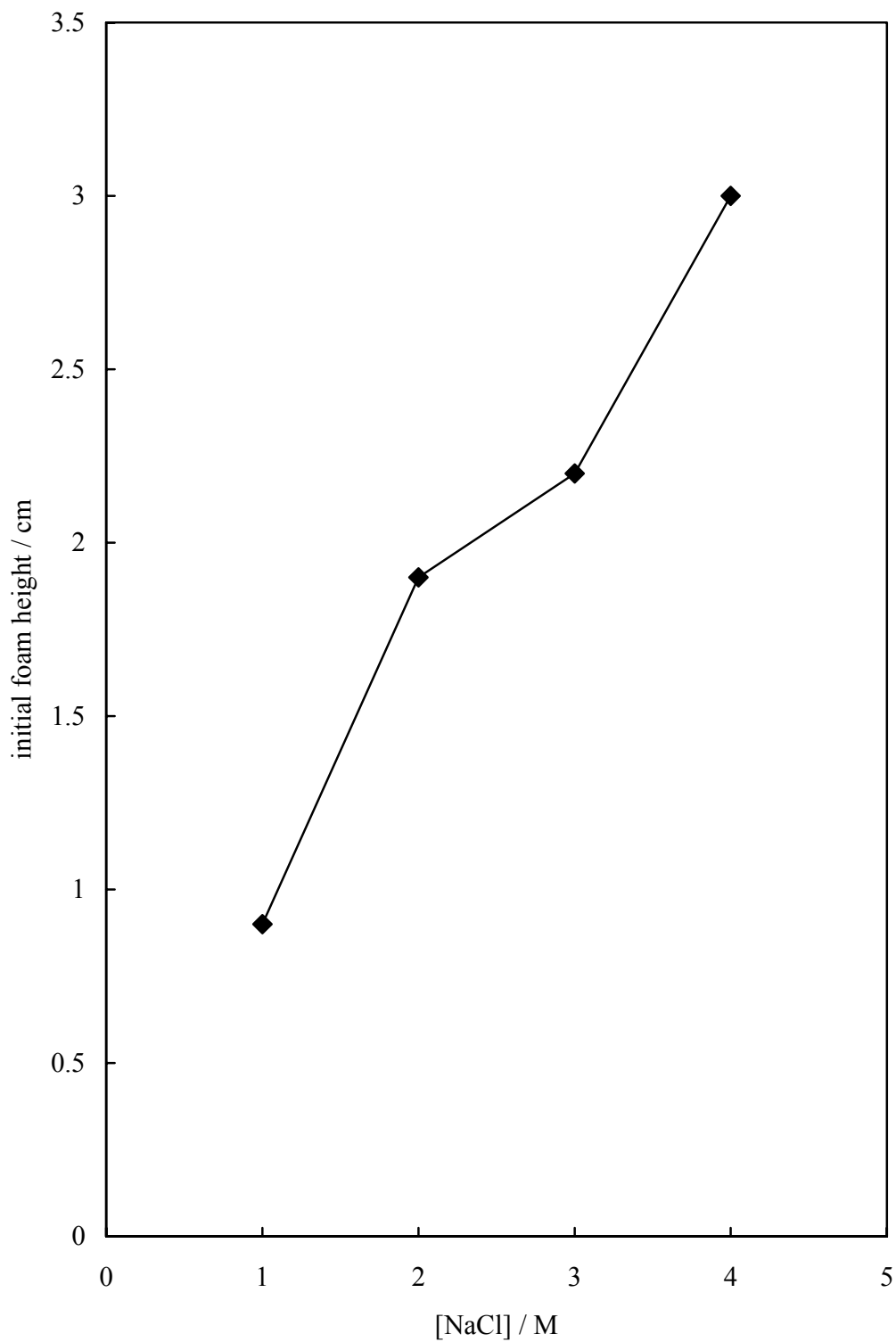
Figure 7.21 shows that very similar results are obtained for a higher clay concentration (*e.g.* 4 wt. %) at 2 M NaCl.

Figure 7.21 Images taken at different time periods after shaking the glass test tubes containing 10 mL Laponite RD dispersions with [Laponite RD] = 4 wt. % and [NaCl] = 2 M, pH around 8.5 (protocol 2).

(a) after 30 sec.   **(b) after 60 sec .**

(c) after 15 min.   **(d) After one day**
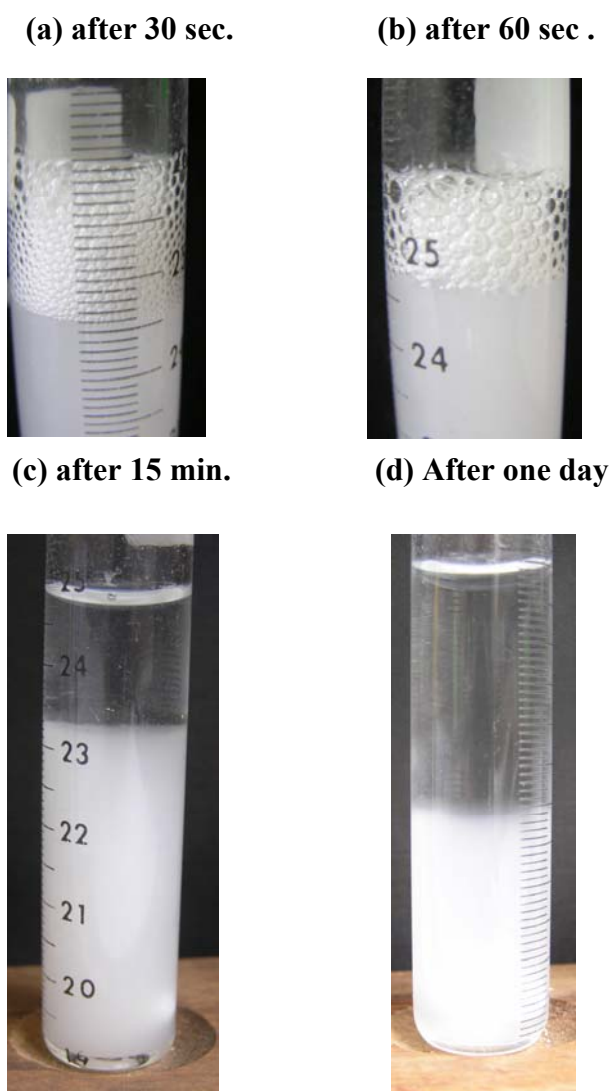
By linking the previous results shown in the phase diagram in Figure 7.15 with the foaming results obtained here it can be concluded that foams only appeared when [NaCl] > 0.5 M and at all Laponite RD concentrations, where flocculation of particles occurred. However, the foams formed were very unstable and particles sediment. As explained before in section 7.3, the clay particles may be too small and therefore easily detached from the air-water interface.

7.5   Other electrolytes

The foaminess of ocean waves, relative to fresh water, has long been attributed to the effect of salts in reducing bubble coalescence. This phenomenon is exploited in extraction processes using froth flotation[22], in which the extraction efficiency increases as the bubble size gets smaller. The bubble-stabilizing effect of surfactants is well understood, whereas the effect of salts is not. A study concerning the stabilization of bubbles by salts has been reported.[23] They found that bubble coalescence is inhibited by some salts whereas others have no effect and that this inhibition occurs only upon the 'matching' of a two-valued empirical property assigned to each anion and cation. They believe that those observations could be explained only by the local influence of the ions on water structure, possibly related to the hydrophobic interaction.[24]Another study concerning the flotation of hydrophobic graphite particles in aqueous solutions of inorganic electrolytes has been reported.[3] They found that electrolytes with divalent or trivalent cations or anions gives a high flotation response when compared with monovalent cations or anions. They have shown a correlation between the double layer length $(1/\kappa)$ and the flotation performance, which suggests that the electrostatic interaction plays an important role in the flotation process. Overall, high flotation recoveries were attributed to an increase in the bubble-particle collision probability and possibly bubble entrainment floc flotation. This resulted from the higher concentration of smaller stable bubbles and also a reduction in the electrostatic interactions between particle and bubble.

The effect of different electrolytes (*e.g.* $MgCl_2$ and $LaCl_3$) on the foamability and foam stability of aqueous Laponite RD dispersions was investigated in order to know whether the cation (*e.g.* Na^+, $Mg^{2+,}$ La^{3+}) have an influence on the wettability of the Laponite RD particles. First, the effect of particle and $MgCl_2$ concentration on the foaming ability and foam stability of Laponite RD aqueous dispersions at pH around 6.3 - 7.8 was investigated using protocol 1. The results revealed that at low $[MgCl_2]$ (Figure 7.22.) only dispersions of [Laponite RD] $\geq$ 2 wt. % become completely gelled (not flowing). With the lowest concentration of Laponite RD studied (Figure 7.23), gels did not formed at any concentration of $MgCl_2$ added. All dispersions sediment with time and a clear supernatant was observed at the top of dispersions.

Figure 7.22 Images taken a few minutes after shaking the glass tubes containing 20 mL dispersions at different [Laponite RD]; (a) 0.5 wt.%, (b) 1 wt.%, (c) 2 wt.%, (d) 2.5 wt.% and (e) 3 wt.% and fixed [$MgCl_2$] = 0.01 M at pH around 7.8.
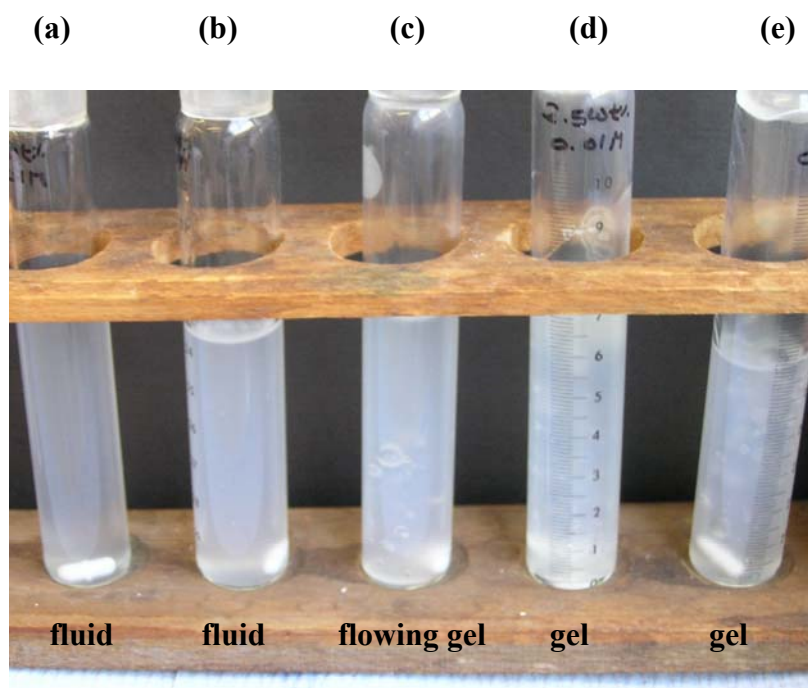
Figure 7.23 Images taken one day after shaking the glass tubes containing 20 mL dispersions of [Laponite RD] = 0.5 wt.% at different [$MgCl_2$]; (a) 0.01 M, (b) 0.05 M, (c) 1 M and (d) 2 M at pH = 6.3 – 7.8.
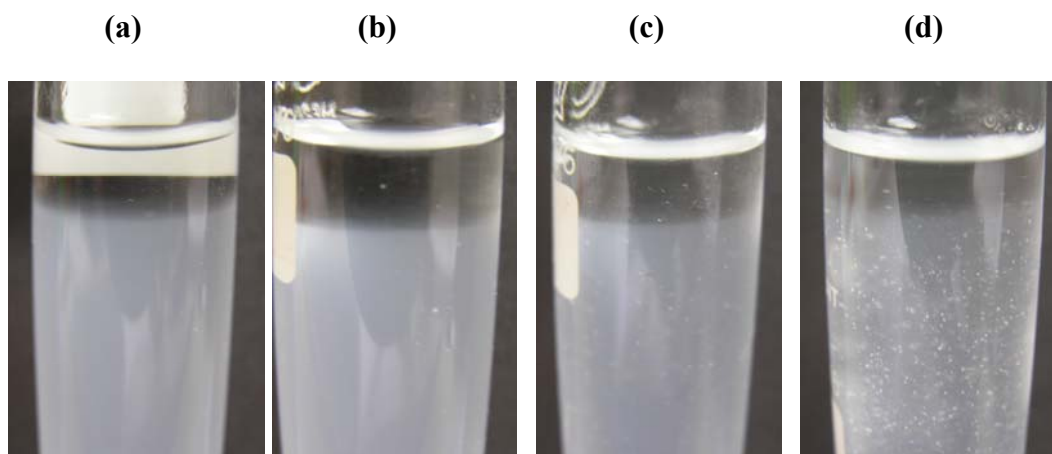
At a fixed $[MgCl_2] = 1$ M, dispersions containing the lowest amount of Laponite RD (*e.g.* 0.5 wt. %) start to sediment quicker due to their fluidic consistence. After a few hours a clear supernatant was observed (see Figure 7.24. (a) and (b)) while the ones with higher concentration were more viscous and therefore only after one day a very small supernatant was observed (see Figure 7.26 (c), (d) and (e)).

Figure 7.24 Photo taken one week after shaking the glass tubes containing 20 mL dispersions at different [Laponite RD]; (a) 0.5 wt.%, (b) 1 wt. %, (c) 2 wt. %, (d) 2.5 wt.% and (e) 3 wt.% , at a fixed $[MgCl_2] = 1$ M and pH ~ 6.8. (a) and (b) are fluid. (c) to (e) are viscous.
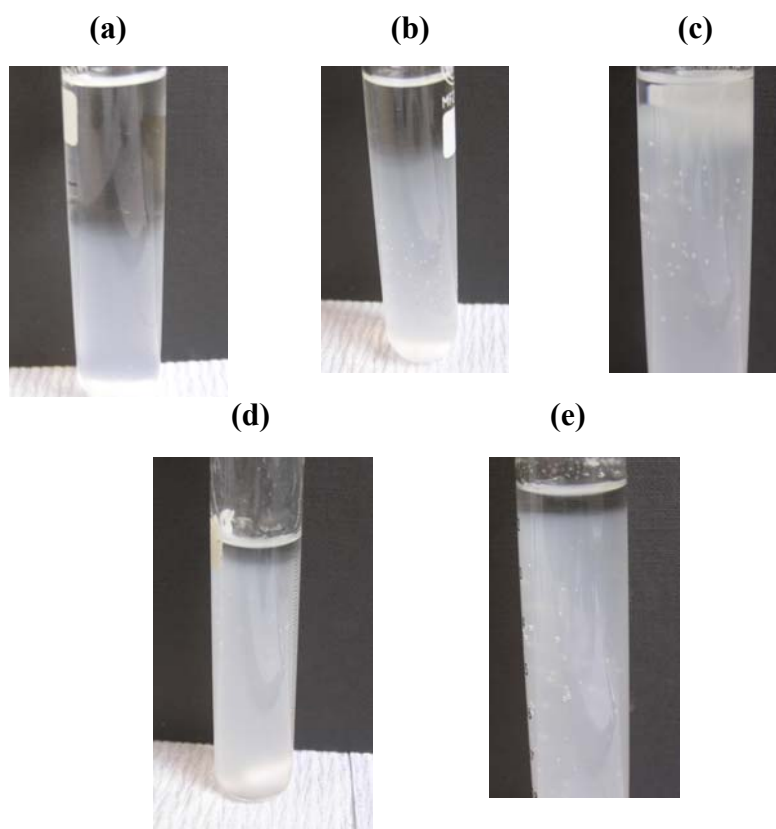
At a fixed [Laponite RD] = 2 wt. %, the lower the $[MgCl_2]$ added to the dispersion the more gelled (not flow) the dispersion becomes (Figure 7.27 (a) to (c)) and only a few bubbles were formed and get trapped in the gel. At a higher concentration of $MgCl_2$ (Figure 7.25 (d) and (e)), more bubbles are formed within the flowing gel and bubbles rise quicker to the surface giving a small foam at the top of dispersion. However, once they reach the surface they burst very quickly. Similar results were obtained when NaCl was used.

Figure 7.25 Images taken 2 minutes after shaking the glass tubes containing 20 mL dispersions of [Laponite RD] = 2 wt. % at different [MgCl₂]; (a) 0.01 M, (b) 0.05 M, (c) 0.1 M, (d) 0.5 M, (e) 1 M and (f) 2 M and pH ~ 6.3 - 7.8.

    (a)   (b)   (c)   (d)   (e)   (f)

pH =   7.8   7.6   7.4   7.0   6.8   6.3
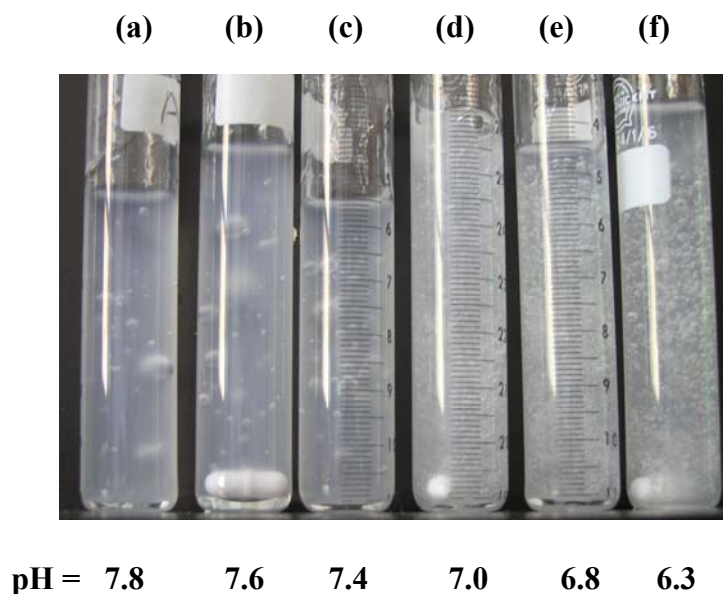
The effect of Laponite RD particles and LaCl₃ concentration on the foaming ability and foam stability of Laponite RD aqueous dispersions was also investigated. When a high concentration of LaCl₃ (*e.g.* 2 M) was dispersed in water without Laponite RD particles, a dark solution was observed which become hot and gas was released (clouds of steamy fumes of hydrogen chloride is produced). Hydrogen ions and chloride ions in the mixture combine together as hydrogen chloride molecules and are given off as a gas. However with a large excess of water, the temperature never gets high enough for that to happen, the ions just stay in solution. After shaking the vessel containing an aqueous solution of LaCl₃ (*e.g.* 2 M), small bubbles appear at the top of vessel but burst immediately. Therefore, it can be concluded that LaCl₃ alone is not surface-active.

The pH is more or less independent of clay concentration but decreases systematically with an increase in [LaCl₃]. By only adding [LaCl₃] = 0.5 M, the pH of the initial Laponite RD dispersion (pH ~ 10) decreases to about 6. Aqueous solutions of LaCl₃ contain moderate concentrations of hydrogen ions and can react as acids to neutralize bases. Figure 7.26 shows images of foams formed by shaking dispersions of Laponite RD particles at a fixed particle concentration of 0.5 wt. % at different [LaCl₃].

Figure 7.26 Images taken after shaking the glass tubes containing 20 mL dispersions of [Laponite RD] = 0.5 wt.% at different [LaCl₃]; (a) 0.5 M, (b) 1 M and (c) 2 M and pH around 4.8 - 6.2 at the times indicated.

Immediately after shake test (30 seconds)
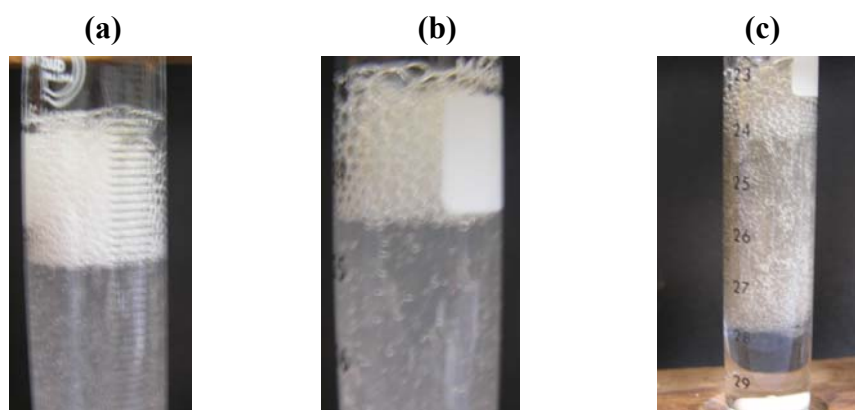
After 5 minutes
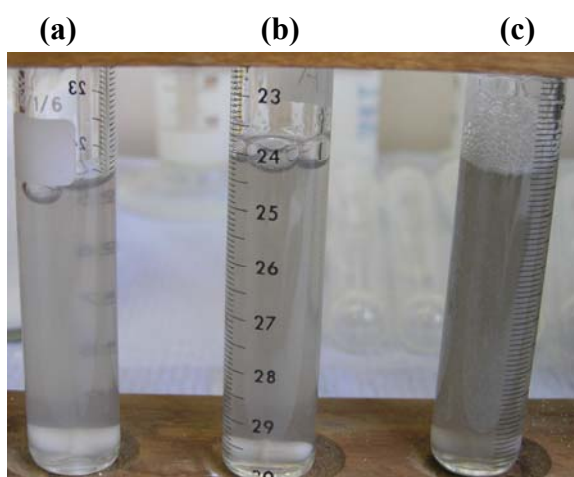
After one day
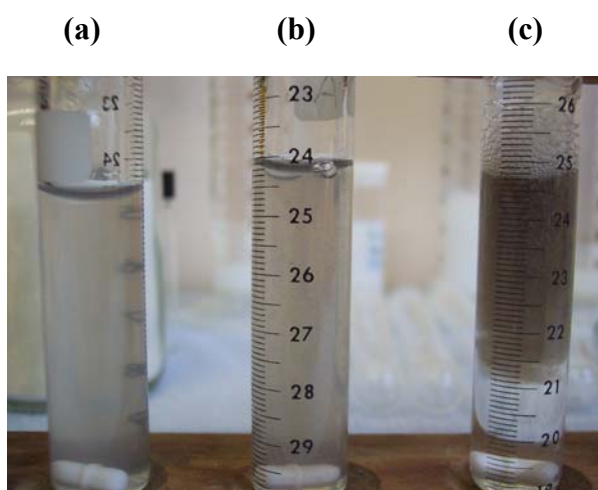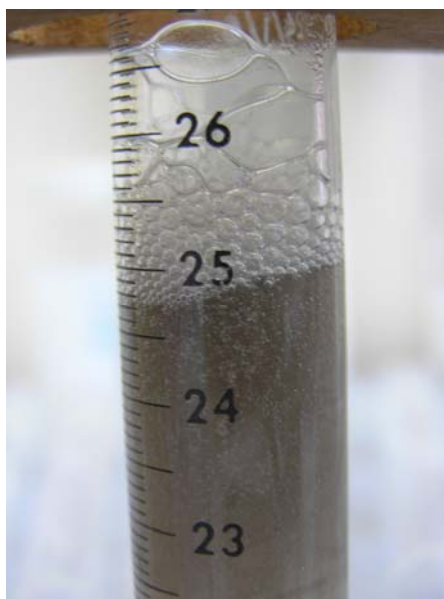
The higher the [LaCl$_3$] added (*e.g.* 2 M) to the Laponite RD dispersions containing a fixed particle concentration of 0.5 wt. %, the darker and viscous the dispersion becomes and a strong exothermic reaction happened. As a result the foam produced was very stable, while at a lower concentration of LaCl$_3$ the dispersions were fluid and the bubbles produced burst completely after a few minutes. The increase in foam stability with a higher concentration of LaCl$_3$ may be linked to the increased bulk viscosity of the dispersion with solids content. Another greater stabilizing action conferred by solid particles is achieved if the particles are partially hydrophobic. They are then kept at the air-water surface by surface forces, in the same way as lipophilic molecules are adsorbed there. Therefore, the presence of LaCl$_3$ may be increasing the hydrophobicity of the Laponite RD particles and foam lamellae carry these particles upward with the foam, a phenomenon on which is based the process of ore flotation. The particles at the surface of the lamellae add considerably to foam stability by adsorbing at the air-water surface.

The effect of [LaCl$_3$] on the foaming ability and stability of aqueous Laponite RD dispersions at a fixed particle concentration of 1 wt. % was also investigated (see Figure 7.27). It was observed that the higher the concentration of LaCl$_3$ used the higher the formation and rising of bubbles to the surface and the more stable the foam formed. Especially, in the case where the dispersion quickly gels (*e.g.* LaCl$_3$ = 2M), the foam formed at the top of the vessel remains stable for months (see Figure 7.28). Figure 7.29 shows images of the stable foam formed by shaking a dispersion of Laponite RD

particles at a fixed particle concentration of 1 wt. % and [LaCl$_3$] = 2 M. As it can be seen in the images, the supernatant at the bottom of the vessel increases with time due to drainage but the bubbles trapped in the gelled dispersion and in the foam (top) are stable against coalescence.

Figure 7.27 Images taken a few seconds after shaking the glass tubes containing 20 mL dispersions of [Laponite RD] = 1 wt.% at different [LaCl$_3$]; (a) 0.5 M, (b) 1 M and (c) 2 M and pH around 4.8 – 6.2.

(a) (b) (c)
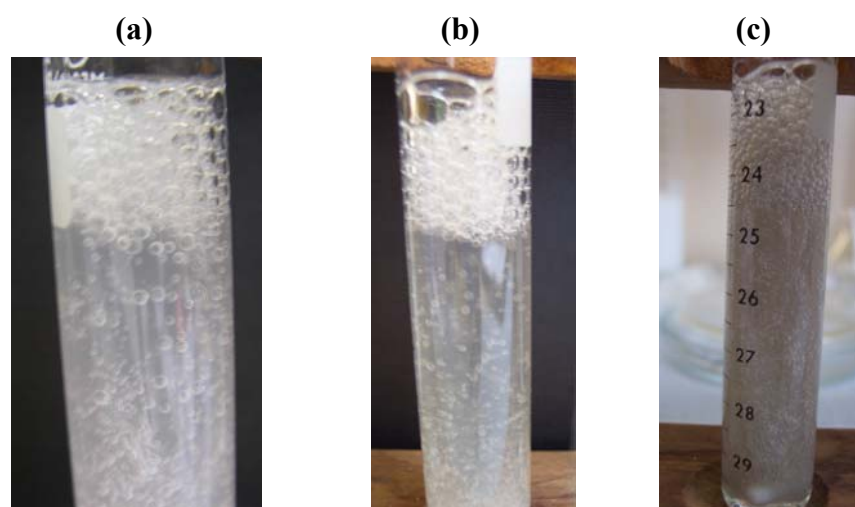
Figure 7.28 Images taken two months after shaking the glass tubes containing 20 mL dispersions of [Laponite RD] = 1 wt.% at different [LaCl$_3$], (a) 0.5 M, (b) 1 M and (b) 2 M and pH around 6.2 - 4.8.

(a) (b) (c)

viscous   flowing gel   gel (does not flow)
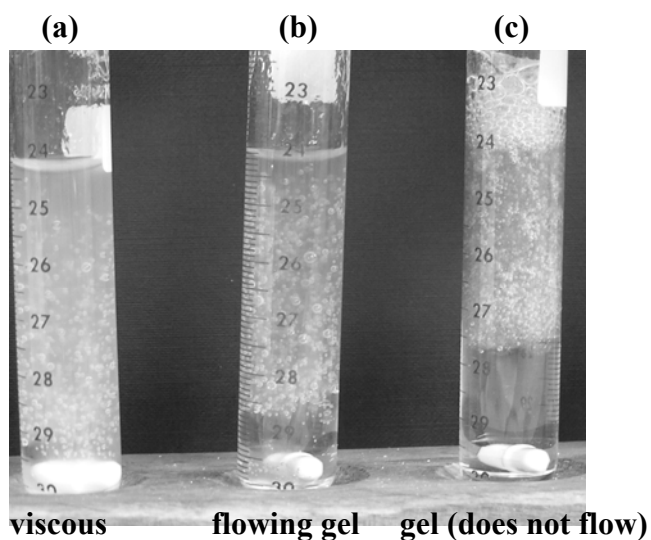
Figure 7.29 Images taken at different times after shaking the glass tube containing 20 mL dispersion of [Laponite RD] = 1 wt. % at [LaCl₃] = 2 M and pH ~ 4.8.

after 30 minutes   after 2 hours   after one month
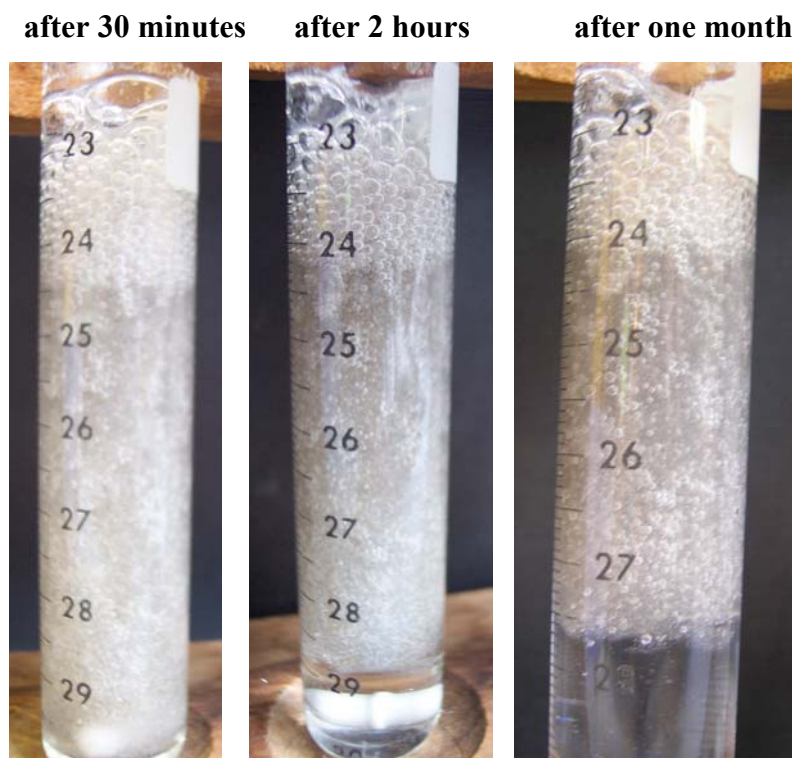
It can be concluded that the foaming ability of the Laponite clay particles increases with the addition of salt (monovalent, divalent or trivalent cations). The higher the concentration of salt (*e.g.* 2-3 M) and the higher the valence of the cation (e.g. LaCl₃) the bigger were the foams produced (see Figure 7.30). However, most of the foams produced here were very unstable and burst in a few seconds. It was clearly observed that not all the particles are in the foam, which could explain their instability. Only the foams produced with the highest concentration of LaCl₃ (*e.g.* 2-3 M) were very stable against coalescence and disproportionation. The long term foam stability achieved with such systems can be attributed to the aqueous dispersion being gelled (solid) after the formation of the bubbles. Therefore, the viscous and elastic nature of the continuous phase and surface of bubbles can be related to the bubble stability observed here. This can be observed with other systems such as ice cream where the long tem bubbles stability is attributed to the thickening of the aqueous phase (*e.g.* polysaccharides) and the fact that the product has being frozen (becomes solid).

Figure 7.30 Initial foam height versus different types of electrolytes concentration (triangles – LaCl$_3$, diamonds – MgCl$_2$, circles – NaCl) for 0.5 wt. % aqueous dispersions of Laponite RD particles (protocol 1).
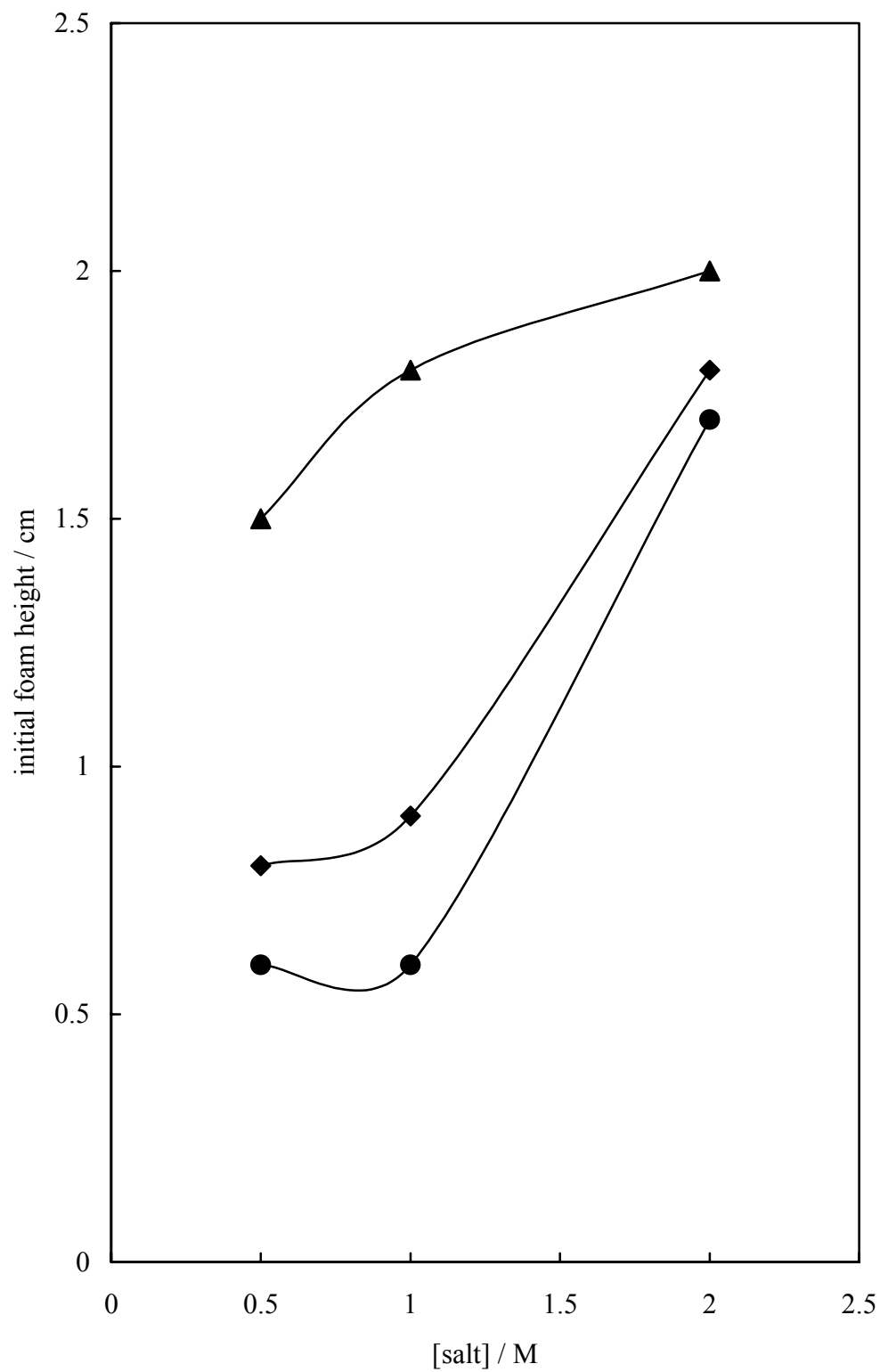
7.6   Conclusions

In order that comparisons can be made with the previous work employing colloidal silica, sodium chloride (NaCl) has been used to investigate the possibility of preparing stable foams containing Laponite RD particles. The aim was to link the foamability and foam stability to the structure of the aqueous dispersions. Laponite RD dispersions have been prepared at either constant particle concentration with increasing concentration of NaCl, or at constant NaCl concentration for a range of clay concentrations by using two different protocols. The effect of others electrolytes such as $MgCl_2$ and $LaCl_3$ on the foaming ability and stability of aqueous Laponite RD was also investigated.

It can be concluded from linking the phase diagrams of NaCl, water and Laponite RD clay particles from both protocols 1 and 2 that foams are only formed under conditions where the particles are flocculated (*via* salt) but not gelled. All foams formed are very unstable (burst within seconds or minutes) and after one day sedimentation of particles occurs, in which a grey, turbid phase separates from a clear, supernatant liquid. When the foam shake test is applied to dispersions of Laponite RD that quickly become gel, bubbles are formed which get trapped within the gel. Addition of salt may be responsible for an increase in the contact angle that Laponite RD particles makes with the air – water surface, therefore increasing their hydrophobicity. However, the fact that these foams are unstable may be attributed to various reasons. One factor is the size of these clay particles, as they are very small and therefore can be easily detached from the air-water interface. Another reason may be the fact that the aqueous phase is gelled quickly and particles lose their mobility, thus hindering foam formation. This could explain why no foams were produced when high concentrations of Laponite RD particles were used as they gelled very quickly.

The results obtained with $MgCl_2$ by using protocol 1 were very similar to those obtained with NaCl. Stable foams were only formed at high $[LaCl_3]$ *e.g.* 2 M, even at lower [Laponite RD] = 1 wt. %, where dispersions become gelled (not flowing) and a supernatant starts to appear at the bottom of the vessel with time. Aqueous dispersions of Laponite RD containing $[LaCl_3]$ < 2 M, also gave reasonable foams at the top of dispersions (foamability), however those foams were very unstable and burst very quickly. These dispersions were viscous (flowing gels) with bubbles trapped in the gel and a supernatant was observed at the bottom with [Laponite RD] $\geq$ 1 wt. % or at the top when [Laponite RD] < 1 wt. %. Foam stability was only achieved with Laponite RD

particles and [LaCl$_3$] > 2 M and this may be attributed to the fact that the foam is formed just before the aqueous phase becomes gelled (solid). So some particles go to the air-water interface, conferring stability to the newly formed bubbles. Also the viscosity and elastic nature of the continuous phase and surface of bubbles gives the long term stability achieved with such systems.

References

1.   R.J. Hunter, Introduction to Modern Colloid Science, Oxford Science Publications, New York (1993).

2.   N.P. Ashby and B.P. Binks, *Phys. Chem. Chem. Phys*., **2**, 5640 (2000).

3.   O. Paulson and R.J. Pugh, *Langmuir*, **12**, 4808 (1996).

4.   B. Dobias, in *Coagulation and Flocculation: Theory and Applications*, Surfactant Science Series, Vol. 45, Marcel Dekker, New York, p. 428 (1993).

5.   Laponite Technical Bulletin, L104.90/A, Laponite − structure, chemistry and relationship to natural clays, Laporte Industries Ltd. (1990).

6.   R. Perkins, R. Brace and E. Matijevic, *J. Colloid Interface Sci*. **48**, 417 (1974).

7.   M. Kroon, Structure and Formation of a Gel of Colloidal Particles, Ph.D. thesis, University of Amsterdam (1998).

8.   Laponite - The Technical Directory, Laport Industries Ltd., Widness, U.K. (1999).

9.   Laponite Performance - Focused attributes in rheology and speciality film forming applications, CommuniClay, Rockwood Specialities Inc., Vol. 1, issue 3 (2001).

10.   D.W. Thompson and J.T. Butterworth, *J. Colloid Interface Sci*., **151**, 236 (1992).

11.   J.M. Saunders, J.W. Goodwin, R.M. Richardson and B. Vincent, *J. Phys. Chem. B*, **103**, 9211 (1999).

12.   K. Norrish, *Discuss. Faraday Soc*., **18**, 120 (1954).

13.   H. van Olphen, An Introduction to Clay Colloid Chemistry, 2nd Ed., Wiley, New York (1977).

14.   S.L. Tawari, D.L. Koch and C. Cohen, *J. Colloid Interface Sci*. **240**, 54 (2001).

15.   C. Martin, F. Pignon, A. Magnin, J.M. Piau, B. Cabane, P. Lindner and B. Cabane, *Phys. Rev. E*, **66**, 021401 (2002).

16.   M. Kroon, W. L. Vos and G. H. Wegdam, *Phys. Rev. E*, **57**, 1962 (1998).

17.   A. Mourchid, A. Delville and P. Levitz, *Langmuir*, **11**, 1942 (1995).

18.   R.G. Avery and J.D.F. Ramsay, *J. Colloid Interface Sci*. **109**, 448 (1986).

19.   M. Bellour, A. Knaebel, J.L. Harden, F. Lequeux and J.P. Munch, *Phys. Rev. E.*, **67**, 405 (2003).

20.   P. Mongondry, T. Nicolai and J.F. Tassin, *J. Colloid Interface Sci*. **275**, 191 (2004).

21. P. Mongondry, J.F. Tassin and T. Nicolai, *J. Colloid Interface Sci.*, **283**, 397 (2005).

22. V.I. Klasson and V.A. Mokrousov, An Introduction to the Theory of Flotation, Butterworths, London (1963).

23. V.S.J. Craig, B.W. Ninham and R.M. Pashley, *Nature*, **364**, 317 (1993).

24. J.N. Israelachvili and R.M. Pashley, *Nature*, **300**, 341 (1982).

CHAPTER 8

CHAPTER 8

PARTICLE - SURFACTANT INTERACTIONS IN FOAMS

8.1   Introduction

Much is known about the behaviour of emulsions, foams and thin films stabilised by surfactant molecules[1] and, more recently, those stabilised solely by solid particles.[2-6] Since many cosmetics (emulsions) or food related foams contain a mixture of both surfactant and particles, it is of interest to study foams stabilised by such mixtures. Addition of surfactant to particle systems or *vice versa* in relation to wetting and emulsification is not new.[7-12] Particle types have included silica, clay, alumina, barium sulphate and carbon with surfactants being cationic, anionic or polymeric.

The hydrophile-lipophile balance number of surfactant molecules is one parameter which determines both the type and stability of foams and emulsions using them.[13] Likewise, the hydrophobicity of particles at the air-water interface has been shown to be crucial in optimising the stability of solid-stabilised foams.[14,15] The hydrophobicity of the particles, as judged from the contact angle they make with an air-water surface, is deemed to be important in whether a particle can adsorb to and remain around bubbles in water. In most cases, particles form a dense layer on bubble surfaces preventing coalescence and slowing down or halting completely disproportionation.[16-19] Evidence also exists that additional stabilisation occurs *via* particle network formation between adsorbed and non-adsorbed particles reducing, in this case, drainage of water between bubbles.[20] Since many particle types are inherently hydrophilic attaching weakly to fluid interfaces, the two ways to increase their hydrophobicity are to hydrophobise the particles *ex situ* by chemisorption and *in situ* by physisorption. For the former, Binks and Horozov[3] using fumed silica nanoparticles coated to different extents with dichlorodimethylsilane groups showed that particles of intermediate hydrophobicity were the only ones capable of stabilising foams. For the latter, Gonzenbach *et al.*[21] achieved the required level of hydrophobisation by addition of short chain amphiphilic molecules which adsorbed on particle surfaces. However, surfactant addition to particle dispersions does not always lead to stable foams. Alargova *et al.*[2] found that mixtures of rod-shaped polymer particles and sodium dodecyl sulphate (SDS) produced foams which were as unstable as pure surfactant ones, whereas foams

of particles alone were stable indefinitely. It was hypothesised that SDS adsorption onto particles rendered them more hydrophilic reducing their affinity for the air-water surface. Subramaniam *et al.*[17] also reported the destabilisation of particle-coated bubbles in water when exposed to surfactant solutions by ejection of particles, explaining their findings in terms of relieving the stress in non-spherical, stable particle-coated bubbles.

This chapter is concerned with the interactions of oppositely charged mixtures of solid particles and a cationic surfactant, i.e. negatively charged silica particles with a positively charged surfactant called cetyltrimethylammonium bromide (CTAB). It's important to emphasise that cationic surfactants are not good detergents or foaming agents, nevertheless they exhibit very important features. Their positive charge allows them to adsorb on negatively charged substrates. For example, minerals with high silica content possess surface – OH groups that engage readily in ion exchange with cationic surfactant leaving the solid with a hydrophobic coating:

$$- SiOH + R_4N^+ \longrightarrow - SiO^- {}^+NR_4 + H^+$$

This capacity also confers to them an antistatic behaviour and a softening action for fabric and hair rising. Their positive charge also enables them to operate as flotation collectors, corrosion inhibitors as well as solid particle dispersants. They are also used as emulsifiers in emulsions and coatings in general, in inks, magnetic slurry, etc.

Despite some activity in this area, systematic studies of the behaviour and properties of foams in mixtures of surfactant and solid particles are lacking. The two materials, particles and surfactants, may act synergistically or antagonistically with respect to foam stabilisation. As a model system, we investigate here the foaming ability and stability of foams stabilised by either pure cationic surfactant, hydrophilic silica particles or their mixture. Additional experiments have been conducted in order to explain the findings including determination of the adsorption of surfactant onto silica, zeta potentials of particle dispersions, equilibrium air-water interfacial tensions and contact angles. Since surfactant adsorbs on particle surfaces, we have investigated the behaviour at different pH, one corresponding to a highly charged surface, another for an intermediate charged surface and the other close to its isoelectric point. If the CTAB surfactant adsorbs on silica particle surfaces, their wettability could be modified which could then affect their efficiency on foaming, either improving or reducing it. This

adsorption could also lead to particle aggregation which may or may not be advantageous to foam stability. However, if the surfactant does not adsorb on particles, *e.g.* they are of the same charge sign, the possibility exists that both species will compete for the air-water interface but one may dominate.

8.2   Properties systems containing CTAB or silica particles alone

A systematic study was carried out on the foaming ability (initial foam volume) and foam stability (time that foam decays) of aqueous dispersions of CTAB or silica nanoparticles alone by using the glass cylinder shaking method. The key parameters investigated were CTAB or particle concentration and the effect of pH. To understand how the concentration of CTAB alone affects the foaming ability and stability, a systematic study was carried out for five different concentrations of CTAB at different pH values. The critical micelle concentration (cmc) of CTAB is reported as 0.9 mM.[22] When the CTAB concentration was increased from 0.01 to 5 mM at a fixed pH, it was found that the foaming ability increased with surfactant concentration at all pH values (Figure 8.1). As a thermodynamically unstable system, the breakdown down of the foam is inevitable and therefore these surfactant – stabilised foams breakdown completely within one day at all concentrations and pH investigated. However, after 24 hours a few polydisperse dry bubbles still remained in the vessels containing the highest concentration of CTAB surfactant, which shows that the foam stability increased with surfactant concentration. The instability of these surfactant foams is mainly attributed to a combination of mechanisms including the drainage of water between bubbles, bubble coalescence and bubble disproportionation. As drainage and disproportionation proceed, bubbles nearer the top of the foam layer increase in size and become polyhedral in shape. The decrease in foam volume after a certain period of time corresponds to the rupture of the thin aqueous film between neighbouring polyhedral bubbles.

Figure 8.1 Effect of CTAB concentration on the foaming ability of solutions of 10 mL CTAB alone at different pH values at room temperature.
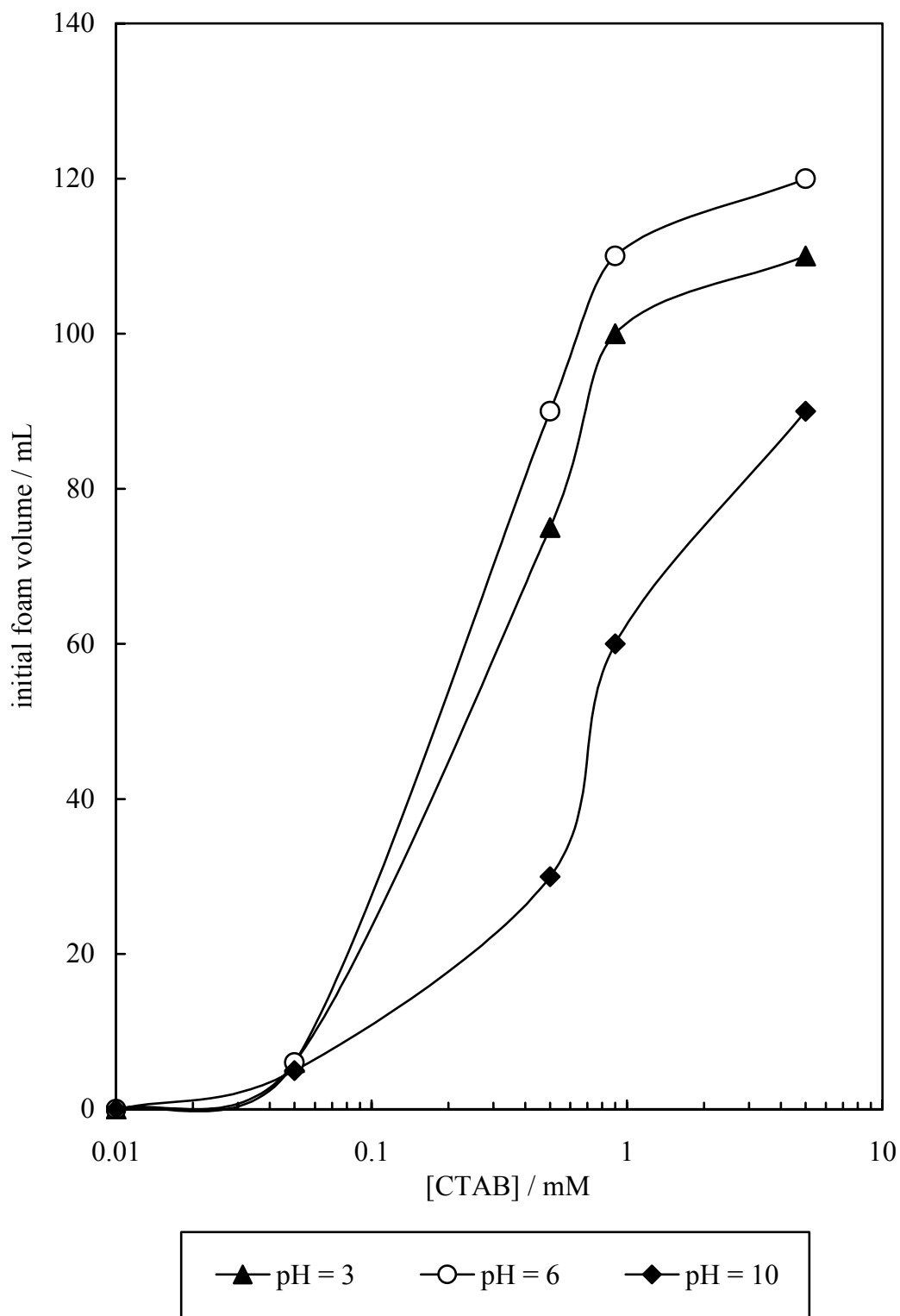
However, at the highest pH = 10 it is worth mentioning that the foamability of the surfactant solutions were slightly lower than at the pH = 3 and 6. Cationic surfactants are generally stable to pH changes, both acid and alkaline.[23] The CTAB surfactant dissociate in water according to $C_{16}H_{33}N(CH_3)_3Br \longrightarrow C_{16}H_{33}N^+(CH_3)_3 + Br^-$ with the positive charge localised at the nitrogen. It is also known that the air-water interface is negatively charged, due to the preferentially adsorption of OH⁻ anions at the interface. Therefore, the adsorption of cationic surfactants is more pronounced at high pH. This can result in the charge reversal at the air-water interface due to increased adsorption of cationic surfactant at the surface of aqueous solutions with increased surfactant concentration.[24, 25]

Velikov et al.[26] have demonstrated that the lifetime of foam films increases linearly with logarithm of surfactant concentration, and not only below the critical micelle concentration (c.m.c.) but also much above this concentration threshold. Bhakta and Ruckenstein[27] developed a theoretical model which explains the effect of surfactant concentration on foam stability in terms of disjoining pressure and surface viscosity. They proposed that an increase in surfactant concentration stabilises the foam by increasing the maximum disjoining pressure. More recent experimental results by Exerowa et al.[28] on foams and wetting films produced using CTAB in the presence of NaCl agree well with this theory. In this case, the electrostatic interactions are found to be the main stabilising forces.

By contrast, at high pH, silica particles are very hydrophilic and poor emulsifiers alone of oil and water.[29] Likewise they are poor foamers of air and water. Therefore, as expected all foams prepared at various particle concentrations (0.1 - 5 wt.%) were extremely unstable to coalescence with no bubbles remaining 3 minutes after aeration. The foamability of these dispersions was also very low, with less than 1 cm³ of foam being generated. This was also observed at all pH values.

8.3   Stability of aqueous dispersions of silica particles and CTAB

Firstly, the effect of adding a single chain cationic surfactant like CTAB to aqueous dispersions of silica particles of diameter 0.6 μm at high pH (e.g. pH = 10) is described. A limited equivalent data set is then presented for an intermediate pH (e.g. pH = 6) and then at a low pH (e.g. pH = 3), in which silica is initially only slightly charged, for comparison.

At pH = 10, particles surfaces are appreciably negatively charged due to dissociation of surface silanol Si-OH groups. Addition of oppositely charged cationic surfactant like CTAB leads to electrostatic adsorption of surfactant monomer onto particle surfaces. As a monolayer forms, particles become increasingly hydrophobic (alkyl chains exposed to solution). Further adsorption of surfactant can occur via chain – chain interaction resulting in a bilayer, now with head-groups exposed to the solution rendering the particles more hydrophilic again.[30] Such changes in the wettability of the silica particles could be sufficient to either stabilise or destabilise the foams produced by them, since hydrophilic particles tend to give rise to unstable foams whilst partially hydrophobic ones tend to make stable foams.

At a fixed concentration of 3 wt.%, addition of CTAB leads to a change in the stability of the dispersions. In Figure 8.2, it can be seen that the initial stable dispersion begins to sediment at intermediate CTAB concentration from 0.05 up to 0.5 mM CTAB, after which the sedimentation falls.

Figure 8.2   Photograph of vessels after 1 hour containing 10 mL aqueous dispersions of silica particles of diameter 0.6 μm (3 wt.%) as a function of CTAB concentration (given in mM) (a) no CTAB, (b) 0.001, (c) 0.01, (d) 0.02, (e) 0.05, (f) 0.09, (g) 0.2, (h) 0.5, (i) 0.9, (j) 5 at pH = 10 and at room temperature.

Before foaming
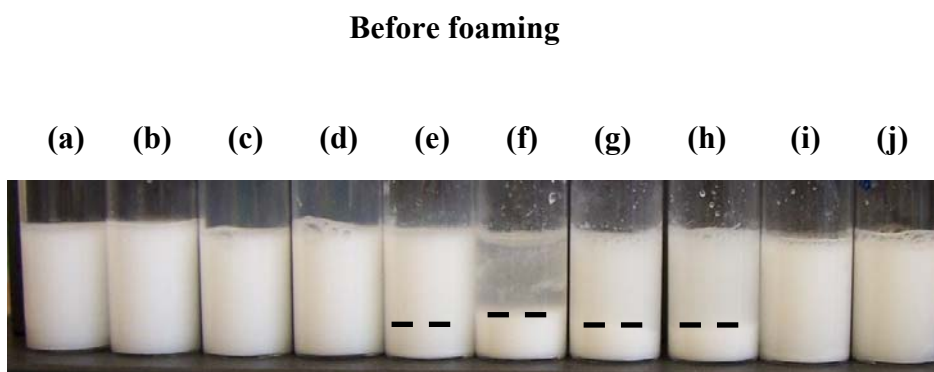
Up to 0.05 mM CTAB, dispersions are stable and bluish since surfactant adsorption is low and repulsion between particles dominates. Between 0.05 and 0.5 mM CTAB, coagulation of particles resulting in their sedimentation occurs progressively as van der Waals attraction between alkyl chains on neighbouring particles dominates. At

0.09 mM CTAB the supernatant is clear compared to the other vessels, which shows that the coagulation extent and sedimentation rate of particles achieves a maximum. Above 0.5 mM CTAB, the sedimentation extent decreases again and particles are re-stabilised as a surfactant bilayer forms on their surfaces leading to charge repulsion. It is likely that the slight flocculation observed here at high surfactant concentration is due to depletion of micelles between particles on close approach, reported in a similar system.[31]

Figure 8.3 shows the height of the sediment (relative to the total volume) as a function of CTAB concentration for the same system and Figure 8.4 shows the hydrodynamic particle diameter measured with the Mastersizer as a function of CTAB concentration. The results obtained here are in very good agreement, as the condition where the particles start to aggregate at intermediate [CTAB] = 0.05 mM is where the hydrodynamic particle size was found to be considerably high achieving a maximum as a result of particle aggregation.

8.3.2   *Aqueous dispersions of silica particles and CTAB at pH = 6 and 3*

Addition of CTAB to the aqueous silica particle dispersions at an intermediate pH = 6 also leads to a change in the stability of the dispersions as previously observed at pH =10. It can be seen in Figure 8.5 that the initial stable dispersion begins to flocculate and sediment very quickly between 0.05 and 0.5 mM CTAB (< c.m.c.), after which the aqueous dispersions is re - stabilised again. Aqueous dispersions of silica particles were also prepared at pH = 3 in the presence of CTAB at different concentrations. At this pH, where the charge of the silica particles is zero (IEP), the particles are found to aggregate. It can be seen in Figure 8.6 that by increasing the concentration of CTAB to the initially unstable silica dispersion at this pH, the aqueous dispersions is re - stabilised again at all concentrations studied. Their stability to sedimentation may be due to the fact that the hydrophobic tail-groups of the CTAB surfactant are adsorbing onto the uncharged silica particles leading to charge repulsion.

Figure 8.3 Sediment height in % after 1 hour *versus* CTAB concentration for the system shown in Figure 8.2.
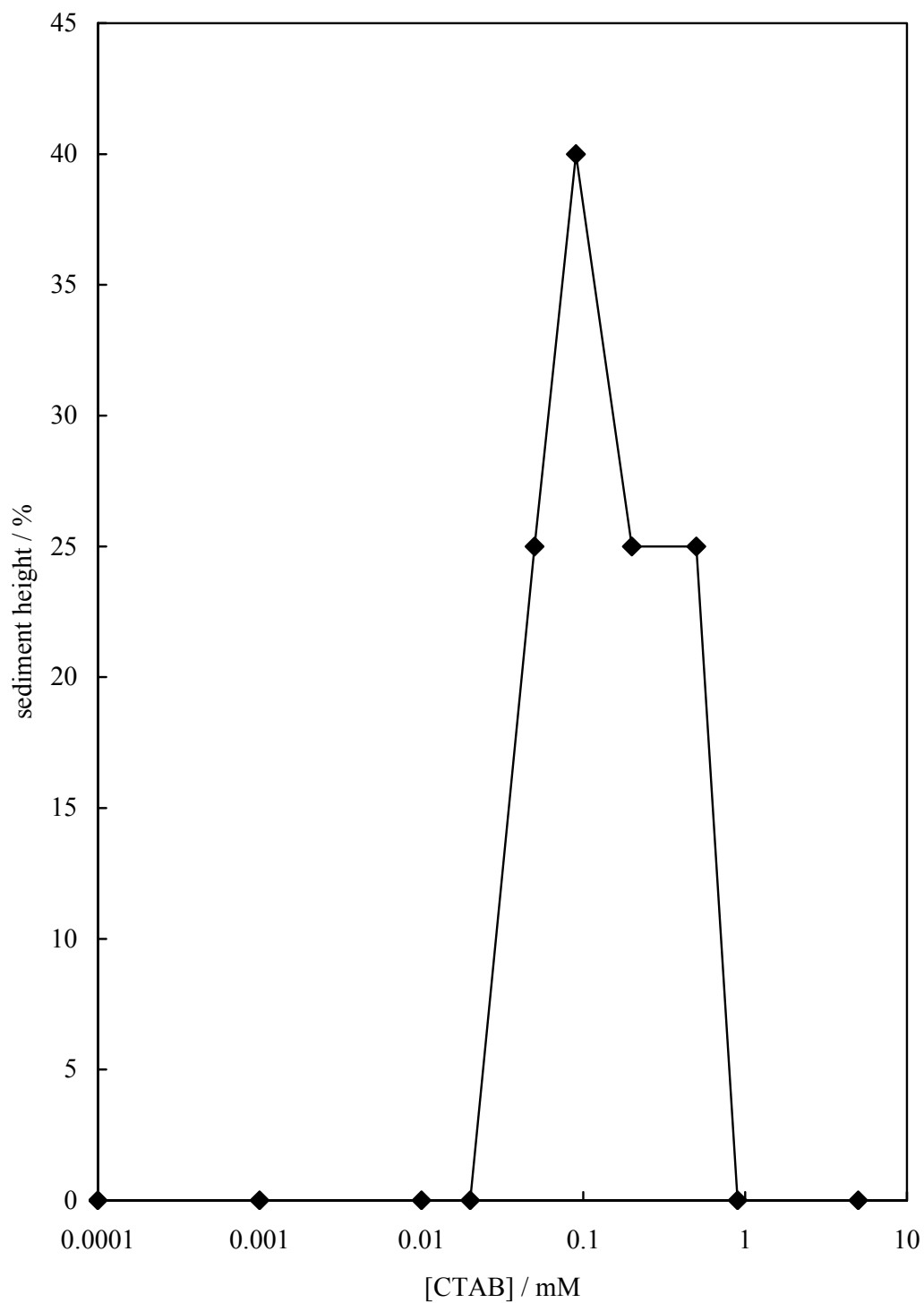
Figure 8.4   Hydrodynamic particle diameter versus [CTAB] for aqueous dispersions of silica particles (0.6 μm), [particle] = 0.1 wt.% at pH = 10. The data 0.00001 mM CTAB corresponds to the aqueous silica dispersion alone (without CTAB).
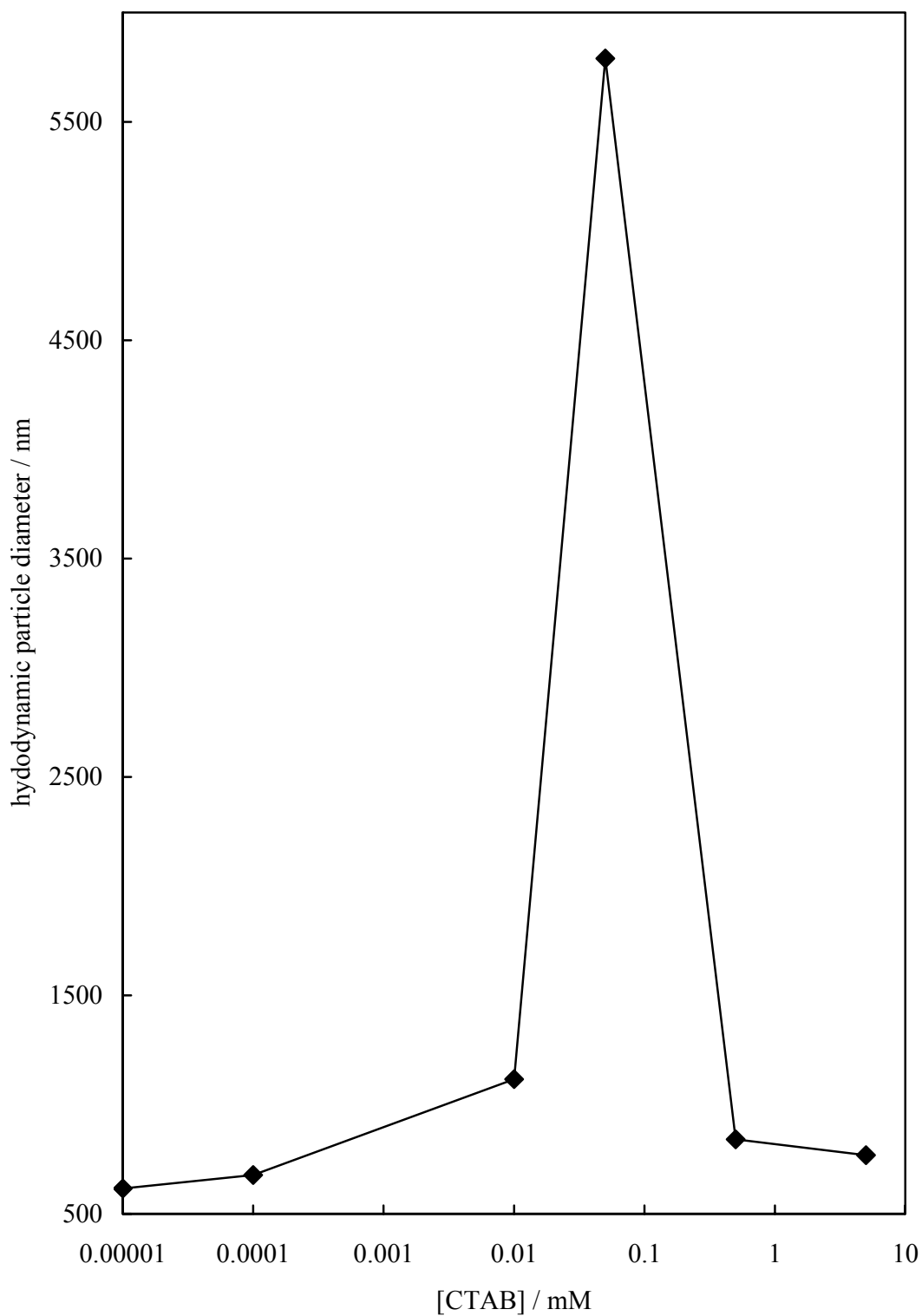
Figure 8.5 Photograph of vessels after 1 hour containing 10 mL aqueous dispersions of silica particles of diameter 0.6 μm (3 wt.%) as a function of CTAB concentration (given in mM), (a) no CTAB, (b) 0.001, (c) 0.02, (d) 0.05, (e) 0.1, (f) 0.2, (g) 0.5, (h) 1 at pH ~ 6 and at room temperature.

Before foaming

(a)   (b)   (c)   (d)   (e)   (f)   (g)   (h)
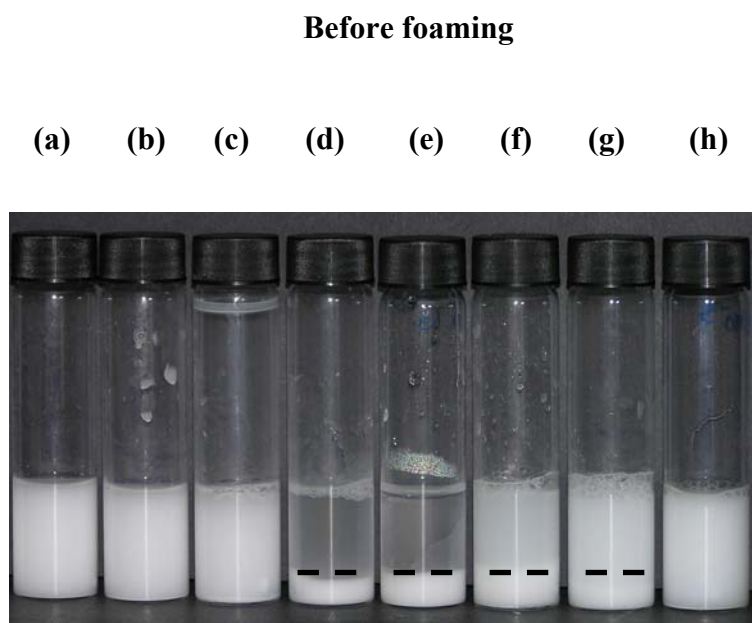
Figure 8.6 Photograph of vessels after 1 hour containing 10 mL aqueous dispersions of silica particles of diameter 0.6 μm (3 wt.%) as a function of CTAB concentration (given in mM), (a) no CTAB, (b) 0.001, (c) 0.02, (d) 0.05, (e) 0.1, (f) 0.2, (g) 0.5, (h) 0.9, (i) 5 at pH = 3 and at room temperature.

(a)   (b)   (c)   (d)   (e)   (f)   (g)   (h)   (i)
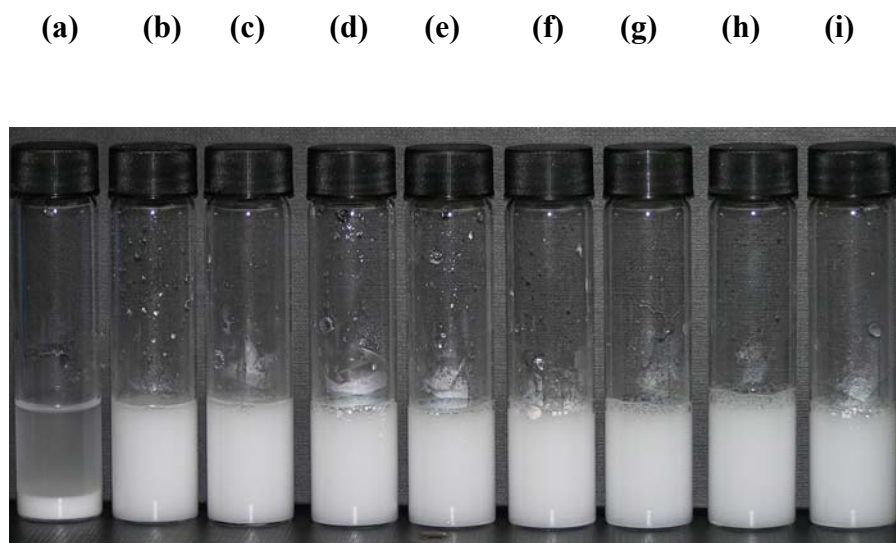
8.4   Effect of CTAB on particle properties in particle-surfactant mixtures

8.4.1   *Adsorption isotherm of surfactant on particles in water at pH = 10*

The adsorption of cationic surfactants on silica surfaces has been investigated by others using ellipsometry,[32] atomic force microscopy,[33,34] depletion from solution,[30,35-37] spectroscopy[38] and combined streaming potential/optical reflectometry.[39] In order to quantify the extent of CTAB surfactant adsorption on silica particles in water, an adsorption isotherm was determined using a surface tension method. This involved measuring the air-water tension as a function of the initial bulk surfactant concentration in the presence and absence of silica particles. Loss of surfactant monomer to particle surfaces leads to an increase in surface tension. The surface tensions were measured using a Krüss K12 apparatus with a du Noüy ring and appropriate correction. The surface tension of pure water is measured first, and then batch solutions of surfactant at different concentrations (at 25 °C) were measured. In addition, the surface tensions for batch samples of surfactant plus particles were determined.

For dilute surfactant solutions (without particles) the plot of surface pressure (π) versus concentration can be well fitted by the Szysykowski equation:[22]

$$\pi = \gamma^0 - \gamma = nRT\, \Gamma_{lg}^{\infty} \ln(1 + KC) = 2.303 nRT\, \Gamma_{lg}^{\infty} \log(1 + KC) \qquad (1)$$

which is derived by combining the Langmuir equation:

$$\Gamma_{lg} = \Gamma_{lg}^{\infty} \frac{KC}{1 + KC} \qquad (2)$$

with the Gibbs adsorption equation:

$$-d\gamma = nRT\, \Gamma_{lg}\, d\ln C = 2.303 nRT\, \Gamma_{lg}\, d\log C \qquad (3)$$

where γ^0 and γ are the surface tensions of pure water and surfactant solution at concentration C, respectively, Γ_{lg} and Γ_{lg}^{∞} are the surface concentration C and of the surfactant at the water/air (liquid/gas) interface, n is the number of ions per molecule of surfactant whose concentration varies with C (n = 2 for a 1-1 type ionic surfactant

without adding salt). *K* is a constant linked to the standard free energy of adsorption of the surfactant ($K = 1/a$, and *a* is a constant in mol/L). The constants Γ_{lg}^{∞} and *K* of various surfactants are found by fitting the measured γ log C (C < c.m.c.) data to equation (1) and are listed in Table 1, which is in good agreement with the literature values.[22]

Table 1. Parameters obtained by fitting the plots of surface tension versus concentration in aqueous solutions for CTAB surfactant at 25 °C.

Parameter	Value
$\Gamma_{lg}^{\infty}/10^{10}$ mol cm^{-2} (measured)	2.5
$\Gamma_{lg}^{\infty}/10^{10}$ mol cm^{-2}	2.7
K/M^{-1}	6.1×10^{-2}

The equilibrium surfactant concentration, C_e, in the silica dispersions is then calculated by the following equation:

$$\pi_c = \gamma_c^0 - \gamma_c = nRT\ \Gamma_{lg}^{\infty} \ln(1 + K\ C_e) \tag{4}$$

where the subscript c refers to the silica dispersions. In order to calculate the adsorbed amount of CTAB on silica particles in water (solid/liquid) Γ_{sl}, the following equation is used

$$\Gamma_{sl} = \frac{V_d(C_{ini} - C_e)}{w_c} \text{ (mmol g}^{-1}) \tag{5}$$

where C_{ini} is the initial concentration of surfactant (mM). V_d is the volume of dispersion, and W_c is the mass of silica particles in the dispersion. The corresponding molecular area A_m of the surfactant can then be calculated using the following equation:

$$A_m = \frac{S_{BET}}{6.02 \times 10^2\ \Gamma_{sl}} \text{ (nm}^2) \tag{6}$$

where S_{BET} is the BET specific surface area of the silica particles (m^2 g^{-1}), and Γ_{sl} has units of mmol g^{-1}. The raw data is plotted in Figure 8.7, where the curve for the silica-containing system is shifted to higher surfactant concentrations, since a fraction of the surfactant adsorbs on the particles and is not available to adsorb at the liquid surface. For the same surface tension, the difference in concentration between the curves allows us to calculate the amount of surfactant adsorbed on silica. A significant drawback of the surface tension method is that the adsorption beyond the c.m.c. is unobtainable. The isotherm derived from such data is given in Figure 8.8. There is a gentle increase in adsorbed amount initially followed by a more significant increase at higher concentrations, ending at the c.m.c.

In a detailed study of similar cationic surfactants (alkylpyridinium chloride) on quartz particles, Fuerstenau and Jia[30] describe four regions in their isotherms. In region I, surfactant ions adsorb individually with their headgroups down. In region II, adsorbed ions associate into patches or hemi-micelles on the surface through chain-chain interaction. This results in an adsorbed monolayer. In region III, a second layer begins to adsorb on the first through hydrophobic interactions of the chains. In region IV occurring close to the c.m.c., the bilayer is complete and the adsorbed amount reaches a plateau value. The last point on the isotherm corresponds to an area per CTAB molecule on particle surfaces equal to 0.63 nm^2. This is to be compared with that measured at the air-water surface of 0.58 nm^2 calculated from the data in Figure 8.7.

8.4.2   *Contact angles of aqueous CTAB drops in air at pH = 10*

In order to explain the effect increasing CTAB has on foamability and foam stability of the silica particles studied a knowledge of the contact angle these particles make with the interface is essential in interpreting some of the phenomena. Since determination of these angles using nanoparticles themselves is not possible, a planar substrate of similar chemical composition to that of particles has been used instead. The close agreement between contact angles on the two substrates types has been shown previously.[40] Figure 8.9 shows the contact angles of CTAB drops at pH = 10 under air on a silicon wafer substrate which possesses a layer of silica on its surface.

Figure 8.7   Variation of air-water surface tension at 25 °C with CTAB concentration at pH = 10 with and without 3 wt.% silica particles of diameter 600 nm.
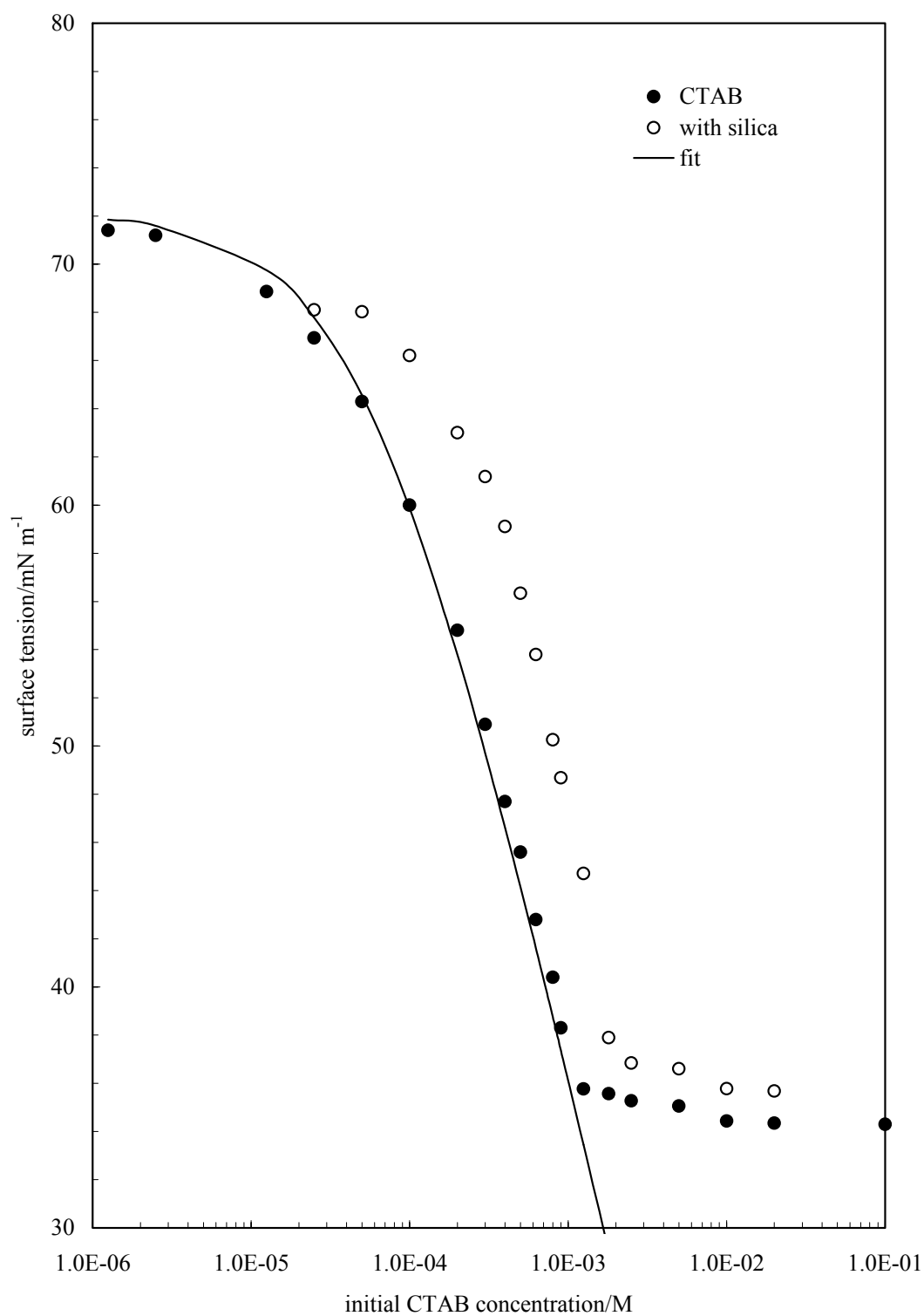
Figure 8.8 Adsorption isotherm of CTAB on silica particles of diameter 600 nm at pH = 10 derived from Figure 8.7.
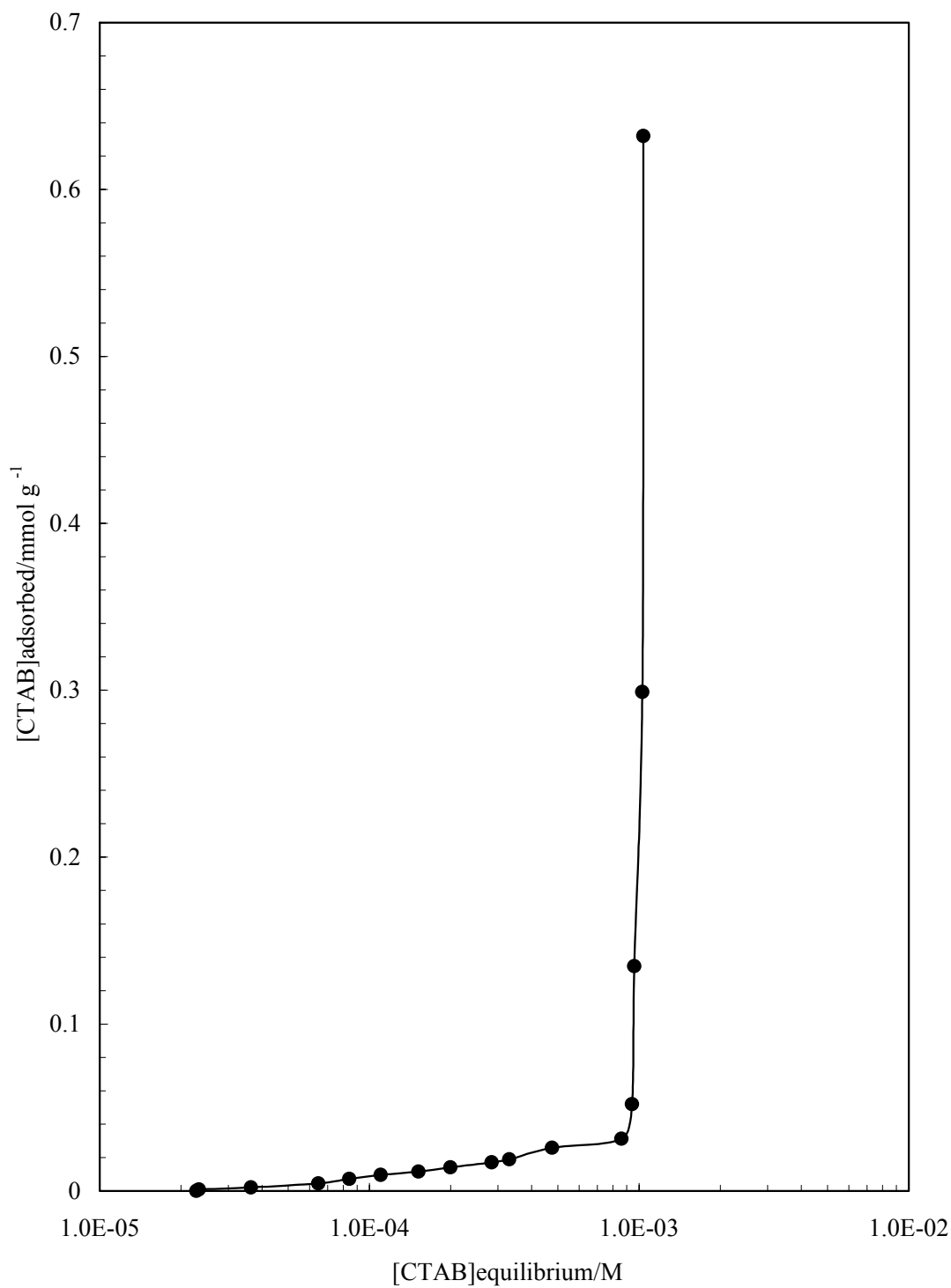
Figure 8.9 Contact angle of aqueous CTAB drops (~ 5 - 10 μL) under air on hydrophilic silicon wafer at pH = 10 versus CTAB concentration. 1×10^{-8} M CTAB corresponds to the aqueous silica dispersion alone (without CTAB).
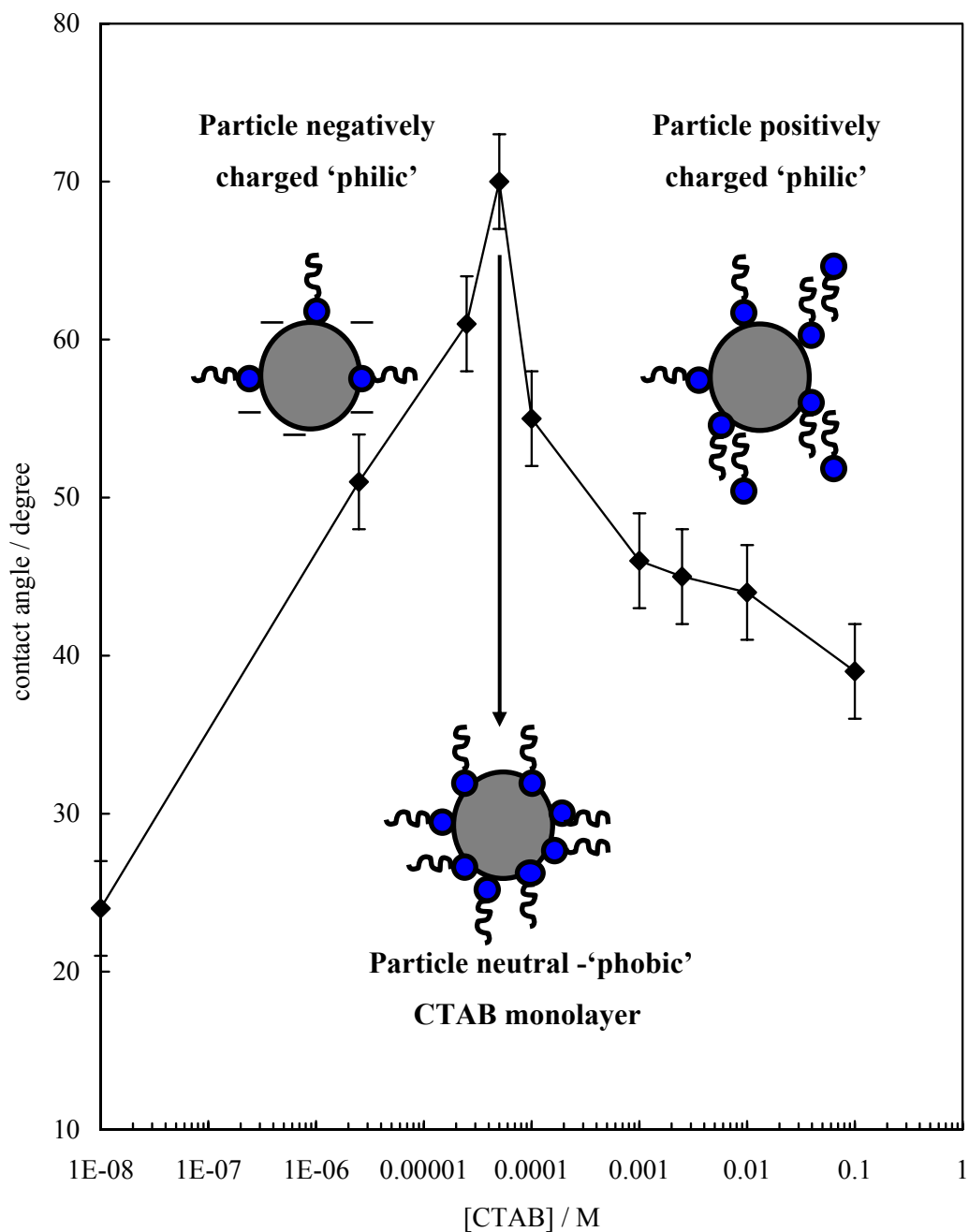
The initially hydrophilic surface in the absence of surfactant exhibits a contact angle through water of approximately 20°. Adsorption of surfactant to both the air-water and the solid-water interfaces results in an increase in θ to a maximum of 70º followed by a significant decrease at higher concentrations. This clearly shows that on addition of CTAB, initially hydrophilic and negatively charged particles become hydrophobic and uncharged at intermediate [CTAB] then hydrophilic again as they become positively charged at higher [CTAB]. Silica surfaces thus undergo a transition from hydrophilic to more hydrophobic to hydrophilic again.[36]

8.4.3 Zeta potential of aqueous silica dispersions and CTAB at pH = 10

The hydrophilic silica surface chemistry must be considered when trying to explain the foaming behaviour and foam stability observed in the system studied. Since the zeta potential of particles directly reflects adsorption in the Stern plane, electrophoretic measurements were conducted with silica particle dispersions as a function of CTAB concentration and are given in Figure 8.10. In the absence of surfactant at this high pH, the zeta potential is around - 70 mV. Addition of CTAB gradually decreases the magnitude of the potential up to 0.05 mM which corresponds to the neutral charge (IEP) and then a sudden reversal of the sign of zeta potential to positive values was observed, as reported by Wang et al.[38] for neutral pH. It can be concluded that on addition of CTAB, initially hydrophilic and negatively charged particles become more hydrophobic and uncharged leading to flocculation and then positively charged and hydrophilic again. As shown previously in section 8.3 (Figure 8.4), a dramatic change in the hydrodynamic size of the silica particles occurs around 0.05 mM CTAB, which corresponds to the same condition were silica particles were found to be uncharged and therefore more flocculated. This condition where particles are least charged is also with agreement with the maximum hydrophobicity as shown previously with the contact angle measurements (Figure 8.9).[41]

Figure 8.10 Zeta potential versus CTAB concentration for aqueous dispersions of monodisperse silica particles of diameter 0.6 μm (0.1 wt.%) at pH around 10. The dotted line corresponds to the aqueous silica dispersion alone (without CTAB).
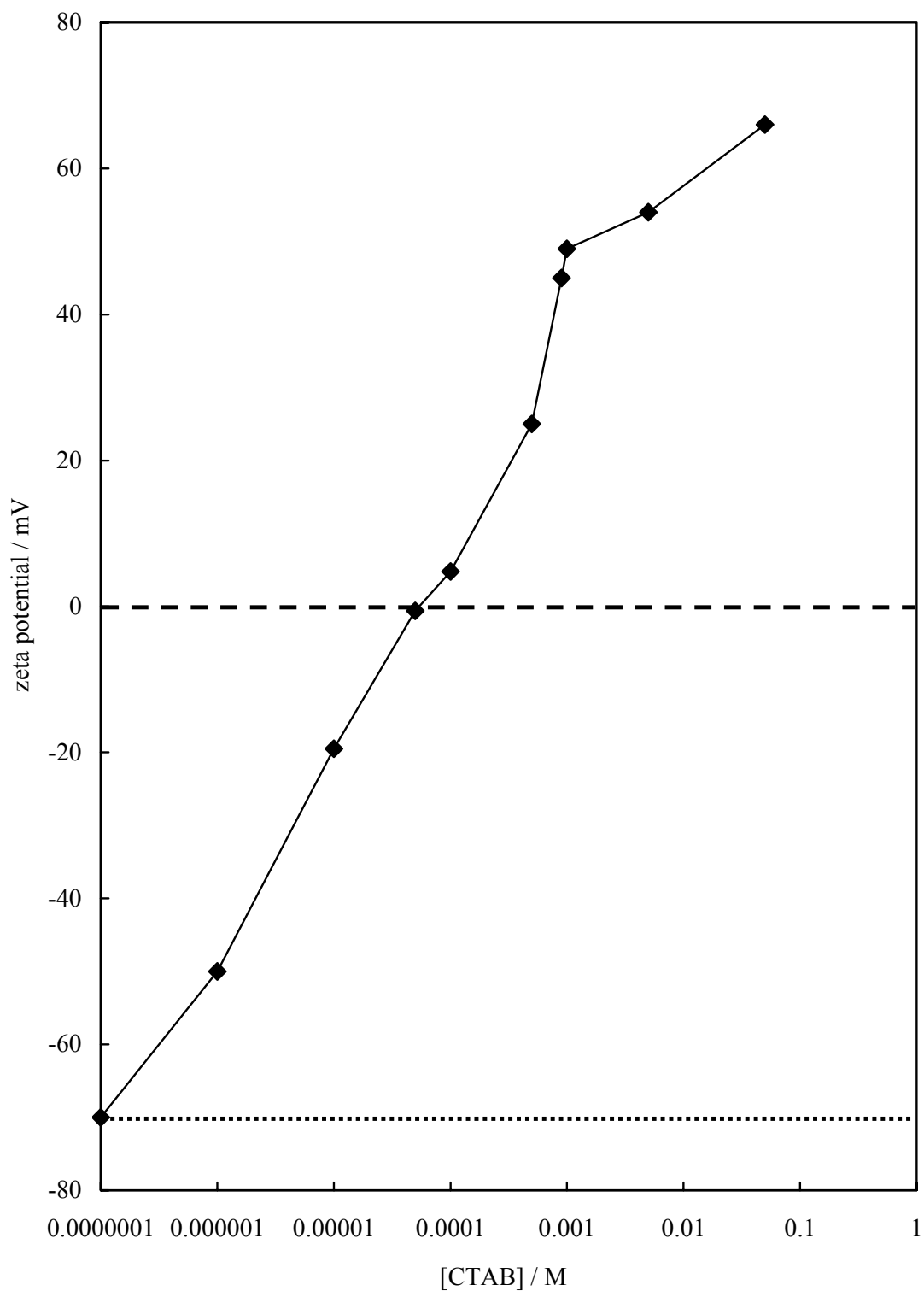
8.5 **Foams stabilised by a mixture of silica particles and CTAB**

As shown previously in section 8.2, no foam could be generated by hand shaking aqueous dispersions of silica particles alone (up to 5 wt.%) at any pH value. Foams prepared from CTAB surfactant solutions alone also collapsed completely within one day at all concentrations (0.01 to 5 mM) and at all pH values. Aqueous foams were prepared from mixtures of silica nanoparticles (3 wt.%) of diameter 0.6 μm and increasing concentrations of surfactant at high pH = 10. Their foamability is compared to that of solutions of surfactant alone. A summary of these findings is given in Table 2.

In mixtures, the initial foam volume increased progressively with surfactant concentration up to 5 mM. However, the foam stability measured after 48 hrs. (and monitored up to 6 months after) passed through a maximum, with the position of the maximum corresponding to the most flocculated dispersions as seen in Figure 8.11. The most stable foams formed between 0.05 and 0.5 mM contained most of the particles originally present as almost none were visible in the aqueous phase following drainage.

Table 2. Foamability (V_0) and a measure of foam stability measured after 48 hrs. (V_{48})/cm^3 of 10 cm^3 aqueous CTAB solutions alone and mixed CTAB/0.6 μm silica dispersions (3 wt. particles) at pH = 10. No foam could be formed from 3 wt.% silica dispersions alone. The stability to flocculation of the mixed dispersions before aeration is also given.

[CTAB]/mM	Surfactant		+ 0.6 μm silica particles		Mixed dispersions
	V_0	V_{48}	V_0	V_{48}	
0.01	0	0	2.5	1.4	stable
0.05	5	0	7.5	7.3	flocculated
0.09	11	0	11	10	most flocculated
0.50	23	0	11	10	flocculated
0.90	30	0	22	0	stable
5.00	60	0	22	0	stable

Figure 8.11 Appearance of foams from mixtures of 10 mL aqueous dispersion of monodisperse silica particles of diameter 0.6 μm (3 wt.%) and CTAB at different concentrations in mM (a) no CTAB, (b) 0.001, (c) 0.01, (d) 0.02, (e) 0.05, (f) 0.09, (g) 0.2, (h) 0.5, (i) 0.9, (j) 5 at pH =10. The times refer to times after foam generation by hand-shaking at room temperature.

Before foaming

After a few minutes

After 48 hours (and monitored up to 6 months after)
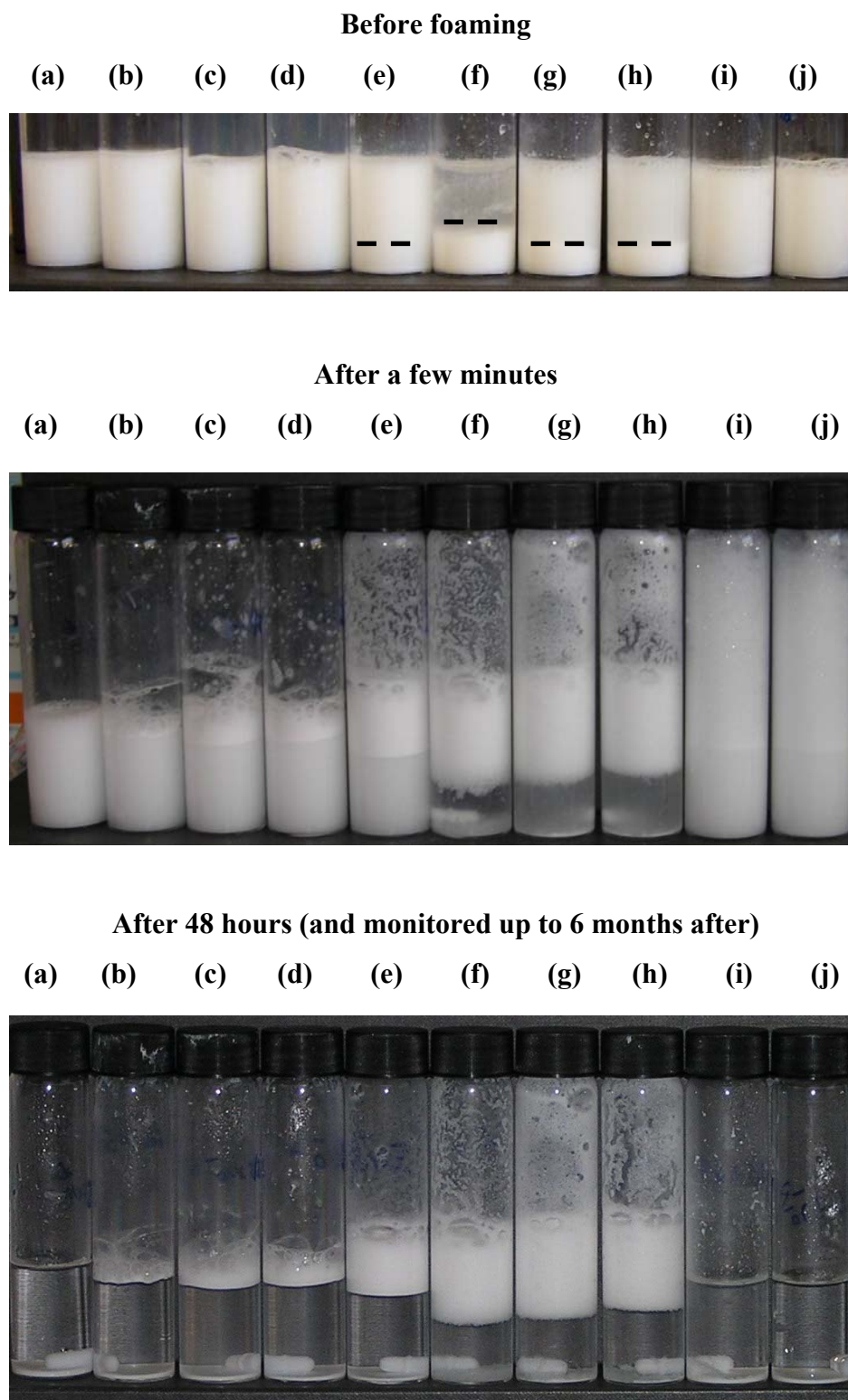
At low surfactant concentration, dispersions are stable as shown in Figure 8.11 and the foam stability is very similar to that of surfactant - stabilised foams alone. At intermediate concentrations (0.05 – 0.5 mM), particles become coated with a surfactant monolayer causing them to aggregate as their hydrophobicity increases. The most stable foams are therefore formed at these intermediate concentrations from dispersions in which the particles are most aggregated. As seen previously from the zeta potentials in Figure 8.10, this is where particles are of low charge and most hydrophobic (Figure 8.9). The adsorption of flocculated, partially coated particles to air bubble surfaces may be responsible for the stabilisation of such foams. It was also noticed that the foams were sensitive to gentle shear or vibration of the vessel causing a fraction of such aggregates to detach from the foam layer and sediment to the bottom of the vessel. The enhanced stability seems to arise from a combination of the adsorption of coated particles around bubbles preventing coalescence as well as the reduction in the extent of drainage between bubbles due to the increased aqueous phase viscosity of a flocculated dispersion. It may be that the adsorbed and non-adsorbed particles are forming a network as shown previously[20]. At high concentrations, a bilayer of surfactant forms on particle surfaces rendering them hydrophilic again and reducing their tendency to adsorb at the air bubble surfaces. Therefore, foam stability decreases as surfactant replaces particles around bubbles.

Since the surface charge density of silica decreases on lowering the pH as charged SiO^- groups become protonated, it is of interest to see if the reduction in the adsorption of surfactant to particle surfaces influenced the foaming behaviour. Silica dispersions may vary greatly with only minor changes in pH. Therefore, the foaming ability and stability of mixtures of silica particles and CTAB surfactant at intermediate pH = 6 and low pH = 3 was also briefly investigated. Figures 8.12 and 8.13 shows the foaming ability and stability of aqueous foams formed by mixtures of silica particles (at a fixed concentration) and CTAB surfactant at different concentrations at pH = 6. Very similar results were observed at intermediate pH and the high pH previously studied. Again, at intermediate CTAB concentrations (0.05 – 0.5 mM), the dispersions before foaming are most flocculated and the foams formed by such dispersions were found to be the most stable. However, at high pH, the foaming ability across the intermediate [CTAB] range studied is very similar, while at the intermediate pH = 6 the foaming ability gradually increases with [CTAB].

Figure 8.12 Appearance of foams from mixtures of 10 mL aqueous dispersion of monodisperse silica particles of diameter 0.6 μm (3 wt.%) and CTAB at different concentrations in mM (a) no CTAB, (b) 0.001, (c) 0.02, (d) 0.05, (e) 0.1, (f) 0.2, (g) 0.5, (h) 1 at pH = 6. The times refer to times after foam generation by hand-shaking at room temperature.
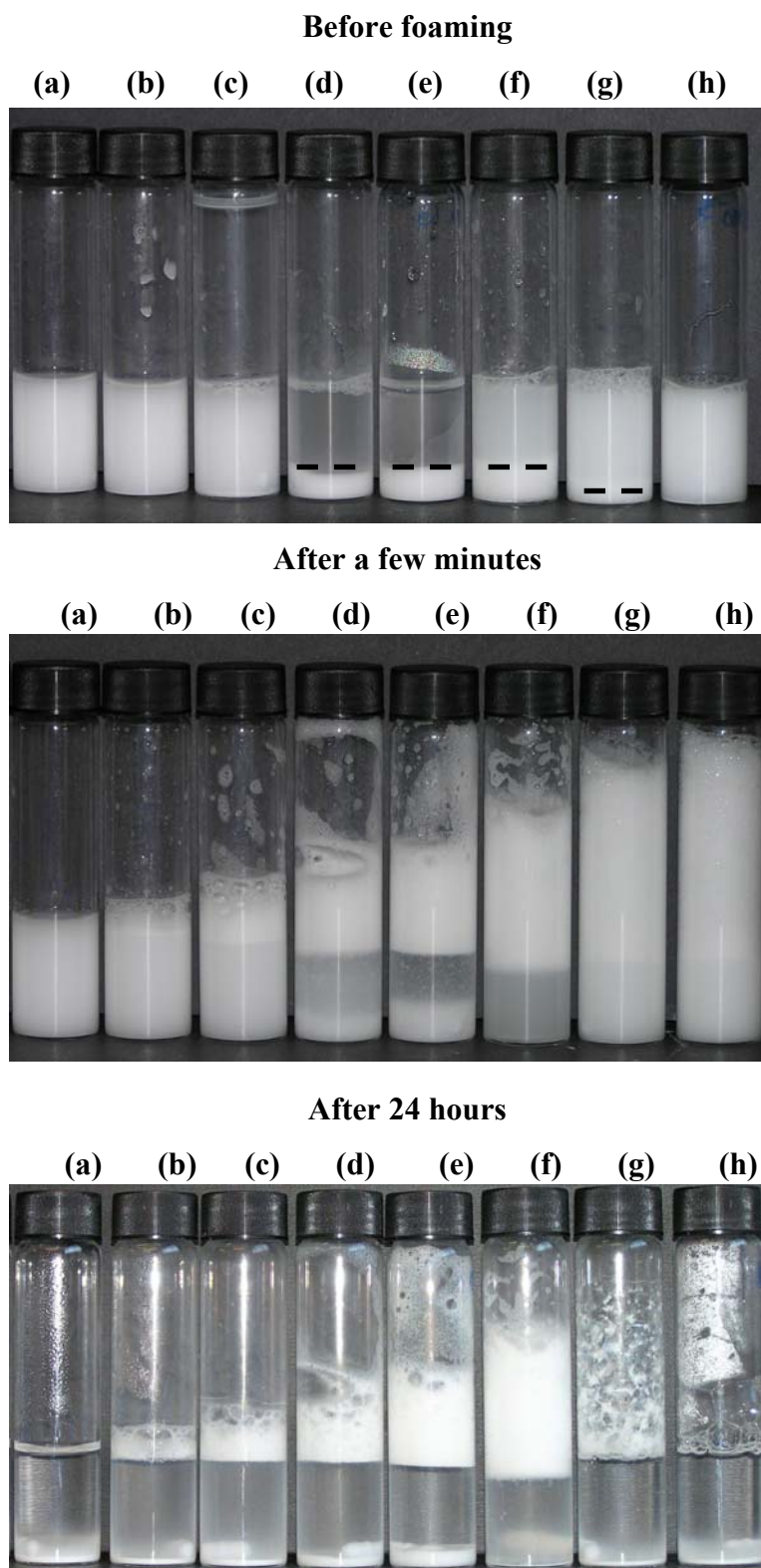
Figure 8.13 Effect of CTAB concentration on the foaming ability (diamonds) and stability after 24 hours (circles) of the system in Figure 8.12.
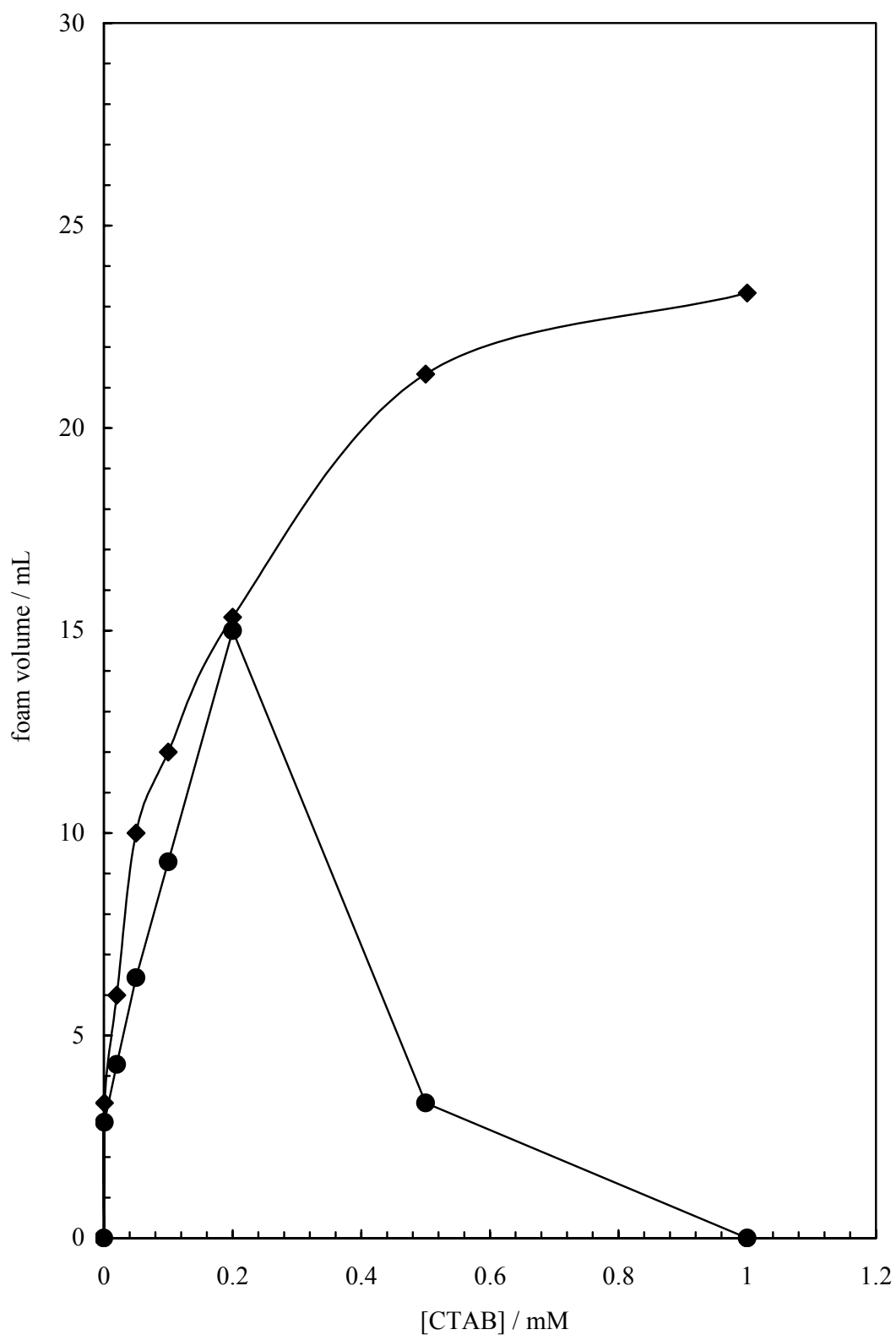
At pH approximately 3, where the charge of silica particles is zero, the particles are found to aggregate. It can be seen in Figures 8.14 and 8.15 that adding different concentrations of CTAB to the initially unstable silica dispersion at this pH, the aqueous dispersions are re - stabilised again and the foaming ability of the mixtures gradually increases with CTAB concentration.

Figure 8.14 Appearance of foams from mixtures of 10 mL aqueous dispersion of monodisperse silica particles of diameter 0.6 μm (3 wt.%) and CTAB at different concentrations in mM (a) no CTAB, (b) 0.001, (c) 0.02, (d) 0.05, (e) 0.1, (f) 0.2, (g) 0.5, (h) 0.9, (i) 1 at pH ~ 3. The times refer to times after foam generation by hand-shaking at room temperature.
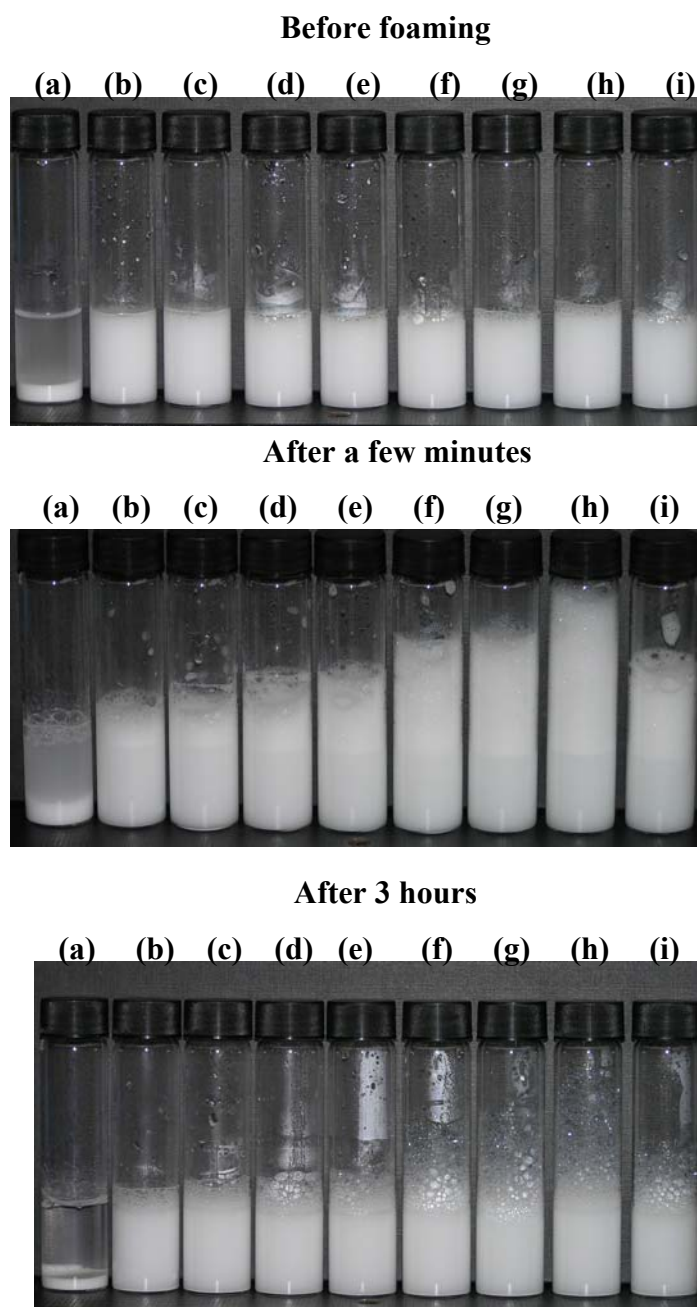
Before foaming

After a few minutes

After 3 hours

Figure 8.15 Effect of CTAB concentration on the foaming ability (diamonds) and stability after 24 hours (circles) of the same system described in Figure 8.14.
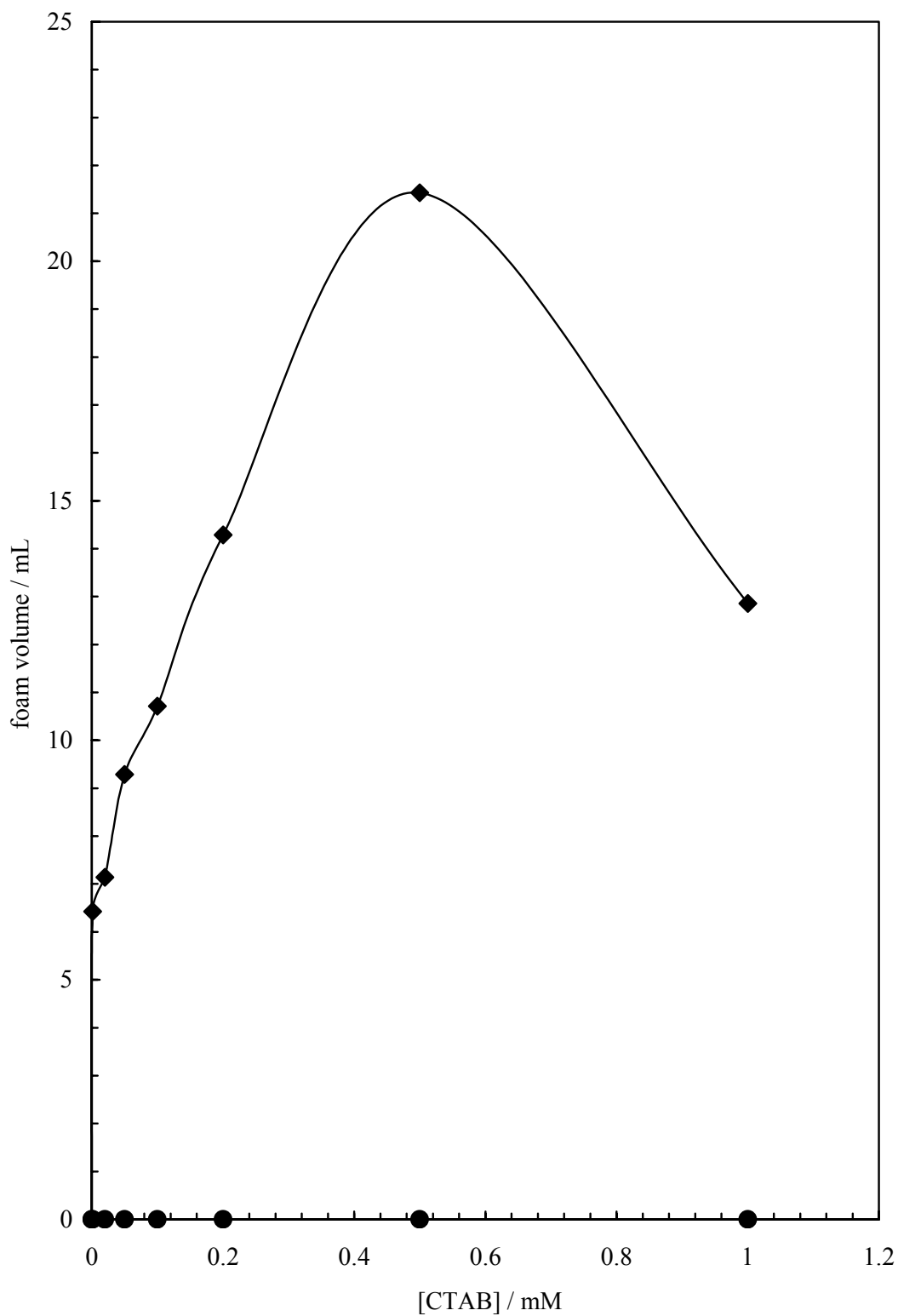
However, the foam stability is poor and very similar to the foam stability of CTAB solutions alone. Here bubble disproportionation is observed after a few hours and after 24 hours almost no foam is observed (only big polyhedral bubbles still remained). A possible explanation regarding the foam stabilisation in particle-surfactant mixtures of opposite charge from results of the present investigation, is schematically represented in Figure 8.16 (A) and (B) for conditions at high and low pH. The change in the particle charge and hydrophobicity induced by adsorption of surfactant triggers the drastic change in foam stability. These results are in close agreement with those described recently for foams stabilised by a mixture of Ludox HS-30 silica nanoparticles and di-C_{10}DMAB cationic surfactant at high pH.[42]

Figure 8.16 Schematic representation explaining the stabilisation or instability of aqueous foams formed by silica particles and CTAB surfactant mixtures at high (A) and low pH (B). Schematic A was adapted from Ref. 39.

(A)

(B)
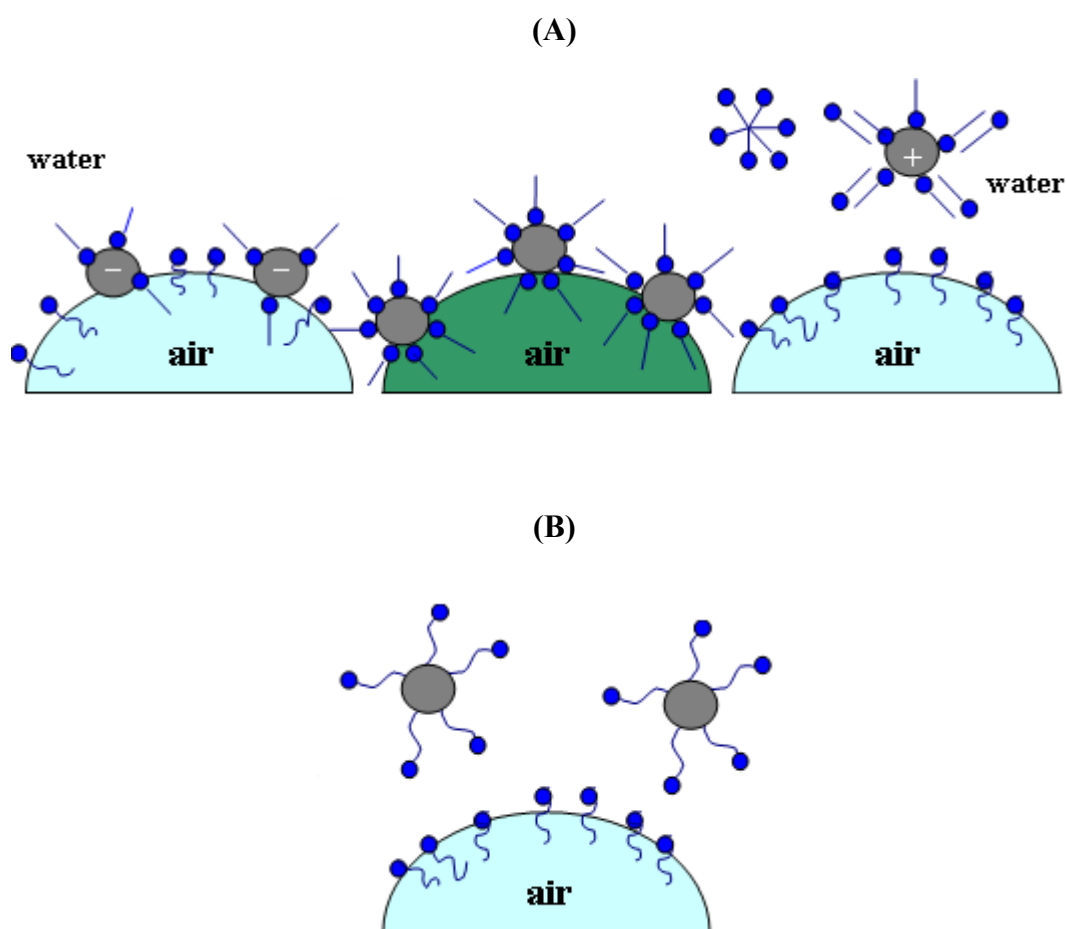
Figure 8.16 (A) shows that at low [CTAB] (left), relatively unstable bubble surfaces contain mainly surfactant molecules with a low percentage of partially coated particles. At intermediate [CTAB] (centre), very stable bubbles are coated with uncharged, hydrophobic particles possessing an adsorbed surfactant monolayer. At high [CTAB] (right), very unstable bubbles contain an adsorbed surfactant layer; cationic particles coated with surfactant bilayers and surfactant micelles remain dispersed in the aqueous phase. However, at low pH = 3 a different picture emerges. At such low pH and no [CTAB], silica particles are uncharged and therefore particles are found to aggregate as shown previously in Figure 8.14. Silica particles do not foam alone and therefore very little and very unstable foam was observed at this condition. When CTAB surfactant is added to the uncharged silica particles at pH = 3 (Figure 8.16 (B)), the hydrophobic tail groups may adsorb down onto the hydrophobic silica particles with its head (polar groups) being exposed to the solution. This type of adsorption is driven both by hydrophobic interactions and electrostatic attraction.[43] As a result silica particles become more hydrophilic again and particles are re-dispersed in bulk on acquiring a net positive charge. This happens because less surfactant is required for the particles to become positively charged due to the reduced number of charged sites at low pH. Therefore, the bubbles produced at this condition are unstable behaving as bubbles-stabilised by surfactant alone, as they contain mainly surfactant monolayer at their surface instead of silica particles. Other studies, have shown tail down adsorption of surfactant onto hydrophobic surfaces such as graphite.[44]

8.6   Foam structure

In order to probe the structure of bubbles and the arrangement of surfactant and particles around air bubbles, Cryo – SEM images of freshly prepared foams (unstable) and very stable foams prepared after a few days were taken for comparison as shown in Figures 8.17 and 8.18. The SEM images shown below of the surface of a bubble stabilised by a mixture of 3 wt.% particles and 0.005 mM CTAB (Figure 8.17) and 0.05 mM CTAB (Figure 8.18) at pH ~ 10, shows that the surface concentration of particles around bubbles increases at low surfactant concentration to an intermediate concentration. Thus it can be concluded that the foam stabilisation changes from surfactant dominated at low concentration (unstable) to particle dominated at intermediate concentration (very stable). These results are in close agreement with those previously described regarding the stability of dispersions before foaming followed by their foaming ability and

stability. At low surfactant concentration (0.005 mM), the dispersion was stable and a small volume of foam was produced (poor foaming ability). The foam stability was very similar to that of surfactant-stabilised foams alone and most of the particles were found in the aqueous phase following drainage. At an intermediate concentration (0.05 mM), silica particles were found to be uncharged and become coated with a surfactant monolayer causing them to aggregate as their hydrophobicity increases. As a result of this, the foams formed were found to be very stable and contained most of the particles within the foam as only very few particles were found in the aqueous phase. The change in the particle charge and hydrophobicity induced by adsorption of surfactant triggers the drastic change in foam stability as particles replace surfactant on bubble surfaces at intermediate concentrations (*e.g.* 0.05 mM).

Figure 8.17 Cryo - freeze fracture SEM micrographs at different magnifications of fragments of aqueous foams stabilised by a mixture containing 3 wt. % silica particles (0.6 μm in diameter) and 0.005 mM CTAB at pH = 10 after a few minutes of foaming.

332
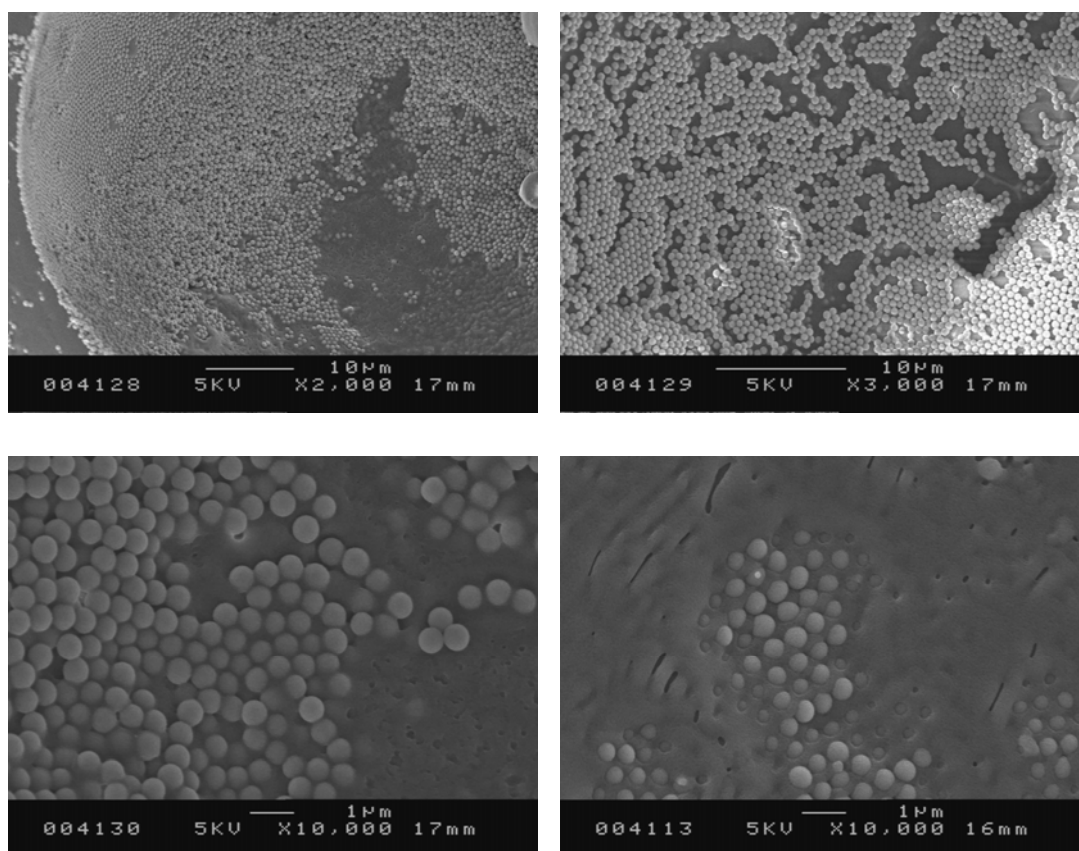
Figure 8.18 Cryo - freeze fracture SEM micrographs at different magnifications of fragments of aqueous foams stabilised by a mixture containing 3 wt. % silica particles (0.6 μm in diameter) and 0.05 mM CTAB at pH = 10 after 3 days.
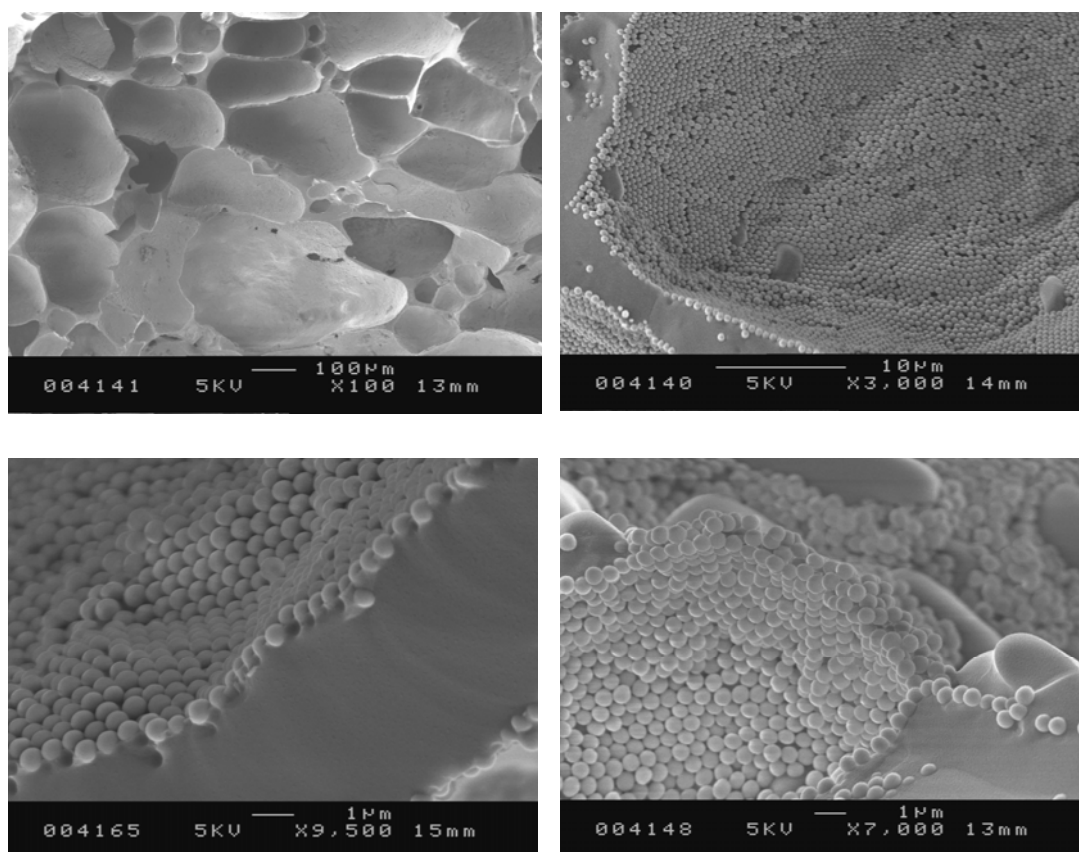
It is also worth mentioning other features, such as the non – spherical wavy nature or rippled texture of a particle-coated bubble surface as evidenced in Figure 8.18. The first observation is a result of the jamming of particles at the fluid interface preventing its relaxation to a sphere.[45] The second observation is due to the compression of a particle layer increasing its surface concentration. Eventually, since such particles are irreversibly adsorbed, further compression causes the air-water surface to undulate giving it the rough appearance seen.[3] In the same system an image of the air-water surface edge reveals the contact angle of particles measured into the aqueous phase of around 90°, while in the system shown in Figure 8.17 the particles are more deeply penetrated into the air bubble surface, revealing a lower contact angle of the particles if measured into the aqueous phase. A monolayer of close-packed particles on a bubble surface is also clearly seen in Figure 8.18 and this could be responsible for the highest foam stability shown here.

8.7   Conclusions

A detailed investigation into the behaviour of foams stabilised by a mixture of hydrophilic silica nanoparticles and CTAB cationic surfactant at various pH has been described. At any particle concentration or pH value, particles alone are ineffective foam stabilisers whereas surfactant-stabilised foams become increasingly stable to coalescence with concentration. Nevertheless, they break down completely within one day at all surfactant concentrations. In mixtures, the synergism between silica particles and CTAB at pH = 10 leads to enhanced foam stability at an intermediate CTAB concentration, where particles were found to be most flocculated. Complementary experiments have been undertaken in order to offer an explanation for the latter synergy. By determining the size of particles in water and CTAB at different concentrations, it was shown that surfactant addition initially leads to particle flocculation followed by re-dispersion. From zeta potential measurements, it is shown that surfactant addition initially transforms particles from anionic to uncharged and hydrophobic and subsequently to cationic as a result of adsorption. Using suitable contact angle measurements at air-water-solid interfaces, it is shown that silica surfaces become increasingly hydrophobic initially upon surfactant addition achieving a maximum in hydrophobicity at intermediate [CTAB] and then particles become hydrophilic again as a result of bilayer surfactant adsorption. The most hydrophobic particles, possessing an adsorbed monolayer of surfactant, yield foams which are completely stable to disproportionation and coalescence. Cryo-SEM analysis of frozen foams also reveals the changeover from surfactant to particle-dominated bubble surfaces in line with the dramatic increase in stability. The foaming ability and stability of mixtures of silica particles and CTAB surfactant at low pH (*e.g.* pH = 3) was also investigated. The main finding was that when CTAB surfactant was added to the unstable silica dispersions at pH = 3, silica particles become positively charged and coated with surfactant tails instead of hydrophilic heads (positively charged). Therefore, the foams formed at such low pH were unstable behaving as foams stabilised by surfactants alone, as they contain mainly surfactant monolayer at their surface instead of silica particles.

One limitation withdrawn from this work is that the initial stable aqueous dispersion containing silica particles become destabilised (particles flocculated) at an intermediate CTAB concentration, where the maximum in foam stability was found. The extensive flocculation of particles could be an issue in certain industries.

References

1. K.L. Mittal and P. Kumar, Emulsions, Foams, and Thin Films, CRC Press (2000).

2. R.G. Alargova, D.S. Warhadpande, V.N. Paunov and O.D. Velev, *Langmuir*, **20**, 10371 (2004).

3. B.P. Binks and T.S. Horozov, *Angew. Chem. Int. Ed.*, **44**, 3722 (2005).

4. S. Fujii, A.J. Ryan and S.P. Armes, *J. Am. Chem. Soc.*, **128**, 7882 (2006).

5. K. Vijayaraghavan, A. Nikolov and D. Wasan, *Adv. Colloid Interface Sci.*, **49**, 123 (2006).

6. B.P. Binks and R. Murakami, *Nature Mater.*, **5**, 865 (2006).

7. V.B. Menon and D.T. Wasan, *Colloids Surf.,* **19**, 89 (1986).

8. D. Johansson, B. Bergenstahl and E. Lundgren, *JAOCS*, **72**, 921 (1995).

9. R. Aveyard, B.P. Binks, P.D.I. Fletcher, T.G. Peck and C. E. Rutherford, *Adv. Colloid Interface Sci.*, **48**, 93 (1994).

10. A.P. Sullivan and P.K. Kilpatrick, *Ind. Eng. Chem. Res.*, **41**, 3389 **(**2002).

11. N.D. Denkov, *Langmuir*, **20**, 9463 (2004), and references therein.

12. P.R. Garrett, S.P. Wicks and E. Fowles, *Colloids Surf. A*, **307**, 282 (2006).

13. B.P. Binks, Modern Aspects of Emulsion Science, Royal Society of Chemistry, Cambridge (1998).

14. B.P. Binks, *Curr. Opin. Colloid Interface Sci.*, **7,** 21 (2002).

15. B.P. Binks and T.S. Horozov, Colloidal Particles at Liquid Interfaces, Cambridge University Press, Cambridge (2006).

16. Z. Du, M.P. Bilbao-Montoya, B.P. Binks, E. Dickinson, R. Ettelaie and B.S. Murray, *Langmuir*, **19**, 3106 (2003).

17. A.B. Subramaniam, C. Mejean, M. Abkarian and H.A. Stone, *Langmuir*, **22**, 5986 (2006).

18. M. Abkarian, A.B. Subramaniam, S-H. Kim, R. J. Larsen, S-M Yang and H.A. Stone, *Phys. Rev. Lett.*, **99**, 188301 (2007).

19. A. Cervantes Martinez, E. Rio, G. Delon, A. Saint-Jalmes, D. Langevin and B.P. Binks, *Soft Matter*, **4**, 1531 (2008).

20. E. Dickinson, R. Ettelaie, T. Kostakis and B.S. Murray, *Langmuir*, **20**, 8517 (2004).

21. U.T. Gonzenbach, A.R. Studart, E. Tervoort and L.J. Gauckler, *Angew. Chem. Int. Ed.*, **45**, 3526 (2006).

22. M.J. Rosen, Surfactants and Interfacial Phenomena, 3rd Ed., John Wiley and Sons, New Jersey (2004).

23. T.F. Tadros, Applied Surfactants: Principles & Applications, Wiley-VCH, (2005).

24. T. Kolarov, R. Yankov, N. E. Esipova, D. Exerowa and Z. M. Zorin, *Colloid Polym. Sci.*, **271**, 519 (1993).

25. K. Hänni-Ciunel, N. Schelero and R. von Klitzing, *Faraday Discuss.*, **141**, 41 (2009).

26. K.P. Velikov, O.D. Velev, K.G. Marinova and G.N. Constantinides, *J. Chem. Soc. Faraday Trans*, **93**, 2069 (1997).

27. A. Bhakta and E. Ruckenstein, *J. Colloid Interface. Sc*i., **1**, 70 (1997).

28. D. Exerowa, N.V. Churaev, T. Kolarov, N.E. Esipova, N. Panchev and Z.M. Zorin*, J. Colloid Interface. Sc*i, **1**, 104 (2003).

29. B.P. Binks and S.O. Lumsdon, *Langmuir,* **16**, 8622 (2000).

30. D.W. Fuerstenau and R. Jia, *Colloids Surf. A*, **223**, 250 (2004).

31. K. Furusawa, A. Sato, J. Shirai and T. Nashima, *J. Colloid Interface Sci*., **53**, 273 (2002).

32. P. Wängnerud and G. Olofsson, *J. Colloid Interface Sci*., **153**, 392 (1992).

33. S.B. Velegol, B.D. Fleming, S.R. Biggs, E.J. Wanless and R.D. Tilton, *Langmuir*, **16**, 2548 (2000).

34. R. Atkin, V.S.J. Craig and S. Biggs, *Langmuir*, **17**, 6155 (2001).

35. T.P. Goloub, L.K. Koopal, B.H. Bijsterbosch and M.P. Sidorova, *Langmuir*, **12**, 3188 (1996).

36. M. Szekeres, I. Dékánya and A. de Keizer, *Colloids Surf. A*, **141**, 327 (1998).

37. L.K. Koopal, T. Goloub, A. de Keizer and M.P. Sidorova, *Colloids Surf. A*, **151**, 15 (1999).

38. W. Wang, B. Gu, L. Liang and W.A. Hamilton, *J. Phys. Chem. B*, **108,** 17477 (2004).

39. O. Theodoly, L. Cascão-Pereira, V. Bergeron and C.J. Radke, *Langmuir*, **21**, 10127 (2005).

40. R. Aveyard, B.P. Binks, P.D.I. Fletcher and C.E. Rutherford, *Colloids Surf. A*, **83**, 89 (1994).

41. L.G.J. Fokkink, J. Ralston, *Colloids Surf.* **36**, 69 (1989).

42. B.P. Binks, M. Kirkland and J.A. Rodrigues, Soft Matter, **4**, 2373 (2008).

43. R. Atkin, V.S.J. Craig, E.J. Wanless and S. Biggs, *Adv. Colloid Interface Sci.*, **103**, 219 (2003).

44. S. Manne, T.E. Schäffer, Q. Huo, P.K. Hansma, D.E. Morse, G.D. Stucky and J. A. Aksay, *Lamgmuir*, **13**, 6382 (1997).

45. A.B. Subramaniam, M. Abkarian, L. Mahadevan and H.A. Stone, *Nature*, **438** 930 (2005).

.

CHAPTER 9

CHAPTER 9

SUMMARY OF CONCLUSIONS AND FUTURE WORK

9.1   Summary of conclusions

The following conclusions were obtained from the work described in this thesis.

It is proposed that in the absence of surface–active agents, *e.g.* surfactants, the hydrophobicity of silica particles can be modified *in-situ* (Chapter 3) or *ex-situ* (Chapter 4) from hydrophilic to hydrophobic by engineering conditions and therefore particles are able to adsorb at the air-water interface. The foaming ability and stability of these aqueous silica particle dispersions has shown to be strongly dependent on the particle hydrophobicity, particle size, particle concentration, pH, NaCl concentration and also on the protocol used for the foam production. Stock of precipitated aqueous silica particles of diameter 3.5 to 100 nm were used in the *in-situ* study, while synthetic amorphous silica particles of diameters ranging from 50 to 2000 nm were used in the *ex-situ* study. It is shown with both studies that by increasing the particle size, the foaming ability and stability of the aqueous silica particles improved significantly. Since the energy of attachment of a particle to an interface, E, depends on the square of the particle radius, it decreases markedly for very small particles and detachment is easy. Therefore, small particles may not be particularly effective as foam stabilisers compared to the larger particles. It can be concluded that the size of particles has implications with respect to the rate at which particles can diffuse and arrive at the surface of newly formed bubbles in order to prevent disproportionation. Particle concentration was also found to be directly proportional to foaming ability and stability in both *in-situ* and *ex-situ* studies. An increase in particle concentration seems to cause a closer packing of particles at the bubbles surface, resulting in an increase in surface viscosity, a decrease in drainage rate and therefore an increase in foam stability.

The *in-situ* study (Chapter 3) shows that by decreasing the pH of the aqueous silica dispersions and by adding salt (*e.g.* 3 M) particles that are initially negatively charged and hydrophilic seem to become uncharged and more hydrophobic and therefore are believed to go to the air-water interface. As silica particles in water and bare air-water surfaces are negatively charged. Addition of salt to water may reduce the surface charge enhancing the transfer of particles to the surface. It is also found that the

particle contact angle increases as hydrophobicity increases, with both of these factors leading to improved foaming ability and stabilisation of the foam. This explains why stable foams could be prepared at such conditions, whereas in the absence of salt, stable foams could not be produced.

In the *ex-situ* study (Chapter 4), unmodified hydrophilic silica particles are shown to be able to stabilise aqueous foams in the presence of a smaller amount of salt (*e.g.* 0.5 M) compared with the *in-situ* study (*e.g.* 3 M). It is also shown that is possible to produce reasonable amounts of foam stabilised only by solid particles. Such particle-stabilised foams could last for several months. By increasing the particle hydrophobicity in the absence of salt a maximum in foamability was observed at a contact angle equal to 95°. However, the most stable foams are those formed with higher particle hydrophobicity ($\theta = 110°$) and in the presence of salt, where the adsorbed particles form a coagulated solid network preventing coalescence and disproportionation of bubbles. Silica particles were found to aggregate in bulk after addition of salt. The extent of aggregation depends on the hydrophobicity of the particle and the concentration of electrolyte. It was found that the more hydrophobic particles and the higher the salt concentration used, the bigger the aggregates formed. It seems that when very dense layers of particles and small aggregates adsorb around air bubbles, foam stability is enhanced in comparison to foams formed with discrete primary particles as they are easily detached form the air-water interface. One consequence of particle aggregation is the increased viscosity of the aqueous phase (gelling) which results in slower drainage of foam films and increased stability of the foam. The densely packed particles at the air-water interface, either in monolayer or multilayer configuration, provide strong steric hindrance to bubble coalescence.

The method of foam production is shown to have an influence on the foaming ability and stability of these aqueous silica particles. A higher volume of foam was obtained with the Ultra–Turrax homogeniser compared with the foams generated by hand–shaking. Foams produced with homogenisation at 17, 000 rpm were found to be more stable to disproportionation or coalescence of bubbles since bubbles seem to be completely covered with the particles, while at 13, 000 rpm some particles still remain in the bulk and eventually sediment.

Vertical foam films with particle monolayers at their surfaces have been studied in order to gain a better understanding of the mechanisms of foam stabilisation by solid particles. The structure and stability of the foam films were strongly dependent on particle contact angle, interactions between particles from the same and the opposite

monolayer and monolayer density. Stable films are observed only in those cases when the particle contact angle, θ, fulfils the condition for a stable particle bridge, that is, $\theta <$ 90° for foam films. These hydrophilic particles seem to possess high lateral mobility during film thinning which is crucial for their rearrangement at the air-water surface and subsequent stabilisation. That is why the hydrophilic particles are expelled out of the thinning foam film, forming eventually a ring of bridging particles at the film periphery. This happens in the case of foam films with dilute particle monolayer at their surfaces. However, in normal conditions, this means that dilute particle monolayer cannot protect the bubbles in real foam systems. Only when close-packed particles are achieved, very stable foams films can be obtained. This can be confirmed with real foam systems, where very stable small bubbles are covered with close-packed silica particles as shown in Chapter 4. Closely packed layers of solid particles are known to prevent the coalescence of bubbles in foams. In the case of foam films with hydrophobic particles at their surfaces is shown that by opening the film slowly particles start to move away from the thinnest part of film and do not bridge the surfaces. When the film is opened quickly, the film breaks immediately as some particles bridge the film surfaces. The hypothesis for stable foam films with close packed bilayers of hydrophobic particles is not supported by our results; probably because the films studied were not fully covered with close-packed particles. More experiments are needed in order to clarify the hypothesis.

A new method has been developed for measuring the contact angle of solid particles at the air-water interface *in-situ*. The results obtained are in excellent agreement with the contact angle values measured with alternative techniques. This new method showed that the air-water contact angle of 3 μm size silica particles hydrophobised to different extents gradually increase with an increases of particle hydrophobicity, in agreement with the trend obtained for the contact angle measured through the water on glass slides hydrophobised simultaneously with the particles.

The foaming ability and stability of hydrophilic Laponite clay particles has also been investigated. It is shown that foams are only formed under conditions where the particles are flocculated (*via NaCl*) but not gelled. Addition of salt may be responsible for an increase in the contact angle that Laponite particles make with the air-water surface, therefore increasing their hydrophobicity. However, this is not sufficient to stabilise the foams. All foams formed with this system are very unstable (burst within seconds or minutes). One reason that could be attributed to the instability of these foams is the size of the clay particles, as they are very small and therefore can be detached easily from the air-

water interface. Another reason may be that the aqueous phase is gelled quickly causing particles to lose their mobility, thus hindering foam formation. The effect of other electrolytes such as $MgCl_2$ and $LaCl_3$ on the foaming ability and stability of Laponite particles was also investigated. The results obtained with $MgCl_2$ were very similar to those obtained with NaCl. Aqueous dispersions of Laponite containing $[LaCl_3] < 2$ M gave rise to some bubbles at the top of dispersions (foamability), however those bubbles were very unstable and burst very quickly. Foam stability was only achieved when $[LaCl_3] > 2$ M and this may be attributed to the fact that the foam is formed just before the aqueous phase becomes gelled. Therefore, some particles go to the air-water interface, conferring stability to the newly formed bubbles. Also the viscosity and elastic nature of the continuous phase and surface of bubbles gives the long term stability achieved with such systems.

It has been shown in Chapter 8 that in mixtures of hydrophilic silica nanoparticles and CTAB cationic surfactant, the synergism between particles and CTAB at pH = 10 leads to enhanced foam stability at an intermediate CTAB concentration, where particles were found to be most flocculated. It is shown that surfactant addition initially leads to particle flocculation followed by re-dispersion. From zeta potential measurements, it is also shown that surfactant addition initially transforms particles from anionic to uncharged and hydrophobic and subsequently to cationic as a result of adsorption. Using suitable contact angle measurements at air-water-solid interfaces, it is shown that silica surfaces become increasingly hydrophobic initially upon surfactant addition achieving a maximum in hydrophobicity at intermediate [CTAB] and then particles become hydrophilic again as a result of bilayer surfactant adsorption. The most hydrophobic particles, possessing an adsorbed monolayer of surfactant, yield foams which are completely stable to disproportionation and coalescence. The foaming ability and stability of mixtures of silica particles and CTAB surfactant at low pH (*e.g.* pH = 3) was also investigated. The main finding was that when the surfactant was added to the unstable silica dispersions at pH = 3, silica particles become positively charged and coated with surfactant tails instead of hydrophilic heads (positively charged). Therefore, the foams formed at such low pH were unstable behaving as foams stabilised by surfactant alone.

Finally, it can be concluded from this research that nanoparticles are effective foaming agents of air and water and by controlling their hydrophobicity, foams that are completely stable to coalescence and disproportionation can be prepared. The behaviour of particles adsorbed at the air-water interface can also be manipulated by changing the pH, particle concentration and the concentration of salt of the aqueous particles systems.

The application of the fundamental knowledge gained in this research project will enable the development of a novel range of products based on particle-stabilised foams for use in food, detergent, and cosmetic formulations.

9.2   Future work

The following ideas are suggested from the work described in this thesis:

The cylinder shake test method and the use of an Ultra-Turrax homogeniser were the two methods used in the generation of all particle-stabilised foams obtained in this research. As a result, all foams were produced by incorporating air at room temperature. Depending on the process used when generating the foam, the size and shape of the bubbles within the foam may vary. Therefore, it is suggested to use other methods for the production of particle-stabilised foams in order to determine if they would improve their foaming ability and stability. Performing controlled studies at different temperatures and the incorporation of different gases is also important in order to determine if the temperature or type of gas would influence the foaming ability and stability of such aqueous particle dispersions. It is expected that the use of other gases less soluble than air (*e.g.* nitrogen), would be effective in producing more stable aqueous foams. One example, where foams could be reproduced under controlled conditions such as constant gas flow rate and constant temperature is the use of a thermostatically controlled foam column, where gas such as nitrogen is added directly to the liquid phase as fine bubbles blown through a sinter underneath the foaming solution. The information gathered from such experiments could prove useful in many industrial applications, as different manufacturing processes are used in different foamed products.

The search for new particles of different chemistry, size and hydrophobicity with potential application at enhancing the foaming ability and stability of foams is suggested. Since many (inorganic) colloidal particles in nature and technology are not spherical, it is also important to understand the influence of particle shape on the foaming ability and stability of the dispersions and be able to compare their rheological properties with spherical particles. Although some work exists on aqueous dispersions of rod-like particles, the behaviour of these particles at the air-water interface is still not well understood. For example, nanofibrous materials are currently being produced using a wide range of manufacturing properties. The surface properties of these materials are

dependent on their structure & size. Therefore, it would be of interest to study their behaviour at the air-water interface. However, understanding the surface properties of nanofibres is challenging due to difficulties in measuring the inherent properties of the fibres themselves.

Another suggestion would be adjusting the hydrophocity of rod-like inorganic materials (*e.g.* attapulgite or microspar particles), disc-like particles (*e.g.* laponite) or amorphous calcium carbonate particles of different sizes by using different types of modifiers (*e.g.* stearic acid) or by addition of surfactants, followed by studying the foaming ability and stability of the chemically modified particles. However, one challenge would be to achieve a uniform and stable hydrophobic coating with this type of particles, due to the large spread in both particle shapes and dimensions. This study would therefore, explore this aspect with a view of utilising the particles as novel foaming agents, as such non-spherical particles are attracting much interest worldwide.

There is a need for more detailed investigation into the foaming ability and stability, on a bulk scale, for systems involving mixtures of more than one surfactant in the presence of colloidal particles or mixtures of proteins, solid particles and surfactants. This would provide a better understanding into the foaming ability and stability of many industrial foams.

Finally, it is suggested to investigate the effect of particle size, salt concentration and particle shape on the stability of thin foam films in order to gain a better understanding on the mechanical behaviour of the foam films and be able to link the results with the bulk particle–stabilised foams.

.

APPENDIX: TABLES OF EXPERIMENTAL RESULTS

Figure 3.1   Initial foam volume (V_0) as a function of particle size for 20 mL aqueous dispersions of silica particles at fixed [particle] = 5 wt. %, pH = 4.20, and [NaCl] = 3 M.

Particle size / nm	Exp.1. V_o / mL	Exp. 2. V_o / mL	Average V_o / mL
3.5	5	3	4
25	9	7	8
34	10	12	11
100	22	20	21

Figure 3.2   Initial foam volume (V_0) as a function of particle concentration for 20 mL aqueous dispersions of silica particles of diameter 100 nm at fixed pH = 4.5 and [NaCl] = 3 M.

[silica] / wt. %	Exp.1. V_o / mL	Exp. 2. V_o / mL	Average V_o / mL
0	0	0	0
1	11	12	11.5
2	14	16	15
5	20	22	21
10	25	24	24.5

Figure 3.3 Variation of foam volume with time for 20 mL aqueous dispersions of silica particles of diameter 100 nm, [NaCl] = 3 M, and pH ~ 4.25 at different particle concentrations.

Time / min	Foam volume at ≠ [particle] wt.% / mL			
	1 %	2 %	5 %	10 %
0	12	15	20	25
5	4	12	18	20
15	3	11	16	17
30	2	10	16	17
60	0	10	15	17
120	-	9	14	16
180	-	9	13	16
240	-	8	12	15
360	-	8	11	14
1440	-	6	8	11
2880	-	3	5	8

Figure 3.5 Variation of initial foam volume with pH for 20 mL aqueous dispersions of silica particles of diameter 100 nm , [particle] = 5 wt.% and 3 M NaCl.

pH	Initial foam volume / mL		
	Exp.1	Exp.2	Average
1.6	9	10	10
2.7	12	15	14
3.2	14	15	15
4.2	20	23	20
4.5	18	22	20
4.7	17	18	18
5.1	14	15	15
5.4	13	16	15
5.9	8	9	9
7.4	8	10	9

Figure 3.6 Variation of foam volume with time for 20 mL aqueous dispersions of silica particles of diameter 100 nm, [particle] = 5 wt. %, [NaCl] = 3M, at different pH.

Time in min.	Foam volume / mL								
	pH=1.6	pH=2.7	pH=3.2	pH=4.3	pH=4.5	pH=4.7	pH=5.1	pH=6	pH=7.4
0	10	15	15	20	20	18	15	9	9
1	0	0	7	18	16	11	7	5	0
5	-	-	6	16	15	10	6	4	-
10	-	-	5	16	14	10	5	4	-
15	-	-	5	15	14	9	5	4	-
30	-	-	5	15	14	8	5	4	-
60	-	-	5	14	13	8	5	4	-
120	-	-	4	13	12	8	5	4	-
180	-	-	4	13	12	8	5	4	-
240	-	-	3	13	11	7	4	3	-
300	-	-	3	12	10	7	4	2	-
360	-	-	2	11	9	7	4	0	-
1200	-	-	0	10	7	5	3	-	-
1320	-	-	-	9	7	5	3	-	-
1440	-	-	-	9	7	4	2	-	-
2880	-	-	-	8	6	4	2	-	-

Figure 3.7 Variation of foam half-life ($t_{1/2}$) with pH for 20 mL aqueous dispersions of silica particles, [particle] = 5 wt. %, [NaCl] = 3M.

pH	$t_{1/2}$ / min.
1.6	0
2.7	0
3.2	0
4.3	1200
4.5	300
4.7	15
5.1	0
6.0	0
7.4	0

Figure 3.8 Variation of initial foam volume with pH for 20 mL aqueous dispersions of silica particles, [particle] = 5 wt. %, [NaCl] = 3 M.

pH	Initial foam volume / mL
4.0	15
4.1	16
4.2	20
4.5	20
4.7	18
4.8	15
4.9	15
5.0	14
5.2	14
5.3	14

Figure 3.9 Variation of foam half-life with pH for 20 mL aqueous dispersions of silica particles, [particle] = 5 wt. %, [NaCl] = 3M.

pH	$t_{1/2}$ / min.
4.0	1440
4.1	1440
4.2	1200
4.5	300
4.7	240
4.8	30
4.9	15
5.0	5
5.2	0
5.3	0

Figure 3.10 Variation of foam volume with time for 20 mL aqueous dispersions of silica particles, [particle] = 5 wt. %, [NaCl] = 3 M, at different pH.

Time in min.	Foam volume / mL						
	pH=4.00	pH=4.22	pH=4.53	pH=4.64	pH=4.78	pH=4.88	pH=5.17
0	15	20	20	18	18	15	14
1	15	17	16	16	12	10	6
5	14	16	14	14	10	6	5
15	14	16	14	13	10	5	4
30	13	15	14	13	9	5	4
60	13	15	13	12	8	5	4
120	13	14	12	11	8	5	4
180	13	14	12	9	7	5	4
240	12	13	11	9	7	5	4
300	11	12	10	9	7	4	4
1440	8	10	7	7	5	4	3
2880	7	9	5	5	4	3	0

Figure 3.11 Initial foam volume versus pH for 20 mL aqueous dispersions of silica particles of diameter 100 nm, [particle] = 10 wt. %, [NaCl] = 3 M.

Initial foam volume / mL		
pH = 4.09	pH = 4.34	pH = 4.73
25	20	18

Figure 3.12 Variation of foam volume with time for 20 mL aqueous dispersions of silica particles of diameter 100 nm, [particle] = 10 wt. %, [NaCl] = 3 M at different pH.

Time in min.	Foam volume / mL		
	pH = 4.09	pH = 4.34	pH = 4.73
0	25	20	18
1	18	16	13.9
5	17	16	14
15	17	16	12
30	17	15	11
60	17	15	10
120	17	14	10
180	16	14	8
240	15	13	7
300	14	12	7
1440	11	9	5
2880	8	6	4

Figure 3.13 Foam volume versus time for 20 mL aqueous dispersions of silica particles of diameter 100 nm, [particle] = 5 wt. %, [NaCl] = 3 M and pH ~ 4.2 for two separate dispersions.

Time in min.	Foam volume / mL	
	pH = 4.22	pH=4.12
0	20	18
5	18	17
15	16	17
30	16	17
60	15	16
120	14	13
180	13	13
360	11	11
1140	8	9
1440	7	9
2880	5	8

Figure 3.15 Initial foam volume and foam volume after different times versus concentration of NaCl for 20 mL aqueous dispersions of silica particles of diameter 100 nm, [particle] = 5 wt. % at pH around 4.5.

[NaCl] / M	Foam volume / mL			
	Initial (v_0)	5 hours	24 hours	48 hours
0	0	0	0	0
1	8	0	0	0
2	12	0	0	0
3	20	12	8	5
4	22	11	8	5
5	23	9	6	5

351

Figure 3.16 Variation of the initial foam volume and foam half-life with [NaCl] for 20
mL aqueous dispersions of silica particles of diameter 100 nm (5 wt. %) at
pH around 4.5.

[NaCl] / M	Initial foam volume / mL	Foam half-life ($t_{1/2}$) / min.
0	0	0
1	12	1
2	15	5
3	20	1080
4	22	240
5	23	180

Figure 3.17 Initial foam volume for 20 mL aqueous silica dispersions of diameter 100
nm, at a fixed [particle] = 5 wt.% at pH = 4.5 and contact angles of
aqueous NaCl drops under air on hydrophilic glass slides versus [NaCl].

[NaCl] / M	Initial foam volume / mL	contact angle (θ) / deg.
0	0	5
1	12	12
2	15	22
3	20	28
4	22	32
5	23	38

Figure 3.19 Foam half-life for 20 mL aqueous silica dispersions of particle diameter 100 nm, [particle] = 5 wt. % at pH = 4.5 and contact angles of aqueous NaCl drops under air on silicon wafer at pH = 4.5 versus [NaCl].

[NaCl] / M	Foam half-life ($t_{1/2}$) / min.	contact angle (θ) / deg.
0	0	14.3
1	1	29.2
2	5	35
3	1080	48.5
4	240	46.8
5	180	36.9

Figure 3.20 Zeta potential versus pH for aqueous dispersions of silica particles of diameter 100 nm, [particle] = 0.1 wt. % in Milli-Q water.

pH	Zeta potential / mV
9.5	- 63.3
6.5	- 53.1
4.5	- 34.8
3	- 17.3

Figure 3.21 Zeta potential versus NaCl concentration for aqueous dispersions of silica particles of diameter of diameter 100 nm, [particle] = 0.1 wt. % at different pH.

[NaCl] / M	Zeta potential / mV		
	pH = 9.5	pH = 4.5	pH = 3
0	-63.3	- 34.8	-17.3
0.25	n/a	-0.5	3.5
0.5	-9	0.4	6.8
1	5.7	10.7	12.2
2	13.9	19.1	20.5
3	17.6	20.4	21
4	20	20.8	21.6
5	20.2	21.9	21.7

Figure 3.22 Zeta potential versus pH for aqueous dispersions of silica particles of diameter 100 nm, [particle] = 0.1 wt. % at different [NaCl].

pH / [NaCl]/M	Zeta potential / mV						
	0	0.5	1	2	3	4	5
9.5	- 63.3	-9	5.7	13.9	17.6	20	20.2
6.5	- 53.1	-7	8.7	16.8	18.6	20.5	19.4
4.5	- 34.8	0.4	10.7	19.1	20.4	20.8	21.9
3	-17.3	6.8	12.2	20.5	21	21.6	21.7

Figure 3.23 Zeta potential versus pH for aqueous dispersions of silica particles of diameter 100 nm, [particle] = 0.1 wt. % with no salt (in this work) and with [NaCl] = 0.4 M (data obtained by George[36]).

pH	Zeta potential / mV	
	No salt	**[NaCl] = 0.4 M**
9.5	- 63.3	-18
8.5	n/a	-17.5
8	n/a	-15
7.5	n/a	-12
6.5	- 53.1	-8
6	n/a	-5
5.5	n/a	-2.5
4.5	- 34.8	-0.4
4	n/a	1
3.5	n/a	2.5
3	-17.3	2.8

Figure 3.26 Viscosity and shear stress versus shear rate for aqueous silica dispersion of diameter 100 nm, 5 wt. %, pH = 4.30, no salt.

Shear rate / s^{-1}	Viscosity / 10^{-3} Pa s	Shear stress / 10^{-2} Pa
3.63	2.36	0.85
4.51	2.24	1.01
5.61	2.17	1.21
7.01	1.78	1.25
8.74	1.70	1.49
10.9	1.99	2.17
13.6	1.79	2.43
17.0	1.81	3.07
21.2	1.47	3.11
26.4	1.40	3.71
33.0	1.39	4.59
41.1	1.40	5.76
51.3	1.39	7.13
63.9	1.44	9.19
79.6	1.48	11.8

Figure 3.27 Viscosity and shear stress versus shear rate for aqueous silica dispersion of diameter 100 nm, 5 wt. %, pH = 4.30, [NaCl] = 5 M.

Shear rate / s^{-1}	Viscosity / 10^{-3} Pa s	Shear stress / 10^{-2} Pa
3.63	12.4	4.49
4.87	10.3	5.02
6.68	9.06	6.05
8.95	8.33	7.45
12.1	7.15	8.63
16.4	6.07	9.94
22.1	5.30	11.7
29.8	4.54	13.5
40.3	4.09	16.5
54.5	3.99	21.7
73.5	3.47	25.5

Figure 3.28 Viscosity at a shear rate 22 s^{-1} versus time for aqueous silica dispersions of diameter 100 nm, 5 wt.%, pH = 4.30 at different NaCl concentration.

[NaCl]/M	Viscosity / 10^{-3} Pa s		
	30 min.	24 hours	48 hours
1	2.08	3.64	3.30
2	2.94	3.86	3.42
3	4.09	5.25	4.68
4	4.92	5.79	5.67
5	7.64	7.94	6.99

Figure 3.29 Viscosity at a shear rate 22 s^{-1} versus [NaCl] for aqueous dispersions of silica particles of diameter 100 nm, 5 wt.%, pH = 4.30 at different times.

Time / hours	Viscosity / 10^{-3} Pa s @ [NaCl]				
	1 M	2 M	3 M	4 M	5 M
30 min.	2.08	2.94	4.09	4.92	7.64
24	3.64	3.86	5.25	5.79	7.94
48	3.30	3.42	4.68	5.67	6.99

Figure 4.3 ΔBS at the bottom of the vessel (0 - 6 mm) versus time for 3 wt. % aqueous dispersions of silica particles of diameter 0.6 μm at different hydrophobicity and no salt.

Time/sec	ABS / % @ bottom of vessel				
	5°	58°	77°	95°	105°
0	0	0	0	0	0
60	0.04579	0.09034	0.4126	2.800	5.098
120	0.01066	0.09636	0.8469	3.102	5.714
180	0.08427	0.08527	0.9403	3.129	5.843
240	0.1312	0.3835	1.159	3.232	5.895
300	0.2215	0.4806	1.415	3.227	5.928
360	0.2899	0.3677	1.393	3.286	5.919
420	0.3550	0.4516	1.505	3.361	5.959
480	0.4413	0.3779	1.611	3.348	5.934
540	0.5085	0.6573	1.756	3.427	5.994
600	0.5778	0.7595	2.049	3.413	6.015
660	0.6223	0.8844	1.972	3.485	6.013
720	0.6886	1.023	2.074	3.507	6.048
780	0.7165	1.315	2.146	3.537	6.009
840	0.7965	1.488	2.256	3.545	6.008
900	0.8469	1.376	2.329	3.547	6.041
960	0.8902	1.486	2.609	3.596	6.069
1080	0.9911	1.910	2.570	3.653	6.039
1200	1.087	2.098	2.759	3.683	6.090
1320	1.174	2.311	2.933	3.767	6.058
1440	1.268	2.049	3.294	3.802	6.101
1560	1.547	2.220	3.488	3.879	6.084
1680	1.418	2.556	3.480	3.880	6.103

Figure 4.4　ΔBS at the top of the vessel (12 - 22 mm) versus time for 3 wt. % aqueous dispersions of silica particles of diameter 0.6 μm at different hydrophobicity and no salt.

Time/sec	ABS / % @ top of vessel				
	5°	58°	77°	95°	105°
0	0	0	0	0	0
60	0.01041	-0.3259	0.02456	-0.5934	-11.40
120	0.004012	-0.4604	0.06748	-0.8426	-11.56
180	0.007287	-0.5157	-0.1188	-1.015	-11.60
240	-0.03041	-0.5653	-0.1660	-1.143	-11.62
300	-0.04517	-0.6616	-0.2188	-1.287	-11.64
360	-0.05105	-0.6991	-0.2734	-1.395	-11.66
420	-0.06366	-0.7266	-0.3243	-1.461	-11.66
480	-0.06020	-0.7711	-0.3859	-1.515	-11.67
540	-0.07803	-0.8232	-0.4423	-1.567	-11.67
600	-0.08329	-0.8821	-0.4958	-1.613	-11.68
660	-0.09968	-0.9254	-0.5594	-1.647	-11.70
720	-0.1090	-0.9399	-0.6257	-1.688	-11.70
780	-0.1278	-0.9591	-0.6893	-1.719	-11.67
840	-0.1403	-0.9737	-0.7637	-1.746	-11.63
900	-0.1359	-1.006	-0.821	-1.781	-11.63
960	-0.1435	-1.040	-0.8872	-1.805	-11.62
1080	-0.1675	-1.056	-1.014	-1.87	-11.63
1200	-0.1877	-1.096	-1.152	-1.936	-11.64
1320	0.2051	-1.115	-1.291	-1.989	-11.64
1440	-0.1954	-1.157	-1.429	-2.040	-11.64
1560	-0.2126	-1.183	-1.61	-2.091	-11.65
1680	-0.2380	-1.194	-1.679	-2.135	-11.65

Figure 4.5 ΔH (phase thickness of the sediment layer) from backscattering data obtained between height limits (0 to 8 mm) versus time for 3 wt. % aqueous dispersion of silica particles of diameter 0.6 μm at different particle hydrophobicity and with no salt.

Time /	ΔH / mm			
sec	5°	58°	95°	105°
0	0	0	0	0
60	0	0	2.25	0.246
120	0	0	2.44	3.70
180	0	0	2.45	3.79
240	0	0	2.45	3.81
300	0	0	2.44	3.85
360	0	0.390	2.44	3.87
420	0	0.408	2.42	3.88
480	0	0.594	2.40	3.88
540	0	0.876	2.41	3.88
600	0	0.854	2.40	3.88
660	0	0.917	2.40	3.93
720	0	0.976	2.38	3.92
780	0	1.04	2.37	3.92
840	0	1.08	2.36	3.94
900	0	1.13	2.35	3.96
960	0	1.25	2.35	3.96

Figure 4.6 ΔH (phase thickness of the sediment layer) from backscattering data obtained between height limits (0 to 8 mm) at long time for 3 wt. % aqueous dispersion of silica particles of diameter 0.6 μm at different particle hydrophobicity and no salt.

Time / sec	ΔH / mm			
	5°	58°	95°	105°
85551	0.815	1.26	3.4	5.99
85611	0.941	1.26	3.39	6.01
85671	1.03	1.28	3.39	6.00
85731	1.06	1.3	3.4	5.99
85791	1.07	1.29	3.44	5.98
85851	1.13	1.29	3.4	6.03
85911	1.10	1.3	3.44	5.99
85971	1.11	1.31	3.39	5.98
86031	1.12	1.31	3.44	5.98
86091	1.15	1.3	3.43	5.97
86151	1.15	1.32	3.39	6.06
86211	1.13	1.33	3.4	5.98
86271	1.16	1.33	3.44	6.07
86331	1.16	1.31	3.46	5.98
86391	1.13	1.31	3.44	6.06
86451	1.12	1.32	3.39	6.01
86511	1.12	1.32	3.44	6.00
86631	1.12	1.32	3.41	5.97

Figure 4.9 Hydrodynamic particle diameter and mean particle velocity versus particle hydrophobicity for 3 wt. % aqueous dispersions of silica particles of diameter 0.6 μm and no salt (data obtained in the first 20 minutes after sample preparation).

air – water θ / deg.	migration velocity V / (μm) min^{-1}	particle diameter / μm
5	11.3397	0.586
58	18.9270	0.829
77	39.5489	1.09
95	44.3149	1.16
105	240.423	2.95

Figure 4.12 Hydrodynamic particle diameter and particle velocity (clarified phase) versus NaCl concentration for 3 wt. % aqueous dispersions of unmodified silica particles of diameter 0.6 μm at different [NaCl] (data obtained in the first 20 minutes after sample preparation).

[NaCl] / M	Particle diameter / μm	migration velocity V / (μm) min^{-1}
0	0.586	11.3397
0.05	2.44	197.316
0.1	2.81	260.272
0.5	3.81	481.191

Figure 4.16 Initial foam height and foam height after 48 hours versus estimated particle hydrophobicity for 10 mL aqueous silica dispersions of diameter 0.6 μm previously silanised at different [DCDMS] at a concentration of 3 wt. %, pH = 6 and no salt.

air – water θ / deg.	Initial foam height / cm	Foam height after 48 hours / cm
5	0	0
58	1.5	1
77	3	2.8
95	3.5	3.3
105	2.5	2.38
110	2.44	2.33

Figure 4.19 Foam height *versus* time for 10 mL (~ 3.2 cm) aqueous silica dispersions of diameter 0.6 μm (θ_{aw} average = 58°) at a concentration of 1.5 wt. %, pH = 5.6 to 4.4 at different [NaCl] given (hand shake test).

Time / min.	Foam height / cm @ [NaCl]			
	0 M	0.05 & 0.1 M	0.5 M	1 M
1	0	1.23	1.48	1.75
30	0	1.21	1.42	1.67
60	0	1.19	1.34	1.64
180	0	1.05	1.21	1.54
360	0	1.04	1.178	1.47
1440	0	1.03	1.17	1.45

Figure 4.21 Foam height *versus* time for 10 mL (~ 3.2 cm) aqueous silica dispersions of diameter 0.6 μm (θ_{aw} average = 58°) at a concentration of 3 wt. %, at pH around 5 at different [NaCl] given (hand shake method).

Time / min.	Foam height / cm @ [NaCl]				
	0 M	0.05 M	0.1 M	0.5 M	1 M
1	0.75	1.13	1.38	2	2.25
30	0.75	1.11	1.38	1.81	2.08
60	0.68	0.95	1.23	1.77	2.05
180	0.64	0.89	1.14	1.65	1.97
360	0.64	0.89	1.14	1.65	1.97
1440	0.64	0.76	0.89	1.53	1.81

Figure 4.28 Hydrodynamic particle diameter and initial foam height versus air-water contact angle for 3 wt. % aqueous dispersions of silica particles of diameter 0.6 μm in the absence of salt.

air – water θ / deg.	Initial foam height / cm	Particle diameter / μm
5	0	0.58
58	1.5	0.829
77	3	1.09
95.1	3.5	1.25
105	2.5	2.95

Figure 4.29 Hydrodynamic particle diameter and initial foam height versus NaCl concentration for 3 wt. % aqueous dispersions of silica particles of diameter 0.6 μm and previously silanised at [DCDMS] = 8 × 10^{-4} M (θ_{aw} average = 58°).

[NaCl] / M	Initial foam height / cm	Particle diameter / μm
0	1.56	0.829
0.05	2.05	2.44
0.1	2.1	2.81
0.5	2.7	3.81
1	3.44	4.72

Figure 4.30 Hydrodynamic particle diameter and initial foam height versus NaCl concentration for 3 wt. % aqueous dispersions of silica particles of diameter 0.6 μm and previously silanised at [DCDMS] = 8 × 10^{-2} M (θ_{aw} average = 105°).

[NaCl] / M	Initial foam height / cm	Particle diameter / μm
0	2.3	2.95
0.05	2.3	3.12
0.1	2.5	4.93
0.5	2.7	6.96
1	2.7	7.39

Figure 4.35 Initial foam height and foam height after 48 hours versus air-water contact angle for aqueous dispersions of silica particles of diameter 0.6 and 2 μm at different concentrations as given.

θ / deg.	Initial foam height / cm		Foam height after 48 hours / cm	
	0.6 μm 3 wt.%	2 μm 10 wt.%	0.6 μm 3 wt.%	2 μm 10 wt.%
5	0	0	0	0
58	1.5	3.58	1	2.84
77	3	3.81	2.8	3.63
95	3.5	3.97	3.3	3.87

Figure 6.4 Radial distance measured from the film centre versus light intensity profile in grey scale units (*g.s.u*). Note: data continues until page 374.

Radial distance, r / μm	Light intensity / *g.s.u.*
5.67	3054
6.30	2977
6.93	3030
7.56	2970
8.19	3032
8.82	2982
9.44	2996
10.07	2976
10.70	3096
11.33	2975
11.96	3067
12.59	3058
13.22	3072
13.85	3063
14.48	3020
15.11	3054
15.74	3069
16.37	3003
17.00	3040
17.63	3062
18.26	2956
18.89	2907
19.52	2906
20.15	2994
20.78	2953
21.41	3056
22.04	2976
22.67	3013
23.30	2907
23.93	3013
24.56	2985
25.18	2931
25.82	2981
26.45	3012
27.07	2996
27.70	2959
28.33	3011
28.96	2965
29.59	2988
30.22	2919
30.85	2965
31.48	3075

Radial distance, r / μm	Light intensity / *g.s.u.*
32.11	2983
32.74	2982
33.37	2945
34.00	2963
34.63	2936
35.26	3006
35.89	2966
36.52	2970
37.15	2903
37.78	2912
38.41	3007
39.04	2954
39.67	2990
40.30	3015
40.93	2963
41.56	2902
42.19	2944
42.82	2981
43.45	2879
44.07	2928
44.70	2896
45.33	2884
45.96	2912
46.59	2929
47.22	2918
47.85	2906
48.48	2878
49.11	2885
49.74	2858
50.37	2917
51.00	2896
51.63	2924
52.26	2875
52.89	2920
53.52	2942
54.15	2908
54.78	2861
55.41	2919
56.04	2865
56.67	2934
57.30	2849
57.93	2852
58.56	2866
59.18	2866
59.82	2842
60.45	2976
61.07	2907

Radial distance, r / μm	Light intensity / *g.s.u.*
61.70	2890
62.33	2934
62.96	2884
63.59	2863
64.22	2869
64.85	2822
65.48	2808
66.11	2851
66.74	2844
67.37	2896
68.00	2891
68.63	2831
69.26	2835
69.89	2850
70.52	2859
71.14	2827
71.78	2822
72.41	2709
73.04	2798
73.67	2792
74.30	2843
74.93	2792
75.56	2756
76.19	2807
76.82	2812
77.45	2808
78.07	2816
78.70	2788
79.35	2900
79.96	2750
80.59	2781
81.23	2729
81.85	2706
82.49	2766
83.13	2835
83.74	2711
84.37	2750
85.00	2741
85.63	2797
86.26	2757
86.89	2745
87.52	2755
88.15	2728
88.77	2716
89.40	2754
90.03	2730
90.67	2681

Radial distance, r / μm	Light intensity / *g.s.u.*
91.29	2724
91.92	2757
92.55	2736
93.18	2684
93.82	2648
94.45	2759
95.07	2714
95.70	2727
96.33	2743
96.96	2665
97.59	2745
98.23	2673
98.85	2746
99.48	2694
100.11	2701
100.74	2683
101.37	2739
102.00	2654
102.63	2666
103.26	2699
103.89	2661
104.52	2662
105.15	2692
105.78	2631
106.41	2587
107.03	2722
107.67	2674
108.30	2649
108.93	2606
109.57	2643
110.19	2736
110.82	2681
111.45	2673
112.07	2608
112.71	2732
113.35	2595
113.97	2708
114.59	2688
115.22	2675
115.85	2678
116.48	2643
117.11	2691
117.74	2606
118.37	2653
119.00	2680
119.63	2673
120.26	2593

Radial distance, r / μm	Light intensity / *g.s.u.*
120.89	2591
121.52	2636
122.15	2607
122.78	2627
123.41	2592
124.03	2531
124.66	2590
125.29	2554
125.92	2656
126.56	2570
127.18	2591
127.82	2538
128.45	2604
129.07	2619
129.71	2615
130.34	2524
130.96	2556
131.59	2627
132.23	2628
132.85	2594
133.48	2538
134.12	2610
134.74	2597
135.37	2528
136.00	2498
136.63	2541
137.26	2593
137.89	2582
138.52	2529
139.15	2643
139.78	2589
140.41	2590
141.04	2488
141.66	2595
142.30	2563
142.93	2531
143.56	2492
144.18	2516
144.82	2517
145.45	2523
146.08	2491
146.71	2560
147.34	2539
147.97	2616
148.59	2515
149.23	2502
149.85	2478

Radial distance, r / μm	Light intensity / *g.s.u.*
150.48	2503
151.11	2462
151.74	2482
152.37	2522
153.00	2479
153.63	2420
154.26	2472
154.89	2522
155.52	2474
156.15	2423
156.78	2425
157.41	2475
158.04	2401
158.67	2383
159.30	2419
159.93	2448
160.56	2442
161.19	2463
161.82	2416
162.45	2393
163.08	2480
163.71	2430
164.34	2425
164.97	2451
165.59	2436
166.23	2424
166.86	2343
167.49	2309
168.11	2404
168.74	2408
169.37	2497
170.00	2475
170.63	2413
171.26	2370
171.89	2357
172.52	2362
173.15	2357
173.78	2290
174.41	2325
175.04	2438
175.67	2347
176.30	2362
176.93	2382
177.56	2295
178.18	2332
178.81	2387
179.45	2339

Radial distance, r / μm	Light intensity / *g.s.u.*
180.08	2329
180.71	2250
181.34	2346
181.97	2293
182.59	2372
183.23	2266
183.86	2371
184.49	2248
185.12	2296
185.75	2248
186.37	2275
187.00	2256
187.63	2340
188.26	2246
188.89	2299
189.52	2309
190.15	2200
190.78	2279
191.41	2249
192.04	2221
192.67	2188
193.30	2277
193.93	2242
194.56	2193
195.19	2199
195.82	2264
196.45	2259
197.07	2276
197.71	2288
198.34	2258
198.97	2226
199.59	2179
200.23	2152
200.86	2175
201.49	2196
202.12	2152
202.75	2220
203.37	2191
204.00	2184
204.63	2127
205.26	2218
205.89	2135
206.52	2178
207.15	2119
207.78	2167
208.41	2128
209.04	2181

Radial distance, r / µm	Light intensity / g.s.u.
209.67	2106
210.30	2116
210.93	2129
211.56	2173
212.19	2087
212.82	2094
213.45	2107
214.079	2141
214.71	2174
215.33	2172
215.97	2129
216.58	2096
217.23	2075
217.8	2104
218.48	2044
219.11	2081
219.74	2051
220.37	1991
221.00	2033
221.63	1978
222.26	2042
222.89	2073
223.52	2023
224.15	2072
224.78	2033
225.41	2010
226.04	1997
226.67	2021
227.30	2028
227.93	1968
228.56	1951
229.19	2023
229.82	2018
230.45	2056
231.08	1943
231.71	1976
232.34	1964
232.96	1900
233.59	1909
234.23	1936
234.85	1895
235.48	1870
236.12	1875
236.74	1890
237.35	1860
238.01	1883
238.63	1852

Radial distance, r / μm	Light intensity / *g.s.u.*
239.26	1827
239.89	1823
240.52	1790
241.15	1804
241.78	1713
242.41	1775
243.04	1777
243.67	1693
244.31	1657
244.93	1691
245.56	1698
246.19	1630
246.82	1614
247.45	1604
248.08	1569
248.71	1580
249.34	1603
249.97	1547
250.59	1601
251.23	1563
251.86	1602
252.49	1593
253.12	1527
253.75	1612
254.37	1632
255.01	1688
255.63	1744
256.26	1766
256.89	1847
257.52	1959
258.15	2135
258.78	2273
259.41	2364
260.04	2506
260.67	2685
261.30	2846
261.93	3107
262.56	3250
263.19	3320
263.82	3390
264.45	3510
265.07	3591
265.71	3594
266.34	3570
266.97	3308
267.59	3165
268.23	2990

Radial distance, r / µm	Light intensity / *g.s.u.*
268.86	2698
269.49	2451
270.12	2149
270.75	1930
271.38	1816
272.00	1667
272.63	1758
273.26	1858
273.89	2090
274.52	2434
275.15	2701
275.78	3097
276.41	3294
277.04	3314
277.67	3405
278.30	3191
278.93	2878
279.56	2570
280.19	2213
280.82	1972
281.45	1824
282.08	1937
282.71	2163
283.34	2511
283.97	2976
284.60	3072
285.23	3287
285.85	3132
286.49	2797
287.12	2508
287.75	2181
288.37	2050
289.01	1985
289.63	2229
290.26	2642
290.89	2914
291.52	3175
292.15	3153
292.78	2876
293.41	2504
294.04	2135
294.67	2109
295.30	2205
295.93	2576
296.56	2814
297.19	3070
297.82	2909

Radial distance, r / μm	Light intensity / *g.s.u.*
298.45	2647
299.08	2346
299.71	2218
300.34	2238
300.96	2497
301.59	2882
302.23	2963
302.86	2769
303.49	2594
304.12	2341
304.75	2231
305.38	2386
306.01	2724
306.64	2800
307.27	2842
307.89	2577
308.52	2344
309.15	2265
309.78	2525
310.41	2801
311.04	2923
311.67	2754
312.30	2420
312.93	2326
313.56	2406
314.192	2739
314.82	2853
315.45	2818
316.08	2543
316.71	2417
317.34	2649
317.97	2927
318.60	3237
319.23	3094
319.86	2817
320.49	2856
321.12	0
321.75	3113
322.38	3092
323.00	2710
323.64	2223
324.27	1961
324.89	2108
325.53	2355
326.15	2200
326.78	2008

Figure 6.5 Film thickness of the meniscus calculated for the interference maxima and minima obtained from the light intensity profile data.

Radial distance, r / μm	Film thickness, h_e / μm
253.75	0.21
266.34	0.31
272.64	0.41
278.30	0.51
282.08	0.62
285.86	0.72
289.64	0.82
292.15	0.92
295.30	1.03
297.82	1.13
300.34	1.23
302.86	1.33
305.38	1.44
307.89	1.54
309.78	1.64
311.67	1.74
313.56	1.85
315.45	1.95
317.34	2.05
319.23	2.16
320.49	2.26
322.38	2.36
324.89	2.46
326.16	2.57
328.04	2.67
329.93	2.77
330.56	2.87
331.82	2.98
333.71	3.08

Figure 6.7 Film thickness, h_e, at the location of one bridging particle of diameter 3 µm versus radial distance from the film centre during the shrinking of the film by pumping water into the meniscus.

Radial distance, r / µm	Film thickness, h_e / µm
321.7	2.3
285.1	2.26
247	2.22
194	2.25
121.3	2.38

Figure 6.10 Contact angles of 3 µm silica particles hydrophobised with HMDS measured at an air-water interface with the new FCM and on glass plates hydrophobised simultaneously with the particles.

[HMDS] / M	Contact angle / deg.	
	particle	glass plate
1×10^{-4}	40 ± 2	46 ± 3
1×10^{-3}	56 ± 1	67 ± 3
1×10^{-1}	67 ± 2	75 ± 2

Figure 6.13 Contact angles of PS sulphate latex particles of diameter 9.6 µm at the air-water interface determined by the side imaging technique (using equations 4 and 5 from page 262) and from the bridging particles in the thin foam films by using the new film calliper method.

Figure no.	FCM contact angle / deg.	Side Imaging Technique contact angle / deg.	
		Sin θ (Eq. 4)	Cos θ (Eq. 5)
1	37.69	37.98	36.75
2	40.61	35.74	34.11
3	41.54	44.62	45.15
4	38.68	43.74	41.77
5	38.68	43.63	40.33
6	41.54	35.74	37.92
7	39.66	42.06	37.69
8	41.54	42.96	42.47
9	39.66	41.92	34.55
10	42.46	40.87	40.33

Figure 7.9 Partial phase diagram of 20 mL aqueous Laponite RD dispersions at pH in around 8.5-10 in the presence of NaCl at room temperature (protocol 1).

Dispersion description	[NaCl] / M	[Laponite RD] / wt.%
Clear Fluid	0.001 0.001	0.5 1.0
Clear gel, flows	0.001	2.0
Turbid gel (reversible from 0.1 M NaCl)	0.1 0.1 0.1 0.1 0.5 0.5 0.5 0.5 1.0 1.0 1.0 1.0 2.0 2.0 2.0	1.5 2.0 2.5 3.0 2.5 3.0 3.5 4.0 2.5 3.0 3.5 4.0 3.0 3.5 4.0
Slightly turbid viscous	0.01	0.5
Slightly turbid gel, flows	0.01 0.1 0.5 1.0 2.0 1.0	1.0 1.0 1.0 1.0 1.0 0.5
Slightly turbid floc + clear supernatant	0.1 0.5 1.0 2.0 3.0	0.5 0.5 0.5 0.5 0.5
Turbid gel (doesn't flow, reversible), clear supernatant at the bottom of vessel	0.5 0.5 1.0 1.0 2.0 2.0 2.0 3.0	1.5 2.0 1.5 2.0 1.5 2.0 2.5 1.5
Turbid gel, flows, clear supernatant at the bottom of vessel	3.0 3.0 4.0 4.0 4.0	2.0 2.5 1.5 2.0 2.5

Figure 7.14 Partial phase diagram of 20 mL aqueous Laponite RD dispersions at pH around 8.5 – 10 in the presence of NaCl at room temperature (protocol 2).

Dispersion description	[NaCl] / M	[Laponite RD] / wt.%
Clear Fluid	0.001	0.5
	0.001	1.0
Clear gel, flows	0.001	2.0
Turbid floc + clear supernatant	0.5	0.1
	0.5	1.0
	0.7	1.0
	1.0	1.0
	1.5	1.0
	2.0	1.0
	2.5	1.0
	3.0	1.0
	1.0	0.1
	1.5	0.1
	1.5	0.5
	1.5	1.0
	1.5	2.0
	1.5	3.0
	1.5	4.0
	2.0	0.05
	2.0	0.1
	2.0	0.5
	2.0	1.0
	2.0	2.0
Slightly turbid viscous	0.01	0.5
	0.01	1.0
Slightly turbid gel (doesn't flow)	0.001	2.5
	0.001	3
	0.001	4
	0.001	5

Figure 7.16 Initial foam height versus NaCl concentration for 0.5 wt. % aqueous dispersions of Laponite RD particles (protocol 1).

[NaCl] / M	Initial foam height / cm
0.5	0.6
1	0.6
2	1.7
3	2.5

Figure 7.20 Initial foam height versus NaCl concentration for 1.5 wt. % aqueous dispersions of Laponite RD particles (protocol 2).

[NaCl] / M	Initial foam height / cm
1	0.9
2	1.9
3	2.2
4	3

Figure 7.30 Initial foam height versus different types of electrolytes concentration ($LaCl_3$, $MgCl_2$, NaCl) for 0.5 wt. % aqueous dispersions of Laponite RD particles (protocol 1).

[NaCl] / M	Initial foam height / cm
0.5	0.6
1	0.6
2	1.7
[MgCl$_2$] / M	**Initial foam height / cm**
0.5	0.8
1	0.9
2	1.8
[LaCl$_3$] / M	**Initial foam height / cm**
0.5	1.5
1	1.8
2	2

Figure 8.1 Effect of CTAB concentration on the foaming ability of solutions of 10 mL CTAB alone at different pH values at room temperature.

[CTAB] / M	initial foam volume / mL		
	pH = 3	pH = 6	pH = 10
0.0000125	0	0	0
0.00005	6	6	4
0.0009	75	90	30
0.005	100	110	60
0.05	110	120	90

Figure 8.3 Sediment height in % after 1 hour *versus* CTAB concentration for the system shown in Figure 8.2.

CTAB / mM	Sediment height / %
0.001	0
0.01	0
0.02	0
0.05	25
0.09	40
0.2	25
0.5	25
0.9	0
5	0

Figure 8.4 Hydrodynamic particle diameter versus [CTAB] for aqueous dispersions of silica particles (0.6 μm), [particle] = 0.1 wt.% at pH = 10.

[CTAB] / mM	Hydrodynamic particle diameter / nm
0.00001	615
0.0001	677
0.01	1116
0.05	5790
0.5	841
5	768

Figure 8.7 Variation of air-water surface tension at 25 °C with CTAB concentration at pH = 10 with and without 3 wt. % silica particles of diameter 600 nm.

[CTAB] / M	CTAB alone	+ silica particles
	γ / (mN) m^{-1}	γ / (mN) m^{-1}
0.00000125	70.8	68.6
0.0000025	70.6	68.5
0.0000125	68.58	68.12
0.000025	66.94	68.1
0.00005	64.3	68.02
0.0001	61	66.21
0.0002	57.8	63
0.0003	54	61.18
0.0004	51.8	59.11
0.0005	48.7	56.34
0.000625	44.95	53.8
0.0008	41.4	50.26
0.0009	39.7	48.68
0.00125	35.77	44.71
0.0018	35.57	37.9
0.0025	35.27	36.84
0.005	35.06	36.6
0.01	34.44	35.78
0.02	34.35	35.68

Figure 8.8   Adsorption isotherm of CTAB on silica particles of diameter 600 nm at pH = 10 derived from data in Figure 8.7.

[CTAB] equilibrium / M	[CTAB] ads / (mmol) g^{-1}
2.28E-05	0.00007
2.33E-05	0.00089
3.64E-05	0.00212
6.46E-05	0.00451
8.41E-05	0.00720
1.10E-04	0.00966
1.52E-04	0.01160
2.00E-04	0.01418
2.84E-04	0.01719
3.30E-04	0.01898
4.75E-04	0.02582
8.60E-04	0.03133
9.41E-04	0.05197
9.60E-04	0.13466
1.03E-03	0.29904
1.04E-03	0.63208

Figure 8.9   Average contact angle of aqueous CTAB drops (~ 5 - 10 μl) under air on hydrophilic silicon wafer at pH = 10 versus CTAB concentration. 1×10^{-8} M CTAB corresponds to the aqueous silica dispersion alone (without CTAB).

[CTAB] / M	Average contact angle / deg.
0.00000001	24
0.0000025	51
0.000025	61
0.00005	70
0.0001	55
0.001	46
0.0025	45
0.01	44
0.1	39

Figure 8.10 Zeta potential versus CTAB concentration for aqueous dispersions of monodisperse silica particles of diameter 0.6 μm (0.1 wt. %) at pH ~ 10. The dotted line corresponds to the aqueous silica dispersion alone (without CTAB).

[CTAB] / M	Zeta Potential / mV
0.0000001	-70
0.000001	-50
0.00001	-19.5
0.00005	-0.6
0.0001	4.8
0.0005	25
0.0009	45
0.001	49
0.005	54
0.05	66

Figure 8.13 Effect of CTAB concentration on the foaming ability and stability after 24 hours of foams produced from mixtures of 10 mL aqueous dispersion of monodisperse silica particles of diameter 0.6 μm (3 wt. %) and CTAB at different concentrations at pH = 6.

[CTAB] / mM	pH = 6	
	Initial foam volume	Foam volume after 24 hours
0	0	0
0.001	3.3	2.9
0.02	6.0	4.3
0.05	10	6.4
0.1	12	9.3
0.2	15.3	15
0.5	21.3	3.3
1	23.3	0

Figure 8.15 Effect of CTAB concentration on the foaming ability and stability after 24 hours of foams produced from mixtures of 10 mL aqueous dispersion of monodisperse silica particles of diameter 0.6 μm (3 wt. %) and CTAB at different concentrations at pH ~ 3.

[CTAB] / mM	pH = 3	
	Initial foam volume	**Foam volume after 24 hours**
0	0	0
0.001	6.4	0
0.02	7.1	0
0.05	9.3	0
0.1	10.7	0
0.2	14.3	0
0.5	21.4	0
1	12.8	0